

THE JOURNAL OF
PHYSICAL
CHEMISTRY

Volume 67

JANUARY—JUNE, 1963

PAGES 1—1398

W. ALBERT NOYES, JR., *Editor*

WALTER J. MOORE, *Assistant Editor*

CHARLES R. BERTSCH, *Senior Production Editor*

RICHARD H. BELKNAP, *Director of Fundamental Journals Division*

EDITORIAL BOARD

A. O. ALLEN
J. BIGEISEN
B. P. DAILEY
F. S. DANTON
D. D. ELEY
D. H. EVERETT
J. R. FRESCO

C. J. HOCHANADEL
W. KLEMPERER
A. D. LIEHR
S. C. LIND
F. A. LONG
J. L. MARGRAVE
J. P. McCULLOUGH

R. G. PARR
G. PORTER
J. E. RICCI
R. E. RUNDLE
W. H. STOCKMAYER
M. B. WALLENSTEIN
W. WEST

EASTON, PA.
MACK PRINTING COMPANY
1963

THE JOURNAL OF PHYSICAL CHEMISTRY

W. ALBERT NOYES, JR., EDITOR

WALTER J. MOORE, ASSISTANT EDITOR

ALLEN D. BLISS, SENIOR PRODUCTION EDITOR

EDITORIAL BOARD

A. O. ALLEN
J. BIGEISEN
B. P. DAILEY
F. S. DAINTON

D. D. ELEY
D. H. EVERETT
S. C. LIND
F. A. LONG

J. L. MARGRAVE
J. P. MCCULLOUGH
G. PORTER
J. E. RICCI

R. E. RUNDLE
W. H. STOCKMAYER
M. B. WALLENSTEIN
W. WEST

© Copyright, 1963, by the American Chemical Society.

Published monthly by the American Chemical Society at 20th and Northampton Sts., Easton, Pa. Second-class postage paid at Easton, Pa.

The Journal of Physical Chemistry is devoted to the publication of selected symposia in the broad field of physical chemistry and to other contributed papers.

Manuscripts originating in the British Isles, Europe, and Africa should be sent to F. C. Tompkins, The Faraday Society, 6 Gray's Inn Square, London W. C. 1, England.

Manuscripts originating elsewhere should be sent to W. Albert Noyes, Jr., Department of Chemistry, University of Rochester, Rochester 20, N. Y.

Correspondence regarding accepted copy, proofs, and reprints should be directed to Senior Production Editor, Allen D. Bliss, ACS Office, Mack Printing Company, 20th and Northampton Sts., Easton, Pa.

Director of Planning, Fundamental Journals: Richard H. Belknap, 1155 Sixteenth St., N.W., Washington 6, D. C.

Advertising Office: Reinhold Publishing Corporation, 430 Park Avenue, New York 22, N. Y.

Articles must be submitted in duplicate, typed, and double spaced. They should have at the beginning a brief Abstract, in no case exceeding 300 words. Original drawings should accompany the manuscript. Lettering at the sides of graphs (black on white or blue) may be pencilled in and will be typeset. Figures and tables should be held to a minimum consistent with adequate presentation of information. Photographs will not be printed on glossy paper except by special arrangement. All footnotes and references to the literature should be numbered consecutively and placed in the manuscript at the proper places. Initials of authors referred to in citations should be given. Nomenclature should conform to that used in *Chemical Abstracts*, mathematical characters be marked for italic, Greek letters carefully made or annotated, and subscripts and superscripts clearly shown. Articles should be written as briefly as possible consistent with clarity and should avoid historical background unnecessary for specialists.

Notes are similar to articles in every way except as to length and are subjected to the same editorial appraisal. In their preparation particular attention should be paid to brevity and conciseness. Material included in Notes must be definitive and may not be republished subsequently.

Communications to the Editor are designed to afford prompt preliminary publication of observations or discoveries whose value to science is so great that immediate publication is imperative. The appearance of related work from other laboratories is in itself not considered sufficient justification for the publication of a Communication, which must in addition meet special requirements of timeliness and significance. Their total length may in no case exceed 1000 words or their

equivalent. They differ from Articles and Notes in that their subject matter may be republished.

Symposium papers should be sent in all cases to Secretaries of Divisions sponsoring the symposium, who will be responsible for their transmittal to the Editor. The Secretary of the Division by agreement with the Editor will specify a time after which symposium papers cannot be accepted. The Editor reserves the right to refuse to publish symposium articles, for valid scientific reasons. Each symposium paper may not exceed four printed pages (about sixteen double spaced typewritten pages) in length except by prior arrangement with the Editor.

The American Chemical Society and the Editors of *The Journal of Physical Chemistry* assume no responsibility for the statements and opinions advanced by contributors.

Business and Subscription Information

Remittances and orders for subscriptions and for single copies, notices of changes of address and new professional connections, and claims for missing numbers should be sent to the Subscription Service Department, American Chemical Society, 1155 Sixteenth St., N.W., Washington 6, D. C. Changes of address for *The Journal of Physical Chemistry* must be received on or before the 30th of the preceding month. Please include an old address label with the notification.

Claims for missing numbers will not be allowed (1) if received more than sixty days from date of issue, (2) if loss was due to failure of notice of change of address to be received before the date specified in the preceding paragraph, or (3) if the reason for the claim is "missing from files."

Subscription rates (1963): members of American Chemical Society, \$12.00 for 1 year; to non-members, \$24.00 for 1 year. Postage to countries in the Pan-American Union, \$0.80; Canada, \$0.40; all other countries, \$1.20. Single copies: \$2.50. Postage, single copies: to Canada and countries in the Pan-American Union, \$0.15; all other countries, \$0.20. Rates for back issues are available from the Special Issues Sales Department, 1155 Sixteenth St., N.W., Washington 6, D. C.

Publications of the American Chemical Society include: *Analytical Chemistry*, *Biochemistry*, *Chemical Abstracts*, *CA Section Groupings*, *Chemical and Engineering News*, *Chemical Reviews*, *Chemical Titles*, *Chemistry*, *Industrial and Engineering Chemistry*, *Inorganic Chemistry*, *Journal of Agricultural and Food Chemistry*, *Journal of the American Chemical Society*, *Journal of Chemical Documentation*, *Journal of Chemical and Engineering Data*, *Journal of Medicinal Chemistry*, *The Journal of Organic Chemistry*, and *The Journal of Physical Chemistry*. Rates on request.

1961 DIRECTORY OF GRADUATE RESEARCH

The newest edition of this unique directory is the fifth to be prepared by the ACS Committee on Professional Training. It covers the 1959-60 and 1960-61 academic years and provides a useful reference to:

- degrees available
- fields of interest and publications
of 3702 faculty members

in 273 departments or divisions of chemistry, biochemistry, and chemical engineering in United States universities offering the Ph.D. degree.

Under each department heading, degrees offered and fields of specialization appear first. Then faculty members are listed alphabetically with an up-to-date record on their education...general fields of major research interest...subjects of current research...publications during the past two years. You can clearly determine where your own field of interest is most actively represented.

The table of contents lists universities under the three main groups. There is another index by faculty names. A summary table shows for each graduate department of chemistry the number on the faculty, number of Ph.D.'s in each department, graduate enrollment, and Ph.D. degrees granted in 1959-60 and 1960-61. It offers a quick comparison by size.

This directory is comprehensive yet concise, and with it you can easily gain full information on the teaching resources of each school. If you counsel students or seek an advanced degree yourself, or if you are interested in knowing the kind of research done in certain academic centers, for whatever purpose, then this book will answer your questions and save you time.

529 pages.

Paper bound.

Price: \$4.00

Order from:

Special Issues Sales / American Chemical Society / 1155 16th Street, N. W., / Washington 6, D. C.

THE JOURNAL OF PHYSICAL CHEMISTRY

VOLUME 67, NUMBER 1

JANUARY, 1963

G. E. Heckler, A. E. Taylor, C. Jensen, D. Percival, R. Jensen, and P. Fung: Uranyl Sensitized Photodecomposition of Organic Acids in Solution.....	1	Peter O'D. Offenhardt, Philip George, and Gilbert P. Haight, Jr.: The Ionization Constants for the Ligand 2,2',2''-Tripyridine.....	116
O. K. Rice: Non-equilibrium Effects in the Dissociation of Diatomic Molecules by a Third Body.....	6	Daniel Cubicciotti: Thermodynamics of Liquid Solutions of Bismuth and Sulfur.....	118
Gilbert J. Mains, H. Niki, and M. H. J. Wijnen: The Formation of Benzene in the Radiolysis of Acetylene..	11	Antonio A. Sandoval, H. C. Moser, and Robert W. Kiser: Ionization and Dissociation Processes in Phosphorus Trichloride and Diphosphorus Tetrachloride.....	124
John E. Gordon: Distribution of Substituted Anilines between Aqueous Dioxane and a Polystyrenesulfonic Acid Ion Exchange Resin.....	16	J. W. Cary: Onsager's Relation and the Non-isothermal Diffusion of Water Vapor.....	126
John E. Gordon: Relative Formation Constants for Some Substituted Dibenzoate Ions.....	19	K. W. Bewig and W. A. Zisman: Investigation of Solution Adsorption on Platinum of Pure and Mixed Films of Fatty Amines by Contact Potentials.....	130
A. Reisman and M. Berkenblit: The Non-detonative Synthesis of Cadmium Selenide and Other II-VI Compounds from the Elements.....	22	Paul Delahay: Coulostatic Study of Adsorption Kinetics at a Metal-Electrolyte Interface.....	135
F. Toussaint, J. J. Fripiat, and M. C. Gastuche: Dehydroxylation of Kaolinite. I. Kinetics.....	26	Louis Watts Clark: Kinetic Studies on the Decarboxylation of Several Unstable Acids in the Molten State.....	138
J. J. Fripiat and F. Toussaint: Dehydroxylation of Kaolinite. II. Conductometric Measurements and Infrared Spectroscopy.....	30	H. K. Bodenseh and J. B. Ramsey: Variation in the K_A -Value of a Salt with Composition of a Binary Solvent.....	140
Michael A. Greenbaum, James N. Foster, M. Louis Arin, and Milton Farber: The Thermodynamics and Physical Properties of Beryllium Compounds. I. Enthalpy and Entropy of Vaporization of Beryllium Fluoride	36	Y. Amenomiya and R. J. Cvetanovic: Application of Flash-Desorption Method to Catalyst Studies. I. Ethylene-Alumina System.....	144
Amallesh Chatterjee and Jacob A. Marinsky: Dissociation of Methacrylic Acid Resins.....	41	R. Waack and M. A. Doran: Solvent Effects in the Electronic Spectrum of Organolithium Compounds.....	148
Jacob A. Marinsky and Amallesh Chatterjee: A Thermodynamic Interpretation of the Osmotic Properties of Cross-Linked Polymethacrylic Acid.....	47	A. J. Kovacs, Robert A. Stratton, and John D. Ferry: Dynamic Mechanical Properties of Polyvinyl Acetate in Shear in the Glass Transition Temperature Range.....	152
D. G. Kolp, R. G. Laughlin, F. P. Krause, and R. E. Zimmerer: Interaction of Dimethyldodecylamine Oxide with Sodium Dodecylbenzenesulfonate in Dilute Solution.....	51	A. D. Kennedy and H. O. Pritchard: The Thermal Isomerization of Cyclopropane at Low Pressures.....	161
Benjamin J. Intorre, Ti Kang Kwei, and Clarke M. Peterson: Sorption Behavior of the Diglycidyl Ether of Bisphenol A.....	55	P. Ausloos and Richard E. Rebbert: Intramolecular Rearrangements. V. Formation of Ethylene in the Photolysis of Ethyl Acetate from 4 to 500° K.....	163
Leslie M. Theard and Milton Burton: Radiolysis of Liquid Methanol and Some Methanolic Salt Solutions.....	59	Isabel B. Burkley and R. E. Rebbert: Reactions of Methyl Radicals with Aromatic Compounds. I. Toluene, Ethylbenzene, and Cumene.....	168
Gerald P. Lewis and Paul Ruetschi: The Oxidation of Hydrogen and Deuterium on a Rotating Disk Electrode	65	William A. Sanders and R. E. Rebbert: Reactions of Methyl Radicals with Aromatic Compounds. II. The Xylenes.....	170
L. A. Errede and J. P. Cassidy: The Chemistry of Xylylenes. XVI. The Trapping of Radicals in Gas Streams by Mutual Quench Techniques.....	69	A. N. Wright and C. A. Winkler: The Active Nitrogen Afterglow and the Quenching Effect of Added Ammonia..	172
L. A. Errede and J. P. Cassidy: The Chemistry of Xylylenes. XVII. The Mechanism for Formation of Xylylenes in Gas Phase.....	73	William P. Sholette and Richard F. Porter: Mass Spectrometric Study of High Temperature Reactions in the Boron-Hydrogen-Oxygen System.....	177
S. Gilman: A Study of the Mechanism of Carbon Monoxide Adsorption on Platinum by a New Electrochemical Procedure.....	78	Norman D. Coggeshall: Comparison of Mass Spectral Regularities for <i>n</i> -Paraffins and <i>n</i> -Terminal Olefins...	183
Gerald Houghton: Band Shapes in Non-linear Chromatography with Axial Dispersion.....	84	Sherril D. Christian, Harold E. Afsprung, and Stanton A. Taylor: The Role of Dissolved Water in Partition Equilibria of Carboxylic Acids.....	187
Clarence J. Wolf and Richard H. Toeniskoetter: Radiolytic and Thermal Decomposition of Borazole.....	88	Pasupati Mukerjee and Ashoka Ray: The Effect of Urea on Micelle Formation and Hydrophobic Bonding.....	190
Terrell N. Andersen and Henry Eyring: Electrode Depolarization Kinetics on Open Circuit.....	92	Pasupati Mukerjee and Ashish K. Ghosh: The Effect of Urea on Methylene Blue, its Self-association, and Interaction with Polyelectrolytes in Aqueous Solution..	193
D. Kummer and J. D. Baldeschwieler: Organo Silylethylenediamine Compounds. II. The Nuclear Magnetic Resonance Spectra of Silylamines.....	98	NOTES	
David A. Schulz and Alan W. Searcy: Vapor Pressure and Heat of Sublimation of Calcium Fluoride.....	103	Edward P. Rack and Adolf F. Voigt: Radiation Dose and Iodine Scavenger Effects on Recoil C ¹¹ Reactions in Cyclohexane.....	198
J. T. Kummer and J. D. Youngs: The Surface Composition of a Dilute Solid Solution of Calcium Chloride in Sodium Chloride.....	107	Marvin F. L. Johnson and Carl D. Keith: The State of Platinum in Re-forming Catalysts.....	200
R. T. Hobgood, Jr., G. S. Reddy, and J. H. Goldstein: Nuclear Magnetic Resonance Spectra of Some Alkyl Vinyl Ethers and Methyl Vinyl Sulfide.....	110	G. Czapski, B. H. J. Bielski, and N. Sutin: The Kinetics of the Oxidation of Hydrogen Peroxide by Cerium(IV)..	201
Norbert Muller and Duane T. Carr: Carbon-13 Splittings in Fluorine Nuclear Magnetic Resonance Spectra.....	112	COMMUNICATION TO THE EDITOR	
		Ted B. Flanagan: On Large Differences in the Equilibrium Solubilities of Hydrogen and Deuterium in Platinum-Palladium Alloys.....	203

AUTHOR INDEX

- Affsprung, H. E., 187
 Amenomiya, Y., 144
 Andersen, T. N., 92
 Arin, M. L., 36
 Ausloos, P., 163
 Baldeschwieler, J. D., 98
 Berkenblit, M., 22
 Bewig, K. W., 130
 Bielski, B. H. J., 201
 Bodenseh, H. K., 140
 Burkley, I. B., 168
 Burton, M., 59
 Carr, D. T., 112
 Cary, J. W., 126
 Cassidy, J. P., 69, 73
 Chatterjee, A., 41, 47
 Christian, S. D., 187
 Clark, L. W., 138
 Coggeshall, N. D., 183
 Cubicciotti, D., 118
 Cvetanovic, R. J., 144
 Czapski, G., 201
 Delahay, P., 135
 Doran, M. A., 148
 Errede, L. A., 69, 73
 Eyring, H., 92
 Farber, M., 36
 Ferry, J. D., 152
 Flanagan, T. B., 203
 Foster, J. N., 36
 Fripiat, J. J., 26, 30
 Fung, P., 1
 Gastuche, M. C., 26
 George, P., 116
 Ghosh, A. K., 193
 Gilman, S., 78
 Goldstein, J. H., 110
 Gordon, J. E., 16, 19
 Greenbaum, M. A., 36
 Haight, G. P., Jr., 116
 Heckler, G. E., 1
 Hobgood, R. T., Jr., 110
 Houghton, G., 84
 Intorre, B. J., 55
 Jensen, C., 1
 Jensen, R., 1
 Johnson, M. F. L., 200
 Keith, C. D., 200
 Kennedy, A. D., 161
 Kiser, R. W., 124
 Kolp, D. G., 51
 Kovacs, A. J., 152
 Krause, F. P., 51
 Kummer, D., 98
 Kummer, J. T., 107
 Kwei, T. K., 55
 Laughlin, R. G., 51
 Lewis, G. P., 65
 Mains, G. J., 11
 Marinsky, J. A., 41, 47
 Moser, H. C., 124
 Mukerjee, P., 190, 193
 Muller, N., 112
 Niki, H., 11
 Offenhartz, P. O'D., 116
 Percival, D., 1
 Peterson, C. M., 55
 Porter, R. F., 177
 Pritchard, H. O., 161
 Rack, E. P., 198
 Ramsey, J. B., 140
 Ray, A., 190
 Rebbert, R. E., 163, 168,
 170
 Reddy, G. S., 110
 Reisman, A., 22
 Rice, O. K., 6
 Ruetschi, P., 65
 Sanders, W. A., 170
 Sandoval, A. A., 124
 Schulz, D. A., 103
 Searcy, A. W., 103
 Sholette, W. P., 177
 Stratton, R. A., 152
 Sutin, N., 201
 Taylor, A. E., 1
 Taylor, S. A., 187
 Theard, L. M., 59
 Toeniskoetter, R. H., 88
 Toussaint, F., 26, 30
 Voigt, A. F., 198
 Waack, R., 148
 Wijnen, M. H. J., 11
 Winkler, C. A., 172
 Wolf, C. J., 88
 Wright, A. N., 172
 Youngs, J. D., 107
 Zimmerer, R. E., 51
 Zisman, W. A., 130

THE JOURNAL OF PHYSICAL CHEMISTRY

(Registered in U. S. Patent Office) (© Copyright, 1963, by the American Chemical Society)

VOLUME 67, NUMBER 1

JANUARY 22, 1963

URANYL SENSITIZED PHOTODECOMPOSITION OF ORGANIC ACIDS IN SOLUTION¹

BY G. E. HECKLER, A. E. TAYLOR, C. JENSEN, D. PERCIVAL, R. JENSEN, AND P. FUNG

Department of Chemistry, Idaho State College, Pocatello, Idaho

Received February 2, 1962

Uranyl sensitized photodecomposition products of various organic acids are presented. Sensitized photodecomposition rates for malonic, succinic, and glutaric acids were determined in the pH range 0.5 to 3.0 by measuring the gas produced in a Warburg micromanometric apparatus. Theoretical analysis of these results shows that the photosensitive species is a 1:1 complex of diionized acid with uranyl ion for malonic acid and a mixture of 1:1 complex and 2:1 complex of monoionized acid with uranyl ion for succinic and glutaric acids.

Photodecomposition of oxalic acid in solution sensitized by uranyl ion has been used extensively for actinometry.² Uranyl sensitized photodecomposition studies of other organic acids have been made.³ Past studies of such systems have involved internal analysis of the organic acid and residual by standard analytical techniques.

In this Laboratory, Taylor and Jarvis^{4,5} used a Warburg apparatus with high intensity ultraviolet lamps and quartz flasks for *external* micromanometric measurement of the amount of gaseous product. This technique permits continuous measurement of the extent of reaction without disturbing the reacting system. However, the nature of the gas evolved must be known to apply theoretical analysis to the experimental measurements.

This paper presents results of investigation for photodecomposition products from a variety of acids; it also discusses the results and makes a theoretical analysis of the nature of the reacting system for photodecomposition of a group of three organic acids.

Experimental

Chemicals.—The melting points of Baker Analyzed Reagent formic, oxalic, succinic, and tartaric acids and of Eastman White Label propionic acid indicated a high degree of purity. These,

(1) This paper is based on work performed under contract with the United States Atomic Energy Commission, contract no. AT(10-1)-310 with Idaho State College.

(2) C. R. Masson, V. Bockelheide, and W. A. Noyes, Jr., "Techniques of Organic Chemistry," Vol. II, 2nd Ed., Ed. by A. Weissberger, Interscience Publishers, Inc., New York, N. Y., 1956, pp. 292-298.

(3) G. K. Rollefson and M. Burton, "Photochemistry and the Mechanism of Chemical Reactions," Prentice-Hall, Inc., Englewood Cliffs, N. J., 1934, pp. 241-244.

(4) A. E. Taylor and F. G. Jarvis, Presented at the Northwest Regional Meeting of the American Chemical Society, June 16, 1958, in Portland, Oregon.

(5) A. E. Taylor, G. E. Heckler, and D. R. Percival, *Talanta*, **7**, 232 (1961).

as well as Baker and Adamson A.C.S. acetic acid, were used as received. Eastman White Label glutaric acid was repurified by crystallization from benzene to give a product of m.p. 97-98°. Tests of Eastman malonic acid indicated high purity, but micro amounts of a photosensitive impurity were revealed during this investigation. These were removed by crystallization from acetone. Eastman White Label valeric anhydride was hydrolyzed to obtain a solution of valeric acid. Uranyl chloride solutions were prepared as described in ref. 5.

Apparatus.—A rectangular Warburg apparatus—modified by introduction of high intensity ultraviolet lamps (G.E. G36T6)—was used for micromanometric determination of the production of gas. According to the manufacturer's specifications, 90% of the output of these lamps is 2537 Å. Hg radiation. For reaction vessels, quartz single side-arm flasks of approximately 25-ml. capacity were used.

Absorbancy measurements were obtained with a Beckman DU spectrophotometer; pH measurements, with a Beckman Model G pH meter; gaseous infrared analysis with a Beckman IR-5.

Method.—A. **Photodecomposition Products.**—Solutions containing UO_2Cl_2 and one of the acids were placed under an argon atmosphere in a 250-ml. quartz flask and irradiated by a bank of six 18-in., 15 w. Sylvania germicidal lamps for periods ranging from 3 to 16 hr., depending upon the organic acid being examined. The gas was transferred to a 10-cm. infrared gas cell by a gas handling apparatus which permitted measurement of the approximate partial pressure of the decomposition product. All solutions were 0.05 *M* in UO_2Cl_2 and 0.5 *M* in acid except the following: valeric acid, 0.038 *M* in UO_2Cl_2 and 0.154 *M* in acid; malonic, 0.062 *M* in UO_2Cl_2 and 0.398 *M* in acid; succinic, 0.288 *M* in acid.

The non-gaseous photodecomposition products were identified by a paper chromatographic method described by Kennedy and Barker.⁶

B. **Micromanometric.**—Of the 14 manometers in the rectangular Warburg apparatus, two were used for barometric corrections and two were used to assure a constant intensity of light produced by the fluorescent lamps. These latter two flasks contained 0.1 *M* oxalic acid and 3.75×10^{-4} *M* UO_2Cl_2 at a pH of 1.30 ± 0.02 during all measurements.

To correct for physical variations between flasks, "pressure constants" were experimentally determined for the other ten flasks. These "pressure constants" were measured by irradiating

(6) E. P. Kennedy and H. A. Barker, *Anal. Chem.*, **23**, 1033 (1951).

TABLE I

Acid	Formula	Acid concn., <i>M</i>	UO ₂ ⁺² concn., <i>M</i>	pH of system	Gaseous photo-decomposition products	Non-gaseous decomposition products
Formic	HCOOH	0.5	0.05	1.5	CO ₂ , CO, ^a (H ₂)	H ₂ O
Acetic	H ₃ C—COOH	.6	.04	1.8	CO ₂ , CH ₄	None
Propionic	H ₃ C—CH ₂ —COOH	.5	.05	1.8	CO ₂ , C ₂ H ₆	None
Valeric	H ₃ C—(CH ₂) ₃ —COOH	.15	.04	1.9	CO ₂ , C ₄ H ₁₀ ^b	None
Oxalic	HOOC—COOH	.5	.05	0.6	CO ₂ , CO	H ₂ O
Malonic	HOOC—CH ₂ —COOH	.4	.06	0.9	CO ₂	H ₃ C—COOH
Tartaric	HOOC—CH(OH)—CH(OH)—COOH	.5	.05	1.1	CO ₂	(H ₂ C(OH)CH(OH)COOH)
Succinic	HOOC—(CH ₂) ₂ —COOH	.3	.05	1.6	CO ₂	H ₃ C—CH ₂ —COOH
Glutaric	HOOC—(CH ₂) ₃ —COOH	.5	.05	1.6	CO ₂	H ₃ C—(CH ₂) ₂ —COOH

^a Moles of CO₂ > moles of CO. ^b *n*-Butane.

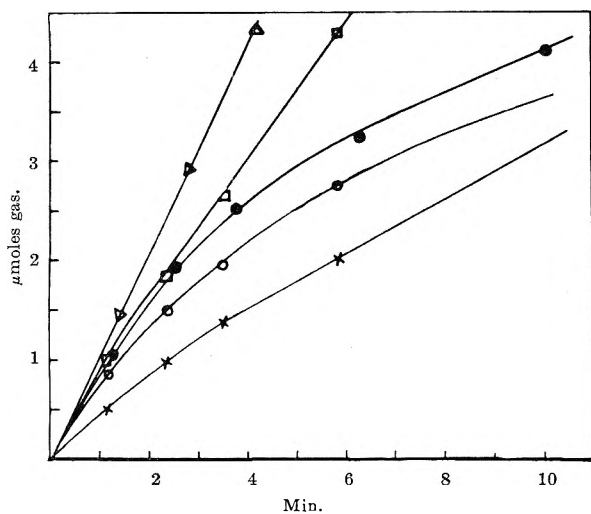


Fig. 1.—Gas produced vs. irradiation time for oxalic acid (pH 1.32), Δ ; malonic acid (pH 1.93), \square ; succinic acid (pH 2.63), \times ; glutaric acid (pH 3.00), \circ ; tartaric acid (pH 1.99), \bullet . Concentrations were 0.1 *M* in acid and 3.75×10^{-4} *M* in uranyl for all cases.

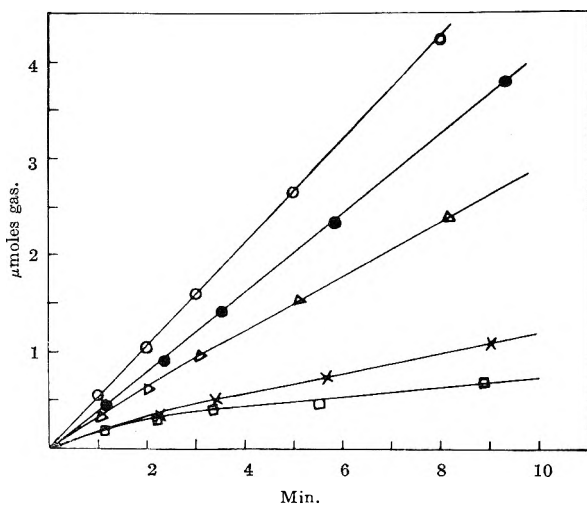


Fig. 2.—Gas produced as a function of time for 0.1 *M* malonic acid at pH 2.20, \circ ; pH 2.00, \bullet ; pH 1.83, Δ ; pH 1.32, \times ; pH 1.10, \square ; UO₂⁺² (moles/l.) = 3.75×10^{-4} .

the same solution in all flasks and calculating correction factors which convert all measured pressures to that measured in an arbitrarily selected "standard flask." These constants permit correction of results from nine of the flasks to that of the "standard flask" and make all measurements comparable.

Before radiation, all flasks were swept free of air by argon, leaving an argon atmosphere above the solution. All measurements were made at $30 \pm 0.02^\circ$, and the volume of reacting solution was 3.2 ml. in all cases. Further details of these measurements may be found in ref. 5.

Results

Photodecomposition Products.—Table I summarizes the product analyses. Two competing reactions appear

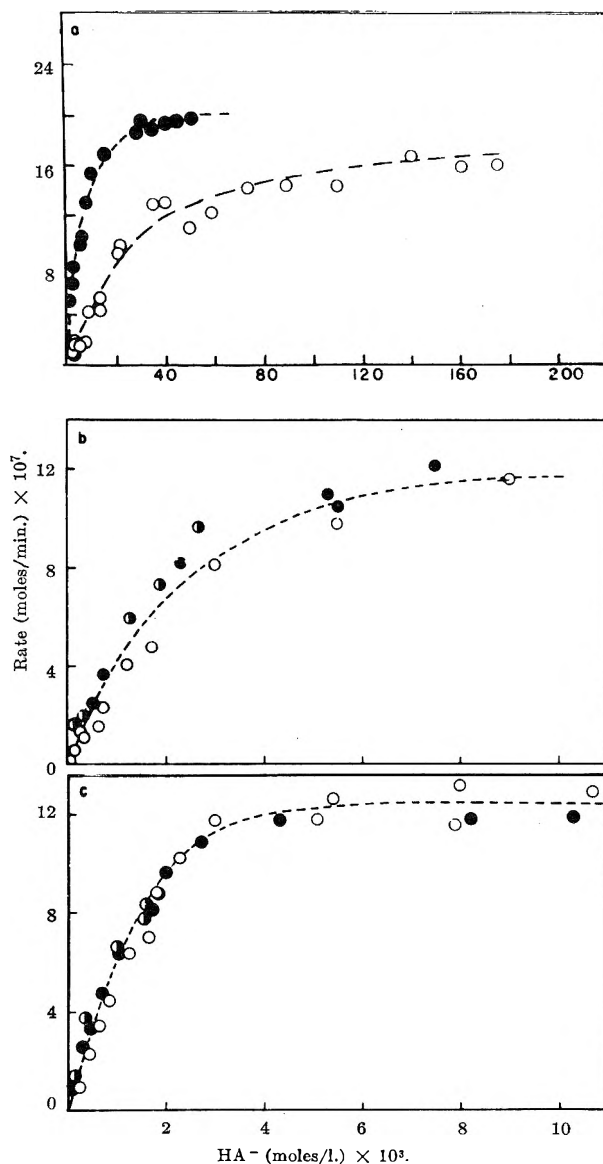
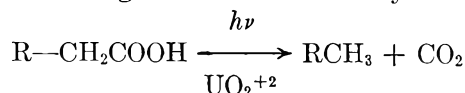


Fig. 3.—Rate as a function of concentration of monoionized acid for (a) malonic, 0.1 *M*, \bullet ; 0.5 *M*, \circ ; (b) succinic, 0.03 *M*, \circ ; 0.1 *M*, \bullet ; 0.3 *M*, \circ ; (c) glutaric, 0.03 *M*, \circ ; 0.1 *M*, \bullet ; 0.3 *M*, \circ .

to take place during radiation of formic acid: both CO₂ and CO were found, the former more predominant. From these reaction products, formation of H₂ and H₂O are hypothesized.³ Glyceric acid was not positively identified as a product of photodecomposition of tartaric acid. However, by analogy with the other acids for which a generalized reaction may be



glyceric acid is the probable non-gaseous product.

Four of these acids (tartaric, malonic, succinic, and glutaric) yield CO_2 as the only gaseous photodecomposition product, and these four were selected for micro-manometric studies. The tartaric acid micromanometric results indicated greater complexity of the solution system than was true for the other three acids. Hence the remainder of this report presents results for malonic, succinic, and glutaric acids only.

Micromanometric.—Figure 1 illustrates experimental measurements for several acids. The rate of gas production was found to decrease with time as acid was depleted or as uranyl concentration was decreased by conversion to the uranic form.⁷ Figure 2 illustrates the effect of pH variations on malonic acid. During the first 1 to 4 min., depending on the system, the rate is linear with time. Over this time scale the rate of photodecomposition (production of CO_2) may be considered a function of the properties of the original solution (*i.e.*, uranyl concentration, acid concentration, etc.). Figure 3 plots the rate of sensitized photodecomposition *vs.* concentration of monoionized carboxylic acid at constant uranyl chloride concentration; Figure 4 plots rate *vs.* concentration of diionized acid for each of the three acids investigated also at constant uranyl chloride concentration. These carboxylate concentrations were controlled by varying both the organic acid concentration and the pH. The concentrations of the ionized organic species were calculated using accepted dissociation constants. Figures 3 and 4 show that rate of photodecomposition is a monotonic function of the *monoionized acid* for succinic and glutaric acids and a monotonic function of the *diionized acid* for malonic acid.

Absorbance data to which the method of continuous variation^{8,9} has been applied are given in Fig. 5. These data indicate that an acid/uranyl ratio of 2:1 for succinic acid and of 1:1 for malonic acid represents a complex. Photodecomposition results indicate that the complex formed with glutaric acid is similar to that for succinic, yet absorbance data did not disclose a complex.

Discussion.—The variation in photodecomposition rates with pH, and with concentration of organic acid and uranyl at low pH, may be explained by assuming (1) that the photosensitive species is a complex formed between uranyl ion and organic acid ion, and (2) that the rate of photodecomposition is proportional to the product of the concentration of complex and the intensity of radiation.

$$\text{rate} = kI(\text{complex}) = dn_{\text{CO}_2}/dt \quad (\text{I})$$

Where I is intensity of radiation, n_{CO_2} is moles of CO_2 formed, t is time, and parentheses indicate concentration.

To determine the effect upon decomposition rate caused by the decrease of radiation due to absorption, the Beer-Lambert law may be applied

$$I_L = I_0 \exp[-(k_1 a_1 + k_2 a_2 + \dots)L] = I_0 \exp[-(\sum_i k_i a_i)L]$$

where k_i is the molar absorptivity index for component i present at concentration a_i , and L represents the length

(7) J. J. McBrady and R. Livingstone, *J. Phys. Chem.*, **50**, 176 (1946).

(8) A. E. Martell and M. Calvin, "Chemistry of the Metal Chelate Compounds," Prentice-Hall, Inc., Englewood Cliffs, N. J., 1952, pp. 28-34.

(9) I. Feldman and J. R. Havill, *J. Am. Chem. Soc.*, **76**, 2114 (1954).

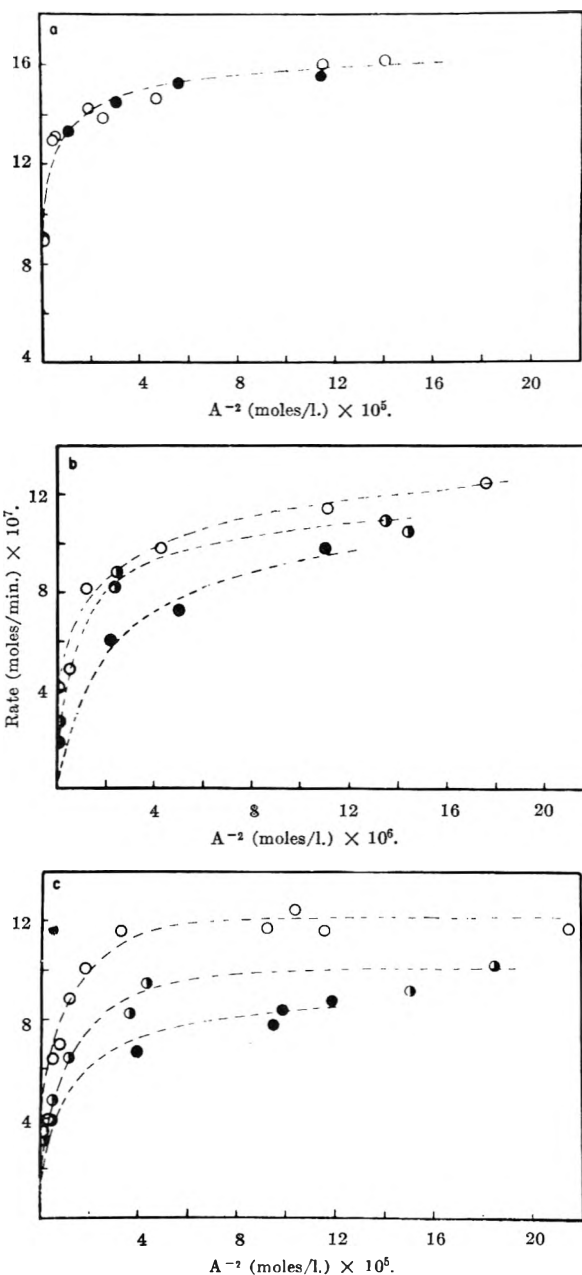


Fig. 4.—Rate as a function of concentration of diionized acid for (a) malonic, 0.1 M , ●; 0.5 M , ○; (b) succinic, 0.03 M , ●; 0.1 M , ●; 0.3 M , ○; (c) glutaric, 0.03 M , ●; 0.1 M , ○; 0.3 M , ○.

of solution through which the light has passed. If the reaction chamber were an ideal system consisting of a vertical cylinder with light entering vertically through the bases of the cylinder, the differential rate of decomposition at height L from a regular volume element of height dL and unit cross-sectional area would be, according to (I)

$$dr = KI_L(\text{complex}) dL = KI_0(\text{complex}) \times \exp[-(\sum_i k_i a_i)L] dL$$

Integration of this expression over the volume of the cell yields

$$r = dn_{\text{CO}_2}/dt = KSI_0(\text{complex}) \times \{(1 - \exp[-(\sum_i k_i a_i)h]) / \sum_i k_i a_i\} \quad (\text{II})$$

Where h is total height of cylinder, S is area of base of cylinder, I_0 is entering light intensity, and K is a pro-

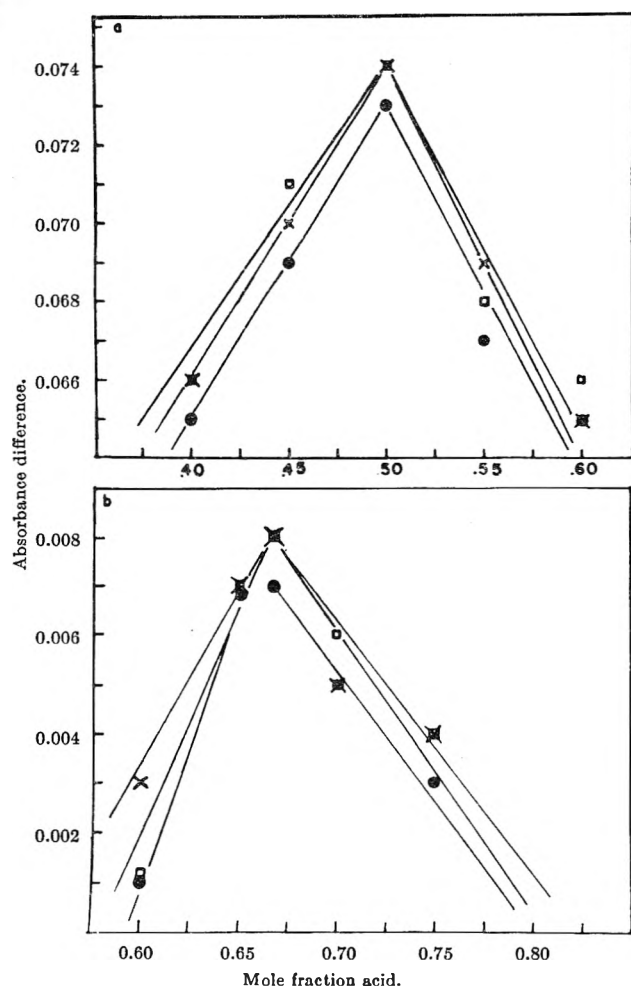


Fig. 5.—Absorbance difference as a function of mole fraction (a) malonic, (b) succinic: ●, $\lambda = 405$ succinic; ×, $\lambda = 415$; □, $\lambda = 425$; ●, $\lambda = 435$ malonic.

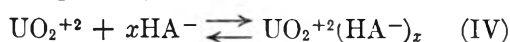
portionality constant. The factors K , S , and I_0 are constant for each acid studied, and $\sum_i k_i a_i$ may be spectrophotometrically determined as $2.303A$, where A is the absorbancy measured for a 1-cm. cell at 2537 \AA . Gathering the constants gives

$$r = k(\text{complex}) \{ [1 - \exp(-2.3Ah)] / 2.3A \} \quad (\text{III})$$

Because the flasks used in these measurements were non-ideal systems, the height, h , must be treated as an empirical constant.

The nature of the photosensitive complex with uranyl ion in solutions of each of the three acids is partially indicated by the data presented in Fig. 3 and 4 together with the continuous variation results. (In the remainder of this paper, chemical formulas appearing in parentheses indicate concentration of that species. The symbol U refers to the total uranyl concentration as complex or as ion.)

The experimental results presented in Fig. 3 and 4 show that the complex formed in either succinic or glutaric acid solutions is directly related to the concentration of *monoionized acid* species present. The continuous variation results indicate that the acid to uranyl ratio is 2:1 for succinic acid. Based on these facts the following equilibrium is hypothesized for both acids (succinic and glutaric).



Wherein x is expected to be 2 for succinic acid but is uncertain for glutaric acid.

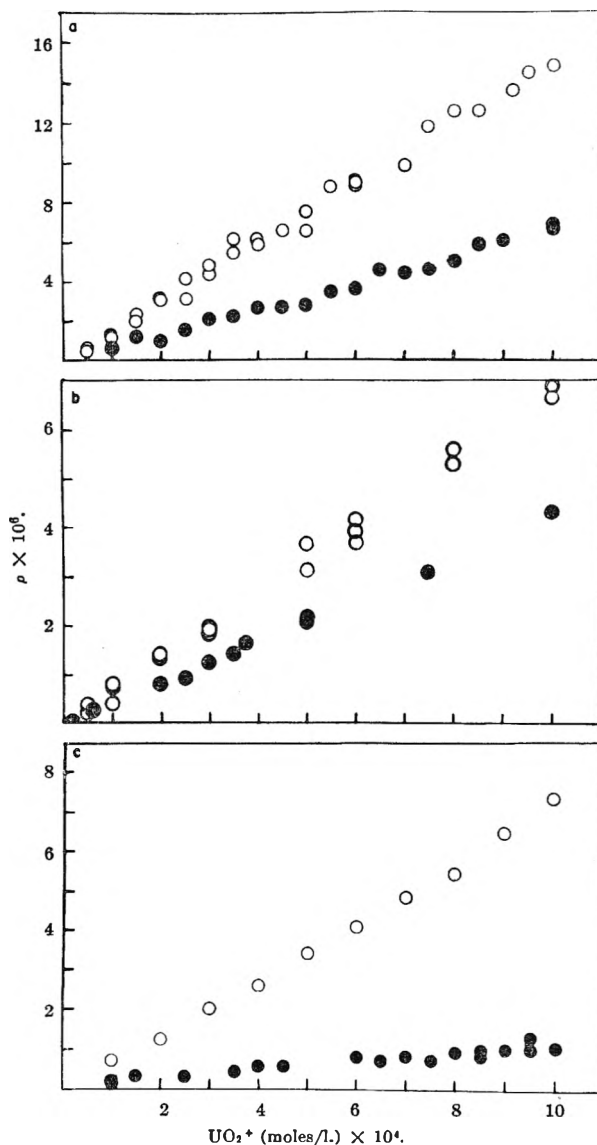


Fig. 6.— ρ as a function of concentration of UO_2^{+2} for (a) malonic, 0.1 M, ●; 0.5 M, ○; (b) succinic, 0.1 M, ●; 0.3 M, ○; (c) glutaric, 0.1 M, ●; 0.3 M, ○.

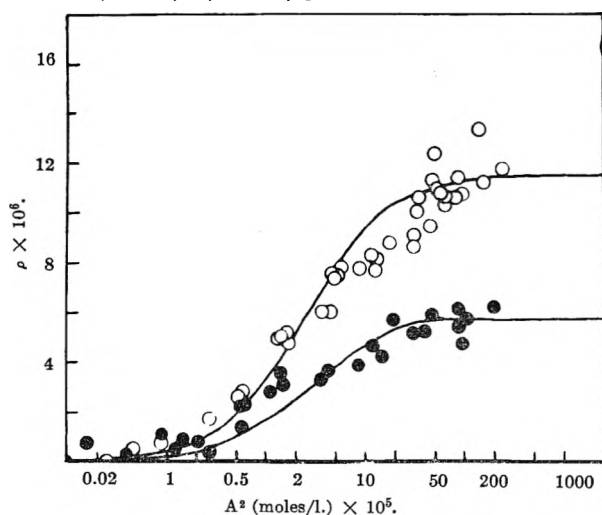


Fig. 7.— ρ as a function of concentration of diionized malonic acid: (UO_2^{+2}) = $3.75 \times 10^{-4} M$, ●; (UO_2^{+2}) = $7.5 \times 10^{-4} M$, ○.

For malonic acid, on the other hand, the results given in Fig. 3 and 4 show that the complex formed is directly related to the concentration of *diionized acid* present. This fact, together with the 1:1 ratio disclosed by the continuous variation data, indicates the equilibrium in eq. V



wherein x is expected to be one. In these formulas HA^- represents HOOCRCOO^- and $-\text{R}-$ represents $-\text{CH}_2-$ for malonic, $-(\text{CH}_2)_2-$ for succinic, and $-(\text{CH}_2)_3-$ for glutaric.

Other reactions appear to interfere as the pH is increased much above 3.0, beyond which quantitative prediction of reaction rate becomes difficult.

During these studies, the organic acid concentration was varied from 0.3×10^{-1} to $5 \times 10^{-1} M$ while the total uranyl concentration was varied from 0.25×10^{-4} to 10×10^{-4} . Over this range, the concentration of mono- and diionized acid may be considered independent of the amount of complex formed, because, as these ions are consumed to form complex, they are replenished by equilibrium reaction with the relatively high concentration of undissociated acid.

From (IV)

$$K_{\text{IV}} = (\text{UO}_2^{+2}(\text{HA}^-)_x) / [U - (\text{UO}_2^{+2}(\text{HA}^-)_x)](\text{HA}^-)^x$$

and solving for concentration of complex

$$(\text{complex}) = (\text{UO}_2^{+2}(\text{HA}^-)_x) = \frac{K_{\text{IV}}(\text{HA}^-)^x U}{[1 + K_{\text{IV}}(\text{HA}^-)^x]} \quad (\text{VI})$$

From (V)

$$K_{\text{V}} = (\text{UO}_2^{+2}(\text{A}^{-2})_x) / [U - (\text{UO}_2^{+2}(\text{A}^{-2})_x)](\text{A}^{-2})^x$$

and solving for concentration of complex

$$(\text{complex}) = (\text{UO}_2^{+2}(\text{A}^{-2})_x) = \frac{K_{\text{V}}(\text{A}^{-2})^x U}{[1 + K_{\text{V}}(\text{A}^{-2})^x]} \quad (\text{VII})$$

Substitution of (VI) into (III) yields

$$r = k \left\{ \frac{K_{\text{IV}}(\text{HA}^-)^x U}{[1 + K_{\text{IV}}(\text{HA}^-)^x]} \right\} \times \left\{ \frac{[1 - \exp(-2.3Ah)]}{2.3A} \right\}$$

which may be converted into a more usable form by multiplying through by the inverse of the last term to obtain

$$\rho = r \left\{ \frac{2.3A}{[1 - \exp(-2.3Ah)]} \right\} = \frac{k K_{\text{IV}}(\text{HA}^-)^x U}{[1 + K_{\text{IV}}(\text{HA}^-)^x]} \quad (\text{VIII})$$

Substitution of (VII) into (III) followed by a similar rearrangement yields

$$\rho = k' K_{\text{V}}(\text{A}^{-2})^x U / [1 + K_{\text{V}}(\text{A}^{-2})^x] \quad (\text{IX})$$

According to (VIII), ρ (hereinafter called the reduced rate), should give a linear graph when plotted *vs.* the total uranyl concentration providing (HA^-) is held constant in photodecomposition measurements on succinic and glutaric acid solutions. Similarly, according to (IX), ρ *vs.* U should yield a linear graph in photodecomposition measurements on malonic acid solutions when (A^{-2}) is held constant. Figure 6 demonstrates that this linear relation holds for each of these acids. An h value of 0.7 cm. was necessary to cause the linear plot of ρ to pass through the origin as shown in Fig. 6. The true height of the solution in the flasks was 0.3 cm., but the system was not ideal because light from the fluorescent tube beneath the flasks entered from various angles.

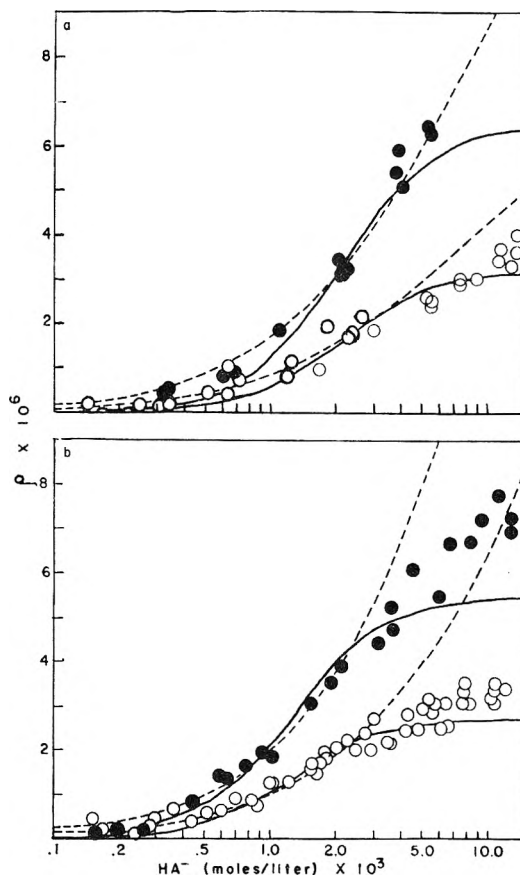


Fig. 8.— ρ as a function of concentration of monoionized acid for $(\text{UO}_2^{+2}) = 3.75 \times 10^{-4} M$, O; $(\text{UO}_2^{+2}) = 7.5 \times 10^{-4} M$, ●; (a) succinic; (b) glutaric. Solid lines—calculated for 2:1 (HA^- : UO_2^{+2}); dashed lines—calculated for 1:1 (HA^- : UO_2^{+2}).

Photodecomposition produces some carbon dioxide when solutions of the organic acids alone are irradiated. Hence, the reduced rates given have been corrected to include only the photodecomposition rate for the sensitized reaction. Corrections were determined by radiating unsensitized samples, for which the absorbance was relatively low. Therefore, the correction measurements so obtained were multiplied by a factor $(A'/A)(1 - \exp[-2.3Ah]) / (1 - \exp[-2.3A'h])$, where A' and A are the absorbances of the unsensitized and the uranyl sensitized systems, respectively, and h has the value 0.7 cm. This factor converts the unsensitized rate to the lower rate it will have in a system of higher absorbance, such as that which exists in the uranyl sensitized solutions. The correction so determined then was subtracted from the total rate of carbon dioxide production to leave only the rate for the sensitized reaction. The relative size of the correction varies with type of acid, total acid concentration, total uranyl concentration, and pH. As the total uranyl concentration approaches zero, the correction approaches 100%. The relative size of the correction term for 0.1 M organic acid and 1×10^{-3} uranyl is 5.7% for glutaric acid, 2.1% for succinic acid, and 3.4% for malonic acid. For 0.1 M organic acid and 1×10^{-4} M uranyl, the correction increases to 30% for glutaric acid, 10% for succinic acid, and 33% for malonic acid.

The empirical rate constant, k , and the stability constant, K_{IV} (or K_{V}), may be evaluated from the slopes of the ρ *vs.* uranyl graphs in Fig. 6. These slopes have been calculated using the method of least squares and

TABLE II

Acid	Concn. (moles/ l.)		$\Delta\rho/\Delta u$ $\times 10^3$	K_1	K_2	K_3		$k \times 10^3$	
	pH					Acid:uranyl		Acid:uranyl	
						1:1	2:1	1:1	2:1
Malonic	0.5	2.54	15.0 ± 0.3	1.397×10^{-3}	2.1×10^{-6}	$4.0 \pm 0.2 \times 10^5$		15.3 ± 0.3	
	.1	1.90	$6.5 \pm .2$						
Succinic	.3	2.29	$6.7 \pm .2$	6.63×10^{-5}	2.8×10^{-6}	$1.3 \pm 0.6 \times 10^2$	$2.2 \pm 0.4 \times 10^5$	20.5 ± 8.0	8.8 ± 0.6
	.1	2.52	$4.3 \pm .1$						
Glutaric	.3	2.35	$7.0 \pm .2$	4.54×10^{-5}	4.54×10^{-5}	53.1 ± 44.5	$8.7 \pm 1.1 \times 10^5$	50.4 ± 30.4	7.8 ± 0.3
	.1	2.00	$1.2 \pm .1$						

the values of the constants are presented in Table II. To calculate these constants, models of the complex have been assumed. The model assumed determines the value of x to be used in eq. VIII and IX. The models which may be assumed for each acid are limited by the results presented in Fig. 3 and 4.

The diionized species of malonic acid could, conceivably, form a six-membered ring with uranyl ion. The constants presented in Table II are calculated from eq. IX with x equal to one. Attempts to calculate constants from eq. IX with x equal to two (*i.e.*, a 3:2 complex) yielded negative results. If a 3:2 complex is hypothesized— x equal to 1.5—a non-linear ρ vs. U curve is predicted; hence, calculations for this model were not attempted. Figure 7 presents experimental reduced rate vs. diionized malonic acid measurements for two concentrations of total uranyl. The solid lines were computed from eq. IX using the constants given in Table II with x equal to one. The reasonable fit indicates the validity of the 1:1 complex.

The monoionized species of glutaric and succinic acids (see Fig. 3 and 4) could form a charged 1:1 com-

plex, or an uncharged 2:1 complex. The constants presented in Table II for glutaric and succinic acids were calculated from eq. VIII for both x equal to one and x equal to two. Hypothesis of a 3:2 complex predicts a non-linear ρ vs. U curve. Figure 8 presents experimental reduced rate vs. monoionized acid measurements for two concentrations of total uranyl in solutions of succinic and glutaric acids. The solid lines were calculated from eq. VIII using the constants for x equal to two in Table II, and the dashed lines were similarly calculated for x equal to one. From these results it is impossible to conclude the precise nature of the complex; however, it seems probable that both photosensitive species are present.

The measurements presented in Fig. 7 and 8 represent a pH range from less than 0.5 to near 3.0 at the upper limit. Within this pH range, the reasonable fit of the calculated reduced rate to that measured shows that the photosensitive species is 1:1 ($A^{-2}:\text{UO}_2^{+2}$) in malonic acid. However, a mixture of 1:1 and 2:1 ($\text{HA}^{-}:\text{UO}_2^{+2}$) is indicated in glutaric and succinic acids.

NON-EQUILIBRIUM EFFECTS IN THE DISSOCIATION OF DIATOMIC MOLECULES BY A THIRD BODY¹

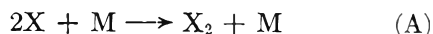
By O. K. RICE

Department of Chemistry, University of North Carolina, Chapel Hill, North Carolina

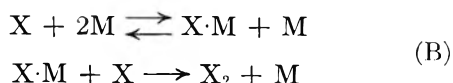
Received March 3, 1962

In the dissociation of diatomic molecules, the population of energy levels near the dissociation limit falls below the equilibrium population. In the present paper this is treated on the assumption that equal amounts of energy are removed in all collisions, but attention is given to the change of density of energy levels near dissociation. The effect of the mass of the third body and the effect of the temperature on the average amount of energy removed at each collision are considered. It is found that a reasonably good qualitative discussion of the relative effect of the different rare gases on the dissociation of I_2 (or association of I atoms) can be given using these ideas. The present considerations are compared with the calculations of Keck, using the so-called variational theory of chemical reactions.

The recombination of atoms in the presence of a third body has been the subject of numerous experimental studies in recent years. It has been found, in general, that the rate constant for the reaction



has a negative temperature coefficient. This can be explained readily if the reaction goes in steps



where $X \cdot M$ is a loosely bound complex (generally resulting from van der Waals forces); however, in cases where the complex $X \cdot M$ is very unstable (as, for ex-

ample, where M is a helium atom), the second mechanism may be expected to be unimportant, and in such cases another cause for the negative temperature coefficient must be sought. It has been suggested² that such a negative temperature coefficient could be explained by redissociation of the vibrationally excited molecules first formed in the recombination, and some details of such a mechanism have been worked out by Polanyi.³

It also has been noted by Nikitin and Sokolov⁴ that

(2) (a) R. L. Strong, J. C. W. Chien, P. E. Graf, and J. E. Willard, *J. Chem. Phys.*, **26**, 1287 (1957); (b) B. Widom, *ibid.*, **34**, 2050 (1961).

(3) J. C. Polanyi, *ibid.*, **31**, 1338 (1959).

(4) E. E. Nikitin, *Dokl. Akad. Nauk SSSR*, **116**, 584 (1957); **121**, 991 (1958) [translations, *Soviet Phys. Doklady*, **2**, 453 (1957); **3**, 701 (1958)]; E. E. Nikitin and N. D. Sokolov, *J. Chem. Phys.*, **31**, 1371 (1959); E. E. Nikitin, *Dokl. Akad. Nauk SSSR*, **132**, 395 (1960) [translation, Physical Chemistry Section, Consultants Bureau, 417 (1961)].

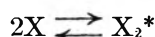
(1) Work supported by the National Science Foundation.

the rate of dissociation of a diatomic molecule, the reverse of reaction A, will be lowered by the lack of equilibrium in the upper vibrational levels when the reaction takes place, and a discussion, with some calculations based on quantum mechanical transition probabilities, has been given by Pritchard.⁵ These phenomena are essentially equivalent, any lowering in the rate constant for association being in exactly the same proportion as that in the rate constant for dissociation.⁶

Most recently, Benson and Fueno⁷ have made a detailed study of the rate of recombination, taking into account the effect of redissociation of excited vibrational states. Their work is based upon the assumption that the transitions take place only between adjacent vibrational levels, and that the transition probabilities depend upon the vibrational level as in the case of a harmonic oscillator. In formulating their results they considered a "species" X_2^* which consisted of a pair of atoms close enough to be bound together, but not actually bound together, *i.e.*, having enough energy to dissociate. Then their formula for the rate constant for association, k_a , was

$$k_a = \lambda ZK^*G(T) \quad (1)$$

Here K^* was the equilibrium constant for



Z was the collision frequency of X_2^* with M , λ , assumed to be unity, was the probability that the collision would result in association, and $G(T)$ was the fraction of those which associate which are not dissociated again in subsequent collisions. K^* was evaluated by some rough but reasonable geometrical considerations, and $G(T)$ was found to be roughly equal to the reciprocal of the number of vibrational states within a range of kT of the dissociation threshold.

As pointed out by Benson and Fueno, this formula is the logical extension of the collisional theory of atom recombination developed by the writer.⁸ Actually the formula is equivalent to one in the later article,^{8b} except for the factor $G(T)$ and for the method of evaluating K^* . Since my method of evaluating K^* makes it about proportional to the number of vibrational states within a range of kT from the dissociation threshold, the presence of $G(T)$ about cancels this particular factor. However, Benson and Fueno's estimate of the number of vibrational states in the range noted is much smaller than mine.

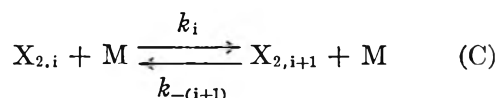
New Calculation of the Dissociation Constants.—This writer's preference generally has been to deal directly with the dissociation constant k_d , since this involves a binary collision. The constant k_a then can be obtained, since the equilibrium constant for reaction (A)

$$K = k_a/k_d \quad (2)$$

can be found. This turns out to have an especial advantage when one wishes to consider the effect of lack of equilibrium in the higher vibrational states, since the problem then can be formulated much more simply, and

a number of relationships which apparently have been overlooked then can be readily seen. We shall, therefore, proceed in this way, and we shall make somewhat different assumptions than those made previously [but compare Nikitin⁴ (1960)]. In particular, we shall not assume that the transitions occur from one vibrational level to the next, but that they take place with a certain energy increment. Of course, the energy increment in X_2 will not, by any means, be the same in all collisions with M , and a change in rotational energy (which would result from a collision crosswise to, rather than along, the line of centers of X_2) also can cause dissociation. In the latter case the effect occurs through a change in the effective potential energy, which is shifted with respect to the vibrational energy of the molecule, so again we may consider that the vibrational state is changed relative to the dissociation energy. We may hope that our assumption of equal vibrational energy increments will give a reasonable approximation if we take the increment equal to the average change of energy actually occurring in collisions in which X_2 is in the range of energy levels close to the dissociation limit. We believe that these are the important levels in determining the rate of dissociation; in general, the dissociating molecule must ascend the ladder of vibrational levels, but not just one rung at a time, since the rungs are not uniformly spaced; instead, the size of the steps is assumed to be uniform. The collision of M with X_2 when the latter has enough energy to be nearly dissociated, at least at the end of the motion when the X 's are widely separated (which will be the most probable situation for a collision), is very much like a collision of M with a free atom X . We may suppose that it can be handled classically, and that, roughly speaking, on the average, exchange of a certain amount of energy takes place. For this reason, it appears that the assumption of uniform energy increments is more reasonable than the assumption that the transitions take place only between adjacent vibrational states; actually, as we will see, the truth may lie somewhere between. In any case, it is to be understood that we are not attempting to present a finished theory, but only what appears to be a convenient basis for discussion of the experimental results.

Let us denote the average transfer of energy as η . Then we may formulate the series of reactions or collisions by means of which the molecule ascends the vibrational ladder by equations of the sort



In this equation $X_{2,i}$ represents a molecule in a certain range of energy of extent η , the energy being marked off in zones of width η , with i representing a higher energy than $i + 1$. We will let $i = 0$ for the zone of width η just below the dissociation limit of X_2 . If the reaction (C) comes to equilibrium, then the following relations hold

$$X_{2,i+1}/X_{2,i} \cong (g_{i+1}/g_i)e^a \quad (3)$$

where the italicized symbols $X_{2,i}$, etc., represent concentrations, where g_i is the number of energy levels in the range i , and where $a = \eta/kT$. From the law of microscopic reversibility, at equilibrium

$$k_i X_{2,i} = k_{-(i+1)} X_{2,i+1} \quad (4)$$

(5) H. O. Pritchard, *J. Phys. Chem.*, **65**, 504 (1961).

(6) O. K. Rice, *ibid.*, **65**, 1972 (1961).

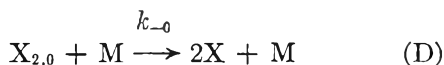
(7) S. W. Benson and T. Fueno, *J. Chem. Phys.*, **36**, 1597 (1962). The author is indebted to Dr. Benson for a preprint of this paper.

(8) (a) O. K. Rice, *ibid.*, **9**, 258 (1941); (b) *Monatsh. Chem.*, **90**, 330 (1959).

From (3) and (4) the usual relation follows

$$k_i/k_{-(i+1)} = (g_{i+1}/g_i)e^a \quad (5)$$

In general, of course, we do not have equilibrium established, and it is exactly the departure from equilibrium which we wish to investigate. The departure from equilibrium occurs because in the case of the reaction which takes place from the uppermost range, $i = 0$, which is the one resulting in dissociation



the back reaction does not occur at the beginning when no X atoms are present. Though the system is not at equilibrium, it will quickly come to a steady state,⁹ and, in the light of the above remarks, we may write

$$dX_{2,0}/dt = k_{-1}X_{2,1} - (k_0 + k_{-0})X_{2,0} = 0 \quad (6)$$

and, in general, for all other $X_{2,i}$ (except the last one)

$$dX_{2,i}/dt = k_{-(i+1)}X_{2,i+1} + k_{i-1}X_{2,i-1} - (k_i + k_{-i})X_{2,i} = 0 \quad (7)$$

The advantage of considering the problem from the point of view of the association reaction is that it is now possible to get all the $X_{2,i}$ in terms of $X_{2,0}$ by simple iteration, provided the k_i are known. We know that for the lower energy ranges (large i) where the deviation from equilibrium is expected to be small, $X_{2,i}$ should be proportional to $g_i e^x$, with $x = (\epsilon_D - \epsilon)/kT$ (where ϵ is the energy and ϵ_D the dissociation energy). We find that if we suppose, and only if we suppose, that X_0 is proportional to e^x , then all the higher X_i also will be proportional to e^x but with different proportionality constants. We expect the quantum weight g_i to be an important part of this proportionality constant; therefore we set

$$X_{2,i} = c_i g_i e^x \quad (8)$$

We substitute this in eq. 7, noting that the exponential factor in X_{i+1} will differ from that in X_i by the factor e^a , and that in X_{i-1} will differ from that in X_i by e^{-a} . We also make use of eq. 5. Thus we obtain

$$k_i c_{i+1} g_i + k_{-i} c_{i-1} g_i - (k_i + k_{-i}) c_i g_i = 0 \quad (9)$$

which may be rewritten

$$y_i c_{i+1} + y_{-i} c_{i-1} - c_i = 0 \quad (10)$$

where $y_i = k_i/(k_i + k_{-i})$ and $y_{-i} = k_{-i}/(k_i + k_{-i})$. Since we wish to use this equation for iteration, starting at the top of the vibrational ladder (small i), it is convenient to rewrite the equation once more by writing i for $i + 1$, which yields

$$c_i = y_{i-1}^{-1} c_{i-1} - (y_{-(i-1)}/y_{i-1}) c_{i-2} \\ = (1 + e^{-a_i}) c_{i-1} - e^{-a_i} c_{i-2} \quad (11)$$

where we have set $y_{-(i-1)}/y_{i-1} = e^{-a_i}$. This, it will be noted, is the ratio of the probability of a jump upward to a jump downward from the same state. It cannot be obtained from microscopic reversibility, but, in general, we may expect a_i to be positive so that the probability of a transition to the higher energy level will be less than that to the lower level. We will be interested only

(9) See O. K. Rice, *J. Phys. Chem.*, **64**, 1851 (1960).

in the relative values of the c_i in order to compare with the equilibrium case, for which, by eq. 8, all the c_i would be equal. Thus we may as well set $c_0 = 1$, and if we let $c_{-1} = 0$ (equivalent to using eq. 6 to start the iteration), we see that we may obtain all the following c_i if e^{-a_i} is known for each i .

Only if special assumptions be made can the problem be solved analytically. If e^{-a_i} be assumed to be constant, and if we set $b = e^{-a_i}$, then it is readily seen, by substitution in eq. 11 starting with $i = 1$, that

$$c_i = 1 + b + b^2 + \dots + b^i \\ = (1 - b^{i+1})/(1 - b) \quad (12)$$

Unless a_i is quite small, this converges fairly rapidly, and for all i greater than that at which convergence is practically complete, the levels will have essentially their equilibrium quota. The ratio c_0/c_∞ will give us the fraction of the equilibrium quota in the interval $i = 0$, and the ratio of the actual rate constant k_a to $k_{a,eq.}$, the constant which would be observed if equilibrium prevailed clear up the vibrational ladder. We see at once, since $b < 1$, that

$$c_0/c_\infty = k_a/k_{a,eq.} = 1 - b = 1 - e^{-a_i} \quad (13)$$

The special case of a "truncated" harmonic oscillator, with uniformly spaced energy levels (but a last one, beyond which dissociation occurs) and in which transition takes place only between adjacent levels and always with the same probability (*i.e.*, all k_i equal and all k_{-i} equal) has been worked out for the case of the association reaction by Benson and Fueno. They find that the rate of dissociation is decreased by a factor $1 - e^{-\eta/kT}$ due to redissociation from the higher levels. We get exactly the same factor for the decrease in the rate of dissociation if we set $a_i = a = \eta/kT$, which corresponds to the case of the truncated harmonic oscillator with all k_i equal,¹⁰ as in this case we would have to have $y_{-(i-1)}/y_{i-1} = e^{-a}$.

It is seen that the result embodied in eq. 13 is by no means confined to the special case of the truncated harmonic oscillator, but has a much greater range of application, the only necessary assumption, aside from the basic approximation that the energy is transferred in definite increments, being that a_i is independent of i . It is a little difficult to see just how restrictive this assumption is, but it seems likely that it is sufficiently good to give us at least a rough idea of the behavior of actual systems. Furthermore, it seems reasonable to suppose that a_i is fairly close to a . For our subsequent purposes we shall set $e^{-a_i} = f e^{-a}$, where f is not far from unity.

Within the limitations imposed by the approximations we have made, we are now in a position to find a formal expression for k_d , as

$$k_d = \left[4\pi\sigma^2 \left(\frac{kT}{2\pi\mu} \right)^{1/2} \right] \left[\frac{ng_0 e^{-\epsilon_D/kT} e^{a/2}}{kT/h\nu_0} \right] \times \\ [1 - f e^{-a}] \left[\frac{f e^{-a}}{1 + f e^{-a}} \right] \left(\frac{r_m}{r_e} \right)^2 \quad (14)$$

In this expression, the first bracket represents the collision frequency for collisions between X_2 and M, having

(10) From this we see that the detailed working out of this special case provides another example, showing, as previously,⁹ that the relation $K = k_a/k_d$ will not be affected by lack of equilibrium in the higher levels.

an effective collision distance σ ; the quantity μ is the reduced mass for such a pair. The second bracket is the equilibrium fraction of the molecules X_2 in the zone $i = 0$ just below the dissociation; the average energy of the levels in this region will be close to $\epsilon_D - \eta/2 = \epsilon_D - akT/2$, so the expression in the numerator represents the partition function for the molecules in this zone, while the expression in the denominator is the partition function for the unexcited molecules¹¹; n is the number of electronic levels which have attractive potential curves with asymptotes at the same energy, and from which transitions ultimately occur to the ground state (actually the various quantities in the equation must be averaged over these electronic states). The third bracket allows for the lack of equilibrium in the higher vibrational states. The fourth bracket is the probability that a collision will result in an increase in energy, with consequent dissociation of those X_2 in zone $i = 0$. Up to this point the expression would be correct for non-rotating molecules. When we average over all rotational states^{8b,12} the factor r_m^2/r_e^2 appears, where r_m is the average distance between the nuclei at the maximum in the effective potential energy curve due to the rotational potential, and r_e is the equilibrium distance. (This now assumes, which may not be quite correct, that f and a do not depend on the rotational state.)

For comparison we write down the expression previously derived,¹³ slightly rearranged

$$k_d = \left[4\pi\sigma^2 \left(\frac{kT}{2\pi\mu} \right)^{1/2} \right] \left[\frac{n(kT/\delta\epsilon_v)e^{-\epsilon_D/kT}}{kT/h\nu_0} \right] \left(\frac{r_m}{r_e} \right)^2 \quad (15)$$

Aside from the lack of the third and fourth brackets this differs from the other expression in the numerator of the second bracket. The quantity $\delta\epsilon_v$ is the energy between adjacent levels at an energy kT below the dissociation energy. A rough relation between g_0 and $kT/\delta\epsilon_v$ readily can be found. The behavior of energy levels near the dissociation limit is such that, roughly¹⁴

$$\epsilon_D - \epsilon_v = \alpha(v_D - v)^2/2 \quad (16)$$

where v_D is the quantum number at the dissociation limit, ϵ_v is the energy corresponding to quantum number v , and α is a proportionality constant. For particular values of $\epsilon_D - \epsilon_v$ let us designate v by a subscript (*i.e.*, $v = v_{kT}$ at $\epsilon_D - \epsilon_v = kT$ and $v = v_{akT}$ at $\epsilon_D - \epsilon_v = akT$). We see that $v_D - v_{kT} = (2kT/\alpha)^{1/2}$, and, by differentiation of eq. 16, $\delta\epsilon_v = \alpha(v_D - v_{kT}) = (2akT)^{1/2}$. Noting that $g_0 = v_D - v_{akT} = (2akT/\alpha)^{1/2}$, we see that

$$g_0 = 2a^{1/2}kT/\delta\epsilon_v \quad (17)$$

Thus the relation between eq. 14 and eq. 15 can be found easily if a and f are known. If we can estimate these quantities, we can use eq. 14 to obtain, from the experimental data, a somewhat more meaningful value of σ , which can then be compared with what we know about the range of the intermolecular forces.

(11) This is the classical partition function; but if the same approximation is made in calculating K , the resulting expression for k_d will be correct.

(12) O. K. Rice, *J. Chem. Phys.*, **21**, 750 (1953).

(13) Reference 8b, eq. 5.

(14) This is the type of relation used to extrapolate band spectra to convergence. It would follow precisely from a Morse potential. Actually, of course, the average molecule has some angular momentum, and its potential-energy curve has an effective centrifugal barrier. A curve with a centrifugal barrier actually may be better described by a Morse function, which is comparatively short-ranged, than would be the curve for a non-rotating molecule. In the latter, the asymptotic approach to the dissociation limit probably is controlled largely by the long-ranged van der Waals forces.

Estimation of the Parameters and Discussion of the Data on Iodine.—The quantity f , as we have remarked, will not be expected to differ greatly from unity, and we shall assume $f = 1$. We now turn our attention to a or η . It seems certain that η will be closely related to the energy of the colliding particle, M . To the extent that the collision may be considered to be a collision between M and one of the atoms X , we may make some estimate of the possible transfer of energy from the conservation laws of momentum and energy. The most probable situation will be that in which the atoms in X_2 are near their positions of maximum displacement, for over a considerable region in this neighborhood the relative velocity will be slow. Let us therefore consider what happens when an atom M of mass m_M , moving with velocity v_M , strikes head on an atom X of mass m_X which at first has zero velocity.^{8b,15} It is readily shown that in a free collision (no force field), the atom X will acquire a kinetic energy equal to $4m_Mm_X/(m_M + m_X)^2$ times the original kinetic energy of M . A glancing collision certainly will not be as effective as a head-on collision; on the other hand, some collisions in which the relative velocity of the X atoms is large may be expected to be more efficient than those in which their velocity is small. We therefore shall assume that¹⁶

$$a = 4m_Mm_X/(m_M + m_X)^2 \quad (18)$$

This is equivalent to the assumption that, if the atoms have equal mass, the average energy transferred is equal¹⁷ to kT , whereas it falls off according to (18) when the masses are different. This is a rough assumption, but seems reasonable for a working hypothesis in such a complicated situation. If it be accepted, it permits an evaluation of σ from the experimental values of k_d (or k_a , using eq. 2) by means of eq. 14. Careful experiments on the recombination of iodine atoms in the presence of the inert gases at room temperature have been made by Christie, Harrison, Norrish, and Porter,¹⁸ and we show in Table I the values of σ calculated from eq. 14, as well as the values previously obtained from eq. 15. The calculations using eq. 15 have been discussed thoroughly,^{8b} and the values of σ appropriate to eq. 14 have been obtained from them by correcting for the effect of the factors involving a .

TABLE I
CALCULATION OF COLLISION DISTANCE σ IN Å. FOR VARIOUS GASES WITH I_2

	He	Ne	Ar	Kr	Xe
σ (eq. 15)	1.1	1.9	3.1	3.9	4.9
a	0.119	0.472	0.729	0.957	0.999
$1 - e^{-a}$.1120	.376	.518	.616	.632
$e^{-a}/(1 + e^{-a})$.470	.384	.325	.277	.270
$2a^{1/2}e^{a/2}$.735	1.737	2.45	3.16	3.29
σ (eq. 14)	5.5	3.7	4.8	5.4	6.6

The unreasonably small value of σ obtained for He has been eliminated; the comparatively large value of σ obtained for He by use of eq. 15 suggests that the correc-

(15) See O. Oldenberg, *Phys. Rev.*, **37**, 194 (1931).

(16) This equation should not be used if the molecule X_2 is lighter than the atom M , since the translational energy of X_2 always could be readily converted to internal energy by collision with a heavy body regardless of eq. 18.

(17) Some recent classical calculations by J. C. Keck, *Discussions Faraday Soc.*, to be published, indicate that most pairs formed by association will be within kT of the dissociation energy. The author is indebted to Dr. Keck for a preprint of this work.

(18) M. I. Christie, A. J. Harrison, R. G. W. Norrish, and G. Porter, *Proc. Roy. Soc. (London)*, **A231**, 446 (1955).

- tions involving a are somewhat too large. This is especially so, since the values of σ for Ar, Kr, and Xe might have to be reduced when one takes into account the contribution to the reaction due to "sticky" collisions, mechanism (B). It was shown in ref. 8b that contributions to the reaction rate from this "complex" mechanism should, in these cases, be comparable to the contribution from the collision mechanism, (A). The contribution from the complex mechanism might have been slightly overestimated in ref. 8b because no account was taken of the effect of the rotational potential in making a complex $X \cdot M$ less stable, but the contribution surely should be of considerable importance for xenon.¹⁹

Although the corrections for lack of equilibrium as obtained by using eq. 21 to calculate a may be somewhat exaggerated, there seems to be no doubt that they should be made, and that our calculation gives the right order of magnitude. It is quite interesting that a major part of the effect of a limited transfer of energy due to difference in mass arises from the factor $1 - e^{-a}$, which expresses the effect of lack of equilibrium in the higher energy levels.

The Temperature Coefficient.—We return now to a consideration of the temperature coefficient of k_d , and in this respect eq. 14 appears at first to be something of a disappointment. Using eq. 17, it readily may be seen that if n , a , σ , f , and r_m are independent of temperature, the expression (14) also will be temperature independent aside from the factor $e^{-\epsilon_D/kT}$. Actually, r_m may be expected to decrease slowly with temperature. If the more distant part of the potential-energy curve may be supposed to have the form $-c/r^6$, where c is a constant, then for any particular value of the rotational quantum number j the value of r_m can be found by setting

$$d[-c/r^6 + j(j+1)h^2/8\pi^2\mu_I r^2]/dr = 0$$

The average value could then be approximated (*i.e.*, the corresponding value of j found) by setting $j(j+1)h^2/8\pi^2\mu_I r_m^2 = kT$, which makes r_m proportional²⁰ to $T^{-1/6}$. Thus r_m^2 is proportional to $T^{-1/3}$ and the increase in the rotational potential probably also will cause a slight decrease in g_0 , so that we may say that there is an over-all factor of about $T^{-1/2}$ if n , a , σ , and f are constant. When we calculate k_a from k_d , using K , the factors $T^{-1/2}$ and $e^{-\epsilon_D/kT}$ both are cancelled, leaving k_a temperature independent. However, actually, as noted in the Introduction, k_a appears to decrease with temperature, varying at least inversely proportionally to temperature with helium as the inert gas, and being somewhat more dependent on temperature with argon. In the case of argon this could be in part

(19) It may be that all the values of σ should be increased by a factor $(5/3)^{1/2}$, since n , the number of attractive potential energy curves to which association can occur, was taken as 5. It is possible that n should have been taken as 3, since the potential energy curve for the $^3\Pi_{1u}$ state (of degeneracy 2) is very shallow, so that re-dissociation from it may occur before stabilization by transition to another potential-energy curve with a deeper minimum. In general, transitions between potential-energy curves should be relatively easy, even if requiring change in multiplicity, in a case like iodine, where the coupling is largely j - j coupling. The argument of D. L. Bunker, *J. Chem. Phys.*, **32**, 1001 (1960), that n should be unity, with only the ground state, $^2\Sigma_g^+$, contributing, does not seem convincing, since the $^3\Pi_{2u}$ probably has a considerably deeper minimum²¹ than he suggests and it will only be necessary for the rate of non-adiabatic transfer to be rapid for a range of energies a few times η below the dissociation limit for any given potential-energy curve to make an effective contribution.

(20) See B. Widom, *J. Chem. Phys.*, **31**, 1027 (1959).

accounted for by the decreasing contribution of the complex mechanism. This, however, apparently cannot account for all the effect. Benson and Fueno believe that the temperature coefficient can be accounted for by increasing lack of equilibrium at higher temperatures, this being based on the assumption that η is independent of temperature, rather than a . It appears to this writer, however, that the average amount of energy transferred at a collision must increase with the amount of energy available. It has been seen, however, that our assumptions are not completely correct, and it may, indeed, be possible that η increases less rapidly with T than was supposed. The classical description of the collision occurring between a rare gas atom and an iodine atom breaks down when the iodine atom moves toward the other iodine atom and comes strongly into its field. It is well known that, because of increasingly poorer overlap of the wave function, large transfers of energy are less probable than small transfers. Thus, the transfer of energy may well fail to keep up with the temperature, causing a to decrease with temperature. This, together with a possible decrease of f and of σ with increasing temperature (the latter because glancing collisions are likely to be less effective at high temperatures where they last a shorter time) may well account for the temperature coefficient. Also, some of the temperature coefficient may, as suggested in reference 8b, arise from an effective decrease in n , since re-dissociation from an excited electronic level would become more likely the higher the temperature. Unfortunately, it is difficult to make quantitative estimates.

It is probably the collisions, which take place when the iodine atoms are close enough together to be in the region where their mutual potential energy changes relatively rapidly and quantum effects are of some importance, which make a greater than given by eq. 21. Therefore, it may be relevant to consider the effect of overlap of wave functions over the range of molecular attraction as a whole to see whether a decrease in a in the relevant range of temperatures, say from 300 to 1500°K., is to be expected. The de Broglie wave length for the vibration of I_2 is given by the well known formula $\lambda = h/p_r = h/(2\mu_{I_2}\epsilon_r)^{1/2}$, where p_r and ϵ_r are, respectively, the radial momentum and the radial kinetic energy. We thus find

$$d\lambda/d\epsilon_r = -1/2\lambda/\epsilon_r$$

whence we estimate that if we change ϵ_r by kT at $T = 300^\circ\text{K.}$ and take ϵ_r as the dissociation energy of I_2 , we would get a relative change in λ of approximately 0.008. However, the average kinetic energy of a pair of iodine atoms in their mutual field in the ground state near the dissociation limit is less than the dissociation energy, so we should perhaps estimate $d\lambda/\lambda$ as about 0.02. Now the number of energy levels in the ground state is about 150, meaning that there are about 75 de Broglie wave lengths near the dissociation, and the change of phase will be about 1.5 wave lengths, which gives relatively good overlapping of the wave function over a range comparable to that in which interatomic forces change appreciably. However, with $d\epsilon_r = kT$ at $T = 1500^\circ\text{K.}$, the overlapping would be much less, so the transition would be considerably less probable. Similar calculations would be expected to give similar results for the excited states, since both ϵ_r and the

number of quantum levels would both be smaller, but these factors would not compensate completely. In any case, the suggestion that a should decrease appreciably with temperature appears to be reasonable.

Comparison with Theory of Keck.—It seems desirable to conclude this paper with a comparison with the recent work of Keck²¹ on what he calls the variational theory of chemical reactions. In this theory a surface in phase space is selected, such that if a representative point crosses it, and does not cross back, the system may be said to have undergone reaction. The difficulty which arises is that a representative point may cross such a surface more than once, so the calculation gives only an upper bound for the rate. It is possible to select the surface in various ways, and an attempt is made to choose it in such a way as to cause the calculated rate to be a minimum. The calculation of the rate of crossing of the surface is reduced to an integral, which is simple in form but difficult to evaluate. Application of this procedure to the recombination of iodine atoms in the presence of the rare gases gives values of the upper bound which agree remarkably well with the experimental results at room temperature. It is, however, to be noted that Keck has made the calculation on the assumption that only recombination to the lowest electronic state is effective, *i.e.*, he takes $n = 1$. If n is assumed to be 3 or 5, his upper bounds will be several times greater than the observed ones, which seems more reasonable. However, in a number of other cases Keck's upper bound is close to or below experimental results, and his calculations presumably are sensitive to the potential-energy curve. The interatomic attraction between a rare gas atom and an iodine atom may be considerably greater than his estimate, since the situation seems favorable for a charge transfer complex.²² The analysis previously made⁸ of the rate of association

(21) J. C. Keck, *J. Phys. Chem.*, **32**, 1035 (1960).

(22) G. Porter and J. A. Smith, *Nature*, **184**, 446 (1959).

of iodine atoms with benzene as a third body indicates that the mutual potential energy of iodine atoms and benzene is almost the same as that of iodine molecules and benzene.

Although the mass of the third body does enter one of his boundary conditions, Keck states that the results are independent of the mass of the third body. There certainly are more collisions the lighter the third body; however, the faster the third body moves, the less time it spends in the neighborhood of the combining atoms, and the density in phase space is the same in any case. The question then arises as to whether the appropriate unit for consideration of the transition is the individual collision or a certain length of time. In any case, the point of view taken in the present paper is that we look at the individual collision. Since the number of collisions depends upon the mass of the third body, and since, if the potentials were always exactly the same, the actual rate of reaction would be the same according to Keck's calculation, it is clear that he predicts different collision efficiencies for the different rare gases. This is not surprising, since the dynamics of collisions involving different relative masses are very different. However, if the collision efficiency for the actual reaction is near unity, we expect the rate for a heavy third body to parallel the rate of collision and so to be less than that for a light one, and we must then suppose that the fact that Keck obtains the same rate (aside from effects of changes in the potential energy) is because he overestimates the rate more in the case of the heavy third body. The rate found by Keck, since it is always an equilibrium rate, should be compared with our rate without the factor $1 - e^{-a}$. If this be done, it is, indeed, found that his rate (corrected for n) exceeds our equilibrium rate by a greater amount the greater the mass of the third body. This still will be true even if we have overcorrected somewhat for helium as the third body.

THE FORMATION OF BENZENE IN THE RADIOLYSIS OF ACETYLENE¹

BY GILBERT J. MAINS, H. NIKI, AND M. H. J. WIJNEN

Department of Chemistry, Carnegie Institute of Technology, Pittsburgh, Pa., and The Radiation Research Laboratories, Mellon Institute, Pittsburgh, Pa.

Received April 3, 1962

The radiolysis of acetylene was studied over the pressure range 10 to 300 mm. and over the temperature range 25 to 262°. The effects of small amounts of free radical scavengers, the effects of excess krypton, and the effects of an excess of mercury vapor on the radiolysis yield of benzene were studied. C₂H₂:C₂D₂, C₂H₂:D₂, and C₂D₂:H₂ mixtures also were subjected to radiolysis. One experiment on the mercury photosensitized formation of benzene in a C₂H₂:C₂D₂ mixture is reported. The data are shown to be consistent with the formation of benzene by free radical reactions. A possible free radical mechanism to explain the formation of benzene and intermediate products is discussed.

The polymerization of acetylene to benzene has been the subject of several photochemical²⁻⁶ and radiation chemical investigations.⁷⁻⁹ The radiation induced

(1) Based partially upon data submitted by H. Niki in partial fulfillment of the requirements for the degree Doctor of Philosophy, Carnegie Institute of Technology.

(2) M. Zelkoff and L. M. Aschenbrand, *J. Chem. Phys.*, **24**, 1034 (1956).

(3) S. Shida, Z. Kuri, and T. Furuoya, *ibid.*, **28**, 131 (1958).

(4) D. J. LeRoy and E. W. R. Steacie, *ibid.*, **12**, 117 (1944).

(5) J. K. Cashion and D. J. LeRoy, *Can. J. Chem.*, **32**, 906 (1954).

(6) H. W. Melville, *Trans. Faraday Soc.*, **32**, 258 (1936).

(7) S. C. Lind, "Radiation Chemistry of Gases," Reinhold Publ. Corp., New York, N. Y., 1961, Chapter 9.

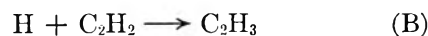
(8) L. M. Dorfman and A. C. Wahl, *Radiation Res.*, **10**, 680 (1959).

(9) L. M. Dorfman and F. J. Shipko, *J. Am. Chem. Soc.*, **77**, 4723 (1953).

polymerization has been explained⁸ in terms of ion-molecule chain reactions of the type



and higher homologs or, as well, by a free radical chain process, such as



and



and higher acetylene addition steps. The formation of benzene can be attributed to cyclization of the ionic or

free radical chain at the appropriate step. Recently,^{8,9} it was postulated that the benzene was formed by a mechanism which was independent of the polymerization mechanism and which involved an excited state of acetylene, probably the triplet state.

The formation of benzene *via* an excited state mechanism also was proposed for the direct photolysis of acetylene^{2,6} and for the mercury sensitized photolysis of acetylene,³ although LeRoy^{4,5} has supported the free radical mechanism of benzene formation.

Owing to the uncertainty of the relative importance of the ionic, free radical, and excited state mechanisms of benzene formation, one of our Laboratories¹⁰ undertook an investigation of the mercury sensitized radiolysis and photolysis of acetylene. The radiolysis of acetylene and acetylene-*d*₂, acetylene and *D*₂, and acetylene-*d*₂ and H₂ mixtures also was studied.

One of us has reported the chlorine atom induced polymerization of acetylene,¹¹ and has identified C₂H₃Cl, C₄H₅Cl, C₆H₆, C₆H₅Cl, and polymer products. The formation and relative abundance of these products strongly suggest that the precursor to benzene is the C₆H₆Cl radical, which then may cyclize by losing either H or Cl or which may continue further polymerization by addition to acetylene. In the light of this new evidence, it seemed desirable to restudy the radiolysis of acetylene and to examine the possibility that benzene may be formed *via* the free radical precursor, C₆H₇. This independent study considered the effect of acetylene pressure, temperature, free radical scavengers, and krypton. Because these two studies^{10,11} have resulted in similar conclusions regarding the formation of benzene, it seemed desirable to report them jointly.

Experimental

Acetylene was obtained from the Matheson Company and, after distillation at low temperature to remove traces of acetone, contained less than 0.5% ethylene by mass spectrometer analysis. Acetylene-*d*₂ was obtained from Merck Company, Canada, and was similarly distilled and analyzed. Less than 1.6% C₂HD was found as impurity. Matheson Company H₂ was used without further purification. Stuart Company D₂, containing less than 0.5% HD, was used without purification. Krypton was obtained from Airco, and was found mass spectrometrically pure. Bethlehem Apparatus Company, triple-distilled, instrument grade mercury was used in the mercury sensitized experiments. Once-sublimed iodine was used.

Co⁶⁰ γ -radiations were performed in cylindrical Pyrex sample vessels equipped with a break seal. All such vessels had an outside diameter of 20 mm. and a volume of 37 \pm 1 cc. Two different Co⁶⁰ sources were used. Source I exhibited a dose rate in water of 8.50 \times 10¹⁴ e.v./cc./sec.; Source II, 4.91 \times 10¹⁵ e.v./cc./sec. The dose rate in the vapor phase was calculated on the assumption that energy absorption is proportional to the electron density of the sample. No correction was made for the relative stopping power of the vapor and glass.¹² The reliability of this extrapolation of dose rates from the liquid phase to the vapor phase was ascertained by calculating the *G*-yield of N₂ from N₂O at 25° and 95 cm. The value obtained was 9.3 \pm 0.3, in fair agreement with the value 9.7 reported earlier.¹³ It seems reasonable to assign a maximum error of 10% to the absolute *G*-yields determined in this way. The relative *G*-yields are, of course, more reliable.

X-Radiations were performed using a Machlett OEG-50 X-ray tube operated at 50 pkev. at anode currents up to 50 ma. The dose rate at 50 pkev. and 40 ma. was 1.04 \times 10¹⁴ e.v./cc./sec. in N₂O at 25° and 93 cm., assuming¹³ a *G*-yield of 9.7 for N₂ formation. The dose rates in the reaction mixtures were computed

from X-ray attenuation coefficients.¹⁴ The error in the absolute *G*-yield probably is no more than 10% by this method. Reaction vessels were Pyrex cylinders, 45 mm. in diameter and 75 mm. long. One end of the vessel was fitted with a thin in-blown window; the other end with a break seal. The volume of the vessels was 100 \pm 5 cc. The reaction vessels were heated under vacuum after cleaning. If mercury was to be present, the vacuum was broken and 20 μ l. of liquid mercury was added. After re-evacuation, acetylene was added to the appropriate pressure, 10 mm. at 25° unless otherwise stated in the text. The reaction vessels then were sealed off and placed in an aluminum block oven fitted with a thin aluminum window. The aluminum oven was wrapped with heating tape and placed in a 3-l. heating mantle. For experiments at 262°, the heating mantle was adjusted to give an air temperature of 260°. The heating tape supplied the additional heat to control the oven temperature at 262 \pm 1°. A Hallikainen Resistotrol automatic temperature regulator controlled the heating tape. The temperature was monitored at several points in the oven by calibrated copper-constantan thermocouples. The same procedure was followed for the experiments at 25° except that the heating tape and heating mantle were not turned on. The system did not increase in temperature more than 1° during these room temperature irradiations.

The products observed in the γ -radiolysis experiments at 25° were benzene, diacetylene, 1,3-butadiene, and polymer. Diacetylene and 1,3-butadiene were minor products and often could not be determined. Approximate *G*-yields for diacetylene and 1,3-butadiene are 1.8 and 0.5, respectively. Analysis of the γ -radiolysis products was carried out by gas chromatography. In these experiments less than 0.1% of the acetylene was converted to benzene.

In the X-radiolysis experiments and the photolysis experiment, benzene, vinylacetylene, diacetylene, phenylacetylene, and cyclooctatetraene were observed as products of decreasing importance. 1,3-Butadiene was observed in trace yields in all 262° experiments. In the experiments in which hydrogen was added, 1,3-butadiene was a major product. All analyses of X-ray products were carried out on a Consolidated 21-103C mass spectrometer. The identification of phenylacetylene and cyclooctatetraene is only tentative. These products are in accord with those observed earlier.²

Results

Isotopic Studies.—The radiolysis of an approximately equimolar mixture of C₂H₂ and C₂D₂ resulted in the mixture of isotopically substituted benzenes shown in Table I. Considering only those experiments in the absence of mercury, it can be seen that relatively large yields of C₆H₅D, C₆H₃D₃, and C₆D₅H were observed at both 25 and 262° in spite of the fact that less than one molecule in 25 was C₂HD at the end of the experiment. The percentage conversion of acetylene to benzene seems too small to attribute these high yields of C₆H₅D, C₆H₃D₃, and C₆D₅H to secondary processes. Furthermore, if the formation of these isotopic benzenes occurred by secondary processes, the relative distribution of the isotopic species should be dose dependent. In experiments in which the dose was varied so that the extent of conversion changed, no variation in the relative distribution of isotopic benzenes was observed. In the presence of excess mercury vapor, the benzene distribution was *independent* of dose up to 8% conversion of the acetylene to benzene.

In order to ascertain whether the presence of C₆H₅D, C₆H₃D₃, and C₆HD₅ resulted from a rapid scrambling of the hydrogens in the benzene after formation, some experiments were carried out in which C₂H₂ was irradiated in the presence of 2% C₆D₆. Although traces of mixed benzenes could be detected, the resultant benzenes were at least 98% C₆H₆ and C₆D₆. It seems reasonable to conclude that the formation of benzene cannot occur exclusively by an excited state mechanism as postulated

(10) H. Niki and G. J. Mains, Carnegie Institute of Technology.

(11) M. H. J. Wijnen, *J. Chem. Phys.*, **36**, 1672 (1962).

(12) J. Weiss and W. Bernstein, *Phys. Rev.*, **98**, 1828 (1955).

(13) P. Hartek and S. Dondes, *Nucleonics*, **14**, 66 (1956).

(14) G. W. Grodstein, Natl. Bur. Std. Circ. 583, 1957.

TABLE I

RELATIVE ABUNDANCE OF ISOTOPIC BENZENES FORMED IN THE X-RADIOLYSIS AND PHOTOLYSIS OF C ₂ H ₂ -C ₂ D ₂ MIXTURES ^a				
Benzene	X-Rays at 25°, %	X-Rays at 262°, %	X-Rays, Hg at 262°, %	Ultraviolet, Hg at 262°, %
C ₆ H ₆	7.2 ± 1.3	5.9 ± 1.9	6.4 ± 1.3	5.6 ± 1.6
C ₆ H ₅ D	6.6 ± 1.9	7.6 ± 1.3	7.3 ± 1.8	9.2 ± 0.9
C ₆ H ₄ D ₂	24.2 ± 0.5	20.7 ± 0.1	21.8 ± 0.1	20.7 ± 0.1
C ₆ H ₃ D ₃	12.0 ± 1.2	16.6 ± 0.6	14.5 ± 0.9	19.6 ± 3.0
C ₆ H ₂ D ₄	28.7 ± 1.4	26.8 ± 1.2	27.3 ± 1.7	23.5 ± 1.2
C ₆ HD ₅	8.6 ± 0.1	11.0 ± 0.6	10.4 ± 0.9	12.9 ± 1.3
C ₆ D ₆	12.9 ± 1.6	12.2 ± 1.5	12.4 ± 1.4	8.7 ± 1.0
% C ₂ HD conversion	1.4	4.9	2.8	8.0
% conversion benzene	0.3	0.5	0.6	0.9

* NOTE: The uncertainties listed above were computed assuming maximum errors in the estimated mass spectrometer patterns for the isotopically substituted benzenes. All experiments were reproducible to within a few per cent. One experiment at 262° in the presence of Hg was carried out to 8% conversion and the benzenes were analyzed using 11.0 e.v. electrons in the mass spectrometer. The distribution of benzenes was in excellent agreement with that reported in column three above.

by earlier investigators.^{8,9} Some mechanism involving C-H bond rupture seems to be operative. Dorfman⁹ first suggested this C-H bond rupture on the basis of a few early isotope experiments but did not consider this process part of the mechanism of benzene formation. It should be noted that a small portion of the C₆H₆, C₆H₄D₂, C₆D₄H₂, and C₆D₆ could be formed by an excited state mechanism. However, the high yields of C₆H₄D₂ and C₆D₄H₂ are not *prima facie* evidence for an excited state mechanism, since these products are favored statistically in both free radical and excited state mechanisms.

It is important that the distribution of isotopic benzenes observed in the ³P Hg photolysis experiment (Table I, column 4) is quite similar to that observed in the radiolysis experiments. A significant yield of C₂HD was obtained, which may account for the increased yields of C₆H₅D, C₆H₃D₃, and C₆D₅H. However, the yields of these products are too large to be accounted for by statistical inclusion of C₂HD by a triplet state mechanism as postulated earlier.³ Additional experiments, planned for the near future,¹⁰ are required to determine whether the triplet state mechanism is required in ³P Hg photolysis experiments.

Influence of Acetylene Pressure and Dose Rate.—The first series of runs in Table II gives the *G*-value for benzene formation as a function of the initial acetylene pressure at 25°. The results, which are shown in Fig. 1, leave no doubt that the *G*-value of benzene increases with decreasing acetylene pressure for both γ -irradiation and X-irradiation. Since the *G*-yields for these two types of radiation differ by a factor of ten, which is considerably outside the estimated errors in these quantities, it seems reasonable to attribute these differences to an intensity effect. At an acetylene pressure of 20 cm., the dose rate in Co⁶⁰ Source I is about 1 × 10¹¹ e.v./cc./sec., whereas the dose rate in the X-ray system is about 1 × 10¹³ e.v./cc./sec. at this pressure. Both Laboratories^{10,11} have considered the possibility that this difference was attributable to different dosimetry techniques. Inasmuch as both laboratories used N₂O dosimetry as a secondary or primary standard, this explanation cannot be valid. In the X-radiolysis experiments it was found that a factor of four increase in anode current increased the rate of benzene formation by a factor of 2.5 (*vide infra*—Influence of Sensitizers). Furthermore, the *G*-yield of benzene was found to be markedly reduced in preliminary experiments using a Van de Graaf accelerator. In the light of these experiments, it seems reasonable to assign the differences in

the abscissa of the curves in Fig. 1 to an intensity effect rather than to any experimental artifact.

It is noteworthy that pressure effects and intensity effects have not been reported previously. Dorfman and Shipko⁹ report a *G*-value of 5.1, independent of acetylene pressure, using tritium beta radiation. However, these authors found it necessary to convert 5–10% of the acetylene to benzene, and the possibility of secondary reactions must be considered. Since the increase in acetylene pressure also results in the increase in dose rate, it is not possible to ascribe the decreases depicted in Fig. 1 to pressure effects alone. In order to

TABLE II
RADIOLYSIS OF ACETYLENE

Run no.	C ₂ H ₂ init. press., cm. at 0°	Additives init. press., cm.	Source	G-C ₆ H ₆
Influence of initial acetylene pressure at 25°				
1	4.3	...	Co ⁶⁰ I	13.6
4	14.8	...	Co ⁶⁰ I	10.3
6	47.7	...	Co ⁶⁰ I	8.6
2	76.7	...	Co ⁶⁰ I	7.4
3	6.9	...	Co ⁶⁰ II	10.6
7	15.4	...	Co ⁶⁰ II	10.0
8	46.5	...	Co ⁶⁰ II	7.7
5	76.8	...	Co ⁶⁰ II	7.0
101C	1.6	...	X-Ray	5.1
109B	4.0	...	X-Ray	2.6
115A	10.5	...	X-Ray	1.6
118A	43.4	...	X-Ray	0.5
Influence of free radical scavengers at 25°				
9	44.7	Oxygen 2.4	Co ⁶⁰ I	No C ₆ H ₆ obsd.
10	46.1	Iodine	Co ⁶⁰ I	No C ₆ H ₆ obsd.
11	15.2	Isobutylene 1.1	Co ⁶⁰ II	0.7
12	47.2	Isobutylene 1.5	Co ⁶⁰ II	2.3
Influence of krypton ^a at 25°				
7	15.4	...	Co ⁶⁰ II	10.0
13	15.7	12.2	Co ⁶⁰ II	20.7
14	15.1	19.0	Co ⁶⁰ II	21.2
15	15.5	42.2	Co ⁶⁰ II	38.6
Influence of temp.				
Temp., °C.				
16	6.3	12	Co ⁶⁰ I	12.6
22	6.2	60	Co ⁶⁰ I	15.2
21	6.1	102	Co ⁶⁰ I	20.1
17	6.3	136	Co ⁶⁰ I	26.6
19	6.2	140	Co ⁶⁰ I	24.6
18	6.2	173	Co ⁶⁰ I	19.1
20	6.2	213	Co ⁶⁰ I	13.3

^a *G*-value based on the mass of C₂H₂ present.

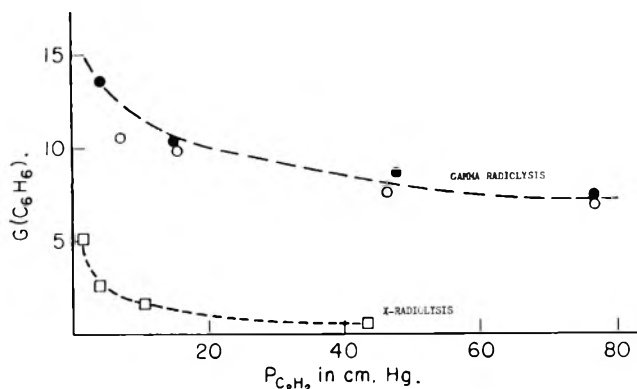


Fig. 1.—Variation of $G\text{-C}_6\text{H}_6$ with pressure and dose rate.

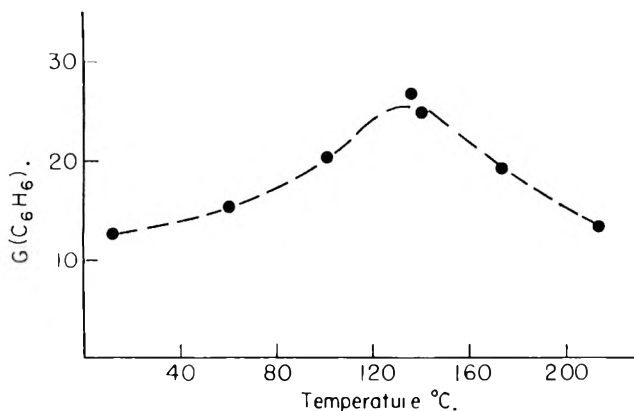


Fig. 2.—Variation of $G\text{-C}_6\text{H}_6$ with temperature.

establish a distinct pressure effect it is necessary to compare experiments at constant dose rates. The dose rates should be essentially the same at a pressure of 76.6 cm. in Source I, at 13.2 cm. in Source II, and 1.26 in the X-ray beam. A comparison of the G -yields, 7.4, 10, and 7-8 (extrapolated), respectively, does not reveal a marked pressure dependence. Therefore, while an intensity effect on the G -yield of benzene is established by the present experiments, a separate and distinct pressure effect has not been proven.

Accepting that the fraction of reacting acetylene forming benzene is 0.2 as reported by Dorfman and Shipko,⁹ the maximum conversion in the experiments reported in Table II may be estimated at 1.5%. Dorfman and Wahl⁸ report that at low pressures (0-2 cm.) the G -value of benzene decreases with decreasing pressure. This observation is not in contradiction with the data of Table II. If benzene is formed *via* a free radical path, it seems reasonable to expect a decreasing G -value at lower pressures due to disappearance of free radicals at the walls. Thus a maximum must occur in both curves in Fig. 1 at low acetylene pressures.

Influence of Temperature.—The data of Table II show the influence of temperature on the formation of benzene. These data are presented graphically in Fig. 2 and clearly indicate that a maximum is obtained in the G -yield at about 140°. A study of the mercury photosensitized polymerization of acetylene has revealed a similar maximum. Melville⁶ reported that the rate of polymerization increases with increasing temperature to a maximum at about 200°. A study¹⁵ of the temperature dependence of the mercury sensitized radiolysis of acetylene also revealed a maximum in the G -yield of benzene formation near 160°.

Influence of Free Radical Scavengers.—Based upon the evidence cited in the preceding sections, free radical scavengers might be expected to reduce the yield of benzene. Runs 9, 10, 11, and 12 in Table II show the effect of addition of free radical scavengers. The formation of benzene is completely suppressed by the addition of oxygen and iodine. Experiments in one of our Laboratories¹¹ have shown that isobutylene is an efficient scavenger of hydrogen atoms. Runs 10 and 11 show that benzene formation is increasingly suppressed by increase of isobutylene concentration. Using isobutylene as a radical scavenger, we have observed the formation of *t*-butylethylene. The formation of benzene decreases while *t*-butylethylene increases with increasing amounts of isobutylene. The failure of isobutylene to scavenge the precursor of benzene completely probably is due to the efficiency of acetylene as a scavenger.

The interpretation of the effects of added free radical scavengers in radiolysis experiments is always subject to question. Some of these compounds are expected to behave as excited state and/or ion scavengers as well as free radical scavengers. For the system reported here it seems reasonable to rule out major contribution of excited states based upon the isotopic studies. Therefore, the marked effect of oxygen, which has a higher ionization potential than acetylene, probably can be attributed to free radical scavenging.

Influence of Sensitizers.—One of the arguments in favor of the duality in the primary process has been the observation that the addition of rare gases to acetylene prevents the cyclization to benzene.⁸ Runs 7, 13, 14, and 15 of Table II fail to confirm this observation for the krypton-acetylene mixtures used in these experiments. These results are not necessarily contradictory. It was noted early in the discussion that an increase in dose rate decreased the yield of benzene. The experiments of Dorfman and Wahl⁸ were done at much higher dose rates using a Van de Graaf accelerator. In the experiments of Table II, the ratio of krypton to acetylene is less than three, whereas Dorfman and Wahl used much higher ratios. Therefore, it is possible to reconcile these superficially contradictory observations in terms of differences in dose rates.

The distribution of X-radiolysis products at 262° in the presence and absence of mercury vapor is reported in Table III. Experiments 47B and 48A demonstrate that the conversion to gaseous products and to benzene is increased by a factor of about 10 in the presence of *ca.* 100 mm. of mercury vapor. Experiments 48A and 47A indicate that a fivefold increase in the initial acetylene pressure increased the yield of products by a factor of 1.7 without significantly altering the distribution of these products.

Owing to the very low conversion in expt. 47B, the product distribution is subject to considerable error. Therefore, it seems unwarranted at the present time to discuss possible variations in product distribution caused by the presence of mercury vapor. Mercury, by virtue of its low ionization potential, may behave as a C_2H_2^+ scavenger in the systems reported here. If mercury is behaving as an efficient ion scavenger, the data of Tables I and II indicate that ionic reactions do not contribute significantly to the benzene formation. Because reliable cross section data for charge transfer

reactions in these systems are unavailable, the extent of suppression of the ionic processes by mercury vapor cannot be evaluated quantitatively.

A comparison of expt. 47C and 48A reveals the dose rate effect noted earlier in the discussion.

TABLE III
X-RADIOLYSIS OF ACETYLENE AT 262°

	Experiment no.			
	47A	47B	47C	48A
$P_{C_2H_2}$, mm. at 25°	50	10	10	10
P_{Hg} , mm. at 262°	100 ^a	0	100 ^a	100 ^a
Anode current, ma.	40	40	10	40
Irradiation time, min.	30	30	30	30
% Conversion to gaseous products	3.5	0.2	0.8	2.0
Gaseous ^b product distribution (%)				
Diacetylene	9.2	13.2	8.3	10.4
Vinylacetylene	14.1	27.6	22.7	15.0
Benzene	71.7	51.5	66.3	72.2
Phenylacetylene	1.9	4.7	1.1	1.2
Cycloöctatetraene	3.1	3.0	1.6	1.2

^a Calculated from the vapor pressure curve for mercury. ^b 1,3-Butadiene was too small for confident analysis and was not included in the table.

Influence of Hydrogen and Mercury.—In order to ascertain the effectiveness with which hydrogen atoms initiate the polymerization of acetylene to benzene, a few X-radiolysis experiments were carried out using an eighteenfold excess of H₂ in the presence of acetylene and mercury at 262°. Ethylene and 1,3-butadiene were found to be major products, although small amounts of benzene, butane, cyclohexadiene, cyclohexane, and cyclohexane also were observed.

Some experiments were performed using H₂-acetylene-*d*₂ and D₂-acetylene mixtures to trace the role of hydrogen. The results of these experiments are presented in Table IV. It is significant that the ratios C₆H₅-D/C₆H₆ and C₆D₅H/C₆D₆ depend upon the ratio of initial reactants. A comparison of expt. 104B with expt. 99A indicates that the ratio C₆H₅D/C₆H₆ is only slightly dependent upon the extent of conversion and, therefore, secondary processes are not the means by which deuterium is being incorporated into the benzene. Furthermore, the extent of exchange to form C₂HD is too small to yield the large amounts of C₆H₅D by statistical inclusion of C₂HD in the polymer chain. Therefore, the mechanism by which benzene is formed most probably involves hydrogen in either the initiating and/or terminating step.

The similarity of the results of Table IV with the results of other experiments in which polymerization of

TABLE IV

THE MERCURY SENSITIZED X-RADIOLYSIS OF ACETYLENE-HYDROGEN MIXTURE AT 262°

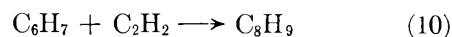
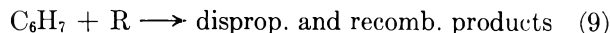
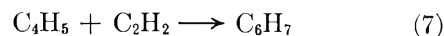
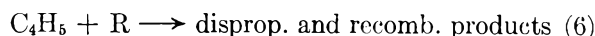
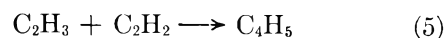
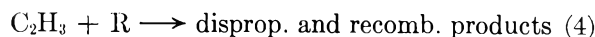
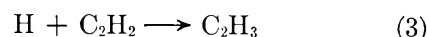
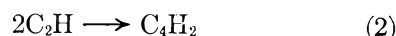
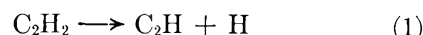
	Experiment no.				
	104B	99A	96B	98A	96A
$P_{C_2H_2}$ (mm. at 25°)	10	10	10
P_{D_2} (mm. at 25°)	180	180	330
P_{Hg} (mm. at 262°)	100 ^a	100 ^a	100 ^a	100 ^a	100 ^a
$P_{C_2D_2}$ (mm. at 25°)	10	10
P_{H_2} (mm. at 25°)	180	330
Irradiation time (min. at 40 mm.)	15	30	30	30	30
C ₆ H ₅ D/C ₆ H ₆	0.28	0.30	0.63
C ₆ H ₅ H/C ₆ D ₆	0.44	0.64
Yield of C ₂ HD, %	2.6	3.5	6.5	3.4	4.2
Conversion to benzene, %	0.6	1.2	0.2	0.6	0.1

^a Calculated from the vapor pressure curve for mercury.

acetylene was affected by other initiating radicals is striking. When chlorine atoms are used to initiate the formation of benzene, the yield of chlorobenzene is much less than the yield of benzene.¹¹ In the experiments of Drew and Gordon,¹⁶ where acetylene was polymerized by radicals formed from the photolysis of deuterioacetone, no deuterated toluene was found.

Discussion

In suggesting that the data may be explained by a free radical mechanism, we have no intention of ruling out partial ionic product formation in the absence of added ion scavengers. We do not express an opinion as to whether free radicals are formed *via* neutralization of ions or by decomposition of excited molecules. By analogy to the formation of benzene in the methyl radical¹⁶ and chlorine atom¹¹ initiated polymerization of acetylene, we suggest that the following mechanism is in agreement with the observed data



etc. to cycloöctatetraene and polymer

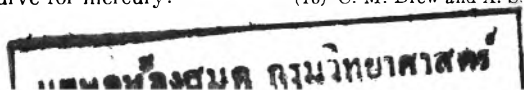
In the above reaction sequence, R denotes a polymeric radical originating from H atom or C₂H radical addition to acetylene. This mechanism offers a qualitative explanation for the observed products, *i.e.*, diacetylene, butadiene, vinylacetylene, benzene, and higher polymers.

The presence of H atoms in the system is indicated by the formation of diacetylene and the simultaneous absence of molecular hydrogen. Further confirmation of the presence of H atoms is afforded by the production of benzenes containing an odd number of D atoms in the experiments utilizing C₂H₂:C₂D₂ mixtures.

It has been pointed out recently¹¹ that C₂H₂Cl radicals react rapidly with acetylene to yield addition products. A similar reactivity might be expected for the C₂H₃ radical. Therefore it is not surprising that only traces of 1,3-butadiene are observed in the radiolysis of acetylene. In the radiolysis of C₂H₂:H₂ mixtures, in which H₂ is in considerable excess, the vinyl radical concentration may be increased to such an extent that recombination to butadiene is favored over addition to acetylene.

The dose rate dependence of benzene formation is explained by reactions 8, 9, and 10. Increasing radical concentrations resulting from increasing dose rates will favor reaction 9 over benzene formation. We also would expect a decrease in benzene formation with increasing acetylene pressure since reaction 10 will com-

(16) C. M. Drew and A. S. Gordon, *J. Chem. Phys.*, **31**, 1417 (1959).



pete with reaction 8 at large acetylene pressures. Unfortunately, present data are insufficient to ascertain whether such a distinct pressure effect is as predicted.

It might be argued that the formation of benzene by reaction 8 is subject to question since elimination reactions involving alkyl radicals are known to have rather high activation energies. However, the reaction postulated here may involve simultaneous cyclization and elimination, thereby reducing considerably the energy requirements of simple elimination reactions. The temperature dependence shown in Fig. 2 corresponds to an over-all activation energy for benzene formation which varies with temperature.

The high G -yields for benzene formation at low dose rates and small acetylene pressure indicate that benzene may be produced by a chain mechanism such as that postulated in the above reaction sequence. If benzene is formed *via* a free radical mechanism, then some polymer also must be formed by a free radical path. This does not mean that part of the polymer formation, possibly even the major part, may not be due to ion-molecule polymerization reactions.

In conclusion, the authors would like to state that they are well aware of the controversial nature of the postulated free radical mechanism for benzene formation. Quantitative information on intermediate formation will be necessary before firm conclusions can be reached regarding specific reactions. The system probably is much more complicated than our mechanism implies. Discussion of the data was, therefore, not intended as proof of this mechanism. Its sole purpose was to point out that objections raised against a free radical mechanism no longer are valid, and that, indeed, the data are quite consistent with information gained on benzene formation in photochemical systems.

Acknowledgment.—This investigation was supported, in part, by the U. S. Atomic Energy Commission in both contributing Laboratories. H. N. wishes to express his gratitude to the U. S. Atomic Energy Commission for financial support during the period of the investigation. The authors wish to thank Dr. L. Dorfman for helpful criticism of an early manuscript and for suggesting some additional experiments.

DISTRIBUTION OF SUBSTITUTED ANILINES BETWEEN AQUEOUS DIOXANE AND A POLYSTYRENESULFONIC ACID ION-EXCHANGE RESIN

BY JOHN E. GORDON

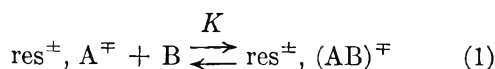
Mellon Institute, Pittsburgh, Pennsylvania

Received April 20, 1962

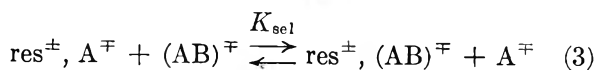
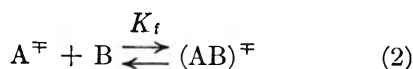
Distribution of four *p*-substituted anilines between 80.5 weight % aqueous dioxane and a polystyrenesulfonic acid ion-exchange resin, Bio-Rad AG50W-X8, has been studied over a wide range of concentration. The data obey a classical mass law expression for the reaction $\text{res}^- + \text{H}^+ + \text{B} = \text{res}^-, \text{BH}^+$. The observed equilibrium constants are related to the acid dissociation constants of the anilinium ions in 82% dioxane by the equation $\log K = 1.17 + 0.831 \text{ p}K_a$.

Introduction

The reaction between a molecule B, in solution, and an ion A^\mp present as the solid ion-exchange resin salt

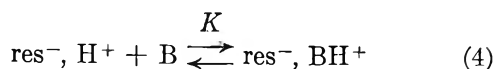


is important in attempts to employ ion exchangers in problems of physical organic chemistry. It provides an approach to measurement of complex ion formation equilibria and of selectivity effects in organic ion-exchange equilibria, as may be seen by expressing (1) as the sum of (2) and (3)



Reaction 1, as an equilibrium analog of the key kinetic process in resin-catalyzed reactions, offers a means of comparing equilibrium and kinetic selectivity effects.

The reaction of bases with the hydrogen form of the exchanger



is one of the simplest examples of (1). The purpose of the present measurements is to find if a true equilibrium

constant can be determined for reaction 4, and to what extent relative values of such K 's for a series of structurally related substrates, B, represent relative values of the complex ion formation constants, in this case the relative basicities. Previous studies of the distribution of bases into acidic exchangers¹⁻⁵ (or acids with basic exchangers⁶⁻⁸) have not provided such equilibrium constants, but often have been interpreted as adsorption phenomena. This often was necessitated by the use of water or a medium approaching water, as solvent, in which case sorption of acid or base independent of chemical reaction with the resin functional groups may be pronounced.⁹

Experimental

Materials.—Reagent grade dioxane and aniline were fractionally distilled; center cuts having properties in agreement with the literature were used. The remaining bases were reagent grade materials, crystallized three or more times and displaying melting points agreeing with literature values; they were sublimed at 10^{-4} mm. shortly before use. The resin was purified Dowex 50W-X8, 200-400 mesh, obtained from Bio-Rad Labora-

- (1) L. Saunders and R. S. Srivastava, *J. Chem. Soc.*, 2111 (1952).
- (2) T. Vermeulen and E. H. Huffman, *Ind. Eng. Chem.*, **45**, 1658 (1953).
- (3) G. W. Bodamer and R. Kunin, *ibid.*, **45**, 2577 (1953).
- (4) G. S. Panson and R. Ellsworth, *J. Org. Chem.*, **35**, 1466 (1960).
- (5) S. R. Watkins and H. F. Walton, *Anal. chim. Acta*, **24**, 334 (1961).
- (6) J. A. Bishop, *J. Phys. Chem.*, **50**, 6 (1946).
- (7) D. A. Robinson and G. F. Mills, *Ind. Eng. Chem.*, **41**, 2221 (1949).
- (8) S. Peterson and E. Gowen, *ibid.*, **45**, 2584 (1953).
- (9) C. W. Davies and G. G. Thomas, *J. Chem. Soc.*, 2624 (1951); S. Peterson and R. W. Jeffers, *J. Am. Chem. Soc.*, **74**, 1605 (1952); R. E. Anderson and R. D. Hansen, *Ind. Eng. Chem.*, **47**, 71 (1955).

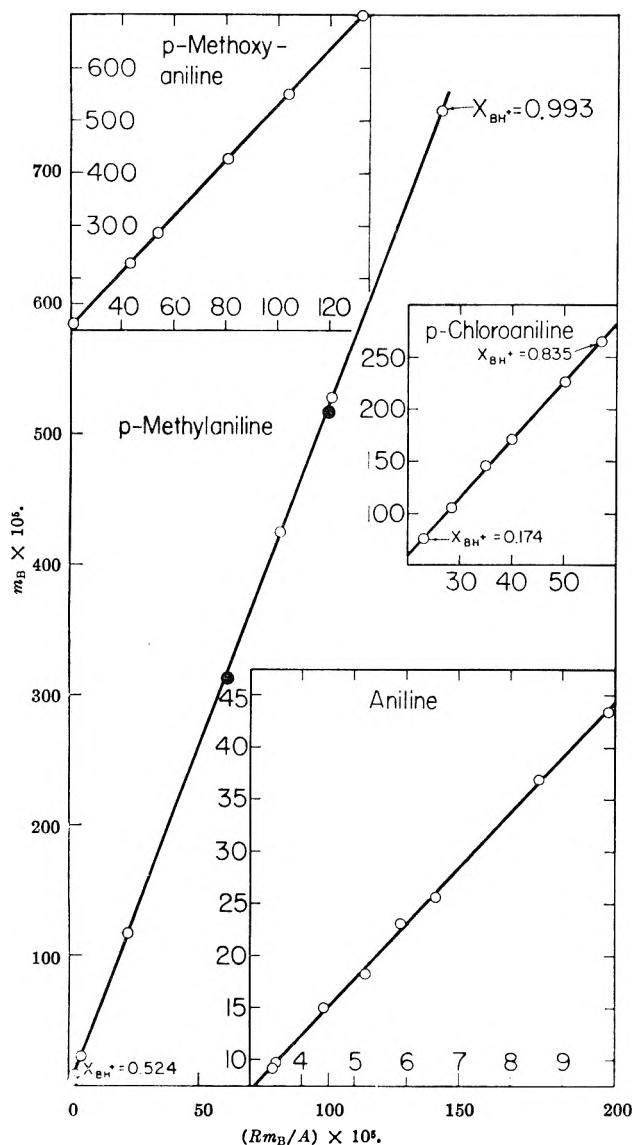


Fig. 1.—Distribution of substituted anilines between 80.50 wt. % aqueous dioxane and a polystyrenesulfonic acid ion exchange resin at 25.0°. Solid circles represent reverse approach to equilibrium (see text).

tories, Richmond, California, as AG 50W-X8. Its 60 Mc. proton magnetic resonance spectrum in water showed no evidence of heterogeneity.¹⁰ The resin was air dried to ca. 20% water, weighed into 1-ml. ampoules (ca. 0.1–0.15-g.), and dried to constant weight at 75–80° and a final pressure of ca. 10⁻⁴ mm. (6–8 hr.); the ampoules were sealed *in vacuo*, recovered, and weighed. The capacity of the dry material by titration in water was 5.21 meq./g. The vacuum-dried resin contained no more than 0.042 mmole of water per meq. of –SO₃H groups, as determined by direct potentiometric Karl Fischer titration under methanol.

Equilibrium Measurements.—A weighed sample of base solution and a sealed ampoule containing a known weight of resin were sealed in a heavy-walled reaction tube, and the ampoule was broken by shaking. The tube was rocked in a constant temperature bath at 25.0 ± 0.1° until equilibrium was attained. After filtration through a hypodermic needle fitted with a modified Swinny adaptor, the solution immediately was analyzed spectrophotometrically on a Cary Model 14 instrument at the wave length shown in Table II, applying a small correction for light absorption due to soluble impurities in the resin. Extinction coefficients used (Table II) were averages of at least two separate determinations. The amount of base taken into the resin phase was computed from the initial and final concentrations. Attainment of equilibrium was assured for each system by increasing the equilibration time until invariant results were obtained. These systems reached equilibrium within 10 hr. As proof of

(10) J. E. Gordon, *J. Phys. Chem.*, **66**, 1150 (1962).

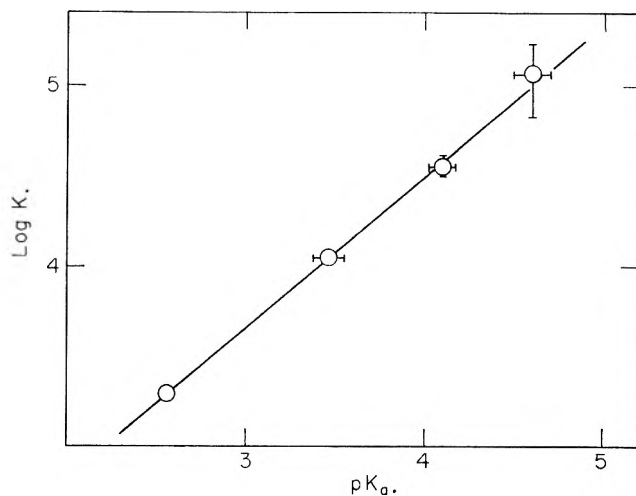


Fig. 2.—Equilibrium constants for reaction 4 vs. acid dissociation constants for the anilinium ions. Maximum experimental uncertainty is indicated by the horizontal and vertical lines.

the attainment of equilibrium, some points were measured from the reverse direction; thus, in Fig. 1, the upper of the two solid circles for *p*-toluidine was determined by the usual procedure; a weighed aliquot of the solution phase then was removed and replaced by a weighed quantity of pure solvent, and the specimen was re-equilibrated and re-analyzed giving the lower solid circle at lower X_{BH^+} which agrees with the forward reaction data within the estimated experimental error for the extended manipulation (ca. 2% in *S*). Possible sorption of base independent of salt formation was eliminated by equilibrating solutions of the bases with an alkali metal salt form of the resin, finding no detectable sorption of base within experimental error (ca. 0.5%) for the solvents used in the equilibrium measurements, though at dioxane contents as low as 60% it is pronounced.

Resin Phase Solvent Composition Measurements.—Resin samples (50–100 mesh) were equilibrated with 80% dioxane and excess solvent was removed by centrifugation.^{11,12} The interior solvent then was distilled off at a final pressure of 10⁻⁴ mm. and a temperature of 80°. The trapped distillate was analyzed by integration of the proton magnetic resonance spectrum on a Varian A-60 spectrometer; the intensities used were averages of at least 10 integrations of the spectrum; standard solutions are determined in this way with an average accuracy of ca. 1.5%. The results for pure hydrogen, for $X_{H^+} = 0.5 = X_{BH^+}$, and for pure *p*-toluidinium resins were 38, 32, and 28% dioxane in the sorbed liquid.

Swelling Measurements.—Swelling of 50–100 mesh resin beads, dried *in vacuo*, was measured microscopically.¹² The results are given in Table I.

TABLE I
SWELLING OF HYDROGEN AND *p*-TOLUIDINIUM RESINATES^a IN AQUEOUS DIOXANE

Solvent, % dioxane	Swelling, ^b %		
	res ⁻ , H ⁺	res ⁻ , } ArNH ₃ ⁺ ^c	res ⁻ , ArNH ₃ ⁺
0	122	58	28
20	133		
40	128		
60	131		
80	108	63	26
90	100	37	16
100	56 ^d		

^a AG 50W-X8, 50–100 mesh. ^b Average precision, ca. 5%. ^c $X_{H^+} = 0.5$. ^d Reference 10.

Results

Data for distribution of four *p*-substituted anilines between the resin and 80% aqueous dioxane and of *p*-toluidine between the resin and 90% aqueous dioxane over a wide range of solution phase concentrations and

(11) H. P. Gregor, D. Nobel, and M. H. Gottlieb, *ibid.*, **59**, 10 (1955).

(12) H. P. Gregor, F. Guttoff, and J. I. Bregman, *J. Colloid Sci.*, **6**, 245 (1951).

TABLE II

EQUILIBRIUM CONSTANTS AND EFFECTIVE CAPACITIES FOR THE REACTION OF SUBSTITUTED ANILINES WITH HYDROGEN RESINATE IN AQUEOUS DIOXANE AT 25.0°

Base	Solvent, wt. % dioxane	$K \times 10^{-3}$	$rK^a \times 10^{-3}$	C , meq./g. resin	rc^b	$\lambda_{\max.}^c$ m μ	$\epsilon^*_{\max.}^d \times 10^{-2}$
<i>p</i> -Chloroaniline	80.50	1.965	0.046	5.526	0.036	302	18.69
Aniline	80.50	11.10	0.31	5.331	.050	238	102.6
						289	18.85
<i>p</i> -Methylaniline	80.50	35.7	4.4	5.267	.005	240	98.80
						295.5	17.67
<i>p</i> -Methoxyaniline	80.50	116	48	5.298	.004	237.5	101.6
						305	24.48
<i>p</i> -Methylaniline	90.00	31.37	4.6	5.111	.004	296	19.38

^a Probable error in K . ^b Probable error in C . ^c Wave lengths used for analysis. ^d ϵ^* = optical density/cell length (cm.) \times molal concentration.

resin phase compositions were analyzed in terms of the mass law expression (5) for reaction 4, where X^r denotes mole fraction in the resin phase, and m_B the base mo-

$$K = \frac{X_{BH^+}^r}{X_{H^+}^r} \times \frac{1}{m_B} \quad (5)$$

lality in the solution phase. In these systems distribution of base into the resin in the absence of reaction with the resin counterions is negligible. Equation 5 was used in the form

$$m_B = -1/K + C(Rm_B/A) \quad (6)$$

according to which a plot of m_B vs. Rm_B/A should be linear and yield K and C from the slope and intercept. Such plots are shown in Fig. 1, and the constants derived by least squares fitting of the data to eq. 6 are given in Table II. The nitroanilines proved too weakly basic to measure.

In Fig. 2 the measured equilibrium constants are compared with the corresponding anilinium ion dissociation constants measured^{13,14} in 82% dioxane. The equation

$$\log K = 1.17 + 0.831 pK_a \quad (7)$$

fits the data with a probable error of 0.02 in $\log K$, well within the experimental uncertainty of these values.

Discussion

Only a moderately stringent test for parallelism between the observed K values and the substrate basicities can be made.¹⁵ However, within the limits of precision attainable in these measurements, a linear relationship is found (eq. 7), implying that differential selectivity effects are absent and that the measurements have the chemical significance attributed to them in (4).

The composition of the solvent within the resin phase is changing with the changing ionic composition of the resin throughout each set of data (see Experimental). Using the solvent dependence of pK_a in pure aqueous

(13) H. P. Marshall and E. Grunwald, *J. Am. Chem. Soc.*, **76**, 2000 (1954).

(14) J. C. James and J. G. Knox, *Trans. Faraday Soc.*, **46**, 254 (1950). The measurements of ref. 13 and 14 are not in perfect agreement; a possible explanation has been given in ref. 13. However, the discrepancies are not large compared to the precision of the present results, and average values were used for comparison.

(15) Marshall and Grunwald¹³ show that proportionality between values of $\log f_B/f_{BH^+}$ in two different homogeneous media does not always exist for a group of bases of the same general structure. However, for a series varying only in a remote substituent, the deviations would not appear to be large (cf. M. A. Paul and F. A. Long, *Chem. Rev.*, **57**, 31 (1957)). Comparison of the resin system with homogeneous solution is more ambiguous than comparison of two different homogeneous media, since the chemical composition of the resin phase is rather different from that of the solution phase, and especially since the measured equilibrium constant is uncorrected for salt effects.

dioxane,¹⁴ and considering reaction 2 (the base protonation equilibrium) to occur in a phase consisting of just the sorbed solvent, an upper limit on the drift in K introduced from this source can be estimated. Only for *p*-chloroaniline should curvature in the data plot be just detectable. That none is in fact detected is consistent with the expectation that the phase appropriate to the acid-base equilibrium is not pure sorbed liquid but the homogeneous gel^{16a} including both sorbed solvent and resin matrix, a medium in which the effects of changing sorbed solvent composition must be much smaller than those estimated above. The equality, within experimental error, of K for *p*-toluidine in 80 and 90% dioxane is also consistent with insensitivity of K to the interior solvent composition.

The apparent absence of strong deviations from the simple mass law expression (5) in what amounts to a concentrated electrolyte solution in a medium of low dielectric constant is of interest. In general, for cation exchange in water, K_{se1} is not independent of the ionic state, and the activity coefficients of the resin salts vary strongly with the resin phase ionic composition.^{16c} The absence of this complexity in the present case appears analogous to the K_{se1} constancy observed by Gregor, Belle, and Marcus¹⁷ for exchanges between large anions in water, and it can be fitted rather well into the ion association model developed by these authors.

Use of (6) whereby the resin capacity, C , is obtained directly from the data is indicated in non-aqueous solvents because of the known manifestation of reduced effective capacities by the resin in such systems.⁴ For example, we have found that although K is too large to measure for the reaction of aniline with hydrogen resinate in anhydrous acetonitrile, the effective capacity is only 2.7 meq./g. This presumably results from an ionic sieve effect^{16b} enhanced under conditions of reduced swelling. The values of C from the present measurements approximate the true capacity, 5.21 meq./g., as expected in view of the high degree of swelling in these solvents (Table I). The slightly high and slightly low values in 80 and 90% dioxane, respectively, are attributable to a small degree of partitioning of free base into the anilinium resinate in the former case, and to the onset of deswelling in the latter.

Acknowledgment.—The writer thanks Dr. A. A. Bothner-By for numerous helpful discussions.

(16) J. A. Kitchener, in "Modern Aspects of Electrochemistry," J. O'M. Bockris, Ed., No. 2, Academic Press, Inc., New York, N. Y., 1959; (a) p. 100; (b) p. 130; (c) p. 116 ff.

(17) H. P. Gregor, J. Belle, and R. A. Marcus, *J. Am. Chem. Soc.*, **77**, 2713 (1955).

RELATIVE FORMATION CONSTANTS FOR SOME SUBSTITUTED DIBENZOATE IONS

By JOHN E. GORDON

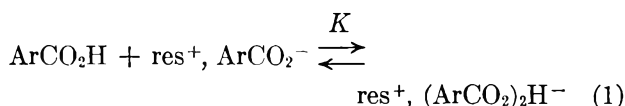
*Mellon Institute, Pittsburgh, Pennsylvania**Received April 20, 1962*

Equilibrium constants for the reaction between the carboxylic acid salt of an anion-exchange resin and the corresponding acid in acetonitrile solution have been measured at 25.0° for five *m*- and *p*-substituted benzoic acids. Relative values of these constants are taken as measures of the relative formation constants of the dibenzoate ions, $(\text{ArCOO})_2\text{H}^-$, and are found to increase with increasing acidity of ArCOOH according to $\log K = 3.48 - 0.200 \text{ p}K_a$. Evidence is found for some formation of tricarboxylate at concentrations higher than those corresponding to 75% completion of the 1:1 reaction.

The complex ions $(\text{BH} \dots \text{B})^\pm$ produced by interaction of an acid with its conjugate base long have been known in the solid state for such diverse bases as $\text{B} = \text{F}^-$,¹ Cl^- ,^{2,3} CO_3^{2-} ,⁴ RCO_2^- ,⁵ ArC^- ,⁶ RO^- ,⁷ R_2O ,^{3,8} RCONHR ,⁹ $\text{H}_2\text{NCH}_2\text{CO}_2\text{H}$,¹⁰ and NH_3 .¹¹ Important information on hydrogen bonding has come from studies of these materials.¹² The BHB^\pm ions exist also in solution in non-water-like solvents, where they have been detected by infrared¹³ and electronic¹⁴ absorption spectroscopy, by conductimetric¹⁵ and potentiometric¹⁶ titrations, and by chemical interpretation of the dependence of acidity functions on composition.¹⁷ Kinetic and equilibrium investigations involving acids and bases in non-water-like media thus require, for their complete understanding, accurate knowledge of the stoichiometry, structure, and stability of any BHB^\pm species present. Although some information on stoichiometry and structure is available in the above studies, few measurements of formation constants^{14,18,19} for BHB^\pm species have been reported, and from these little information on the systematic dependence of stability on structure is derivable. This article presents measurements on a series of dibenzoate ions, $(\text{ArCO}_2)_2\text{H}^-$, in which a substituent remote from the reaction center is

varied and from which the dependence of the formation constant upon the acidity of the parent acid is obtainable.

A distribution method^{20a} was employed in which the acid ArCO_2H was partitioned between a liquid phase (acetonitrile) and the carboxylate salt of an anion exchange resin, res^+ , ArCO_2^- . In this system the distribution coefficient for partition of ArCO_2H into the resin phase in the absence of reaction with the resin counterions is zero, and the observed distribution equilibrium is in a first approximation described simply by the stoichiometric reaction



Experimental

Materials.—Acetonitrile (Fisher reagent) was fractionally distilled twice from phosphorus pentoxide, collecting a constant-boiling middle cut; typically this had b.p. 80.5° (740 mm.), n_D^{20} 1.3413 [reported²¹ b.p. 80.8° (740 mm.), n_D^{20} 1.3416]. Karl Fisher titration revealed less than 0.008% water. Potentiometric titration showed that acetic acid (or stronger acid) was present to the extent of no more than $10^{-4} m$. The material was homogeneous to vapor phase chromatography. Some batches were subjected to a further fractionation from freshly-fused potassium carbonate; however, there was no detectable difference in the results obtained with the different preparations. Acids were reagent materials, crystallized several times from water, whose melting points agreed with published values; they were sublimed at about 10^{-4} mm. shortly before use. The resin used was a purified grade of Dowex 1-X4, obtained as AG 1-X4, 200–400 mesh, in the chloride form, from Bio-Rad Laboratories, Richmond, California; the p.m.r. spectrum of a water suspension of the OH^- form showed no evidence of heterogeneity.^{20b} The anhydrous material possessed a capacity = 4.57 meq./dry g. after cycling. The resinium carboxylates were prepared by column treatment of 9.1–9.5 meq. of air-dried resinium chloride with 2 l. of carbonate-free *N* sodium hydroxide, followed by 500 ml. of de-ionized water, then with 24.6 mmoles of the appropriate acid in 500 ml. of 50% (by volume) ethanol, and finally with 1.23 mmoles of the acid in 250 ml. of ethanol. The resin was dried in a stream of nitrogen overnight and 0.1–0.12 g. samples were weighed into 1-ml. ampoules and dried to constant weight (6 hr.) at 70° and a final pressure of ca. 10^{-4} mm. These products were analyzed by eluting with 250 ml. of a solution prepared by mixing 50 ml. of *N* sodium hydroxide with 450 ml. of saturated potassium perchlorate and analyzing the eluates spectrophotometrically for carboxylate ion. Results are given in Table I. Karl Fischer titration^{20a} showed that the vacuum-dried resins contained no more than 0.034 mmole of water/mmole of resin.

Equilibrium Measurements.—Solutions of the acids in acetonitrile were equilibrated with the corresponding resinium carboxylates at 25.0° as in the previous work.^{20a} Equilibrium was

- (1) S. W. Peterson and H. A. Levy, *J. Chem. Phys.*, **20**, 704 (1952).
- (2) R. West, *J. Am. Chem. Soc.*, **79**, 4568 (1957).
- (3) No direct spectroscopic or diffraction evidence for the BHB^\pm structural unit is available, but its presence is highly probable.
- (4) G. Bacon and N. Curry, *Acta Cryst.*, **9**, 82 (1956).
- (5) (a) P. Peiffer, *Ber.*, **47**, 1580 (1914); (b) J. E. Kench and T. Malkin, *J. Chem. Soc.*, 230 (1939); (c) A. W. Davidson, *Chem. Rev.*, **8**, 180 (1931); (d) J. C. Speakman, *J. Chem. Soc.*, 3357 (1949).
- (6) G. J. van Meurs, *Z. physik. Chem.*, **91**, 313 (1916); D. Hadži and J. E. Gordon, unpublished results.
- (7) P. J. Wheatley, *J. Chem. Soc.*, 4270 (1960); J. G. Pritchard and H. M. Nelson, *J. Phys. Chem.*, **64**, 795 (1960).
- (8) F. Klages, H. Meuresch, and W. Steppich, *Ann.*, **592**, 81 (1955).
- (9) E. H. White, *J. Am. Chem. Soc.*, **77**, 6215 (1955); N. Albert and R. M. Badger, *J. Chem. Phys.*, **29**, 1193 (1958).
- (10) W. S. Frost, *J. Am. Chem. Soc.*, **64**, 1286 (1942); M. J. Buerger, E. Barney, and T. Hahn, *Z. Krist.*, **108**, 130 (1956); T. Hahn and M. J. Buerger, *ibid.*, **108**, 419 (1957).
- (11) J. Kendall and J. G. Davidson, *J. Am. Chem. Soc.*, **42**, 1141 (1920); I. Olovsson, *Acta Chem. Scand.*, **14**, 1453, 1466 (1960).
- (12) R. Blinc and D. Hadži, *Spectrochim. Acta*, **16**, 853 (1960); R. Blinc, D. Hadži, and A. Novak, *Z. Elektrochem.*, **64**, 567 (1960), and references therein.
- (13) G. M. Barrow and E. A. Yerger, *J. Am. Chem. Soc.*, **76**, 5211 (1954); E. A. Yerger and G. M. Barrow, *ibid.*, **77**, 4474, 6206 (1955); G. M. Barrow, *ibid.*, **78**, 5802 (1956).
- (14) M. M. Davis and H. B. Hetzer, *J. Res. Natl. Bur. Std.*, **48**, 381 (1952).
- (15) (a) A. A. Maryott, *ibid.*, **38**, 527 (1947); (b) P. Bryant and A. Wardrop, *J. Chem. Soc.*, 895 (1957).
- (16) H. B. van der Heijde, *Anal. chim. Acta*, **16**, 392 (1957).
- (17) (a) H. Van Looy and L. P. Hammett, *J. Am. Chem. Soc.*, **81**, 3872 (1959); (b) R. P. Bell, "The Proton in Chemistry," Cornell University Press, Ithaca, N. Y., 1959, p. 81.
- (18) I. M. Kolthoff, S. Bruckenstein, and M. K. Chantooni, Jr., *J. Am. Chem. Soc.*, **83**, 3927 (1961).
- (19) von F. Römlberg and K. Cruse, *Z. Elektrochem.*, **63**, 404 (1959).

(20) (a) J. E. Gordon, *J. Phys. Chem.*, **67**, 16 (1963); (b) **66**, 1150 (1962).

(21) J. A. Riddick and E. E. Toops, Jr., in "Technique of Organic Chemistry," A. Weissberger, Ed., Vol. VII, Interscience Publishers, Inc., New York, N. Y., 1955, p. 224.

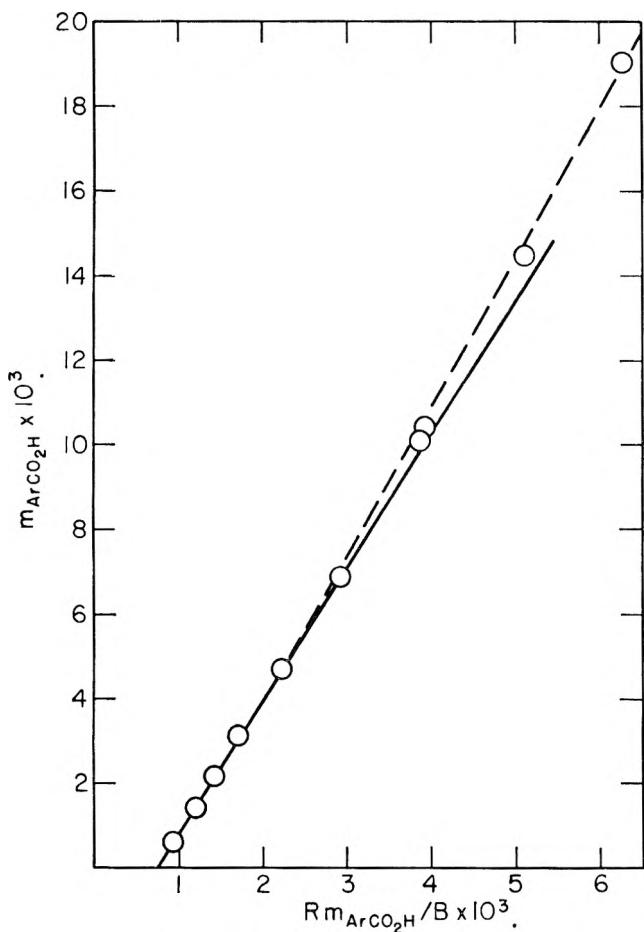


Fig. 1.—Distribution of benzoic acid between anhydrous acetonitrile and resinium benzoate at 25.0°, plotted according to eq. 3.

TABLE I
ANALYSIS OF RESINIUM CARBOXYLATES, Y-C₆H₄COO⁻, Res⁺
C (meq. ArCOO⁻/g. of dry resin)

Y	Calcd.	Found	$\lambda_{\max.}^a$ m μ	$\epsilon_{\max} \times 10^{-2}$
p-OCH ₃	2.99	2.98	247	136
p-CH ₃	3.14	3.15	234	112
H	3.28	3.31	268	5.28
m-Cl	2.95	2.94	277	6.71
p-NO ₂	2.86	2.86	273	101

^a Wave lengths used for analysis.

reached within 10 hr. As before, it was possible to approach equilibrium from both directions. For example, a sample in the anisic acid system gave a point at $Rm_{ArCOOH}/A = 4.50 \times 10^{-3}$; 3.639 g. of the solution phase ($m_{ArCOOH} = 1.028 \times 10^{-2}$) was replaced with 4.381 g. of pure acetonitrile, followed by shaking for 10 hr., while the reverse reaction occurred to give a measured value of $Rm_{ArCOOH}/A = 3.33 \times 10^{-3}$ at $m_{ArCOOH} = 7.105 \times 10^{-3}$ which falls on the line defined by the forward points (Rm_{ArCOOH}/A calcd. = 3.40×10^{-3}) within the estimated experimental error for the extended operation (ca. 2% in A).

Control Experiments.—Correction for ultraviolet-absorbing material leached from the resin was negligible. Distribution of substrate into the resin phase in the absence of reaction with the resin counterions was tested for by equilibrating the resin with acetonitrile solutions of the generally similar, but non-acidic, acetophenone; thus, the concentration of 7.78 g. of an acetonitrile solution ($m = 1.2 \times 10^{-3}$) of acetophenone did not diminish detectably on equilibration with 91.8 mg. of resinium benzoate.

Results

The data were analyzed in terms of the mass law expression for reaction 1

$$K = \frac{X_{(ArCOO)_2H^-}}{X_{ArCOO^-}} \times \frac{1}{m_{ArCOOH}} \quad (2)$$

which was employed in the form

$$m_{ArCOOH} = -\frac{1}{K} + CRm_{ArCOOH}/A \quad (3)$$

where the symbols have the meanings previously used.^{20a} Each system obeyed (3) accurately up about $x_{(ArCOO)_2H^-} = 0.75$; data for benzoic acid are shown in Fig. 1. At higher conversions deviations²² from (3) appeared, and these were of the form expected for simultaneous operation of the reaction



(see below). The entire set of data for benzoic acid, $5 \times 10^{-4} < m_{ArCOOH} < 5 \times 10^{-2}$, was reproduced rather well with $K_2 = K/100$; part of the calculated curve is shown in Fig. 1. Values of C and K determined by the method of least squares applied to the linear portions of the m_{ArCOOH} vs. Rm_{ArCOOH}/A plots are given in Table II.

TABLE II
EQUILIBRIUM CONSTANTS FOR THE REACTION OF RESINIUM BENZOATES WITH BENZOIC ACIDS IN ACETONITRILE AT 25.0°

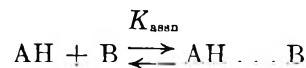
Substituent	K	r_K^a	C	r_C^b	C_0^c	C/C ₀	$\lambda_{\max.}$ m μ^d	$\epsilon_{\max}^e \times 10^{-2}$
p-OCH ₃	383	2	2.86	0.007	2.99	0.956	253	133.6
p-CH ₃	409	13	3.00	.04	3.14	.955	236	114.4
H	427	4	3.16	.02	3.28	.962	272	7.21
m-Cl	528	10	2.81	.02	2.95	.952	280	8.06
p-NO ₂	609	14	2.46	.02	2.86	.861	259	94.4

^a Probable error in K. ^b Probable error in C. ^c True capacity from Table I. ^d Wave lengths used for analysis. ^e $\epsilon^* =$ optical density/cell length \times molal concentration.

Discussion

Equilibrium Constants.—Variation of the stability constants for BH...B[±] species with the acid dissociation constants of BH measures the relative sensitivity of hydrogen bridge strength to proton donor acidity vs. proton acceptor basicity. From Table II it is clear that for B = ArCOO⁻, stability increases with increasing BH acidity. Conductimetric titrations of RCOOH with amines in acetonitrile performed by Bryant and Wardrop^{15b} are consistent with this result, as the conductance maxima at half equivalence (attributed to formation of dicarboxylate ions) become more pronounced with increasing acid strength of RCOOH.

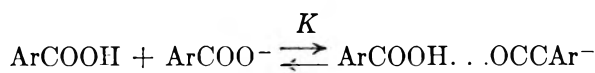
These relations can be made more quantitative by use of the expressions $\Delta \log K_{\text{assn}} = a \Delta \log K_a^{\text{HA}}$ and $\Delta \log K_{\text{assn}} = b \Delta \log K_b^{\text{B}}$ previously employed²³ to describe the dependence of the association equilibrium



upon the acidity of the proton donor moiety and the basicity of the proton acceptor, respectively. Application to the reaction

(22) These cannot be due to association of the acid in the solution phase, since infrared measurements show benzoic acid to be negligibly dimerized in acetonitrile solutions as concentrated as 1 M (C. J. W. Brooks, G. Eglinton, and J. F. Morman, *J. Chem. Soc.*, 106 (1961)).

(23) J. E. Gordon, *J. Org. Chem.*, **26**, 738 (1961).

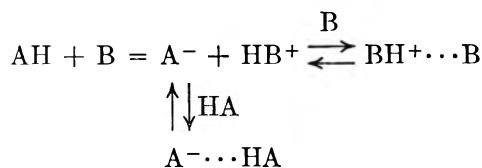


gives

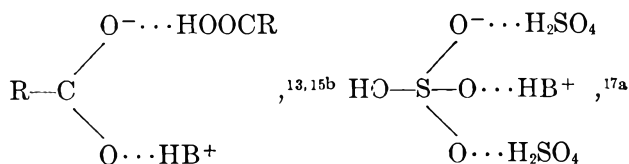
$$\begin{aligned} \Delta \log K &= a \Delta \log K_a^{\text{ArCOOH}} + b \Delta \log K_b^{\text{ArCOO}^-} = \\ &= a \Delta \log K_a^{\text{ArCOOH}} - b \Delta \log K_a^{\text{ArCOOH}} = \\ &= -(a - b) \Delta pK_a^{\text{ArCOOH}} \quad (4) \end{aligned}$$

which implies a linear plot of $\log K$ vs. pK_a . Figure 2 shows such a plot for the results of Table II; the equation of the least squares line is $\log K = 3.48 - 0.200 pK_a$, which reproduces the data well within the probable error of the measured K values. The value of $(a - b) = 0.20$ shows that the dependence on donor acidity exceeds that on acceptor basicity by a sizable fraction of the structure dependence for complete ionization of ArCOOH .²⁴ In other words, in the complex $\text{AH} \cdots \text{A}^-$ the proton donor moiety is closer to its dissociated state than the acceptor is to its protonated state, which suggests the structure $\text{A}^- \cdots \text{H}^+ \cdots \text{A}^-$ as an important contributor to the valence-bond formulation. This also is suggested by spectroscopic observations on solid sodium tristrifluoroacetate by Klemperer and Pimentel,²⁵ who found substantial carboxylate ion character in the bonded HOOCR moieties.²⁶

Stoichiometry.—On passing from water, where acidic protons and basic atoms of dissolved acids and bases are hydrogen-bridged to solvent, through non-water-like solvents toward the solid state, the hydrogen-bridging potentialities of the products of the primary acid-base reaction $\text{AH} + \text{B} = \text{A}^- + \text{BH}^+$ are realized through (a) formation of hydrogen-bridged ion pairs, and (b) secondary incorporation of extra acid or base molecules to form complex species



The stoichiometry of AHA^- species can be predicted rather successfully with the rule: all basic atoms bearing part of the charge in an ion A^- tend to bridge to extra AH molecules except those already engaged in a bridge to the counter ion. Illustrative are the formation of



(24) Since the reactant state actually involves ArCOOH bridged to solvent, eq. 4 should contain a term to include the acidity dependence of the breaking of this bridge $\Delta \log K = (a - b - a_s) \Delta pK_a^{\text{ArCOOH}}$. This bridge, however, is weak, and a_s is estimated to be less than 0.1. Hence the determined slope is a good approximation to $(a - b)$, and represents its minimum value.

(25) W. Klemperer and G. C. Pimentel, *J. Chem. Phys.*, **22**, 1399 (1954).

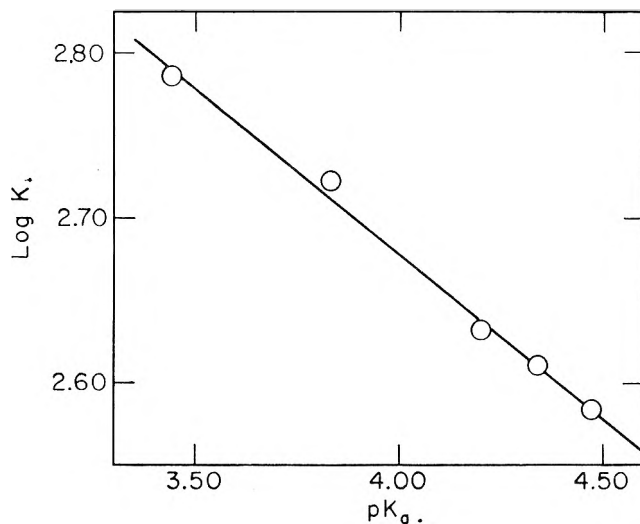
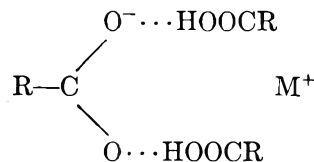


Fig. 2.—Formation constants for res^+ , $(\text{ArCOO})_2\text{H}^-$ vs. acidity, plotted according to eq. 4.

and others of the ions cited in the Introduction.²⁷ This pattern persists to some extent even in the solid state where other forces contribute to determination of the stoichiometry. Solid alkali metal tricarboxylates



are well known^{5c,25} in addition to the dicarboxylates, but the normal ammonium carboxylates decompose spontaneously to the dicarboxylates,^{5a,5b} with the ammonium tricarboxylates apparently remaining unknown. The ammonium salt ammoniates¹¹ also are understandable on this basis.

Thus, in the present system, with a poly-quaternary ammonium cation, one would expect possible interference from the formation of tricarboxylate, though it would be difficult to predict the extent to which formation equilibria for the two species might overlap. The results are indeed in agreement with this expectation, and suggest a ratio of 1:1 to 2:1 equilibrium constants of ~ 100 .

Acknowledgment.—The writer thanks Dr. A. A. Bothner-By for numerous helpful discussions.

(26) Some other acid carboxylates do not show such pronounced behavior [D. Hadzi and A. Novak, "Infrared Spectra of, and Hydrogen Bonding in, Some Acid Salts of Carboxylic Acids," University of Ljubljana, 1960].

(27) With phenols the situation is less clear. There is strong indication of interaction of ArOH with ArO^- , R_4N^+ , where there is no bridge to counterion¹⁶; and there is no indication of such interaction with primary, secondary, and tertiary ammonium 2,4-dinitrophenolates,²⁸ although the phenol concentration probably is too low to make this a good test. Picrate ion is variously considered to bridge to one²⁹ or two¹⁸ molecules of picric acid at concentrations in excess of 0.1 M in acetonitrile; with these nitrophenols, the rule becomes ambiguous due to the delocalization of charge over a large number of oxygens. Römberg and Cruse found AHA^- formation necessary to account for the shape of the titration curves for 0.01 M picric acid with amines in acetonitrile.¹⁹

(28) R. G. Pearson and D. C. Vogelsong, *J. Am. Chem. Soc.*, **80**, 1038 (1958).

(29) C. M. French and I. G. Roe, *Trans. Faraday Soc.*, **49**, 314 (1953).

THE NON-DETONATIVE SYNTHESIS OF CADMIUM SELENIDE AND OTHER II-VI COMPOUNDS FROM THE ELEMENTS¹

BY A. REISMAN AND M. BERKENBLIT

Thomas J. Watson Research Center of International Business Machines, Yorktown Heights, New York

Received April 25, 1962

The cause of detonations in the direct synthesis of CdSe and other II-VI compounds from the elements has been shown to be due to the formation of insoluble passivating layers around the reactants. These passivating layers do not rupture until temperatures high enough to achieve appreciable solubility of the desired compound in melts rich in the elemental constituents are attained. It is demonstrated that single stage, non-detonative low temperature synthesis of each of the compounds can be effected *via* use of reactant powders whose particle sizes apparently are less than twice the thickness of the passivating layer which tends to form, such that the reactants are completely consumed during the passivating layer formation. The method appears to be general for binary compounds which melt appreciably higher than either of the elemental constituents.

Introduction

CdSe is a wide gap representative of the II-VI class of compound semiconductors with current interest focused on its photoconductive properties. Considering the length of time that such properties have been known and studied, however, it is surprising that so little is published about the detailed chemistry of this compound. For example, little is known about the nature of the problems associated with synthesis of the selenide, or for that matter, the other II-VI compounds, directly from the elements. This paper will discuss the origin of such problems and their resolution.

Experimental Procedure

A. Thermal Investigations.—The reaction behaviors of the materials were studied with differential thermal analysis (d.t.a.). Discussions of the high gain circuitry employed, as well as other pertinent features of the method, have been presented in earlier publications.² The furnace used was a modified version of the low heat capacity designs described in ref. 2. To enable operation in controlled atmospheres or vacuum, sleeves of non-porous, recrystallized Al₂O₃ were inserted in the furnace. Since the reactants, Cd, Zn, S, Se, and Te are volatile in the temperature intervals surveyed, all analyses were effected in sealed evacuated silica containers which incorporated a thermocouple well in their design. In practice, the reactants were introduced into the sample container, which was evacuated to the 10⁻⁶ mm. region, then sealed at a constriction. The suitability of silica crucibles was evaluated *via* duplicate determinations of the CdCl₂ melting point, 565°, in conventional platinum assemblies² and silica. The results were within the expected limits of experimental variation normally observed, ±2°. Because silica devitrifies rapidly in air above 800–900°, the d.t.a. sample holders were maintained in an atmosphere of purified nitrogen. The method of purification involved moisture removal with P₂O₅, and oxygen removal with heated copper wire. Protected in this manner, the containers remained clear even after sustained treatments in the 1200° temperature region. Al₂O₃ powder was used as a reference material and temperatures were measured with Pt-Pt 10% Rh thermocouples. Differential signals were preamplified to provide a chart span of 15 μv./inch; d.t.a. heating and cooling cycles were conducted at 3.5°/min. or less.

B. Reagents.—The Zn and Te had manufacturers' assays of 99.9999%, while the S was purchased as a 99.999% material. None of these values was verified. The Cd and Se whose reaction and synthesis was of prime interest were purchased as 99.999% elements and were analyzed here by emission spectroscopic techniques. Aside from oxygen contamination, removal of which is described subsequently, the Cd was found to assay >99.995% with the major impurities detected in several lots being Si (0.1–3

p.p.m.), Cu (0.1–10 p.p.m.), Mg (0.3–1 p.p.m.), Al (0.1–3 p.p.m.), and Ca (0.3–1 p.p.m.). The Se always met specifications with major contaminants being Cd (1–3 p.p.m.), Cu (3–5 p.p.m.), Mg (0.1–1 p.p.m.), and Si (1–3 p.p.m.). The impurity content of synthesized CdSe will be discussed subsequently.

C. X-Ray Analysis.—All reaction mixtures were examined by the Debye-Scherrer technique using Philips Electronic equipment.

Experimental Results and Discussion.

A. Interaction of Elemental Cd and Se.—Commercially, CdSe is synthesized by solid state reaction or aqueous precipitation techniques. Analytical studies conducted on products offered by several vendors and materials synthesized in this Laboratory by a variety of dry and wet synthetic methods, other than direct synthesis from the elements, revealed the following: CdSe derived from aqueous precipitations generally was contaminated by quantities of carbon up to 5–10% by weight and in general exhibited bulk cadmium content up to 2% excess by weight relative to bulk selenium content. CdSe resulting from solid state processes was contaminated in general by unreacted starting materials, free cadmium and/or selenium, which on a bulk basis showed excesses of one or the other, generally selenium up to 6% by weight. Attempts at controlling these syntheses were unsuccessful and the next approach was to prepare the selenide directly from the elements in silica receptacles. In three out of five initial experiments conducted in evacuated sealed containers containing 1/8-in. Cd and 1/16-in. Se shot, severe detonations occurred when the samples, heated at between 0.2 and 0.5°/min., reached the 900–1000° temperature range. Since pure Cd was observed to melt at 320 ± 1° and pure Se at 215 ± 1°, the results were unexpected because the detonations, indicative of first reaction, occurred some 600–700° above the melting point of the higher melting component. Heat treatments just below the detonation range for up to two weeks also generally were unsuccessful in preventing the explosions when the samples subsequently were heated to higher temperatures. Those reaction mixtures which did not result in broken reaction vessels still were unusable because they were highly contaminated with Si. Reactions then were studied in the d.t.a. apparatus, using the silica containers mentioned above. The latter, because of their small size, were sufficiently strong to contain the reaction and enable subsequent heating past the melting point of CdSe observed at 1239 ± 3°. Figure 1 shows a typical heating study conducted at 3.5°/min. While other traces differed in detail in the higher temperature portions, the effects were always qualitatively the

(1) This paper was presented in part at the Symposium on Non-stoichiometric Compounds, 141st National Meeting of the American Chemical Society, March 20–29, 1962, Washington, D. C.

(2) See for example: A. Reisman, Ph.D. Thesis, Univ. Mic. No. 58-2876, Chem. Phys.; A. Reisman, *Anal. Chem.*, **32**, 1566 (1960); A. Reisman and J. Mineo, *J. Phys. Chem.*, **64**, 748 (1960); A. Reisman and J. Karlak, *J. Am. Chem. Soc.*, **80**, 6500 (1958) F. Holtzberg, A. Reisman, M. Berry, and M. Berkenblit, *ibid.*, **79**, 2039 (1957).

same, the chief variations being the precise temperature of initial reaction and the number of successive exothermic bursts accompanying the reaction. At approximately 77° , a slowly generated small peak (1) representative of a non-isothermal exothermic process always was observed. Upon completion of this exotherm, cooling of the sample did not reveal a corresponding cooling anomaly. Reheating of the sample failed to yield the exotherm again unless the first endothermic peak (2) corresponding to the melting of Se was exceeded. Thermal analysis of pure selenium gave identical results. X-Ray analyses were performed on the as-received Se as well as on Se heated slightly higher than the 77° anomaly and cooled. Crystalline patterns were given by each of the samples. Samples of Se then were heated to the melting point and permitted to melt partially or completely. X-Ray examination of the partially melted samples, quenched or slowly cooled from the melting temperature, were essentially indistinguishable from the as-received Se. X-Ray examination of completely melted materials, quenched or slowly cooled from above the melting point, showed them to be amorphous to X-rays. D.t.a. of a partially melted sample which was slowly cooled gave a barely perceptible exothermic peak at around 77° . Samples permitted to undergo greater amounts of melting exhibited larger heating exotherms. Fully melted samples, whether quenched or slowly cooled, gave rise to the largest exotherms. From these data it is concluded that selenium tends to solidify in the amorphous state and that upon heating, the irreversible conversion, amorphous to crystalline, becomes rapid around 77° . Since this conversion is thermodynamically spontaneous, the observed transformation temperature, 77° , is undoubtedly fortuitous. However, d.t.a. studies at heating rates between 0.5 and $2.5^\circ/\text{min}$. never yielded values differing by more than a few degrees, indicating that below 77° the amorphous phase is thermally frozen-in. What is not understood is the observation that the irreversible conversion could not be effected during a cooling cycle either with pure Se or binary mixtures of Se and Cd.

Returning now to Fig. 1, an endotherm, (3), attributable to the melting of Cd is seen at 320° . From this point to the 900 – 1000° range, no further anomalies are in evidence and X-ray examination of samples heated between 350 and 850° showed only the diffraction maxima of Cd, not even a trace of CdSe being detected. The samples, when removed from the d.t.a. sample containers, revealed that the Cd pellets had retained their initial shapes and were imbedded in the dark red-black Se glass. This behavior is reminiscent of the melting of Al shot, the shot being prevented from coalescing by the tenacious skin of Al_2O_3 surrounding them. As will be discussed subsequently, the behavior of Cd shot in a Se matrix is due to a related but different phenomenon.

At anywhere from a low value of 900° to a high of 995° , d.t.a. peaks similar to (4) of Fig. 1 were observed to generate, frequently at speeds faster than the recorder pen could follow. The spontaneity of these exotherms often results in adiabatic elevations of sample temperatures up to several hundred degrees above the existing furnace temperature. Examination of samples subsequent to the exotherms revealed conversion of the elemental constituents to CdSe.

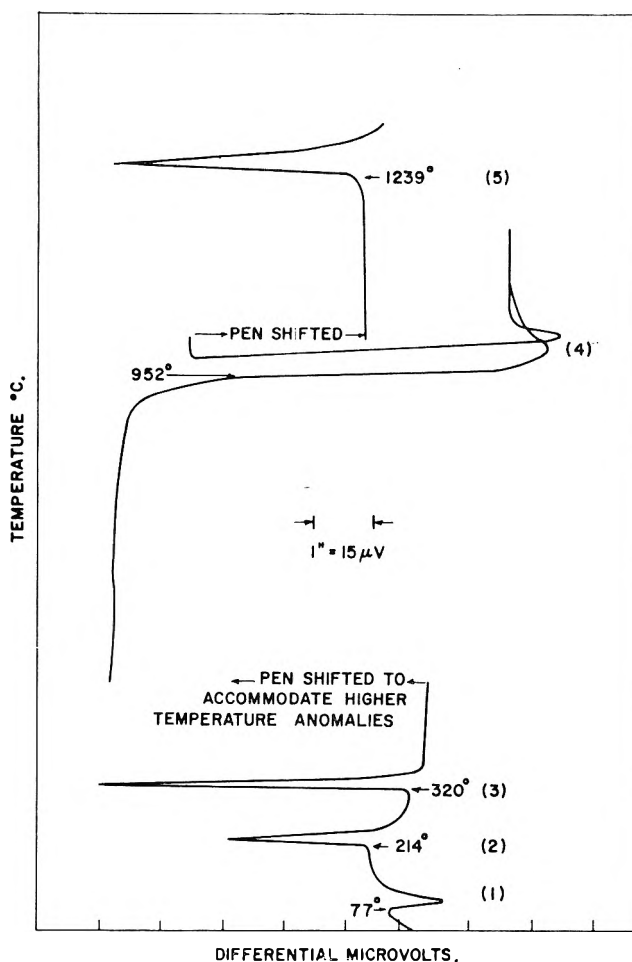


Fig. 1.—D.t.a. Cd-Se pellet reaction trace at a heating rate of $3.5^\circ/\text{min}$.

On some occasions the reaction was observed to occur in successive stages, sometimes as many as six. In these instances, the sample temperatures were not elevated more than 20 – 30° during any stage. D.t.a. heating studies of samples having undergone reaction did not reveal any of the lower temperature anomalies and showed only the melting of CdSe (5) at $1239 \pm 3^\circ$.

Because of the retention of shape by the Cd shot past the melting point, it was initially thought that the reaction failed to occur at low temperatures, owing to the coating of each Cd bead by a skin of CdO, which was impervious to the vapors of Cd and Se and restricted Cd-Se contact. Melting experiments of Cd quickly dispelled this idea. While each bead was covered by an oxide skin, this skin did not prevent coalescence of the individual shot or vaporization of the metal, clearly demonstrating that the reaction Cd-Se is not restricted by an oxide coating. A quartz system then was fabricated which permitted vacuum distillation of Cd to a central chamber to separate the metal from its oxide skin, severance of the distillation chamber by fusion of a capillary connection, and final vapor intermixing of Se (contained in a third bulb) with the distilled Cd. The reaction system remaining after the Cd distillation was completed and the distillation bulb severed was dumbbell shaped, permitting the Se and Cd to be maintained at different temperatures. The unreacted elements were heated to above their respective melting points, at which time they began to distil toward the interconnection between the chambers.

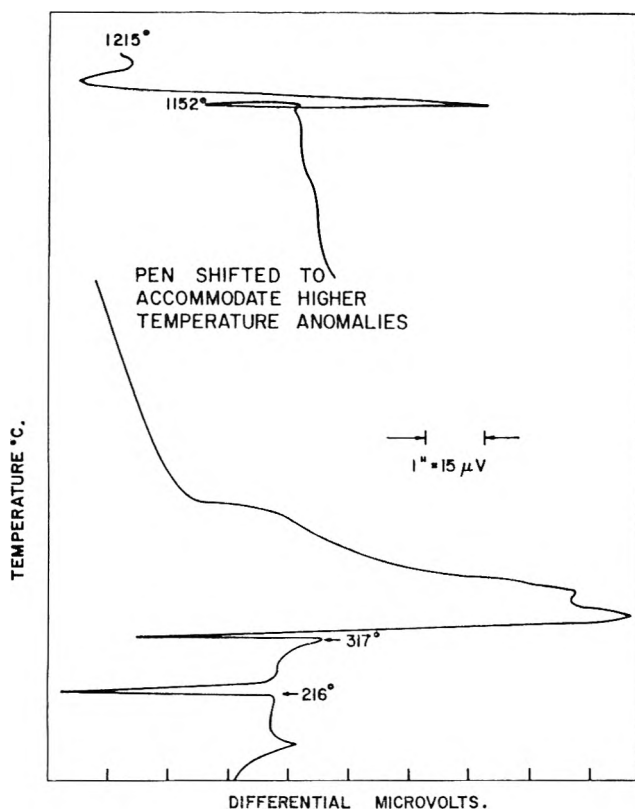


Fig. 2.—D.t.a. Cd-Se powder reaction trace at a heating rate of $3.4^{\circ}/\text{min}$.

Very shortly thereafter, the walls of both chambers, as well as the interconnections, became covered with a black, relatively involatile material, later identified as CdSe. Simultaneously, a similar film formed over the molten pool of Cd. With this latter occurrence, the distillation of Cd abruptly ceased, and continued treatment for 12 days failed to result in conversion to the selenide. During this period, however, the Se continued to froth violently. It appears, therefore, that the failure of a mixture of Cd and Se to react when both are hundreds of degrees above their melting points is due to the formation of a tenacious skin of CdSe (impervious to both Cd and Se vapor) around the Cd particles, concurrent with the melting of the Cd. It has been observed that the deposit of CdSe does not form until the melting point of Cd has been achieved. This skin apparently remains intact up to the $900\text{--}1000^{\circ}$ temperature range where it was initially assumed that a vapor pressure buildup caused destruction of the skin. The vapor pressure of CdSe at 900° is of the order of 20 mm.,³ which might be expected to result in a mechanical weakening of the CdSe skin. At 765° , Cd metal exhibits a pressure of 1 atm.,⁴ which indicates that at 900° this pressure would reach several atmospheres. Such pressures, coupled with the high vapor pressure of CdSe in the temperature range in question, would tend to rupture the passivating skin. It appeared in fact, based on these pressure considerations, that rupture of the passivating skin should have occurred at appreciably lower temperatures than were observed. Examination of the phase diagram of the system Cd-Se⁵ revealed that the solubility of CdSe in Cd rich melts is small until approximately 900° , while the

solubility of CdSe in Se rich melts does not become appreciable until approximately 1000° . The reaction mixtures that had been examined contained attributes of both extremes since the Cd globules surrounded by a passivating layer of CdSe each constituted a Cd rich melt in the system Cd-CdSe, while the CdSe layer-molten Se mixture constituted a Se rich melt in the system Se-CdSe. The above suggested an approach to the low temperature direct synthesis of CdSe from the elements. It appeared also that the problem attending synthesis might be a general one for other compounds which melt much higher than their constituent elements and other II-VI reactions and syntheses also were studied.

B. Synthesis of CdSe from the Elements.—It was reasoned that direct synthesis of CdSe from the elements could be effected by reaction of the elements in sufficiently small mesh size, such that the average Cd particle size was less than a double thickness of the reaction-inhibiting layer which formed. In so doing, the reactants would be consumed entirely in forming this layer and synthesis would be complete. Such a low temperature synthesis has many obvious advantages.

A d.t.a. trace, Fig. 2, was taken on a sample composed of an equimolar mixture of 325 mesh Cd and Se powders at a rate of $3.4^{\circ}/\text{min}$. The Cd powder was found to be highly surface contaminated with oxide, which was readily detected when the Cd melted. This oxide could be removed effectively in either of two ways. The first involved passage of hydrogen over the Cd powder contained in a silica boat at 200° for 4 hr. These experiments indicated initial surface oxide contamination, of from 5–8% by weight, which is inadvertently introduced in fabrication of the powder by a spraying technique. The second method of oxygen removal, which is simpler, involves treatment of the powder with concentrated reagent grade NH_4OH for 10–15 min. at room temperature followed by 20 rinses in $5\times$ -distilled water and vacuum drying to an ultimate pressure of 2×10^{-6} mm. at 50° . The products obtained by both methods do not reoxidize detectably when stored for up to two weeks and do not show formation of a CdO skin when melted. The Se powder was vacuum baked at 300° for a short period to decompose SeO_2 and then reground. Returning to Fig. 2, at 77° , the exothermic conversion amorphous-crystalline Se occurred, followed at 216° by the endothermic melting of Se. At around the Cd melting point, an endotherm initiated which was interrupted by a broad, slowly generated exotherm. At a higher temperature, 1152° , a very rapid exotherm occurred. A second sample treated in the same way was cooled and analyzed with X-rays after the low temperature exotherm at around 320° . This analysis showed the presence of CdSe plus small amounts of Cd metal. Another sample prepared in the same way was heated at the same rate to 500° , cooled, and reheated. The d.t.a. trace revealed small peaks at 215 and 318° , providing further verification that the low temperature reaction had not gone to completion.

A series of five samples then was prepared in d.t.a. containers and these were heated in a muffle furnace at different heating rates and to different final temperatures. Subsequent to these reaction treatments, the samples were examined with d.t.a., yielding the following results.

A sample heated initially to 400° at $0.44^{\circ}/\text{min}$. gave

(3) G. A. Somorjai, *J. Phys. Chem.*, **65**, 1059 (1961).

(4) "Handbook of Chemistry and Physics," 1960–1961, p. 2339.

(5) A. Reisman, M. Berkenblit, and M. Witzel, *J. Phys. Chem.*, **66**, 2210 (1962).

small endothermic peaks attributable to the Se and Cd meltings. Similar results were obtained for samples heated to 445° at 0.9°/min. and 510° at 1.1°/min. A sample heated to 500° at 1.0°/min. and another sample heated to 500° at 0.44°/min. did not yield the Se and Cd melting peaks, and when heated to the melting point of CdSe neither exhibited any high temperature exotherm coincident with final reaction. These data indicated that the synthesis of the selenide could be effected from 325 mesh powders at heating rates below 1°/min. to a maximum temperature of 500°. Further studies revealed that this maximum temperature could be reduced to 450° with a heating rate of 0.5°/min.

Attempts then were made to effect the synthesis using Cd powder and Se shot. These always showed the presence of small quantities of unreacted Cd and Se. If such samples then were ground and reheated to 450° at less than 5°/min., the reaction went to completion as shown by the absence of Se and Cd melting peaks and the high temperature reaction exotherm. The latter, incidentally, being spontaneous, gives an amplification effect, providing an extremely sensitive test for unreacted Cd and Se. It is interesting that all samples of CdSe prepared by the solid state reaction techniques mentioned earlier (whether prepared here or commercially purchased) showed high temperature reaction exotherms which when first observed were believed to be due to a monotropic phase change which could not be verified by X-ray analysis, and represented an enigma.

An explanation for the heating rate and maximum temperature dependence of the synthesis is deduced from the experiment involving Se shot and Cd powder. It has been determined that the low temperature synthesis does not initiate at appreciable rates until the Cd begins to melt, before which all of the Se already has melted. Since the experiments involving Se shot and Se powder differ only in the degree of initial reactant contact, it appears that the heating rate and maximum temperature dependence are simply a question of allowing sufficient time for the molten selenium to contact all of the Cd particles uniformly *via* diffusion through the matrix of CdSe which forms. The time required in the Se shot experiment is expected to be greater since there is no intimate contact of the reactants and the Cd particles would not be coated with a molten layer of selenium. In the powder reaction, as the Se powder (which is in intimate contact with the Cd powder) melts, it would tend to coat neighboring Cd particles.

The synthesis has been extremely reliable in literally hundred of attempts involving quantities of reactants ranging from only a few grams to 200 g. and may be conducted in Pyrex tubes with starting pressures of $1-3 \times 10^{-6}$ mm. Spectroscopic analysis of this CdSe shows a contamination level not much worse than that present in the unreacted elements. This is not, of course, unexpected since the maximum temperature attained in the synthesis does not exceed 450° and the temperature range in which appreciable liquid phase is present is from approximately 215-350°. Typical analysis data shows the major impurity values to be, Ca < 3 p.p.m.; Si, 3 p.p.m.; Cu < 1 p.p.m.; Mg < 1 p.p.m.; and Al 1-3 p.p.m.

C. Synthesis of CdS, CdTe, ZnS, ZnSe, and ZnTe.— In general, reaction behavior in each of the systems Cd-S, Cd-Te, Zn-S, Zn-Se, and Zn-Te more or less

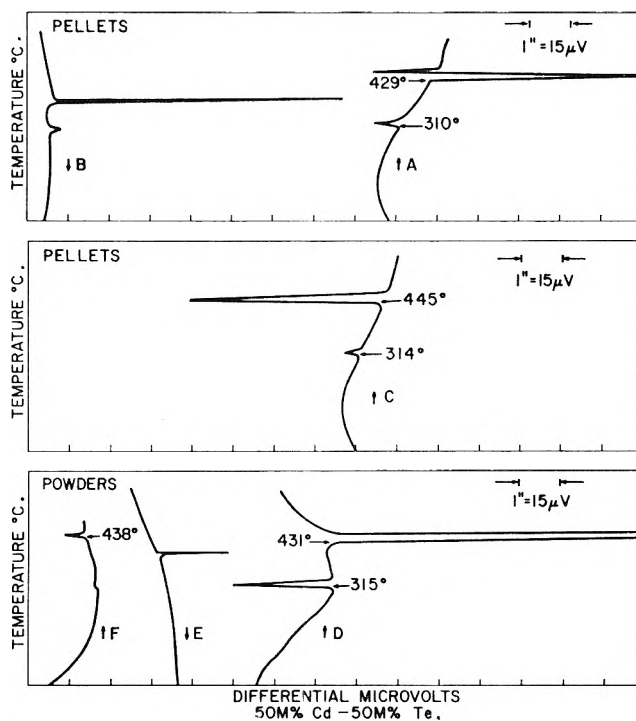


Fig. 3.—D.t.a. Cd-Te pellet and powder reaction traces at a heating rate of 2.5°/min.

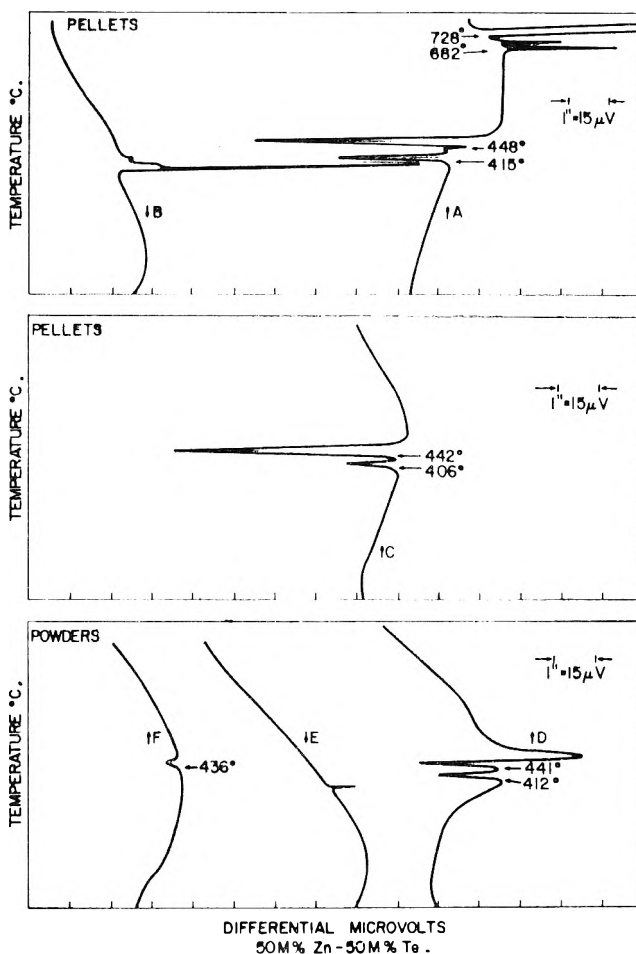


Fig. 4.—D.t.a. Zn-Te pellet and powder reaction traces at a heating rate of 2.5°/min.

approximates that described above and need not be discussed in too great detail.

1. The reaction of Cd-S was studied using Cd pellets and S powder and Cd and S powders (325 mesh or less). The results of such studies were analo-

gous to those obtained with CdSe, and CdS synthesis can be effected completely in a single stage by employing the exact procedure defined for CdSe, *viz.*, heating at 0.5°/min. or less to 450°.

2. The reaction Cd-Te, unlike any of the others, proceeds to some extent even with pellets. The results are shown in Fig. 3. Trace 3A shows a reaction exotherm at 429°, while in 3B and 3C the subsequent cooling and heating cycles still show the presence of large quantities of unreacted elements.

The powder reactions are shown in 3D-3F, from which it is discerned that these reactions are much more complete. The single stage synthesis from powders is accomplished using the exact procedure defined for CdSe. What is evident from these results is that the solubility curves in the systems CdTe-Cd and CdTe-Te move away from the end member axes at low temperatures, which results are in agreement with the published information on phase equilibria in the system.⁶ From these results it appears also that the controlling factor

(6) D. deNobel, Ph.D. Thesis, Univ. of Leiden, 1958.

in the powder reactions is the higher melting elemental constituent.

3. The reaction Zn-S is very similar to that observed for Cd-Se and Cd-S. Preparation of this material in a one-stage synthesis also follows the procedure defined for CdSe.

4. The reaction Zn-Se also closely resembles the Cd-Se reaction, with the notable difference that a single stage complete powder synthesis can be effected at rates as high as 3°/min.

5. The Zn-Te reaction is shown in Fig. 4 and, as can be seen, its behavior resembles that for the other binary reactions excluding the Cd-Te reaction. From the data it is observed that in the system Zn-Te, the solubility of ZnTe in melts rich in either Zn or Te becomes appreciable at around 600-700°.

The method of synthesis is being studied for other reactions whose products melt at appreciably higher temperatures than their elemental constituents. These include a number of III-V, III-VI, and II-V compounds.

DEHYDROXYLATION OF KAOLINITE. I. KINETICS

BY F. TOUSSAINT, J. J. FRIPIAT, AND M. C. GASTUCHE

Laboratoire des colloïdes (INEAC) et de chimie minérale, Institut Agronomique, University of Louvain, Héverlé-Louvain (Belgium)

Received April 30, 1962

The kinetics of kaolinite dehydroxylation has been studied by thermogravimetry. Two diffusion processes must be taken into consideration: gross diffusion of water vapor from the clay surface toward the gas phase, and inner diffusion of water molecules, nucleated in the lattice, outward from the crystal. The first process may be controlled by working at relatively low temperature (430°). When this condition is fulfilled, the order of the rate process with respect to the solid phase is unity but no definite order exists with respect to the vapor phase. This is explained by the existence of a water film operating as a diffusion barrier at the reaction interface. Dehydroxylation occurs by removal of constitution water from a complete octahedral layer and not by random nucleation in the lattice. This conclusion agrees with previous deductions from n.m.r.

I. Introduction

The object of this paper and of a following one is the study of the dehydroxylation process of kaolinite, the properties of samples taken at intermediate stages between kaolinite and metakaolin having been described elsewhere.¹ Although numerous papers already have been devoted to this subject,² the dehydroxylation mechanism never has been completely explained.

For the kinetic studies the two methods of differential thermal analysis and thermogravimetry were used in an attempt to distinguish between the two different diffusion processes which must be considered. These are: (1) the diffusion of water molecules, nucleated inside the lattice, toward the crystal surface ("inner" diffusion process); and (2) the diffusion of water molecules in the powder mass ("gross" diffusion process).

The first diffusion mechanism, nucleation and growth of nuclei, cannot be distinguished, but the second one can be controlled by careful adjustment of the experimental parameters.

The influence of particles size distribution upon the dehydroxylation process, as emphasized by Eyraud, Prettre, *et al.*,³ Schmidt and Heckroodt,⁴ Van Nieuwen-

berg and Pieters,⁵ Laws and Page,⁶ and Robertson-Brindley, and Mackenzie,⁷ can be accounted for by the adoption of both diffusion mechanisms.

As shown by Grim⁸ and Caillère and Hénin,⁹ the first diffusion process is determined by crystalline properties while the partial vapor pressure of water mainly affects diffusion through the sample mass.^{10,11} References 3-11 are mainly concerned with dehydroxylation studies by d.t.a., that is to say under non-isothermal conditions.

The requirement that the diffusion mechanisms shall be controlled as well as possible limits the value of d.t.a. In general, isothermal thermogravimetry is better adapted to kinetic investigations.

Murray and White¹² made a thorough study of the rate process by this method and showed that it obeys a

(3) C. Eyraud, R. Goton, Y. Trambouze, T. H. The, and M. Prettre, *Compt. Rend.*, **240**, 862 (1955).

(4) E. R. Schmidt and R. O. Heckroodt, *Mineral. Mag.*, **32** [247], 314 (1959).

(5) C. J. Van Nieuwenberg and H. A. Pieters, *Rec. trav. chim.*, **48**, 27 (1929).

(6) W. Laws and J. B. Page, *Soil Sci.*, **62**, 319 (1936).

(7) R. H. S. Robertson, G. W. Brindley, and R. C. Mackenzie, *Am. Mineralogist*, **39**, 118 (1954).

(8) R. E. Grim, *ibid.*, **32**, 493 (1947).

(9) S. Caillère and S. Hénin, *Actes. Congr. Ceram. Intern.*, 137 (1948).

(10) R. L. Stone, *J. Am. Ceram. Soc.*, **35**, 50 (1952).

(11) W. Schraunli and F. Becker, *Ber. Deut. Keram. Ges.*, **37** [5], 227 (1960).

(12) P. Murray and J. White, *Clay Minerals Bull.*, **1**, 84 (1949); *Trans. Brit. Ceram. Soc.*, **48**, 151 (1949); **54**, 187 (1955).

(1) M. C. Gastuche, F. Toussaint, J. J. Fripiat, R. Touillaux, and M. Van Meersche, *Clay Minerals Bull.*, 1962, to be published.

(2) E. B. Allison, *ibid.*, **2**, 242 (1955); H. E. Kissinger, *Anal. Chem.*, **29**, 1702 (1957); E. C. Sewell, *Clay Minerals Bull.*, **2**, 233 (1955); T. Jacobs, *Nature*, **182**, 1086 (1958); R. Guennelon, *Bull. Groupe Franç. Argiles*, **6**, 27 (1959).

first-order law for samples of different origins and for degrees of transformation less than 75%. Unfortunately, they did not investigate the diffusion phenomena specifically and from this viewpoint their results are open to criticism. Brindley and Nakahira¹³ surveyed the influence of size and shape of the sample and clarified the gross diffusion mechanism reported above. They also found a first-order law, below the limit established by Murray and White.

The process of dehydroxylation belongs to the class of heterogeneous reactions, the rate of which can be expressed as

$$V = kC_s^{n_s}C_v^{n_v} \quad (1)$$

where n_s and n_v are the orders with respect to the solid and to the vapor phase and C_s and C_v the concentrations of the products of the reaction. In order to understand the mechanism, the values of n_s and n_v must be established. To our knowledge, no attempt in this direction has ever been performed.

Therefore, the field of this first paper is clearly delineated: taking in account the two diffusion mechanisms and by controlling the second one, to compute n_s and n_v and derive the reaction characteristics.

II. Experimental

Apparatus.—A Ugine Eyraud (D.A.M., France) thermobalance was used for this study. It permits one to obtain a continuous record of the sample weight when heating under vacuum or under constant water vapor pressure. Care is taken to bring the sample to the working temperature as fast as possible and stationary thermal conditions generally are reached within 5 min. The furnace is held within $\pm 1^\circ$ by an electronic programmer. Temperature measurements are made using a thermocouple inserted in a calcinated kaolinite sample located a few mm. below the reacting sample, and water vapor pressure is measured by means of an oil manometer.

Material.—The kaolinite used for this study was taken from a very pure sample collected in the Busirian sediment of Yangambi (Congo Republic). The pseudo-hexagonal morphology is perfectly developed, the average length of hexagons being 1600 Å, while the average thickness is approximately 740 Å. Dehydroxylation does not change these characteristics appreciably; thus the B.E.T. surface area is $16 \text{ m}^2 \text{ g}^{-1}$ for the initial sample and $12.0 \text{ m}^2 \text{ g}^{-1}$ after dehydroxylation at 550° under atmospheric pressure. The initial hydroxyl content amounts to 14.2% (by weight) and decreases to 1.25% after the same treatment.

Most of the work was performed with 10.6 mm. tall clay cylinders, 7.4 mm. in diameter and weighing approximately 0.4 g. They are made from a clay paste dried at 100° .

The holder used for this kind of sample was made from a platinum screen, hanging on the balance arm. Kaolinite also has been used in a powdered form: in this case, a 0.4-g. sample is introduced into a quartz cell of 10 mm. inner radius and filled up to three fifths of the height.

III. Results

A. Diffusion Process.—The gross diffusion phenomenon that now will be considered includes the transport of water molecules escaping from the reaction interface and driven through the sample toward the gaseous phase. Experimental conditions were sought that would reduce its influence upon the "true" rate process of dehydroxylation.

Aggregated clay cylinders were used for this purpose: the reaction is stopped at average α -values, respectively, equal to 30 and 70%. Runs were made under a low and a high water pressure (0.75 and 12.9 mm.) and at both extremes of the suitable temperature range (430

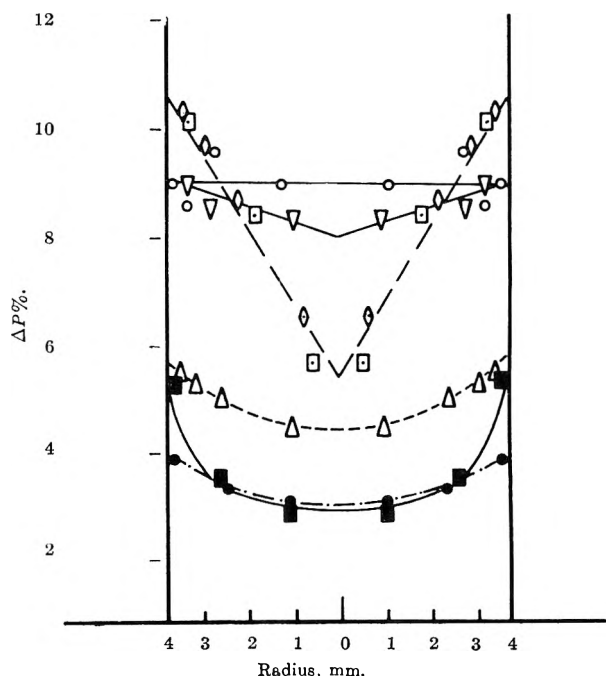


Fig. 1.—Gross diffusion process. Water loss ($\Delta P\%$) as a function of the radius in mm. Upper curves, $\alpha \approx 70$: \diamond , 490° , $P_{\text{H}_2\text{O}} = 12.9 \text{ mm.}$; \square , 490° , $P_{\text{H}_2\text{O}} = 1 \text{ mm.}$; \circ , 431° , $P_{\text{H}_2\text{O}} = 0.6 \text{ mm.}$; ∇ , 430° , $P_{\text{H}_2\text{O}} = 11 \text{ mm.}$ Lower curves $\alpha \approx 30$: \triangle , 435° , $P_{\text{H}_2\text{O}} = 11.3 \text{ mm.}$; \bullet , 430° , $P_{\text{H}_2\text{O}} = 11.6 \text{ mm.}$; \blacksquare , 485° , $P_{\text{H}_2\text{O}} = 0.7 \text{ mm.}$

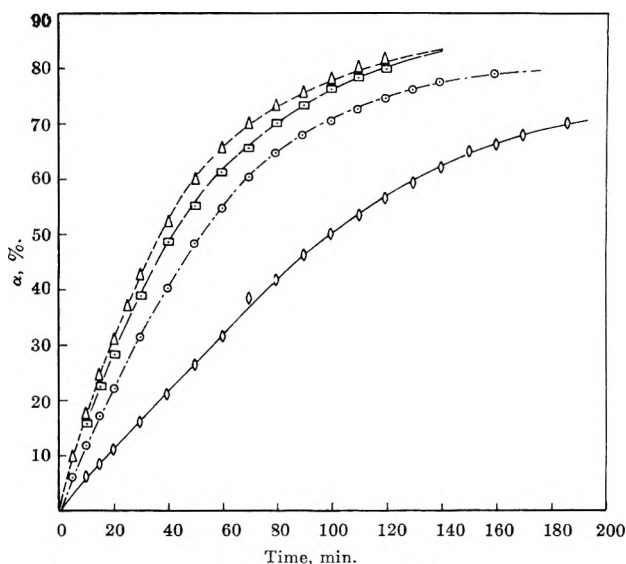


Fig. 2.—Dehydroxylation process at constant temperature (431°) under different pressures: $P_{\text{H}_2\text{O}} = 0.8 \text{ mm.}$, \triangle ; 0.9 mm. , \square ; 4.3 mm. , \circ ; 11.2 mm. , \diamond .

and 490°). Cylinders then were carefully cut into concentric rings and each sample then was calcinated to determine the residual water.

Figure 1 shows the experimental results. They clearly demonstrate that whatever the pressure, the water content distribution within the samples is more homogeneous when the reaction is performed at lower (430 – 435°) rather than at higher temperatures.

Therefore, the kinetic study which follows was performed below 435° .

B. The Two Orders of the Rate Process.—The object of these investigations is to compute the orders of the reaction with respect to the solid (n_s) and to the vapor (n_v) phases according to relationship 1. Therefore, a set of experiments was run either under constant pressure at different temperatures or at constant temperature under different pressures. Figures 2 and 3

(13) G. W. Brindley and M. Nakahira, *Clay Minerals Bull.*, **3**, 114 (1957); *Mineral. Mag.*, **31** [240], 781 (1958); *Clays and Clay Min. Publ.* 566, 1958, pp. 267–278; *J. Am. Ceram. Soc.*, **42** [7], 311 (1959).

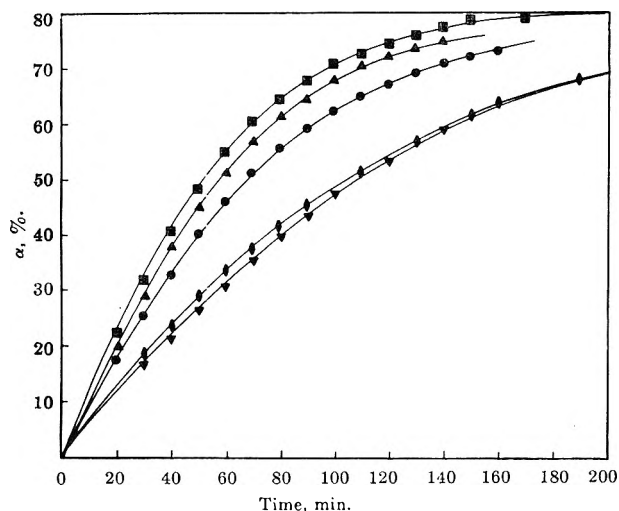


Fig. 3.—Dehydroxylation process under constant pressure (4.3 mm.) at different temperatures: ■, 431°; ▲, 424°; ●, 422°; ◆, 408°; ▼, 404°.

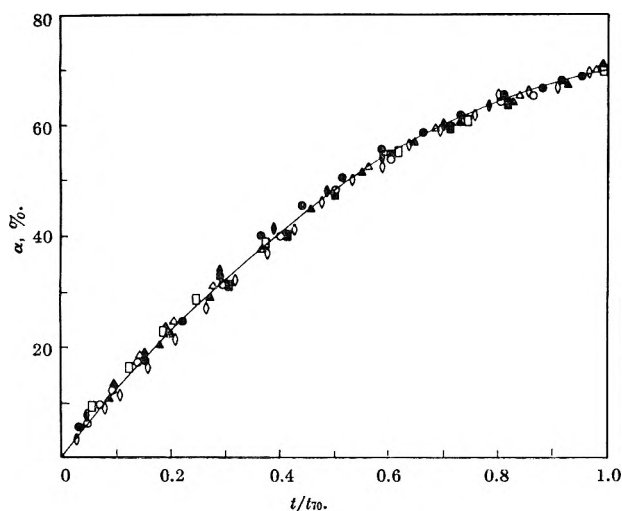


Fig. 4.—Dehydroxylation process expressed in reduced coordinates for clay cylinders. Symbols are those given in Fig. 2 and 3.

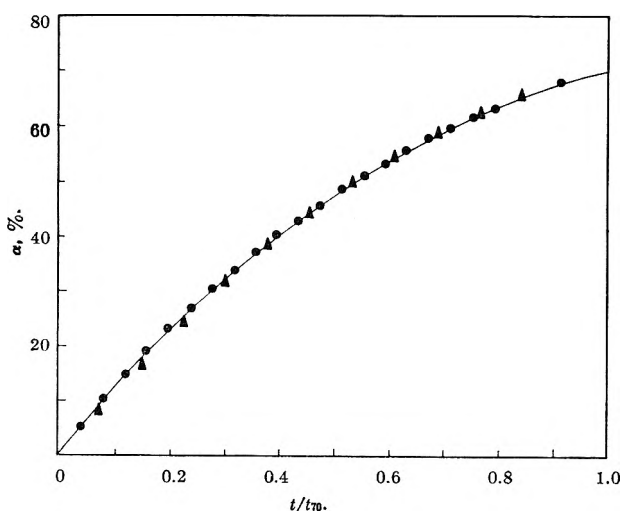


Fig. 5.—Dehydroxylation process expressed in reduced coordinates for powdered clay: $P_{\text{H}_2\text{O}} = 4.8$ mm.; ▲, at 427°; ●, at 398°.

give experimental plots of α against the time. Figure 4 summarizes the data expressed in relative coordinates α and $t/t_{70\%}$. The reduced time $t/t_{70\%}$ is calculated with respect to the time necessary to complete 70% of the reaction (t corresponding to $\alpha = 70\%$).

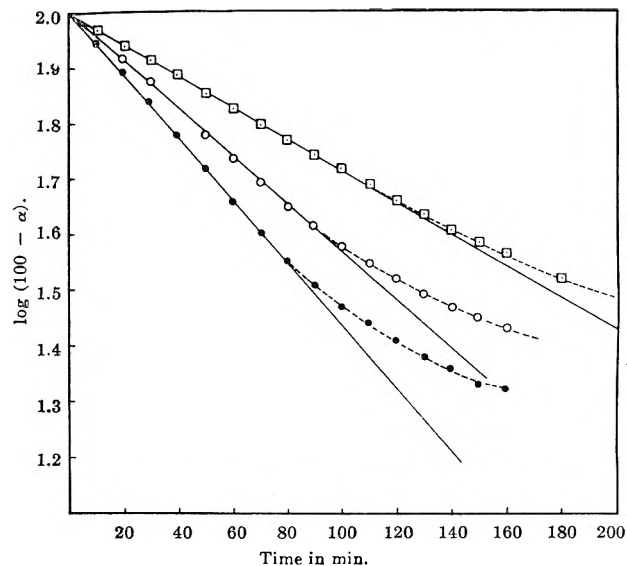


Fig. 6.—First-order rate law with respect to the solid phase: $P_{\text{H}_2\text{O}} = 4.3$ mm., □ at 408°; ○ at 422°; ● at 431°.

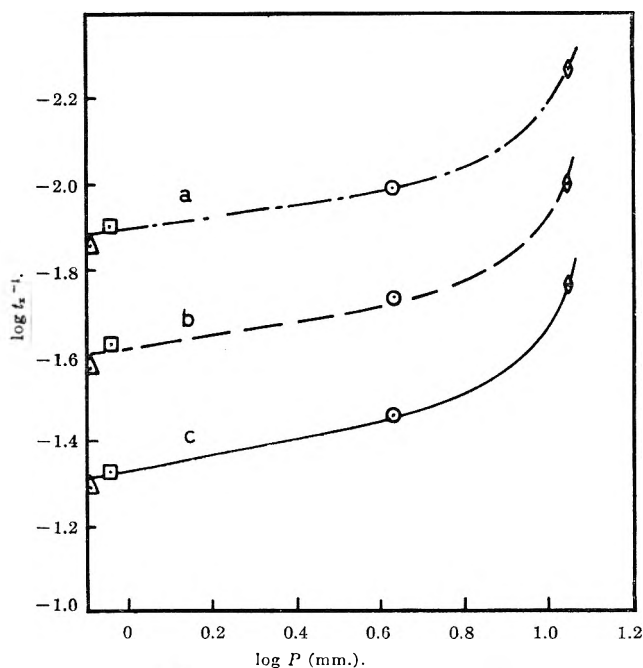


Fig. 7.— $\log t_x^{-1}$ against $\log P$. t_x represents the time necessary to reach $\alpha = 70$ (for a), $\alpha = 50$ (for b), and $\alpha = 30\%$ (for c) of the reaction; temperature, 431°.

Figures 2–4 include data obtained from clay cylinders while Fig. 5 represents results given by powdered samples: plots of Fig. 5 and 4 can be perfectly superimposed.

The reaction order with respect to the solid is calculated under a constant pressure condition (4.3 mm.). By plotting $\log(100 - \alpha)$ vs. time it is found that n_s is equal to unity as long as α remains lower than approximately 70% (Fig. 6), whereas the order with respect to the vapor phase (n_v) is obtained by plotting $\log t_x^{-1}$ with respect to $\log P_{\text{H}_2\text{O}}$, where t_x is the time required to reach a given $\alpha = x$ value. Figure 7 contains such plots for three different α -values and demonstrates that n_v is not constant. For $P_{\text{H}_2\text{O}} = 4.3$ mm., the slope of $\log t_x^{-1}$ vs. $\log P_{\text{H}_2\text{O}}$ is approximately 0.2, but it increases with the pressure regardless of the extent of dehydroxylation.

C. Activation Energy.—The activation energy is calculated as usual from the slope of $\log t_{50}^{-1} P_{\text{H}_2\text{O}}^{n_v}$

plotted *vs.* the inverse of absolute temperature. The Arrhenius law holds satisfactorily and the activation energy amounts to 25 kcal. under the following conditions: $P_{\text{H}_2\text{O}} = 4.3$ mm., $\alpha = 50\%$, $n_v = 0.2$, and 676°K . $< T < 704^\circ\text{K}$.

This value is noticeably lower than the ones reported by other workers, none of which have worked at so a low temperature. For instance, around 770°K , Brindley and Nakahira¹³ found 65 kcal. Such discrepancies cannot be explained by differences in mineralogical or morphological characteristics, but indicate intervention of diffusion phenomena at higher temperature.

IV. Discussion

The first order with respect to the solid permits the representation of α , under constant pressure, as an exponential function of the time

$$\alpha = (1 - e^{-kt}) \quad (2)$$

Relationship 2 reflects the fact that dehydroxylation becomes slower toward the end of the reaction. This may be interpreted from two different viewpoints: (1) The nucleation probability decreases as the concentration of hydroxyl radicals within the lattice is reduced. (2) The deeper the locus of nucleation, the slower the molecules are removed.

According to the first hypothesis, we assume nucleation occurs randomly, the average OH...OH distance increasing as reaction proceeds. According to the second hypothesis, we may suppose nucleation and growth of nuclei affect complete crystal domains, the process being limited by inner diffusion. On the basis of nuclear magnetic resonance, it has been suggested¹ that the second hypothesis is correct. Van Vleck¹⁴ has established that the "second moment," calculated from n.m.r. spectra, is inversely proportional to the sixth power of the average OH-OH length; thus if this function is computed for partially dehydroxylated material, any significant change with respect to α will reflect a perturbation in the distribution of hydroxyls belonging to the lattice.

Experimental results collected in Table I show that the second moment is constant but the low sensitivity of the method as applied to solids prevents n.m.r. spectra to be recorded for $\alpha > 70\%$.

TABLE I

DEHYDROXYLATION EXTENT α (IN %) AND "SECOND MOMENT" (S.M.) (IN GAUSS²) CALCULATED FROM N.M.R. SPECTRA

Frequency: 58 Mc./sec. field modulation: 2.32 gauss. (The contribution of aluminum has been taken into account¹)

α	S.M.
0	4.6
15	4.4
32	4.6
40	4.6
51	4.6
67	4.3

According to these observations, the interpretation of the first order with respect to the solid may be expressed as follows: the time required for nucleation and growth of the nuclei is very short as compared with the time required for a water molecule to diffuse inside the lattice toward a reaction interface. In other words,

(14) J. H. Van Vleck, *Phys. Rev.*, **74**, 1168 (1948).

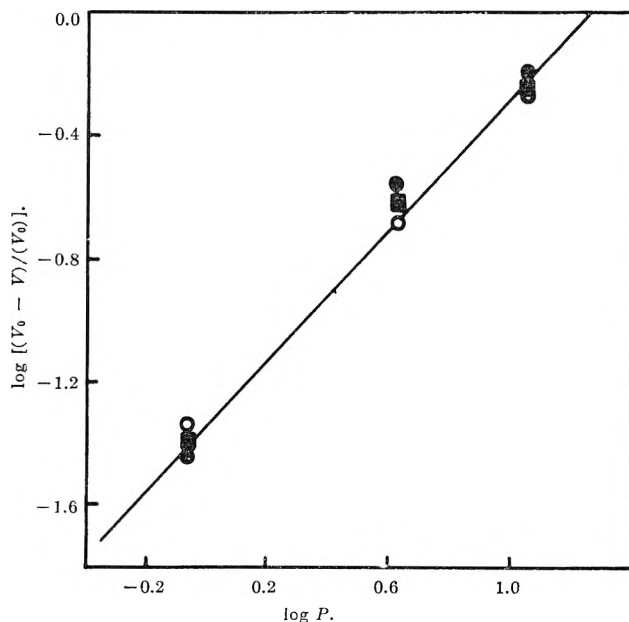


Fig. 8.—Log $(V_0 - V)/V_0$ against log P at 431° .

dehydroxylation proceeds by successive destruction of complete octahedral layers and the reaction probability is proportional to the amount of unreacted material. These conclusions agree with Brindley and Nakahira's¹³ deductions. As we have eliminated the perturbations arising from gross diffusion of water molecules through the powder, the effect of external water vapor pressure must be to control "internal" diffusion processes. If V_0 and V are the rate of reaction under vacuum and under a water pressure P , respectively, Fig. 8 shows that relationship 3 holds regardless of the extent of dehydroxylation.

$$\ln \frac{V_0 - V}{V_0} = \text{constant} + \ln P \quad (3)$$

Assuming an adsorbed water film behaves as a diffusion barrier, the rate process V can be divided into two components: one associated with the rate of emergence of water molecules from the crystals (V_1) and the other with the rate of evaporation (V_2).

$$V = V_1 - V_2 \quad (4)$$

V_1 is proportional to the interface area S and V_2 to the covered fraction θ represented, for instance, by the Langmuir isotherm: $\theta = P/(P + b)$.

$$V = S(k_1 - k_2\theta) \quad (5)$$

If $P \rightarrow 0$, $V \rightarrow V_0 = Sk_1$. Therefore

$$\frac{V_0 - V}{V_0} = \frac{k_2}{k_1} \frac{P}{P + b} \quad (6)$$

which is identical with the empirical relationship 3 insofar as P is negligible as compared with b . A high value for b can be expected since relatively high temperature and low pressure preclude the saturation of the surface. It follows that the effect of pressure accounts for the existence of a stationary water film covering the reaction interface and limiting the diffusion of water outside the crystal. This explains also why the concept of reaction order with respect to the vapor phase has, in this case, no physical meaning and why the slope of $\log t_x^{-1}$ *vs.* $\log P_{\text{H}_2\text{O}}$ increases with pressure (Fig. 7).

V. Conclusions

The mechanism of kaolinite dehydroxylation may be described as follows. (1) Reaction proceeds by successive destruction of complete octahedral layers. (2) The rate process is limited mainly by diffusion of water molecules inside the lattice toward the external surface of the crystal. (3) Water vapor pressure affects the diffusion through the interface where a water film probably operates as a diffusion barrier. (4) The reaction order with respect to the solid is unity, though no defi-

nite order with respect to the vapor phase can be determined. (5) Under our experimental conditions, gross diffusion mechanism through the sample can be eliminated if dehydroxylation is run below 435°. (6) The activation energy (25 kcal.) is noticeably lower than determined by other authors.

The following paper will attempt to give a more detailed mechanism from physical data obtained by electrical conductivity measurements and infrared spectroscopy.

DEHYDROXYLATION OF KAOLINITE. II. CONDUCTOMETRIC MEASUREMENTS AND INFRARED SPECTROSCOPY

BY J. J. FRIPIAT AND F. TOUSSAINT

Laboratoire des colloïdes (I.N.E.A.C.) et de chimie minérale, Institut Agronomique, University of Louvain, Héverlé-Louvain (Belgium)

Received April 30, 1962

When kaolinite is heated from 100 to 500°, conductivity measurements demonstrate that three successive processes occur. The first one, between 100 and 360°, corresponds to a slow increase in conductivity and is assumed to represent a proton delocalization process which involves the free hybrid orbitals of octahedral oxygens. The second one, between 360 and 420°, is associated with removal of water from the crystals and is marked by a conductivity decrease. Above 420°, lattice defects in the metakaolin phase contribute to a sharp increase in the conductivity. The assumed proton delocalization process is clearly observed by modifications occurring in the OH (or OD) stretching vibration band. Components of this band are supposed to represent vibrations of different hydrogen bonded hydroxyls. Their frequencies shift closer to each other when the clay film is heated up to 360°. These modifications may be translated in terms of OH...O lengthening or shortening and permit an approximate representation of lattice distortions.

I. Introduction

Electrical conductivity measurements on solid clay powders have been used by Shimizu¹ and De Keyser² in order to differentiate hydration from constitution water. According to Shimizu, three conductance levels are observed when heating kaolinite. The first one corresponds to the removal of hydration water around 100°; the second, extending from 300–500°, has an activation energy of approximately 6 kcal., determined as usual from the slope of $\log \sigma$ vs. T^{-1} (where σ is the conductance). Its significance is not described. The third one, corresponding to dehydroxylation, is marked by a sharp increase in σ . Freund³ has followed the disorganization of the metakaolin structure at high temperature by the same kind of measurement.

The direct observation of OH stretching vibrations by infrared spectroscopy has been studied by several workers. Thus, Stubican⁴ and more recently Miller⁵ undertook such a study, but they mainly observed samples "frozen" at different dehydroxylation levels and did not investigate spectral modifications at high temperature while the reaction proceeds. In a preliminary attempt, Fripiat and Toussaint⁶ gave some evidence that, before the rate process becomes measurable, some reorganization occurs in the octahedral layer, indicating some proton delocalization. As electrical measurements might be correlated with proton mobility, an attempt was made to explain some dehydroxylation features by collecting information from both infrared and conductometric measurements. The

present contribution follows a first paper dealing with kinetics⁷ and a previous one where properties of partially dehydroxylated samples were studied by nuclear magnetic resonance, X-ray fluorescence, and acid dissolution techniques.⁸

II. Experimental

A. Samples.—Kaolinite used for this investigation has been described previously.⁷ For conductometric measurements, clay cylinders 5 mm. in height, 8 mm. in diameter, and weighing approximately 0.27 g. were prepared by drying clay paste at 100°. Platinum was evaporated under vacuum onto the ends of the cylinders for use as electrodes. For runs where the weight loss and conductance were measured simultaneously, a conductivity cell made from two concentric platinum screen electrodes of 10 mm. height, the radii of which were, respectively, 6 and 2 mm., was used. The electrodes were embedded in a clay paste and the whole "cake" was allowed to dry at 100°.

Conductivity measurements obtained from the first kind of sample were reproducible, but it was quite impossible to reproduce the geometry for the second set. It follows that in this last case, the results have only a relative significance. For infrared spectroscopy, clay films were prepared by evaporation of a few drops of a concentrated suspension upon a flat platinum screen. The crystals were perfectly oriented, as shown by the exclusive presence of 001 reflections in X-ray diffraction diagrams, the *c*-axis standing perpendicular to the film surface. Deuterated kaolinite was prepared by the method of Romo⁹ by heating in a "bomb" at 290° under a D₂O vapor pressure of 90 kg./cm.² for 9 days; approximately 50% of constitution hydroxyls were exchanged.

B. Apparatus.—The cell, represented schematically by Fig. 1, is used in order to measure the conductivity of clay cylinders. When weight and conductance are recorded simultaneously the clay "cake" is suspended on the thermobalance arm by means of two rigid tungsten wires soldered to the platinum electrodes. Two very short and thin tungsten wires (10 μ) make the electrical connection at the point where the system is hanging free. The

(1) S. Shimizu, *Sci. Rep. Tohoku Imp. Univ. Ser. III, Petrol. Min. Minerals Deposits*, **22**, 633 (1933).

(2) W. De Keyser, *Ber. Deut. Keram. Ges.*, **21**, 29 (1940).

(3) F. Freund, *ibid.*, **37**, 209 (1960).

(4) V. Stubican, *Mineral Mag.*, **32**, 38 (1959); V. Stubican and R. Roy, Technical Report No. 3, A.P.I. project 55, 1960.

(5) J. G. Miller, *J. Phys. Chem.*, **65**, 800 (1961).

(6) J. J. Fripiat and F. Toussaint, *Nature*, **186**, 627 (1960).

(7) F. Toussaint, J. J. Fripiat, and M. C. Gastuche, *J. Phys. Chem.*, **67**, 26 (1963).

(8) M. C. Gastuche, F. Toussaint, J. J. Fripiat, R. Touillaux, and M. Van Meersche, *Clay Minerals Bull.*, in press (1962).

(9) L. A. Romo, *J. Phys. Chem.*, **60**, 987 (1956).

weight calibration is checked under these conditions. Conductivity data are obtained from a "Kerr" bridge working at 1.5 kc. With this apparatus, conductance may be measured in the range extending from 10^{-10} to 10^{-1} mho and corrected for any capacitance change.

For spectroscopic investigations, the platinum screen bearing the clay film is pressed between two copper blocks fitted with heating elements and thermocouples. The whole system may be oriented in such a way that the angle between the c crystal axis and the infrared beam can be increased from 0 to 50° without the loss of too much radiant energy. Spectra are recorded between room temperature and 500° for various orientations. In a few cases, spectra at -190° were obtained by cooling the cell with liquid nitrogen, care being taken to prevent condensation of atmospheric moisture by purging the spectrograph with dry nitrogen. A Beckman I-R4 fitted with CaF_2 optics was used with the following settings; 2.7 μ region: gain 9%, period 8 sec., slit $2 \times$ standard, scanning speed 0.02 $\mu/\text{min.}$, double beam; 3.7 μ region: gain 10%, period 8 sec., slit 0.2 mm, scanning speed 0.04 $\mu/\text{min.}$, single beam.

III. Results

A.—Conductometric Measurements.—Figure 2 reproduces the change in conductivity (σ) observed under various pressures when the temperature of the cell given by Fig. 1 is increased stepwise from 100 to 500° . It must be emphasized that each experimental point corresponds to an "equilibrium" measurement; that means after each temperature increment, the conductivity is recorded until it becomes constant. In fact, a rapid increase followed by a slow decrease is observed. The time required to reach a constant value is extremely variable and may be of the order of several hours, especially in the low temperature range. Diffusion of minute traces of water liberated when the temperature is rising can explain these variations. Fripiat and Dondeyne¹⁰ have shown that partial surface dehydroxylation occurs in kaolinite at temperatures as low as 100° *in vacuo*.

In spite of the scatter of experimental results, Fig. 2 shows that conductivities measured *in vacuo* below 350° are a little lower than the ones observed under water vapor pressures ranging from 0.7 to 10.7 mm. Three main features appear when σ is plotted against temperature: a rather slow increase occurs between 100 and 360° , followed by a fall extending from 360 to 420° ; a very sharp increase is observed beyond this limit. The change observed at temperatures higher than 490° is not reproduced in Fig. 2 because a jump of one order of magnitude occurs. Activation energies of 4 and 18 kcal., respectively, were obtained from the linear variations of $\log \sigma$ against T^{-1} in the ranges from 100 to 360° and from 420 to 490° .

Figure 3 records conductivity against extent of dehydroxylation at 390° . As explained previously, these data obtained with electrodes embedded in a clay cake have a relative value only, since sample geometry is not easily reproduced. Plots of Fig. 3 correspond to the second step observed in the function $\sigma(T)$ given by Fig. 2. If the conductivity decrease observed between 360 and 420° originates from removal of constitution hydroxyl groups, it may be suggested that the continuous rise occurring between 100 and 360° arises from the increasing mobility of protons inside the lattice.

Moreover, the rapid conductivity change beyond 420° may be attributed to metakaolin lattice defects and does not relate to the dehydroxylation process. In other words, experimental results suggest that the increase in conductivity occurring between 100 and

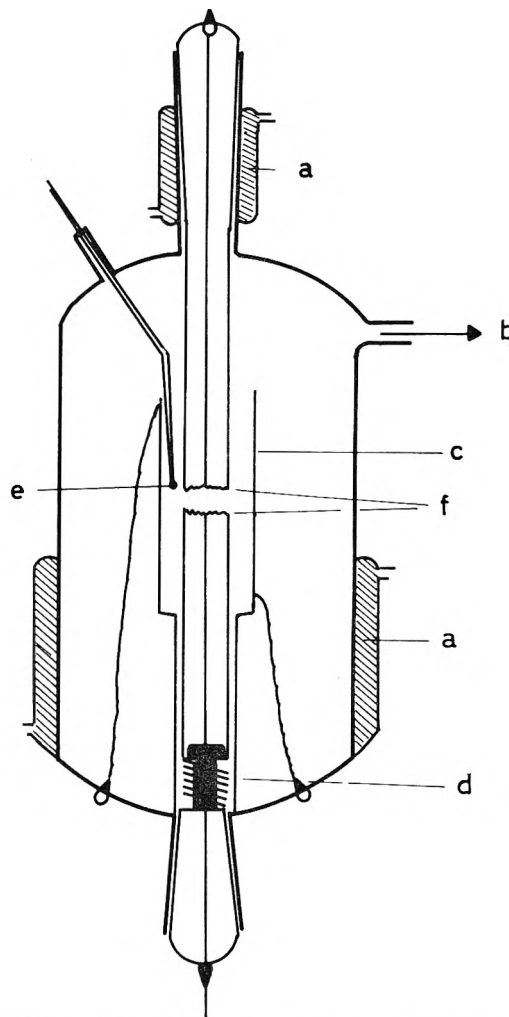


Fig. 1.—Conductivity cell: a, water cooler; b, vacuum line; c, furnace; d, spring; e, thermocouple; f, platinum electrodes.

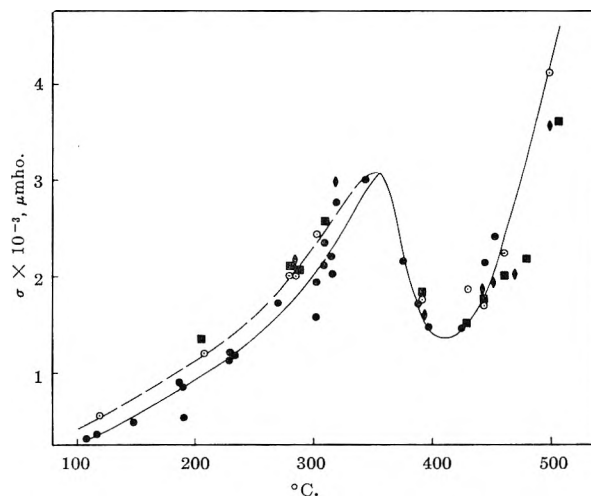


Fig. 2.—Conductivity σ against temperature: $P_{\text{H}_2\text{O}} = 10^{-6}$ mm., \circ ; $P_{\text{H}_2\text{O}} = 0.7$ mm., \bullet ; $P_{\text{H}_2\text{O}} = 4.8$ mm., \blacksquare ; $P_{\text{H}_2\text{O}} = 10.7$ mm., \blacklozenge .

360° originates from increasing mobility of structural protons since removal of constitution hydroxyls between 360 and 420° provokes a rapid depletion of the charge carriers. The activation energy value of 4 kcal. calculated for the first step is of the expected order of magnitude for the mobility of hydrogen ions in an environment of oxygens in close packing. Thus, in ice, the activation energy for the breaking of one hydrogen bond amounts to 5.2 kcal., according to Murphy.¹¹

(10) J. J. Fripiat and P. Dondeyne, *J. Chim. phys.*, 543 (1960).

(11) E. J. Murphy, *J. Chem. Phys.*, 19, 1516 (1951).

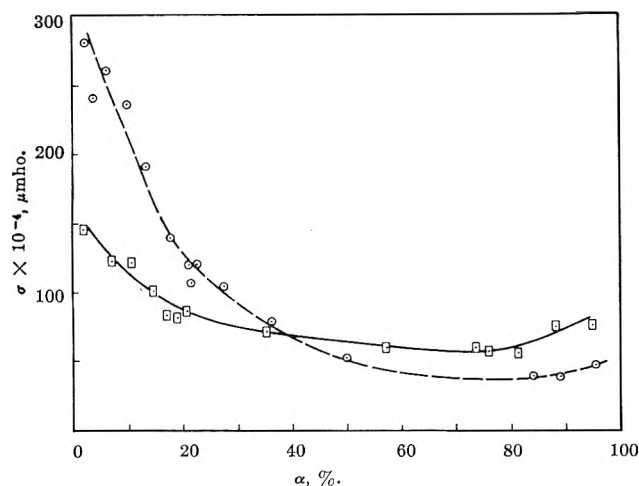


Fig. 3.—Conductivity σ against dehydroxylation extent α (in %) at 420°. Curves correspond to two different runs.

In water, the proton transfer $\text{H}_3\text{O}^+ \leftrightarrow \text{H}_2\text{O}$ requires an activation energy that Conway, Bockris, and Linton¹² theoretically estimate to be 3.9 kcal.

The suggested proton delocalization process also is supported by theoretical considerations. Among the 24 oxygen sp^3 orbitals of the octahedral unit cell, 14 are used for bonding aluminum and silicon to oxygen and 10 are available to the 4 protons. At low temperature, it might be assumed each proton is localized upon one specific oxygen atom, while at high temperature, delocalization occurs and they can move on all the “free” orbitals. The number of distinguishable ways in which A indistinguishable protons can occupy N distinguishable orbits is given by the relationship $N!/A!(N-A)!$. The entropy of A localized protons in the unit cell thus is given by A times the entropy for each proton, *viz.*, $R \ln 2!$. The entropy of A completely delocalized protons in the unit cell is given by $R \ln N!/A!(N-A)!$. Thus it follows that the “delocalization entropy” ΔS^* is given by

$$\Delta S^* = [R \ln N!/A!(N-A)! - AR \ln 2!] \quad (1)$$

For kaolinite, $\Delta S^* = 5.9$ e.u. As the energy change corresponding to such a delocalization process may be expected to be mainly entropic, we assume that: $\Delta E^* \approx T\Delta S^*$.

If delocalization should be complete at 360°, just before the dehydroxylation process becomes measurable, ΔE^* would reach 3.2 kcal. This theoretical result compares well with the value of 4 kcal. obtained from conductivity measurements and supports the proposed hypothesis.

B. Infrared Spectroscopy.—If progressive proton delocalization occurs below 360°, the OH and OD stretching bands, located, respectively, in the 2.7 and 3.7 μ regions, will change accordingly. Figures 4, 5, and 6 reproduce the observed spectra not only at increasing temperature but also for different orientations: θ represents the angle between the normal of the clay film and the direction of the infrared beam. Four components are observed in the OD stretching band where spectral resolution is the highest; they are called, respectively, LF, MF_1 , MF_2 , and HF according to their frequencies; LF, MF_1 , and HF components only are distinguishable in the 2.7 μ region (OH band). When the temperature is rising, the frequencies of HF, MF_1 ,

and LF shift closer to each other as shown in Fig. 7 for hydroxyls. These shifts are responsible for the disappearance of “transmission barriers” separating LF from MF_1 and MF_2 from HF. If ν_0^0 is the stretching frequency of free hydroxyls or deuterioxyls and ν^0 the actual frequency in kaolinite obtained for each component by extrapolation at 0°K., we may write

$$\Delta\nu = (\nu_0^0 - \nu^0)(1 + \gamma T) = \Delta\nu^0(1 + \gamma T) \quad (2)$$

Table I contains the $\Delta\nu^0$ and γ values.

TABLE I
 $\Delta\nu^0$ AND γ VALUES OBTAINED FOR OH AND OD BANDS

	$\Delta\nu^0$ (cm.^{-1}) for OH	$\gamma \times 10^3$, $\text{cm.}^{-1} (\text{°K.})^{-1}$ for OH	$\gamma \times 10^3$, $\text{cm.}^{-1} (\text{°K.})^{-1}$ for OD	$\beta \times 10^6$, $\text{Å.} (\text{°K.})^{-1}$
HF	33	+0.862	+0.862	-41.3
MF_1	76	-0.132	-0.130	+11.0
LF	132	-0.297	-0.302	+21.5

On the other hand, Lippincott and Schroeder¹³ have correlated $\Delta\nu$ and OH...O distance for hydrogen bonded hydroxyls using a different formula. From their results it follows that

$$\Delta\nu_{\text{OH}} = 680e^{-5.025(r-2.7)} \text{ cm.}^{-1} \quad (3)$$

where r is the OH...O distance in Å. From relationships 2 and 3, the thermal expansion coefficients β of the three different OH...O lengths, to which should correspond the three main spectral features HF, MF_1 , and LF, are calculated. As seen in Table I, the length of the OH...O bond corresponding to HF shortens while the two others increase when the temperature rises. It is interesting to compare these β coefficients with the ones obtained recently by McKinsty¹⁴ for thermal expansion of the kaolinite unit cell. For the c -axis, he found 20×10^{-6} Å. ($\text{°K.})^{-1}$ and 5×10^{-6} Å. ($\text{°K.})^{-1}$ for the b -axis; no result is given in his preliminary paper for the a -axis. These values are of the same order of magnitude as the ones calculated above.

The isotopic ratios also change a little with temperature as shown in Table II. According to Pimentel and McClellan,¹⁵ it is believed that the isotopic ratio is lower for stronger hydrogen bonds and consequently higher vibrational anharmonicity. The lower value obtained for the LF component corresponding with a shorter OH...O bond is therefore exceptional.

TABLE II
ISOTOPIC RATIOS AT DIFFERENT TEMPERATURES

Temp.	30°	205°	280°
LF	1.3580	1.3596	1.3601
MF_1	1.3614	1.3621	1.3619
HF	1.3612	1.3617	1.3621

Figures 4 and 5 clearly demonstrate that the intensities of the different band components remain constant whatever the temperature, but that they are sensitive to change in film orientation. Figure 6 represents spectra recorded in the OD region at a temperature of 30°. Under these conditions where there is a loss in transmission caused either by the optical path lengthening, arising from the sample rotation, or by a partial beam reflection, correction is applied by increasing the instrument gain.

(13) E. Lippincott and R. Schroeder, *ibid.*, **23**, 1099 (1955).

(14) H. A. McKinsty, A.P.I. Project 55, 1960.

(15) G. C. Pimentel and A. L. McClellan, “The Hydrogen Bond,” Reinhold Publ. Corp., New York, N. Y., 1960.

(12) B. E. Conway, J. O. M. Bockris, and H. Linton, *J. Chem. Phys.*, **24**, 834 (1956).

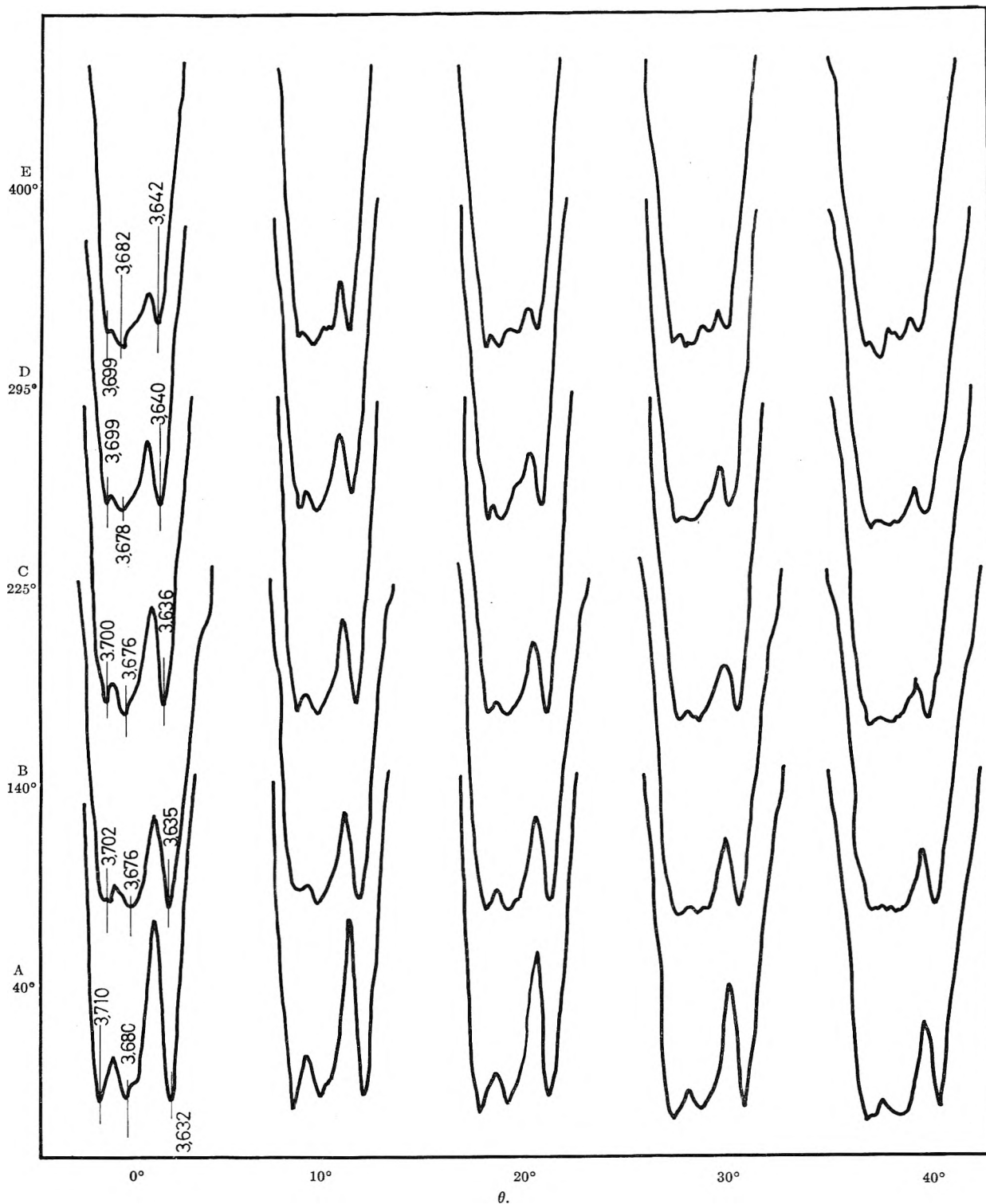


Fig. 4.—OH stretching vibration band at five temperatures (40–400°) under atmospheric pressure and for five different film orientations measured by θ (0–40°). Ordinate represents transmission.

The intensity of LF component is almost constant while HF, MF_1 , and MF_2 become more pronounced when the clay film rotates. In order to explain these observations, one may consider the orientation of the ten "free sp^3 " orbitals with respect to the normal to the clay film (Fig. 8). The c -axis in kaolinite is tilted at 104° to the lattice 001 plane. Four among these ten orbitals run parallel to this axis; they are represented in Fig. 8 by a vector to which a length of four arbitrary units has been attributed. One among these four orbitals belongs to the inner hydroxyl layer, the three others are directed outside the octahedral layer, toward the

contiguous sheet. Two orbitals, one belonging to the upper octahedral layer and the other to the inner layer, point in the opposite direction; they are represented by a vector to which a length of two arbitrary units has been given. The two remaining vectors, each of them being one unit long, correspond with the four remaining orbitals tilted at 110° with respect to the main ones.

Absorbances for each "potential" OH bond would be, as a first approximation, proportional to the value of the projection of the corresponding vector upon the plane containing the electrical field E of the infrared radiation. This assumption results from the assumed

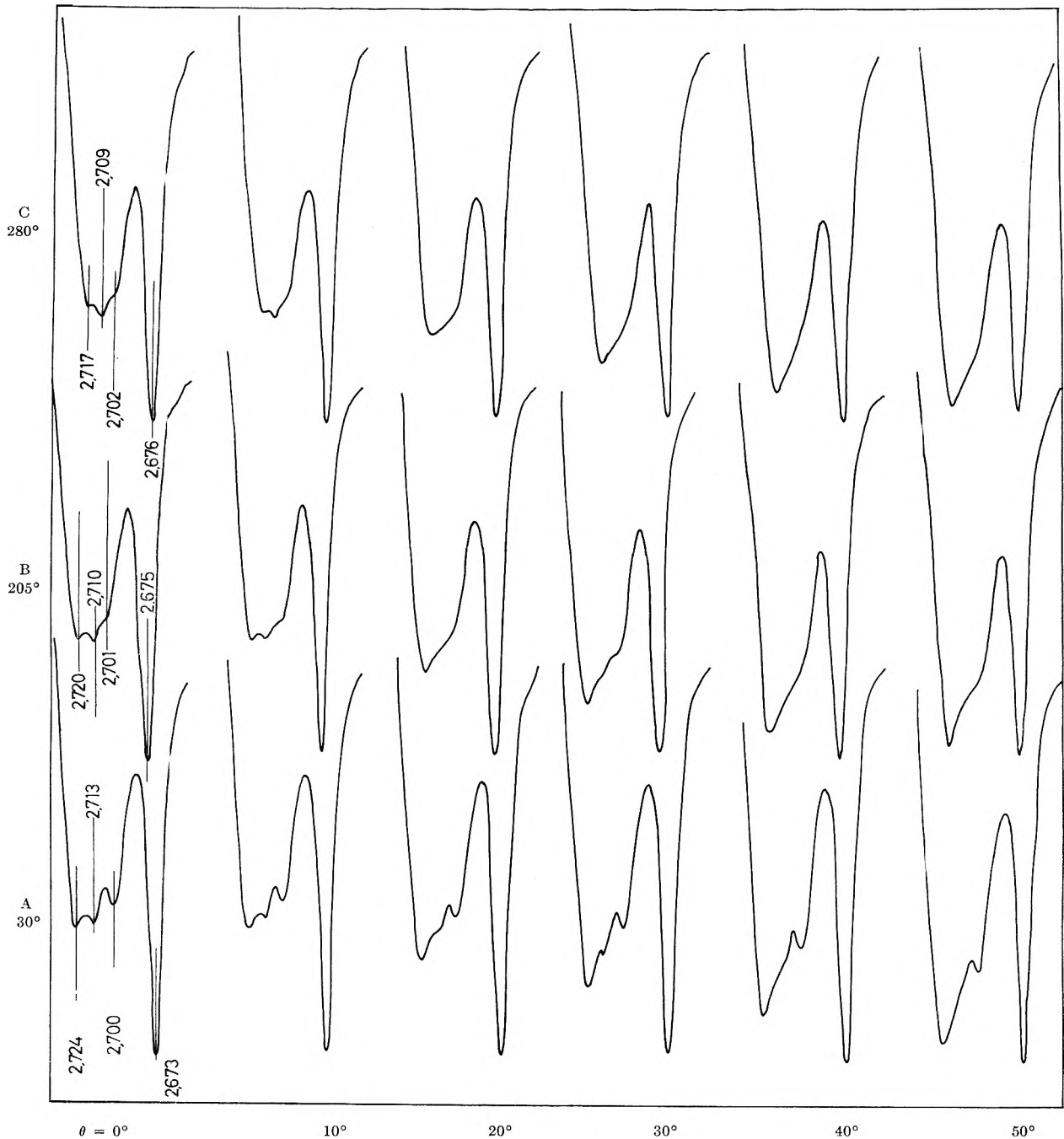


Fig. 5.—OD stretching vibration band at three temperatures (30–280°) under atmospheric pressure and for six different film orientations measured by θ (0–50°). Ordinate represents transmission.

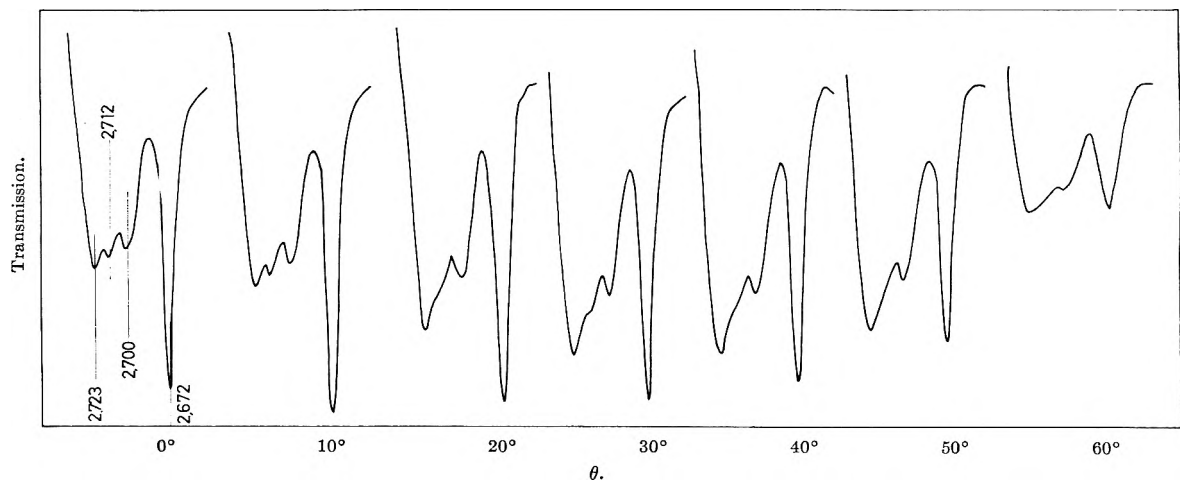


Fig. 6.—OD stretching vibration band at 30° for different film orientation given by θ . Ordinate represents transmission.

equivalence of all the hybrid orbitals. The electrical vector being located in a plane perpendicular to the infrared beam, projections easily may be computed from the rotation angle. The values are given in Fig. 8; it is only the absorbance of the vibrations corresponding to the OH bonds oriented following the *c*-axis which increase noticeably with θ .

The results of the spectroscopic investigations are summarized in Table III, assuming each band component corresponds to a specific OH class.

TABLE III

Band component	Frequency and OH...O length with rising temp.	Absorbance with increasing θ	Probable orientation for OH bond
HF	Decrease	Increases	Parallel to <i>c</i>
MF ₂	Increases	
MF ₁	Increase	Increases	
LF	Increase	Does not change	Tilted at 110° to <i>c</i>

IV. Discussion

The first point to be discussed concerns the origin of the OH band multiplicity in kaolinite. It should originate from combination with low frequency vibrations of the lattice as proposed by Wickersheim¹⁶ in order to explain some spectral features of alkali hydroxides. Let ν and ν' be two hypothetical combination frequencies of either ν_{OH} or ν_{OD} with a lattice frequency ν_x such as

$$\nu = \nu_{OH} + \nu_x \text{ and } \nu' = \nu_{OD} + \nu_x$$

The isotopic ratio R is given as follows since ν_x is much smaller than ν_{OH} and ν_{OD}

$$R = \frac{\nu_{OH}}{\nu_{OD}} \left[1 + \nu_x \left(\frac{\nu_{OD} - \nu_{OH}}{\nu_{OH} + \nu_{OD}} \right) \right] = \frac{\nu}{\nu'} \quad (4)$$

When LF, MF₁, and HF are compared (Table II), the largest difference quoted for R is approximately equal to 0.003. If multiplicity could arise from combinations, such a small discrepancy would require ν_x to be smaller than 25 cm.⁻¹. Therefore this hypothesis probably can be excluded.

It has been proposed by Beutelspacher¹⁷ and Van der Marel and Zwiers¹⁸ that the OH band components should correspond with inner and surface hydroxyls, but, according to Romo⁹ and Roy and Roy,¹⁹ the deuteration process does not permit the distinction of specific fluctuations in their relative intensities as would be expected from different locations. So the only rational hypothesis appears to be that multiplicity originates from different bond orientation in the lattice together with specific OH...O interactions. Serratosa and Bradley²⁰ obtained strong evidence for this viewpoint by studying polarization effects in the infrared spectra of trioctahedral and dioctahedral micas. In the trioctahedral lattice, all the OH bonds are oriented perpendicular to the 001 planes. In dioctahedral micas they distinguish three possible orientations, two of them being symmetrically equivalent. One is perpendicular to the 001 planes while the two others

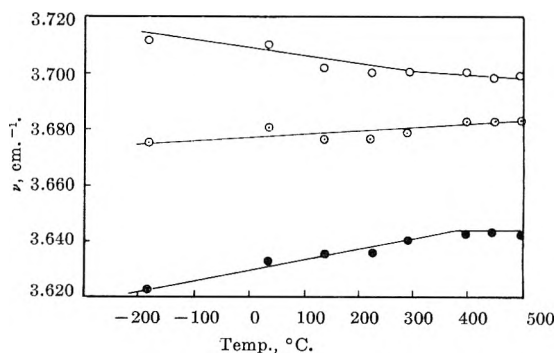


Fig 7.—Frequency shifts of HF (○), MF (○), and LF (●) components of the OH band against temperature.

correspond with orbitals tilted at 110° to the *c*-axis as represented in Fig. 8. In fact, in the trioctahedral layer as already pointed out by Krebs,²¹ there is, per oxygen atom, only one free sp² orbital available for hydrogen and it is directed along the *c*-axis. In addition, a calculation of the "second moment" as proposed by Van Vleck²² has been reported in a previous paper.⁷ If three of the four protons of the unit cell are located on the orbitals directed outwards from the octahedral layer along the *c*-axis, a second moment equal to 4.7 ± 0.2 gauss² is obtained; 2.55 and 2.79 Å. are chosen, respectively, as the oxygen distances in the lower silica layer and the hydroxyl distance in the upper octahedral layer of two contiguous sheets. The contribution of the remaining proton is very weak and is not taken into consideration.

The experimental value derived from nuclear magnetic resonance spectra is 4.6 gauss², in close agreement with the theoretical value given above.

All these considerations together with the conclusions derived from the spectroscopic study strongly suggest that, in the localized state, the protons of the upper octahedral layer give rise to the HF, MF₁ components of the hydroxyl stretching band. The LF component, the intensity of which does not change with the film orientation, should be attributed to the proton located in the inner hydroxyl layer, the corresponding OH bond being tilted with respect to the *c*-axis. If this hypothesis is correct, the frequency shifts which appear when the temperature is raised may be interpreted. The hydrogen bond length corresponding with "HF" hydroxyls shortens while the length of the ones which are responsible for MF₁ and LF components increases.

As the upper octahedral layer contains one hydrogen atom belonging to the OH-2Al-OH chain and two atoms included in a OH-Al-O bond, more than one frequency (HF and its satellites MF₁ and MF₂) may be associated with their vibrations.

The strong lattice distortion which occurs with increasing temperature shifts some hydroxyls closer to each other and lengthens the distances between others. It is impossible to be more precise, but this may be accounted for to some extent by a collapse of interlamellar space and by an expansion of the octahedral layer. During these changes, proton delocalization occurs; at 360° conductometric measurements indicate that the process is complete. It is a remarkable coincidence that above the same temperature limit, the frequency shift shown by Fig. 7 no longer appears. According to these deductions, at 360°, kaolinite may be

(16) K. A. Wickersheim, *J. Chem. Phys.*, **31**, 863 (1959).

(17) H. Beutelspacher, *11^d Congr. Intern. Sci. du Sol*, **1**, 329, Paris (1956).

(18) H. W. Van der Marel and J. H. L. Zwiers, *Silicates Ind.*, **24**, 359 (1958).

(19) D. M. Roy and R. Roy, *Geochim. Cosmochim. Acta*, **11**, 72 (1957).

(20) J. M. Serratosa and W. F. Bradley, *J. Phys. Chem.*, **62**, 1164 (1958).

(21) H. Krebs, *Z. anorg. allgem. Chem.*, **278**, 82 (1955).

(22) J. H. Van Vleck, *Phys. Rev.*, **74**, 1168 (1948).

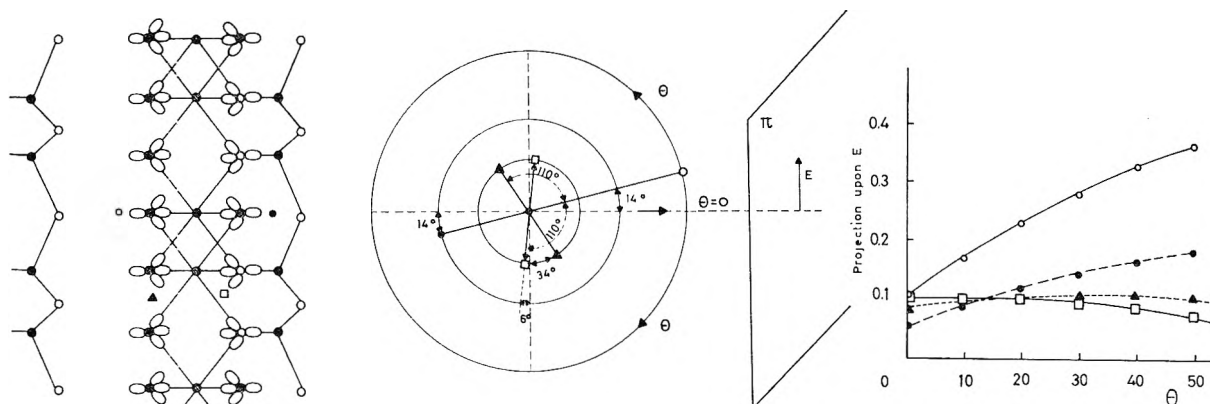


Fig. 8.—Left: hybrid orbitals of octahedral oxygens in the unit cell. Center: orbital orientation with respect to the normal ($\theta = 0$) to the film. The beam electrical field E is located in the plane " π ", parallel to the film. Right: orbital projection upon π as a function of the rotation angle θ .

considered as being in a "predehydroxylation" state, the definition of which includes all the characteristics enumerated above.

Above 360° , the dehydroxylation process becomes measurable, the kinetics of which has been reported in an earlier paper.⁸

V. Conclusions

The dehydroxylation process of kaolinite is preceded by complex changes which bring the lattice into a "predehydroxylation" state characterized as follows: (1) proton delocalization occurs within the octahedral

layer; (2) the frequencies of the components of the hydroxyl stretching vibration shift toward each other; (3) interlamellar space collapses to some extent while the octahedral layer expands.

The protons located in the upper octahedral layer may be associated with the high and medium frequency components of the OH band, while the low frequency component can be attributed to the vibration of hydroxyls belonging to the inner octahedral layer.

The changes in the relative distances between hydroxyls and oxygen suggest a strong lattice distortion in the predehydroxylation state.

THE THERMODYNAMIC AND PHYSICAL PROPERTIES OF BERYLLIUM COMPOUNDS. I. ENTHALPY AND ENTROPY OF VAPORIZATION OF BERYLLIUM FLUORIDE^{1,2}

BY MICHAEL A. GREENBAUM, JAMES N. FOSTER, M. LOUIS ARIN, AND MILTON FARBER

Rocket Power, Inc., Research Laboratories, Pasadena, California

Received May 1, 1962

Using torsion effusion, gravimetric effusion, and transpiration techniques, the enthalpy and entropy of vaporization of BeF_2 were determined over the temperature range 550 – 950° . The enthalpy of vaporization in this temperature range was found to be 53.25 ± 0.25 kcal, while the corresponding entropy was found to be 38.7 ± 0.6 cal./deg./mole. A determination of the melting point of crystalline BeF_2 by means of vapor pressure measurements yielded a value of $542 \pm 3^\circ$. Torsion effusion measurements of the effusing vapor show the gaseous species over liquid beryllium fluoride to consist of BeF_2 .

I. Introduction

Thermodynamic data concerning the vaporization of BeF_2 have been controversial in published work^{3–7} during the past several years. The heat of vaporization of BeF_2 was first reported by Sense³ in 1954. Based on the results of transpiration experiments in the temperature range 745 – 968° , the author obtained a value of 50.88 kcal. for the heat of vaporization of BeF_2 . Subsequently, Sense⁴ repeated his previous work in the temperature range 802 – 1021° and reported the value

of 50.1 kcal. for ΔH_{vap} . Novoselova, *et al.*,⁵ in 1958, reported a value of 46.98 (calculated ± 0.65) kcal. for ΔH_{vap} of BeF_2 . This calculation was made from a series of vapor pressure measurements in the range of 821 – 1002° , using the transpiration technique. No values for the entropy of vaporization of BeF_2 are reported in the literature.

The reported values for the melting point of BeF_2 vary over a very wide temperature range. The first value reported was by Novoselova,⁶ in 1944, who reported the melting point as being "somewhere under 600° ." In 1954, Roy, Roy, and Osborn⁷ determined the melting point by differential thermal analysis, obtaining a value of $543 \pm 5^\circ$. The same year, Sense³ reported a value of 803° for the melting point.

The present work has been undertaken to clarify these heats and entropies of vaporization and to answer some of the ambiguities on status of molecular species, accommodation coefficients, and the melting point.

(1) Presented in part before the Division of Physical Chemistry of the American Chemical Society at the 141st National Meeting in Washington, D. C., March 21–29, 1962 (abstract page 49-R).

(2) This research was supported by the Air Research and Development Command of the Air Force.

(3) K. A. Sense, M. J. Sryder, and J. W. Clegg, *J. Phys. Chem.*, **58**, 223 (1954).

(4) K. A. Sense, *ibid.*, **62**, 453 (1958).

(5) A. V. Novoselova, *et al.*, *Vestnik Moskov Univ. Ser. Mekh., Astron., Fiz., Khim.*, **13**, No. 6, 181 (1958).

(6) A. V. Novoselova, *J. Gen. Chem. USSR*, **14**, 385 (1944).

(7) D. Roy, R. Roy, and E. F. Osborn, *J. Am. Ceram. Soc.*, **37**, 300 (1954).

A determination of the heat and entropy of vaporization and the melting point of BeF_2 has been made by three established experimental techniques: torsion and gravimetric effusion and transpiration. The combination of these experimental methods has allowed the use of a greatly extended temperature range over the studies previously reported.³⁻⁶

II. Experimental

A. Gravimetric Effusion.—The effusion cells used in this study were machined from high density graphite having an ash content of less than 0.08%. Non-reactivity of the graphite with BeF_2 was proven experimentally in the temperature range of the investigation. The cells were made from a block with a square cross section of 20 mm. and with a height of 22 mm. A cylindrical cavity 18 mm. in diameter and 20 mm. deep was drilled along the long axis of the block. The effusion holes were drilled at the points of minimum wall thickness about 10 mm. from the top of the cell. In order to decrease the length of the effusion hole and to increase the Clausing factor, a 0.5-mm. cut 14 mm. wide was taken across the face of each effusion hole. The size of the hole and the number of holes used were determined by the pressure of the BeF_2 vapors which were estimated to be encountered. In the region of high vapor pressure, one 1-mm. hole was used, in the intermediate region either two or four 1-mm. holes were used, whereas in the lower pressure region either four 2-mm. or four 3-mm. holes were used. The use of different orifice areas allowed control over the amount of vapor effusing. In this manner the rate of weight loss was maintained fast enough to decrease reading errors and slow enough to avoid a too rapid depletion of material from the cell or kinetic effects of the evaporation from the surface. The sample chambers were closed with tapered graphite stoppers.

The orifice areas were determined in two ways: (1) by a direct measurement of the orifice diameter and wall thickness with a measuring microscope capable of direct measurement to 0.001 mm., and (2) by experimental determination of the Clausing factor by measuring the vapor pressure of high purity zinc metal and comparing these values with previously reported values.⁸

The effusion cell was supported by a 2-mil molybdenum wire which in turn was attached to a quartz helix (0.1027 mm./mg. sensitivity, 9 g. capacity). Calculations of actual specifications for the spring can be made by the use of a series of equations.⁹ A molybdenum radiation shield was used to ensure uniform temperature over the distance traveled by the cell. The thermocouple junction was placed in a graphite reference block which was supported in its position under the effusion cell by the thermocouple leads. The vapor pressure of BeF_2 was determined in the temperature range of 530° to 780°, using a cylindrical resistance furnace. The temperature was regulated manually by means of a variable powerstat. With small manual adjustments of the powerstat the temperature in the furnace was controlled within $\pm 1^\circ$. A Chromel–Alumel thermocouple was inserted in a graphite block situated just below the effusion cell. The temperature of the block was taken to be the temperature of the effusion cell. Three Chromel–Alumel thermocouples were used to measure the vertical thermal gradient within the radiation shield which showed a maximum temperature variation of $\pm 1^\circ$.

Initially, the effusion cell was washed with distilled water and soaked in reagent grade acetone. After air drying the effusion cell, crystals of high purity beryllium fluoride (99.5–99.7% as prepared by Brush Beryllium Co.) were placed in the cell and a tight fitting graphite cap secured on the cell. The cell was positioned in the quartz tube and the system evacuated to better than 10^{-7} mm. Prior to setting the furnace to the desired temperature the loaded effusion cell was maintained overnight under the high vacuum at around 300° to ensure thorough outgassing of the cell and its contents. After reaching the desired temperature, the position of the calibrated spring was measured with a cathetometer. After a selected period of time, depending on the rate of effusion, the position of the calibrated spring was measured again. In this manner the weight loss of the effusion cell per unit time was measured. At each cathetometer reading the temperature was measured. A minimum of five weight loss measurements were made at each temperature. The temperature of the furnace then was raised or lowered to another temperature and

the weight loss measurements repeated. In all measurements the total distance traveled by the effusion cell was not more than 1.5 in. above the reference block. At the end of each series of determinations the apparatus was dismantled, the cell opened, inspected, and filled again with sample.

B. Torsion Effusion.—Vapor pressure measurements of BeF_2 also were carried out by means of the torsion effusion procedure between 550–610°. The apparatus consisted of a torsion system enclosed within a vertical quartz and Pyrex vacuum chamber. A one pound lead block was inserted between the torsion suspension and the remainder of the apparatus to absorb and lessen the vibrations originating from the mechanical pump and movement in the environs.

The torsion system consisted of a 5-ft. length of 2 mil molybdenum wire to which was attached a mirror and an aluminum vane (to permit magnetic damping). The torsion constant of the molybdenum wire (D) was calculated from the following measurements: the oscillation period (t_1) for the suspension plus graphite disk which has a moment of inertia I_1 (where $I_1 = Dt_1^2/4\pi^2$) and the oscillation period (t_2) for the aforementioned suspension system (with graphite disk) plus a graphite body of known moment of inertia, I_2 (where $I_1 + I_2 = Dt_2^2/4\pi^2$). For the torsion system in terms of the measured quantities t_1 , t_2 , and I_2 , $D = 4\pi^2 I_2 / (t_2^2/t_1^2)$. The values obtained for the torsion wire systems ranged from 0.6367 to 0.6831 dyne-cm./radian. The constants obtained were an average of at least three separate determinations. The torsion constant of the suspension system was measured before and after vapor pressure determinations were made and remained constant to within 1%.

The angle of rotation of the torsion cell was measured by the displacement of a beam of light by a galvanometer mirror which was cemented to the quartz rod. The distance from the cathetometer telescope to the mirror on the torsion wire and the distance resulting from the movement of the beam of light reflected from the galvanometer mirror were measured on the cathetometer scale.

The regulation of the resistance furnace used in this investigation and measurement of the temperatures has been described above. The torsion effusion cell was situated approximately 2 cm. above a graphite reference block containing a Chromel–Alumel thermocouple. Because of the absence of a radiation shield, the furnace was positioned at the same point around the quartz tube for each determination. With the furnace in this position, the temperature gradient above the reference block was measured to a height of 1.5 in. for nine different temperatures. These measurements were accomplished with three thermocouples spaced above the reference block at 0.5-in. intervals. These calibrations were used to make the approximate temperature corrections which have been employed. Conditioning of the cell was similar to the procedure employed in the gravimetric studies.

A minimum of 20 min. was required to establish equilibrium at a given temperature. When the temperature was raised it also was observed that the oscillation of the mirror would increase. This oscillation could be lessened by quickly lowering the temperature of the furnace about 10° and then slowly raising it again to the desired point. When the torsion system picked up vibrations from the environment, the oscillations could be damped rapidly by placing a strong permanent magnet around the aluminum vane. This was done only to slow down the turning until the reference line was in the mirror since it was found that the presence of the magnet shifted the zero point. It was observed, however, that the displacement of the mirror was a constant factor which left the slope of the vapor pressure curves unaffected. This was indicated by the fact that the slopes of the $\log P$ vs. $1/T$ plots were the same with or without the presence of a magnet. Zero points were taken with and without the magnet and then readings were taken at the highest temperatures with and without the magnet. In both cases the differences in readings were identical, approximately 0.80 cm. Intermediate temperatures also demonstrated the same difference in readings. After equilibrium was attained at least three readings were taken before changing the temperature. During all determinations the pressure in the system was 10^{-5} mm. or less.

C. Transpiration.—The transpiration apparatus consisted of a transpiration tube, a high temperature furnace, and auxiliary equipment. The transpiration tube was a 30-mm. o.d. quartz tube. In order to avoid any possible reactions between BeF_2 gas and quartz, a reaction which is thermodynamically favored, a nickel liner was placed inside the transpiration tube.

The carrier gas used in the experiments was highly purified

(8) R. F. Barrow, *et al.*, *Trans. Faraday Soc.*, **51**, 1354 (1955).

(9) F. M. Ernsberger and C. M. Drew, *Rev. Sci. Instr.*, **24**, 117 (1953).

argon which was passed over heated copper for further removal of oxygen. The gas flow rate in all experiments was measured with a calibrated flowmeter. The nickel boats used in this experiment were constructed from high purity nickel sheet and were 1 in. long, $\frac{3}{8}$ in. wide, and $\frac{3}{8}$ in. deep. The temperature gradients across the nickel boat were established by placing a Chromel-Alumel thermocouple on each side of the nickel boat. The temperature gradient, in most cases, was less than 1° . The temperature of the sample boats during a run was controlled to $\pm 1^\circ$ with a Leeds-Northrup controller-recorder.

III. Results and Discussion

A. Melting Point of BeF_2 .—To determine an exact melting point of BeF_2 a series of effusion runs was commenced with a cell having four 3-mm. holes. The observed rate of weight loss from an experiment at 550° was more than 2.5 times that at 530° with the same cell in which, by subsequent examination of the BeF_2 , the solid was shown to be present. Since a drop of 20° in temperature produced less than a twofold drop in rate for BeF_2 liquid, it appeared that fusion was occurring between 530 and 550° . Examination of the contents of the cell indicated that the BeF_2 had indeed melted and on cooling had formed a glass. This behavior is similar to that of B_2O_3 and other compounds. Since glasses are considered supercooled liquids it is to be expected that the vapor pressure data for the BeF_2 glass would fall on the liquid vapor pressure curve as it actually does.

A more precise determination of the melting point of BeF_2 was carried out by making weight loss measurements of fresh samples of crystalline BeF_2 at 530 , 535 , 540 , 541 , 543 , and 545° . The vapor pressures were calculated from these weight loss data by means of the Knudsen effusion equation. In addition, inspection of the cell contents was made after each run. A discontinuity in the slope of $\log P$ vs. $1/T$ was found to occur at approximately 542° . Inspection of the BeF_2 in the cell after the run at 541° showed no fusion had occurred. The BeF_2 after the 543° run, however, had completely fused. The combination of discontinuity in the slope of $\log P$ vs. $1/T$ coupled with physical inspection of the BeF_2 samples establishes the melting point of BeF_2 as $542 \pm 3^\circ$, in excellent agreement with the value reported by Roy, Roy, and Osborn⁷ ($543 \pm 5^\circ$) obtained by differential thermal analysis.

B. Vapor Pressure of BeF_2 .—The vapor pressure of BeF_2 was studied initially over the temperature range 550 – 780° at 10° intervals by means of the Knudsen gravimetric effusion procedure. The results of these runs in terms of rate of weight loss and partial pressures are listed in Table I. Five different effusion cells with varying orifice areas were used with frequent duplication of temperature points to assure that the experimental data were independent of orifice area. The cells employed had from one 1-mm. hole to four 3-mm. holes. Comparison of the data from these cells is presented in Table II. From these data it can be seen that the vapor pressures are independent of orifice area. The Clausing factors for each cell were calculated from the hole dimensions which were determined to within 5 parts in 10,000 and are presented in Table III.

For the calculations of the vapor pressure of BeF_2 the modified Knudsen equation

$$P_{\text{min}} = 17.14 \frac{G}{W_0 a} (T/M)^{1/2} \quad (1)$$

TABLE I
WEIGHT LOSS AND PRESSURE DATA FOR $\text{BeF}_2(l)$ FROM GRAVIMETRIC EFFUSION STUDIES

Temp., $^\circ\text{K.}$	Rate of wt. loss, (g./sec.) $\times 10^6$	Pressure, mm. $\times 10^3$	Temp., $^\circ\text{K.}$	Rate of wt. loss, (g./sec.) $\times 10^6$	Pressure, mm. $\times 10^3$
1053	116 ^a	1730	933	5.8 ^a	82
1043	83 ^a	1220	924	4.0 ^a	56
1034	73 ^a	1080	923	69 ^b	50
1023	72 ^a	1060	913	44 ^b	32
1013	47 ^a	690	903	33 ^b	24
1004	43 ^a	620	893	22 ^b	16
1002	39 ^a	560	883	18 ^b	13
993	30 ^a	440	874	14.3 ^b	10.2
983	21 ^a	300	863	10.4 ^b	7.3
973	15 ^a	210	853	8.3 ^b	5.9
963	14 ^a	200	843	4.5 ^b	3.2
953	10.2 ^a	145	834	3.7 ^b	2.5
943	7.2 ^a	101	823	2.1 ^b	1.5

^a Effusion cell has one 1-mm. hole. ^b Effusion cell has four 2-mm. holes.

TABLE II
VAPOR PRESSURE OF BeF_2 FOR CELLS OF VARIOUS ORIFICE AREAS

Temp., $^\circ\text{K.}$	Cell	Pressure, mm. $\times 10^2$	Temp., $^\circ\text{K.}$	Cell	Pressure, mm. $\times 10^2$
883	d	1.30	943	a	10.1
892	c	2.1	943	c	11.8
893	d	1.61	953	a	14.5
903	d	2.4	953	b	11.7
913	d	3.2	964	a	20
923	b	4.8	963	c	20
923	d	5.0	923	a	21
923	c	5.3	983	a	30
923	a	5.6	993	a	44
933	a	8.2			

TABLE III
GEOMETRICAL FACTORS OF EFFUSION CELLS

Cell	Description	$1/a$	Clausing factor	Area, $\text{cm.}^2 \times 10^3$
a	1 hole \times 1 mm. diam.	1.00	0.6720	8.107
b	2 hole \times 1 mm. diam.	1.00	.6720	16.214
c	4 hole \times 1 mm. diam.	1.00	.6720	32.43
d	4 hole \times 2 mm. diam.	0.80	.8013	129.72

was employed to yield P directly in mm., where G is given in grams of material effusing during the length of the run, W_0 is the Clausing factor, a is the orifice area, and M is the molecular weight of effusing species. Farber and Darnell¹⁰ showed that it is possible to ascertain that the pressure calculated from eq. 1 is the equilibrium pressure

$$P_{\text{eq}} = P \left(I + \frac{a}{\alpha A_t} \right) \quad (2)$$

where A_t is the surface area of material and α is the accommodation coefficient by using several different orifice to surface area ratios. The present work essentially follows this experimental procedure since five effusion cells with varying orifice areas were employed (a/A_t ratios varying from 1 to 36).

During each run at a given temperature a minimum of five observations were made on the position of the helix. A line of the form $v = at + b$ was fitted to the data by the least squares method. The rate of change of the length of the helix, a , was multiplied by the reciprocal of the sensitivity to obtain the rate of weight

of loss per unit time. A temperature reading was taken concurrently with the observation of the helix. The average of the temperature readings was used for the value of the temperature. The molecular weight of the effusing vapor was assumed to be the molecular weight of BeF_2 , 47.0 g./mole.

The Clausing factor calculated from the ratio of the length of the effusion hole to the radius was found to be in good agreement with that obtained from a direct measurement of the vapor pressure of zinc metal.⁸ The Clausing factor used and the values for the ratio of the length of the effusion hole (l) to the radius (a) are listed in Table III for each cell. The corrections for mean free path in the effusion cell are negligible at the lower temperatures where the vapor pressures are of the order of 10^{-8} atm. At the high end of the temperature range where the pressures were of the order of 10^{-5} to 10^{-4} atm. the corrections to the vapor pressure range between 1 and 2%.

A summary of the effusion data is shown in Table I. The least squares plot of ΔF vs. T yields a value of 38.7 ± 0.6 cal./deg./mole for ΔS_{vap} . The van't Hoff calculation from a least squares plot of $\log P$ vs. $1/T$ of the experimental data leads to a value for ΔH_{vap} of 53.22 ± 0.18 kcal.

The experimental determination of the vapor pressure of BeF_2 (liquid) was extended to a temperature range between 850 and 950° by means of the transpiration method.

It is necessary in a transpiration experiment to establish equilibrium definitely.^{11,12} Low flow rates may cause diffusion of material in and out of the reaction zone, causing high weight losses. If the flow rate is too fast, insufficient time is available for establishment of the equilibrium; therefore a non-steady state rate of vaporization is obtained, resulting in a low weight loss per unit volume.

In order to establish the equilibrium flow rate,^{11,12} a series of runs was made at 930° using different flow rates. The trial flow rates were in the range of 2.5 to 16.5 cc. per min. of argon. As the flow rate was increased up to 10 cc./min. the weight loss per unit volume of gas (and thus the vapor pressure) decreased. In the range of 10 to 14 cc. per min. the vapor pressure measured was constant within experimental error. For flow rates higher than 14 cc. the weight loss was found to decrease as the flow rate increased. These results are presented in Fig. 2. Table IV presents the transpiration results for the vapor pressure of BeF_2 obtained in the temperature interval of 850–950°. These data are shown on the vapor pressure plot (Fig. 1)

TABLE IV
VAPOR PRESSURE OF LIQUID BeF_2 FROM TRANSPARATION EXPERIMENTS

Temp., °K.	Pressure, ^a mm.	Pressure, ^b mm.
1223	50.2	50.5
1198	36.2	36.5
1173	22.1	20.5
1148	11.6	12.1
1123	8.7	7.8

^a Transpiration experiment. ^b Extrapolated values from effusion experiment.

(11) M. Farber and A. J. Darnell, *J. Chem. Phys.*, **23**, 1460 (1955).

(12) M. Farber, *ibid.*, **36**, 661 (1962).

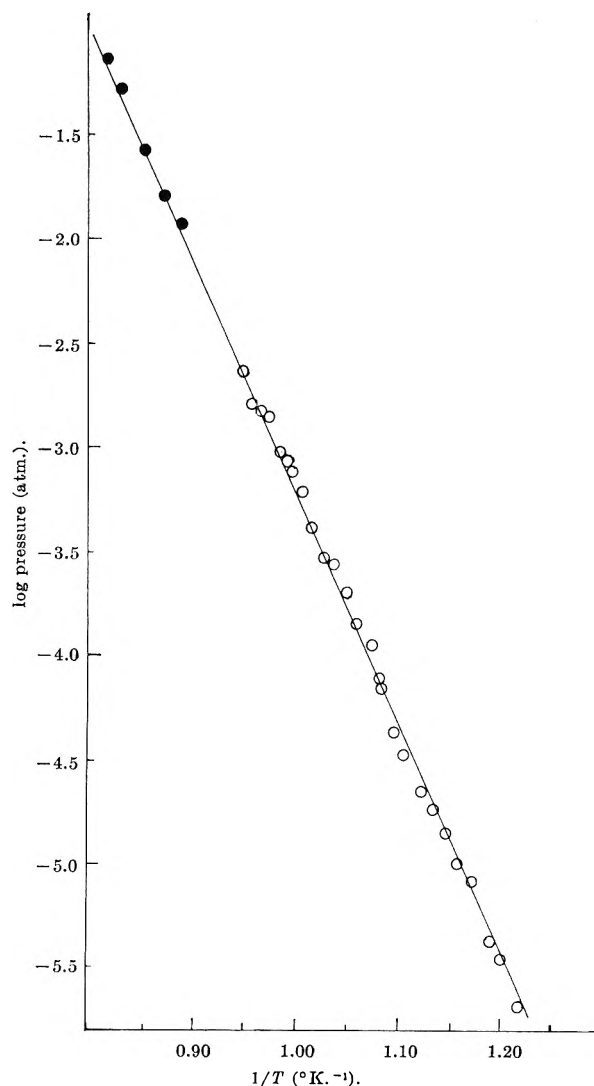


Fig. 1.—Vapor pressure of $\text{BeF}_2(l)$ as a function of temperature: O, effusion method; ●, transpiration method.

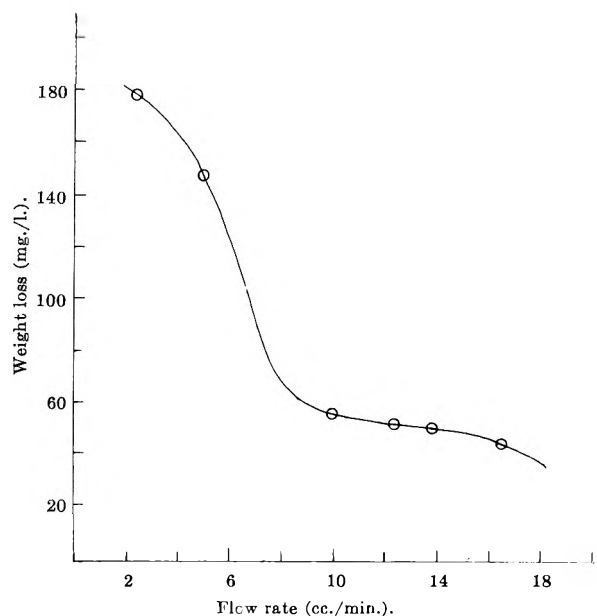
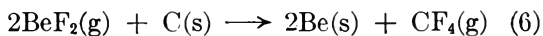
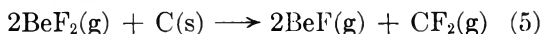
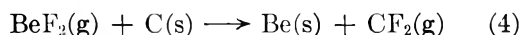


Fig. 2.—Weight loss of BeF_2 as a function of argon flow rate. as a temperature extension of the effusion experiments. They are in good agreement with the enthalpy and entropy data reported.

C. Vapor Species over Liquid BeF_2 .—The ΔH_{vap} value was based on the assumption that all vapor

effusing from the cells was, in fact, BeF_2 , and that no dissociation, association, or chemical reaction occurs. Preliminary calculations at a temperature of 1300°K . show no significant dissociation of BeF_2 occurring at the pressures encountered in this work. These calculations were based on an experimental value for the heat of formation of BeF of -45 ± 2 kcal./mole recently determined at this Laboratory.¹³

The possibility for producing effusion vapors other than pure BeF_2 exists through the reaction of BeF_2 with the carbon of the cell. Among possible reactions are



These reactions could lead to values for M above and below the value of 47 of BeF_2 . If, however, any reactions were occurring between BeF_2 and the graphite effusion cell, visual indications of this would be discernible. No signs of attack on the carbon could be observed, however. Further, accurate measurements of the orifice dimension (using a measuring microscope) of the effusion cells after extensive use showed that within the accuracy of measurement (1 part in 1000) no change in dimensions had occurred. Since reaction of BeF_2 with the cell almost certainly would have led to erosion of the orifices, it seems fairly safe to say that no such reactions occurred.

Brewer¹⁴ has reported that BeCl_2 , BeBr_2 , and BeI_2 are appreciably associated in the temperature region in which the current experiments have been carried out, and that BeF_2 might associate in the gas phase appeared as a possibility. If association of BeF_2 were occurring, not only would absolute values of vapor pressure be in error, but the slope of the plot of $\log p$ vs. $1/T$, and consequently the ΔH_{vap} value, could be in error. The effect on the slope would result from the sensitivity of association to temperature, thus shifting all vapor pressure values a non-constant amount.

The value for the heat of vaporization of BeF_2 reported above is based on the experimental data obtained using the Knudsen gravimetric effusion and transpiration techniques. The vapor pressure values calculated from the Knudsen equation depend upon the molecular weight (M) of the effusing vapor. The

(13) M. Greenbaum, R. Yates, L. Arin, M. Arshadi, J. Weiher, and M. Farber, unpublished data.

(14) L. Brewer, Metal. Lab. Report CC-3455, National Bureau of Standards.

original values for P in the temperature range 550 – 780° were calculated on the assumption that M was equal to 47.0, the molecular weight of BeF_2 . However, to confirm this fact, torsion experiments were carried out to determine the average molecular weight of the species effusing from the cells at the experimental temperatures.

The torsion effusion technique provides a direct measurement of the pressure exerted by a vapor effusing from an orifice and has been employed previously to study vapor pressures of a variety of compounds.^{15–25} The sample is enclosed in an effusion cell suspended from a fine wire or fiber and the vapor is allowed to stream out in a horizontal direction from two eccentrically located holes. This effusion of vapors imparts a torque to the effusion cell. The angle through which the cell rotates is observed with a cathetometer and the vapor pressure is calculated, in dynes/cm.², from the equation

$$P = \frac{2DB}{\sum a_i f_i q_i} \quad (7)$$

where P is the vapor pressure in dynes/cm.², D is the torsion constant of suspension in (dyne-cm.)/radian, B is the angle of deflection in radians, a_i is the cross-sectional area of hole i in cm.², f_i is the Searcy correction factor (the force exerted by effusing molecules depends on the number escaping from an orifice and upon their radial distribution), and q_i is the horizontal distance of hole i from suspension in cm. (moment arms).

Since the vapor pressure calculated from the torsion equation (7) is independent of the molecular weight of the effusing vapor, it is possible to calculate the average molecular weight of effusing vapors by the use of both effusion procedures. Using the torsion effusion technique, vapor pressures were measured for BeF_2 between 550 and 610° . These values then were substituted into the gravimetric effusion equation and the values of M calculated. Over the temperature range investigated, the average value obtained for M was 44.7 ± 2.0 . On the basis of these results it is possible to conclude reasonably that no association of BeF_2 is occurring in this temperature range.

(15) M. Volmer, *Z. physik. Chem. Boden. Fest.*, **863** (1931).

(16) K. Neumann and E. Volker, *Z. physik. Chem.*, **A767**, 33 (1932).

(17) K. Neumann and E. Lichtenberg, *ibid.*, **A184**, 89 (1939).

(18) K. Nina and Z. Sibata, *J. Chem. Soc. Japan*, **61**, 660 (1940).

(19) K. Nina, *ibid.*, **61**, 770 (1940).

(20) K. Nina and M. Yoshiyama, *ibid.*, **61**, 1055 (1940).

(21) M. Yoshiyama, *ibid.*, **62**, 204 (1941).

(22) G. Wessel, *Z. Physik.*, **130**, 539 (1951).

(23) A. W. Searcy and R. D. Freeman, *J. Am. Chem. Soc.*, **76**, 5229 (1954).

(24) A. W. Searcy and R. D. Freeman, *J. Chem. Phys.*, **23**, 88 (1955).

(25) R. D. Freeman and A. W. Searcy, *ibid.*, **22**, 762 (1954).

DISSOCIATION OF METHACRYLIC ACID RESINS

BY AMALESH CHATTERJEE¹ AND JACOB A. MARINSKY²*Department of Chemistry, University of Buffalo, Buffalo, N. Y.**Received February 6, 1962*

The electrolytic dissociation of two differently cross-linked polymethacrylic acid resins has been investigated. Its water absorption properties and its potentiometric behavior have been measured for this purpose. The basic Gibbs-Donnan equation for a membrane equilibrium in the presence of a hydrostatic pressure has been combined with the theoretical treatment of polyelectrolytes due to Katchalsky and co-workers to examine the data. An equation is developed in which the potentiometric and water absorption behavior of the gel is well described. An intrinsic dissociation constant of 5.16 ± 0.35 is calculated for the monomeric unit of the gel. This value is in good agreement with the 4.86 value obtained by earlier workers for linear and very low cross-linked polymethacrylic acid.

Introduction

An attempt has been made in the present investigation to evaluate the intrinsic dissociation constant of a 1 and 5% copolymer of divinylbenzene and methacrylic acid.³ Potentiometric titrations and water absorption measurements have been made in order to facilitate the investigation. Measurements of this nature have been reported previously by other investigators. See, *e.g.*, Gregor and Bregman,⁴ Kunin and Barry,⁵ Michaeli and Katchalsky,^{6,7} Gregor,⁸ Gregor, *et al.*,⁹ Howe and Kitchener,¹⁰ Hale and Reichenberg,¹¹ and Fisher and Kunin.¹²

The Henderson-Hasselbach equation, $\text{pH} = \text{p}K_a - n \log ((1 - \alpha)/\alpha)$, where α is the degree of neutralization, n is a constant characteristic of a given system, and K_a is the apparent or average ionization constant, was employed by Gregor⁹ to consider and compare the titration of methacrylic acid resins with linear polyacids. The postulate was made that the pH of the solution outside of the polymer coils was being measured for both the soluble as well as the cross-linked materials, thereby attributing equal significance to the pH measurement. Parallel behavior of both systems was observed, but the cross-linked acids were found to be apparently weaker at the same salt concentration. This was attributed to imbibement of salt by the gel systems, negating the initial postulate.

Gregor also observed that the apparent dissociation constant of the cross-linked acids decreased with increasing degrees of cross-linking. Fisher and Kunin,¹² using the Henderson-Hasselbach equation, confirmed this result. Divinylbenzene and several other vinyl compounds were used as cross-linking agents in their study. The magnitude of the change was observed to depend on the mole percentage of acrylate in the polymer. The limiting values of $\text{p}K_a$ as cross-linking reagent was reduced to zero equaled the $\text{p}K_a$ value of the linear polymers of the corresponding acids.

The limitation of the Henderson-Hasselbach equation is that it contains the two parameters, $\text{p}K_a$ and n ,

which vary with ionic strength, n approaching unity and K decreasing to a limiting $\text{p}K_a$ value at higher ionic strength. In addition, no correction term for the equilibrium distribution of neutral electrolyte between gel and solvent phases is provided to differentiate linear and cross-linked polyacid behavior.

A more general analysis of gel systems, which leads to an "intrinsic" dissociation constant characteristic of the ionizable group of the polymer and independent of ionic strength, degree of dissociation, and cross-linking, was shown to be valid for polymethacrylic acid of very low cross-linking by Katchalsky and co-workers,¹³ who employed a modified statistical treatment of polyelectrolytes for this purpose. Two alternate treatments of Donnan invasion of the gel by electrolyte were incorporated by Michaeli and Katchalsky⁶ to account for the effect of the presence of a neutral salt on the potentiometric properties of the solution. Successful use of polyelectrolyte theory has most recently been made by Kuhn, Ebner, Kuhn, and Walters¹⁴ to obtain the intrinsic dissociation constant for differently cross-linked polyacrylic acid gels prepared by them for study in $10^{-3} N$ NaCl.

Howe and Kitchener,¹⁰ however, were unable to make the statistical theory of polyelectrolyte gels quantitatively applicable to their more concentrated gel systems, which were similar to those employed in this investigation, even though they controlled the preparation of their samples and were aware of parameters necessary for employment in the Katchalsky treatment.

It is believed that the present treatment which follows has led to the first quantitative interpretation of potentiometric and water absorption data obtained with relatively highly cross-linked, commercially produced polymethacrylic acid. An intrinsic $\text{p}K$ value that is independent of cross-linking, degree of dissociation, and ionic strength results from the treatment. The basis for its calculation, the Gibbs-Donnan equation for a membrane equilibrium in the presence of a hydrostatic pressure,^{15a,b} is presented below for the ion-exchange reaction involving the replacement of H_3O^+ ion by Na^+ ion

$$\ln \frac{(m_{\text{H}_3\text{O}^+})(m_{\text{Cl}^-})(\gamma_{\text{H}_3\text{O}^+})(\gamma_{\text{Cl}^-})}{(m_{\text{Na}^+})(m_{\text{Cl}^-})(\gamma_{\text{Na}^+})(\gamma_{\text{Cl}^-})} = \frac{(\bar{m}_{\text{H}_3\text{O}^+})(\bar{m}_{\text{Cl}^-})}{(\bar{m}_{\text{Na}^+})(\bar{m}_{\text{Cl}^-})} \frac{(H_3O^+)(Cl^-)}{(Na^+)(Cl^-)} + \frac{\Pi}{RT} (\bar{V}_{\text{HCl}} - \bar{V}_{\text{NaCl}}) \quad (1)$$

(1) Postdoctoral Fellow, 1960-1961. On leave of absence from Vidyasagar College, Calcutta, India.

(2) Correspondence to be addressed to this author.

(3) Amberlite IRC-50, a product of Rohm and Haas Co., Philadelphia, Pa.

(4) H. P. Gregor and J. I. Bregman, *J. Am. Chem. Soc.*, **70**, 2370 (1948).

(5) R. Kunin and R. E. Barry, *Ind. Eng. Chem.*, **41**, 1269 (1949).

(6) I. Michaeli and A. Katchalsky, *J. Polymer Sci.*, **23**, 683 (1957).

(7) A. Katchalsky and I. Michaeli, *ibid.*, **15**, 69 (1955).

(8) H. P. Gregor, *J. Am. Chem. Soc.*, **73**, 642 (1951).

(9) H. P. Gregor, M. J. Hamilton, J. Becker, and F. Bernstein, *J. Phys. Chem.*, **59**, 874 (1955).

(10) P. G. Howe and J. A. Kitchener, *J. Chem. Soc.*, 2143 (1955).

(11) D. K. Hale and D. Reichenberg, *Discussions Faraday Soc.*, **7**, 79 (1949).

(12) S. Fisher and R. Kunin, *J. Phys. Chem.*, **60**, 1030 (1956).

(13) A. Katchalsky, N. Shavit, and H. Eisenberg, *J. Polymer Sci.*, **13**, 69 (1954).

(14) W. Kuhn, G. Ebner, H. J. Kuhn, and D. H. Walters, *Helv. Chim. Acta*, **43**, 502 (1960).

(15) (a) F. G. Donnan and E. A. Guggenheim, *Z. Physik Chem.*, **162A**, 356 (1932); (b) F. G. Donnan, *ibid.*, **168A**, 369 (1934).

In this equation m refers to molal concentrations, γ is the ionic activity coefficient, \bar{V} represents the partial molal volume of electrolyte, and Π is the contractile pressure of the resin network. A bar placed over all terms on the right-hand side of the equation identifies the particular function with the resin phase.

The cross-linked resin gel may be considered to contain n_m monomeric units associated with n_m carboxylic groups arranged in chains of z monomeric units that extend from one cross-linking point to the next. The product of the number of chains (n_p) and monomer units per chain (z) defines the resin macromolecule (R).

Dissociation of the macromolecule, $H_{n_p z}R$, is governed by the usual laws of equilibrium and may be described in $n_p z$ dissociation constants

$$\ln k_1 = \ln \frac{R(\bar{m}_{H_3O^+})}{HR}; \ln k_2 = \ln \frac{HR(\bar{m}_{H_3O^+})}{H_2R}$$

$$\ln k_{n_p z} = \frac{H_{n_p z-1} R(\bar{m}_{H_3O^+})}{H_{n_p z} R} \quad (2)$$

Since the $n_p z$ dissociating sites are identical, they may be assumed to have little effect upon one another and the $n_p z$ conventional equilibrium constants can then be related to a single equilibrium constant K_{HR} by

$$\ln K_{HR} = \ln \frac{\alpha}{1-\alpha} (\bar{m}_{H_3O^+}) \quad (3)$$

where α is the degree of dissociation at any dissociation site.¹⁶

The above constant is not a true constant, expressed in terms of concentration as it is, and terms are included in eq. 4 to allow for deviation of the free energy of the hydrogen ion ($\gamma_{H_3O^+}$) and the polyanion ($1/kT(\partial F_e/\partial \nu)_\kappa$) from that of the idealized mixture

$$\ln K_{HR} = \ln \frac{\alpha}{1-\alpha} (\bar{m}_{H_3O^+}) +$$

$$\ln \bar{\gamma}_{H_3O^+} + \frac{1}{kT} \left(\frac{\partial F_e}{\partial \nu} \right)_\kappa \quad (4)$$

where F_e is the electrostatic free energy of the ionized polyanion carrying ν negatively charged groups, and κ is the inverse Debye radius¹⁷ determined by the concentration of the small ions in the resin phase.

Rearranging eq. 4

$$\ln \bar{m}_{H_3O^+} \bar{\gamma}_{H_3O^+} = \ln K_{HR} -$$

$$\ln \frac{\alpha}{1-\alpha} - \frac{1}{kT} \left(\frac{\partial F_e}{\partial \nu} \right)_\kappa \quad (5)$$

and substituting eq. 5 in eq. 1

$$\ln \frac{(m_{H_3O^+})(\gamma_{H_3O^+})}{(m_{Na^+})(\gamma_{Na^+})} = \ln K_{HR} - \ln \frac{\alpha}{1-\alpha} +$$

$$\ln \frac{1}{\bar{m}_{Na^+} \bar{\gamma}_{Na^+}} - \frac{1}{kT} \left(\frac{\partial F_e}{\partial \nu} \right)_\kappa + \frac{\Pi}{RT} (\bar{V}_{HCl} - \bar{V}_{NaCl}) \quad (6)$$

(16) C. Tanford, "Physical Chemistry of Macromolecules," John Wiley and Sons, Inc., New York, N. Y., 1961, pp. 532-535.

(17) The reciprocal of Debye's radius is given by $\kappa^2 = 4\pi^2 \sum n_i z_i^2 / DkT$, where n_i is the number per ml. of ions of type i each carrying z_i elementary charges, $\sum n_i z_i$ is the sum of all small ions in the gel phase, ϵ is the charge of the electron, D is the dielectric constant of the medium, k is Boltzmann's constant, and T is the temperature in $^\circ K$.

Further simplification of eq. 6 yields

$$\ln (m_{H_3O^+})(\gamma_{H_3O^+}) = \ln K_{HR} - \ln \frac{\alpha}{1-\alpha} +$$

$$\ln \frac{m_{Na^+} \gamma_{Na^+}}{\bar{m}_{Na^+} \bar{\gamma}_{Na^+}} - \frac{1}{kT} \left(\frac{\partial F_e}{\partial \nu} \right)_\kappa + \frac{\Pi}{RT} (\bar{V}_{HCl} - \bar{V}_{NaCl}) \quad (7)$$

$$\log a_{H_3O^+} = \log K_{HR} - \log \frac{\alpha}{1-\alpha} + \log \frac{a_{Na^+}}{\bar{a}_{Na^+}} -$$

$$\frac{0.4343}{kT} \left(\frac{\partial F_e}{\partial \nu} \right)_\kappa + \frac{0.4343\Pi}{RT} (\bar{V}_{HCl} - \bar{V}_{NaCl}) \quad (8)$$

$$pH = pK_{HR} - \log \frac{1-\alpha}{\alpha} + \log \frac{\bar{a}_{Na^+}}{a_{Na^+}} +$$

$$\frac{0.4343}{kT} \left(\frac{\partial F_e}{\partial \nu} \right)_\kappa + \frac{\Pi \cdot 0.4343}{RT} (\bar{V}_{NaCl} - \bar{V}_{HCl}) \quad (9)$$

The form of eq. 9 is comparable with that of the general relation that is obtained from the theoretical treatment of Michaeli and Katchalsky for a similar system.⁶

The electrostatic free energy and contractile pressure terms and the activity coefficient of the Na^+ ion in the gel phase are the only parameters of eq. 9 that are not easily accessible for the evaluation of the intrinsic dissociation constant of the acid form of the resin. The quantitative relation between the degree of dissociation of the resin and the pH of the external equilibrium solution is determinable by controlled neutralization of the acid form of the exchanger in the presence of electrolyte at constant ionic strength. The activity coefficient of the Na^+ ion in the equilibrating solution is calculable from published mean activity coefficient values for the electrolyte.¹⁸

Contractile Pressure Term.—The contractile pressure for the cross-linked ion-exchange resin may be computed according to eq. 10.^{8,19}

$$\Pi = \frac{RT}{\bar{V}_w} \ln \left(\frac{a_w'}{a_w} \right) \text{ at constant } N_m \quad (10)$$

where \bar{V}_w is the partial molal volume of the water, a_w' is the activity of the water in the cross-linked exchanger, a_w is the activity of the water in a chemically identical exchanger without cross-linking, and N_m is the weight normality ($1000/\text{g. H}_2\text{O} \times \text{equiv.}^{-1}$) at the respective water activity values. Proper use of this equation requires that values of a_w' that are encountered in a cross-linked exchanger be compared with a_w values for the chemically identical unrestrained resin containing exactly the same amount of water per equivalent. The uptake of water by a completely unrestrained resin is, however, not experimentally measurable and the standard procedure has been to use a_w values that are obtained as a function of N_m in isopiestic vapor pressure experiments with the most weakly cross-linked exchanger that will permit valid measurement of this resin property.²⁰

In this investigation an estimate of this property of the hypothetically unrestrained exchanger has been

(18) R. A. Robinson and R. H. Stokes, "Electrolyte Solutions," Butterworth Scientific Publications, London, England, 1959.

(19) G. E. Boyd and B. A. Soldano, *Z. Elektrochem.*, **57**, 162 (1953).

(20) E. Glueckauf, *Proc. Roy. Soc. (London)*, **214**, 207 (1952).

made by using eq. 11 given below to convert practical osmotic coefficient values experimentally determined by Alexandrowicz²¹ for dilute solutions of polymethacrylic acid and computed for the more concentrated polymethacrylate systems encountered by employing the theoretically based equations due to Lifson and Katchalsky.²²

For an aqueous solution¹⁸

$$\nu\phi = - \frac{\log a_w}{m(0.03782)} \quad (11)$$

ϕ being the practical osmotic coefficient and ν the number of ions in solution. The polyelectrolyte solutions of interest are 1, n electrolytes where n is very large as a consequence of the large number of positive charges due to the polyanion. The colligative properties of the solution are, as a result, almost exclusively determined by the mobile counterions and ν in this case is very close to unity.^{19, 20, 23}

Comparison between the cross-linked exchanger and the polyelectrolyte solution is presumed in this treatment to be valid after correcting for the differences in their free energies of swelling, *i.e.*, it is assumed that the cross-linking of the resin does not change the thermodynamic properties of the polyelectrolyte. The convergence that is observed in the experimental program for the isopiestically derived osmotic curves for the 1 and 5% cross-linked resin at moderately low water activity support this postulate.

Activity Coefficient of Mobile Counterion.—It has been shown by Alexandrowicz²¹ that for solutions of polymethacrylic acid and sodium bromide in which $\alpha m_{NaBr} \gg m_{NaBr}$, the activity coefficient of the salt approaches the value of ϕ_p , the practical osmotic coefficient of the polyelectrolyte. By presuming the same behavior in the cross-linked polymethacrylic acid-sodium chloride system that was investigated by us and by limiting the equilibration experiments to sodium chloride concentrations no greater than 0.3 *m* to minimize electrolyte invasion, the activity coefficient of Na⁺ ion in the resin phase can be identified with the computed ϕ_p values.²²

Electrostatic Free Energy Term.—Estimate of the electrostatic free energy term of the polyanion is made using the equation of Katchalsky, Shavit, and Eisenberg¹³ that is derived using a randomly kinked molecule model.

Experimental

Materials.—The weakly acidic cation exchanger, Amberlite IRC-50, a product of the Rohm and Haas Co., Philadelphia, Pa., was employed in the experimental program. Resin samples containing approximately 1 and 5% divinylbenzene as the cross-linking agent for the polymethacrylic acid were used in a parallel series of experiments. The 1% cross-linked resin, consisting of large irregularly shaped beads, was converted to the salt and acid forms several times with normal NaOH and HCl prior to use. Finally, it was washed with de-ionized water until free from imbibed electrolyte and was stored over saturated NH₄NO₃. The 5% cross-linked resin was obtained in reagent grade form and was not subjected to any pretreatment.

The exchange capacity of the resin was determined either by adding standard alkali to a weighed quantity of the dry acid form of the resin and back titrating the excess alkali or by pH titration. The dry weight of the resin was determined by heating aliquot portions of the moist resin to constant weight at 60° over silica gel and under vacuum.

Reagent grade sodium chloride and sodium hydroxide were purchased from the J. T. Baker Co. and were used without further purification. Carrier-free 2.6 yr. Na²² was purchased from the Nuclear Science and Engineering Corporation. Pyrex vessels were used in all the experiments.

Equilibrium Procedure.—The equilibration was carried out by adding weighed samples of dry resin to standard sodium chloride solution containing a known amount of the 2.6 yr. Na²² nuclide. Accurately measured quantities of NaOH were added to attain the desired degree of conversion to the salt form. The solutions were then diluted to a volume of 50.00 ml. and a final NaCl concentration of 0.10 or 0.30 *m*. The fractional sodium content of the resin samples that were employed ranged from about 0.01 to as high as 1.0. The stoppered samples were shaken gently at the ambient room temperature during the equilibration procedure.

The H₃O⁺ ion in solution was determined by pH measurement. The Na⁺ ion concentration, already accurately known from the design of the experiment, was checked by radiometric analysis of Na²² in both phases. The pH measurement of the equilibrium mixtures was made while nitrogen gas passed over the surface of the solutions to prevent dissolution of CO₂ from the atmosphere. For the Na⁺ ion measurement, the resin beads were separated from the solution by centrifugation-filtration. The solution was decanted into a glass cylinder fitted with a fritted glass disk and supported in a 50-ml. centrifuge tube by means of constrictions near its bottom. After filtration of most of the solution by a brief centrifugation, the resin beads were quantitatively transferred to the fritted glass cylinder in the centrifuge tube. Centrifugation for 1.5 to 2 hr. was needed to remove adhering supernatant solution as completely as possible. The centrifuge tubes were kept covered with Saran Wrap secured by rubber bands to prevent evaporation.

The centrifuged resin samples as well as the 2.0-ml. aliquot portions of the separated solution phase of each equilibrated sample were then transferred to test tubes and the Na²² activity present in each sample was measured in a 1.25 × 2 in. well-type thallium-activated sodium iodide crystal detector. The activity of 2.0-ml. aliquot samples of original solution containing the same quantity of the Na²² nuclide that was employed in the exchange reaction was also measured for comparison. Whenever necessary, solution volumes were modified to compare with resin volumes to avoid introduction of error due to different sample geometry.

Water Absorption Measurements—Static Method.—After analysis of the equilibrium mixtures, the resin samples were quantitatively transferred to weighed silver crucibles for the isopiestic vapor pressure experiments. The silver crucibles then were placed on a 0.5 in. thick copper plate inside a vacuum desiccator, together with a saturated solution of known water activity¹⁸ that was contained by a platinum dish. The high thermal conductivity that was ensured by this experimental arrangement minimized thermal gradients. The system was evacuated at the start of a measurement to hasten approach to equilibrium and was kept immersed in a thermostated water bath at a constant temperature of 25 ± 0.05°. After several weeks, N₂ gas passed through concentrated sulfuric acid and over desiccant CaCl₂ was bled into the desiccator slowly to remove the vacuum. On opening the desiccator, pre-weighed rubber stoppers were used to cover the samples, thereby preventing weight changes prior to and during the weighing of samples. The samples after weighing were uncapped and replaced in the desiccator, which was then resubmerged in the bath without evacuation. Weighings were repeated at regular intervals until constant weight of the samples was achieved.

The amount of water absorbed by the resin was determined from the calculated weight of the dry resin salt and total weight of the moist sample, since residual water tightly held by the salt-form of the resin was not removed in the drying procedure.

Dynamic Method.—Isopiestic equilibration with solution of high water activity (>0.98) was achieved relatively rapidly by passing N₂ gas previously equilibrated with vapor due to saturated K₂Cr₂O₇ solution over the resin samples. A Fisher-Porter flow meter measured the flow of N₂ gas from a cylinder into a series of gas-washing bottles that were packed with glass beads to keep the size of the bubbles small, thereby facilitating a more rapid approach to equilibrium of the liquid and gas phases. A check valve inserted into the line precluded the possibility of back-up of liquid. The first gas-scrubber contained 0.6 *M* NaCl solution; the others contained saturated K₂Cr₂O₇ as the reference solution

(21) Z. Alexandrowicz, *J. Polymer Sci.*, **43**, 325 (1960).

(22) S. Lifson and A. Katchalsky, *ibid.*, **13**, 43 (1954).

(23) W. Kern, *Z. physik. Chem.*, **181A**, 249, 283 (1938).

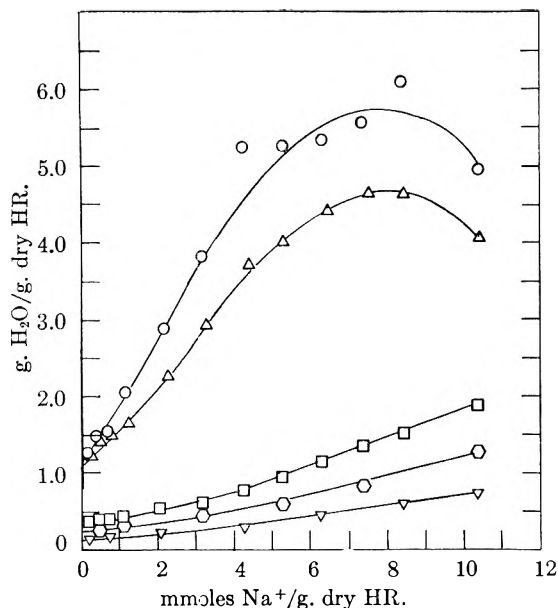


Fig. 1.—Water absorption properties of 1% cross-linked Amberlite IRC-50 in contact with: 0.1 *m* NaCl (—○—○—) and 0.3 *m* NaCl (—△—△—); isopiastically equilibrated with: saturated BaCl₂ (—□—□—), saturated NaCl (—○—○—), and saturated LiNO₃ (—▽—▽—).

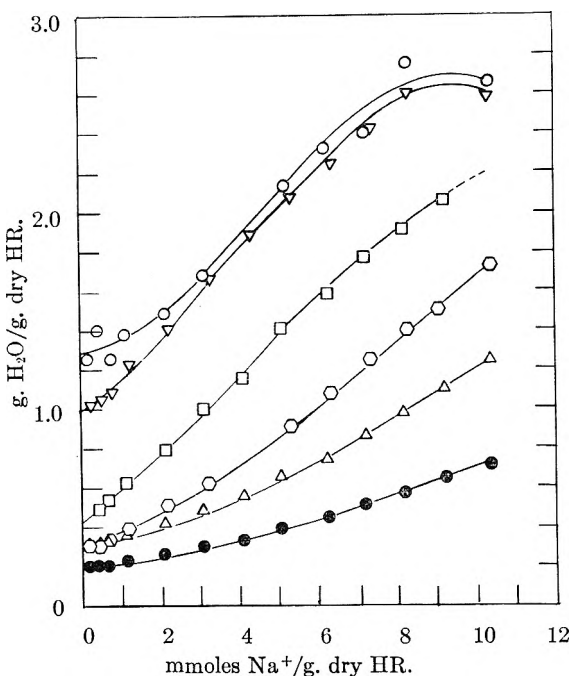


Fig. 2.—Water absorption properties of 5% cross-linked Amberlite IRC-50 in contact with: 0.1 *m* NaCl (—○—○—) and 0.3 *m* NaCl (—▽—▽—); isopiastically equilibrated with: saturated K₂Cr₂O₇ (—□—□—), saturated BaCl₂ (—○—○—), saturated NaCl (—△—△—), and saturated LiNO₃ (—●—●—).

and were completely submerged inside the thermostated water bath. Use of 0.6 *M* NaCl with a water activity about equal to that of the saturated reference solution in the first gas-washing bottle situated outside of the bath prevented evaporation of the reference solution in the next washing bottle, thereby preventing crystallization of K₂Cr₂O₇ and the possibility of restriction of gas flow through the system during an experiment. The level of water was maintained in the NaCl solution to keep its water activity reasonably constant. The N₂ gas, after leaving the last scrubber, passed into a large reservoir containing saturated K₂Cr₂O₇ solution to provide a large residence time for the gas in contact with the reference solution. The gas then passed through a glass wool filter which served to remove entrained liquid prior to its entry into a desiccator containing the resin samples and

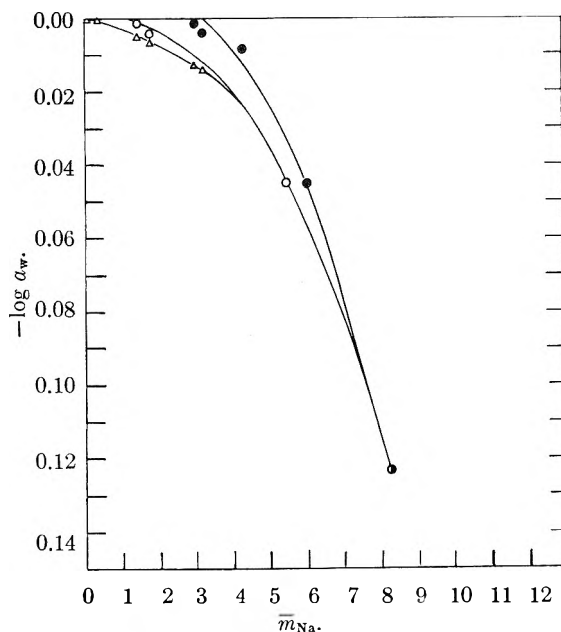


Fig. 3.—Plot of the logarithm of the water activity vs. the resin molality in the 80% dissociated gel: 5% cross-linked resin (—●—●—), 1% cross-linked resin (—○—○—), and hypothetical unrestrained resin (—△—△—).

saturated K₂Cr₂O₇ solution. Small stirrers extended into the reservoir and desiccator through pressure shielded sleeves assured uniform mixing of gas and water vapor prior to their removal to the atmosphere through another gas bubbler containing additional reference solution.

All connections in the above assembly were made with Pyrex glass and polyethylene tubing to avoid contamination of the flowing gas. Pyrex brand stopcocks and ball-joints were provided at the influent and effluent ends of the desiccator to facilitate withdrawal of the desiccator from the bath while keeping the remainder of the assembly immersed. Paraffin was used to ensure a water-tight seal of the desiccator cover.

At regular intervals the desiccator was taken out of the bath by disengaging the ball joints and the samples were weighed until constant weight of the samples was obtained.

Contact Method.—An alternative approach to the accurate estimate of water contained by resin in equilibrium with solution of high water activity employed direct contact of the dried resin salt with 0.1 and 0.3 *m* NaCl solutions. For these measurements an estimate of water absorption was first made by centrifugation-filtration of the equilibrated samples to constant weight. The separated resin samples were then redried over silica gel under vacuum at 60° to constant weight. Small, accurately weighed portions of 0.100 and 0.300 *m* NaCl were added to the dried resin samples and accurately weighed portions of additional water based upon the earlier determined absorption behavior were added to the samples so that at equilibrium the 0.1 and 0.3 *m* concentration would be nearly maintained. Analysis of the actual NaCl content of weighed portions of the supernatant liquid yielded an accurate estimate of the water absorbed by each resin sample.

Results and Discussion

Water Absorption Data.—The water absorption data that were obtained with the 1 and 5% cross-linked resin, respectively, are presented graphically in Fig. 1 and 2. The water contained per dry gram of resin is plotted as a function of the millimoles of sodium per dry gram of resin in these figures, the dry weight of resin initially in the hydrogen form being used as the reference state. The sodium content of these resin samples, controlled by varying the degree of neutralization employed in the sample preparation, extends over the complete salt-fraction range from about 0.01 to unity.

The two upper curves in these figures are based upon water absorption data that were obtained for sizable resin samples in contact with 0.1 and 0.3 *m* NaCl solu-

tions, respectively. They are S-shaped and resemble water absorption curves that have been reported previously for polymethacrylic acid resin.^{10,24} The curves obtained by using the static isopiestic method lose this characteristic shape at lower water activity, exhibiting a linear relationship between water and sodium content from 100 to 50% neutralization of the acidic form of the resin. The one curve obtained when the 5% cross-linked IRC-50 resin was equilibrated with saturated $K_2Cr_2O_7$ ($a_w = 0.9801$) by employing the dynamic isopiestic method parallels the two curves that were obtained by direct contact with the equilibrating solution, indicating that the shape of the curve is not affected by the method of equilibration that is employed.

Evaluation of the Activity Coefficient of Sodium in the Gel.—The resin molality values, \bar{m}_{Na^+} , that are computed from the water absorption data that were obtained for the 1 and 5% cross-linked resin samples at $\alpha = 0.8$ are plotted vs. the logarithm of the water activity in equilibrium with each resin sample in Fig. 3. The water activity properties of the hypothetical unrestrained resin (polymethacrylate solution) are also presented in Fig. 3 and show the contribution of the contractile pressure term, Π . The first two points in this curve are based on the osmotic measurements of Alexandrowicz.²¹ The remaining points are estimated from practical osmotic coefficient values computed with the theoretically derived equations of Lifson and Katchalsky.²² These equations²⁵ are based on a model of cylindrical symmetry that is assigned to the macromolecule in a fully stretched state. Justification for their use is the accurate prediction of osmotic coefficient values over a large range in α that their solution provides. Predicted and experimental ϕ values compare favorably with each other at α values as low as 0.2.

The osmotic coefficient values, ϕ_r , that are computed for the hypothetical unstrained resin at the monomer molalities encountered in the 1 and 5% cross-linked resins at the different neutralization values are plotted in Fig. 4 together with the experimental values due to Alexandrowicz.²¹ Those ϕ_r values are equated with the activity coefficient of the Na^+ ion in the gel phase ($\bar{\gamma}_{Na^+}$).²⁶

Estimate of the Contractile Pressure Term.—The contractile pressure that the 1 and 5% cross-linked resin

(24) H. P. Gregor, B. Sundheim, K. Held, and M. Waxman, *J. Colloid Sci.*, **7**, 511 (1952).

(25)

$$\phi = \frac{1 + \beta^2}{\lambda^2} - \frac{1}{R^2/a^2 - 1}$$

where

$$\lambda = \frac{\alpha \epsilon^2 / D b k T}{1 + |\beta| \cot |\beta| \ln \frac{R}{a}}$$

$$\ln R/a = \frac{1}{2} \ln \frac{1000}{\bar{V}_m} - \frac{1}{2} \ln m_{Na^+} = \gamma$$

$$R^2 = \frac{1000}{\Pi b m_{Na^+} L}$$

and

$$\alpha^2 = \frac{V_m}{\Pi b L}$$

R being the average mid-distance between 2 polymer rod centers, m_{Na^+} the monomeric polymer concentration, b the length of the monomer unit, a the radius of the monomolecular rod, L , Loschmidt's number, \bar{V}_m , the partial volume of the polymer in solution, and β a constant of integration in the solution of the differential equation for $\psi(r)$, the electrostatic potential of rod-like parallel polyelectrolyte molecules.

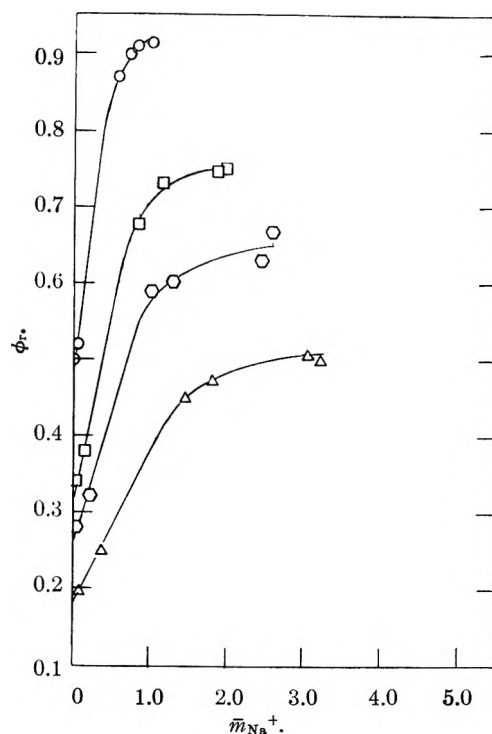


Fig. 4.—Plot of practical osmotic coefficient vs. resin molality: $\alpha = 0.1$ (—○—○—○—); $\alpha = 0.3$ (—□—□—□—), $\alpha = 0.5$ (—△—△—△—), and $\alpha = 0.8$ (—▽—▽—▽—).

endures when equilibrated with 0.1 and 0.3 m NaCl at different dissociation values has been estimated using eq. 10 and its variation with α is shown in Fig. 5. The value of Π decreases with decreasing α , approaching zero as α approaches zero. This behavior correlates well with the swelling data obtained by Katchalsky and Michaeli⁷ for loosely cross-linked polymethacrylate gels. The disappearance of the Π term is to be expected as the completely associated hydrogen form of the resin is approached.

The behavior of the Π term as a function of resin molality at a constant α value is shown in Fig. 6 for the two resins at three different α values. Points with curls attached are experimentally based; points not

(26) This treatment derives from the following precise description by Alexandrowicz²¹ of the experimental behavior of polymethacrylic acid-sodium bromide systems investigated by him

$$\lim_{m_{NaBr} \rightarrow 0} (\Delta \log \gamma_{NaBr}) = \log \phi_p$$

where

$$\begin{aligned} \Delta \log \gamma_{NaBr}(m_{NaBr}, m_m) &= \log \gamma_{NaBr}(m_{NaBr}, m_m) - \log \gamma_{NaBr}(m_{NaBr}, m_m = 0) \\ &= \log \gamma_{+Na^+}(m_{NaBr}, m_m) + \log \gamma_{-Br^-}(m_{NaBr}, m_m) - \log \gamma_{+Na^+}(m_{NaBr}, m_m = 0) - \log \gamma_{-Br^-}(m_{NaBr}, m_m = 0) \end{aligned}$$

Since experiment has shown that the addition of a polyelectrolyte does not appreciably change the activity coefficient of the by-ion^{27,28}

$$\gamma_{-Br^-}(m_{NaBr}, m_m) - \gamma_{-Br^-}(m_{NaBr}, m_m = 0) \approx 0$$

and

$$\begin{aligned} \Delta \log \gamma_{NaBr}(m_{NaBr}, m_m) &\sim \log \gamma_{+Na^+}(m_{NaBr}, m_m) - \log \gamma_{+Na^+}(m_{NaBr}, m_m = 0) \approx \Delta \log \gamma_{+Na^+}(m_{NaBr}, m_m) \end{aligned}$$

so that

$$\log \phi_p = \lim_{m_{NaBr} \rightarrow 0} (\Delta \log \gamma_{NaBr}) \approx \Delta \log \gamma_{+Na^+}$$

and

$$\log \phi_p = \log \gamma_{+Na^+}$$

(27) I. Kagawa and K. Katsura, *J. Polymer Sci.*, **9**, 405 (1952).

(28) M. Nagasawa, M. Izumi, and I. Kagawa, *ibid.*, **37**, 375 (1959).

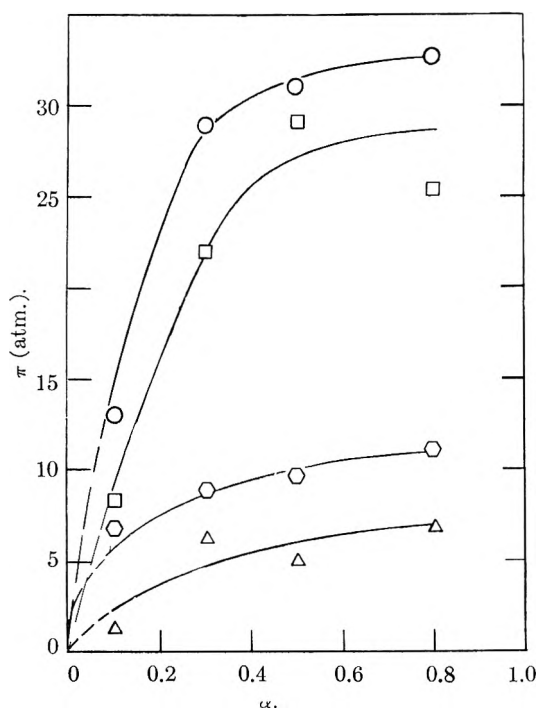


Fig. 5.—Plot of contractile pressure vs. degree of dissociation: 5% cross-linked resin equilibrated with 0.1 *m* NaCl (—○—○—○—) and 0.3 *m* NaCl (—□—□—□—); 1% cross-linked resin equilibrated with 0.1 *m* NaCl (—△—△—△—) and 0.3 *m* NaCl (—▽—▽—▽—).

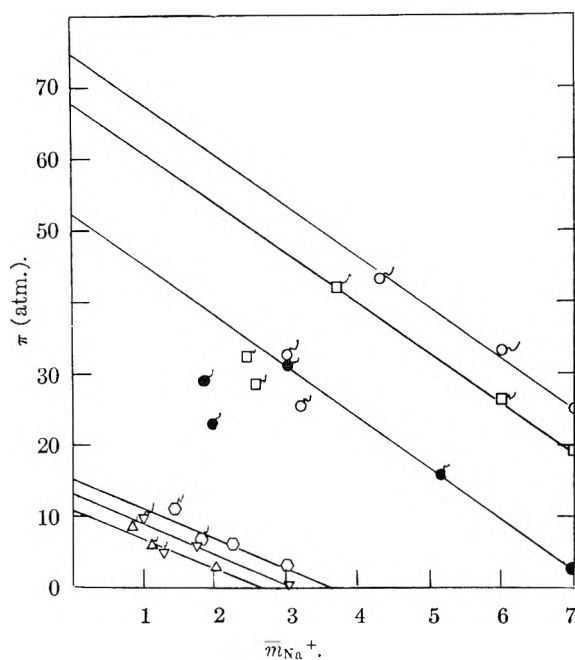


Fig. 6.—Plot of contractile pressure vs. resin molarity. 5% cross-linked resin: $\alpha = 0.8$ (—○—○—○—), $\alpha = 0.5$ (—□—□—□—), and $\alpha = 0.3$ (—△—△—△—); 1% cross-linked resin: $\alpha = 0.8$ (—○—○—○—), $\alpha = 0.5$ (—▽—▽—▽—), and $\alpha = 0.3$ (—△—△—△—).

designated in this manner are interpolated from the best smooth curves drawn through the experimental values (e.g., Fig. 3). The scatter of the first two points in each set of data may be attributed to uncertainty in the water absorption measurement made *via* direct contact of sample and equilibrating solution. The resin is a porous material²⁹ and physical sorption of solvent is a possible source of error in these points. A minor discrepancy in the water content measurement

(29) R. Kunin, "Porous Resins," Gordon Research Conference on Ion-exchange, June 29, 1961.

can produce a significant distortion of the Π value since the difference between two small numbers is involved in its calculation. The Π values that are obtained from the isopiastically based points and from the smooth curves are considered most reliable, and lines to represent the variation of Π with m_{Na^+} for the differently cross-linked resins consequently favor these points. The linear relationship that is observed is expected for an exchanger in which Hooke's law is obeyed.²⁰

TABLE I
THEORETICAL EVALUATION OF THE ELECTROSTATIC FREE ENERGY TERM

Degree of dissociation (α)	Electrostatic free energy $\left(\frac{0.4343}{kT} \left(\frac{\partial F_e}{\partial \alpha}\right)_\kappa\right)$
1% Cross-linked resin; 0.1 <i>m</i> NaCl	
0.8	0.66
.5	.43
.3	.28
.1	.11
1% Cross-linked resin; 0.3 <i>m</i> NaCl	
0.8	0.53
.5	.39
.3	.26
.1	.10
5% Cross-linked resin; 0.1 <i>m</i> NaCl	
0.8	0.43
.5	.29
.3	.20
.1	.095
5% Cross-linked resin; 0.3 <i>m</i> NaCl	
0.8	0.41
.5	.28
.3	.19
.1	.086

TABLE II
THE INTRINSIC DISSOCIATION CONSTANT OF CROSS-LINKED POLYMETHACRYLIC ACID

System	pH	$\log \frac{1-\alpha}{\alpha}$	$\log \frac{a_{Na}}{a_{Na^+}}$	$\frac{0.4343}{kT} \left(\frac{\partial F_e}{\partial \alpha}\right)_\kappa$	pK
IRC-50-1%; 0.1 <i>m</i> NaCl	7.20	-0.640	0.918	0.657	4.96
	6.40	-.008	.881	.431	5.08
	5.68	.363	.855	.278	4.91
	4.75	.935	.786	.110	4.79
IRC-50-1%; 0.3 <i>m</i> NaCl	6.80	-.635	.60	.527	5.04
	6.00	-.013	.55	.386	5.05
	5.45	.359	.583	.260	4.92
	4.5	.913	.475	.100	4.84
IRC-50-5%; 0.1 <i>m</i> NaCl	7.80	-.602	1.297	.425	5.48
	6.70	-.016	1.284	.290	5.11
	6.10	.359	1.252	.197	5.01
	5.22	.917	0.968	.0945	5.07
IRC-50-5%; 0.3 <i>m</i> NaCl	7.22	-.590	.878	.411	5.34
	6.27	-.015	.909	.283	5.06
	5.63	.344	.837	.192	4.94
	4.75	.891	.424	.086	5.13

The Electrostatic Free Energy Term.—The treatment of Katchalsky and Lifson³⁰ for estimating the electrostatic free energy of polyelectrolyte solutions

(30) A. Katchalsky and S. Lifson, *J. Polymer Sci.*, **11**, 409 (1953).

(31) The equation that is employed is

$$\frac{0.4343}{kT} \left(\frac{\partial F_e}{\partial \alpha}\right)_\kappa = \frac{2\alpha\epsilon^2}{DbkT} \log 1 + \frac{6}{\kappa sb}$$

where b is the hydrodynamic length of the monomer (2.55×10^{-8} cm.) and s is the number of monomers per statistical element.³⁴

using a randomly kinked model³¹ has been adopted to compute the electrostatic free energy term of eq. 9 for the systems investigated in this study. This model has proved useful in the interpretation of potentiometric measurements carried out on polymethacrylic solutions¹³ and gels⁶ and is similarly useful for correlation of the data compiled herein.

The values that have been computed for the electrostatic free energy term are presented in Table I.

The Intrinsic Dissociation Constant.—The experimental pH values corresponding to α values of 0.8, 0.5, 0.3, and 0.1 for the 1 and 5% cross-linked resins equilibrated with 0.1 and 0.3 *m* NaCl are listed in Table II together with the *pK* values that are computed from these potentiometric data. The various parameters

employed for this evaluation also are presented in the table. Only the swelling term of eq. 9 is neglected since the product of the contractile pressure, Π , and the partial molal volume difference ($\bar{V}_{\text{HCl}} - \bar{V}_{\text{NaCl}}$) is too small to be of importance.

The constancy of the *pK* values that are obtained is reasonably satisfactory. The *pK* value of 5.16 ± 0.35 that results compares favorably with the value of 4.86 reported for polymethacrylic acid solutions by earlier workers.^{6,14,32}

Acknowledgment.—Financial support through Contract No. At(30-1)-2269 with the U. S. Atomic Energy Commission is gratefully acknowledged.

(32) A. Arnold and J. Th. Overbeek, *Rec. trav. chim.*, **68**, 879 (1949).

A THERMODYNAMIC INTERPRETATION OF THE OSMOTIC PROPERTIES OF CROSS-LINKED POLYMETHACRYLIC ACID

BY JACOB A. MARINSKY¹ AND AMALESH CHATTERJEE²

Department of Chemistry, University of Buffalo, Buffalo, New York

Received May 5, 1962

A thermodynamic interpretation of the osmotic properties of cross-linked polymethacrylic acid ion exchange resins (1 and 5% cross-linked Amberlite IRC-50) at several different dissociation values and solvent activities has been attempted. The results of this treatment are compared with the results of theoretically based computations that were reported in the preceding paper and which employed Katchalsky's randomly kinked macromolecule model for polymethacrylic acid. The value of $1/\alpha \log \bar{\gamma}_r$ at different experimental conditions that is determined from the thermodynamic treatment by using the computed electrostatic contribution to the free energy of the resin at one experimental condition as an arbitrary reference point is observed to compare favorably with the corresponding computed value of the electrostatic free energy term, indicating that the calculations are self-consistent. An estimate of the thermodynamic properties of the macro-ions in the concentration range in which short-range forces due to ion-ion and ion-solvent interaction predominate is possible by extension of the thermodynamic treatment of the osmotic data and the results of these computations are also included. The internal consistency between both approaches that is obtained at higher solvent activities is felt to justify this extension.

Introduction

The water absorption properties and the potentiometric behavior of cross-linked polymethacrylic acids have been reported by us in the preceding paper.³ The equation that was used to examine the data is

$$\text{pH} = \text{p}K_{\text{HR}} - \log \frac{1 - \alpha}{\alpha} + \log \frac{\bar{a}_{\text{M}^+}}{a_{\text{M}^+}} + \frac{0.4343}{kT} \left(\frac{\partial F_e}{\partial \nu} \right)_\kappa \quad (1)$$

where α is the degree of dissociation, and \bar{a}_{M^+} and a_{M^+} represent the activity at equilibrium of the univalent cation in the gel and solution phases, respectively. The value of \bar{a}_{M^+} was obtained from the simple relationship, $\log \phi_p^4 \approx \log \bar{\gamma}_{\text{M}^+}$, that has been demonstrated to prevail in polymethacrylate systems.^{3,5}

In the course of the earlier investigation,³ osmotic data were obtained with the 1% and 5% cross-linked ion exchange gel by varying the degree of dissociation while maintaining the solvent activity constant or by varying the solvent activity while keeping the degree of dissociation at a fixed value. Correction for restraint by the cross-linked matrix of the exchanger was made for those systems which were equilibrated at high solvent

activity. The value of ϕ_p , in these instances, was computed for the hypothetically unrestrained exchanger at the experimentally observed monomer molality values by using the Katchalsky model of cylindrical symmetry for the macromolecule in the fully stretched state.⁶

The last term in the equation refers to the change in the electrostatic free energy of the ion exchanger with the degree of dissociation. The model of Katchalsky and Lifson,⁷ which considers the gel to be a randomly kinked macromolecule carrying ionized groups in a medium of finite ionic strength, was used for its evaluation.

The electrostatic free energy, F_e , of the macromolecule is defined as the difference between the free energy of the actual polyelectrolyte and the free energy of the same polyelectrolyte in a hypothetical state in which all of the ions, fixed or free, carry no charge. This choice of reference state is made since electrostatic interaction in the macromolecule does not disappear with dilution and the polyelectrolyte never approaches "ideality." The only interest, however, is in the deviation of the free energy of the macromolecule from the ideal entropy of mixing of ionized and un-ionized groups among the ionizable groups fixed by the gel network and this term accurately evaluates the deviation of the free energy of the mixture due to electrostatic forces.

(1) Correspondence to be addressed to this author.

(2) Postdoctoral Fellow 1960-1961. On leave of absence from Vidyasagar College, Calcutta, India.

(3) A. Chatterjee and J. A. Marinsky, *J. Phys. Chem.*, **67**, 41 (1963).

(4) ϕ_p = practical osmotic coefficient.

(5) Z. Alexandrowicz, *J. Polymer Sci.*, **43**, 325 (1960).

(6) S. Lifson and A. Katchalsky, *ibid.*, **13**, 43 (1954).

(7) A. Katchalsky and S. Lifson, *ibid.*, **11**, 409 (1953).

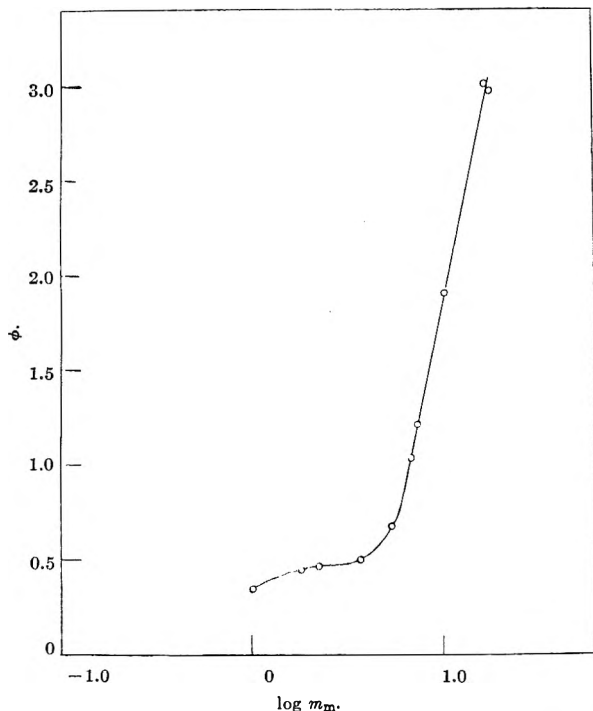


Fig. 1.—Plot of the practical osmotic coefficient, ϕ , vs. the logarithm of the molality of the gel monomeric units ($\alpha = 0.8$).

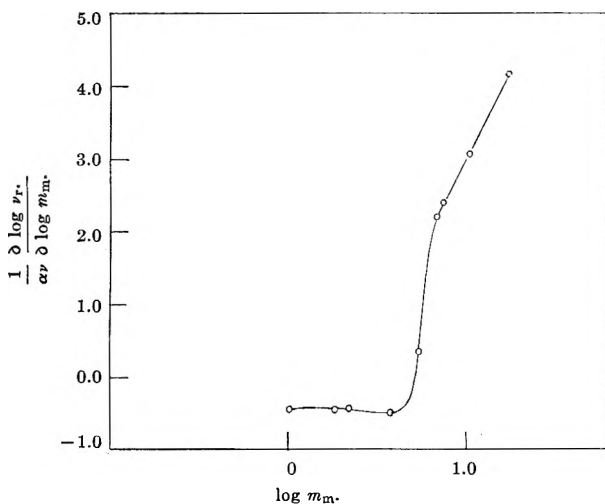


Fig. 2.—Plot of the function, $(1/\alpha\nu)(\partial \log \gamma_r/\partial \log m_m)$, vs. the logarithm of the molality of the gel monomeric units ($\alpha = 0.8$).

It is the objective of the thermodynamic treatment which follows to demonstrate (1) the self-consistency of the approach that was employed in the preceding paper³ for the analysis of the water absorption properties and the potentiometric behavior of the cross-linked polymethacrylic acid resins and (2) to justify extension of estimates of the thermodynamic properties of the counter- and macro-ions to the highest concentration range that was encountered in the previous study.

Theory

For the restricted case of a system maintained at constant temperature

$$-VdP + \sum_i m_i d\bar{G}_i = 0 \quad (2)^8$$

where \bar{G}_i is the partial molal Gibbs free energy of the i th species and m_i indicates its molality. Equation 2, modified to describe the system of interest, becomes

(8) R. A. Robinson and R. H. Stokes, "Electrolyte Solutions," Butterworths Scientific Publications, London, 1959, p. 33.

$$-\bar{V}_{H_2O} d\pi + m_{H_2O} d\bar{G}_{H_2O} + m_{NaCl} d\bar{G}_{NaCl} + \sum_i m_{r_i} d\bar{G}_{r_i} = 0 \quad (3)$$

r representing the resinate macromolecule and π the osmotic pressure within the resin phase. The imbibement of NaCl by the gel phase in each of the experiments that was performed is small enough to neglect and

$$V_{H_2O} d\pi + m_{H_2O} d\bar{G}_{H_2O} + \sum_i m_{r_i} d\bar{G}_{r_i} = 0 \quad (4)$$

A complex spectrum of species is encountered as a result of dissociation of the macromolecule, e.g., Na^+ , $H_{(1-\alpha)\nu}R^{-\alpha\nu}$, $Na_{\alpha\nu}H_{(1-\alpha)\nu}R$, H^+ , $H_{(1-\alpha)\nu-1}R^{-(\alpha\nu-1)}$, \dots , $H_{(1-\alpha)\nu-n}R^{-(\alpha\nu-n)}$, where ν is the charge of the completely dissociated macroanion. When α is kept constant one principal species is presumed to predominate and eq. 4 becomes

$$-\bar{V}_{H_2O} d\pi + m_{H_2O} d\bar{G}_{H_2O} + m_r d\bar{G}_r = 0 \quad (5a)$$

or

$$\frac{-\bar{V}_{H_2O} d\pi}{RT} + m_{H_2O} d \ln a_{H_2O} + m_r d \ln a_r = 0 \quad (5b)$$

The osmotic properties of the hypothetical unrestrained resin were computed in the earlier paper³ for the various experimental conditions that were studied to eliminate the $\bar{V} d\pi$ term of eq. 5 and

$$m_{H_2O} d \ln a_{H_2O} + m_r d \ln a_r = 0 \quad (6)$$

By using the definitions

$$\ln a_{H_2O} = \frac{-\phi}{m_{H_2O}} [\alpha\nu + 1] m_r \quad (7)$$

and

$$\ln a_r = \ln m_r + \alpha\nu \ln \alpha\nu m_r + \ln \gamma_r \quad (8)$$

and by differentiating eq. 6 with respect to m_r

$$m_{H_2O} \frac{\partial \ln a_{H_2O}}{\partial m_r} + m_r \frac{\partial \ln a_r}{\partial m_r} = 0 \quad (9)$$

the useful expression given below results

$$\phi - 1 + 0.4343 \frac{\partial \phi}{\partial \log m_m} = \frac{1}{\alpha\nu} \frac{\partial \log \gamma_r}{\partial \log m_m} \quad (10)$$

where m_m is the concentration of the monomeric units of which the cross-linked gel consists. A plot of ϕ vs. $\log m_m$ to obtain $\partial \phi / \partial \log m_m$ from the tangent at any point permits evaluation of $(1/\alpha\nu)(\partial \log \gamma_r / \partial \log m_m)$. The value of $(1/\alpha\nu) \partial \log \gamma_r$ may then be computed from graphical integration of the function $(1/\alpha\nu)(\partial \log \gamma_r / \partial \log m_m)$ plotted vs. $\log m_m$.

Essentially the same treatment as is outlined above was used earlier by Alexandrowicz⁵ to calculate the activity coefficient of the linear polymer of polymethacrylic acid.

Calculation of the Activity Coefficient of Cross-Linked Polymethacrylic Acid.—The absolute value of $\log \gamma_r$ cannot be determined independently by the above approach since electrostatic interaction in the macromolecule does not disappear with dilution. However, the electrostatic contribution to the free energy of the resin has been computed previously³ and it is possi-

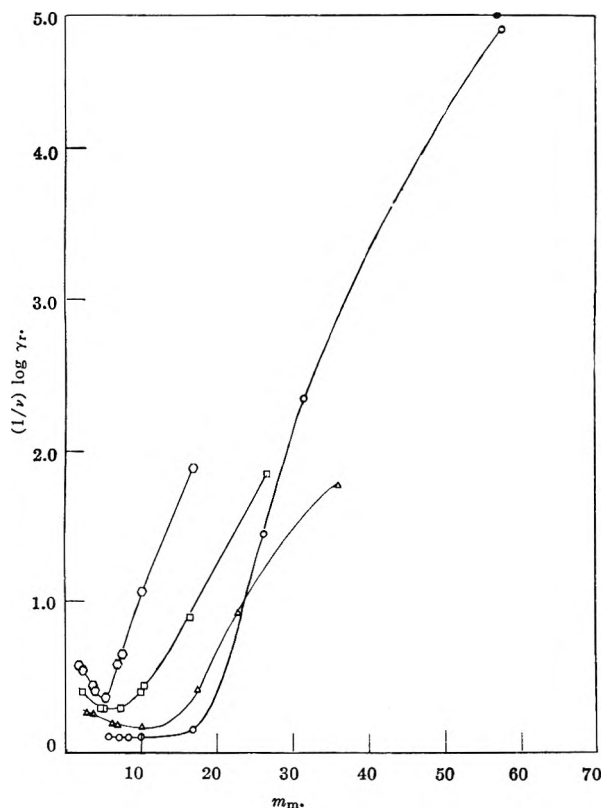


Fig. 3.—Resinate activity coefficient values: $\alpha = 0.1$, $\circ\text{-}\circ\text{-}\circ\text{-}$; $\alpha = 0.3$, $\text{-}\Delta\text{-}\Delta\text{-}\Delta\text{-}$; $\alpha = 0.5$, $\text{-}\square\text{-}\square\text{-}\square\text{-}$; and $\alpha = 0.8$, $\text{-}\bigcirc\text{-}\bigcirc\text{-}\bigcirc\text{-}$.

ble to compare these theoretical computations with the behavior of $(1/\alpha\nu) \log \gamma_r$, that is predicted from the above thermodynamic treatment.

For this purpose the values that were estimated to be the electrostatic contribution to the free energy of the variously dissociated 5% cross-linked resin equilibrated with 0.1 *m* NaCl have been equated with $(1/\alpha\nu) \log \bar{\gamma}_r$, to provide an arbitrary reference point for the evaluation of $(1/\nu) \log \gamma_r$ at the other experimental situations. The results of these computations are listed in Table I together with the corresponding $(0.4343/kT)(\partial F_e/\partial \nu)_\kappa$ values. Figures 1 and 2 present graphs of $\log m_m$ vs. ϕ and $(1/\alpha\nu)(\partial \log \gamma_r/\partial \log m_m)$, respectively, for the $\alpha = 0.8$ condition to demonstrate the important steps in the calculation of $(1/\alpha\nu) \log \gamma_r$. The curve that is presented in Fig. 1 is based upon the best smooth curve that can be drawn through the ϕ values that are computed for the 1 and 5% cross-linked resin at the monomer molality that is observed after equilibration with solvent at various water activity values (see Fig. 3 of ref. 3 and Fig. 6). In the lower molality region of the curve correction for restraint by the cross-linked matrix has been made. Several points corresponding to the 1% cross-linked resin in the intermediate monomer molality region and the two points in the highest monomer molality region which correspond to the 1 and 5% cross-linked resins, respectively, need no correction for restraint and are experimentally based.

The good agreement that is obtained between the electrostatic term that is based upon our interpretation of the theoretical treatment of Katchalsky⁷ and the corresponding $(1/\alpha\nu) \log \gamma_r$ term that is derived from the above thermodynamic treatment of osmotic data demonstrates the self-consistency of the approach that was used in the preceding paper, and justifies extension

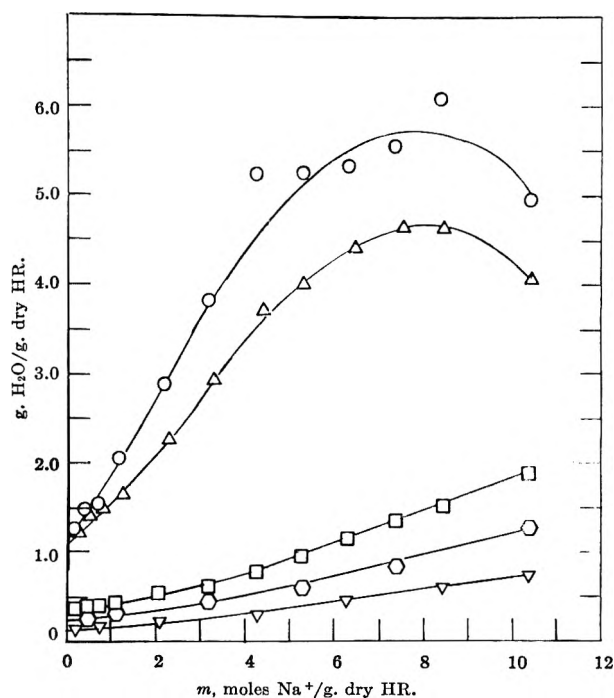


Fig. 4.—Water absorption properties of 1% cross-linked Amberlite IRC-50 in contact with: 0.1 *m* NaCl, $\circ\text{-}\circ\text{-}\circ\text{-}$ and 0.3 *m* NaCl, $\text{-}\Delta\text{-}\Delta\text{-}\Delta\text{-}$, isopiastically equilibrated with: saturated BaCl₂, $\text{-}\square\text{-}\square\text{-}\square\text{-}$, saturated NaCl, $\text{-}\bigcirc\text{-}\bigcirc\text{-}\bigcirc\text{-}$, and saturated LiNO₃, $\text{-}\nabla\text{-}\nabla\text{-}\nabla\text{-}$.

TABLE I
RESINATE ACTIVITY COEFFICIENTS DEDUCED FROM A THERMODYNAMIC INTERPRETATION OF OSMOTIC DATA

Degree of dissociation (α)	Electrostatic free energy $\frac{0.4343}{kT} \left(\frac{\partial F_e}{\partial \nu} \right)_\kappa$	$\frac{1}{\alpha\nu} \log \gamma_r$
1% cross-linked resin; 0.1 <i>m</i> NaCl		
0.8	0.66	0.57
.5	.43	.41
.3	.28	.27
.1	.11	.10
1% cross-linked resin; 0.3 <i>m</i> NaCl		
0.8	0.53	0.54
.5	.39	.38
.3	.26	.25
.1	.10	.09
5% cross-linked resin; 0.1 <i>m</i> NaCl		
0.8	0.43	
.5	.29	
.3	.20	
.1	.095	
5% cross-linked resin; 0.3 <i>m</i> NaCl		
0.8	0.41	0.41
.5	.28	.29
.3	.19	.19
.1	.086	.10

of the thermodynamic treatment to the osmotic data that were obtained at lower water activities. The activity coefficient values which derive from this analysis are plotted in Fig. 3 as a function of the monomer molality of the polymethacrylate gel at several degrees of dissociation. The corresponding water absorption data are presented in Fig. 4 and 5. The variation of the practical osmotic coefficient of the resin gel ($\phi_r = \bar{\gamma}_r^+_{Na^+}$) with sodium ion molality is plotted in Fig. 6 at several different dissociation values.

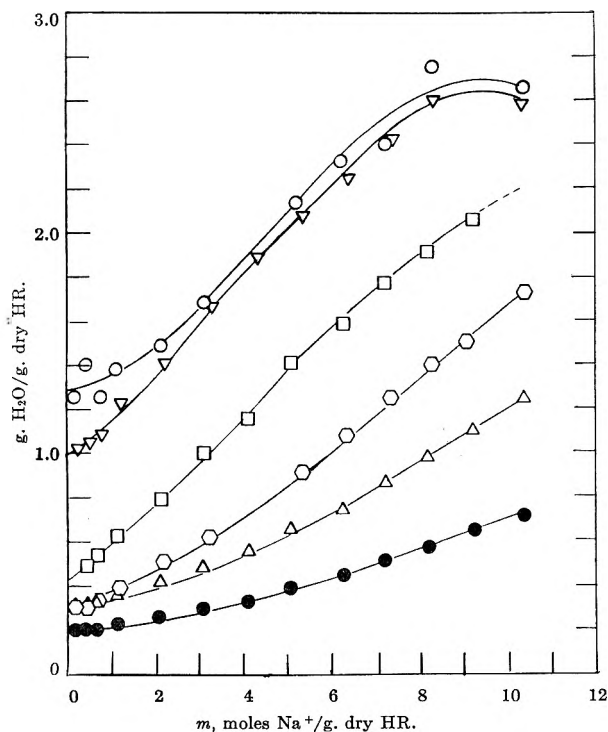


Fig. 5.—Water absorption properties of 5% cross-linked Amberlite IRC-50 in contact with: 0.1 *m* NaCl, $\circ\text{---}\circ\text{---}\circ$ and 0.3 *m* NaCl, $\nabla\text{---}\nabla\text{---}\nabla$; isopiastically equilibrated with: saturated $\text{K}_2\text{Cr}_2\text{O}_7$, $\square\text{---}\square\text{---}\square$; saturated BaCl_2 , $\hexagon\text{---}\hexagon\text{---}\hexagon$; saturated NaCl, $\triangle\text{---}\triangle\text{---}\triangle$; and saturated LiNO_3 , $\bullet\text{---}\bullet\text{---}\bullet$.

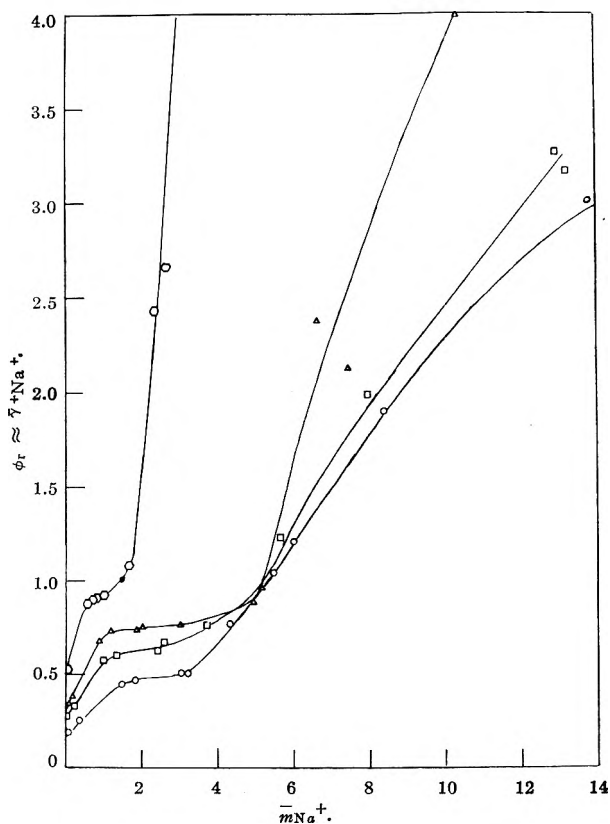


Fig. 6.—The variation of practical osmotic coefficient with sodium ion molality: $\alpha = 0.8$, $\circ\text{---}\circ\text{---}\circ$; $\alpha = 0.5$, $\square\text{---}\square\text{---}\square$; $\alpha = 0.3$, $\triangle\text{---}\triangle\text{---}\triangle$; and $\alpha = 0.1$, $\hexagon\text{---}\hexagon\text{---}\hexagon$.

Discussion

The behavior of $(1/\alpha\nu) \log \gamma_r$ with increasing molality of the polyelectrolyte that is observed in Fig. 3 is as expected. In the Katchalsky treatment⁷ the transition of the randomly kinked polyelectrolyte molecule from its uncharged reference state to its final state is performed by charging the ions isothermally in infinitesimal steps to their actual charge. Three separate steps are introduced in the charging process: (a) the ionic atmosphere is produced, (b) the macromolecules are gradually stretched, and (c) the repulsive energy of the fixed ions, screened by their atmospheres, is accumulated. Screening by counterions is minimized in the more dilute polyelectrolyte system ($\alpha m_m < 4$) since the geometry of the macromolecule is relatively unchanged while the counterion atmosphere is more dilute. As a result the repulsive energy due to the fixed charges of the macromolecule, and consequently $(1/\alpha\nu) \log \nu_r$, is larger the more dilute the system.

As the concentration of the polyelectrolyte increases $(1/\alpha\nu) \log \gamma_r$ decreases because of more effective screening of the fixed charges of the macromolecule by the greater population of counterions. Eventually, however, short-range interactions due to ion-ion and ion-solvent involvement predominate and result in the rapid increase in $(1/\alpha\nu) \log \gamma_r$, paralleling the behavior of electrolyte solutions at high concentration values.

The behavior (Fig. 6) of the activity coefficient of the sodium counterion, $\bar{\gamma}_{\text{Na}^+}$, with counterion concentration at several different degrees of ionization of the polyelectrolyte also is consistent with previous observations.^{7,9,10} The activity coefficient of a counterion in solutions of polyelectrolyte free of extra electrolyte always decreases strongly with the degree of ionization of the polyelectrolyte and the concentration of the polyelectrolyte. This result is attributable to association of the counterion with the macro-ion because of strong electrostatic attraction to the highly charged poly-ion, the degree of counterion association increasing with poly-ion dissociation as a result of the increasing charge of the poly-ion. The rapid increase in $\bar{\gamma}_{\text{Na}^+}$ with counterion molality at high concentration values parallels the rise in the mean activity coefficient values of strong electrolytes and is attributable to the complication of short-range forces which originate from ion-ion and ion-solvent interactions.

On the basis of the moderate success that is obtained in this paper and the preceding one³ by treating an ion exchanger as a polyelectrolyte rather than as a simple strong electrolyte as has been suggested by Glueckauf¹¹ it is recommended that the polyelectrolyte model of the ion exchanger be used for the fundamental analysis of the ion exchange phenomenon.

Acknowledgment.—Financial support through Contract No. At(30-1)-2269 with the U. S. Atomic Energy Commission is gratefully acknowledged.

(9) W. Kern, *Makromol. Chem.*, **2**, 279 (1948).

(10) F. T. Wall and W. B. Hill, *J. Am. Chem. Soc.*, **82**, 5599 (1960).

(11) E. Glueckauf, *Proc. Roy. Soc. (London)*, **214**, 207 (1952).

INTERACTION OF DIMETHYLDODECYLAMINE OXIDE WITH SODIUM DODECYLBENZENESULFONATE IN DILUTE SOLUTION

BY D. G. KOLP, R. G. LAUGHLIN, F. P. KRAUSE, AND R. E. ZIMMERER

Miami Valley Laboratories, The Procter & Gamble Co., Cincinnati, Ohio

Received May 7, 1962

By studies of pH, light transmission, and diffusion coefficient, dimethyldodecylamine oxide and sodium dodecylbenzenesulfonate have been found to interact in aqueous solution in the following ways: (1) Below the critical micelle concentration of the mixture, the protonated form of the amine oxide and the dodecylbenzenesulfonate precipitate metathetically. This consumption of the protonated form results in protonation of additional amine oxide, which results in an increase in pH. The pK_{SP} of the precipitate is found to be 10.8. (2) Above the critical micelle concentration, the phenomenon of mixed micelle formation is added to the metathetical interaction. The critical micelle concentration of the system containing a 2:3 mole ratio of DBS to DDAO is 0.706×10^{-3} mole/l. (DBS + DDAO), lower than the critical micelle concentration of either of the surfactants alone. The molar ratio in the micelles is about 1:2 DBS:DDAO. It is concluded that only mixed micelles are present in the system.

Introduction

Aliphatic amine oxides are weak bases having about the same basicity as the acetate anion.¹ At any particular pH, the amine oxide is in equilibrium with its cationic form, which is produced by protonation of the amine oxide molecule at the oxygen atom; or, expressed symbolically for dimethyldodecylamine oxide (DDAO)

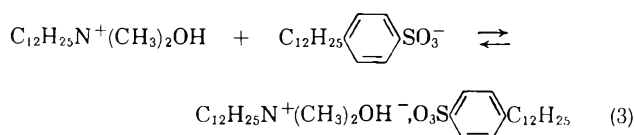


For this equilibrium, the equilibrium constant has been found by potentiometric titration to be

$$K_A = \frac{[\text{H}^+][\text{DDAO}]}{[\text{DDAOH}^+]} = 10^{-4.90} \quad (2)$$

where the quantities in brackets are the activities of the indicated species relative to a standard state such that, at infinite dilution, the activity equals the molar concentration. The value shown above was used in this work.

When DDAO and sodium dodecylbenzenesulfonate (DBS) are present together in solution at low pH, a precipitation occurs according to the equation

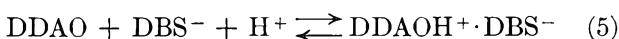


The composition of the precipitate has been established in this work by analyses for S and N. The structure shown is supported by the infrared absorption spectrum, which shows sulfonate bands and hydrogen-bonded OH bands at 3.7–3.8 μ . Amine oxide bands are absent.

The quantitative aspect of the precipitation is expressed by the solubility product

$$K_{SP} = [\text{DDAOH}^+][\text{DBS}^-] \quad (4)$$

where the activities relative to the standard state mentioned above are used. Combination of eq. 1 and 3 gives



The equilibrium constant for the reverse of this process is

$$K = \frac{[\text{DDAO}][\text{DBS}^-][\text{H}^+]}{[\text{DDAOH}^+ \cdot \text{DBS}^-]} = K_A K_{SP} \quad (6)$$

(1) P. Nylen, *Z. anorg. allgem. Chem.*, **246**, 227 (1941).

where the symbols are used as before.

Since protons are used in the formation of the precipitate, it is clear that precipitation is accompanied by an increase in pH. Above a final pH of about 8, however, the rise in pH occurs without apparent precipitation. The following sections of this paper are devoted to presenting and explaining this pH effect.

Results and Discussion

The Behavior of DBS-DDAO Solutions below the Critical Micelle Concentration. Measurements of pH.

—The data of Table I and Fig. 1 show the pH values obtained for a typical group of solutions containing DDAO and DBS at 25°. The pH is found to go through a maximum at the 1:1 mole ratio of DDAO to DBS. A number of other series of solutions in the concentration range 0.4×10^{-3} to 1.10×10^{-3} mole/l. were subjected to pH measurements with results similar to those presented.

TABLE I

Initial concn. DDAO, moles/l. $\times 10^3$	Initial concn. DBS, moles/l. $\times 10^3$	Mole fraction DBS	pH ^a	pK_{SP}
0.035	0.314	0.90	7.72	10.78
.078	.313	.80	8.10	10.81
.133	.311	.70	8.33	10.82
.200	.307	.60	8.55	10.86
.240	.306	.55	8.63	10.86
.304	.304	.50	8.77	10.86
.332	.222	.40	8.65	10.88
.336	.145	.30	8.46	10.87
.338	.085	.20	8.25	10.89
.00	.315	1.00	7.0 ± 0.1	
.342	.00	0.00	7.3 ± 0.15	
Average				10.85 ^b

^a Obtained from smooth curve drawn through points in Fig. 1.

^b Average K_{SP} from all applicable pH data is 10.8₈.

Although no precipitation was observed in these pH measurements, the mechanism of the pH increase probably is identical with that found at lower pH values. In that event, the absence of visible precipitate may be due to one or both of the following causes:

1. The amount of precipitate necessary to account for the increase in pH is very small—about 3 mg./l. for the system at the 1:1 mole ratio shown in the table.

2. The precipitate may be so finely divided initially that its ability to scatter light is not sufficient to give a visible turbidity. Nevertheless, the precipitate must form immediately because the pH change is immediate.

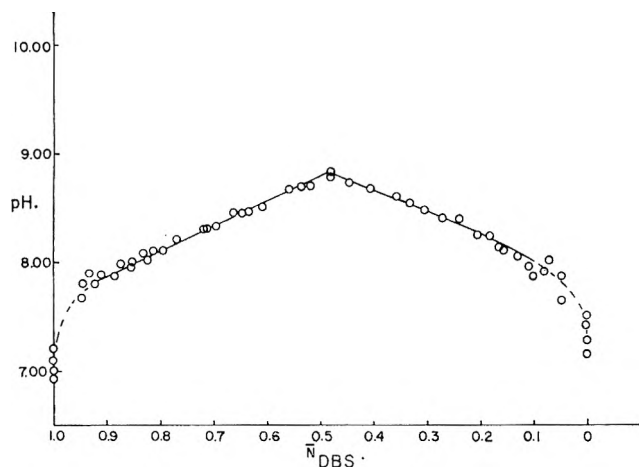


Fig. 1.—pH vs. mole fraction of DDAO-DBS mixtures below the critical micelle concentration.

If the increase in pH on mixing DDAO and DBS is in fact due to the precipitation process described, the final pH, with certain assumptions, can be used to calculate the solubility product of the precipitate. From eq. 6

$$\bar{K}_{SP} = \frac{[H^+][DDAO][DBS^-]}{K_A} \quad (7)$$

or, in logarithmic form

$$pK_{SP} = pH + p[DDAO] + p[DBS] - pK_A \quad (8)$$

By means of eq. 8, the values of pK_{SP} shown in Table I were calculated. This calculation involves the assumption that the activities of the various species are approximately equal to molar concentrations. This is believed to be valid in these dilute solutions but is definitely invalid above the critical micelle concentration. That the solutions considered here are probably below the critical micelle concentration is indicated by the diffusion data presented later in this paper and by the constancy of the pK_{SP} values shown in Table I.

In using eq. 8 it is necessary to find the equilibrium concentrations of DDAO and DBS. These are found from eq. 9

$$[DDAO] = C_{DDAO} - x \quad (9)$$

where C_{DDAO} is the initial concentration of DDAO and x is the extent of reaction of DDAO to form $DDAOH^+$ and the precipitate, $DDAOH^+ \cdot DBS^-$, as measured by the uptake of protons. The value of x can be found from the pH by the following argument.

Since each mole of DDAO in reacting to form $DDAOH^+$ or $DDAOH^+ \cdot DBS^-$ uses a mole of protons, the equilibrium condition involves a deficiency of protons relative to hydroxide ions. If the number of protons is taken to be equal initially to the number of hydroxide ions, then at equilibrium, the number of protons will be deficient by the extent of reaction, x , while the number of hydroxide ions will not be reduced. Although additional protons will be produced by dissociation of water, hydroxide ions will be produced in equal number to maintain the inequality.

Thus

$$[H^+] + x = [OH^-] \quad (10)$$

and, from the ionization constant of water

$$pH + p(H + x) = 14.00 \quad (11)$$

Then

$$x = 10^{pH-14.00} - 10^{-pH} \quad (12)$$

The extent of reaction of DBS is somewhat smaller because a part of the reaction with protons produces $DDAOH^+$ rather than $DDAOH^+ \cdot DBS^-$. Specifically

$$y = x - [DDAOH^+] = x - \frac{[DDAO][H^+]}{K_A} \quad (13)$$

where y is the extent of reaction of DBS. Then

$$[DBS] = C_{DBS} - y \quad (14)$$

where C_{DBS} is the initial concentration of DBS.

The inclusion of x and y in the calculations affects the values of pK_{SP} by 0.06 at most. The contribution of y to pK_{SP} is less than 0.01.

The constancy of pK_{SP} supports the supposition that the pH change is due to the formation of a precipitate as supposed in the calculation. Further substantiation is given in the next section of the paper.

Measurement of K_{SP} .—The solubility of the $DDAOH^+ \cdot DBS^-$ precipitate can be found in a more direct way by measuring the light transmission of aged solutions as a function of pH. Although turbidity is not immediately visible, it develops as the solutions stand. Also, turbidities which are not readily visible can be measured. As the pH increases, a point is reached at which the protonation of the amine oxide becomes insufficient to maintain the precipitate. At this point eq. 8 may be applied somewhat more simply than before. Since the precipitate disappears at this pH, the concentrations of DDAO and DBS are undiminished by precipitation. The DDAO concentration is affected by the extent of protonation, but this is negligible at the pH values at which data were obtained. It still is necessary to assume the activities equal to the molar concentrations. From these considerations, the data given in Table II are obtained.

TABLE II

Concn. DDAO, moles/l. 10^3	Concn. DBS, moles/l. 10^3	pH of turbidity threshold	pK_{SP}
0.080	0.300	8.10	10.82
.340	.085	8.05	10.69
.200	.200	8.20	10.70
.550	.550	9.15	10.77
.380	.380	8.90	10.84
Average			10.76

The agreement between the pK_{SP} values from turbidity measurements and pH measurements, respectively, is such as to support the conclusion that the increase in pH is due to precipitation.

The previous sections of this paper have dealt with the behavior of solutions containing DDAO and DBS below the critical micelle concentration. Above the critical micelle concentration, the interaction of these two species is complicated by the possibility of formation of micelles containing both of the surfactants. Also the assumptions used in the interpretation of pH and turbidity data are invalid above the critical micelle concentration.

The Behavior of DBS-DDAO Solutions in the Micellar Region. pH Behavior.—The pH of solutions con-

taining DBS and DDAO above the critical micelle concentration follows a course such as that shown in Fig. 2. The behavior is qualitatively similar to that observed below the critical micelle concentration except that the maximum in the curve is much flatter. For reasons already stated, the pH behavior above the critical micelle concentration cannot be interpreted in terms of ionic equilibria.

Diffusion.—DBS-DDAO solutions of sufficient concentration for the formation of micelles were investigated by diffusion coefficient measurements. From such measurements can be learned (1) the critical micelle concentration of surfactant mixtures, (2) the concentration of the micellized and unmicellized forms of each surfactant in solution, and (3) the concentration and composition of the micelles. The procedures used in these determinations are based on principles found to hold for single detergent solutions.² The diffusion coefficients, or rather self-diffusion coefficients, were determined by the open-ended capillary method using tagged solutes.³

The diffusion coefficient of a single surfactant is independent of concentration at concentrations smaller than the critical micelle concentration. Above the critical micelle concentration, it decreases, at first rapidly and then more and more gradually with increasing concentration. In this region, the following formula holds²

$$cD = c_1D_1 + c_mD_m \quad (15)$$

where D is the diffusion coefficient as observed in the solution at concentration c , D_1 and c_1 are the diffusion coefficient and the concentration of the unmicellized (monomeric) fraction, and D_m and c_m the diffusion coefficient and concentration of the micelles. Of course, $c = c_1 + c_m$. For single detergents, c_1 is equal to the critical micelle concentration.

The diffusion coefficient of the micelles can be determined from a series of diffusion coefficient measurements or, directly, by "tagging" of the micelles with a trace amount of a radioactive material that is completely solubilized by them. Lauryl alcohol was found to be a suitable material for this purpose.² Used at a level of 10 p.p.m., it does not affect the structure of surfactant solutions.

The determination of the micellized and unmicellized fractions of a surfactant in a surfactant mixture is based on formula 15, which can be written in the following two forms

$$c_1 = c \frac{D - D_m}{D_1 - D_m} \text{ and } c_m = c \frac{D_1 - D}{D_1 - D_m} \quad (16)$$

All diffusion coefficients entering the formulas are determinable: D and D_m in the solution under consideration, D by having the tag in the surfactant, and D_m by tagging the micelles with radioactive lauryl alcohol, while D_1 is determined separately in a solution containing only monomeric surfactant. The over-all concentration of the surfactant, c , of course, is known. After the c_1 and c_m values have been determined for each surfactant in the solution, it is a simple matter to compute the concentration and composition of the micelles.

(2) Unpublished work.

(3) J. Wang, *J. Am. Chem. Soc.*, **73**, 510 (1951).

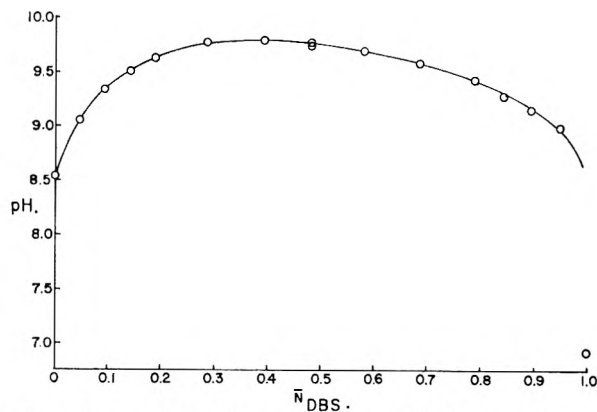


Fig. 2.—pH vs. mole fraction of DDAO-DBS mixtures above the critical micelle concentration.

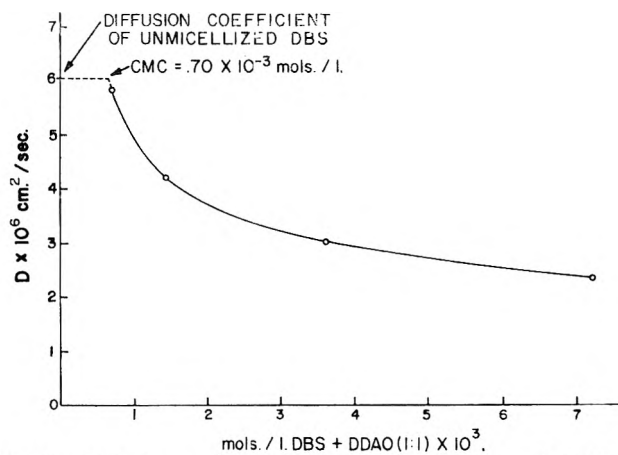


Fig. 3.—Diffusion coefficient of unmicellized DBS and DBS in DBS-DDAO (1:1) solutions buffered with 0.02% $\text{Na}_2\text{H}_2\text{O}_4\text{CO}_3$.

Only solutions containing DBS and DDAO at a weight ratio of 1.0 (molar ratio 0.66) were investigated. The solutions were buffered to a pH of 10 with 0.01% each of NaHCO_3 and Na_2CO_3 in order to minimize the protonation of DDAO. The buffer had little effect on the diffusion coefficients. The results are summarized in Fig. 3 and Table III.

Figure 3 shows that the diffusion coefficient of DBS in the presence of DDAO decreases markedly with increasing concentration. A short extrapolation to the magnitude of the diffusion coefficient of the unmicellized DBS gives the critical micelle concentration of the surfactant mixture as 0.70×10^{-3} mole/l. Note that this is considerably smaller than the critical micelle concentration of either DBS, which is approximately 1.4×10^{-3} mole/l., or DDAO, which is 1.9×10^{-3} mole/l.

From the data in Table III it is seen that the unmicellized surfactant concentrations change little on doubling the concentration, almost all of the added surfactant becoming micellized. It is not clear whether the small changes actually observed are real or due to the non-uniformity of DBS. For if the DBS contained isomers that do not micellize at low concentrations, these would concentrate in the unmicellized fraction of DBS.

From the fact that the concentrations of the unmicellized fractions of both surfactants are considerably smaller than their critical micelle concentrations, it follows that micelles consisting solely of one or the other surfactant cannot form in the solutions. In other words, only mixed micelles exist. Whether all mixed

TABLE III
THE COMPOSITION OF DBS-DDAO SOLUTIONS AT 30°
(Solutions buffered with 0.02% $\text{Na}_2\text{H}_2\text{O}_7\text{CO}_3$, pH 10)

	—0.1% DBS-DDAO (1:1)—			—0.2% DBS-DDAO (1:1)—		
	DBS	DDAO	Micelles	DBS	DDAO	Micelles
A. Diffusion coefficients $\times 10^6$ cm. ² /sec.						
(1) D , surfactant in test soln.	3.04	2.00		2.26	1.56	
(2) D_1 , monomeric surfactant ^a	6.06	5.80		6.06	5.80	
(3) D_m , tagged micelles ^b			1.09			0.97
B. Concentrations in moles/l. $\times 10^4$						
(1) Unmicellized fraction	0.58	0.46		0.72	0.57	
(2) Micellized fraction	0.86	1.75		2.16	3.80	
(3) Total	1.44	2.21		2.88	4.37	
(4) Micellar concn. (in terms of monomer)			2.61			5.96
C. Composition of micelles						
(1) DBS-DDAO weight ratio			43/57			46/54
(2) DBS-DDAO molar ratio			33/67			36/64

^a Determined in separate solution. ^b Test solutions with 0.001% lauryl alcohol-C¹⁴ added.

micelles are of the same size and composition remains unknown.

The DBS-DDAO molar ratio of very nearly 1:2 in the micelles is considered to be fortuitous.

Experimental

1. pH Measurements. Apparatus.—A Beckman model G pH meter equipped with a No. 8970-13 calomel reference electrode and a No. 1190-80 general purpose glass electrode was used to determine the pH of all solutions except where noted. The solutions under test were contained in a specially constructed cell. The cell body was either a 250-ml. short form beaker cut off and beaded or a 300-ml. tall form beaker. The cover of the cell consisted of a No. 13 rubber stopper fitted with reference and glass electrodes, gas inlet and outlet tubes, and four glass tips for Ultramax burets. These buret tips were connected to 25-ml. automatic burets, equipped with Ascarite filled U-tubes and drying tubes, by means of polyethylene tubing. The burets were equipped with No-Lub (Teflon) stopcocks to which the polyethylene tubing was connected by means of a machined nylon bushing. The cell was mounted in a Sargent Type NSI-12 constant temperature bath at $25.0 \pm 0.2^\circ$. It was shielded from the stirrer motor by a stainless steel wire screen. Nitrogen, free of CO₂ (prepared by passing water-pumped nitrogen through a tower of Ascarite followed by two cotton-filled towers, a water-filled tower, and finally another cotton-filled tower) was swept slowly through the cell at all times.

In order to eliminate field effects induced by the stirring motor and static electrical effects, the pH meter, the constant temperature bath, the motor screen, and even the operator were grounded. In addition, static charges would develop in the cell from time to time, giving rise to erratic pH measurements. This source of error was eliminated by rinsing the cell with dilute KCl solution followed by distilled water.

The pH values are believed to be accurate within the limits of the meter (± 0.02 pH unit). New electrodes, properly soaked prior to use, and fresh pH 7.00 Beckman 3501 buffer for standardizing the meter were used.

Procedure for pH Determinations.—Stock solutions (ca. 8 mM) of DBS and DDAO were made up by dissolving a weighed amount in neutral (pH 7.0 \pm 0.2) water, obtained by boiling distilled water in a clean stainless steel beaker and cooling under nitrogen. The pH of the DBS solution was adjusted to 7.0 ± 0.1 with 0.01 N HCl and carbonate-free 0.01 N NaOH. The concentration of the stock solution of DBS was determined by cationic titration with standardized cetyltrimethylammonium bromide solution, following the standard method.⁴ The concentration of the DDAO was determined by titration of the excess DBS in a mixture of known volumes of standard DBS and unknown DDAO solutions, using the same method. Under the acidic conditions of the titration, DDAO is quantitatively converted to the cationic form.

The data for each pH vs. mole fraction curve were determined in two separate runs. The mole fraction values from 1 to 0.5 were included in one run and the values 0.5 to 0 in another.

This was done by adding a measured amount (usually 25.00 ml.) of DBS to the cell, measuring the pH, adding appropriate aliquots of amine oxide to the cell, mixing the contents by swirling, and measuring the pH to the nearest 0.01 unit after each addition. The initial concentration was adjusted where necessary by first adding neutral water. The second run was identical with the first except that DBS was added to amine oxide.

2. Measurements of Light Transmission.—Solutions of DBS and DDAO for turbidity measurement were prepared at a pH of 6-7 and allowed to stand at room temperature for at least 16 hr. Small increments of a suitable NaOH solution were used to adjust the pH of an aliquot to the desired value. pH was measured at room temperature (about 25°) on a Beckman model GS pH meter equipped with a sleeve-type calomel electrode and a general purpose glass electrode.

Light transmission was measured at room temperature (about 25°) with a Lumetron colorimeter using unfiltered incandescent light and a cell of 5-cm. light path. Distilled water, taken to have 100% transmission, was used as standard. In some cases a single aliquot of solution was used for several successive adjustments of pH and measurements of light transmission. Nevertheless, the critical point at which transmission becomes essentially complete, as pH increases, always was determined on fresh aliquots.

In most cases, the light transmission becomes constant at 97-99%. The deviation from 100% transmission is attributed to the presence of minor amounts of debris (cellulose fibers from filter paper, etc.) in the solutions.

3. Diffusion Measurements.—The self-diffusion coefficients were determined by the open-ended capillary³ method using radiotagged DBS (S³⁵), DDAO (C¹⁴), and lauryl alcohol (C¹⁴). Two solutions of the same composition, one radioactive and the other inactive, were prepared. The radioactive solution was filled into two capillaries 2-4 cm. long and 0.7 mm. in diameter. The capillaries were placed in 50-100 ml. of the inactive solution in a closed vessel that was kept in a water bath at $30 \pm 0.05^\circ$. Diffusion was allowed to proceed until roughly half the activity had diffused out of the capillaries. The capillaries then were removed, emptied by centrifugation or rinsing, and the activity of the contents was determined in a Packard Co. Tri-Carb liquid scintillation spectrometer. From the initial and final activity contents, the length of the capillaries, and the time of diffusion, the self-diffusion coefficients were calculated. For details of the calculation see, for instance, ref. 3.

4. Untagged Materials. DDAO.—Armour's Armeen DMCD (dimethyl-coconutamine) was distilled once through a 2-ft. column of glass helices. The C₁₂ cut was redistilled through a 3-ft. spinning gauze band column and the cuts analyzed by gas chromatography.⁵ Two fractions totaling 76 g. and containing 99% dimethyldodecylamine were oxidized with a 30% excess of H₂O₂ in a 67% alcohol (in water) solution at 50°. The excess H₂O₂ was decomposed with platinum black and the unoxidized amine (nil) removed by petroleum ether extractions. Most of the

(5) The following conditions applied to the gas chromatographic analyses; column: 30% Apiezon L on 100-200 mesh Celite in a 10-ft. \times 1/4-in. o.d. copper tube; conditions: column temperature, 180°; block temperature, 310°; 91 cc. He carrier gas/min.; inlet pressure 25 p.s.i.

(4) T. Barr, J. Oliver, and W. V. Stubbings, *J. Soc. Chem. Ind.*, **67**, 45 (1948).

alcohol was removed under a current of N_2 at 40–50° and the residual solution freeze-dried, yielding 75 g. (91%) of crude amine oxide. Recrystallization from 1 l. of acetone (dried over Drierite) gave 55 g. (66%) of product.

Anal. Calcd. for $C_{14}H_{20}NO$: C, 73.3; H, 13.6; N, 6.10. Found: C, 72.7; H, 13.2; N, 6.09.

DBS.—The sodium dodecylbenzenesulfonate for this work was made by polymerization of propylene to the tetramer, which was used to alkylate benzene. The resulting alkyl benzene was sulfonated with sulfuric acid. Each step of the preparation introduces isomerism, and in addition the polymerization of propylene gives a distribution of molecular weight. No attempt was made in this work to isolate a single isomer or homolog.

A sample of DBS from a commercial source was purified by recrystallization from alcohol. Analytical data indicate the following compositions for the separate samples used in the pH and light transmission measurements, respectively.

	DBS used for pH measurements, %	DBS used for light transmission measurements, %
DBS	98.5	95.6
Na_2SO_4	..	2.6
Dodecylbenzene	0.5	..
H_2O	1.2	2.5

5. Radiotagged Materials.—The radiological purity of the S^{35} -labeled DBS was 97% according to a test that involved extraction of the DBS acid from strongly acidified solution with ethyl ether. The methyl- C^{14} -labeled DDAO retained a constant specific activity on recrystallization from ethanol, hence it was pure by this test. The chemical purity of the radioactive surfactants, which were prepared and purified in essentially the same way as the inactive surfactants, probably was the same as the purity of the inactive surfactants. The purity of the C^{14} -labeled lauryl alcohol was estimated at 95%.

SORPTION BEHAVIOR OF THE DIGLYCIDYL ETHER OF BISPHENOL A

BY BENJAMIN J. INTORRE, TI KANG KWEI, AND CLARKE M. PETERSON

Central Research Laboratories, Interchemical Corporation, New York, N. Y.

Received May 12, 1962

The sorption, desorption, and exchange behavior of molecularly thin films of the diglycidyl ether of bisphenol A (DGE) on chrome plate were investigated in benzene, hexane, and chloroform solution. Surface potentials of these films prepared by sorption from the three solvents are compared at various surface coverages. The results are interpreted in terms of different orientations of DGE in the first sorbed molecular layer. Sorption data and desorption kinetics data support these interpretations. Exchange experiments, as well as the desorption experiments, demonstrate the difficulty of removing the first sorbed molecular layer.

Introduction

The sorption characteristics of polar organic molecules onto solid surfaces are of interest from both the fundamental and applied points of view. Recently, data have been reported for a variety of sorbants,^{1–12} but in most cases the sorbants were either simple monofunctional molecules or high polymers with a large number of potentially sorbable segments.

The sorption behavior of the diglycidyl ether of bisphenol A (DGE), I, is of special interest for several reasons. This compound is a simple low molecular weight substance whose sorption behavior may be compared to that of other simple compounds. On the other hand, the molecule has four polar oxygen atoms distributed along a hydrocarbon backbone, which suggests the possibility of considering its structure as intermediate between simple monofunctional molecules and multifunctional macromolecules.

In an earlier investigation at these Laboratories of the sorption behavior of octadecyl acetate and polyvinyl acetate (PVAc), Gottlieb⁷ demonstrated the usefulness of surface potential measurements in determining the orientation of sorbed molecules on metal substrates. It was postulated in the case of PVAc that nearly all the segments of the polymer chain are in contact with the surface up to one monolayer surface coverage. Additional sorbed polymer did not

affect the surface potential. It was suggested that the segments of these additional chains probably are randomly oriented.

A later study, conducted in these Laboratories, of the kinetics of PVAc sorption⁹ suggests instead that the first flat monolayer may revert to the coiled configuration at higher surface coverage. In this region of higher surface coverage only a fraction of the polymer segments in each chain are in contact with the surface.

Conceivably, DGE could also be sorbed in more than one configuration depending on the number of groups in contact with the surface. It has been shown that DGE and its higher polymeric modifications form compressible films on water,¹³ and that the configuration attained is a function of the film pressure applied on the surface balance. It was felt that a study of the surface potential of the sorbed molecule might lead to a knowledge of its orientation at a metal surface. Benzene, hexane, and chloroform, three typical solvents having different polarity and affinity for DGE, were used. The surface potential of films of DGE sorbed or deposited from each solution was investigated. Supplementary evidence was obtained on the sorption behavior of DGE in these systems through sorption, desorption, and exchange experiments.

Experimental

The techniques used were those described earlier by Gottlieb.⁷

Materials.—Radioactively labeled DGE, tagged with carbon-14 at the central carbon atom (specific activity—0.13 mc./g.) was obtained through the courtesy of the Shell Chemical Corporation. This compound was received in crystalline form and was of exceptional purity. Non-radioactive DGE was obtained as a pure crystal (m.p. 43.5°) from the same source.

Commercial grade hexane (obtained from Chemical Solvents Inc., Newark, New Jersey), and reagent grade benzene (obtained from Mallinckrodt Chemical Works) were purified immediately before use by passage through a silica gel–alumina chromatographic column to remove traces of polar impurities.

(13) J. Glazer, *J. Polymer Sci.*, **13**, 355 (1954).

- (1) J. J. Bordeaux and N. Hackerman, *J. Phys. Chem.*, **61**, 1323 (1957).
- (2) H. D. Cook and H. E. Ries, Jr., *ibid.*, **63**, 226 (1959).
- (3) F. M. Fowkes, *ibid.*, **64**, 726 (1960).
- (4) H. L. Frisch, M. Y. Hellman, and J. L. Lundberg, *J. Polymer Sci.*, **38**, 441 (1959).
- (5) H. L. Frisch and R. Simha, *J. Chem. Phys.*, **27**, 720 (1957).
- (6) G. L. Gaines, *J. Colloid Sci.*, **15**, 321 (1960).
- (7) M. Gottlieb, *J. Phys. Chem.*, **64**, 427 (1960).
- (8) R. L. Patrick and G. O. Payne, Jr., *J. Colloid Sci.*, **16**, 93 (1961).
- (9) C. M. Peterson and T. K. Kwei, *J. Phys. Chem.*, **65**, 1330 (1961).
- (10) J. W. Shepard and J. P. Ryan, *ibid.*, **60**, 127 (1956); **63**, 1729 (1959).
- (11) H. A. Smith and T. Fort, Jr., *ibid.*, **62**, 519 (1958).
- (12) R. R. Stromberg and G. M. Kline, *Modern Plastics*, **1** (April 1961).

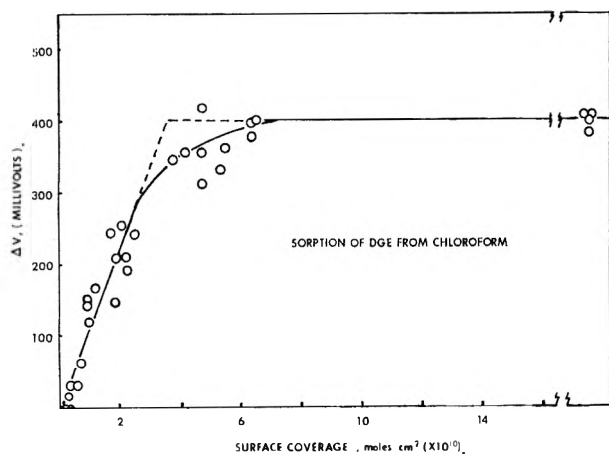


Fig. 1.—Sorption of DGE from chloroform; sorption time, 1 min.

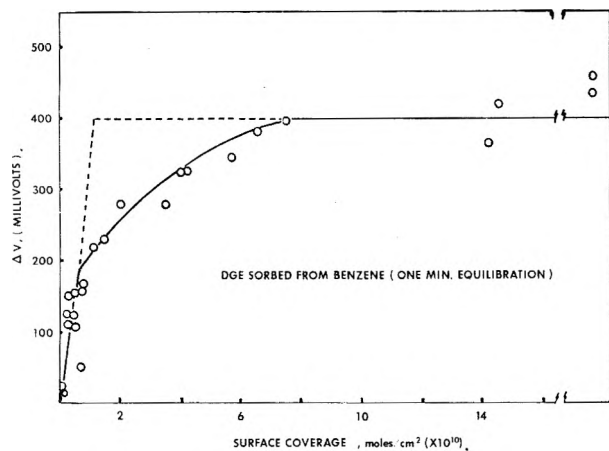


Fig. 2.—Sorption of DGE from benzene; sorption time, 1 min.

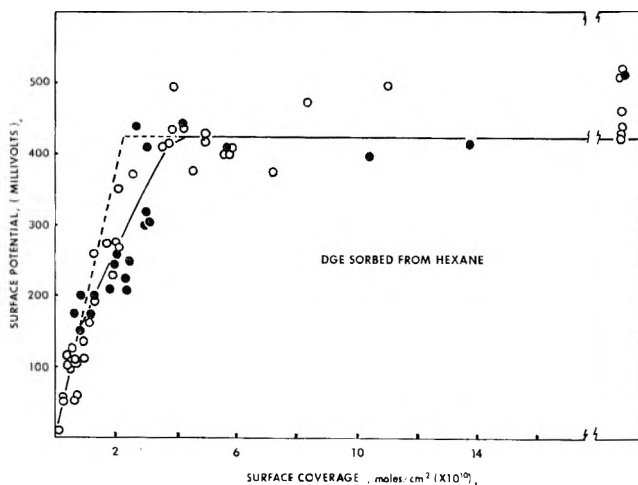


Fig. 3.—Sorption of DGE from hexane: filled circles overnight sorption; open circles, 1 min.

Reagent grade chloroform (obtained from Mallinckrodt Chemical Works) was freshly distilled before use, and only the center fraction was used.

Chrome plates (0.5 × 0.5 in.) were prepared from commercial ferrotype plates and cleaned by extraction with hot benzene. Each plate was gently flamed in a bunsen flame immediately prior to use.

Freshly prepared solutions at concentrations ranging from 0.1 to 0.0001% were used in these experiments.

Apparatus.—A Zisman type vibrating electrode surface potential apparatus¹⁴ was used to measure the surface potentials of thin films of sorbed DGE on flamed chrome plate.

A thin window gas flow counter (Nuclear-Chicago Model D47, fitted with a "Micro-mil" window) was used to measure radioactivity.

Procedure.—The change in the surface potential of a flame-cleaned chrome plate due to the sorption of DGE was measured as the difference between an initial surface potential V_0 and the final surface potential V_t . V_0 was determined in the following way. In each case the chrome plate was first flame cleaned for about 10 sec. in a blue bunsen flame. Before measuring V_0 , the plate was cooled to ambient temperature. It was found that cooling in air or in any one of the three solvents caused little variation in V_0 . As a standard practice, flamed plates were cooled for 1 min. in purified benzene. The plate was then drained, allowed to air dry for a few seconds, and the initial surface potential, V_0 , was measured. The same plate then was immersed in a solution of the radioactive DGE in a given solvent for 1 min. (overnight for the "equilibrium" measurements), rinsed quickly with pure solvent, and quickly air dried. The final surface potential of the plate, V_t , then was measured. The difference between these two measurements, $\Delta V = V_t - V_0$, is the change in surface potential caused by the sorption of the compound on the surface. A few samples were treated similarly but were not given the solvent rinse after removal from radioactive DGE solution. This allowed the measurement of the surface potential under conditions of excess coverage of the chrome plate with DGE.

Desorption kinetics curves were obtained from measurements on a number of chrome plates, each plate representing one point on the curve. The plates were flame-cleaned and cooled in benzene as described above. They then were equilibrated with a solution of DGE for 1 hr. and then immersed in solvent for measured time intervals. Residual DGE on the plates was determined by radiometric measurement.

Exchange kinetics data were obtained in a similar manner. After equilibration with a solution of radioactive DGE, chrome plates were re-equilibrated with a solution of non-radioactive DGE at the same concentration, for a measured time interval. Radioactive DGE remaining on the chrome plates was assayed radiometrically.

Results

A plot (Fig. 1) of the change in surface potential ΔV against surface coverage of DGE sorbed from chloroform shows that the surface potential increases linearly at low surface coverage. Thereafter the surface potential increases more slowly with increasing surface coverage and finally reaches a plateau. The experimental points clustered at the extreme right edge of Fig. 1, 2, and 3 are made at surface coverages of 20 to 30 moles/cm.² and are included to show the constancy of surface potential at very high surface coverage.

The surface potential–surface coverage curve of DGE sorbed from benzene onto chrome plate also shows a steep region at low surface coverage. However, before the plateau region is reached at high surface coverage the curve passes into a marked region of lesser slope. The surface potential continues to increase through this region with increasing surface coverage until it reaches the plateau voltage. With benzene the plateau is reached at a surface coverage of about 4.0×10^{-10} mole/cm.² or 18 counts per minute per square centimeter (c./min./cm.²) when equilibration has occurred over long periods of time (overnight), and at 7.0×10^{-10} mole/cm.² (30 c./min./cm.²) in the case of 1-min. equilibrations (see Fig. 2). This difference suggests a slow equilibration of DGE with the surface in benzene solvent.

The surface potential–surface coverage curve for DGE sorbed from hexane (Fig. 3) is similar in shape to that found with DGE sorbed from benzene. From hexane solution, overnight (filled circles) and 1-min. (open circles) equilibrations give the same results within the experimental error. The plateau in the surface

(14) W. Zisman, *Rev. Sci. Instr.*, **7**, 367 (1932).

potential curve is reached at a surface coverage of about 4.0×10^{-10} mole/cm.² (18 c./min./cm.²).

The scatter of the experimental data in the surface potential experiments is due in part to the low specific activity of the DGE and to the general difficulties experienced in obtaining surface potential measurements.

Sorption Isotherms.—The equilibrium amounts of DGE sorbed onto chrome plate from each of the three solvents was determined as a function of solution concentration. In the procedure chrome plates were each given a quick rinse in the solvent after sorption in order to remove any adhering solution and allowed to drain. It was considered desirable to know the magnitude of this "carry-out" effect. A "no-rinse" curve therefore was determined using samples from which adhering solution had not been rinsed but which were allowed to drain.

Figure 4 shows the sorption isotherm and the "no-rinse" curve obtained from benzene solution. It can be seen that the sorption isotherm levels off at about 4.2×10^{-10} mole/cm.² (or 18.5 c./min./cm.²). The "no-rinse" curve rises linearly with solution concentration, reflecting the amount of DGE deposited on the plate in addition to the amount sorbed.

The corresponding sorption isotherm and "no-rinse" curves obtained with hexane as solvent and rinse were qualitatively similar to those obtained with benzene. The sorption isotherm levels off at about the same coverage (4.3×10^{-10} mole/cm.², or 19.0 c./min./cm.²). At low solution concentration, appreciably more DGE is sorbed from hexane than from benzene solution. The "no-rinse" curve also rises with solution concentration, and has a considerably greater slope than the "no-rinse" curve obtained from benzene solution, demonstrating the poor affinity of DGE for hexane.

The sorption isotherm for chloroform solution of DGE could not be obtained since the quick rinse with chloroform after sorption removed all but 2 to 3 c./min./cm.² of DGE from the plates. Apparently, chloroform effectively competes with DGE for the chrome surface by virtue of its polar nature. The "no-rinse" curve from chloroform solution was essentially identical with that obtained with benzene.

Desorption and Exchange.—The interaction between DGE and chrome plate was characterized further with additional information obtained in desorption and exchange experiments. In the exchange experiments, radioactive DGE sorbed on chrome plates was allowed to exchange with non-radioactive DGE in solution.

Both desorption and exchange from each of the three solvents were found to be extremely rapid at surface coverages above 1×10^{-10} mole per cm.². Below this amount of coverage removal of sorbed DGE was a slow process (see Fig. 5).

In the case of benzene as solvent, the extent of surface coverage remaining after the initially rapid desorption (*i.e.*, the height of the horizontal portion of the curve) appears to be somewhat dependent upon the length of time the DGE had equilibrated with the surface in the sorption stage. The residual amount of DGE was greater when the longer sorption equilibration periods were used. This suggests again that the equilibration of DGE with the surface from benzene solution is a slow process. This is consistent with the sur-

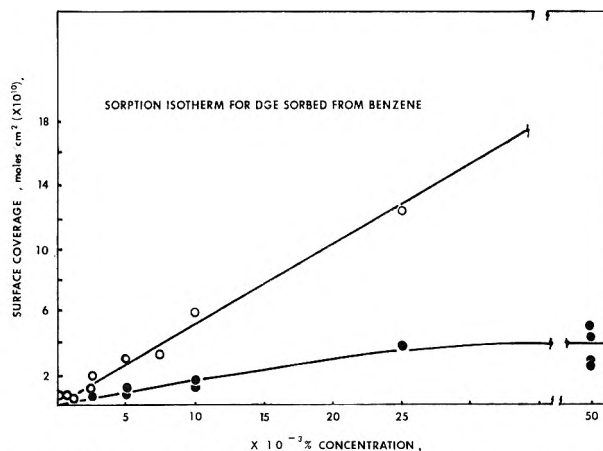


Fig. 4.—Sorption isotherm for DGE sorbed from benzene: solid circles, "no-rinse" curve; open circles, rinsed samples.

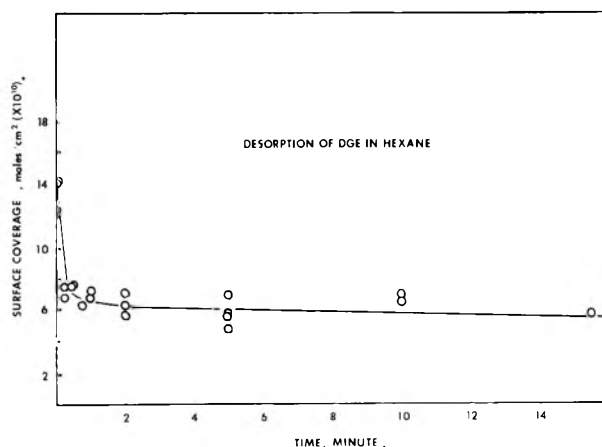
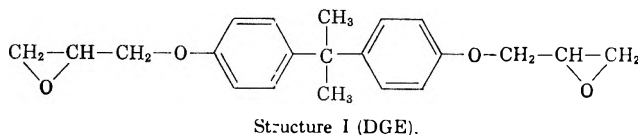


Fig. 5.—Desorption kinetics of DGE in hexane; sorption time, 1 hr.

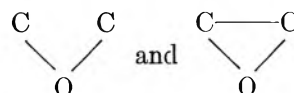
face potential data. This slow process may involve either a reorientation and redistribution of sorbed molecules to a more ordered arrangement, or chemisorption.

Discussion

The DGE molecule (see Structure I) contains four oxygen atoms distributed along a hydrocarbon back-



bone. It is assumed that only oxygen atoms in direct contact with the surface affect the surface potential. It also may be reasonable to assume that the four oxygen atoms are equivalent in their effect on the surface potential, since the metal (oxide) surface "sees" very similar structures



This molecule therefore may be considered intermediate in functionality between simple molecules such as stearic acid, and larger molecules such as polyvinyl acetate. Therefore the results obtained with DGE may be useful in describing the behavior of polymer molecules at an interface.

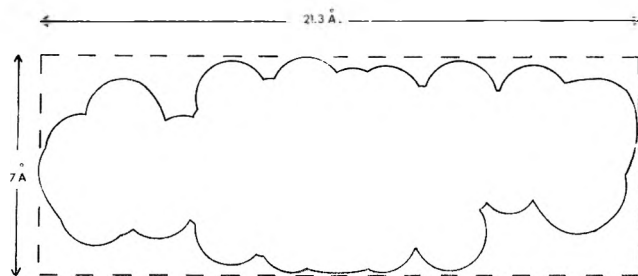


Fig. 6.—Projection of DGE molecule on surface, with estimated molecular dimensions.

In order to interpret the surface potential data, it is first necessary to estimate the area occupied by a DGE molecule when it is sorbed on chrome plate. Film balance measurements on the higher homologs of DGE¹³ on water indicate that the area occupied on the water surface is largely determined by the surface pressure applied. A consideration of the Fischer-Hirschfelder model of DGE demonstrates the possibility of widely divergent surface areas occupied by sorbed molecules, depending on whether a vertical or horizontal (flat) orientation of the molecule is assumed. The minimum and maximum surface areas which would be occupied by the molecule lying flat or standing vertically were estimated as follows.

The minimum area of the DGE molecules lying flat was estimated from a projection of the Fischer-Hirschfelder molecular model on a plane surface (see Fig. 6). The corresponding maximum area was estimated from the product of the maximum length and maximum width of the molecular model.

The minimum area occupied by the DGE molecule sorbed in a vertical orientation can be conveniently estimated from the molecular volume calculated from the measured specific gravity of DGE and the maximum length of the molecule estimated from the model. The maximum area occupied by the molecule standing vertically was taken as the area swept out by the rotation of the methyl groups around the molecule "backbone." The results of these calculations, and the calculated surface coverage for a monolayer of DGE for each case, are shown in Table I. These estimated values of the molecular area of sorbed DGE can be used to interpret the data as follows.

TABLE I
MINIMUM AND MAXIMUM AREAS COVERED BY THE DGE MOLECULE SORBED IN HORIZONTAL AND VERTICAL ORIENTATIONS

	Horizontal		Vertical	
	Area per molecule, Å. ²	Coverage (moles/cm. ²)	Area per molecule, Å. ²	Coverage (moles/cm. ²)
Minimum	100	1.6×10^{-10}	22.9	7.2×10^{-10}
Maximum	150	1.1×10^{-10}	38.5	4.3×10^{-10}

When DGE is sorbed from chloroform solution it is found that the surface potential increases linearly with surface coverage, extrapolating to the plateau voltage at about 3.7×10^{-10} mole per cm.² sorbed (Fig. 1). This curve is similar to that reported by Gottlieb for the surface potential of a sorbed monofunctional molecule, octadecyl acetate. The extrapolated surface coverage corresponds approximately to the maximum expected area per DGE molecule in the vertical orientation as estimated from the molecular dimensions (see Table I). This correspondence suggests that at total coverage DGE molecules may be sorbed vertically

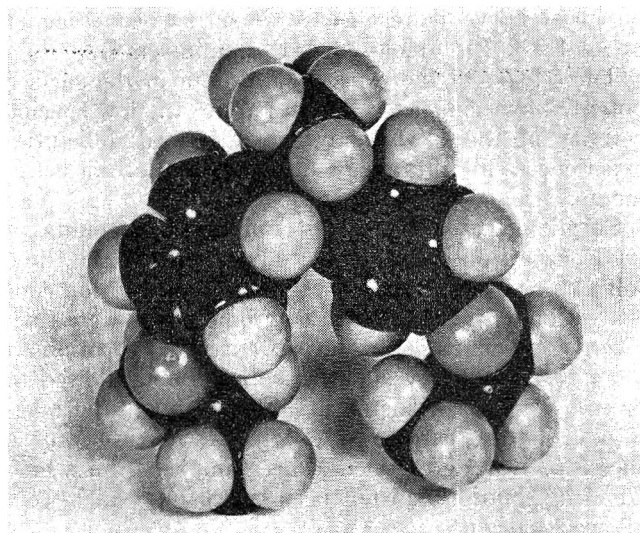


Fig. 7.—DGE molecular model, in horseshoe configuration.

with only one oxirane oxygen in contact with the surface. It seems likely that DGE may be sorbed from chloroform solution in the vertical configuration even at low coverages.

The surface potential-surface coverage curves for DGE sorbed from benzene and from hexane are different from that obtained from chloroform solution.

The rate of increase of surface potential with sorption of DGE from benzene (Fig. 2) is initially four times that found when DGE is sorbed from chloroform solution. This finding is understandable if the DGE molecules are pictured in this case as being sorbed with their four oxygen groups each in contact with the chrome surface and contributing to an increase in surface potential. The flat configuration for sorbed DGE molecules would satisfy this condition. From an extrapolation of the initial slope of the surface potential-surface coverage curve to the plateau voltage, it would also appear that each molecule in this configuration occupies 150 Å.² surface area. It is interesting to note that this is the same area per monomer unit found by Schick¹⁵ for an ethoxilin polymer at the water-carbon tetrachloride interface.

The onset of the plateau region occurs at about 4.0×10^{-10} mole per cm.² sorbed. Therefore, the completed monolayer may be composed of DGE molecules sorbed in the vertical configuration. Evidence of the change in configuration of sorbed DGE molecules is seen in the marked transition region separating the initial steep-sloped part of the curve from the plateau. From the shape of the curve in the transition region it appears that the rearrangement from the flat to the vertical configuration at high surface coverages results from the (partial) displacement of each DGE molecule originally sorbed in the flat configuration by subsequently sorbed DGE.

When DGE was sorbed onto the chrome plate from hexane solution the initial slope of the surface potential-surface coverage curve (Fig. 3) was found to be twice that obtained in sorption from chloroform solution. This suggests that at initial low coverages DGE molecules may be sorbed from hexane with two oxygen groups in contact with the chrome surface contributing to surface potential. A "horseshoe" bent conformation determined with the molecular model satisfies

(15) M. J. Schick, *J. Polymer Sci.*, **25**, 465 (1957).

this condition by permitting sorption of DGE molecules with only the two epoxide oxygens on the surface (see Fig. 7). The plateau is reached at about 4.0×10^{-10} mole/cm.², as in the experiments with benzene and chloroform solutions. A transition region also appears between the plateau and the initial steep-sloped part of the curve. This suggests that as the surface coverage increases, additional molecules pack in at the surface and force a vertical orientation on the sorbed molecules.

Our results at low surface coverage indicate that DGE is sorbed in different configurations depending upon the solvent. Since at low coverage the DGE molecules are essentially surrounded by solvent only, these differences may reflect different configurations of DGE molecules in these solutions. A mixed solvent-solute monolayer may exist here, similar to that described by Cook and Ries.² At higher coverage, the DGE molecules are sorbed vertically from all three solvents. It therefore appears that this orientation

is energetically preferred where solute-solute interactions are more prominent.

The kinetics of desorption of DGE into hexane, benzene, and chloroform are very rapid down to surface coverages of about 75 to 150 Å.² per molecule; thereafter desorption is very slow. This suggests that desorption of the vertically oriented molecular layer (where one oxygen per molecule interacts with the surface) is rapid, but when sufficient surface is available for two or more oxygens per molecule to interact with the surface, the rate of desorption is greatly diminished. It is felt that this interpretation may be generalized to the case of desorption of polymer molecules from surfaces.

Acknowledgment.—We wish to express our appreciation to the management of Interchemical Corporation for permission to publish this work. We also wish to thank Mr. C. A. Kumins for his constant encouragement and helpful suggestions.

RADIOLYSIS OF LIQUID METHANOL AND SOME METHANOLIC SALT SOLUTIONS

BY LESLIE M. THEARD AND MILTON BURTON

Department of Chemistry and Radiation Laboratory,¹ University of Notre Dame, Notre Dame, Indiana

Received May 21, 1962

In the concentration range 10^{-3} to 10^{-1} M, KI decreases yields of glycol and of H₂ and increases formaldehyde yield in Co⁶⁰-gamma radiolysis of liquid methanol according to the stoichiometric relationship $-\Delta G(\text{glycol}) + \Delta G(\text{H}_2) \simeq \Delta G(\text{H}_2\text{CO})$. CsCl has similar but less pronounced effects and KBr and KCl are without effect. The chlorides of La, Gd, Dy, Y, and Lu, at concentrations >0.05 M, have effects on $G(\text{glycol})$ and $G(\text{H}_2\text{CO})$ which are qualitatively similar to that of KI (changes in $G(\text{H}_2)$ are attributable to an "acid effect"); effects within the group differ quantitatively in a manner independent of atomic number or magnetic character (paramagnetic or diamagnetic). The effects of the salts other than KI are discussed in terms of the influence of degree of solvation. The effect of KI on $G(\text{glycol})$ and $G(\text{H}_2\text{CO})$ is concluded to be attributable to the chemistry of the I⁻ ion itself and to be non-dependent on its mass or atomic number as such. The important mode of behavior which leads to H₂CO enhancement and equal glycol decrease is suggested to be $\text{CH}_3\text{O} + \text{I}^- \rightarrow \text{CH}_3\text{O}^- + \text{I}$.

Introduction

In the radiolysis of methanol, addition of potassium iodide increases the 100-e.v. yield of formaldehyde and decreases that of ethylene glycol.² Two possible explanations have been suggested: a single sequence of chemical reactions responsible for both effects or, alternatively, an essentially physical phenomenon, namely a Stark effect-induced internal conversion (by the heavy I⁻ ion), which might in turn determine the state decomposing to the observed product or precursor of that product. The investigation here reported was motivated by the desire to discover whether excited states of sufficient persistence for occurrence of the latter process might exist in liquid methanol.

The work described was confined to observation of a limited number of phenomena, which neither required nor permitted kinetic analysis. Instead, it rather directly tested the possible merits of the mechanisms proposed by comparison of the effects of KI with those of CsCl (Cs⁺ and I⁻ are of approximately the same atomic mass), LiCl, and KCl. Further, because internal conversion induced paramagnetically (*i.e.*, by a Zeeman effect) is known to be more probable than the electro-

statically induced process, various other chlorides of both paramagnetic and diamagnetic rare earths and related elements were studied for their effects; the former included GdCl₃ and DyCl₃, the latter LaCl₃, YCl₃, and LuCl₃.

Experimental

Materials.—Stopcocks and ground-glass tapered joints were greased with Apiezon stopcock-grease type N.

The following chemicals were employed without further purification: cesium chloride, Fisher Purified; potassium chloride, potassium bromide, potassium iodide, and lithium chloride, Fisher Certified Reagent; Baker and Adamson magnesium metal (ribbon form) and lanthanum chloride; Baker Purified magnesium turnings; Baker Analyzed Reagent sulfuric acid and hydrochloric acid; Eastman 2,7-naphthalene-disulfonic acid-4,5-dihydroxy sodium salt; Fisher sodium metal.

The two grades of methanol used were Eastman's Spectrograde and Fisher's Certified. Typical stated impurities for the latter and their amounts are: water, 0.01 to 0.05%; acidity, 0.002%; alkalinity, 0.0003%; acetone, aldehydes, 0.0003%. Impurities, including water, in the Spectrograde material were undetectable by vapor phase chromatography. However, the presence of water was detected during the drying procedure by precipitate formation after reaction of magnesium with methanol.

CD₃OH was obtained from the Volk Radiochemical Co. and had a stated isotopic purity of 99%.

Samples of lanthanum, yttrium, gadolinium, dysprosium, and lutetium chlorides were prepared from the rare earth oxides³:

(3) The high purity oxides were graciously supplied by Professor F. H. Spedding of Iowa State University and of the Ames Laboratory of the Atomic Energy Commission.

(1) The Radiation Laboratory is operated under contract with the Atomic Energy Commission. This paper was presented at the 141st National Meeting of the American Chemical Society, Washington, D. C., March 21, 1962.

(2) G. Meshitsuka and M. Burton, *Radiation Res.*, **8**, 285 (1955).

with minor variations, the method was that described by Moeller and Brantley.⁴

Sodium methylate solution in methanol was prepared by vacuum distillation of a known volume of methanol into a flask containing a weighed sample of sodium metal. Agitation during and after reaction ensured homogeneity of the solution.

Radiation Sources and Dosimetry.—Two types of Co⁶⁰ γ -ray sources were used: an underground source⁵ and a Ghormley-Hochanadel type source. Energy absorption in methanol and in methanolic solutions was determined with the Fricke dosimeter using the value $G(\text{Fe}^{+3}) = 15.6$ with correction on the basis that absorption of energy per unit volume by the various liquid media at the same position in the source is proportional to their electron densities. Dose rates were approximately 8×10^{20} and 1.5×10^{20} e.v./min.

Apparatus.—Most of the degassing and gas collection was carried out by a reflux method. Apparatus for both procedures included a small cold finger atop a glass rod-packed column having a round-bottom flask connected at the lower end. The outer jacket of the cold finger was constructed of 15-mm. o.d. tubing; 10-mm. o.d. tubing formed the finger. A 6-mm. diameter rod extended almost the entire length inside the 35-cm. long, 10-mm. o.d. column. A 50-ml. and a 500-ml. round-bottomed flask were connected below the gas collection and degassing columns, respectively. Both columns had side arms connected just above the flasks for introduction of samples.

Drying of methanol on the vacuum line was carried out in a 500-ml. round-bottom flask fitted with water-cooled condenser. Atop the condenser was attached a tapered joint modified by inside connection of a length of tubing by ring seal just below the taper. The tubing was of sufficient length to protrude through the joint, and it thereby limited contact of methanol vapor with stopcock grease during distillation.

Sample Preparation and Exposure.—Except where otherwise indicated, all the degassing and gas collection employed the microstill reflux method described by Van Dusen and Hamill.⁶ Methanol was dried on the vacuum line by reaction with magnesium; much of the residual hydrogen was pumped off in several repeated expansions. After 3–6 hr. of stirring and refluxing at 40° the material was transferred under vacuum to the microstill for further treatment with magnesium and purification.

Methanol was treated with 2,4-dinitrophenylhydrazine, DNP, by several methods. One method, adapted from that of Siggia,⁷ included 3-hr. refluxing (on a 50-theoretical-plate column) of a mixture of 0.08 g. of DNP and 800 ml. of methanol 0.025 *M* in sulfuric acid. Thereafter, a 500-ml. middle fraction was collected and treated with sufficient sodium hydroxide to neutralize all the acid originally present in the lot. Refluxing of this fraction was followed by collection of a 300-ml. middle fraction which was dried *in vacuo*. In a second method, a solution of 4 g. of DNP and 1 ml. of concentrated H₂SO₄ in 2 l. of methanol was refluxed overnight, and a middle fraction was collected and then degassed without drying. A third method included refluxing of a solution of 10 g. of DNP, 2.2 ml. of concentrated H₂SO₄, 8 ml. of water, and 2 l. of methanol. Thereafter, the procedure followed that of the second method.⁸ All samples of methanol were degassed prior to irradiation.⁹ All *G* values reported are

(4) T. Moeller and J. C. Brantley, *Anal. Chem.*, **22**, 433 (1950).

(5) M. Burton, J. A. Ghormley, and C. J. Hochanadel, *Nucleonics*, **13**, 74 (1955).

(6) W. Van Dusen and W. H. Hamill, *J. Am. Chem. Soc.*, **84**, 3648 (1962).

(7) S. Siggia, "Quantitative Organic Analysis via Functional Groups," John Wiley and Sons, Inc., New York, N. Y., 1954, p. 31.

(8) In the second and third methods we followed J. H. Baxendale and F. W. Mellows, *J. Am. Chem. Soc.*, **83**, 4720 (1961). We are indebted to Dr. Mellows for his kind advice and assistance with this portion of our work.

(9) According to R. P. Porter, *J. Phys. Chem.*, **61**, 1260 (1957), studies involving methanol can be complicated by formation of trimethylborate in Pyrex vessels. The situation, when it occurs, is particularly notable in the vapor. Consequently, we made several attempts to detect trimethylborate impurity or an effect of its presence. Methanol vapor from liquid samples stored in Pyrex containers was analyzed by mass spectrometry with no indication of the presence of trimethylborate. Two samples of methanol vapor which had stood in Pyrex cells for three months under conditions prevalent in our Laboratory showed no detectable trimethylborate by mass spectral analysis. Repeated mass spectral analyses of methanol vapor throughout the course of the work likewise revealed no trimethylborate content. *G*(H₂) values for samples distilled from methanol lots which had been refluxed with ~5% water (for conversion of any borate to boric acid) prior to drying with magnesium were not significantly different from values for samples not so treated. Furthermore, there was no dependence of *G*-values on possible aging of methanol in Pyrex storage flasks.

for samples irradiated within a few hours after vacuum distillation into radiolysis cells.

Most of the salt solutions to be irradiated were prepared from solutions of the salts in vacuum-distilled methanol. Predetermined amounts of these solutions were added to irradiation cells; after partial degassing, the methanol was distilled off and discarded. Solutions of LiCl and rare earth chlorides had to be heated (by hot water) for complete removal of methanol. Afterwards, 5 or 10 ml. of dry, degassed methanol was distilled into the evacuated cells to make up the final solutions. The samples were exposed to irradiation in 10-ml. sealed Pyrex cells according to the usual technique.

Product Collection and Analysis.—The bulk of the gases (*ca.* 85%) was first collected by freeze-thaw technique. The microstill reflux method enabled collection of the last remnants of gas; a minor modification in this work was the employment of liquid nitrogen instead of Dry Ice as coolant for the copper rod inserted in the still head.

Analysis for formaldehyde was by a variant of MacFadyen's technique¹⁰ of colorimetric quantitative determination of the complex formed by formaldehyde and chromotropic acid (2,7-naphthalene-disulfonic acid-4,5-dihydroxy). In the present work it was found that methanol markedly affects the extinction coefficient of the complex when chromotropic acid solution, prepared according to MacFadyen's technique, is treated with methanolic solutions of formaldehyde of known concentration. Plots of optical density *vs.* concentration become increasingly non-linear with increasing methanol concentration. However, a tenfold dilution of the methanol solution with 9 *M* sulfuric acid prior to treatment with chromotropic acid solution results in a linear Beer-Lambert relationship for solutions in which formaldehyde and chromotropic acid concentrations are 0.1 to 1.1 γ /ml. and 2 mg./ml., respectively. The extinction coefficient of the complex determined therefrom is 0.64 ml./ γ -cm.

Procedure for analysis of an irradiated sample began by dilution of 1 ml. of the sample to a volume of 10 ml. by 9 *M* sulfuric acid; 1 ml. of this solution in a 25-ml. volumetric flask then was treated with 10 ml. of chromotropic acid solution, prepared by the method of MacFadyen. The mixture, in the stoppered flask, was heated for 1.5–2 hr. in boiling (or near-boiling) water along with a blank solution (in another flask) prepared from pure methanol. (For convenience, several analyses were conducted at the same time.) Because the reaction is light sensitive, heating was always in darkness. Optical densities were measured on a Beckman Model DU spectrophotometer at 570 $m\mu$ using the tungsten-lamp light source. Accuracy of determination of known samples was $\pm 6\%$.

Analysis for glycol was by oxidation of the glycol to formaldehyde and analysis of formaldehyde with chromotropic acid. Correction was made for formaldehyde already present. The procedure used is an adaptation of the method of Lambert and Neish for determination of glycerol.¹¹ Considerable spread in analysis of known samples warranted the assignment of accuracy at $\pm 14\%$.

Results

Gas yields were determined for a variety of samples of pure methanol. The latter differed in method of degassing, presence or absence of water impurity, and use either directly from the manufacturer's bottle or after distillation. Values of *G*(H₂) were in the range 3.7 to 5.2 and were of good reproducibility only when the microstill reflux method of degassing (for initial purification) was used. All reported yields are from samples degassed by this method.

Figure 1 shows yields from samples which were dried *in vacuo* prior to degassing. Only the values of *G*(CH₄) based on the reflux gas-collection technique are shown. Such yields are *ca.* 33% higher than less trustworthy ones determined by freeze-thaw gas collection. The difference is attributable to better collection of CH₄ by the reflux method; difficulty of removal of methane from methanol has been reported previously.²

(10) D. A. MacFadyen, *J. Biol. Chem.*, **158**, 107 (1945).

(11) M. Lambert and A. C. Neish, *Can. J. Res.*, **28B**, 83 (1950).

Approximately one-third of the yields shown in Fig. 1 were obtained with purified Eastman Spectrograde methanol. All other runs were made with purified Fisher Certified methanol. There is no detectable difference in yields with pure methanol which is attributable to the brand of methanol used.

Table I lists gas yields from Fisher methanol samples which were treated by various techniques prior to irradiation (*cf.* Sample Preparation and Exposure). The methanol employed in the last run shown in Table I was prepared like that in the runs represented by Fig. 1.

TABLE I
GAS YIELDS FROM LIQUID METHANOL RADIOLYSIS
Dose: $ca. 3 \times 10^{19}$ e.v./ml.

Description of purification technique	G		
	H ₂	CH ₄	CO
DNP (0.1 g./l.)	5.02	0.31	0.06
DNP (2 g./l.) + H ₂ SO ₄ (0.02 N)	4.98	.42	.14
DNP (2 g./l.) + H ₂ SO ₄ (0.02 N)	5.00	.44	.12
DNP (5 g./l.) + H ₂ SO ₄ (0.04 N) + H ₂ O (0.03 M)	5.03	.43	.10
DNP (5 g./l.) + H ₂ SO ₄ (0.04 N) + H ₂ O (0.03 M)	4.94	.46	.10
10 ⁻⁴ M acetone in MeOH prepared with DNP	4.90	.45	.11
Stock MeOH	4.85	.43	.16
Stock MeOH	4.94	.45	.20
No DNP, dry	4.57	.41	.17

The value of $G(\text{H}_2)$ from samples which were treated with DNP is close to 5.0, as shown in Table I; an average $G(\text{H}_2)$ from all samples not so treated is *ca.* 4.7 (Fig. 1). Before too much significance is attached to this difference, it should be noted that $G(\text{H}_2)$ from stock methanol not treated with DNP and degassed without drying is *ca.* 4.9 (Table I). Further, addition of 10⁻⁴ M acetone to methanol which had been treated with DNP resulted in $G(\text{H}_2) = 4.9$ (Table I). The amount of added acetone is comparable to the 0.0005% acetone and aldehydes initially present in the methanol (Fisher Certified Reagent) as stated by the manufacturer. All the samples represented in Table I, with the exception of the first, were prepared from the sample lot of Fisher Certified Reagent methanol.

Values of $G(\text{H}_2)$, $G(\text{H}_2\text{CO})$, $G(\text{glycol})$, and $G(\text{CH}_4)$ extrapolated to zero dose (*cf.* Fig. 1) are 4.63, 1.99, 2.69, and 0.44, respectively. The average value of $G(\text{CO})$ is 0.07.

Figure 2 shows the effect of KI on methanol radiolysis yields. A few low-concentration runs on DNP-treated methanol containing KI (Table II) indicate that the yields differ from those obtained for solutions of KI in solvent not treated with DNP. Because of such differences observed for solutions and the effect of DNP treatment observed for pure methanol radiolysis, the discussion of results is concerned only with the concentration-dependent trends of yields; such trends apparently are unaffected by solvent treatment with DNP.

The data of Table III show that at 0.05 and 0.1 M concentrations the qualitative effect of CsCl is similar to that of KI; quantitatively, CsCl is less effective. Solutions with concentrations less than 0.05 M (Table II) were prepared with DNP-treated solvent. Although values of $G(\text{glycol})$ are in poor agreement, the slight rise of $G(\text{H}_2\text{CO})$ between 2×10^{-3} and 2×10^{-2} M indi-

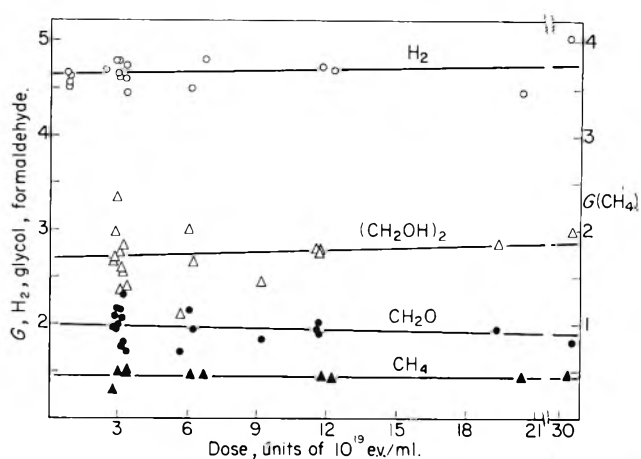


Fig. 1.—Effect of dose on yields from radiolysis of methanol.

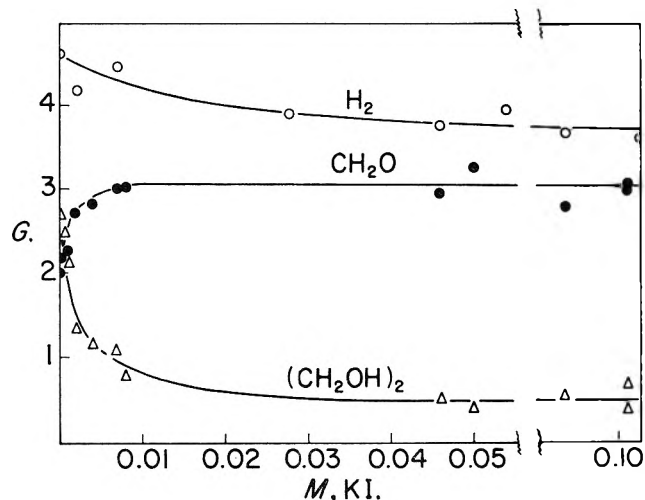


Fig. 2.—Effect of KI on yields of some methanol radiolysis products: O, H₂; ●, CH₂O; Δ, (CH₂OH)₂.

cates an effect of CsCl considerably less than that shown for KI.

The solutes LiCl, KCl, KBr, and CH₃ONa (Tables II and III) are practically without effect at 0.05 M concentration.

TABLE II
RADIOLYSIS YIELDS FROM SOLUTIONS OF SALTS IN DNP-TREATED METHANOL

Solute	Concn., M	G				
		H ₂ CO	(CH ₂ OH) ₂	H ₂	CH ₄	CO
..	0	1.96	2.99	4.99	0.41	0.10
KI	0.002	3.25	1.37	4.95	.43	.07
	.004	3.35	0.95	4.90	.47	.09
	.015	3.75	1.12	4.79	.46	.05
CsCl	.002	2.12	3.35			
	.004	2.03	2.92			
	.01	2.29	3.07			
	.02	2.46	2.82			
LiCl	.05	2.26	3.52			
	.1	2.04	2.91			
	.5	3.18	2.36			

Figure 3 shows yields from solutions of LaCl₃, GdCl₃, and YCl₃ in methanol (no DNP was used in the solvent purification). The effect of GdCl₃ on $G(\text{H}_2)$ is almost identical with that shown for LaCl₃. Table IV shows effects of DyCl₃ and LuCl₃; the data for these compounds cover a smaller range of concentration and

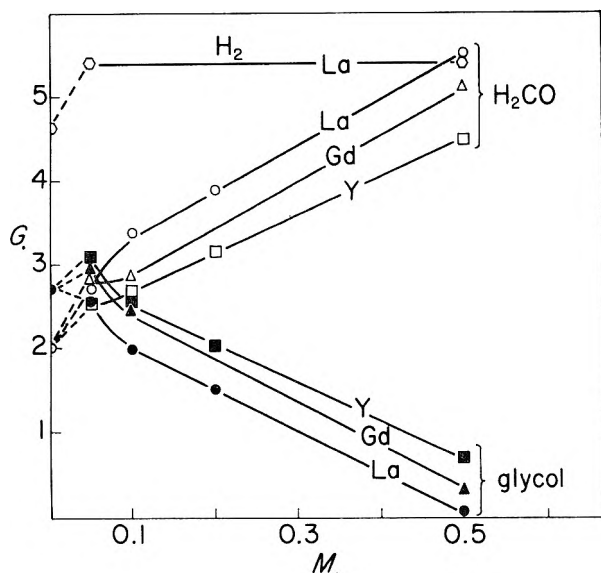


Fig. 3.—Effects of some rare earth chlorides on some methanol radiolysis yields: (\square) $G(\text{H}_2)$ vs. $[\text{LaCl}_3]$; (\circ), $G(\text{CH}_2\text{O})$ vs. $[\text{LaCl}_3]$; (\bullet), $G(\text{glycol})$ vs. $[\text{LaCl}_3]$; (Δ), $G(\text{CH}_2\text{O})$ vs. $[\text{GdCl}_3]$; (\blacktriangle), $G(\text{glycol})$ vs. $[\text{GdCl}_3]$; (\square), $G(\text{CH}_2\text{O})$ vs. $[\text{YCl}_3]$; (\blacksquare), $G(\text{glycol})$ vs. $[\text{YCl}_3]$.

TABLE III
RADIOLYSIS YIELDS FROM METHANOLIC SALT SOLUTIONS
Dose: ca. 3.1×10^{19} e.v./ml.

Solute	Concn., M	G				
		H_2CO	$(\text{CH}_2\text{OH})_2$	H_2	CH_4	CO
..	0	1.99	2.69	4.63	0.44	0.07
CsCl	0.05	2.19	1.75	4.14	.47	.11
	.1	2.74	1.19	3.80	.45	.11
	.5	2.72	2.36			
LiCl	0.03	2.03	2.61			
	.05	2.61	1.92	4.48	.44	.14
	.1	2.13	2.50			
KCl	.05	1.76	2.32	4.47	.45	.14
	.05	1.64	2.96	4.44	.44	.13
	.5	1.79	2.91			
CH_3ONa	.05	1.95	2.59	4.46	.54	.09
	.1	1.95	2.93			
	.5	1.79	2.91			

would confuse the curve beginnings if included in Fig. 3. The effect of 0.05 M DyCl_3 on $G(\text{glycol})$ is striking. All the chlorides represented by Fig. 3 and Table IV were prepared from the corresponding oxides by us. It was found that a LaCl_3 sample obtained from the Allied Chemical and Dye Corporation had effects on $G(\text{H}_2\text{CO})$ and $G(\text{glycol})$ qualitatively similar to, but quantitatively different from, the effects observed for LaCl_3 synthesized by us from the oxide. For example, at 0.5 M yields determined for a solution of the Allied product were $G(\text{H}_2\text{CO}) = 3.90$ and $G(\text{glycol}) = 1.43$.

TABLE IV
FORMALDEHYDE AND GLYCOL YIELDS FROM METHANOL SOLUTIONS
OF DyCl_3 AND LuCl_3
Dose: ca. 3.1×10^{19} e.v./ml.

Solute	Concn., M	G	
		H_2CO	$(\text{CH}_2\text{OH})_2$
..	0	1.99	2.69
DyCl_3	0.05	2.42	3.63
	.1	2.83	2.45
	.2	3.22	2.26
	.2	3.05	2.43
LuCl_3	.05	2.54	3.16
	.1	2.73	2.88
	.2	3.05	2.43

Table V gives relative gas radiolysis for 0.5-ml. samples of liquid CD_3OH and solutions of KI and LaCl_3 in CD_3OH .

TABLE V
RELATIVE GAS RADIOLYSIS YIELDS FROM LIQUID CD_3OH AND
SOLUTIONS OF LaCl_3 AND KI IN CD_3OH
Dose: ca. 2×10^{20} e.v./ml.

Solute	M	%			
		H_2	HD	D_2	$\text{CD}_4/\text{CD}_3\text{H}$
..	..	11	78	11	2.4
LaCl_3	0.05	11	78	11	1.5
LaCl_3	.2	17	72	11	1.0
KI	.01	13	75	12	2.4
KI	.12	17	68	15	1.6

Discussion

General Statements.—The effect of KI shown in Fig. 2 is described by the relationship

$$-\Delta G(\text{glycol}) + \Delta G(\text{H}_2) \simeq \Delta G(\text{H}_2\text{CO})$$

The sharp increase of $G(\text{H}_2\text{CO})$ and the sharp decrease of $G(\text{glycol})$ occur in the same KI concentration region; apparently, the two changes result from interdependent processes. Similarly, the more gradual decrease of $G(\text{H}_2)$ may be attributable to processes which lead also to gradual decrease of $G(\text{glycol})$.

The relative lack of effect of KCl indicates that I^- is responsible for the KI effect. Further, although the qualitative effects of CsCl and KI are similar, the quantitative difference argues against attribution of the I^- effect to a nuclear charge-dependent process.

Yttrium chloride and the rare earth chlorides studied affect methanol radiolysis yields, but no effect of these compounds is attributable to paramagnetism. Absence of a paramagnetic effect is evidenced by Fig. 3, which shows that at concentrations greater than 0.05 M , paramagnetic GdCl_3 has a qualitative effect similar to diamagnetic LaCl_3 and YCl_3 and a quantitative effect which is between that of the latter two compounds.

The over-all effects of the rare earth compounds are attributable to two processes, one of which occurs at low concentration, and another which occurs at high concentration.

It appears that the low-concentration effect is attributable to acidity. Other workers^{3,12,13} have shown that increased acidity (from addition of H_2SO_4) causes increase of $G(\text{H}_2)$, $G(\text{H}_2\text{CO})$, and $G(\text{glycol})$; acidity of methanolic solutions of rare earth chlorides may be assumed from known acidity of the corresponding aqueous solutions.¹⁴

Increase of $G(\text{H}_2\text{CO})$ and decrease of $G(\text{glycol})$ in the concentration range 0.1 to 0.5 M (cf. Fig. 3) are not accompanied by further change in $G(\text{H}_2)$; such a result does not fit what is known about an acid effect.¹² Because of the high salt concentration, some consideration of possible effects of direct energy absorption by the salts is desirable. For example, it may be considered that behavior of the salts subsequent to absorption of energy leads to the observed effects on $G(\text{H}_2\text{CO})$ and $G(\text{glycol})$. However, at equal concentration, YCl_3 , LaCl_3 , and GdCl_3 absorb energy in the order written, *i.e.*, with increasing mass, but the magnitude

(12) G. E. Adams and J. H. Baxendale, *J. Am. Chem. Soc.*, **80**, 4215 (1958).

(13) N. N. Lichtin, *J. Phys. Chem.*, **63**, 1440 (1959).

(14) T. Moeller and H. E. Kremers, *Chem. Rev.*, **37**, 120 (1945).

of the effect of $GdCl_3$ is between that of $LaCl_3$ and YCl_3 . Further, the two heaviest of the rare earth chlorides studied, $DyCl_3$ and $LuCl_3$, have effects nearest to that of the lightest compound of the group, YCl_3 .

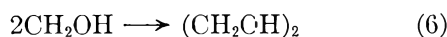
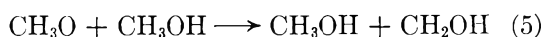
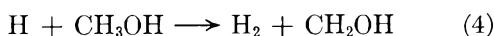
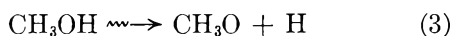
The extent of increase of $G(H_2CO)$ and decrease of $G(\text{glycol})$ in the presence of rare earth chlorides at equal concentration decreases in the order $LaCl_3$, $GdCl_3$, $DyCl_3$, YCl_3 , and $LuCl_3$, which also is the order of decreasing basicity of the cations. Basicity is indicative of relative tendency to lose or gain electrons. The greater the basicity of cations, the less is their attraction for electrons, either free or combined in anions.¹⁴ This view implies that at equal concentration in methanol the degree of dissociation of the salts listed decreases in the order given; it would also mean that the number of methanol molecules involved in solvation sheaths about the solutes decreases in the same order. This latter point suggests that absorption, or perhaps more precisely the localization, of excitation energy in molecules in the solvation sheath may lead to enhanced formaldehyde yield and depressed glycol yield. Thus, a mode of methanol decomposition which leads to glycol formation may be so affected by solvation that formaldehyde formation is favored.

Remarks on Mechanism.—The reaction



is a plausible primary interaction which may account for the effect of I^- on $G(H_2CO)$ and part of its effect on $G(\text{glycol})$. Reaction 1 is analogous to the scavenging of OH radicals by halide ions (presumed to occur in the radiolysis of aqueous acid solutions of halide salts).¹⁵

An over-all mechanism of methanol radiolysis fits the following chemical features.

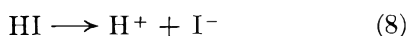


Iodine atoms produced through reaction 1 presumably would encounter CH_2OH radicals. Reaction *via*

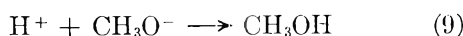


would cause increased $G(H_2CO)$, and reactions 1 and 7 account for equal depression of $G(\text{glycol})$ because reactions 5 and 6 are thus made to occur to a lesser extent.

Dissociation of HI



and neutralization of CH_3CO^-

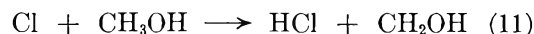


complete the over-all process.¹⁶

Similar removal of methoxy radicals by Cl^- ions

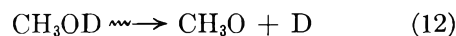


is not expected to affect yields because Cl atoms would readily react with methanol

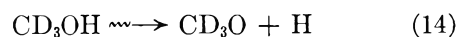


to yield CH_2OH radicals. Thus, the net result would be replacement of reaction 5 by reactions 10 and 11 without change in ultimate consequences.

Production of methoxy radicals by methanol radiolysis seems likely on the basis of compositions of hydrogens produced from radiolysis of liquid CD_3OD and of liquid CD_3OH . Meshitsuka, *et al.*,¹⁷ reported 60% HD, 4% D_2 , and 36% H_2 produced from CH_3OD . Burr, Dalton, and Meyer¹⁸ reported similar results for CH_3OD ; for radiolysis of liquid CD_3OH they found 75% HD. The data of Table V agree with the latter result. The large contribution of hydroxyl hydrogen to over-all molecular hydrogen production is clearly indicated, and a reasonable inference is that considerable initial decomposition occurs *via* reaction 3. According to previous work (on effect of so-called scavengers) formaldehyde appears to be formed, at least in part, by a process unimolecular in excited methanol.^{2,8,12} In this view, in radiolysis of CH_3OD and CD_3OH , HD production is expected to accompany formaldehyde production. However, since $G(CH_2O)$ is only *ca.* 40% of $G(H_2)$, it seems likely that there is some other mode of formation of HD. If methoxy radicals are produced, further production of HD may occur by the reactions

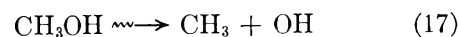


or



Assuming that, in the presence of KI, the process which leads to formaldehyde enhancement results also in equal glycol depression, the remaining unaccounted-for glycol depression equals hydrogen depression (*cf.* eq. 1). The latter two effects probably are related and perhaps are attributable to a process which suppresses methanol decomposition. Suppression of reaction 2 leads to the required stoichiometry. Of the 1-1 electrolytes studied, only KI and CsCl show an effect on $G(H_2)$.

Production of H, CH_3 , and radical precursors of glycol, which may be CH_2OH or CH_3O , is well evidenced by previous work on methanol radiolysis.^{2,8,12} Furthermore, it is known that all the formaldehyde and ~40% of the hydrogen found have no scavengable radical precursors.^{2,8,12} Accordingly, decomposition steps 2 and 3 and, in addition, decomposition *via* the over-all processes



account for much of the radiation chemistry of liquid methanol. It is interesting to note that these decom-

(17) G. Meshitsuka, K. Ouchi, K. Hirota, and G. Kusumoto, *J. Chem. Soc. Japan*, **78**, 129 (1957).

(18) J. G. Burr, C. K. Dalton, R. A. Meyer, Abstracts of the 137th National Meeting of the American Chemical Society, Cleveland, Ohio, 1960, p. 42-R; NAA-SR-5350.

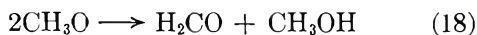
(15) M. Burton and K. C. Kurien, *J. Phys. Chem.*, **63**, 899 (1959).

(16) I_2 is not a product of radiolysis of methanolic KI solutions. Therefore, if I atoms are produced, either they do not combine to form I_2 , or if they combine, some further process results in total consumption of I_2 .

position steps have been proposed by Porter and Noyes¹⁹ to explain the ultraviolet photolysis ($\lambda < 2000 \text{ \AA}$.) of CH_3OH vapor. The similarity suggests that radiolytic decomposition of the liquid may occur, at least in part, from neutral electronically excited species. Meshitsuka and Burton² indicated that such a mechanism can explain all the decomposition. To the contrary, Hayon and Weiss²⁰ suggested that the radiolysis may involve dissociation of primarily formed polarons. Baxendale and Mellows⁸ attribute *ca.* 60% of the over-all decomposition to processes which may involve decomposition of the neutral species. Decomposition of excited methanol *via* reaction 16 was proposed by Baxendale and Sedgwick²¹ as the principal source of H_2CO produced in the vapor phase radiolysis of methanol.

The suggestion that rare earth chlorides may increase formaldehyde and decrease glycol by altering primary methanol decomposition may be considered with reference to reactions 2, 3, and 16. If decomposition *via* reaction 16 is enhanced by the solute at the expense of reaction 2 or 3, the net effect is enhancement of $G(\text{H}_2\text{CO})$ and equal depression of $G(\text{glycol})$; $G(\text{H}_2)$ is unaffected.

Implications of Methoxy Radical Production.—In pure methanol the probable fate of CH_3O radicals which diffuse away from the ionization track is reaction 5. In the ionization track, reactions of CH_3O radicals may contribute to part of the H_2CO yield *via* disproportionation



In the gas phase reaction 18 is exothermic by 74 kcal.²² Further, in a study of oxidation of methyl radicals, Dever and Calvert²³ compared reaction 18 to the reaction



and found that $k_{18}/k_{19} \geq 60$.

It is possible that methane may be produced in the

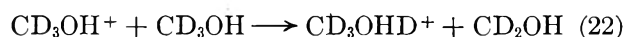
ionization track by a biradical reaction unaffected by scavenger.



Wijnen²⁴ has found that the activation energy for reaction 20 is 1.5 kcal.

Reaction 18 can account for the trend of relative formaldehyde and glycol yields as a function of LET. The ratio of ethylene glycol to formaldehyde is greater for γ -ray irradiation of methanol than it is for irradiation by 28-Mev. helium ions.²⁵ In the latter case the more densely ionizing helium ions may yield higher local CH_3O radical concentration (near the end of the ionization track) with resultant greater probability for occurrence of reaction 18.

Recent studies of ion-molecule reactions of CH_3OH vapor and of CD_3OH vapor suggest an ionization mechanism for production of CH_3O radicals. L. P. Theard and Hamill²⁶ studied the reactions



by mass spectrometry (at 10^{-5} mm. pressure). They found that $Q_{21}/Q_{22} = 1.3$, where Q_{21} and Q_{22} are cross sections of reactions 21 and 22, respectively. The total cross section of reactions 21 and 22 is very high and is about equal to the cross section of the ion-molecule reaction which produces CH_3OH_2^+ in CH_3OH vapor. Thus, if CH_3OH^+ enters an H-atom abstraction reaction in liquid CH_3OH , abstraction of H-atoms from OH groups seems more probable than abstraction from CH_3 groups by a factor of *ca.* 1.3 on the basis of the simple reactions 21 and 22 alone. In addition, in view of the favorable orientation resultant from hydrogen bonding, such abstraction from OH groups would appear to be even more favored in the liquid.²⁷

Acknowledgment.—The authors wish to thank Professor G. Meshitsuka for his help in the early stages of this work and Professors W. H. Hamill and J. L. Magee for several helpful suggestions and discussions.

(24) M. H. J. Wijnen, *J. Chem. Phys.*, **27**, 710 (1957).

(25) W. R. McDonell and S. Gordon, *ibid.*, **23**, 208 (1955).

(26) L. P. Theard and W. H. Hamill, *J. Am. Chem. Soc.*, **84**, 1134 (1962).

(27) *Cf.* the analogous reaction of radiolytically produced H_2O^+ in water in a model considered by Magee, "Summary of the Proceedings of an Informal Discussion of the Radiation Chemistry of Water," G. von Bünau, *et al.*, Editors, January, 1959, University of Notre Dame, Notre Dame, Indiana.

(19) R. P. Porter and W. A. Noyes, Jr., *J. Am. Chem. Soc.*, **81**, 2307 (1959).

(20) E. Hayon and J. J. Weiss, *J. Chem. Soc.*, 3970 (1961).

(21) J. H. Baxendale and R. D. Sedgwick, *Trans. Faraday Soc.*, **57**, 2157 (1961).

(22) P. Gray, *ibid.*, **52**, 344 (1956).

(23) D. F. Dever and J. G. Calvert, *J. Am. Chem. Soc.*, **84**, 1362 (1962).

THE OXIDATION OF HYDROGEN AND DEUTERIUM ON A ROTATING DISK ELECTRODE

BY GERALD P. LEWIS¹ AND PAUL RUETSCHI

The Carl F. Norberg Research Center, The Electric Storage Battery Company, Yardley, Pennsylvania

Received May 22, 1962

The oxidation of hydrogen and deuterium in alkaline solutions was studied by use of a rotating disk platinized platinum electrode. The variables investigated were KOH concentration, speed of rotation, electrode potential, and temperature. The rates for diffusion and ionization were determined. The currents decreased significantly as the KOH concentration was increased from 0.1 to 5.0 *N*. The product $k = DS^{3/2}$, where D is the diffusion coefficient and S the solubility, was determined for hydrogen and deuterium. The ratio of the k values of H₂ and D₂ was 3.5 in 0.1 *N* KOH at 30° and 3.3 at 50°. The ratios decreased successively as the KOH concentration increased and in 5.0 *N* KOH were 1.5 and 1.4 at 30 and 50°, respectively. The ratio of the maximum hydrogen ionization current to the maximum deuterium ionization current in the absence of diffusion effects was 1.8 in 0.1 *N* KOH at 30° and decreased to 1.5 in 5.0 *N* KOH at 30°. An increase in temperature from 30 to 50° increased the ionization current in both cases, but the hydrogen current increased at a faster rate than the deuterium current. The difference in the rate of oxidation between hydrogen and deuterium suggests that a separation of the isotopes during the ionization process is possible.

Introduction

The electrochemical ionization of hydrogen gas has been studied by Eucken and Weblus.^{2,3} The plot of ionization current vs. applied electrode potential exhibited two maxima which were attributed to two different forms of adsorbed hydrogen. These results were subsequently confirmed by Breiter.^{4,5} Franklin, *et al.*,⁶ also investigated the oxidation of hydrogen on platinized platinum electrodes. In their experiments, the potential was varied at a constant rate and the current was continuously recorded. Three maxima in the ionization current were observed. The first two again were attributed to different forms of adsorbed hydrogen, while the third, occurring at the most positive potential, was felt to be due to the ionization of hydrogen absorbed in the platinum. The experiments described above were performed with stationary electrodes, and the currents measured were influenced also by the diffusion of the hydrogen to the electrode. Levich⁷ first showed that the diffusion currents for a reaction could be determined separately by using a rotating disk electrode. The limiting diffusion currents are proportional to the square root of the speed of rotation of the electrode, the concentration, and the diffusion coefficient to the power ²/₃ of the reacting species, and inversely proportional to the sixth root of the kinematic viscosity of the electrolyte. Frumkin^{8,9} studied the ionization of hydrogen on smooth and platinized platinum using a rotating disk electrode. When diffusion is rate controlling, the current is dependent on the speed of rotation of the electrode; when the rate of diffusion becomes greater than the actual rate of ionization at the electrode, the ionization reaction becomes rate limiting. At high speeds of rotation, therefore, the ionization current should become independent of the speed of rotation. Frumkin determined the ionization currents for hydrogen as a

function of electrode potential, and found a maximum ionization current at an electrode potential of 45 mv. positive to the reversible potential. The current was dependent upon the rate of application of the potential and his results therefore are valid only for the specified rate of change. Schuldiner¹⁰ studied the ionization of both hydrogen and deuterium on stationary palladium electrodes and found that at small positive potentials relative to the reversible potential the current was linear with potential. The deuterium ionization current was lower than that of hydrogen for any given potential.

The present work was initiated to investigate the ionization of both hydrogen and deuterium on a rotating disk electrode and to determine the limiting diffusion currents and the limiting ionization currents for both species. The potential was changed in discrete steps, so as to eliminate the dependence of the current on the rate of change of the potential.

Experimental

The apparatus consisted entirely of Pyrex glass including the seals to the electrodes and the associated equipment to introduce gas into the electrolyte. A water-cooled bearing on the rotating shaft allowed speeds up to 20,000 r.p.m. The rotating electrode was a platinum cylinder, 0.5 cm. in diameter, sealed coaxially in acrylic tubing so that the base of the cylinder was flush with the end of the tubing. The acrylic tubing enclosed tightly the lower end of the rotating shaft, which was a stainless steel rod, 0.475 cm. in diameter, inserted at the upper end in a special high speed, water-cooled bearing. A small stainless steel spring between the lower end of the shaft and the platinum cylinder provided electrical contact to the electrode. A belt and pulley system was used to drive the shaft as well as a tachometer-generator to measure the speed of rotation. The generator was purchased from Servo-Tek Co., and was accurate to within 1%. Electrical contact between the rotating stainless steel shaft and the external system was maintained with a silver slip-ring, and silver-graphite brushes, purchased from Graphite Metallizing Co.

The glass cell was designed to allow dispersion of the gas into the electrolyte through a fritted glass disk. A Luggin capillary was centrally placed at the bottom of the cell, and extended up to within 1 cm. of the rotating electrode. The capillary was connected to a Hg/HgO reference electrode compartment. The auxiliary electrode was a platinum sheet 0.12 mm. thick, bent into a cylindrical form, 1.5 cm. in diameter and 1.5 cm. high.

An electronic potentiostat was used to vary the potential of the working electrode with respect to the reference electrode. It maintained a constant potential between the rotating disk

(1) Submitted in partial fulfillment for the degree of Doctor of Philosophy in Chemical Engineering at the Polytechnic Institute of Brooklyn.

(2) A. Eucken and B. Weblus, *Z. Elektrochem.*, **55**, 114 (1951).

(3) E. Wicke and B. Weblus, *ibid.*, **56**, 169 (1952).

(4) M. Breiter and C. Knorr, *ibid.*, **59**, 153 (1955).

(5) M. Breiter and C. Knorr, *ibid.*, **59**, 681 (1955).

(6) T. Franklin and S. Cooke, *J. Electrochem. Soc.*, **107**, 557 (1960).

(7) G. Levich, *Zh. Fiz. Khim.*, **32**, 1565 (1958); D. P. Gregory and A. C. Riddiford, *J. Chem. Soc.*, 3756 (1956).

(8) A. Frumkin and E. Aikazyan, *Izv. Akad. Nauk SSSR*, **2**, 202 (1959).

(9) A. Frumkin and E. Aikazyan, *Dokl. Akad. Nauk SSSR*, **100**, 315 (1955).

(10) S. Schuldiner and J. Hoare, *J. Electrochem. Soc.*, **105**, 279 (1958).

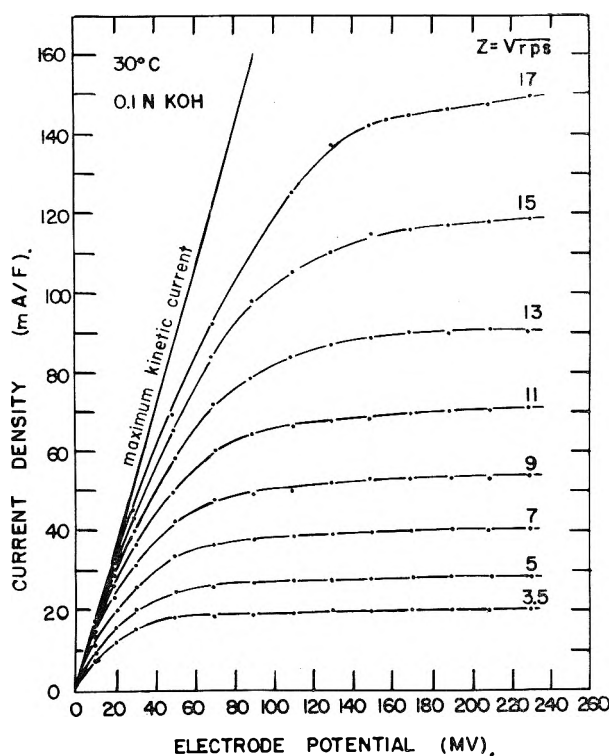


Fig. 1.—Ionization currents for hydrogen, expressed in ma./f., as a function of the electrode potential. The total current is obtained by multiplying the figures on the ordinate by 0.02 f. The parameter Z is the square root of the number of rotations per second.

and the reference electrode, independent of current. The potential of the electrode was measured with a Hewlett Packard Model 410A vacuum tube voltmeter, accurate to 2%. Ionization currents were measured with a 0.25% Sensitive Research microammeter, and the tachometer voltage was measured with a 0.5% Sensitive Research voltmeter. The rotating platinized electrode was prepared as suggested by Janz.¹¹ The smooth platinum disk electrode was dipped first in a dilute aqua regia solution, and then in warm concentrated nitric acid. Hydrogen was evolved cathodically from the disk electrode in a dilute sulfuric acid solution for 5 min. at a current of 5 ma. The electrode then was washed and placed in the standard platinizing solution of 3% chloroplatinic acid with 0.1% lead acetate present. Platinum was electro deposited on the surface at 5 ma. for 5 min. The electrode then was washed, the shaft inserted through the bearing, and the cell clamped in place and filled with the desired KOH electrolyte. The electrolyte was subsequently saturated with hydrogen or deuterium for 1 hr.

The hydrogen and deuterium were purchased from the Matheson Co. Mixtures of the gases also were supplied and analyzed by the Matheson Co. The potassium hydroxide solutions were prepared from Fisher Certified Reagent Grade pellets. The KOH was recrystallized four times to ensure maximum purity of the electrolyte. The water was distilled from an alkaline permanganate solution to oxidize organic impurities, and subsequently was distilled two additional times. The prepared electrolyte solutions were stored in "aged" polyethylene bottles and subjected to standard pre-electrolysis procedures at 100 ma./l. between platinum electrodes for at least 24 hr. In order to compare the data for each electrode, the double layer capacities of the disk electrode were measured prior to each experiment by means of the constant current charging technique. A 1-sec. Honeywell recorder, with chart speed of 720 in./hr., driven by a Hewlett Packard vacuum tube voltmeter, was used to record the voltage-time curve. A charging current of 100 μ a. was applied and five separate charge and decay cycles were taken for each electrode. For the ionization rate measurements, the potentiostat was set to give the desired positive electrode potential vs. the reversible potential, and the speed of rotation of the motor then was adjusted using a powerstat. The current was read 20

sec. after each speed change; it remained constant for 20–50 sec. The entire speed range was covered at constant potential before the potential was changed to a new value. The following variables were investigated:

Speed:	735 to 17,340 r.p.m.
Electrode potential:	5 to 240 mv. positive to the reversible potential
Temperature:	30 and 50°
KOH concn.:	0.1, 1.0, 3.0, 5.0 N
Gas:	Pure H ₂ , pure D ₂ , H/D ratio = 1.07/1

Results

The KOH concentration was found to influence the results significantly. It was observed that on open circuit, prior to the measurements, the electrode did not maintain the reversible potential when it was at rest, even though gas was continually bubbled through the solution. This effect became very pronounced as the KOH concentration increased, and the reversible potential was obtained only when the electrode was being rotated at high speeds. The cathodic current required to maintain the reversible potential with the electrode at rest was measured prior to each experiment, and the results were corrected for this effect. This cathodic current increased from 5×10^{-6} to 5×10^{-5} amp. with increasing KOH concentration from 0.1 to 5.0 N. The double layer capacities of the various electrodes were 0.020 and 0.019 f. for 0.1 N KOH, 0.046 and 0.064 f. for 1 N KOH, 0.076 and 0.055 f. for 3 N KOH, and 0.063 and 0.064 f. for 5 N KOH, for the H₂ and D₂ experiments, respectively. For the 1:1 mixture of H₂ and O₂ the capacities were 0.018, 0.067, 0.082, and 0.060 f. for the respective KOH concentrations. These values refer to the experiments at 30°.

Typical results are shown in Fig. 1. The current density expressed in ma./f. (total electrode area is 0.02 f.) is plotted against the potential of the electrode in mv. positive to the reversible hydrogen potential. The parameter Z is the square root of the speed of rotation. At low KOH concentrations, the currents fluctuated about an average value. The family of curves in Fig. 1 for hydrogen and 0.1 N KOH shows the dependence of current on the speed of rotation and on the electrode potential. The general shape and relative positions of the curves are typical for all of the data at all KOH concentrations. The current is at first linear with potential and then tends to a constant value. For the lowest speed of rotation ($\sqrt{\text{r.p.s.}} = 3.5$, r.p.m. = 735) the current becomes independent of the potential at about 60 mv. positive to the reversible potential. Above this potential the current is limited by diffusion and no longer depends on potential. As the speed of rotation is increased, the currents increase. The slopes of the linear portion of the current-voltage curve increase with the speed of rotation to a limiting value. With increasing rate of rotation, the diffusion plateaus start at increasingly higher electrode potentials.

The maximum kinetic current was reached only within a small potential interval (between 0 and 20 mv. positive to the OCV).

The data for deuterium ionization in 0.1 N KOH are similar to the data for hydrogen except that the currents generally are only one-fourth to one-third as large. The maximum kinetic current was reached at potentials up to 20 mv. positive to the reversible po-

(11) D. G. Ives and G. J. Janz, "Reference Electrodes, Theory and Practice," Academic Press, New York, N. Y., 1961, p. 106.

tential; it was smaller than the corresponding hydrogen current.

The ionization currents were greatly reduced at increased KOH concentration. The current-voltage curves for different speeds of rotation were very close together when compared on the same scale to the results in 0.1 *N* KOH.

The reduction in current due to the change in KOH concentration is illustrated in Fig. 2. The currents observed at the maximum rotational speed of 17,345 r.p.m. are plotted *versus* potential for hydrogen at 30°. The maximum hydrogen current in 0.1 *N* KOH is almost 40 times that in 5.0 *N* KOH. Identical experiments with deuterium showed that the maximum deuterium current in 0.1 *N* KOH is almost 10 times the deuterium current in 5.0 *N* KOH. These unexpected results possibly indicate that kinetic and diffusion control are involved simultaneously.

The variation of the ionization current with the deuterium content in the gas mixture is shown in Fig. 3, where ionization currents for H₂, D₂, and a hydrogen to deuterium mixture of 1.07/1, all in 0.1 *N* KOH, are plotted. The currents for the 1.07/1 gas mixture were approximately halfway between the hydrogen and deuterium data, as expected. The currents for the same gases in 5.0 *N* KOH were very small and close together, indicating low diffusion and ionization rates for both gases at high KOH concentration. An increase of 15 to 20% in the ionization current density was observed with an increase in temperature from 30 to 50°.

Discussion

1. **Determination of Diffusion Coefficients.**—From these results the diffusion coefficients of hydrogen and deuterium can be calculated with the Levich⁷ equation

$$i = 0.62nFD^{1/2}\omega^{1/2}S\nu^{-1/4}$$

where *i* is the limiting current density in amp./cm.², *n* is the number of electrons in the reaction, *F* is the faraday, *D* is the diffusion coefficient, ω is the number of rotations per second, *S* is the solubility of the gas in the electrolyte (moles per cm.³), and ν is the kinematic viscosity of the electrolyte (cm.²/sec.). The current density was obtained by dividing the experimental current by the geometrical area of the electrode, 0.196 cm.². Since the activity of the electrode should not influence the current in the limiting diffusion region, use of the geometrical area instead of the true area is proper. The physical properties of KOH solutions were taken from Bulletin 15 on caustic potash from Allied Chemical Co. Because the solubility of deuterium in KOH could not be obtained, the results were calculated as $D = k/S^{2/3}$, where *k* is experimentally determinable. The data at speeds above $\sqrt{r.p.s.} = 13$ did not agree generally with the rest of the results, but since the Levich equation is applicable to laminar flow only, the discrepancy in the data at higher speeds may be due to turbulence at the electrode surface. Using only the data at speeds equal to and below $\sqrt{r.p.s.} = 13$, the diffusion values in Table I were obtained.

In all cases the deuterium diffusion coefficient is smaller than the hydrogen diffusion coefficient. Thus, in 0.1 *N* KOH the hydrogen diffusion is about 3.5 times the deuterium diffusion, but since the solubility of D₂ in KOH probably is less than that of H₂, the actual diffusion coefficient ratio is less than 3.5. If the inter-

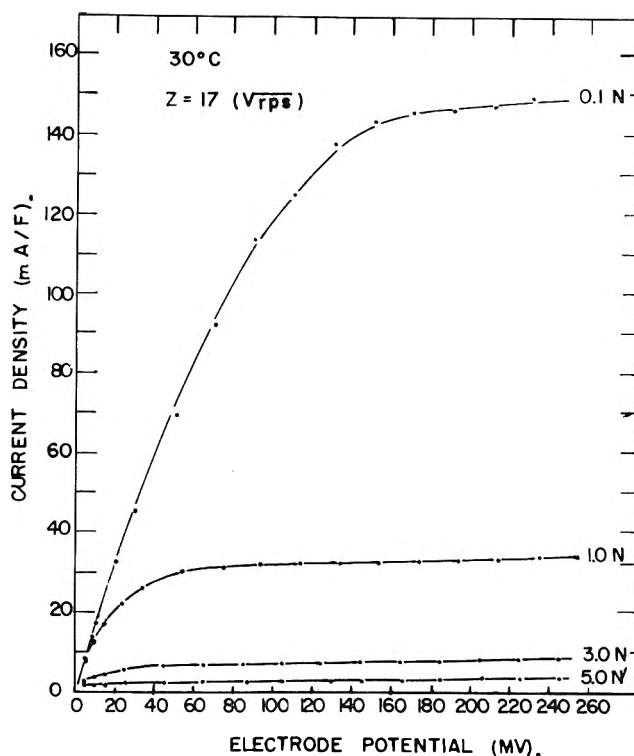


Fig. 2.—Dependence of the ionization current on the KOH concentrations at 30°.

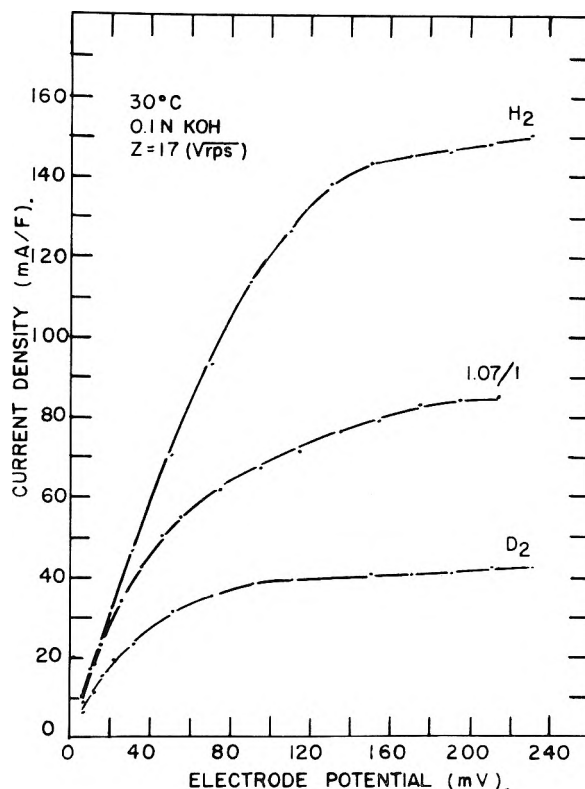


Fig. 3.—Dependence of the ionization current on the deuterium content of the gas.

action forces for H₂ with the solvent are assumed to be similar to those for D₂, then one would expect the ratio of the hydrogen to deuterium diffusion coefficients to be inversely proportional to the square root of the molecular weight ratio, namely 1.41. From Table I it can be seen that this ratio of 1.41 is approached as the KOH concentration increases to 5.0 *N*.

The solubility of hydrogen in KOH is reported in the

TABLE I

VALUES FOR ($k \times 10^{15}$) IN THE EQUATION $D = k/S^{3/2}$ FOR THE DIFFUSION COEFFICIENTS FOR HYDROGEN AND DEUTERIUM

		KOH concentration			
		0.1 N	1.0 N	3.0 N	5.0 N
H ₂	30°	113.0	68.4	17.0	3.60
D ₂	30°	33.3	6.43	2.71	2.40
H ₂	50°	122.0	72.6	18.2	6.1
D ₂	50°	36.4	14.0	7.1	4.3

literature.^{12,13} From these data the following diffusion coefficients were calculated for hydrogen: 18.2×10^{-5} , 13.8×10^{-5} , 9.9×10^{-5} , and 4.0×10^{-5} cm.²/sec., in 0.1, 1.0, 3.0, and 5.0 N KOH, respectively, at 30°. At 50° the coefficients are 23.7×10^{-5} , 22.0×10^{-5} , 12.4×10^{-5} , and 7.9×10^{-5} cm.²/sec. in the respective KOH concentrations. These diffusion coefficients are higher than those reported in the literature.^{14,15} The latter cannot, however, be compared directly with the present results, since they were determined in different solutions under different experimental conditions. It should be pointed out that the Levich equation is valid only for smooth electrode surfaces. It is possible that the mass transport of H₂ and D₂ is enhanced by the surface roughness due to platinizing. It appears, however, that the form of the Levich equation holds, since the values of $k = DS^{3/2}$ were relatively constant up to $\sqrt{r.p.s.} = 13$.

2. **Determination of the Rate of Ionization.**—When the effect of diffusion is eliminated, the maximum kinetic ionization current can be determined as a function of potential. The maximum kinetic current for a given potential, reached at infinite speed of rotation, can be determined as shown in Fig. 1, by drawing a straight line through the origin, tangent to the curves in the low potential region where diffusion has been eliminated. The slopes of the lines so obtained are a measure for the rate constants of the ionization process and the results are listed in Table II.

TABLE II

SLOPES OF THE PLOTS OF MAXIMUM KINETIC CURRENT *vs.* POTENTIAL (ma./f./mv.)

	H ₂		D ₂	
	30°	50°	30°	50°
0.1 N KOH	1.9	2.2	1.0	1.10
1.0 N KOH	1.5	1.6	0.35	0.47
3.0 N KOH	0.33	0.70	.19	.27
5.0 N KOH	0.34	0.80	.23	.30

The maximum kinetic current for hydrogen ionization is greater than the deuterium current. The ratio

(12) "The Solubility of Gases in Solution," International Critical Tables, Vol. 3, McGraw-Hill Book Co., Inc., New York, N. Y., 1928, pp. 271-283.

(13) A. Seidell, "Solubilities of Inorganic and Metal Organic Compounds," 4th Ed., Vol. 1, McGraw-Hill and Werner, Inc., Washington, D. C., 1958.

(14) V. V. Ipatiev and V. I. Tikhomirov, "Diffusion of Gases Under Pressure," *J. Gen. Chem. USSR*, **1**, 736 (1931).

(15) W. Jost, "Diffusion in Solids, Liquids, Gases," Academic Press, Inc., New York, N. Y., 1952.

of the hydrogen current to that of deuterium in a 0.1 N KOH solution is 1.8 at 30° and 2.0 at 50° and for 5.0 N KOH solution it is 1.5 at 30° and 2.7 at 50°. With increasing temperature, therefore, the rate of hydrogen ionization increases faster than that of deuterium.

It should be pointed out again that the electrode areas are expressed in terms of the double layer capacity, and that the KOH concentration influences this capacity. If the capacities, as measured in each solution by means of charging curves, were proportional to the active area of the electrode, the results could be interpreted readily, as above. If, however, the active electrode area remains constant, even though the double layer capacities differ in the various KOH solutions, the geometric surface area of the electrode must be used to calculate a current density figure. The ionization rate constant then is readily obtained from the plot of the actual current *vs.* potential.

Summary

The following conclusions can be drawn from the data.

1. In all experiments the rate of ionization for hydrogen was greater than for deuterium, and a separation of the isotopes during the ionization process is possible.

2. The diffusion coefficient for hydrogen in 0.1 N KOH is about 3.5 times greater than the deuterium coefficient. The ratio of hydrogen to deuterium diffusion coefficients in 5.0 N KOH at 30° is 1.5. The corresponding ratios of diffusion coefficients for 0.1 and 5.0 N KOH at 50° are 3.3 and 1.4, respectively.

3. The diffusion coefficients for H₂ decreased with increasing KOH concentration. The coefficient was 18.2×10^{-5} cm.²/sec. for 0.1 N KOH at 30° and decreased to 4.0×10^{-5} cm.²/sec. in 5.0 N KOH. The coefficients at 50° were 23.7×10^{-5} cm.²/sec. in 0.1 N KOH and 7.9×10^{-5} cm.²/sec. in 5.0 N KOH.

4. The maximum kinetic current for the ionization of hydrogen is 1.8 times the deuterium kinetic ionization current in 0.1 N KOH at 30° and the corresponding ratio at 50° is 2. For 5.0 N KOH solutions at 30° the maximum kinetic current ratio is about 1.5.

5. The limiting diffusion currents for deuterium were reached at smaller positive potentials, with respect to the reversible potential, than for hydrogen. This is due to the greater activation energy needed to ionize the deuterium molecule, and to the lower deuterium diffusion coefficient. Therefore hydrogen is ionized (in 0.1 N KOH solutions at 30°), in the range where the reaction is diffusion limited, three to four times faster than deuterium, even though the predicted maximum kinetic current ratio is only 1.8.

6. An increase in temperature from 30 to 50° increases the maximum kinetic currents for hydrogen or deuterium ionization. The rate of increase with temperature is greater for hydrogen than for deuterium, resulting in an increase in the ratio of the maximum kinetic currents at the higher temperature.

THE CHEMISTRY OF XYLYLENES. XVI. THE TRAPPING OF RADICALS IN GAS STREAMS BY MUTUAL QUENCH TECHNIQUES

By L. A. ERREDE AND J. P. CASSIDY

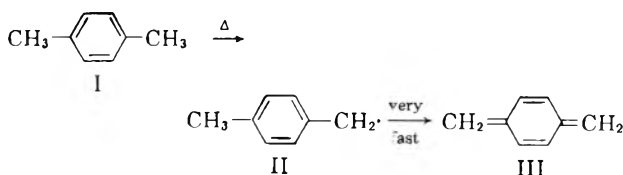
Contribution No. 222 from the Central Research Laboratories of the Minnesota Mining and Manufacturing Company,¹ St. Paul, Minn.

Received May 23, 1962

Fast flow co-pyrolysis of *p*-xylene and CCl₄ at low pressure affords a mixture having *p*-methylbenzyl chloride and β,β -dichloro-*p*-methylstyrene as its two major components. On the other hand, pyrolysis of *p*-xylene and carbon tetrachloride in separate coaxial tubes to give two pyrolyzate streams that blend at a point beyond the furnace affords a mixture having *p*-methylbenzyl chloride and *p*-xylylene dichloride as its two major components. It was shown that the products are formed *via* coupling of *p*-methylbenzyl radicals with chlorine and with trichloromethyl radicals and *via* reaction of *p*-xylylene with chlorine. The reactions of chlorocarbon radicals with *p*-xylene and hydrocarbon radicals with carbon tetrachloride in the quenched stream are relatively unimportant under the reaction conditions used in these experiments.

Introduction

Szwarc^{2,3} has shown that *p*-methyl benzyl radicals (II) and *p*-xylylene (III) are formed sequentially when *p*-xylene is subjected to fast flow pyrolysis at low pressure.



Attempts⁴⁻⁶ have been made to convert these reactive intermediates to mono- and difunctional derivatives by pyrolysis of *p*-xylene with other thermolabile compounds or by mixing a second gas stream with the fast flowing *p*-xylene pyrolyzate as it leaves the furnace. It was reported⁵ that "of all the materials used, only iodine reacted to yield a definite identified product, *viz.*, *p*-xylylene diiodide, in significant quantities." *p*-Methylbenzyl halides, however, were isolated in small amounts when bromine and chlorine were used in lieu of iodine.⁵ In other cases, little or no polymer was produced, indicating that some form of interaction might have occurred with the *p*-methylbenzyl and *p*-xylylene intermediates, but no isolable species were reported.⁵

The co-pyrolysis of carbon tetrachloride with *p*-xylene was studied in our Laboratories and the present paper reports some of the positive results obtained in that investigation.

Results and Discussion

It was reported⁷ that fast flow pyrolysis of *p*-xylene at 1065°, 4×10^{-3} sec. residence time, and 4 mm. pressure converts 14% of the feed stock per pass to *p*-methylbenzyl radicals (II), about 80% of which are isolated as *p*-xylylene (III). When carbon tetrachloride was subjected to fast flow pyrolysis at about these same conditions, Cl₂, C₂Cl₆, C₂Cl₄, and C₆Cl₆ were isolated as the major products as shown in Table I.

(1) This work was carried out in the laboratories of the M. W. Kellogg Co. The data were acquired by Minnesota Mining and Mfg. Co. with the purchase of the Chemical Manufacturing Division of the M. W. Kellogg Co. in March, 1957.

(2) M. Szwarc, *J. Chem. Phys.*, **16**, 128 (1948).

(3) M. Levy, M. Szwarc, and J. Thrusseil, *ibid.*, **22**, 1904 (1954).

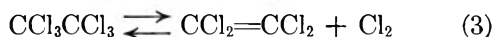
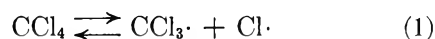
(4) M. Szwarc, *J. Polymer Sci.*, **6**, 519 (1951).

(5) L. A. Auspos, L. A. R. Hall, J. K. Hubbard, W. Kirk, Jr., J. R. Schaeffgen, and S. B. Speck, *ibid.*, **15**, 9 (1955).

(6) J. R. Schaeffgen, *ibid.*, **15**, 203 (1955).

(7) L. A. Errede and J. P. Cassidy, *J. Am. Chem. Soc.*, **82**, 3653 (1960).

These data are consistent with a stepwise formation of C₆Cl₆ from CCl₄ *via* reactions 1 to 4. A similar reaction scheme was postulated^{8,9} to account for the formation of C₆F₆ *via* pyrolysis of CBrF₃.



It has been shown by Dainton and Ivin¹⁰ that pyrolysis of hexachloroethane leads to the formation of tetrachloroethylene in good yield; and it was shown in our Laboratory that appreciable amounts of hexachlorobenzene are produced when tetrachloroethylene is subjected to the relatively mild conditions of fast flow pyrolysis (Table I). Moreover, carbon tetra-

TABLE I
PYROLYSIS OF CHLOROCARBONS

Feed stock	Pyrolysis conditions			% Carbon atoms of feed stock isolated as			
	T, °C.	t (sec.)	P (mm.)	CCl ₄	CCl ₂ =	CCl ₂	C ₆ Cl ₆
CCl ₄	1005	0.003	2	73	7	20	0
CCl ₄	1000	.005	4	48	6	45	0.6
CCl ₄	1000	.015	10	14
CCl ₄	1000	.03	30	49
CCl ₂ =CCl ₂	1005	.01	3	55	39

chloride was converted to hexachlorobenzene in high conversion by increasing the severity of the pyrolysis conditions. These experiments demonstrate that thermal degradation of carbon tetrachloride is more facile than that of *p*-xylene under the same pyrolysis conditions. This is consistent with the relative bond strengths of the weakest links in the respective molecular structures [$D(\text{CCl}_3-\text{Cl}) = 69$ kcal.; $D(\text{CH}_3-\text{C}_6\text{H}_4\text{CH}_2-\text{H}) = 77$ kcal.].¹¹ Hence we were reasonably sure that co-pyrolysis of *p*-xylene with CCl₄ would afford a more than adequate amount of chlorine and chlorocarbon radical fragments (*via* reaction 1) to accommodate the hydrocarbon radicals produced from *p*-xylene.

Accordingly, an approximately equimolar gas mixture of *p*-xylene and carbon tetrachloride was pyrolyzed

(8) Y. Desirant, *Bull. Classe Sci., Acad. Roy. Belg.*, [5] **41**, 759 (1955).

(9) M. Hellman, E. Peters, W. J. Plummer, and L. A. Wall, *J. Am. Chem. Soc.*, **79**, 5654 (1957).

(10) F. S. Dainton and K. J. Ivin, *Trans. Faraday Soc.*, **46**, 295 (1950).

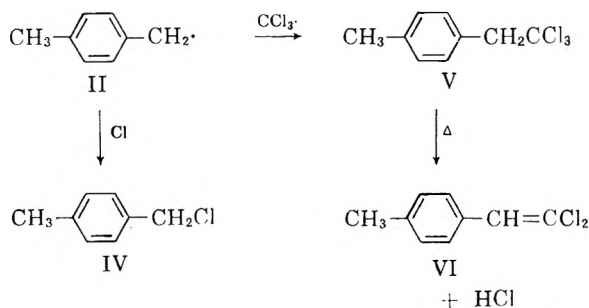
(11) L. A. Errede, *J. Phys. Chem.*, **64**, 1031 (1960).

TABLE II
 THE PYROLYSIS OF *p*-XYLYLENE AND CARBON TETRACHLORIDE AT 1000° AND 5 MM. FOR 0.005 SEC.^a

Pyrolysis stream	Non-pyrolyzed quench stream	Blend point ^b	<i>p</i> -Xylene to CCl ₄ ratio ^c	% Conversion to interaction products ^d			
				<i>p</i> -CH ₂ C ₆ H ₄ CH=CCl ₂	<i>p</i> -CH ₂ C ₆ H ₄ CH ₂ Cl	<i>p</i> -CICH ₂ C ₆ H ₄ CH ₂ Cl	Others
<i>p</i> -Xylene and CCl ₄	None	-20	1/1.1	3.7	4.7	0	3.2 ^e
<i>p</i> -Xylene and CCl ₄	None	4.5	1/1.2	0	5.4	1.5	3.9 ^f
<i>p</i> -Xylene	CCl ₄	4.5	1/0.65	0	0	0	0
CCl ₄	<i>p</i> -Xylene	4.5	1/0.32	0	0.03	0	0.04 ^h

^a These conditions are known to cause 11% conversion of *p*-xylene to *p*-methylbenzyl radicals (L. A. Errede and F. DeMaria, *J. Phys. Chem.*, **66**, 2664 (1962)) which are isolated subsequently as various products.⁷ ^b Blend point in inches away from the end of the pyrolysis zone. ^c Molar ratio. ^d Based on moles of *p*-xylene metered to the system. ^e Calculated as *p*-xylyl equivalents with 0.7 Cl atom per unit. Average molecular weight was 631; % Cl = 17.2. Infrared spectrum indicated this product to be a mixture of alkylated aromatics. ^f Calculated as *p*-xylyl equivalents as (C₈H₆Cl_{0.7})_n having an average molecular weight of ca. 2000. ^g Five % isolated as poly(*p*-xylylene) and 5% as the usual low molecular weight products of *p*-xylene pyrolysis.⁷ ^h 2-Chloro-*p*-xylylene.

at 1005°, 0.003 sec. residence time, and 5 mm. pressure. Poly(*p*-xylylene) was not obtained in the condensate nor was it possible to isolate any difunctional derivative of *p*-xylylene, such as *p*-xylylene dichloride, despite all efforts to do so. On the other hand, *p*-methylbenzyl chloride (IV) and β,β -dichloro-*p*-methylstyrene (VI) were isolated in about equal amounts as the major products (see Table II). *p*-Methylbenzyl chloride (IV) would form *via* reaction of *p*-methylbenzyl radical with chlorine or chlorine atoms; β,β -dichloro-*p*-methylstyrene (VI) could form *via* coupling of *p*-methylbenzyl radical with trichloromethyl radical to afford the corresponding β,β,β -trichloroethyltoluene (V) which then could split out HCl. The β,β -dichloro-*p*-methylstyrene was identified

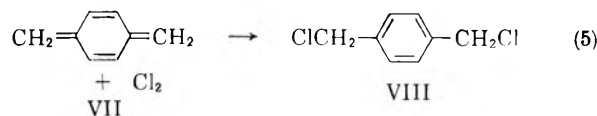


by elementary analysis, n.m.r., infrared spectral analysis, and by oxidation to *p*-toluic acid as described in the Experimental section.

Apparently, coupling with chlorine and trichloromethyl radicals occurred faster than dehydrogenation of *p*-methylbenzyl radicals to afford *p*-xylylene, since no difunctional derivative of the latter intermediate was isolated. It was speculated that difunctional derivatives might be obtained if the compounds were pyrolyzed in separate gas streams and then made to blend after a sufficient time was allowed for *p*-xylylene molecules to form in the hydrocarbon stream.

Accordingly, *p*-xylene and carbon tetrachloride were pyrolyzed in concentric tubes at 1000° and the resultant pyrolyzates were mixed downstream. The more thermolabile chlorocarbon was metered through the inner tube and the hydrocarbon through the outer tube. Confluence was allowed to occur at a point 4.5 in. beyond the pyrolysis zone and the resultant gas mixture was condensed in hexane kept at -78°. Again no polymer was formed, but this time the major products of interaction were *p*-methylbenzyl chloride (IV) and *p*-xylylene dichloride (VIII). No β,β,β -trichloroethyltoluene nor bis-trichloromethyl-*p*-xylylene was isolated, indicating that the trichloromethyl

radicals had been consumed in the chlorocarbon stream *via* reactions 1 and 2 before mixing had occurred. The isolation of *p*-xylylene dichloride, however, indicated that *p*-xylylene might have formed in the hydrocarbon stream after it left the pyrolysis zone and then reacted with Cl₂ at the blend point.



It was probable that some of the products of interaction might have formed by attack of hydrocarbon radicals on carbon tetrachloride or by attack of Cl₂ and CCl₃ on *p*-xylene. To check this possibility, a stream of *p*-xylene was pyrolyzed in the usual way and then mixed with a stream of non-pyrolyzed carbon tetrachloride at the same blend point used in the previous experiments. The confluent stream was collected at -78° in a cold solvent. The resultant solution was warmed to room temperature and poly(*p*-xylylene) was obtained in good yield as described previously.^{12,13} Neither the polymer nor the low molecular weight products of *p*-xylene pyrolysis⁷ contained chlorine, indicating that little or no interaction of the pyrolyzed hydrocarbon stream occurred with non-pyrolyzed CCl₄.

In the next experiment, a stream of carbon tetrachloride was pyrolyzed and then mixed with a large excess of non-pyrolyzed *p*-xylene at the same blend point. A considerable amount of the usual products of CCl₄ pyrolysis was isolated but only minute amounts of *p*-methylbenzyl chloride and 2-chloro-*p*-xylylene were obtained, indicating that very little interaction (relative to co-pyrolysis) of the two gas streams had occurred. Actually, the traces of *p*-methylbenzyl chloride and 2-chloro-*p*-xylylene isolated in this experiment may have formed in solution when the condensate rich in *p*-xylene and chlorine was warmed from -78° to room temperature.

These results (summarized in Table II) indicate that the products of interaction were produced almost entirely by coupling of the radical fragments. It appeared probable that the pyrolyzed hydrocarbon and chlorocarbon streams were serving one another as mutual radical quenches. These results suggested that this technique might be used to help elucidate the mechanism of *p*-xylylene formation from *p*-methylbenzyl radicals as described in another publication.¹⁴

(12) L. A. Errede and B. F. Landrum, *J. Am. Chem. Soc.*, **79**, 4952 (1957).

(13) L. A. Errede, R. S. Gregorian, and J. M. Hoyt, *ibid.*, **82**, 5218 (1960).

(14) L. A. Errede and J. P. Cassidy, *J. Phys. Chem.*, **67**, 73 (1963).

Experimental

Pyrolysis of CCl_4 .—Pyrolysis of carbon tetrachloride was carried out using the apparatus shown in Fig. 1 of ref. 12 according to the procedure described previously for the pyrolysis of *p*-xylene.^{7,12,13} The system was evacuated to the desired pressure and the furnace was adjusted to afford the desired maximum temperature and temperature profile. About 10 moles of carbon tetrachloride was metered at the rate of ca. 0.04 mole/min. to the evacuated system through a calibrated capillary. Pyrolysis occurred in a 1-in. i.d. quartz tube. The pyrolysis zone (*i.e.*, the distance along the tube through which the gas was no less than 50° below its maximum temperature) was about 5 in. long. The pyrolyzate was collected in heptane (3 l.) kept at -78° so that the chlorine condensed therein would be converted to chloroheptanes. A smaller liquid nitrogen trap was used in series with the large Dry Ice trap. At the end of the pyrolysis, the cold traps were warmed to room temperature. The resultant solutions were combined. The solvent and volatile product of pyrolysis were separated by distillation at atmospheric pressure to afford four fractions: (1) b.p. 77–117°; (2) b.p. 117–127°; (3) b.p. 140–148°; and (4) residue. Fractions 1 to 3 were analyzed by means of a mass spectrometer. Fraction 1 was a mixture of *n*-heptane, tetrachloroethane, and carbon tetrachloride. Fraction 2 was essentially all tetrachloroethane, and fraction 3 was a mixture of chloroheptanes. The residue was a mixture of hexachloroethane and hexachlorobenzene. The former was separated from the latter by leaching the residue with methanol. Hexachloroethane crystallized in the form of white platelets (m.p. 181–183°) from the hot concentrated alcohol extract.

Anal. Calcd. for C_2Cl_6 : C, 10.15; Cl, 89.84; mol. wt. 236.8. Found: C, 10.14; Cl, 90.1; mol. wt. 221.

The methanol insoluble residue was recrystallized from hot CCl_4 and hexachlorobenzene was obtained in the form of fine white needles (m.p. 224–226°).

Anal. Calcd. for C_6Cl_6 : C, 25.29; Cl, 74.69; mol. wt. 284.8. Found: C, 25.19; Cl, 74.36; mol. wt. 269.

Pyrolyses were repeated at 2, 4, 10, and 30 mm. pressures and the data are summarized in Table I. Although the amount of chloroheptanes obtained in these experiments indicated that most of the chlorine produced pyrolytically was converted to chloroheptanes and HCl in the condenser, the results were by no means quantitative. Hence, one pyrolysis was repeated at 1000°, 4 mm. pressure, and 0.005 sec. residence time and the pyrolyzate of CCl_4 (10 moles) was collected in a one to one mixture of CCl_4 and HCCl_3 kept at -78°. The cold traps (-78° and -190°) were warmed to room temperature and the chlorine contained therein was passed through an aqueous solution of KI. A slow stream of N_2 was used to remove the last traces of Cl_2 from the cold traps and this gas stream was led into a fresh KI solution. A total of 4.9 moles of I_2 was liberated as determined by titration with sodium thiosulfate. This amount represents about 25% of the chlorine metered to the system as CCl_4 , which agrees well with the amount of Cl_2 anticipated (24%) from products isolated in previous similar runs.

Pyrolysis of Tetrachloroethylene.—Tetrachloroethylene (1.54 moles) was metered at the rate of 0.009 mole/min. to the pyrolysis system evacuated to 3.3 mm. The gas stream was pyrolyzed at 1005° for 0.014 sec. residence time in the pyrolysis zone of the 1-in. i.d. quartz tube and the pyrolyzate was condensed in a Dry Ice-acetone trap. The condensate was separated by distillation at atmospheric pressure and 0.86 mole of C_2Cl_4 was recovered, leaving 0.12 mole of non-volatile impure hexachlorobenzene (m.p. 205–215°) which after one recrystallization from hexane was obtained as fine white needles (m.p. 222–224°).

Co-pyrolysis of *p*-Xylene and Carbon Tetrachloride.—*p*-Xylene (12.1 moles) and carbon tetrachloride (13.9 moles) were metered to the pyrolysis system through separate calibrated capillaries at the rate of 0.035 and 0.040 mole/min., respectively. The two gas streams were mixed within the 1-in. i.d. quartz tube where co-pyrolysis occurred at 1005° and 4.7 mm. for 0.003 sec. residence time. The pyrolyzate was collected in 4.0 l. of hexane kept at -78°. The resultant solution was warmed to room temperature. No polymer formed, indicating the absence of any residual *p*-xylylene in the gas stream when it reached the condenser. The solvent of the clear solution was removed by rapid evaporation at 60 mm. and 100° in a solvent evaporator. The liquid was metered through the top of the evacuated apparatus. The volatile components were vaporized as the liquor

cascaded down the steam heated column, and were removed through an overhead side arm. The non-volatile components were collected in a receiving flask at the bottom of the reactor. A previous trial run using a synthetic mixture showed that virtually all the hexane and xylene are removed in this way with only a negligible loss (<1%) of *p*-methylbenzyl chloride, β,β -dichloro-*p*-methylstyrene, and *p*-xylylene chloride. The last traces of *p*-xylene were removed by evaporation under a stream of N_2 . The residue (291 g.) was a dark oil that contained 28.6% chlorine. This was dissolved in 1 l. of hexane and the resulting solution was chilled to -78° in an attempt to cause precipitation of any *p*-xylylene dichloride that might have been present. No precipitate was obtained, indicating that very little if any of this compound was present since the solubility of *p*-xylylene dichloride in 1 l. of similar solutions at -78° is less than 1 g. The hexane was removed by evaporation and the residue was separated by distillation at 1.0 mm. pressure. Four major fractions were obtained: (1) 80 g., amber oil, b.p. 40–46°; m.p. -2° to 0°; (2) 82 g., b.p. 65–79°; m.p. 28–30°; (3) 39 g., amber oil, b.p. 100–120°; and (4) 50 g., residue which did not distil below 200°.

Fraction 1 gave a strong positive test for active halogen using alcoholic AgNO_3 . The infrared spectrum of this fraction was about the same as that of *p*-methylbenzyl chloride (IV) and this assignment was supported by elementary analysis.

Anal. Calcd. for $\text{C}_9\text{H}_9\text{Cl}$: C, 68.38; H, 6.40; Cl, 25.26; mol. wt. 140.5. Found: C, 68.7; H, 5.82; Cl, 25.3; mol. wt. 141.

A sample of the chloride was converted to the corresponding nitrile by treatment with NaCN in methanol-water solution. Subsequent hydrolysis and acidification yielded *p*-tolylacetic acid which, after one recrystallization from hexane was obtained in the form of white flat needles (m.p. 86–88°; no depression when mixed with authentic sample).

Fraction 2 was recrystallized from MeOH at -78° and β,β -dichloro-*p*-methylstyrene (VI) was obtained in the form of tiny white platelets (m.p. 32.0–32.5°) having a characteristic licorice-like odor. The assigned structure was verified by its infrared spectra in Nujol (strong bands at 6.23, 7.90, 11.07, 11.60, 12.00, 12.47, 13.25, 14.13, and 14.85 μ), n.m.r. spectrum [τ values 7.68 for CH_3 , 3.25 for olefinic CH, 2.63 and 2.90 (A-B type peak) for aromatic CH], and by elemental analysis.

Anal. Calcd. for $\text{C}_9\text{H}_8\text{Cl}_2$: C, 57.77; H, 4.33; Cl, 37.90; mol. wt. 187.1. Found: C, 57.5; H, 4.01; Cl, 38.0; mol. wt. 184.

A sample of the compound was oxidized by KMnO_4 in acetone to give *p*-toluic acid (m.p. 176–177°; no depression when mixed with authentic sample).

Fraction 3 was dissolved in methanol and chilled to -78°, causing 13 g. of 1,2-di-*p*-tolylethane to crystallize from solution in the form of white platelets (m.p. 74–76°, no depression when mixed with authentic sample). The infrared spectrum of this product was identical with that of an authentic sample.⁷ The methanol mother liquor was evaporated to constant weight (26 g.) and the residue was redistilled under vacuum. The infrared spectrum of the distillate indicated that this was a mixture composed mostly of alkylated diphenylmethanes⁷ with a small amount of 1,4-di-*p*-tolylethane. A routine qualitative test for chlorine (sodium fusion followed by AgNO_3) indicated the presence of chlorine in only trace amounts.

Fraction 4 was not separated further. The infrared spectra of this fraction indicated that it was a complex mixture of alkylated aromatics. The average molecular weight was 631, as determined by freezing point depression of cyclohexane, and it contained 17.2% chlorine, which corresponds roughly to about 0.6 chlorine atom per xylyl unit.

In summary, co-pyrolysis of 12.1 moles of *p*-xylene and 13.9 moles of CCl_4 gave 0.57 mole of *p*-methylbenzyl chloride, 0.44 mole of β,β -dichloro-*p*-methylstyrene, 0.35 mole of *p*-methylbenzyl equivalents isolated as 1,4-di-*p*-tolylethane or diphenylmethanes, and 0.40 mole of *p*-methylbenzyl equivalents isolated as ill-defined partially chlorinated non-distillable residue.

Pyrolysis of *p*-Xylene and Carbon Tetrachloride in Separate Coaxial Streams.—The pyrolysis system shown in Fig. 1 of ref. 12 was modified such that the internal thermowell (no. 17) was replaced by an open quartz tube (3-mm. i.d., 7-mm. o.d.) through which the chlorocarbon stream was metered for pyrolysis. The temperature was measured by an external thermocouple that traveled parallel to the quartz pyrolysis tube between the tube and the furnace. The open end of the inner tube extended

1.5 in. beyond the furnace to a point where the temperature was about 600°, at a point 4.5 in. beyond the pyrolysis zone where the temperature was above 990 to 1040° at its center. The system was evacuated to 4.5 mm. and *p*-xylene (7.6 moles) was metered through the outer concentric tube at the rate of 0.032 mole/min., while carbon tetrachloride (8.8 moles) was metered through the inner concentric tube at the rate 0.037 mole/min. Pyrolysis occurred independently in the two concentric tubes for 5×10^{-3} and 4×10^{-4} sec. residence time, respectively, and confluence occurred at the blend point 1 in. beyond the furnace, where the temperature was about 600°. The resultant gas mixture was collected in 4 l. of hexane kept at -78° (no. 7). The resultant solution was warmed to room temperature and the excess solvent was removed by rapid evaporation at 60 mm. pressure and 100° as described previously, and the non-volatile products of interaction were collected as residue. The pyrolysis experiment was repeated three more times so that totals of 30.5 moles of *p*-xylene and 35.2 moles of CCl₄ were passed through the outer and inner concentric tubes, respectively, to afford a total of 684 g. of non-volatile mixture of reaction products.

The residues were combined and then dissolved in 3.4 l. of hexane. The resultant solution was chilled to -78° and *p*-xylylene dichloride (77 g.) precipitated in the form of grayish crystals (m.p. 90–95°). A sample was recrystallized from methanol to afford this compound as white crystals that melted at 95–97°. The compound was characterized further by reaction with NaCN in aqueous ethanol to give *p*-xylylene dicyanide (m.p. 95.5–96.5°). The dicyanide then was hydrolyzed in aqueous NaOH to the salt of *p*-phenylenediacetic acid. Acidification with mineral acid afforded the free acid (m.p. 243–245°). The melting points and infrared spectra of the *p*-xylylene dichloride and its subsequent derivatives were identical with those of authentic samples.

The hexane mother liquor from which *p*-xylylene dichloride was removed by filtration was evaporated to dryness under a stream of nitrogen. The residue was separated by distillation at 1.5 mm. and the following fractions were isolated: (1) 231 g. of *p*-methylbenzyl chloride, b.p. 54–60°, m.p. -2 to 0°; (2) 5 g. of amber oil, b.p. 85–100°. The sample was dissolved in hot methanol and then chilled to room temperature to afford 1.1 g. of *p*-xylylene dichloride, m.p. 97–98°. The solute in the mother liquor was recovered by evaporation to dryness. The infrared spectrum of this residue indicated that it was mostly a mixture of diarylmethanes and 1,2-di-*p*-tolylethane. (3) An amber oil (154 g.), b.p. 100–126° at 1–2 mm. This oil was dissolved in methanol and chilled to -78° to afford 20 g. of di-*p*-tolylethane (m.p. 74–76°). The solute was recovered from the mother liquor by evaporation to dryness. The amber residue was the usual mixture of diarylmethanes and 1,2-di-*p*-tolylethane.⁷ (4) A non-distillable residue (150 g.). The elemental analysis (19.1% Cl; 4.70% H; and 74.8% C) of this fraction corresponds to an average empirical formula of (C₈H₆Cl_{0.7})_n. Its average molecular weight was ca. 2000. An attempt was made to separate the dark oily residue by liquid chromatography using a 6-ft. column filled with 4 lb. of Al₂O₃. The column was developed with hexane as described previously.⁷ Ill-defined tars were obtained in each eluted fraction and only trace amounts of cyclic-tri-*p*-xylylene and 1,4-bis-(2-*p*-tolylethyl)-benzene were isolated.

Thus the pyrolysis of 30.5 moles of *p*-xylene and 35.2 moles of CCl₄ in two concentric streams that blended at a point 4.5 in.

beyond the pyrolysis zone produced 1.65 moles of *p*-methylbenzyl chloride, 0.45 mole of *p*-xylylene dichloride, 1.46 moles of *p*-methylbenzyl equivalents isolated as diarylmethanes and 1,2-di-*p*-tolylethane, and 1.18 moles of ill-defined non-volatile residue whose average empirical formula was (C₈H₆Cl_{0.7})_n.

Pyrolyzed CCl₄ Quenched with Non-pyrolyzed *p*-Xylene.—The pyrolysis system shown in Fig. 1 of ref. 12 was modified such that manometer 8 and stopcock 9 were replaced by a 7 mm. quartz tube that extended to within 1 in. of the furnace. Provisions were made so that *p*-xylene could be metered into the system through this tube. The system was evacuated to 10 mm. and 1.8 moles of CCl₄ was metered to the system through vaporizer no. 15, at the rate of 0.026 mole/min., while 5.6 moles of *p*-xylene was being metered to the system at the other end at the rate of 0.08 mole/min. Pyrolysis of CCl₄ occurred at 1000° for 0.015 sec. and the chlorocarbon pyrolyzate was quenched with non-pyrolyzed *p*-xylene at a point 4.5 in. away from the pyrolysis zone. The gas mixture was collected in cold (-78°) heptane (4 l.). The resulting solution was warmed to room temperature and the excess solvent was separated by rapid evaporation at 60 mm. and 100° as described previously to afford 32 g. of non-volatile residue. This residue was dissolved in hot methanol and hexachlorobenzene (19 g.) crystallized in the form of white needles (m.p. 205–210°) when the solution was cooled to room temperature. The methanol mother liquor was separated by distillation at 1.5 mm. to give 5 g. of distillate (b.p. 50–70°) which was a mixture of *p*-methylbenzyl chloride (ca. 2 g.) and 2-chloro-*p*-xylene (ca. 3 g.) as indicated by infrared analysis and mass spectrometric analysis. The non-volatile residue (5 g., b.p. > 100° at 1.5 mm.) was essentially hexachlorobenzene as indicated by its infrared spectrum.

Pyrolyzed *p*-Xylene Quenched with Non-pyrolyzed CCl₄.—The pyrolysis system shown in Fig. 1 of ref. 12 was modified as described previously for the pyrolysis of CCl₄ and subsequent quench with non-pyrolyzed *p*-xylene. The system was evacuated to 4.5 mm. *p*-Xylene (6.4 moles) was metered at the rate 0.035 mole/min. into the system and pyrolyzed at 1100° for 6×10^{-3} sec. The hydrocarbon pyrolyzate was quenched at a point 4.5 in. away from the pyrolysis zone with non-pyrolyzed CCl₄ entering (at 0.023 mole/min.) through the inlet at the other end of the pyrolysis system. The gas mixture was collected in 3.5 l. of hexane kept at -78°. The resulting clear solution was warmed to room temperature and poly-(*p*-xylene) precipitated throughout the flask. This was removed by filtration to give 33 g. of dry polymer that contained no chlorine. The solvent of the mother liquor was separated by rapid evaporation at 60 mm. and 100° as described previously. The non-volatile residue (29 g.) also contained no chlorine and was a mixture of the usual products of *p*-xylene pyrolysis⁷ as indicated by infrared analysis. The distillate was a mixture of hexane, carbon tetrachloride, *p*-xylene, and some toluene, as indicated by infrared analysis.

Acknowledgments.—The authors are indebted to Drs. H. L. Dinsmore and H. F. White, then of the M. W. Kellogg Co., for interpretation of the infrared spectra and mass spectrometer data, and to Dr. J. J. McBrady of the Minnesota Mining and Mfg. Co. for interpretation of the nuclear magnetic resonance data.

THE CHEMISTRY OF XYLYLENES. XVII. THE MECHANISM FOR FORMATION OF XYLYLENES IN GAS PHASE

BY L. A. ERREDE AND J. P. CASSIDY

Contribution No. 223 from the Central Research Laboratories of the Minnesota Mining and Manufacturing Company,¹ St. Paul, Minn.

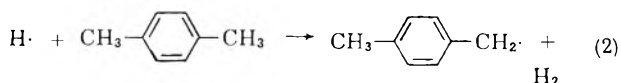
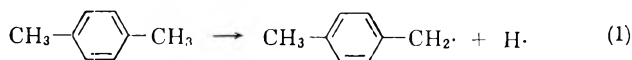
Received May 23, 1962

Fast flow co-pyrolysis of *p*-xylene and carbon tetrachloride at low pressure was used to elucidate the mechanism for conversion of *p*-xylene to *p*-xylylene. It was demonstrated that *p*-methylbenzyl radicals are converted catalytically to *p*-xylylene as the hydrocarbon gas stream travels away from the furnace. Each *p*-xylylene molecule is formed from one *p*-methylbenzyl radical and not *via* collision and disproportionation of two radicals as heretofore believed. The catalyst for dehydrogenation of *p*-methylbenzyl radicals is the carbonized material deposited along the post-pyrolysis zone of the pyrolysis system. Coupling to give 1,2-di-*p*-tolylethane is a homogeneous second-order reaction that competes with dehydrogenation. The ratio of *p*-xylylene to 1,2-di-*p*-tolylethane produced *via* these two reactions increases with increase in catalyst surface and decreases with increase in pressure. The half-life of the *p*-methylbenzyl radicals in the hydrocarbon stream was about 0.01 sec. In contrast, trichloromethyl radicals disappeared completely from the chlorocarbon stream within 0.002 sec. after leaving the pyrolysis zone.

Introduction

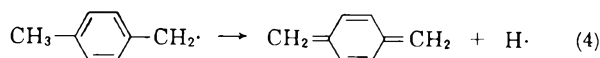
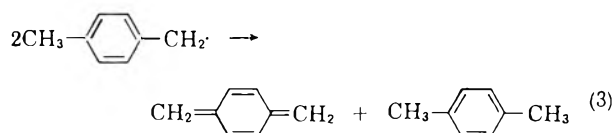
In the preceding paper² of this series, it was reported that fast flow co-pyrolysis of *p*-xylene and carbon tetrachloride at low pressure yielded a pyrolyzate having *p*-methylbenzyl chloride and β,β -dichloro-*p*-methylstyrene as two major components. On the other hand, *p*-methylbenzyl chloride and *p*-xylylene dichloride were the two major products of interaction when *p*-xylene and carbon tetrachloride were pyrolyzed in separate coaxial tubes and the two streams were allowed to blend at a point one inch beyond the furnace. No products of interaction were produced in significant amount when the pyrolyzed stream of one was allowed to blend with an unpyrolyzed stream of the other, proving that the chlorohydrocarbons isolated were produced primarily *via* coupling of the radical fragments. These results suggested that *p*-xylylene might be produced in the hydrocarbon gas stream as the pyrolyzate traveled away from the furnace. It was reasoned that a systematic study of the product distribution as a function of blend point might help elucidate the mechanism whereby *p*-methylbenzyl radicals are converted to *p*-xylylene.

Szwarc has shown unequivocally that thermal rupture of the C-H bond of *p*-xylene to give a *p*-methylbenzyl radical and a hydrogen atom is a first-order homogeneous gas phase reaction.³ Subsequent reaction of the hydrogen atom with *p*-xylene gives another *p*-methylbenzyl radical and molecular hydrogen.



Szwarc postulated that *p*-methylbenzyl radicals are converted to *p*-xylylene in one of two ways, namely, *via* disproportionation (3) and/or decomposition (4).

Reaction 4 as written leads to a chain reaction. The work of Szwarc, however, had shown that the



pyrolysis of xylenes does not involve a chain mechanism. Furthermore, the results of kinetic studies^{3,4} appeared to favor reaction 3. Consequently, it was concluded tentatively that under the usual conditions of fast flow pyrolysis, *p*-xylylene was formed primarily *via* reaction 3. This conclusion was supported by the observation that fast flow pyrolysis of 1,2-bis-*p*-tolylethane gave, among other products, *p*-xylylene and *p*-xylene in about equal amounts.^{5,6}

Results and Discussion

If it is assumed that *p*-methylbenzyl radicals are converted to *p*-xylylene in the gas phase *via* disproportionation as indicated in reaction 3, then it follows that the concentration of reactive species (*i.e.*, *p*-methylbenzyl radicals plus *p*-xylylene) should decrease as the gas stream travels away from the furnace. Hence, the yield of chlorocarbons obtained by quenching this hydrocarbon stream with a gas stream of chlorocarbon radicals should decrease as the blend point is moved farther into the post-pyrolysis zone.

Accordingly, fast flowing gas streams of *p*-xylene and carbon tetrachloride were pyrolyzed in separate concentric tubes, as shown schematically in Fig. 1. The two streams were made to blend at a fixed point having the temperature indicated by the temperature profile shown directly below the diagram of the pyrolysis system. At a point 3 ft. beyond the furnace, the resulting gas stream was collected in hexane kept at -78° . Much of the chlorine generated in this reaction was condensed in the second cold trap cooled by liquid nitrogen. The reaction products were separated as described in detail in our preceding publication.² A series of these coaxial pyrolyses was carried out at approximately the same temperature and residence time. In successive experiments the two gas streams were mixed at -4.5 , -2.5 , 0.5 , 1.5 , 3.5 , 4.5 ,

(1) This work was carried out in the laboratories of the M. W. Kellogg Co. The data were acquired by the Minnesota Mining and Mfg. Co. with the purchase of the Chemical Manufacturing Division of the M. W. Kellogg Co. in March, 1957.

(2) L. A. Errede and J. P. Cassidy, *J. Phys. Chem.*, **67**, 69 (1963).

(3) M. Szwarc, *Discussions Faraday Soc.*, **2**, 46 (1947).

(4) M. Levy, M. Szwarc, and J. Throssell, *J. Chem. Phys.*, **22**, 1904 (1954).

(5) J. R. Schaefgen, *J. Polymer Sci.*, **15**, 230 (1955).

(6) L. A. Errede and J. P. Cassidy, *J. Am. Chem. Soc.*, **82**, 3653 (1960).

TABLE I
PRODUCTS ISOLATED *via* COAXIAL PYROLYSIS OF *p*-XYLENE AND CARBON TETRACHLORIDE

Pyrolysis temp., °C.	Reaction conditions							
	1030	1020	1000	1010	1000	1040	1030	1030
Residence time, 10 ⁻³ sec.	6	6	6	6	6	5	6	8
Blend point, ^a in.	-4.5	-2.5	0.5	1.5	3.5	4.5	7.5	10.5
Temp. of blend point	1030	1020	990	950	700	600	400	300
Moles <i>p</i> -xylene used	12.1	9.2	11.1	8.3	18.5	30.6	7.18	5.75
Moles CCl ₄ used	13.9	7.3	12.0	5.6	25.4	35.6	9.00	7.27
Products isolated (moles)								
<i>p</i> -ClCH ₂ C ₆ H ₄ CH ₂ Cl	0	0	0	0.04	0.15	0.45	0.25	0.33
<i>p</i> -CH ₂ C ₆ H ₄ CH ₂ Cl	0.57	0.30	0.20	.34	.74	1.65	.38	.23
<i>p</i> -CH ₂ C ₆ H ₄ CH=CCl ₂	.44	.26	.13	.05	0	0	0	0
(C ₆ H ₅) ₂ ^b	.37	.22	.16	.21	0.38	1.51	0.22	0.32
(C ₈ H ₆ Cl _{0.7}) _{ca. 0.7} ^c	.39	.32	.37	.24	.39	1.18	.17	.13
Sum total xylyl units	1.77	1.10	0.86	0.88	1.66	4.79	1.02	1.01
% yield ^d	15	12	8	11	9	16	14	18
Expected yield ^e	13	10	7	9	7	15	13	16

^a Point of mixing measured in inches away from pyrolysis zone (see Fig. 1). ^b Mixture of 1,2-di-*p*-tolylethane and methylated diphenylmethane. ^c Residue isolated as decomposition products formed during separation by vacuum distillation. ^d Moles of *p*-xylyl equivalents isolated $\times 100 \div$ moles of *p*-xylene pyrolyzed. ^e Based on *p*-xylene pyrolysis data that related conversion of *p*-xylene to *p*-methylbenzyl radicals as a function of temperature and residence time⁷ (see eq. 5, 6, and 7).

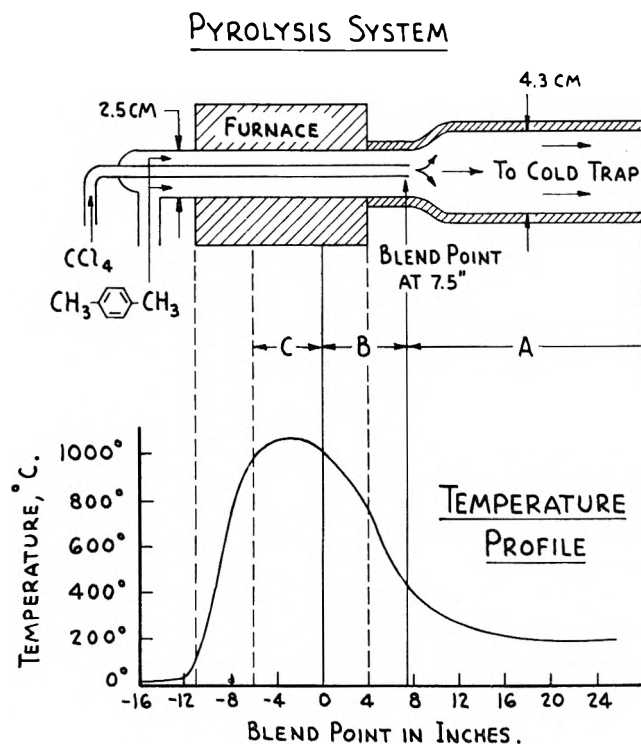


Fig. 1.—Diagram of pyrolysis system showing the corresponding temperatures in the pyrolysis zone C and the post-pyrolysis zones B and A with internal diameters of 2.5 and 4.3 cm., respectively.

7.5, and 10.5 in. beyond the end point of the pyrolysis zone. The numbers of moles of various components isolated in each run are shown in Table I.

The per cent yield of total products of interaction is independent of the distance the hydrocarbon gas stream travels before it is quenched with the chlorocarbon stream. In fact, the yield of interaction products in each run is about equal to the corresponding per cent conversion of *p*-xylene to *p*-methylbenzyl anticipated on the basis of an earlier study. The latter demonstrated that the fractional conversion of *p*-xylene to *p*-methylbenzyl radicals (C) is given by

$$C = At \exp(-Bt) \quad (5)$$

where t is the residence time in seconds, and A and B are temperature dependent variables given by

$$A = 2.6 \times 10^{15} \exp(-83/RT) \quad (6)$$

$$B = 8.5 \times 10^{14} \exp(-80/RT) \quad (7)$$

These results prove that eq. 3 does not represent the mechanism for conversion of *p*-methylbenzyl radicals to *p*-xylylene, since this equation requires that the amount of interaction products decrease as the quench point is moved farther away from the pyrolysis zone.

It also was shown⁷ that the ultimate distribution of products from fast flow pyrolysis of *p*-xylene does not change appreciably as conversion increases at the same reaction pressure. If it is assumed that this also is true in co-pyrolysis, the data given in Table I can be used to calculate the number of moles of each component that would be isolated when 10 moles of *p*-xylene are pyrolyzed to give 1 mole of *p*-methylbenzyl radicals for interaction with the chlorocarbon radicals. Accordingly, the data in Table I were recalculated to determine the yield of individual reaction products at 10% conversion of *p*-xylene, and the results are summarized in Fig. 2.

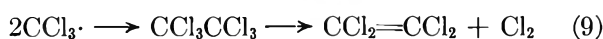
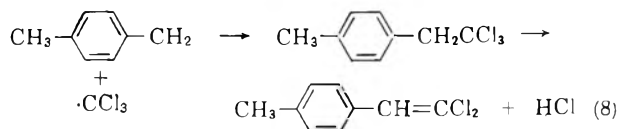
This diagram shows a continuous change in product distribution as a function of blend point. No *p*-xylylene derivative was isolated until the blend point of the two pyrolysis streams was outside the pyrolysis zone; thereafter, the amount of *p*-xylylene dichloride isolated increased linearly with distance away from the pyrolysis zone. These results demonstrate clearly that *p*-xylylene is formed as the pyrolyzate streams away from the furnace. Apparently any *p*-xylylene that might form in the pyrolysis zone is destroyed before it can couple with chlorine or chlorocarbon radicals to give stable compounds. For example, *p*-xylylene produced in the pyrolysis zone could rearrange to cyclooctatetraene, which in turn is known to undergo

(7) L. A. Errede and F. DeMaria, *J. Phys. Chem.*, **66**, 2664 (1962).

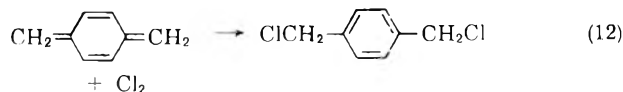
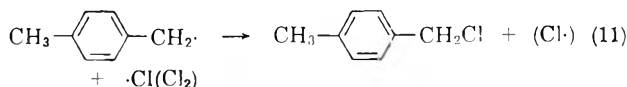
(8) E. J. Prosen, W. H. Johnson, and F. D. Rossini, *J. Am. Chem. Soc.*, **69**, 2068 (1947).

thermal rearrangement to styrene.⁸ Indeed, styrene was identified as one of the products of fast flow pyrolysis of *p*-xylene, and cyclooctatetraene probably was another product of this reaction⁶ as indicated by mass spectrometric analysis. Moreover, other experiments showed that the proportion of styrene (and cyclooctatetraene) produced from *p*-xylene increases with increase in severity of the pyrolysis conditions.⁷ Another possibility is that *p*-xylylene generated in the pyrolysis zone is decomposed to non-condensable gases such as ethylene and acetylene.⁷

The amount of β,β -dichloro-*p*-methylstyrene isolated in these experiments remained constant so long as the blend point was located within the pyrolysis zone. It fell off rapidly when the blend point was extended beyond the furnace. Undoubtedly, β,β -dichloro-*p*-methylstyrene is formed *via* coupling of *p*-methylbenzyl radicals with trichloromethyl radicals to afford *p*-(β,β -trichloroethyl)-toluene, which splits out hydrogen chloride at the high temperatures that exist in the zone of coupling, as indicated by reaction 8.



The rapid decrease in formation of β,β -dichloro-*p*-methylstyrene accompanies a corresponding increase in *p*-methylbenzyl chloride formation, which occurs *via* coupling of methylbenzyl radicals with chlorine (reaction 11). Apparently all of the trichloromethyl radicals in the chlorocarbon stream are consumed *via* eq. 9 and 10 before the gas stream travels 2 in. beyond the pyrolysis zone. Thereafter, the only reactive species in the chlorocarbon stream is chlorine. Consequently, *p*-methylbenzyl chloride and *p*-xylylene dichloride are the only interaction products isolated (eq. 11 and 12) when the two streams are made to blend at a distance greater than 2 in. beyond the pyrolysis zone.



It is conceivable that *p*-CH₃C₆H₄CH₂CCl₃ was produced in small amount despite the fact that it was not isolated, since an appreciable fraction of the condensate of each experiment was obtained as the ill-defined, non-distillable residue having an average empirical formula of (C₈H₆Cl_{0.7})_{ca. 0.7}. This residue was shown by infrared analysis to be a mixture of alkylated aromatics. It was found that residues of this type are formed when a synthetic mixture of the compounds isolated in these experiments is separated by vacuum distillation. The amount of this chlorine containing residue decreased as the proportion of *p*-methylbenzyl halide derivatives decreased in the mixture.

Figure 2 shows that the amount of *p*-methylbenzyl

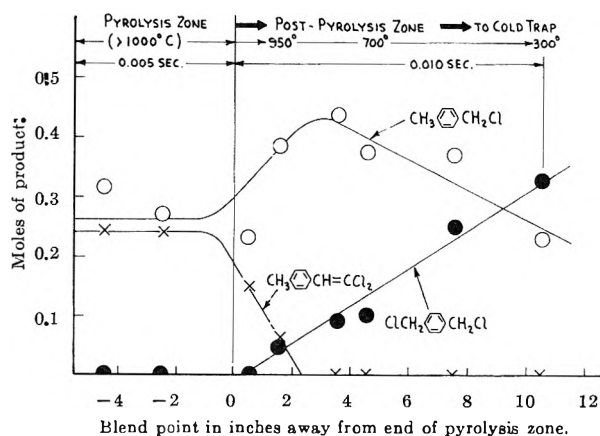


Fig. 2.—Product distribution as a function of the point where the pyrolyzed *p*-xylene stream was allowed to blend with the pyrolyzed carbon tetrachloride stream.

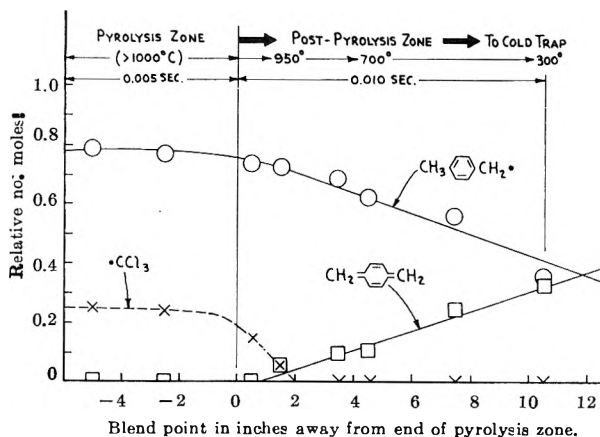


Fig. 3.—Relative concentration of reactive species as a function of distance away from the end of the pyrolysis zone.

chloride isolated decreases steadily and the amount isolated as *p*-xylylene dichloride increases as the blend point is moved beyond the furnace.

The proportion of *p*-methylbenzyl radical isolated as 1,2-di-*p*-tolylethane and methylated diphenylmethanes does not increase appreciably until the blend point is well past the pyrolysis zone. The diarylmethanes were consistently a major portion of this fraction when the blend point was less than 2 in. beyond the pyrolysis zone. The proportion of ditolyethane isolated, however, increased as the blend point was moved beyond 2 in. This is consistent with earlier results which proved that dibenzyls are converted in good yield at 1000° to diarylmethanes *via* fast flow pyrolysis.⁶ Most of the *p*-methylbenzyl units isolated as diarylmethanes must have formed within the pyrolysis zone. The increase in proportion of 1,2-ditolyethane as the distance to the blend point increases can be attributed to the greater time allowed for coupling of *p*-methylbenzyl radicals before quenching with the chlorocarbon pyrolyzate.

The relative amount of *p*-methylbenzyl radicals still present in the hydrocarbon stream at the blend point in question is given by the sum total yield of interaction products isolated as *p*-methylbenzyl chloride, β,β -dichloro-*p*-methylstyrene, and units of non-volatile residue. The yield of *p*-xylylene dichloride represents the corresponding relative concentration of *p*-xylylene. In Fig. 3 the sum total moles of *p*-methylbenzyl radical equivalents and *p*-xylylene equivalents are plotted as a function of blend point. The *p*-methyl-

benzyl units isolated as 1,2-di-*p*-tolylethane and methylated diphenylmethane have not been included in the data shown in Fig. 3, since these products result from side reactions that consume *p*-methylbenzyl radicals *via* coupling and subsequent rearrangement⁶ in the pyrolysis zone.

Figure 3 illustrates the relative stability (with respect to reactivity) of *p*-methylbenzyl and trichloromethyl radicals. At the fast flow pyrolysis conditions described for the present experiments, *p*-methylbenzyl radicals have a half-life of about 0.01 sec. in the hydrocarbon stream, whereas the trichloromethyl radicals disappear completely from the chlorocarbon stream within 0.002 sec.

Figure 3 also shows that the disappearance of *p*-methylbenzyl radicals in the hydrocarbon pyrolyzate is accompanied by a corresponding equivalent increase in *p*-xylylene, implying that each *p*-methylbenzyl radical is converted to one *p*-xylylene molecule. Equation 4, however, does not represent the true picture, since this equation as written is part of a chain sequence that includes eq. 2 and 4. As mentioned earlier, it was shown by Szwarc^{3,4} that the pyrolysis of *p*-xylylene does not involve a chain mechanism. The data shown in Fig. 3 for conversion of *p*-methylbenzyl radicals to *p*-xylylene as a function of distance along the post-pyrolysis zone were studied from the standpoint of elapsed time for the pyrolyzate to reach the respective quench points. It was noted that the rate of conversion of *p*-methylbenzyl radicals to *p*-xylylene in the post-pyrolysis zone of a tube having a 1-in. diameter was virtually constant despite large changes in temperature and concentration of *p*-methylbenzyl radical. On the other hand, the dehydrogenation rate decreased sharply when the pyrolyzate entered the expanded post-pyrolysis tube of 4.3-cm. diameter (Table II) beginning at a point 8 in. away from the pyrolysis zone, as shown in Fig. 1. These results suggest that the dehydrogenation is heterogeneous and zero order.

TABLE II

RELATIVE EFFICIENCY FOR DEHYDROGENATION OF *p*-METHYLBENZYL RADICALS TO *p*-XYLYLENE IN *p*-XYLYLENE GAS STREAM AT 4 MM. PRESSURE

Dehydrogenation zone ^a	Surface/volume ratio of dehydrogenation zone	Relative zero order rate constant
A	0.18/1	25
B	0.59/1	91
C	0.91/1	200

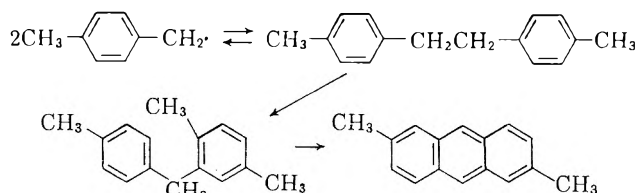
^a Refers to pyrolysis tube system shown in Fig. 1: (A) portion of the post-pyrolysis zone having a 4.3-cm. diameter; (B) portion of the post-pyrolysis zone having a 2.5-cm. diameter; (C) post-pyrolysis zone B fitted with 5 tubes (4 in. long, 8 mm. o.d., and 6 mm. i.d.) inserted in the form of a bundle around the inner pyrolysis tube between the pyrolysis zone and the quench point.

To test this hypothesis, the surface area in the path of the pyrolyzed hydrocarbon stream was increased by packing the reaction tube between the pyrolysis zone and the quench point with small quartz tubes. Pyrolysis of *p*-xylylene again was carried out under conditions that produce 10% conversion to *p*-methylbenzyl radicals in the pyrolysis zone. The pyrolyzate, after flowing through the quartz tube packing, was quenched with pyrolyzed carbon tetrachloride at a point 6 in. beyond the pyrolysis zone. The resulting gas stream

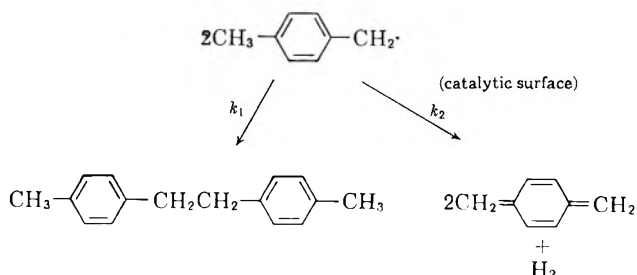
was collected in hexane kept at -78° and the products were separated in the usual way, as described in detail in a previous publication.² Thirty-one per cent of the *p*-methylbenzyl radicals were isolated as *p*-xylylene dichloride, 27% as *p*-methylbenzyl chloride, 24% as methylated diphenylmethanes, 5% as 1,2-di-*p*-tolylethane, and 14% as the ill-defined residue^{2,3} believed to be produced from chlorohydrocarbon products during vacuum distillation of the reaction mixture. Thus, at a point 6 in. beyond the pyrolysis zone, the ratio of *p*-xylylene to *p*-methylbenzyl radicals in this experiment was 31/27 (or 1.15 to 1), whereas Fig. 2 shows that without the packing in the post-pyrolysis zone, the corresponding ratio at the same quench point was only 19/27 (or 0.70/1).

The relative zero-order rate constants for dehydrogenation of *p*-methylbenzyl radicals to *p*-xylylene were calculated as a function of the surface to volume ratio along the post-pyrolysis zones A and B of the apparatus shown in Fig. 2 and for the zone B when modified by addition of the quartz packing. The data, summarized in Table II, show that the dehydrogenation efficiency increases with increase in surface to volume ratio of the post-pyrolysis zone. These results virtually prove that the conversion of *p*-methylbenzyl radicals to *p*-xylylene is a heterogeneous reaction.

This conclusion can be tested further by noting the product distribution as a function of reaction pressure. It was demonstrated⁹ that the *p*-xylylene produced in this dehydrogenation can be collected in a cold solvent and then polymerized at -78° to give insoluble poly(*p*-xylylene) almost exclusively. It also was demonstrated⁶ that coupling of two *p*-methylbenzyl radicals gives 1,2-di-*p*-tolylethane that can rearrange under the existing pyrolysis conditions to give *o*-methylated diarylmethanes which in turn give anthracenes.



The 1,2-di-*p*-tolylethane, diarylmethanes, and anthracenes are collected in the cold solvent along with *p*-xylylene, but these components remain soluble after polymerization of *p*-xylylene is completed. Hence, the secondary products of *p*-methylbenzyl radicals that form *via* bimolecular coupling and those that form *via* heterogeneous dehydrogenation can be separated easily by filtration. The latter are isolated as poly(*p*-xylylene) by filtration and the former are isolated as a mixture by evaporating the mother liquor to constant weight. The weight ratio of soluble products (μ) to



(9) L. A. Errede, R. S. Gregorian, and J. M. Hoyt, *J. Am. Chem. Soc.*, **82**, 5218 (1960).

insoluble products (W) is then a measure of the relative rates for bimolecular coupling (R_1) and dehydrogenation (R_2) which are concurrent reactions as indicated schematically by k_1 and k_2 .

It follows that

$$\frac{u}{W} = \frac{R_1}{R_2} = f\left(\frac{k_1 P^2}{k_2}\right) \quad (13)$$

Bimolecular coupling, a second-order reaction, should increase as the square of the reaction pressure. Dehydrogenation, here suggested to be zero order, should be essentially independent of reaction pressure. Hence, $(u/W)^{1/2}$ should increase linearly with increase in pressure (P) as indicated by

$$(u/W)^{1/2} = KP + C \quad (14)$$

where k and C are constants.

Accordingly, *p*-xylene was subjected to fast flow pyrolysis conditions that afford 3–4% conversion to *p*-methylbenzyl radicals, and the weight ratio of products produced *via* bimolecular reaction (u) to those produced *via* dehydrogenation (W) was determined as described in the Experimental section. Pyrolyses were carried out at pressures ranging from 1.5 to 45 mm. and the results are summarized in Fig. 4. It is seen that $(u/W)^{1/2}$ increases linearly with pressure as required by eq. 13 and 14. Extrapolation of the line to zero pressure gives an intercept for this particular pyrolysis system at 0.5. The value is a function of the geometry of the system as shown in Table II. Probably these results can be improved in favor of dehydrogenation by increasing the surface to volume ratio in the post-pyrolysis zone.

It was surmised immediately that the carbonized material deposited as a film along the walls of the post-pyrolysis zone might be the active catalyst for dehydrogenation, since the *p*-methylbenzyl radicals generated in the carbon-free pyrolysis zone were not converted to *p*-xylylene until the pyrolyzate entered the post-pyrolysis zone of carbonized film.

Szwarc had shown that *p*-methylbenzyl radicals generated from *p*-methylbenzyl bromide *via* relatively mild pyrolysis conditions ($<800^\circ$) afforded only 1,2-di-*p*-tolylethane.¹⁰ The quartz pyrolysis tube was still free of carbon at the end of the experiment.¹¹ *p*-Xylylene was not formed in any amount until pyrolysis temperatures that decompose *p*-xylene itself were used. His results were verified in our Laboratory. A gas mixture of *p*-xylene and *p*-methylbenzyl chloride in the ratio of 10 to 1 was pyrolyzed at 750° and 4 mm. pressure for an average of 0.01 sec. residence time in a fresh, carbon-free quartz tube that was a replica of the ones used in the previous experiments. About 2% of the mixture was converted to *p*-methylbenzyl radicals that were isolated almost entirely as 1,2-di-*p*-tolylethane. Only a trace amount was isolated as polymerized *p*-xylylene. A liberal amount of carbonized material then was deposited along the post-pyrolysis zone of the apparatus by pyrolyses of *p*-xylene at high temperature (*ca.* 1050°). Szwarc's pyrolysis experi-

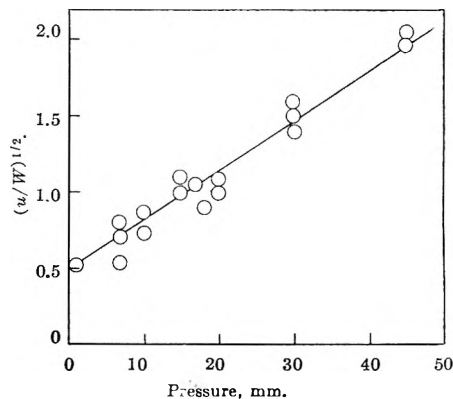


Fig. 4.— $(u/W)^{1/2}$ as a function of the reaction pressure, where u is the weight of *p*-methylbenzyl radicals isolated as 1,2-di-*p*-tolylethane, diarylmethanes, and anthracenes, and W is the weight of *p*-xylylene isolated as poly-*p*-xylylene.

ment again was repeated using the *p*-xylene and *p*-methylbenzyl chloride (10 to 1) feed stock. The conversion of the gas mixture to *p*-methylbenzyl radicals was again about 2% but this time 70% of the radicals produced were isolated as poly-*p*-xylylene and only 30% as 1,2-di-*p*-tolylethane. Similar results were obtained when pyrolysis of this gas mixture was carried out at 700° , although the conversion of *p*-methylbenzyl radicals was understandably much lower at this temperature. Our previous study demonstrated that dehydrogenation of *p*-methylbenzyl radicals to *p*-xylylene occurred at temperatures as low as 300° (see Fig. 1, 2, and 3); hence it is believed that the threshold temperature (*ca.* 800°) reported by Szwarc for isolation of poly-*p*-xylylene is a manifestation of the temperature at which some carbonization occurs to afford the necessary catalyst for the dehydrogenation.

Experimental

The Effect of Pressure on Bimolecular Coupling and Catalytic Dehydrogenation of *p*-Methylbenzyl Radicals.—A pyrolysis system similar to that shown in Fig. 1 of ref. 12 was used for this comparative study. About 5 moles of *p*-xylene metered to the system at the rate of 0.03 mole/min. was pyrolyzed at 950° for 0.01 sec. residence time in the pyrolysis zone of the 1 in. i.d. quartz pyrolysis tube. These pyrolysis conditions afford 3–4% conversion of *p*-xylene to *p*-methylbenzyl radicals.⁶ The pyrolyzate passed through a post-pyrolysis zone (2 ft. long, 1 in. i.d.) along which the temperature decreased from 950 to 200° , and then was collected in heptane (4.5 l.) kept at -78° . The *p*-xylylene solution prepared in this way was agitated vigorously to create numerous polymerization sites⁹ and then allowed to polymerize at -78° for one week. This polymerization procedure precipitates virtually all the *p*-xylylene as poly-*p*-xylylene.⁹ The solution was warmed to room temperature and the polymer was collected by filtration. The 1,2-di-*p*-tolylethane and daughter products were recovered from the mother liquor by evaporation to dryness. The weight ratio of soluble products (u) to insoluble products (W) was taken to indicate the relative rates for bimolecular coupling (R_1) and dehydrogenation (R_2) of *p*-methylbenzyl radicals as indicated in eq. 13 and 14. The reaction pressure was varied from 1.5 to 45 mm. in a series of experiments giving the results summarized in Fig. 4.

The Effect of Carbon Char on Dehydrogenation of *p*-Methylbenzyl Radicals.—The pyrolysis system shown in Fig. 1 of ref. 12 and diagrammatically in Fig. 1 of this publication was modified so that the space around the internal pyrolysis tube of the post-pyrolysis zone was packed with five quartz tubes (4 in. long, 8 mm. o.d., and 6 mm. i.d.) inserted in the form of a bundle that surrounded the inner pyrolysis tube between the pyrolysis zone and the quench point. The pyrolysis system was evacuated to 4 mm. pressure. A solution of *p*-methylbenzyl chloride (0.86 mole) in *p*-xylene (8.6 moles) was metered to the pyrolysis

(10) M. Levy, M. Szwarc, and J. Throssel, *J. Chem. Phys.*, **22**, 1904 (1954).

(11) M. Szwarc, private communication. A clean pyrolysis tube was used for each run and the tube was checked routinely at the end of each experiment to determine the extent of carbonization, if any.

(12) L. A. Errede and B. F. Landrum, *J. Am. Chem. Soc.*, **79**, 4952 (1957).

system at the rate of 0.017 mole/minute. The solution was vaporized at 323° in the vaporizer (no. 15 in Fig. 1 of ref. 12) and was pyrolyzed at 750° for 0.01 sec. in a fresh, quartz pyrolysis tube. The pyrolyzate was passed through the fresh quartz packing in the post-pyrolysis zone which was also free of carbon char and the pyrolyzate was collected in 4 l. of hexane kept at -78°. The resulting solution was warmed to room temperature and only a trace of insoluble poly-(*p*-xylylene) was obtained (ca. 0.5 g.). The polymer was removed by filtration and the mother liquor was separated by distillation at atmospheric pressure. The residue (b.p. > 140°) then was separated by distillation at 3.5 mm. to give three main fractions: (1) *p*-methylbenzyl chloride, 59 g., b.p. 63-67°; (2) 1,2-di-*p*-tolylethane, 21 g., b.p. 125-135°, m.p. 77-78° after one recrystallization from methanol; (3) residue (2 g.), b.p. > 135°. The infrared spectrum of this residue indicated a mixture of 1,2-di-*p*-tolylethane, diarylmehanes, anthracenes, and a small amount of another component that could be cyclo-tri-*p*-xylylene. Thus,

9.3 moles of pyrolysis feed stock was converted to about 0.2 mole of *p*-methylbenzyl units that were isolated as 1,2-*p*-tolylethane (2% yield) and as polymerization products of *p*-xylylene (trace amounts only).

In order to test the effect of freshly deposited carbon char, the apparatus was used for pyrolysis of 10 moles of *p*-xylylene at 1050° and 0.01 sec. residence time. This "conditioning run" caused a uniform layer of carbon char to be deposited over the entire quartz surfaces of the post-pyrolysis zone.

The pyrolysis apparatus then was used to repeat the original pyrolysis experiment. An equal amount of pyrolysis feed stock solution (8.6 moles of *p*-xylylene and 0.86 mole of *p*-methylbenzyl chloride) was pyrolyzed as described before, to generate the equivalent amount of *p*-methylbenzyl radicals (about 0.2 mole) in the pyrolysis zone. The reaction products were isolated as described previously and the 0.2 mole of *p*-methylbenzyl radicals, generated in the pyrolysis zone, were isolated as poly-(*p*-xylylene) (0.11 mole), cyclo-tri-(*p*-xylylene) (0.03 mole), and 1,2-bis-*p*-tolylethane (0.06 mole of *p*-methylbenzyl equivalents).

A STUDY OF THE MECHANISM OF CARBON MONOXIDE ADSORPTION ON PLATINUM BY A NEW ELECTROCHEMICAL PROCEDURE¹

BY S. GILMAN

Research Laboratory, General Electric Co., Schenectady, N. Y.

Received May 25, 1962

The adsorption of CO has been studied by means of a new electrochemical procedure utilizing a complex potential-time wave form. By means of this method, information on the type of bonding is obtained as a function of total surface coverage. Also, a minimum rate constant is estimated for the rapid chemisorption of CO from solution. Information is presented to reveal unusual reproducibility of the Pt surface before adsorption. Hydrogen adsorption is shown to be measurable with high precision using linear sweep speeds of up to 800 v./sec.

Introduction

There is increasing interest in the mechanism of electrochemical oxidation of carbonaceous fuels in connection with fuel cell technology. A knowledge of the mechanism of fuel adsorption is of fundamental importance to the elucidation of the over-all electrode reaction mechanism.

The electrochemical techniques previously described² for measuring CO adsorption have now been further developed and make possible a more detailed study of the system.

The bonding of CO to platinum at the gas-solid interface has been studied by Eischens and Pliskin³ using infrared techniques. These investigators uncovered evidence for both a linear (one-site) and bridged (two-site) adsorption structure on cabosil and alumina-supported platinum. The linear structure was found to account for approximately 15% of the total coverage on the former and 50% of the total coverage on the latter support. Gruber,⁴ using conventional gas-phase volumetric techniques, studied the total adsorption of CO and, alternately, hydrogen on alumina-supported platinum of varying dispersion. Assuming a combination of linear and bridged structures, he derived the contribution of each at saturation coverage as a function of platinum dispersion. None of the previous approaches to the problem could easily lead to information on the type of bonding as a function of total coverage.

(1) This work was made possible by the support of the Advanced Research Projects Agency (Order No. 247-61) through the United States Army Engineer Research and Development Laboratories under Contract Number DA-44-009-ENG-4853.

(2) S. Gilman, *J. Phys. Chem.*, **66**, 2657 (1962).

(3) R. D. Eischens and W. Pliskin, "Advances in Catalysis," Vol. X, Academic Press, Inc., New York, N. Y., 1958, p. 18.

(4) H. L. Gruber, *J. Phys. Chem.*, **66**, 48 (1962).

In this work, the rapid electrochemical techniques employed permit us to determine the contribution of the bridged and linear structures to the coverage as it is increased from zero to saturation. It also allows us to place a minimum limit on the rate of the rapid chemisorption of CO from solution.

Experimental

The electrochemical cell and reagents have been described previously.² The electrolyte was 1 *N* HClO₄; the working electrode had a geometric area of 0.08 cm.². All potentials are referred to a hydrogen electrode in 1 *N* HClO₄. A diagram of the circuit used appears in Fig. 1. The signal generator consisted of two Exact Model 250 signal generators whose ramp output was added by means of a network. Separation between ramps was achieved by means of a Tektronix Type 161 delay pulse generator. Potential "staircases" were generated using relays and batteries for signals of longer than 15-sec. duration and with Tektronix Type 161 delay units for step signals of shorter duration. The potentiostat used was a Wenking "Fast Rise" potentiostat. The current-time (potential) signals were measured with a Tektronix Type 536 oscilloscope using type D and type T plug-ins.

The potential function employed in this work is diagrammed in Fig. 2. The significance of steps A-E is covered below.

I. For Adsorption of 100% CO by Linear Diffusion.—(A) Pretreatment step (15-sec.) to remove adsorbed oxidizable impurities, and to produce a layer of adsorbed oxygen which serves to block adsorption. CO is kept bubbling through the solution. Some molecular oxygen is evolved at a steady-state rate of approximately 1 ma./cm.².

(B) Potential step during which the oxygen layer formed in (A) is maintained, molecular oxygen from (A) is swept away, and the concentration of the adsorbate is brought to its bulk value. CO is kept bubbling through the solution for 0.5 min. The flow of gas is then stopped and the solution allowed to become quiescent for 1.5 additional min. to allow for linear diffusion. No measurable current (less than 1 μa./cm.²) flows after the first second of pretreatment during this step.

(C) Reduction and adsorption step. The adsorbed oxygen layer is reduced within a few milliseconds, exposing a reproducibly

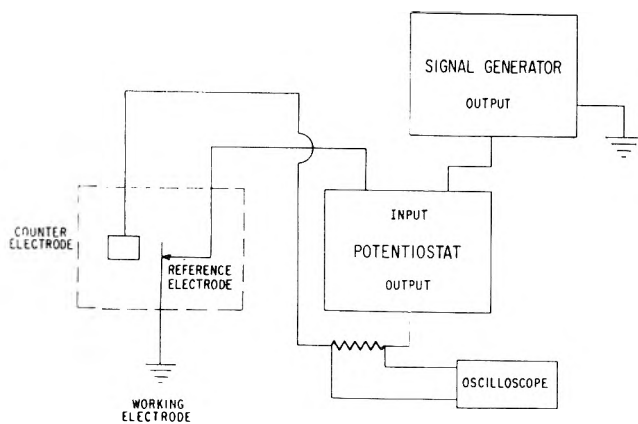


Fig. 1.—Circuit diagram.

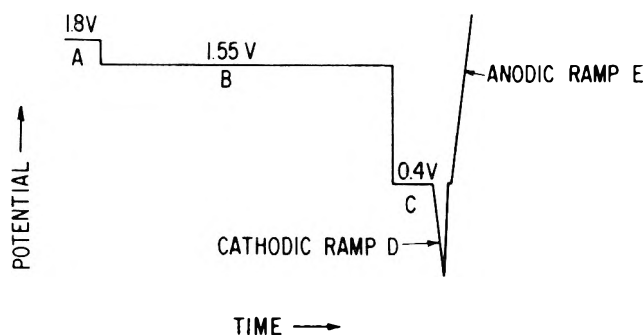


Fig. 2.—Complex signal used for electrochemical study of adsorption.

clean surface to the adsorbate. The duration of step (C) is the adsorption time, τ .

(D) Cathodic sweep. During this sweep hydrogen is electrolytically deposited on sites not previously covered with CO. The sweep speeds used are specified below. Step (D) is eliminated if only step (E) is of interest. For measurements of Q_H (see below) the oscilloscope is triggered at the beginning of the sweep.

(E) Anodic Sweep. During this sweep, adsorbed CO is oxidized and the surface is covered with a layer of adsorbed oxygen. Subtraction of the charge due to the surface oxidation ("solvent correction") from the total charge yields the charge due to CO oxidation (1). If step (D) is included in the sequence of signals, step (E) serves to indicate whether cathodic step (D) causes displacement or reduction of adsorbed CO. For the measurement of Q'_{CO} , the oscilloscope is triggered at the beginning of this sweep.

II. For Adsorption of 1% CO with Stirring.—The procedure is the same as for steps I(A) through I(E) with the following exceptions.

(1) Steps (A) through (E) are conducted with constant flow of a mixture of 1% CO, 99% argon, and with mechanical stirring by a paddle stirrer rotating at 200 r.p.m.

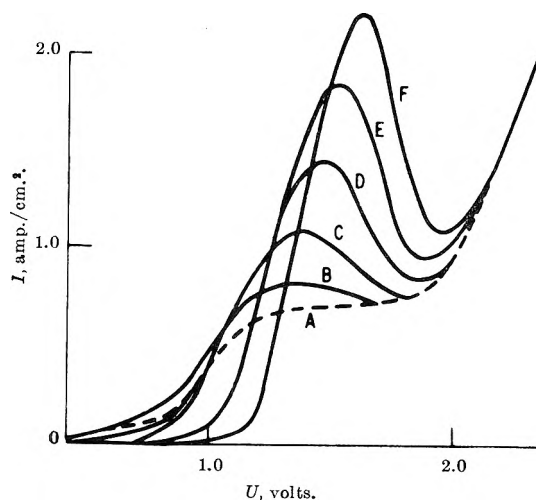
(2) Step (B) is only of 0.5 min. duration with the "quiet period" of 1.5 min. eliminated.

III. For Measurement in the Absence of Adsorbate.—Steps (A) through (E) are conducted as in (I) above with argon substituted for the adsorbate.

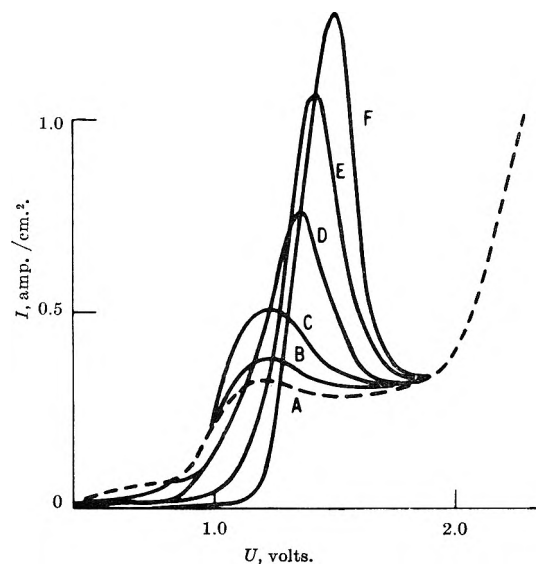
All potentials were adjusted to within 2 mv. using a Rubicon portable potentiometer.

Results and Discussion

I. Anodic Sweep Experiments.—Figures 3A and 3B presents the series of traces obtained at anodic sweep speeds of $v = 1100$ and 360 v./sec., respectively. Figure 3A corresponds to adsorption of CO from the unstirred solution saturated with the gas at 1 atm. Figure 3B corresponds to adsorption of CO from a stirred solution saturated with 1% CO, 99% argon. The temperature was 30° in both cases. The charge density (mcoul./cm.²) due to oxidation of CO, Q'_{CO} , is

A. Adsorption of CO from a quiet saturated solution of 100% CO. Sweep speed, $v = 1100$ v./sec.

Trace	τ , msec.
A	0. (solvent corn.)
B	4.8
C	30
D	98
E	195
F	910

B. Adsorption of CO from a stirred solution saturated with 1% CO, 99% argon; $v = 360$ v./sec.

Trace	τ , sec.
A	0. (solvent corn.)
B	1.0
C	3.0
D	6.0
E	13.0
F	100

Fig. 3.—Typical anodic pulse traces (30°).

obtained by subtracting the area under the solvent (dashed) curve from that under the curve corresponding to any value of τ (the adsorption time) to the point of coincidence of the two curves. The solvent curve is obtained at $\tau = 10$ msec. in the presence of argon (see section IV below). The assumptions involved in this procedure have been discussed previously.² The technique was previously found to give constant Q'_{CO} over a large range of sweep speeds.

Figure 4 plots Q'_{CO} against adsorption time, obtained by evaluating oscillograms typified by Fig. 3A. Let us

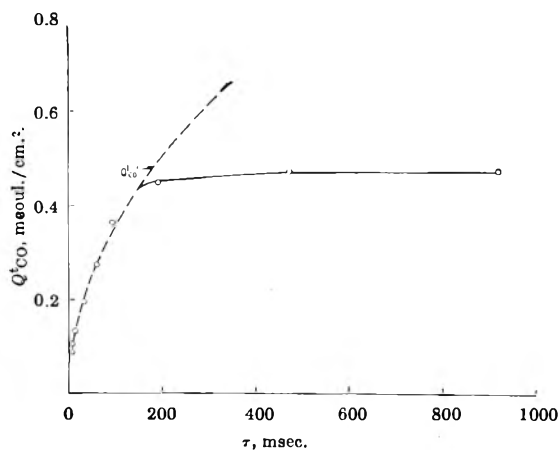


Fig. 4.—Charge due to oxidation of CO during the anodic sweep as a function of total adsorption time. The dashed line is for semi-infinite linear diffusion.

assume that the adsorption of CO is limited by diffusion to the surface. For the short adsorption times involved, let us further assume semi-infinite linear diffusion. The hypothetical charge, Q'_{CO} , might then be regarded as the integral of a "diffusion current density," i_d , of CO to the surface.

$$Q'_{CO} = \int_0^t i_d dt \quad (1)$$

For semi-infinite linear diffusion⁵

$$i_d = n\pi^{-1/2}FD^{1/2}_{CO}C_{CO}t^{-1/2} \quad (2)$$

Hence

$$Q'_{CO} = 2n\pi^{-1/2}FD^{1/2}_{CO}C_{CO}\tau^{-1/2} \quad (3)$$

where

$n = 2$ electrons/molecule

$F =$ Faraday constant

$D = 3.1 \times 10^{-5}$ cm.²/sec. (ref. 2)

$C = 8.92 \times 10^{-7}$ mole/cm.³ (ref. 6)

Substituting numerical values for the constants in eq. 3

$$Q'_{CO} = 1.22\tau^{1/2} \text{ moul./cm.}^2 \quad (4)$$

The theoretical curve for Q'_{CO} is plotted in Fig. 4 where it serves as an excellent fit for the experimental points corresponding to Q'_{CO} until the surface is largely covered with CO. The value of Q'_{CO} at $\tau = 4.8$ msec. is 0.068 moul./cm.² as compared with $Q'_{CO} = 0.062$ moul./cm.², implying that diffusion control commences at values of τ less than 5 msec. Reduction of the surface oxygen layer is not complete until after 1 msec. (see below), and so it is likely that rapid adsorption begins on the partly or largely oxygen-covered surface, and that the adsorption becomes diffusion limited at $\tau < 5$ msec. Let us assume that at small τ and zero CO coverage

$$i_{ads} = nFk_{ads}C_{CO} \quad (5)$$

and that diffusion control commences at 1 msec. Then⁷

(5) H. A. Laitinen and I. M. Kolthoff, *J. Am. Chem. Soc.*, **61**, 3344 (1939).

(6) "Lange Handbook of Chemistry," Tenth Edition, McGraw-Hill Book Co., Inc., New York, N. Y., 1961.

(7) "New Instrumental Methods in Electrochemistry," Interscience Publishers, Inc., New York, N. Y., 1959, p. 76.

$$\frac{K_{ads}\tau^{1/2}}{D^{1/2}_{CO}} > 5 \quad (6)$$

and $k_{ads} = 1$ cm./sec. is the minimum rate constant for adsorption of CO at 30° and 1 atm. Determination of the actual value of k_{ads} at low coverage would likely require measurement at much smaller values of τ and another technique is therefore required. Measurement of k_{ads} at larger coverages with CO will be discussed in a future publication.

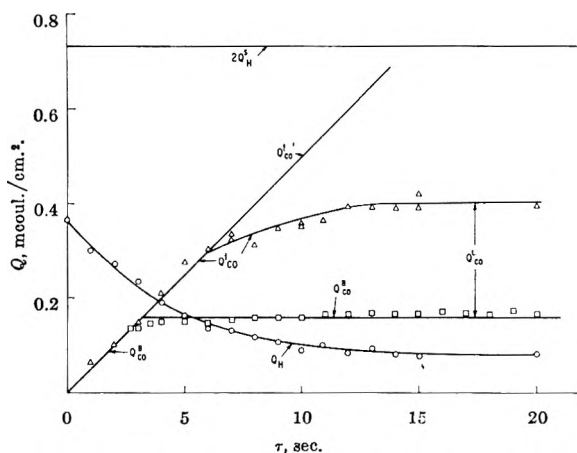


Fig. 5.—Adsorption time-dependence of several different charge densities. Determined in stirred 1 N HClO₄ solution saturated with 1% CO, 99% argon at 30°.

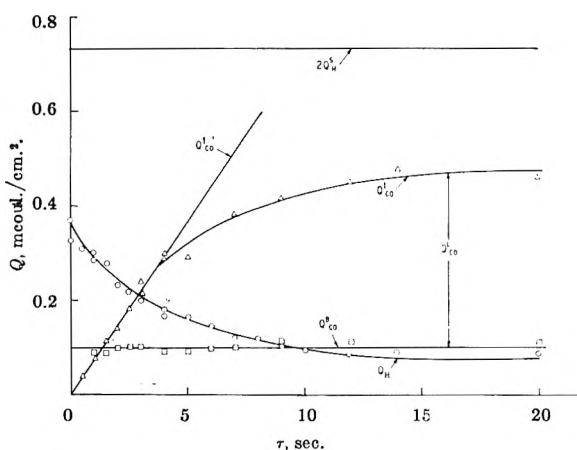


Fig. 6.—Adsorption time-dependence of several different charge densities. Determined in stirred 1 N HClO₄ solution saturated with 1% CO, 99% argon at 83°.

Since rates of adsorption at low coverages with CO are rapid, adsorption may be made to occur at a linear rate by decreasing the CO concentration and employing reproducible mechanical stirring. Figure 5 plots the results obtained by analysis of the traces typified by Fig. 3B ($v = 360$ v./sec., 30°). Figure 6 plots similar results for Q'_{CO} obtained at 83° with a sweep speed of $v = 400$ v./sec. Q'_{CO} is seen to follow the expected linear law until higher coverages are achieved in each case.

II. Cathodic Sweep Experiments.—Figure 7 compiles typical current-time (voltage) traces for the reduced electrode surface in the argon-saturated quiet solution. The reduction time, τ , is kept constant at 100 msec.; each curve corresponds to a different sweep speed v . Figure 7B demonstrates the manner in which the charge due to saturation hydrogen adsorption, Q^S_H is evaluated. The horizontal dashed line partially cor-

rects for double-layer changing. The vertical line approximately locates the point at which molecular hydrogen begins to evolve. Table I lists the values of

TABLE I

Q_H^S AS A FUNCTION OF v EMPLOYING A SINGLE CATHODIC SWEEP

v , v./sec.	Q_H^S , mcoul./cm. ²
5	0.360
10	.362
60	.358
800	.350
2 ^a	.350

^a Method of Will and Knorr.⁸

Q_H^S so obtained. These results are constant to within 1% from $v = 5$ to 60 v./sec., and agree within a few per cent with the value obtained at 800 v./sec., and the value obtained by the method of Will and Knorr⁸ employing a repetitive triangular sweep with $v = 2$ v./sec. The latter investigators were limited to sweep speeds less than approximately 2.0 v./sec. because of the problem of overlap of oxygen adsorption and hydrogen adsorption inherent in the use of a repetitive sweep. The technique here employed may be employed at speeds even in excess of 800 v./sec., although the ease with which point C (Fig. 7B) may be resolved becomes more difficult, especially when the surface is partially covered with CO. A sweep speed of 60 v./sec. was found convenient for use in the remainder of this work.

In Fig. 8, typical hydrogen adsorption traces are assembled for several different values of CO adsorption time, τ . The charge due to adsorption of hydrogen on the surface partially covered with CO, Q_H , is estimated in the same manner as was Q_H^S . The conditions of Fig. 8 are the same as those employed in measuring Q_{CO}^S for Fig. 5 (30°, 1% CO, stirring rate, 200 r.p.m.) and the results are plotted on the same axes in Fig. 5. The experiment was repeated at 83°, and the results are plotted in Fig. 6. Q_H^S is taken as Q_H at $\tau = 0$. Q_H^S has a somewhat smaller value at 83° than at 30°. Both values are reproducible to less than 1% (see IV below).

In the analysis of the data which follows, the assumption will be made that Q_H is the charge due to adsorption of hydrogen on sites not previously covered with CO. This in turn depends on the assumptions that: (1) no CO-Pt bonds are broken in the course of hydrogen-deposition; (2) no reduction of CO occurs in the course of hydrogen-deposition. A test of these assumptions is made by comparing the traces obtained during the anodic pulse with and without an immediately preceding cathodic pulse. Such comparisons were made over the entire range of adsorption times covered by Fig. 5 and 6. Typical traces are assembled in Fig. 9. It is seen that the anodic CO maximum is completely unaffected. The additional currents are due to oxidation of molecular hydrogen generated during the cathodic pulse. This is taken as evidence that assumptions (1) and (2) above are valid. Prolonged evolution of hydrogen at potentials more cathodic than 0 volt was found to cause some desorption of CO and to introduce an anomalous maximum. Such prolonged cathodic treatment is, however, not otherwise encountered in this work.

III. Evaluation of CO-Pt Bonding from Cathodic and Anodic Pulse Data.—For the purpose of this

(8) F. G. Will and C. A. Knorr, *Z. Elektrochem.*, **64**, 258 (1960).

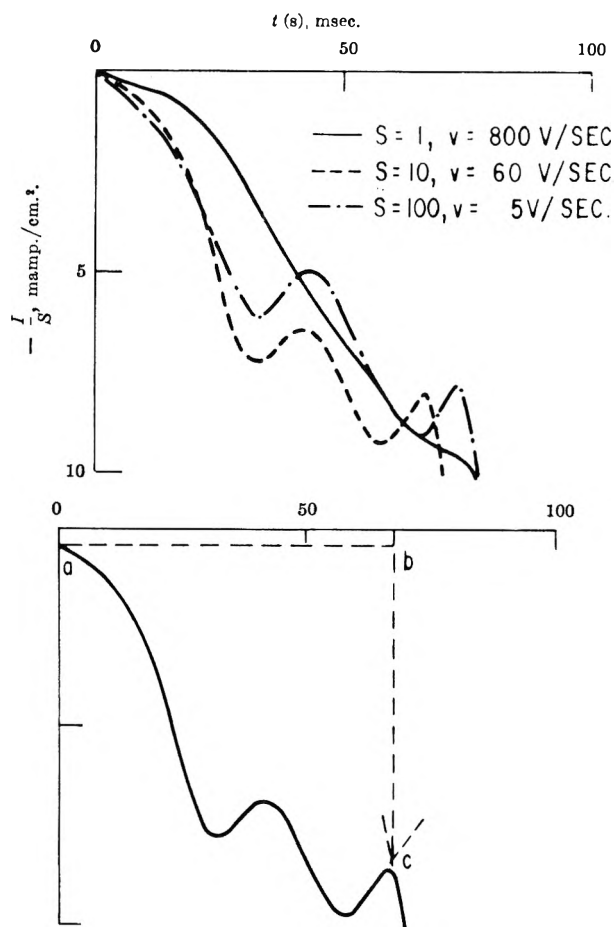


Fig. 7.—Cathodic pulse traces in argon-saturated solution, $\tau = 100$ msec. ("S" is a scale factor).

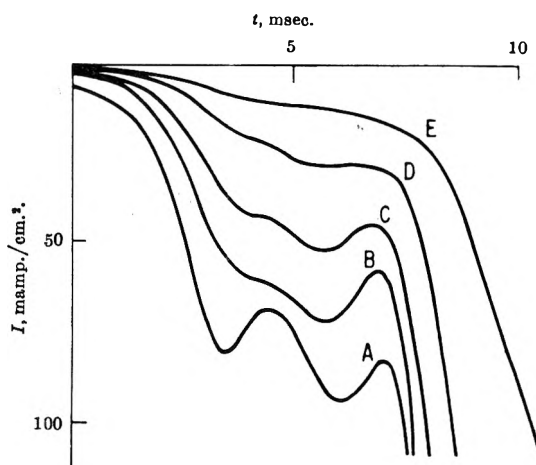


Fig. 8.—Typical cathodic traces during adsorption of CO from stirred solution saturated with 1% CO, 99% argon (30°).

Trace	Adsorption time, τ (sec.)
A	0.1, no CO
B	2.0
C	4.0
D	8.0
E	20.0

treatment, we will make the assumption that bonding is a combination of the bridged (two-site) or linear (one-site) structures.³ Then

$$S_T = S_H + S_B + S_L \quad (7)$$

where S_H , S_B , and S_L are the concentration of sites (mmoles/cm.²) available for simultaneous hydrogen,

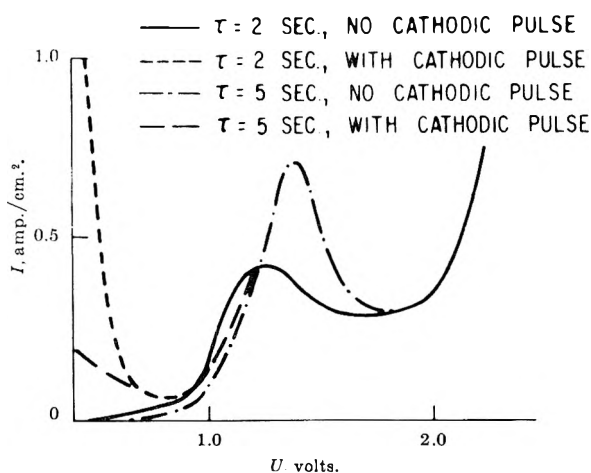


Fig. 9.—Typical anodic traces (with and without cathodic pre-pulse) during adsorption of CO from stirred solution at 30°.

bridged CO, and linear CO adsorption, respectively, and S_T is the total concentration of sites available for adsorption. Then

$$Q_H^S = n_H S_H^S F = n_H S_T F \quad (8)$$

$$Q_H = n_H S_H F \quad (9)$$

$$Q_{CO}^B = n_B S_B F \quad (10)$$

$$Q_{CO}^L = n_L S_L F \quad (11)$$

$$Q'_{CO} = Q_{CO}^B + Q_{CO}^L \quad (12)$$

where

n_H and n_B = one electron/site

n_L = two electrons/site

Q_{CO}^B = charge density due to oxidation of bridged CO during the anodic sweep

Q_{CO}^L = charge density due to oxidation of linear CO during the anodic sweep

S_H^S = concn. of sites available for saturation hydrogen-coverage in the absence of CO

Equation 8 involves the assumption that all adsorption sites available for CO adsorption are also available for hydrogen adsorption. This is already implied by the suggestion that coverage with hydrogen is approximately a monolayer at room temperature.⁹ It will be shown below that eq. 8 appears to be rigorously correct at 30°, but inexact at 83°.

Substituting eq. 8 to 11 into eq. 7 and rearranging, we obtain

$$Q_{CO}^B = Q_H^S - Q_H - Q'_{CO}/2 \quad (13)$$

substituting eq. 12 into 13, we obtain

$$Q_{CO}^B = 2Q_H^S - 2Q_H - Q'_{CO} \quad (14)$$

Q_{CO}^B is determined on Fig. 5 (30°) by performing the required subtractions graphically. The bridged structure alone appears to contribute to Q'_{CO} until a maximum value of $Q_{CO}^B = 0.16$ mcoul./cm.² is achieved, when the linear structure begins to contribute its share to the total charge. The adsorption is diffusion-controlled (following the plot for Q'_{CO}) through maximum

(9) M. Becker and M. Breiter, *Z. Elektrochem.*, **60**, 1080 (1956).

coverage with the bridged structure and through partial coverage with the linear structure, when the rate is obviously no longer determined by mass transport. The fact that Q_H extrapolates back to Q_H^S is evidence that $S_T = S_H^S$, since the adsorption of the first small amount of CO causes the maximum possible decrease in S_H . This would not occur if some of the sites available to CO adsorption were not available to hydrogen adsorption.

At 83°, we are first struck by the observation that Q_H^S has the value 0.327 rather than 0.365 mcoul./cm.². Since S_T could not depend on temperature, we must conclude that all adsorption sites do not cover with hydrogen at the higher temperature. This may in turn be due to an increase in the rate of hydrogen desorption, or to the evolution of molecular hydrogen on a surface only partially covered with hydrogen at the higher temperature. The possibility that it is due to adsorption of accumulated decomposition products of perchloric acid was investigated by retaining the original solution, lowering the temperature to 30°, and again measuring Q_H^S . Q_H^S was found to have its usual 30° value and the possibility of contamination was disproved.

When the value of Q_H^S at 30° is used, as Q_H at $\tau = 0$, the results (Fig. 6) at 83° are qualitatively quite similar to those at 30°. The striking *quantitative* difference is that the charge due to the bridged structure contributes a maximum of only 0.10 mcoul./cm.² as compared with 0.16 mcoul./cm.² at the lower temperature. Judging from the scatter of Q_{CO}^B points at either temperature, this difference is probably significant to 0.01 mcoul./cm.². The resulting larger contribution of the linear structure at the higher temperature results in a larger saturation value of Q'_{CO} at 83°. For 100% CO at saturation coverage (30°) Q'_{CO} was found to have the value 0.511 mcoul./cm.² and Q_H the value 0.081 mcoul./cm.². Solving eq. 14 using these values, $Q_{CO}^B = 0.08$ mcoul./cm.², which is only 50% of the value found at lower coverages using 1% CO as adsorbate. This difference could be accounted for by a difference in Q_H of only 0.04 mcoul./cm.², part of which could be due to adsorption of impurities at the relatively long adsorption time, and to the difficulty with which Q_H is estimated at high coverage with CO (point C of Fig. 7B is not easily resolved). It is therefore not unlikely that the maximum value of $Q_{CO}^B = 0.16$ mcoul./cm.² is actually maintained through saturation coverage. It is also possible that the final CO molecules adsorbed (with difficulty, judging from the decreased rate) tend to convert some bridged CO to linear CO, by partial displacement.

The fractional surface coverage with the bridged and linear species may be defined as

$$\theta_{CO}^B = S_B/S_T \quad (15)$$

$$\theta_{CO}^L = S_L/S_T \quad (16)$$

Then employing (9)–(11)

$$\theta_{CO}^B = Q_{CO}^B/Q_H^S \quad (17)$$

$$\theta_{CO}^L = Q'_{CO}/2Q_H^S, \quad Q_H^S \text{ always taken at } 30^\circ \quad (18)$$

Hence, at 30° $\theta_{CO}^L = 0$ until θ_{CO}^B reaches the maximum value of 0.44, when θ_{CO}^L rises to its saturation value of 0.46. At 83°, θ_{CO}^B reaches its maximum value of 0.30

before θ_{CO}^L increases from 0 to its saturation value. If we define the coverage with the bridge structure in terms of the saturation surface coverage with CO, rather than in terms of the concentration of total adsorption sites, then

$$\theta_{CO}^{B'} = S_B / (2S_L + S_B) \text{ saturation} = Q_{CO}^B / Q_{CO}^L \text{ saturation} \quad (19)$$

and $\theta_{CO}^{B'}$ has the value 0.31 at saturation at one atmosphere and 30°. This is approximately the average of the results obtained on cabosil and alumina-supported platinum by Eischens and Pliskin.³

IV. Examination of the Reproducibility of the Electrode Surface.—The results presented thus far depend strongly on the ability to exactly reproduce and measure S_T . S_T directly determines Q_H^S and the "solvent correction" for the anodic sweep experiments. Both of these latter quantities therefore serve as a sensitive indication of surface reproducibility. The subject of surface reproducibility is introduced at this point, since the reasoning previously applied to CO adsorption may be now applied to impurity adsorption. The latter seems to be the key consideration in this matter.

On applying a 60 v./sec. linear cathodic sweep to the electrode in the quiet, argon-saturated solution, the trace obtained at $\tau = 10$ msec. is that which appears in Fig. 7a (30°). The trace is identical after 100 msec. of reduction, but thereafter Q_H decreases gradually with time. Such reduction in hydrogen adsorption was observed by Will and Knorr⁸ and Breiter and Kennel¹⁰ in sulfuric acid solutions, and ascribed to "surface recrystallization." This implies that the surface has no true constant and reproducible area, but increases with pretreatment and decreases with time. It was observed in this work, however, that decrease in Q_H is accelerated by stirring. This serves as a first indication that the effect is, in fact, due to adsorption of im-

purities on the freshly reduced and active surface. The values of Q_H obtained with and without mechanical stirring are recorded in Table II. If the maximum value of Q_H ($\tau = 10$ to 100 msec.) is taken as Q_H^S , then

$$\theta^c = (Q_H^S - Q_H) / Q_H^S \quad (20)$$

and θ^c has the significance of the fractional sites covered with impurities, if (as for CO) no interaction between deposited hydrogen and adsorbed impurities occurs. The impressive reproducibility of Q_H for any particular value of τ is immediately obvious. For $\tau = 10$ sec., the second entry in the table was taken several days, and the third entry several weeks after the first, during which time the electrode had been exposed to several hundred activation and pulse cycles. The average deviation of 0.3% for these values clearly established the reproducibility of S_T under carefully controlled circumstances. To determine whether our procedure leads to maximum "activation," the potential of step A (see Experimental section) of the pretreatment was increased to 2.0 v. and maintained for 10 min. (maximum pretreatment of Will and Knorr.⁸ Only a small (1%) decrease in Q_H was observed, possibly due to extensive multiple-layering of oxygen during pretreatment.

When an anodic sweep ($v = 360$ v./sec.) was applied to the electrode in quiet, argon-saturated solution, the trace obtained for $\tau = 10$ msec. was identical with that appearing in Fig. 3B as the "solvent curve," the currents which flow are due to a combination of double-layer charging and surface oxidation.² Any difference in integrated charge ΔQ between this trace and that corresponding for large values of τ may be taken as due to oxidation of an adsorbed impurity, by analogy with the work on CO. Further, let us define a quantity θ^{a_c}

$$\theta^{a_c} = \Delta Q / 2Q_H^S \quad (21)$$

θ^{a_c} would be equal to θ^c if the adsorbed material were all oxidizable, with two electrons required per adsorption site. ΔQ and θ^{a_c} are presented in Table II for various values of τ . ΔQ is negative at $\tau = 1$ msec., since the surface is not yet completely reduced. ΔQ and θ^{a_c} are zero from $\tau = 10$ msec. to 10 sec. in the unstirred solution. Thereafter, ΔQ becomes positive, but the values of θ^{a_c} bear no simple constant relationship to θ^c . This might be explained by a combination of events.

(1) Some adsorbed impurities do not oxidize during the anodic sweep until the region of molecular oxygen evolution is entered.

(2) A variety of impurities are adsorbed; the number of electrons per site required depends on the structure of the particular impurity adsorbed. The average number of electrons per site might be expected to vary with composition and, hence, time.

In support of argument (1) above, it may be remarked that for large τ , one pulse does not clear the electrode surface, as evidenced by the distorted appearance of the subsequent trace. Further, the traces for high ΔQ (and τ) often do not coincide with the trace for $\tau = 10$ msec. in the region of molecular oxygen evolution, suggesting that the surface still is partially covered.

TABLE II
ELECTRODE SURFACE REPRODUCIBILITY

τ , sec.	ΔQ , mcoul./cm. ²	θ^c ^a	Q_H , mcoul./cm. ²	θ^{a_c}
		Initially		
0.001	-0.138	-0.17	0.310	0.14
.010	.000	.00	.365	.00
.100	.000	.00	.365	.00
1.00	.000	.00	.356	.02
10.0	.000	.00	.360	0.360
			.358	av. .01
			.362	
10.0 ^a	0.0121	0.02	.334	.09
100	.0300	.04	.337	.08
100 ^a	.0583	.08	.236	.27
1000	.0714	.10	.186	.49
1000 ^a	.242	.75	.114	.70
After 12 hr. of anodic pulsing on 10 cm. ² electrode				
10	0.000	0.00	0.360	0.01
10 ^a	.000	.00	.357	.04
100	.000	.00	.357	.04
100 ^a	.0156	.02	.288	.21
1000	.0258	.04	.328	.09
1000 ^a	.244	.33	.178	.51

^a With stirring at 200 r.p.m.

The fact that some impurities, at least, are oxidizable suggests that they might be removed by adsorbing on a clean electrode surface, and then applying an anodic pulse. Our experience with CO suggests that this adsorption might be transport-limited at low coverages, and kinetically retarded at higher coverages, so that frequent anodic pulses are advantageous. A 10 cm.² smooth Pt electrode was inserted in the cell and pulsed for 12 hr. with stirring. One pulse ($v = 6$ v./sec.) was applied every 12 sec. The table records the various parameters measured after the purification. Judging from θ_c^e , the surface is covered to the extent of only 4% after $\tau = 100$ sec., and 9% after $\tau = 1000$ sec. in the "quiet" solution (transport by convection). This may be compared at comparable times with the 50% reduction observed before purification, and in the work of

Will and Knorr⁸ and Breiter and Kennel.¹⁰ No attempt was made to trace the origin of impurities in this work.

All measurements of CO reported above were made on the pulse-purified solution. The method of purification by the use of anodic pulses may have advantages over more conventional electrochemical methods of purification by evolution of hydrogen and oxygen at auxiliary electrodes,¹¹ since the adsorption of impurities is retarded by these latter conditions and the catalytic efficacy of the electrode reduced.

Acknowledgment.—The author wishes to thank Mr. J. Adamchick for his valuable assistance with the electronic instrumentation.

(11) J. O'M. Bockris and E. C. Potter, *J. Electrochem. Soc.*, **99**, 169 (1952).

BAND SHAPES IN NON-LINEAR CHROMATOGRAPHY WITH AXIAL DISPERSION

BY GERALD HOUGHTON

Department of Chemical Engineering, Division of Engineering Research, University of Pittsburgh, Pittsburgh, Pennsylvania

Received May 28, 1962

By the use of a polynomial type of adsorption isotherm, a nonlinear partial differential equation has been developed that applies to the nonlinear equilibrium chromatography of a single solute in the presence of axial dispersion. Analytic solutions to this equation have been obtained for the case where the nonlinearity is small, or the initial solute concentration is small, or both. Discontinuous solutions for no axial diffusion also have been generated. The effects of a nonlinear isotherm and axial dispersion on band broadening, peak height, and band shape are discussed by evaluating the analytical solutions under typical conditions found in chromatography.

The equation of continuity for the exchange of solute between a mobile phase and a fixed bed of solid adsorbent particles is usually taken as¹⁻⁷

$$\frac{\partial C}{\partial t} + u \frac{\partial C}{\partial z} = E \frac{\partial^2 C}{\partial z^2} - \frac{1}{\epsilon} \frac{\partial n}{\partial t} \quad (1)$$

where C is the moles of solute per unit volume of mobile phase, n the moles of adsorbed solute per unit volume of packed adsorbent, u is the constant mobile phase velocity through the interstices, ϵ the void fraction, and E the coefficient of axial dispersion. Equation 1 assumes uniform column temperature and pressure and neglects radial variations in solute concentration and velocity within the interstices.

The term $(1/\epsilon)(\partial n/\partial t)$ in equation 1 represents the exchange of solute between the phases and is evaluated either by using a finite rate of interfacial transport^{1-3,5-8} or by introducing the concept of instantaneous equilibrium,^{2,4,7-14} when the values of n at each axial position, z , would be given by the adsorption isotherm $n = f(C)$. In the absence of axial diffusion, a linear isotherm causes a pulse of solute to pass through the column unchanged but delayed,⁹ whereas if the isotherm

is concave toward the C -axis the trailing edge develops a finite slope and the leading edge remains vertical, the reverse being true for isotherms concave to the n -axis.⁸⁻¹³ Lapidus and Amundson² have demonstrated that, in the presence of a linear isotherm, axial dispersion causes the sharp boundaries to be smoothed out and the bands to become broader. Analytical solutions for instantaneous equilibrium with axial dispersion and a nonlinear isotherm have been attempted by Glueckauf, *et al.*,¹ who obtained approximate results limited to the case of partial enrichment with a single boundary, no solution being obtained for the diffuse rear boundary. Lightfoot,⁴ using instantaneous equilibrium, and Acrivos,⁵ using a finite rate, have obtained asymptotic approximations for a single boundary with axial dispersion that are only applicable to distances far removed from the column entrance and to nonlinear isotherms concave toward the C -axis. Numerical solutions for a solute pulse using a high-speed digital computer have been obtained by Funk and Houghton^{6,7} for gas-liquid partition chromatography in the most general case involving finite transfer rates, axial dispersion, column pressure drop, and using a nonlinear isotherm of the polynomial form

$$n = f(C) = K_0 + K_1 C + K_2 C^2 \quad (2)$$

This form of isotherm has the advantage that it is concave to the n -axis for positive K_2 as above, concave to the C -axis for negative K_2 , and linear for $K_2 = 0$. Furthermore, the constant K_0 has been introduced so that eq. 2 might be used to approximate a highly curved isotherm without the use of higher order terms such as $K_3 C^3$, $K_4 C^4$, ---; in such cases the constants K_0 , K_1 , and K_2 would be adjusted to represent the equilibrium curve by a curved line segment in the region of

(1) E. Glueckauf, K. H. Barker, and G. P. Kitt, *Discussions Faraday Soc.*, **7**, 199 (1949).

(2) L. Lapidus and N. R. Amundson, *J. Phys. Chem.*, **56**, 984 (1952).

(3) W. C. Bastian and L. Lapidus, *ibid.*, **60**, 816 (1956).

(4) E. N. Lightfoot, *ibid.*, **61**, 1686 (1957).

(5) A. Acrivos, *Chem. Eng. Sci.*, **13**, 1 (1960).

(6) J. E. Funk and G. Houghton, *Nature*, **189**, 389 (1960).

(7) J. E. Funk and G. Houghton, *J. Chromatog.*, **6**, 193, 281 (1961).

(8) H. C. Thomas, *Ann. N. Y. Acad. Sci.*, **49**, 183 (1948).

(9) J. N. Wilson, *J. Am. Chem. Soc.*, **62**, 1583 (1940).

(10) D. DeVault, *ibid.*, **65**, 532 (1943).

(11) J. Weiss, *J. Chem. Soc.*, 297 (1943).

(12) J. E. Walter, *J. Chem. Phys.*, **13**, 229 (1945).

(13) E. Glueckauf, *J. Chem. Soc.*, 1302 (1947).

(14) I. Fatt and M. A. Selim, *J. Phys. Chem.*, **63**, 1641 (1959).

concentration where most of the mass transfer occurs. However, in most cases where the non-ideality is not too great, the true physical situation then would be represented by setting $K_0 = 0$ and adjusting K_1 and K_2 accordingly. Since it is well known that both axial dispersion and a nonlinear isotherm have a profound effect upon the shape, size, and position of elution bands in chromatography and ion exchange, it is the purpose of the present communication to show that, when nonlinear isotherm (2) is combined with continuity eq. 1, the resulting partial differential equation is amenable to solution when the solute is in small concentration, or the nonlinearity is small, or both. The analytical solutions also will be used to show how the elution time, peak height, band width, and band shape are influenced by the physical parameters in the system.

The present discussion will be confined to the case of elution development chromatography in which an isolated section of adsorbent of length L_0 is first saturated with a single solute such that the equilibrium concentration in the mobile phase is uniformly C_0 . Development of the chromatogram then is started by releasing the solute pulse into a stream of pure solvent. Thus, for an infinite column with $C(t, \infty) = 0$ the above conditions correspond to the following initial value problem

$$\left. \begin{aligned} C(0, z) &= C_0 \\ n(0, z) &= K_0 + K_1 C_0 + K_2 C_0^2 \end{aligned} \right\} -L_0/2 < z < L_0/2 \quad (3)$$

$$\left. \begin{aligned} C(0, z) &= 0 \\ n(0, z) &= 0 \end{aligned} \right\} |z| > L_0/2$$

Equilibrium will be assumed initially and at each subsequent point in the column. In this connection initial conditions (3) also might approximate the rapid sample injection technique used in gas chromatography if equilibrium is reached instantaneously.

Partial Differential Equation of Nonlinear Equilibrium Chromatography.—If nonlinear isotherm (2) is substituted for n in continuity eq. 1 the result, after some rearrangement and redefinition of variables, is

$$\frac{\partial C}{\partial t} - \frac{\lambda UC}{1 + \lambda C} \frac{\partial C}{\partial \xi} = \frac{E_0}{1 + \lambda C} \frac{\partial^2 C}{\partial \xi^2} \quad (4)$$

where

$$U = u/(1 + K_1/\epsilon); \quad \lambda = 2K_2/\epsilon(1 + K_1/\epsilon)$$

$$E_0 = E/(1 + K_1/\epsilon); \quad \xi = z - Ut$$

In nonlinear eq. 4 U is the velocity the solute band would possess if the adsorption isotherm were linear or $\lambda = 0$. The parameter λ is proportional to K_2 of eq. 2 and therefore is a measure of the nonlinearity of the isotherm, being positive for an isotherm concave to the n -axis and negative for an isotherm concave to the C -axis. It is clear that if the isotherm is linear, or $\lambda = 0$, eq. 4 will reduce to the parabolic diffusion equation

$$\frac{\partial C}{\partial t} = E_0 \frac{\partial^2 C}{\partial \xi^2} \quad (5)$$

The new variable, ξ , represents the axial coordinate, z , referred to an origin moving with a velocity U . The effects of axial dispersion are represented by E_0 , which is lower than E by the factor $(1 + K_1/\epsilon)$. However,

this reduced axial diffusion coefficient will be compensated by a greater retention time which will permit a longer time for dispersion to occur. In this connection the retention time, t_R , for linear chromatography is given by L/U , where L is the length of the chromatographic column so that

$$t_R = \frac{L}{u} \left(1 + \frac{K_1}{\epsilon} \right) \quad (6)$$

The so-called apparent retention time will be t_R minus L/u .

The nonlinear term $\lambda UC/(1 + \lambda C)$ in eq. 4 is equivalent to a convective velocity that is a function of the solute concentration so that all parts of the elution band will not be traveling at the same rate, whereas the term $E_0/(1 + \lambda C)$ corresponds to a diffusion coefficient that is a function of concentration. Both these effects will result in different solute concentrations being dispersed at different rates, thus causing the elution band to become asymmetric in a direction that depends upon the sign of λ . Although eq. 4 is a complicated nonlinear partial differential equation, it can be made amenable to solution by limiting considerations to either dilute solutions or to small nonlinearities or both such that $|\lambda C| \ll 1$, when

$$\frac{\partial C}{\partial t} - \lambda UC \frac{\partial C}{\partial \xi} = E_0 \frac{\partial^2 C}{\partial \xi^2} \quad (7)$$

The limitation of small $|\lambda C|$ is not critical since even small values can lead to quite a large amount of asymmetry if the elution time is long enough. However, if the residence time is too long, the asymmetry may become progressively reduced because the effects of prolonged axial dispersion will tend to reduce the concentration C and hence the distortion velocity λUC . The velocity λUC will cause the high concentrations at the peak of the pulse to travel faster than the lower concentrations at the base, thus producing an elution band that is skewed in a direction determined by the sign of λ and hence the shape of the adsorption isotherm.

Band Broadening in Linear Chromatography.—Although band broadening in linear chromatography has been considered by a number of workers,^{1-3,6,7} it is useful to obtain the particular solution for development chromatography and to produce a relationship between band breadth and the physical parameters in the system. The solution to eq. 5 for an infinite one-dimensional column with an initial condition $C(0, \xi)$ is¹⁵

$$C(t, \xi) = \int_{-\infty}^{\infty} \frac{C(0, \xi')}{2\sqrt{\pi E_0 t}} \exp \left[- \left(\frac{\xi - \xi'}{2\sqrt{E_0 t}} \right)^2 \right] d\xi' \quad (8)$$

The particular solution for initial conditions (3) then is readily found by integration to be

$$\frac{C}{C_0} = \frac{1}{2} \operatorname{erf} \left(\frac{\xi + 1/2 L_0}{2\sqrt{E_0 t}} \right) - \frac{1}{2} \operatorname{erf} \left(\frac{\xi - 1/2 L_0}{2\sqrt{E_0 t}} \right) \quad (9)$$

The peak concentration, C_p , of the elution band will occur at $\xi = 0$ and pass the measuring point in the column at the retention time $t_R = L/U$, so that

$$\frac{C_p}{C_0} = \operatorname{erf} \left(\frac{L_0}{L} \sqrt{\frac{U}{LE_0}} \right) \quad (10)$$

(15) H. S. Carslaw and J. C. Jaeger, "Conduction of Heat in Solids," Oxford University Press, New York, N. Y., 1959.

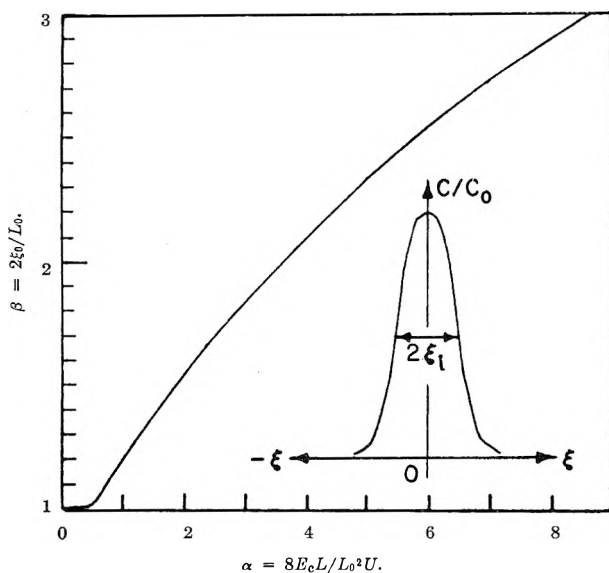


Fig. 1.—Effect of parameters on band broadening in linear chromatography.

Equation 9 gives a symmetrical dispersion around the peak which travels at the solute velocity, U , so that a measure of the band broadening can be obtained by determining the distance of the point of inflection in the elution curve from the center of the band. This may be accomplished by determining the value of ξ , designated ξ_1 (cf. inset of Fig. 1), for which $\partial^2 C/\partial \xi^2 = 0$ in eq. 9 and then setting $t = L/U$. The following transcendental equation results

$$1 - \beta \tanh(\beta/\alpha) = 0 \quad (11)$$

where

$$\alpha = 8E_cL/L_0^2U = 8EL/L_0^2u$$

$$\text{and } \beta = 2\xi_1/L_0$$

The dimensionless parameter β represents the ratio of the band width at time t to the initial sample size, while α is another dimensionless parameter whose value determines the band broadening as shown in Fig. 1, which represents a plot of eq. 11. At low values of α , particularly for $\alpha < 0.5$, it is apparent that band broadening is relatively insensitive to the operating variables. In order to determine the factors that influence α and hence β , it is necessary to have a relationship for E in packed beds. At the present time the only relationship available is that obtained theoretically by Beran,¹⁶ McHenry and Wilhelm,¹⁷ and Aris and Amundson,¹⁸ namely, $E = adu$, where d is the particle diameter and a is a dimensionless constant that appears to have a value in the range 0.5–15, depending upon the nature of the flow. If this form for E is used in the present case, we find $\alpha = 8adL/L_0^2$, so that band broadening is reduced by increasing the initial pulse length, decreasing the column length, and reducing the particle diameter. Decreasing the grain size as a method of increasing resolution in chromatography has been mentioned by Glueckauf, *et al.*¹ It is interesting that the model used for E predicts that band broadening should be independent of eluent velocity, an observation that could be tested readily by experiment.

(16) M. J. Beran, *J. Chem. Phys.*, **27**, 270 (1957).

(17) K. W. McHenry and R. H. Wilhelm, *A.I.Ch.E. J.*, **3**, 83 (1957).

(18) R. Aris and N. R. Amundson, *ibid.*, **3**, 280 (1957).

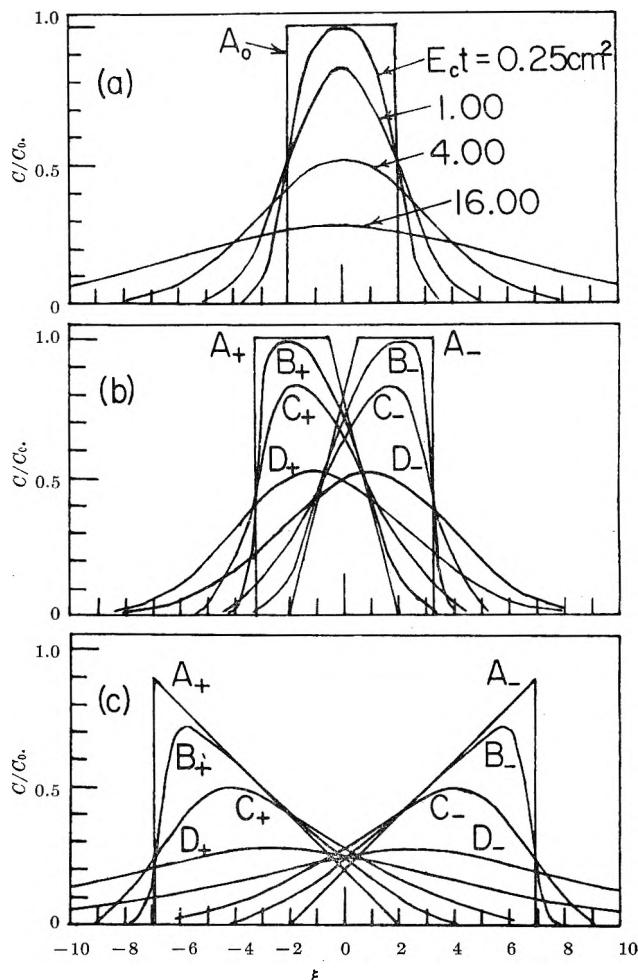


Fig. 2.—Effects of axial dispersion in linear and nonlinear chromatography for $L_0 = 4$ cm. and $U = 0.5$ cm./sec.; (a) linear chromatography, $\lambda = 0$ with the product $E_c t$ as a parameter; (b) partly developed elution band at $t = 100$ sec.; (c) fully developed elution band at $t = 400$ sec.

Letter on graph	E_c , cm. ² /sec.	Subscripts for letters	Extent of nonlinearity
A	0.0000	0	$\lambda = 0.00$
B	.0025	+	$\lambda C_0 = +0.05$
C	.0100	-	$\lambda C_0 = -0.05$
D	.0400		

Figure 2(a) shows plots of C/C_0 vs. ξ according to eq. 9 using the product $E_c t$ as a parameter. It is apparent that dispersion occurs symmetrically around the peak as discussed by Funk and Houghton,^{6,7} so that the peak concentration ratio, C_v/C_0 , and the band broadening ratio, β , will adequately represent the effects of axial dispersion in linear chromatography. However, when the adsorption isotherm is nonlinear, changes in band shape may occur simultaneously with changes in height and width, so that nonlinear chromatography requires a much more complicated mathematical formulation. In this connection Glueckauf, *et al.*,¹ have pointed out that because of the mathematical difficulties involved, the case of nonlinear chromatography with axial dispersion represents an important gap in our knowledge of chromatography, particularly in view of the fact that both of these phenomena usually are present in practice.

Band Shapes in Nonlinear Chromatography.—The effect of a nonlinear isotherm on band shape can be obtained by noting that nonlinear equations of type 7 can be reduced to the parabolic diffusion equation by the following change of variable due to Hopf¹⁹

(19) E. Hopf, *Comm. Pure Appl. Math.*, **3**, 201 (1950).

$$C = \frac{2E_c}{\lambda U} \frac{1}{\phi} \frac{\partial \phi}{\partial \xi} \quad (12)$$

Thus, substituting expression 12 for C in eq. 7, we obtain $\partial \phi / \partial t = E_c \partial^2 \phi / \partial \xi^2$, a result similar to eq. 5, so that the solutions to eq. 7 will be given by eq. 8 with C replaced by ϕ . Furthermore, if $C(0, \xi)$ represents a general initial condition for the introduction of solute into the column, then $\phi(0, \xi)$ may be obtained by direct integration of relation 12

$$\phi(0, \xi) = \phi(0, -\infty) \exp \left[\frac{\lambda U}{2E_c} \int_{-\infty}^{\xi} C(0, \eta) d\eta \right] \quad (13)$$

Accordingly, eq. 12 and 13 may be combined with eq. 8, in which C is replaced by ϕ , to yield the solution

$$C = \frac{-\int_{-\infty}^{\infty} \left(\frac{\xi - \xi'}{\lambda Ut} \right) \exp \left[-\left(\frac{\xi - \xi'}{2\sqrt{E_c t}} \right)^2 + \frac{\lambda U}{2E_c} \int_{-\infty}^{\xi'} C(0, \eta) d\eta \right] d\xi'}{\int_{-\infty}^{\infty} \exp \left[-\left(\frac{\xi - \xi'}{2\sqrt{E_c t}} \right)^2 + \frac{\lambda U}{2E_c} \int_{-\infty}^{\xi'} C(0, \eta) d\eta \right] d\xi'} \quad (14)$$

When initial conditions (3) are introduced into eq. 14, the following analytic solution results for a pulse input

$$\frac{C}{C_0} = \frac{\exp(g) [\operatorname{erf}(p + h) - \operatorname{erf}(q + h)]}{1 - \operatorname{erf}(p) + \exp(g) [\operatorname{erf}(p + h) - \operatorname{erf}(q + h)] + \exp(m) [1 + \operatorname{erf}(q)]} \quad (15)$$

where

$$\begin{aligned} p &= (\xi + 1/2 L_0) / 2\sqrt{E_c t} \\ q &= (\xi - 1/2 L_0) / 2\sqrt{E_c t} \\ g &= \lambda C_0 U (2t\xi + \lambda C_0 U t^2 + L_0 t) / 4E_c t \\ h &= \lambda C_0 U t / 2\sqrt{E_c t} \\ m &= \lambda C_0 U L_0 / 2E_c \end{aligned}$$

It is important to note that eq. 15 correctly reduces to eq. 9 if λ is set equal to zero, corresponding to a linear isotherm.

Although eq. 15 is a complete solution representing the combined effects of axial dispersion with a nonlinear isotherm, it also is necessary to have a solution to eq. 7 with $E_c = 0$ in order to separate the effects of diffusion from those of the nonlinear isotherm. Solutions to eq. 1 with $E = 0$ and $\partial C / \partial t = 0$ for various types of nonlinear isotherm have been discussed by DeVault,¹⁰ Weiss,¹¹ Glueckauf,^{1,13} and Thomas.⁸ However, the particular case of polynomial isotherms of type 3 has not been treated previously. Furthermore, it appears that in addition to neglecting axial dispersion, earlier workers often did not include transient effects represented by the term $\partial C / \partial t$ in eq. 1, the equation of continuity being simply $\epsilon u \partial C / \partial z = \partial n / \partial t$. Thus, in order to establish connections between results 9 and 15 and the equivalent solutions for the cases where $E_c = 0$ in eq. 7, these latter solutions will now be developed for the polynomial adsorption isotherm (3). The general solution to eq. 7 with no axial dispersion ($E_c = 0$) is

$$C = \psi(\xi + \lambda C U t) \quad (16)$$

The function ψ must satisfy the initial conditions (3) and also reduce to the correct form for linear chromatography as $\lambda \rightarrow 0$. For linear chromatography ($\lambda = 0$) the function ψ that satisfies initial conditions (3) is clearly the difference between two unit step functions

$$\frac{C}{C_0} = S_0(\xi + 1/2 L_0) - S_0(\xi - 1/2 L_0) \quad (17)$$

S_0 is the Heaviside unit step function defined by

$$S_0(\xi) = \begin{cases} 0; & \xi < 0 \\ 1/2; & \xi = 0 \\ 1; & \xi > 0 \end{cases} \quad (18)$$

It is interesting to note that the error functions of eq. 9 become the step functions of eq. 17 as $E_c \rightarrow 0$. Solution 17 demonstrates the well known result^{9,11} that, in the absence of axial diffusion, linear chromatography yields a pulse that passes through the column unchanged in either size or shape as shown by the discontinuous curve A_0 in Fig. 2(a). When $\lambda \neq 0$ the solutions that satisfy

eq. 16 as well as initial conditions (3) and also give a solution of the form (17) as $\lambda \rightarrow 0$ might be formed by combining the step functions $S_0(\xi + 1/2 L_0 + \lambda C U t)$ and $S_0(\xi - 1/2 L_0 + \lambda C U t)$; again the similarity between the arguments of these step functions and those of the error functions in eq. 15 should be noted. However, the arguments of S_0 in this case are continuous in C inside the interval $0 \leq C \leq C_0$ so that for a fixed value of t the possible relationships between C and ξ are given by $\xi + 1/2 L_0 + \lambda C U t = 0$ and $\xi - 1/2 L_0 + \lambda C U t = 0$. Accordingly, if $\lambda > 0$ then C must increase linearly as ξ decreases, whereas for $\lambda < 0$ there will be a linear increase in C with an increase in ξ . Thus, if ξ_0 is the value of ξ when $C = 0$, then $\xi_0 = 1/2 L_0$ for $\lambda > 0$ and $\xi_0 = -1/2 L_0$ for $\lambda < 0$. Taking the case of positive λ first, the value of ξ , designated ξ_1 , at which $C = C_0$ on the continuous curve, will be given by the linear form $\xi_1 = 1/2 L_0 - \lambda C_0 U t$. A discontinuity in C will be present at the remaining boundary, $\xi = \xi_2$, where $C = 1/2 C_0$, so that $\xi_2 = -1/2 L_0 - 1/2 \lambda C_0 U t$. Since ξ_2 may be smaller than ξ_1 , a region can exist in which the concentration is uniformly C_0 , a band of this type being termed partly developed. The discontinuous curves A_+ and A_- of Fig. 2(b) illustrate the asymmetrical trapezoidal shapes of partly eluted bands. Thus, for positive λ the discontinuous solution for a partly eluted band is summarized by

$$\lambda C U t = \begin{cases} 0; & 1/2 L_0 < \xi \\ 1/2 L_0 - \xi; & 1/2 L_0 - \lambda C_0 U t < \xi < 1/2 L_0 \\ C_0 U t; & -1/2 L_0 - 1/2 \lambda C_0 U t < \xi < 1/2 L_0 - \\ & \lambda C_0 U t \\ 0; & \xi < -1/2 L_0 - 1/2 \lambda C_0 U t \end{cases} \quad (19)$$

The analogous solution for a partly eluted band with negative λ similarly can be shown to be

$$|\lambda| C U t = \begin{cases} 0; & -1/2 L_0 > \xi \\ 1/2 L_0 + \xi; & |\lambda| C_0 U t - 1/2 L_0 > \xi > -1/2 L_0 \\ |\lambda| C_0 U t; & 1/2 |\lambda| C_0 U t + 1/2 L_0 > \xi > |\lambda| C_0 U t - \\ & 1/2 L_0 \\ 0; & \xi > 1/2 |\lambda| C_0 U t + 1/2 L_0 \end{cases} \quad (20)$$

It is evident from solutions 19 and 20, plotted as curves A₊ and A₋ in Fig. 2(b), that a partly eluted band will drift in the direction of negative ξ if λ is positive and *vice versa* for negative λ . However, the point ξ_1 always moves faster than ξ_2 so that, if elution is continued, ξ_1 will eventually become equal to ξ_2 , when

$$L_0 = \begin{cases} 1/2\lambda C_0 Ut; & \lambda > 0 \\ -1/2|\lambda|C_0 Ut; & \lambda < 0 \end{cases} \quad (21)$$

Thereafter the band assumes a triangular shape with one boundary always vertical and is termed fully developed. Since the sloping boundary still obeys the equation $\lambda C_0 Ut = 1/2L_0 - \xi$ for $\lambda > 0$ and $|\lambda|C_0 Ut = 1/2L_0 + \xi$ for $\lambda < 0$, another equation is necessary to define the triangular band completely, this additional equation being the material balance for the solute in the pulse. If the original solute in the pulse is L_0C_0 and the point (ξ_3, C_3) defines the apex of the triangular elution band, then a material balance gives

$$|\lambda|C_3 Ut = 2L_0C_0/C_3 = \begin{cases} 1/2L_0 - \xi_3; & \lambda > 0 \\ 1/2L_0 + \xi_3; & \lambda < 0 \end{cases} \quad (22)$$

Triangular elution bands A₊ and A₋ in Fig. 2(c), corresponding to $\lambda > 0$ and $\lambda < 0$, respectively, are typical examples of fully developed chromatograms in the absence of axial diffusion.

In order to determine the effects of axial dispersion on both partly developed and fully developed chromatograms, eq. 15 has been plotted in Fig. 2(b) and 2(c) for values of E_c of 0.0025, 0.010, and 0.040 cm.²/sec. with $U = 0.5$ cm./sec. and $L_0 = 4$ cm. A partly developed band is obtained by calculating the concentration profile after 100 sec., while a fully developed band is obtained when $t = 400$ sec. A value of $|\lambda C_0| = 0.05$ has been chosen so that $|\lambda C| \leq 0.05$ and the criterion $|\lambda C| \ll 1$ is satisfied. It is evident from Fig. 2 that

even a relatively small value of $|\lambda C|$ can produce considerable distortion and displacement of the band if the retention time is long enough. It may be noted that if λ is negative and the adsorption isotherm is concave to the C -axis, the peak moves faster through the column than it would if the isotherm were linear, the leading edge having a much steeper slope than the trailing edge—the reverse being true for the positive value of λ . In the absence of axial diffusion, one of the boundaries is always vertical, as discussed by earlier workers.⁸⁻¹³ However, the effect of axial dispersion is to cause both edges to slope and to round off the sharp corners, yielding shapes of the type that is commonly observed in practice. That the bands observed experimentally rarely even approximate the discontinuous forms expected for no axial dispersion was discussed quite early by Wilson.⁹ It is evident from the present analysis that the effect of a nonlinear isotherm is to produce distortion of the elution band, while the effect of axial dispersion is to cause the band to become more symmetrical, the final shape being a balance between these two phenomena (*cf.* Fig. 2). In addition, eq. 15 for small $|\lambda C_0|$ yields elution bands for positive and negative λ that are mirror images of each other in the plane $\xi = 0$.

Finally, the analytic solutions to eq. 5 and 7 with and without axial dispersion have revealed a basic difference between linear and nonlinear chromatography, namely that in the linear case the initial concentration of solute has no effect on the final elution curve if C/C_0 is used as the variable (*cf.* eq. 9 and 17), whereas in the case of the nonlinear isotherm the shape and location of the final elution curve is profoundly affected by the initial solute concentration, C_0 , through the term $\lambda C_0 Ut$ (*cf.* eq. 15, 19, and 20). Thus, in analyzing different mixtures of the same solute having a nonlinear isotherm, some changes in the shape and position of the chromatogram can be expected.

RADIOLYTIC AND THERMAL DECOMPOSITION OF BORAZOLE

BY CLARENCE J. WOLF AND RICHARD H. TOENISKOETTER

Parma Research Laboratory, Union Carbide Corporation, Parma 30, Ohio

Received May 29, 1962

The hydrogen yield from the Co⁶⁰ γ -ray radiolysis of borazole is constant ($G(\text{H}_2) = 0.36$) from -196 to -120° and then increases to 2.90 at 30° . Diphenylpicrylhydrazyl scavenger experiments indicate a yield of 7.5 ± 0.5 radicals per 100 e.v. absorbed. At 24° , borazole decomposes thermally, producing hydrogen at a rate of 4×10^{-8} moles/l.-sec. for 24-hr. periods. The decomposition reaction at 30.8 and 40.8° appears to be autocatalytic since the rate of hydrogen production increases with time.

Introduction

Previous work¹ indicated that methyl substituted borazoles resembled aliphatic hydrocarbons with respect to radiation yields. It was of interest, therefore, to study the radiation chemistry of borazole. Since borazole is isoelectronic with benzene and is sometimes referred to as "inorganic benzene," it is of interest to compare the radiolysis of borazole with benzene and with the saturated cyclic hydrocarbon, cyclohexane. The radiation chemistry of benzene²⁻⁶ and cyclo-

hexane⁷⁻¹⁸ has been studied extensively. Hydrogen yields of 0.038 and 0.044 molecule per 100 e.v. have

- (1) C. J. Wolf and R. H. Toeniskoetter, *J. Phys. Chem.*, **66**, 1526 (1962).
- (2) S. Gordon and M. Burton, *Discussions Faraday Soc.*, **12**, 88 (1952).
- (3) J. P. Manion and M. Burton, *J. Phys. Chem.*, **56**, 560 (1952).
- (4) S. Gordon, A. R. Van Dyken, and T. F. Doumani, *ibid.*, **62**, 20 (1958).
- (5) R. H. Schuler, *ibid.*, **60**, 381 (1956).

- (6) L. Bouby, A. Chapiro, M. Magat, E. Migirdicyan, A. Prevot-Bernas, L. Reinsch, and J. Sebban, *Proc. Intern. Conf. Peaceful Uses At. Energy*, **7**, 526 (1955).
- (7) M. Hamashima, M. P. Reddy, and M. Burton, *J. Phys. Chem.*, **62**, 246 (1958).
- (8) M. Burton, J. Chang, S. Lipsky, and M. P. Reddy, *Radiation Res.*, **8**, 203 (1958).
- (9) H. A. Dewhurst, *J. Phys. Chem.*, **63**, 813 (1959).
- (10) J. Dyne and W. H. Jenkinson, *Can. J. Chem.*, **38**, 539 (1960).
- (11) R. W. Fessenden and R. H. Schuler, *J. Am. Chem. Soc.*, **79**, 273 (1957).
- (12) L. J. Forrestal and W. H. Hamill, *ibid.*, **83**, 1535 (1961).
- (13) P. J. Horner and A. J. Swallow, *J. Phys. Chem.*, **65**, 953 (1961).
- (14) W. S. Guentner, T. J. Hardwick, and R. P. Njsjak, *J. Chem. Phys.*, **30**, 601 (1959).
- (15) G. R. Freeman, *ibid.*, **33**, 71 (1960).

been reported for the γ -ray radiolysis of benzene by Schuler⁵ and Gordon, *et al.*,⁴ respectively. The reported hydrogen yields from irradiated cyclohexane vary between 4.85 found by Horner and Swallow¹³ and 5.85 molecules per 100 e.v. as found by Burton, *et al.*,⁸ and Forrestal and Hamill.¹²

Although borazole is known to decompose at room temperature,¹⁹ little is known about the kinetics of decomposition. Laubengayer, Moews, and Porter²⁰ studied the decomposition of gaseous borazole in the temperature range 337 to 371°. Hydrogen was the principal gaseous product and evidence was found for production of diphenyl- and naphthalene-type compounds. Similar results recently have been reported for the decomposition of liquid borazole.²¹ We report here the rate of hydrogen production from liquid borazole at 30.8 and 40.8°.

Experimental

Borazole was prepared by reduction of B-trichloroborazole with lithium aluminum hydride¹⁹ in tetraethylene glycol dimethyl ether. The crude product (obtained in 45% yield) was separated from the reaction mixture by distillation through a water cooled spiral reflux condenser at a pressure of 10^{-3} mm. Redistillation at atmospheric pressure gave a fraction boiling at 54.2°. The borazole then was vacuum fractionated through traps at -45, -78, and -196° until the vapor pressure of the fraction trapped at -78° was 85 mm. at 0° (lit. 85 mm. at 0° for pure borazole²²). This fractionation procedure was repeated prior to loading of the sample tubes and the samples were stored at -196° to minimize thermal decomposition. Borazole was recovered from irradiated or thermally decomposed samples and was purified in the same manner and reused.

Samples of borazole, weighing approximately one gram, were vacuum distilled into Pyrex tubes 10 mm. \times 100 mm. All samples were irradiated at the desired temperature in a 3200-c. cobalt-60 γ -ray source. The dose rate was 1.1×10^{20} e.v./g.-hr. measured by means of a ferrous sulfate dosimeter assuming a ferric yield of 15.6.²³ All doses were corrected for the decay of the cobalt-60 source and for the difference between the electron density of the sample and that of the dosimeter. For irradiations below room temperature the samples were immersed in appropriate boiling liquids and liquid-solid mixtures.

Sample tubes were opened in the vacuum system and hydrogen was pumped through a -196° trap with the aid of a Toepler pump and measured in a calibrated gas buret. The quantity and purity of the hydrogen were then checked in a gas chromatograph. In preparation of the borazole samples, mercury contamination was minimized by passing the borazole vapor through a U-trap packed with glass wool and cooled to -45°. Within the limits of experimental error, it was found that the presence of small but visible amounts of mercury affected neither the radiation-induced reactions nor the thermal reactions.

The samples used for the thermal decomposition measurements were held in a thermostated water bath controlled to better than $\pm 0.3^\circ$ for periods of time ranging from 6 to 160 hr.

In order to determine the effect of the glass vessel composition on the thermal reaction, borazole was loaded into sample tubes made from several types of glasses including one Pyrex tube which had been irradiated to a total dose of 2×10^{21} e.v./g. Samples were stored at 24° for 70 hr. and the amounts of hydrogen produced, in units of micromoles of H₂ per gram of borazole, were: Pyrex, 11.9; Vycor, 11.9; quartz, 9.8; Nonex, 10.5; cobalt glass, 11.2; uranium glass, 9.1; and irradiated Pyrex, 12.6.

(16) T. D. Nevitt and L. P. Remsberg, *J. Phys. Chem.*, **64**, 989 (1960).

(17) G. E. Adams, J. H. Baxendale, and R. D. Sedgwick, *ibid.*, **63**, 854 (1959).

(18) E. S. Waight and P. Walker, *J. Chem. Soc.*, 2225 (1960).

(19) R. Schaeffer, M. Steindler, L. Hohnstedt, H. S. Smith, Jr., L. B. Eddy, and H. I. Schlesinger, *J. Am. Chem. Soc.*, **76**, 3303 (1954).

(20) A. W. Laubengayer, P. C. Moews, Jr., and R. F. Porter, *ibid.*, **83**, 1337 (1961).

(21) G. Mamantov and J. L. Margrave, *J. Inorg. Nucl. Chem.*, **20**, 347 (1961).

(22) E. Wiberg and A. Bolz, *Ber.*, **73B**, 209 (1940).

(23) S. C. Lind, "Radiation Chemistry of Gases," Reinhold Publ. Corp., New York, N. Y., 1961, p. 59.

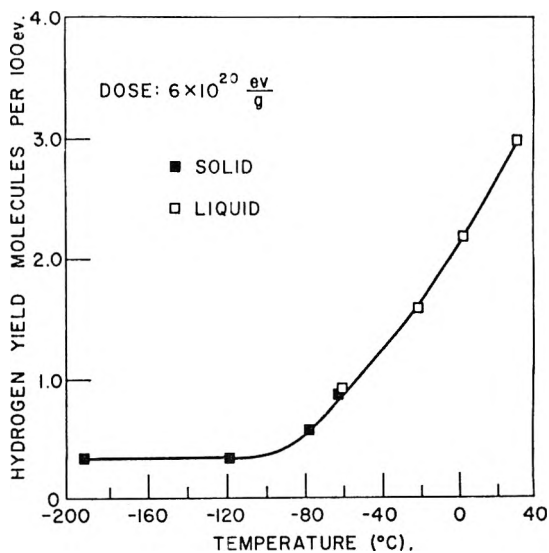


Fig. 1.—Temperature dependence of the hydrogen yields from irradiated borazole.

These values indicate little, if any, effect of glass composition on the rate of decomposition of borazole at 24°.

Diphenylpicrylhydrazyl was obtained from Distillation Products Industries. Its molar magnetic susceptibility was found to be 1255×10^{-6} c.g.s./mole, indicating a high state of purity (theoretical susceptibility of pure DPPH is 1270×10^{-6} c.g.s./mole).²⁴ DPPH concentration in the scavenger experiments was determined spectrophotometrically at 520 $m\mu$ (molar extinction coefficient 12,100) in a Cary Model 14 recording spectrophotometer. A known concentration of DPPH in the liquid to be studied was degassed by conventional techniques in a 1 mm. fused silica absorption cell prior to irradiation. The sample was irradiated, the optical density determined, and the sample then re-irradiated. This sequence was continued until all of the DPPH was consumed.

Borazole was found to react with DPPH at room temperature in the absence of radiation. In the time interval used, the thermal rate of DPPH consumption was approximately linear. In order to determine the radical yields during irradiation, it was necessary to correct for the decrease in DPPH concentration due to the thermal reaction during the irradiation period and while the sample was in transit between the source and the spectrophotometer. This was done by following the thermal reaction spectrophotometrically before and after irradiation and then extrapolating the thermal curves to the midtime of the irradiation period.

Results

Radiolysis of Borazole.—The quantity of hydrogen produced from the γ -ray radiolysis of borazole at 30° is a linear function of dose to 25×10^{20} e.v./g. Thermal decomposition represented approximately 5% of the total hydrogen obtained. After suitable corrections $G(\text{H}_2)$ was found to be 2.90 ± 0.08 molecules per 100 e.v.

$G(\text{H}_2)$ as a function of temperature is shown in Fig. 1. The hydrogen yield from borazole irradiated at or below -120° is 0.36 molecule per 100 e.v. In the liquid phase the hydrogen yield increases from 0.93 to 2.90 molecules per 100 e.v. in the temperature interval -63 to 30°. At the melting point it appears that the physical state of borazole does not affect the hydrogen yield.

Diphenylpicrylhydrazyl (initial concentrations between 0.5 and 1.5×10^{-3} molar) was used to determine the total free radical yield. Figure 2 shows the decrease in DPPH concentration as a function of time and irradiation. The thermal reaction occurs at a

(24) J. V. Zanchetta, Thesis, University of Bordeaux, 1961.

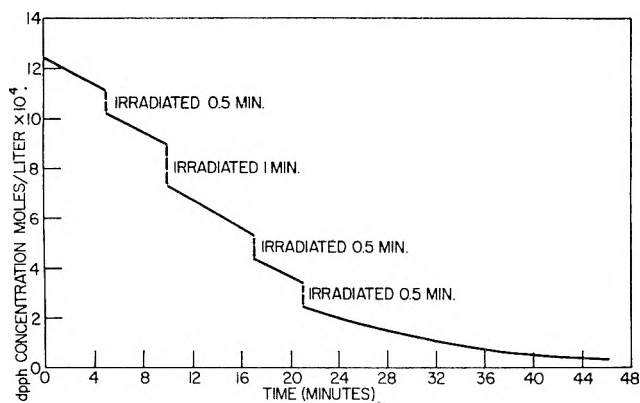


Fig. 2.—Radical yield from irradiated borazole using DPPH as scavenger.

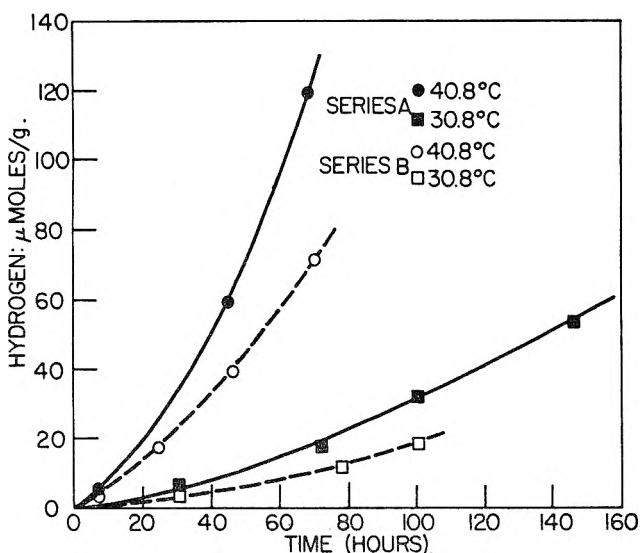


Fig. 3.—Hydrogen from the thermal decomposition of borazole.

rate of 4×10^{-7} mole/l.-sec., ten times faster than the rate of thermal hydrogen production. From the decrease in DPPH concentration with dose, a yield of 7.5 ± 0.5 radicals per 100 e.v. was calculated.

Thermal Decomposition of Borazole.—Initially, the thermal decomposition of borazole was studied in order to correct the results of the radiation experiments. Over periods of time less than 24 hr. the rate of hydrogen production at 24° was found to be about 1.7×10^{-7} mole of H_2 /g.-hr. However, difficulties in storage of our stock supply of borazole led us to suspect autocatalysis in the thermal reactions. For this reason the rate of hydrogen production from borazole as a function of time was investigated at 30.8 and 40.8° . Two sets of seven samples each were used, the seven samples of series (A) being prepared simultaneously from a single batch of purified borazole while the series (B) samples were taken from another batch of borazole.

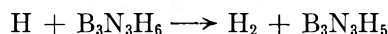
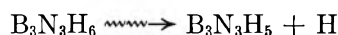
The hydrogen obtained from the thermal decomposition of borazole at 30.8 and 40.8° as a function of time is shown in Fig. 3. The results for series (A) do not coincide with the results for series (B) but the over-all effects are similar. The shapes of these curves indicate that the rate of hydrogen production increases with time. This suggests that the decomposition may be autocatalytic.

Discussion

Radiation induced reactions which occur at low temperatures generally are considered to result from

one or more of three processes: (1) molecular detachment, (2) excited atom or molecule reactions, and (3) recombination reactions within a spur. All three processes should be essentially independent of temperature. Ionic reactions may also occur but they usually can be recognized by their inverse temperature characteristics. Free radical reactions normally require energy of activation and are, therefore, temperature dependent. Thus, a study of the temperature dependence of radiation yields can help in formulating a mechanism.

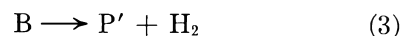
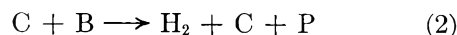
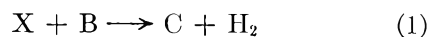
Below -120° H_2 probably is produced by some combination of processes (1), (2), and (3). In the temperature range -80 to 35° the temperature coefficient for hydrogen production is about 2 kcal./mole. This, together with the observation that many radicals are present during radiolysis [$G(\text{radical})_{\text{DPPH}} = 7.5$], suggests that at room temperature H_2 is primarily formed by a conventional radical mechanism, such as



Aromatic compounds in general, and benzene in particular, are well known to be relatively radiation resistant with respect to hydrogen production. Cyclooctatetraene, which has a low degree of aromatic character,²⁶ is similarly resistant to radiation. The mechanisms for energy dissipation which render stability to benzene and cyclooctatetraene, however, must not be operative in borazole, although the aromatic character of the borazole ring appears to be about 24%.²⁶ The hydrogen yield from borazole ($G(H_2) = 2.90$) more closely resembles that from cyclohexane ($G(H_2) = 5.5$)⁷⁻¹⁸ than that from benzene ($G(H_2) = 0.038$)^{4,5} or cyclooctatetraene ($G(H_2) = 0.020$).²⁷

Approximately 80% of the hydrogen obtained during radiolysis of cyclohexane is produced by molecular and hot atom reactions.¹⁰ The low temperature yield of hydrogen^{7,9,28} from cyclohexane reflects the temperature independence of such processes. In the case of borazole radiolysis, the low hydrogen yield at low temperature ($G(H_2)_{-196^\circ} = 0.36$) suggests that molecular and hot atom reactions are relatively unimportant.

The thermal decomposition of borazole appears to involve autocatalysis. Autocatalytic schemes involving one catalyst or an induction period may be written which are consistent with the data of either series (A) or series (B) (see Fig. 3). However, in order to account for the variance of results between the two series, a more complex scheme must be considered, such as



where B is borazole, X is an impurity which reacts

(25) H. D. Springall, T. R. White, and R. C. Cass, *Trans. Faraday Soc.*, **50**, 815 (1954).

(26) H. Watanabe, K. Ito, and M. Kubo, *J. Am. Chem. Soc.*, **82**, 3294 (1960).

(27) S. Shida, H. Yamazaki, and S. Arai, *J. Chem. Phys.*, **29**, 245 (1958).

(28) Unpublished results. For cyclohexane we find: $(G(H_2))_{-196^\circ} = 4.50$.

with B, C is a catalyst for the decomposition of borazole, and P and P' are products.

According to eq. 1, 2, and 3, the rate of hydrogen production is given by

$$dH_2/dt = k_1BX + k_2BC + k_3B \quad (4)$$

The rate of production of C is

$$dC/dt = k_1BX \quad (5)$$

integrating (5) gives

$$C = k_1BXt + C_0 \quad (6)$$

and substitution of (6) into (4)

$$dH_2/dt = k_1BX + k_2BC_0 + k_3B + k_1k_2B^2Xt \quad (7)$$

Integrating eq. 7 and making use of the initial conditions, $H_2 = 0$ at $t = 0$, and dividing both sides by t gives

$$H_2/t = k_1BX + k_2BC_0 + k_3B + \frac{1}{2}k_1k_2B^2Xt \quad (8)$$

The maximum conversion of borazole in our experiments corresponds to about 2% decomposition so that the terms B and B^2 in eq. 7 may be considered constant. If X may be assumed constant, then according to eq. 8, a plot of H_2/t vs. t should give a straight line. Figure 4 shows this linear relation for the experimental values of H_2/t vs. t .

According to this scheme, at either temperature, the ratio of the slopes of the series (A) line to the series (B) line gives the ratio of X in the two sets of samples. This ratio is 2.2 at 30.8° and 2.2 at 40.8°. The intercept term of eq. 8 contains five unknowns, k , k_2 , k_3 , X , and C_0 , which cannot be evaluated. However, for the special case where $k_1BX \ll k_2BC_0 \gg k_3B$, eq. 8 reduces to

$$H_2/t = k_2BC_0 + \frac{1}{2}k_1k_2B^2Xt \quad (9)$$

This simplification follows if hydrogen is not obtained via reaction 1 and reaction 3 is very slow. The reaction scheme then reduces to

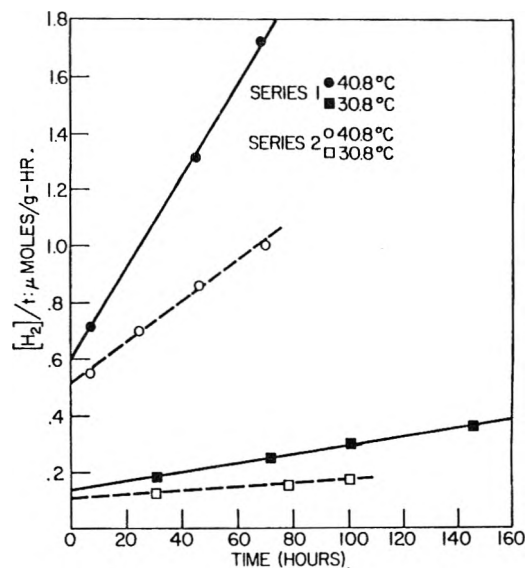
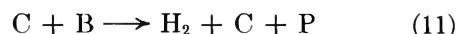


Fig. 4.— H_2/t vs. t (eq. 7) for thermally decomposed borazole.



Using eq. 9 and the intercepts from Fig. 4, the ratio of C_0 (series A) to C_0 (series B) is 1.3 at 30.8° and 1.2 at 40.8°. For each series of data the ratio of the intercepts at the two temperatures gives $k_2(40.8^\circ)/k_2(30.8^\circ)$. This ratio, together with the corresponding slopes, permits estimation of $k_1(40.8^\circ)/k_1(30.8^\circ)$ for each series. From the data for series (A), activation energies of 17 and 28 kcal./mole are calculated for reactions 10 and 11, respectively; series (B) data lead to activation energies of 15 and 29 kcal./mole for the same reactions.

The linearity of hydrogen vs. dose for borazole suggests that trace impurities do not appreciably alter $G(H_2)$. Thus, one suspects that the mechanisms for radiolytic and thermal decomposition are distinct and independent.

Acknowledgment.—We are indebted to Dr. A. W. Czanderna for the magnetic susceptibility measurements and Dr. J. A. Ghormley's continued interest and advice are appreciated.

ELECTRODE DEPOLARIZATION KINETICS ON OPEN CIRCUIT¹

BY TERRELL N. ANDERSEN AND HENRY EYRING

*Department of Chemistry, University of Utah, Salt Lake City, Utah**Received May 31, 1962*

Platinum wire electrodes, in nitrogen-saturated, aqueous solutions containing Fe^{+3} , MnO_4^- , Ce^{+4} , $\text{Fe}(\text{CN})_6^{-3}$, or $\text{Cr}_2\text{O}_7^{-2}$ ions, were cathodically polarized to potentials at or near that of a reversible hydrogen electrode. The polarizing circuit then was broken and the ensuing chemical oxidation of the electrode surface was studied kinetically by following the potential with respect to time. Three segments were observed in the open circuit potential-time depolarization curves. The first was a decay in less than 0.005 sec. from the hydrogen overpotential to the reversible hydrogen potential. During the second segment, the chemisorbed hydrogen was diminished in concentration at a rate equal to the limiting current of the oxidant. The rate of change of potential during the third segment was controlled by the rate at which oxidant accumulated at the electrode and reductant was transported away from the electrode. A mathematical analysis was given which satisfactorily predicted the shape of the second and third segments. Between these latter portions of the curve, the potential was a mixed one, and the shape of the curve was not correlated with the concentrations of species present. However, this somewhat linear slope corresponded to a charging of the double layer (of constant capacity) at a rate near that of the limiting current of the oxidant. The results indicated that the electrode, at the reversible hydrogen potential, had a hydrogen coverage of approximately one monolayer. Similar experiments were performed with a palladium electrode to study the importance of absorbed (or occluded) hydrogen. It was found in this case that the flux of absorbed hydrogen to the electrode surface was important throughout most of the depolarization, to potentials very close to the steady state.

Introduction

If a hydrogen electrode is subjected to an oxidative environment, at least two processes must take place before the potential attains a steady state. These are (1) the removal of chemisorbed hydrogen from the electrode surface and (2) the arrangement of a new double layer corresponding to the potential of the oxidant or of the new environment. During such processes, potential-time curves exhibit inflections and current-potential curves exhibit maxima, which indicate that more than one rate-controlling mechanism is important in establishing the new potential.²⁻¹¹

It is the object of this paper to study the kinetic processes taking place during the chemical oxidation of smooth platinum cathodes by following the potential change. Palladium cathodes also are studied in order to emphasize the importance of absorbed hydrogen.

The oxidizing system chosen was nitrogen-saturated, dilute sulfuric or hydrochloric acid containing Fe^{+3} , MnO_4^- , Ce^{+4} , $\text{Cr}_2\text{O}_7^{-2}$, or $\text{Fe}(\text{CN})_6^{-3}$ ions. The hydrogen was supplied to the electrode by cathodic polarization, whereupon the polarizing circuit was broken and the electrode was allowed to depolarize on open circuit.

For any electrode we may write, in general

$$\dot{i}_{\text{ext}} = \Sigma \dot{i}_f + \frac{dq_{\text{dL}}}{dt} = \Sigma \dot{i}_f + \frac{d(C_{\text{dL}}E)}{dt} \quad (1)$$

(1) This is an essential portion of a thesis submitted to the Chemistry Department, University of Utah, in partial fulfillment of the requirements for a Ph.D. Degree.

(2) J. K. Lee, R. N. Adams, and C. E. Bricker, *Anal. Chim. Acta*, **17**, 321 (1957).

(3) H. P. Agarwal and D. R. Sikka, *Bull. India Sect. Electrochem. Soc.*, **6**, 1, 11 (1957).

(4) J. Giner, *Z. Elektrochem.*, **64**, 491 (1960).

(5) T. C. Franklin and S. L. Cooke, Jr., *J. Electrochem. Soc.*, **107**, 6, 556 (1960).

(6) A. L. Ferguson and M. B. Towns, *Trans. Electrochem. Soc.*, **83**, 271 (1943).

(7) F. P. Bowden, *Proc. Roy. Soc. (London)*, **A125**, 446 (1929).

(8) J. A. V. Butler and G. Armstrong, *ibid.*, **A137**, 604 (1932).

(9) A. Frumkin and E. E. Aikasyan, *Dokl. Akad. Nauk SSSR*, **100**, 35 (1955).

(10) M. Breiter, C. A. Knorr, and W. Volkl, *Z. Elektrochem.*, **59**, 681 (1955).

(11) J. D. Pearson and J. A. V. Butler, *Trans. Faraday Soc.*, **34**, 1163 (1938).

where i_{ext} is the external current, $\Sigma \dot{i}_f$ is the sum of the currents for the faradaic processes at the electrode, C_{dL} is the differential capacitance of the double layer, q_{dL} is the charge on the electrode side of the double layer, and E is the potential of the electrode compared to that of a reference electrode (using the Gibbs-Stockholm sign convention). $\Sigma \dot{i}_f$ may be expressed as a difference of the sums of the cathodic and anodic reactions, and is related exponentially to the potential.^{12,13}

In the event that mass transfer to or from the electrode is slow, equations may be set up for the conservation of mass of each species at the interface. If both charge transfer and mass transfer are rate controlling, the system of differential equations describing the over-all process cannot be solved to give potential explicitly as a function of time. This results from the complex nature of the equations as well as from the lack of knowledge concerning the initial conditions, rate constants, and the diffusion mechanism of hydrogen in the metals.

In order to make simplifications in the analysis, an experimental analysis is first made to determine which processes predominate at any given potential.

Experimental

The cell consisted of a 600-ml. Pyrex electrolytic beaker tightly fitted with a rubber stopper,¹⁴ which held the various inlet tubes. 250 ml. of electrolyte (dilute H_2SO_4 or HCl with oxidant added) was chosen for each experiment; by using this volume the bulk concentration of any species would not change by as much as 1% during a run. The electrolyte was vigorously stirred in all of the experiments (unless specified otherwise) by means of a magnetic stirring bar. The solution was kept N_2 -saturated by bubbling 99.997% pure nitrogen through it prior to each experiment.

The indicator electrode consisted of 99.9% purity platinum (the palladium content was less than 0.01%), or palladium wire of 0.0406-cm. diameter (B&S gage 26), with 10.2 cm.

(12) S. Glasstone, K. J. Laidler, and H. Eyring, "The Theory of Rate Processes," McGraw-Hill Book Co., New York, N. Y., 1941, p. 575.

(13) P. Delahay, "New Instrumental Methods in Electrochemistry," Interscience Publishers, Inc., New York, N. Y., 1954, p. 32.

(14) The rubber stopper enclosing the top of the cell was presoaked in dilute base and acid solutions. Prior to and during the experiments neither the electrodes nor the electrolyte came in contact with the stopper. The experiments were run within a few minutes after transferring the electrolyte to the cell, with N_2 vigorously bubbling through the solution in the meantime. Therefore it is considered that the rubber stopper in no way affected the accuracy of the results within the ascribed precision.

immersed in the solution. The immersed portion of the electrode was in the shape of an inverted horseshoe with the two ends protruding out of the cell through ceramic tubes which insulated the wire from the rubber stopper. Therefore, the wire could be heated in the cell by passing current through it to clean its surface.

A saturated calomel electrode was used as the reference half-cell and made contact with the electrolyte by means of a KCl-agar salt bridge drawn to a capillary at its tip. The working electrode also consisted of platinum; it was enclosed in an inverted Pyrex tube which allowed oxygen gas produced during polarization to be evolved. A glass tube was contained in the stopper as an inlet for reagents; otherwise it was closed. The tubes and electrodes were positioned relative to one another so that the salt bridge and working electrode were on opposite sides of the indicator electrode.

The potential difference between the indicator and reference electrodes was recorded by means of an Offner Type P dynograph assembly with a Type 9405 cathode follower coupler inserted between the amplifier and electrode leads. The limit of precision of the instrument was ± 5 mv. except at potentials positive of 600 mv. and negative of -150 mv. (*vs. s.c.e.*). A Model G Beckman pH meter was used to read steady-state potentials within ± 2 mv.

A constant polarizing current was supplied by means of a d.c. battery connected in series with an ammeter and variable resistor.

The electrolyte was prepared and purified following methods set forth by Bockris.^{15,16} The water was doubly-distilled from basic permanganate solution, chemically pure acid was added, and the resulting solution was pre-electrolyzed. Electrolyte transference was made by means of N_2 pressure or vacuum.

The indicator electrode was flamed, placed in the cell, and heated to approximately 900° for 1 min. in a nitrogen atmosphere (by means of a powerstat), and then successively anodized and cathodized at 10 ma. for a few seconds. The latter treatment probably removed trace amounts of impurities, and may have produced a fresh coating of spongy platinum¹⁷ on the electrode. The electrolyte was introduced into the cell and nitrogen-saturated, after which analytical grade depolarizer, dissolved in solution, was added to the cell (along with product salt, if desired). The oxidizing agents used were $X_2Cr_2O_7$, $KMnO_4$, $Ce(SO_4)_2$, $Fe_2(SO_4)_3$ or $Fe(NO_3)_3$, and $K_3Fe(CN)_6$ and the product solutions were $CrK(SO_4)_4$, $MnSO_4$, $Ce(NO_3)_3$, $FeSO_4$, and $K_4Fe(CN)_6$. The range of concentrations studied was 10^{-4} to 5×10^{-3} M.

The electrode then was cathodically polarized,¹⁸ the nitrogen was turned off, and the polarizing circuit was broken, allowing the indicator electrode to depolarize on open circuit. The nitrogen was turned off to prevent bubbles from impinging on the electrode or on the tip of the salt bridge during depolarization. The cleanliness of the electrode was ascertained by the overvoltage corresponding to a given current density and by the length of time necessary for the depolarization to take place. The electrode was considered "clean" in the above tests, as well as in actual experiments, when (1) good reproducibility was obtained in the repetition of experiments, and (2) when further purification of the solution or electrodes did not yield different results. Any data presented here were remeasured several times, and the relative precision was better than 15% unless otherwise stated. Except for the experiments in which the stirring rate was varied, the speed of the stirring bar was 670 ± 25 r.p.m. The temperature was $25 \pm 1^\circ$ in all experiments except when T was varied and the nitrogen pressure was approximately 0.85 atm. in each experiment. The time of depolarization in the absence of oxidant was 30 or more times that obtained in the presence of oxidant at its lowest concentration, so oxygen and other stray depolarizers were considered to have negligible effect on the results.

Experimental Results and Conclusions

The typical shapes of the depolarization curves for platinum and for palladium are shown in Fig. 1, although the particular curves shown were obtained in MnO_4^- .¹⁹ In each case the polarization current was

(15) A. M. Azzam, J. O'M. Bockris, B. E. Conway, and A. J. Rosenberg, *Trans. Faraday Soc.*, **46**, 918 (1950).

(16) J. O'M. Bockris, "Modern Aspects of Electrochemistry," Academic Press, New York, N. Y., 1954, p. 135.

(17) F. C. Anson, *Anal. Chem.*, **33**, 934 (1961).

(18) It made no difference in the results whether polarization was begun before or after oxidant was added.

(19) Any effects illustrated in the case of a particular solution were observed in any of the depolarizers, unless specified otherwise.

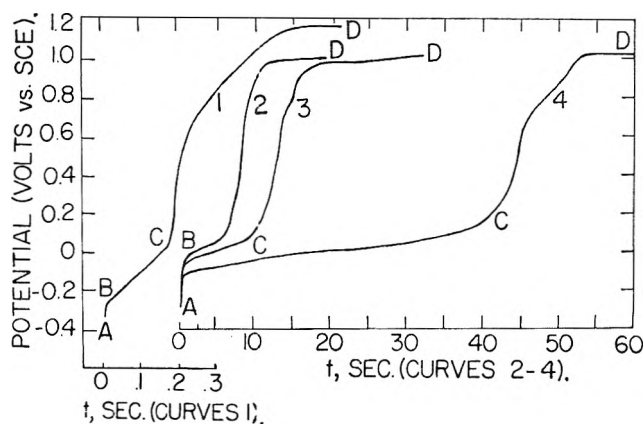


Fig. 1.—Depolarization curves for Pt and Pd showing the effect of polarization time: curve 1, Pt; $t_{pol} = 0.5$ to 120 sec., curves 2 to 4, Pd; $t_{pol} = 5.5, 11,$ and 30 sec., respectively. Solution: 0.45 M H_2SO_4 containing 3.2×10^{-4} M MnO_4^- .

greater than the limiting current of the oxidant, so liberation of hydrogen occurred. It can be seen that the depolarization curves each consist of three distinct segments, AB, BC, and CD, by which these segments shall be referred to throughout the remainder of this paper. The length of BC (in seconds) will hereafter be referred to as τ or the transition time. Interpretation of the results along with experimental and theoretical justification is given below.

Depolarization during AB.—When the battery circuit is opened, the hydrogen concentration on the platinum electrode immediately decreases to that coverage which can be supported by atmospheric pressure; any hydrogen more than this immediately leaves the electrode as gas, due to a pressure difference across the interface. Thus the potential rises from E_A to E_B , the reversible hydrogen potential, in less than 0.005 sec. Since hydrogen overvoltage decay has been studied extensively elsewhere^{20,21} segment AB was not studied kinetically here.

In the case of palladium, $(Pd-H)_\alpha$ and/or $(Pd-H)_\beta$ are/is formed inside the metal at some concentration.^{22,23} When the current ceases, the surface hydrogen immediately is absorbed or evolved to the extent that the palladium surface and interior are approaching equilibrium with respect to hydrogen (although, of course, the surface hydrogen is being oxidized rapidly by the oxidant). If very little hydrogen is present in the metal, the potential E_B will be positive with respect to the hydrogen potential, while if the interior is nearly saturated, the potential will lie near the hydrogen electrode potential.

Depolarization during BC.—From B to C the only net change taking place at the electrode-solution interface is the decrease of adsorbed hydrogen, due to its oxidation by depolarizer. The oxidant ions are reduced as rapidly as they reach the electrode surface, so their concentration at the interface, as well as that of the production, is not changing. The chemistry thus consists of a competition between (a) diffusion of adsorbed hydrogen from the metal interior, and (b) mass transport of oxidant from the solution to the electrode surface. In the case of platinum there is very little ab-

(20) P. C. Milner, *J. Electrochem. Soc.*, **107**, 343 (1960).

(21) P. Ruetschi, *ibid.*, **105**, 819 (1959).

(22) S. Schulzinger, G. W. Castellan, and J. P. Hoare, *J. Chem. Phys.*, **28**, 16 (1958).

(23) T. B. Flanagan and F. A. Lewis, *J. Electrochem. Soc.*, **108**, 437 (1961).

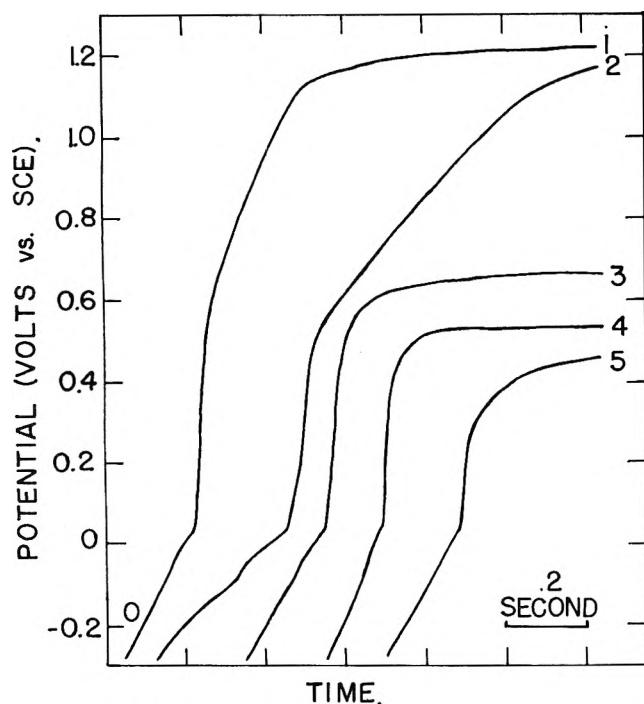


Fig. 2.—Depolarization curves for Pt in 0.45 M H_2SO_4 containing the various oxidants at $16 \pm 1 \times 10^{-4}$ equiv./l.: (1) MnO_4^- ; (2) Ce^{+4} ; (3) $Cr_2O_7^{-2}$; (4) Fe^{+3} ; (5) $Fe(CN)_6^{-3}$.

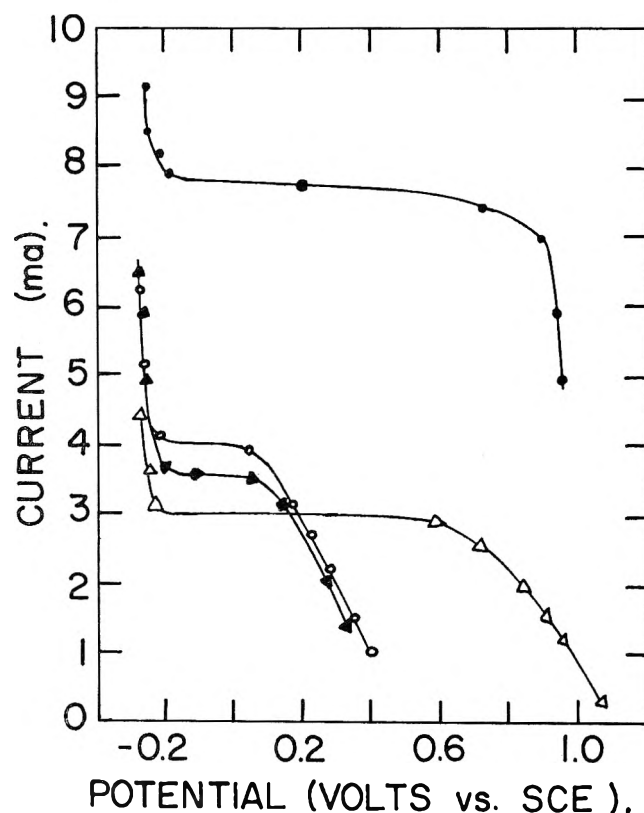


Fig. 3.—Experimental determination of limiting currents in 0.45 M H_2SO_4 containing 36×10^{-4} N solutions of various oxidants: (●) MnO_4^- ; (○) Fe^{+3} ; (▲) $Fe(CN)_6^{-3}$; (Δ) Ce^{+4} . Geometric electrode area = 1.3 cm.².

sorbed hydrogen, so (b) is the slowest step during τ , while in the case of palladium there is an abundance of absorbed hydrogen, and both (a) and (b) are comparably slow. The supporting evidence for the preceding explanation of BC is plentiful.

(a) **Platinum.**—(1) All of the oxidants studied gave similar type curves as shown in Fig. 2. The break

potentials E_B and E_C were independent of the type or concentration of oxidant studied, but depolarization was more rapid in more concentrated solutions of oxidant.

(2) The break potentials, E_B and E_C , were independent of any variables in the experiment except the hydrogen ion concentration. E_B corresponded to the reversible-hydrogen electrode potential at a hydrogen pressure of 1 atm. E_C increased with an increase of hydrogen ion concentration in a manner commensurate with a hydrogen electrode from pH 0 to 3; for pH greater than 3, concentration polarization of H^+ occurred and masked the bulk pH effect. E_B varied with pH in the same manner as did E_C , but the precision of the potential reading was quite poor (± 25 mv.).

(3) Limiting currents were obtained in solutions containing Fe^{+3} , Ce^{+4} , MnO_4^- , and $Fe(CN)_6^{-3}$; Figure 3 shows the potential-current plots for each of these oxidants at a concentration of 36×10^{-4} equivalents/l. in 0.45 M H_2SO_4 solutions stirred at 670 r.p.m. The points were obtained by applying a constant current and observing the steady-state potential to which the electrode relaxed within 1 sec. The limiting currents were found experimentally to be directly proportional to the oxidant concentration. It can be seen from Fig. 3 that the oxidants are being transported to the electrode at their limiting currents at all potentials positive of E_C . In the case of $Cr_2O_7^{-2}$, the potential at constant current slowly drifted toward negative values and did not reach a steady-state within 1 min., except for potentials more negative than -250 mv. As many authors have stated^{24,25} a film is formed on platinum, upon reducing dichromate, which prevents further reduction of the dichromate but which supports reduction of H^+ . This explains the negative drift of potential with time: $Cr_2O_7^{-2}$ reduction sites are continuously poisoned, so the effective current density for dichromate reduction increases while the total current is being held constant.

(4) The depolarization rate at BC was independent of the product ion concentration in the bulk of the solution, from very low concentrations (none added) to 10^{-1} M. High concentrations (10^{-2} to 10^{-1} M) of Mn^{+2} reacted with MnO_4^- to form MnO_2 , and hence slowed down the depolarization rate by lowering the effective MnO_4^- concentration.

(5) The depolarization rate was independent of hydrogen ion concentration from pH 0.2 to 4, at constant ionic strength (by the addition of K_2SO_4 to the H_2SO_4).

(6) The rate was independent of K_2SO_4 concentration within the concentration region for which the activity coefficient of oxidant ions did not vary greatly. In solutions of 0.1 N HCl containing $Cr_2O_7^{-2}$ and Fe^{+3} , τ was identical with that in dilute sulfuric acid solutions over the entire range of concentration of oxidant. The anion was not varied in the case of the other oxidants.

(7) τ decreased significantly with an increase in stirring rate throughout the complete stirring range. In the range 300–900 r.p.m., τ decreased by 32–35% for every 100% increase in stirring rate. In non-stirred solutions there was present an additional arrest starting

(24) Yu. Yu. Matutis and A. Yu. Mitskene, *Lietuvos TSR Mokslu Akad. Darbai Ser. B*, 1, 45 (1959).

(25) H. Gerischer and M. Kappel, *Z. physik. Chem.*, 20, 83 (1959).

at E_B and ending approximately 60 mv. positive of E_B . This was due to hydrogen gas near the electrode being oxidized.

(8) The depolarization rate in vigorously stirred solutions was independent of the polarization time from $t_{pol} = 0.5$ sec. to 2 min. Longer times were not studied due to the greater relative importance of impurities which were slowly plated out during cathodization.

(9) The depolarization rate was essentially insensitive to the polarization potential unless hydrogen gas was liberated, in which case the slope of the entire depolarization curve was noticeably decreased.

Since τ for platinum is independent of polarization time, and $E_C - E_B$ is a constant, we can assume that roughly the same amount of hydrogen is oxidized in each depolarization during the transition time. From the limiting current data we may further say that this rate is constant [electron/(cm.² sec.)], and is proportional to $1/\tau$. From the above deductions, several results can be obtained which further strengthen the previous discussion.

(10) An apparent activation energy may be found for the slow process during τ by employing the Arrhenius rate equation

$$\text{rate} = \frac{K_1}{\tau} = A \exp\left(-\frac{E}{RT}\right) \quad (2)$$

where E is the activation energy, T is the absolute temperature, R equals the gas constant, and A and k_1 are constants. Therefore

$$\log\left(\frac{1}{\tau}\right) = \log\left(\frac{A}{K_1}\right) - \frac{E}{2.3RT} \quad (3)$$

The slope of the $\log(1/\tau)$ vs. $(-1/T)$ curve (for the oxidant $8 \times 10^{-4} M$ Fe³⁺) gave an activation energy of 4.94 kcal./mole with a standard deviation of 0.4% between the experimental points and the line. The viscosity of aqueous solutions changes slowly enough between 2 and 85° (the range in which the temperature variation was carried out) that the increase in reaction rate may be assumed to apply only to the diffusion coefficients of the ions (or the slow surface process, if there is one which is rate determining). The low activation energy obtained is typical of diffusion, and in fact very closely agrees with the 2.6% per degree increase in the diffusion coefficients of the ions in excess electrolyte as given by Jander.²⁶

(11) We can compare the relative rates of reaction, as well as the relative limiting currents of the various depolarizers, to their diffusion coefficients. This is done in Table I at the same stirring rate and concentration ($9 \times 10^{-4} M$) for each oxidant species. Column 2 shows the diffusion coefficients²⁷ of the various ions in excess electrolyte (as the experiments here employed) at 22°. These values were chosen from the data of Jander.²⁶ It has been shown that D , for ions in excess electrolyte, is independent of concentration in the range 10^{-3} to $10^{-1} M$,²⁸ so these values are considered applicable in all the work here reported. Column 3 shows the limiting currents for the various depolarizers, re-

ferred to that for Fe³⁺, at concentrations of $9 \times 10^{-4} M$. Column 4 indicates the relative reaction rates, given by $1/\tau$, for section BC of the curve. Column 5 shows the relative flux (compared to that for Fe³⁺) for the several oxidants. Since $i_{lim} = AnFmC_{Ox}^0$ and we have no theoretical way of knowing to what power D enters into m , the ratio of nD is taken to be the ratio of the flux for the various depolarizers. This approximates m by D/δ where δ is an effective diffusion layer which is nearly the same for each oxidant. Since several products could result from the reduction of MnO₄⁻, three values for the corresponding flux are listed which represent n values of 3, 4, and 5, respectively. Both experimental methods (transition times and limiting currents) show the same relative reaction rates among the depolarizers as do the diffusion coefficients. Since

$$-F \frac{dC_H}{dt} = \frac{d(CE)}{dt} = i_{lim} = AF_n C_{Ox}^0 m_{Ox} \quad (4)$$

the rate of reaction during τ , as given by the over-all amount of hydrogen oxidized per unit time, should be first order with respect to the bulk concentration of oxidant. This is assuming $\Delta(CE)$ is constant (as is ΔE) during τ , and is independent of C_{Ox}^0 . Therefore $(C_{Ox}^0 \tau)$ should be constant in the case of each depolarizer over differing concentrations. This is shown to be nearly so in Table II. It is to be noted that C in eq. 4 and 5 is the total measured capacity of the electrode and includes the so-called pseudocapacity due to hydrogen atoms.

TABLE I
COMPARISON OF REACTION RATES USING DIFFERENT METHODS OF CALCULATION

Depolarizer	D (cm. ² /day)	$\frac{i_{lim}}{i_{lim(Fe^{3+})}}$	$\frac{1/\tau}{1/\tau(Fe^{3+})}$	$\frac{i_{lim}(\text{calcd.})}{i_{lim(Fe^{3+})}(\text{calcd.})}$
Fe ³⁺	0.54	1.0	1.0	1.0
MnO ₄ ⁻	1.5	9.8	6.7	8.3, 11.1, 13.8
Ce ⁴⁺	0.43	0.76	0.34	0.79
Fe(CN) ₆ ⁻³	0.52	0.91	1.35	0.96
Cr ₂ O ₇ ⁻²	0.93	..	5.8	10.3

TABLE II
CONCENTRATION DEPENDENCE OF τ

nC_{Ox}^0 (equiv./l.) $\times 10^4$	$(C^0)_{Fe^{3+}}$ $\times 10^4$	$(nC^0)_{Cr_2O_7^{-2}}$ $\times 10^4$	$(C^0)^{+4}$ $\times 10^4$
36	2.70	2.70	5.25
24	2.52	2.76	6.0
16	2.4	2.72	6.0
10	2.5	2.8	7.6
6	2.37	2.82	8.2
2	1.78	2.6	

Although it has been established previously that the slow step, in the case of platinum, is the linear rate of oxidation of hydrogen, it is still necessary to explain the shape of the potential-time curve. Since the solution is nitrogen-saturated, the Nernst equation cannot be used to describe the electrode potential. Rather, the time dependence of the charge distribution along the coordinate vertical to the electrode surface, or of the electrode capacity, must be taken into account. Considering eq. 1 we have, therefore, during section BC of the platinum depolarization curve: $\Sigma i_t = -d(CE)/dt$. Consider the H_{ads} and protons to be essentially in equilibrium. The rate of oxidation of the reductant is negligible, and the reduction of the depolarizer proceeds

(26) G. Jander, C. Blohm, and B. Grüttner, *Z. anorg. allgem. Chem.*, **258**, 205 (1949).

(27) No value for DCe^{+4} in excess electrolyte could be found; 0.43 was approximated as $DCe^{+4}(DFe^{3+}/DFe^{+2})$. The value agrees quite closely with $D_{Th^{+4}}$, and is assumed to be accurate to within 15%.

(28) B. Grüttner and G. Jander, *Z. anorg. allgem. Chem.*, **266**, 225 (1951).

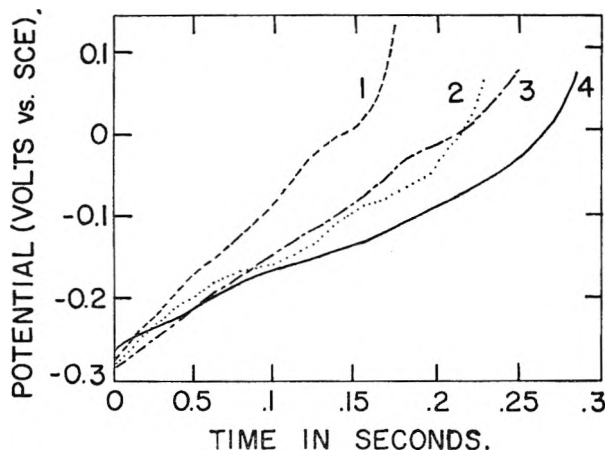


Fig. 4.—Experimental and calculated E vs. t curves from $t = 0$ to τ for Pt. Solutions $1.6 \times 10^{-4} M$ MnO_4^- : (1) calcd.; (2) exptl.; $1.8 \times 10^{-4} M$ Ce^{+4} : (3) calcd.; (4) exptl.

at the constant rate, i_{lim} , throughout τ . Then, neglecting adsorbed or gaseous hydrogen, we have

$$i_{lim} = \frac{d(CE)}{dt} \quad (5)$$

Since no explicit expression for C as a function of E was available, an experimentally determined capacity was used. The C - E curve was graphically integrated to obtain q as a function of E . Then using the relationship $q = q_{init} - i_{lim}t$, E was found as a function of t . The capacitance-potential curve was taken from the paper of Breiter¹⁰ as determined and confirmed by several authors^{10,29-33} for smooth platinum in H_2SO_4 solutions. In converting Breiter's data (θ , the surface coverage) to q , it was assumed that there was present one hydrogen atom for each surface platinum atom at a θ value of 1. The value of 1.5×10^{15} surface platinum atoms per $cm.^2$ of electrode was used³⁴ and the true area of the present electrode was taken as twice its apparent area. Potential-time curves, as calculated and as obtained experimentally, are shown in Fig. 4 for two of the systems studied.

It can be seen that the agreement in shape as well as slope of the calculated and experimental curves is very good. Since the roughness factor of the electrode surface was only estimated, the agreement of the slopes is not too important except that they agree to approximately 30%. The important agreement is the general linear curve with its slight inflection. The two slight maxima which occur on either side of the inflection also occur as maxima in polarography, and have been interpreted in the case of electrolytic oxidation of hydrogen electrodes as adsorbed, as well as adsorbed, hydrogen in the platinum.^{5,35} That the amount of adsorbed hydrogen is very small is evidenced by the short lived nature of the second arrest, as well as by the independence of the depolarization time on the polarization time. This is confirmed by other techniques which measure hydrogen in platinum.³⁶

(29) E. Wicke and B. Weblus, *Z. Elektrochem.*, **56**, 169 (1952).

(30) A. Eucken and B. Weblus, *ibid.*, **55**, 114 (1951).

(31) P. Dolin and B. Ershler, *Acta Physicochim. URSS*, **13**, 747 (1940).

(32) P. Dolin, B. Ershler, and A. Frumkin, *ibid.*, **13**, 779 (1940).

(33) M. Breiter, H. Kammermaier, and C. A. Knorr, *Z. Elektrochem.*, **60**, 37 (1956).

(34) H. A. Laitinen and C. G. Enke, *J. Electrochem. Soc.*, **107**, 773 (1960).

(35) A. Frumkin and E. E. Aikasyan, *Dokl. Akad. Nauk SSSR*, **100**, 35 (1955).

(36) D. P. Smith, "Hydrogen in Metals," Univ. of Chicago Press, Chicago, Illinois, 1958.

It is interesting to calculate the amount of hydrogen oxidized during τ . The amount of hydrogen will be reported as the number of surface platinum atoms covered assuming one hydrogen atom per surface platinum atom. Calculating the quantity of hydrogen as $i_{lim}\tau$, we obtained the results in Table III. θ is the fraction of surface platinum atoms covered with hydrogen. The results are consistent with one another (considering that the capacity of the electrode might vary somewhat from one system to another). The results also agree with other authors who have anodically oxidized platinum from the hydrogen equilibrium potential, and who have concluded that the metal is covered largely with atomic hydrogen.^{10,11,30,37}

To realize further the importance of occluded hydrogen (as compared to that of adsorbed and gaseous hydrogen) experiments were run with palladium similar to those for platinum.

TABLE III

SURFACE COVERAGE OF PLATINUM ELECTRODE

Oxidant	i_{lim} , ma.	τ , sec.	θ
$36 \times 10^{-4} M$ Fe^{+3}	4.05	0.075	0.49
$16 \times 10^{-4} M$ Fe^{+3}	1.8	.15	.43
$18 \times 10^{-4} M$ Ce^{+4}	1.52	.32	.78
$18 \times 10^{-4} M$ $Fe(CN)_6^{-3}$	1.8	.14	.40
$5 \times 10^{-4} M$ MnO_4^-	5.42	.092	.80

(b) Palladium.—A palladium electrode gave results which were very different from those of platinum in two respects: (1) at a given polarization time or current (with other variables also being fixed), the depolarization time was very many times longer; and (2) in stirred solutions, the depolarization time for palladium was very sensitive to the time and current of polarization—*i.e.*, to the amount of hydrogen discharged at the surface. (1) and (2) above are exemplified in Fig. 2, which shows the depolarization curve for platinum and palladium in $0.45 M$ H_2SO_4 containing $3.2 \times 10^{-4} M$ MnO_4^- .

Palladium shows the same type of dependence on stirring rate and oxidant concentration as platinum.

Depolarization during CD.—When the rate of supply of internal hydrogen has become slow enough (due to the diminution of its source), and the surface concentration is sparse enough that oxidant can accumulate at the electrode surface, the potential rises sharply (C in Fig. 2). At this stage of the depolarization, reactions (i) and (ii) become important in determining the potential. The reason that the depolarization during part CD (as well as BC) for palladium is slower than that for platinum is also due to adsorbed hydrogen; this may be shown by slowing down the rate of transport of oxidant to the surface. If this is done (by suddenly decreasing the rate of stirring of the solution) the depolarization curve changes direction and the potential becomes negative again. When the transport rate of oxidant is decreased, the hydrogen concentration on the electrode actually increases since the diffusion rate of adsorbed hydrogen to the surface overtakes the rate of transport of oxidant.

When MnO_4^- or Ce^{+4} was used as the depolarizer, the depolarization curve leveled out much more slowly than in the case of the other oxidants (see Fig. 2 and 3). This was due to the formation of platinum (or pal-

(37) B. Ershler, *Acta Physicochim.*, **7**, 327 (1937).

ladium) oxide,^{2,38} which took place before the steady state could be attained.

The depolarization rate during CD depended on the concentration of oxidant and stirring rate qualitatively in the same manner as did $1/\tau$. In order to evaluate the idea that mass transport was the slow step a model was set up and compared with the experimental results with platinum. The Fe^{+2} - Fe^{-3} system was considered, since oxides were absent, and the oxidation-reduction reaction was assumed to be in equilibrium. Because of the geometry of the cell, the approximation was made that there was a diffusion layer of thickness δ around the electrode, beyond which the stirring of the solution kept the depolarizer concentration constant—the bulk concentration. Between the electrode surface and δ , a diffusion which obeyed Fick's law was assumed to be the only mode of mass transport. This model is very approximate since the immobile layer would vary in thickness from one part of the electrode to the other because of the motion of the liquid.

During the transition time, τ , Fe^{+3} does not accumulate at the electrode, so the initial condition is $\partial C_{\text{Fe}^{+3}}/\partial t = 0$. Therefore, from Fick's second law, $\partial C_{\text{Fe}^{+3}}/\partial x = \text{constant}$ where x is the radial distance out from the surface of the wire. Linear diffusion, rather than cylindrical diffusion, is sufficient here since the diffusion layer, δ , is small compared to the radius of the wire. We shall assume, for calculation purposes, that $C_{\text{Fe}^{+3}}$ is constant and equals $C^0_{\text{Fe}^{+3}}$ throughout CD, although the concentration of Fe^{+2} near the electrode is larger than its value in bulk and decreases with time. From the initial and boundary conditions $C_{\text{Fe}^{+2}}$ was obtained as a function of time using a Fourier series for the product solution to Fick's second law. Since the series converged very slowly, a Burroughs 205 Datatron was used to obtain numerical results to the resulting equation

$$C_{\text{Fe}^{+2}} = C^0_{\text{Fe}^{+2}} \left[1 - \sum_{n=1}^{\infty} \frac{8}{n^2 \pi^2} \exp\left(-\frac{n^2 \pi^2 D t}{4\delta^2}\right) \right] \quad (6)$$

The computer was set to calculate values for the series at a given t until two successive values differed by less than 10%, at which time the computer increased t and calculated the next series.

The experimental values were compared with the calculated ones by converting the experimental potential to $C_{\text{Fe}^{+2}}/C^0_{\text{Fe}^{+2}}$, and comparing the result with the calculated ratio. The theoretical results are shown in Fig. 5a for different values of the parameter δ , and the experimental curve, for $C^0_{\text{Fe}^{+2}} = 1.6 \times 10^{-3} M$ and $C^0_{\text{Fe}^{+3}} = 3.2 \times 10^{-3} M$ (in $0.45 M \text{H}_2\text{SO}_4$) is shown in Fig. 5b. Since there is no way of knowing at which

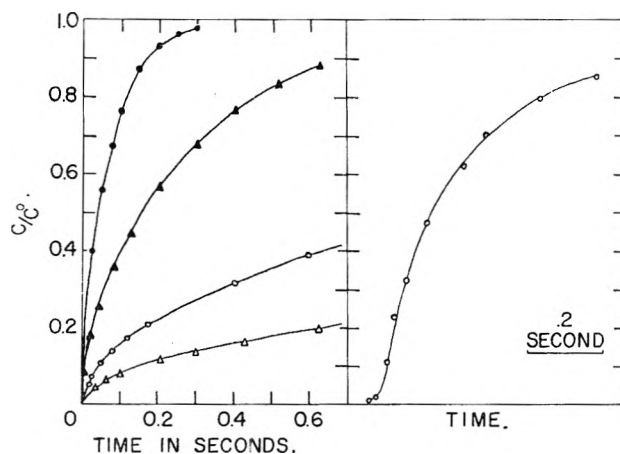


Fig. 5a (left).—Calculated values of C/C^0 : (●) = 0.001 cm.; (▲) = 0.002 cm.; (○) = 0.005 cm.; (△) = 0.01 cm. Fig. 5b (right): C/C^0 taken from experimental decay curve.

potential the oxidation-reduction couple becomes rate controlling, there is no way to choose $t = 0$ for the experimental curve. Therefore the upper half of the curves were compared to determine an optimum δ ; this can be seen to be approximately 0.0015 cm. The theoretical and experimental curves agree well from E_D down to C/C^0 values near 0.25, which is below the sharp bend in the depolarization curve (between C and D). Below this value the calculated C/C^0 drops much faster than the experimental one. This is because the Nernst equation no longer applies. The potential can change no faster than the double layer can be charged and this rate is at least as slow as the limiting current. Considering a constant double layer capacity of approximately $20 \mu\text{f./cm.}^2$, the dE/dt curve can never attain the steep asymptotic slope which the diffusion equation predicts. Some hydrogen probably is present during part of this potential climb. Neglecting the concentration polarization of Fe^{+2} would tend to make the curve less steep also. It is interesting to note that the limiting current obtained in this work resulted in a calculated value for δ of 0.0011 cm. ($i_{\text{lim}} = ADC^0 n F / \delta$). This calculation also uses the diffusion layer concept which must be considered only approximate.

Acknowledgments.—The authors wish to express appreciation for financial support of this work to the U. S. Army Ordnance under OOR Project Number 1889, Contract No. DA-04-495-ORD-959, to the U.S. Atomic Energy Commission under Contract No. AT-(11-1)-1144, and T. N. A. wishes to express appreciation to the National Science Foundation for a Coöperative Fellowship. They also wish to thank Mr. Edwin Dallin, Department of Chemical Engineering, for coding the computer for the diffusion problem.

(38) I. M. Kolthoff and N. Tanaka, *Anal. Chem.*, **26**, 632 (1954).

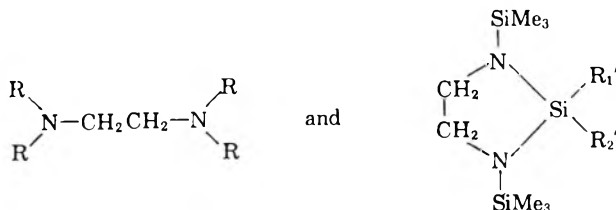
ORGANO SILYLETHYLENEDIAMINE COMPOUNDS. II. THE NUCLEAR MAGNETIC RESONANCE SPECTRA OF SILYLAMINES

BY D. KUMMER AND J. D. BALDESCHWIELER¹

Department of Chemistry, Harvard University, Cambridge 38, Massachusetts

Received May 31, 1962

The n.m.r. spectra of a series of known compounds of the types



indicate that the CH₂ group resonances in the heterocyclic molecules are characteristically about 0.30 p.p.m. downfield from the CH₂ resonances in the chain compounds. When one or two of the R groups in the chain compounds are hydrogen, the CH₂ group resonance shows complex fine structure. This structure is consistent with spectra calculated for XA₂B₂ or XA₂A₂'X' systems with reasonable values for the coupling constants. The NH protons are located by H¹-{N¹⁴} double resonance for these cases. The CH₂ group resonances in the heterocyclic systems show some structure when R₁' and R₂' are very different. It is shown that these features are very useful in the determination of the structures of mixed ring and chain compounds.

Introduction

There recently has been considerable interest in the synthesis of linear and cyclic silylamines.²⁻⁶ Simple linear and cyclic silylamines, for example, are of particular interest as model compounds for the study of silicon-nitrogen polymer systems.⁷ The structures of a number of simple silylamines have recently been determined by chemical methods.^{5,6} It is of interest to characterize the n.m.r. spectra of these compounds since the simple silylamines often appear as functional units in more complex silicon-nitrogen compounds.

The n.m.r. spectra of four known linear silylamines and four known cyclic silylamines are discussed in this paper. It is shown that the n.m.r. spectra of these compounds are consistent with the structures proposed from chemical evidence.^{5,6} The n.m.r. spectra of three new silylamines then are discussed in terms of the general features of the known compounds. It is shown that considerable information on the structure of even complex silylamines can be obtained directly from n.m.r. spectra.

Experimental

The preparation and properties of most of the linear and cyclic silylamines discussed here have been described previously.^{5,6} However, the preparation of compounds IV and VI has not been given previously.

Compound IV was prepared by reaction of Me₃SiNHCH₂CH₂NHSiMe₃ and C₆H₅SiCH₃Cl₂ in benzene according to the method described by Henglein and Lienhard⁸ (50% yield based on C₆H₅SiCH₃Cl₂), b.p. 64-65° (1 mm.), n_D²⁰ 1.4957.

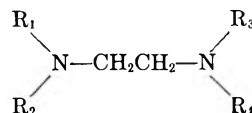
Anal. Calcd. for Si₃C₁₅H₃₀N₂: C, 55.83; H, 9.37; N, 8.68; (322.7). Found: C, 55.93; H, 9.26; N, 8.61; (319).

Compound VI was obtained by the reaction of CH₃NHCH₂CH₂NHCH₃ and (CH₃)₃SiN(C₂H₅)₂⁹ (30% yield), b.p. 211-212°, n_D²¹ 1.4340.

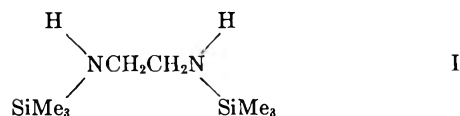
Anal. Calcd. for Si₂C₁₀H₂₈N₂ (232.5): C, 51.65; H, 12.14; N, 12.06. Found: C, 51.67; H, 11.97; N, 12.10; (209).

The n.m.r. spectra were obtained with Varian Associates A-60 and V-4300 high resolution n.m.r. spectrometers. The second radiofrequency field for the proton-nitrogen-14 double resonance experiments was supplied with a locked oscillator system that has been described previously.^{9a,b}

Linear Silylamines.—The proton chemical shifts in four compounds of the type



where the R groups include H, CH₃, and Si(CH₃)₃, are given in Table I. The preparation and chemical properties of these compounds have been discussed previously.^{5,6} The spectrum of compound I



includes a sharp peak at 9.99 τ , a complex multiplet centered at 7.38 τ , and a very broad peak centered at about 9.42 τ . These features are readily assigned from relative intensities to the SiMe₃ groups, the CH₂ bridge protons, and the N-H protons, respectively.

The spectrum of the CH₂ bridge protons consists of an unsymmetrical "triplet" structure as shown in Fig. 1. This spectrum arises from the mutual coupling of the NH protons with the bridge methylene groups. The spin system of interest can be described as an XA₂A₂'X' or XABA'B'X' type, where A and A' for example refer to protons that have the same chemical shift, but are not magnetically equivalent.¹⁰ A complete analysis of the XA₂A₂'X' system with the assumption of reasonable values of the coupling constants gives the calculated spectrum of the bridge protons that is also shown in Fig. 1. The value of J_{AA}

(9) (a) J. D. Baldeschwieler, *J. Chem. Phys.*, **36**, 152 (1962); (b) J. D. Baldeschwieler and E. W. Randall, *Chem. Rev.*, in press.

(10) J. A. Pople, W. G. Schneider, and H. J. Bernstein, "High-resolution Nuclear Magnetic Resonance," McGraw-Hill Book Co., Inc., New York, N. Y., 1959, p. 116.

(1) Alfred P. Sloan Foundation Fellow.

(2) C. Eaborn, "Organosilicon Compounds," Academic Press, New York, N. Y., 1960, p. 339.

(3) R. Fessenden and J. S. Fessenden, *Chem. Rev.*, **61**, 361 (1961).

(4) J. M. Maselli, "The Present State of Silicon-Nitrogen Chemistry," Technical Report Nonr-1866(13), October 11, 1961.

(5) D. Kummer and E. G. Rochow, *Z. anorg. allgem. Chem.*, in press (paper I in this series).

(6) F. A. Henglein and K. Lienhard, *Makromol. Chem.*, **32**, 218 (1959).

(7) (a) R. N. Minné and E. G. Rochow, *J. Am. Chem. Soc.*, **82**, 5625 (1960); (b) **82**, 5628 (1960).

(8) H. Pfeiffer, "A Contribution to the Chemistry of Silylamines and Silazanes," Technical Report Nonr-1866(13), Sept., 1961.

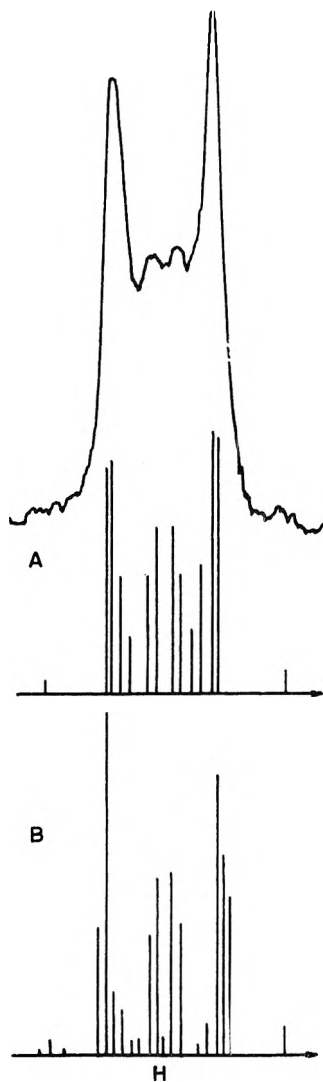


Fig. 1.—CH₂ bridge proton resonance of compound I and spectra calculated for (A) the XA₂A₂'X' case with $J_{AA} = J_{A'A'} = 10.4$ c./sec.; $J_{AA'} = J_{A'A} = 6.9$ c./sec.; $J_{XA} = J_{A'X'} = 7.1$ c./sec.; $J_{X'A} = J_{XA'} = 0.5$ c./sec., and (B) the XABA'B'X' case with the above coupling constants, and $\delta_{AB} = 2.0$ c./sec.

= $J_{A'A'}$ was assumed to be 10.4 c./sec.,^{11,12} the value of $J_{AA'} = J_{A'A}$ was taken as 6.9 c./sec.,¹³ and $J_{XA} = J_{X'A'} = 7.1$ c./sec. and $J_{X'A} = J_{XA'} = 0.5$ c./sec. were assumed.

It is of course possible that the methylene protons are not chemically equivalent, and that the spin system must be described as XABA'B'X' type. If the nitrogen atoms were tetrahedrally hybridized, and the rate of nitrogen inversion were very low, the nitrogen atoms could be considered as asymmetric centers (including the lone pair). In this case the two protons of a methylene group could be non-equivalent even if the populations of the three conformers were equal. Numerous examples of this type of non-equivalence have been reported.^{11,12,14,15}

An upper limit on δ_{AB} can be set by an examination of the spectrum of compound IV, where the NH protons have been replaced by CH₃ groups, but the nitrogen

- (11) J. S. Waugh and F. A. Cotton, *J. Phys. Chem.*, **65**, 562 (1961).
 (12) P. R. Shafer, D. R. Davis, M. Vogel, K. Nngarajan, and J. D. Roberts, *Proc. Natl. Acad. Sci. U.S.A.*, **47**, 49 (1961).
 (13) S. Stafford and J. D. Baldeschwieler, *J. Am. Chem. Soc.*, **83**, 4473 (1961).
 (14) H. Finegold, *Proc. Chem. Soc.*, 283 (1960).
 (15) P. M. Nair and J. D. Roberts, *J. Am. Chem. Soc.*, **79**, 4565 (1957).

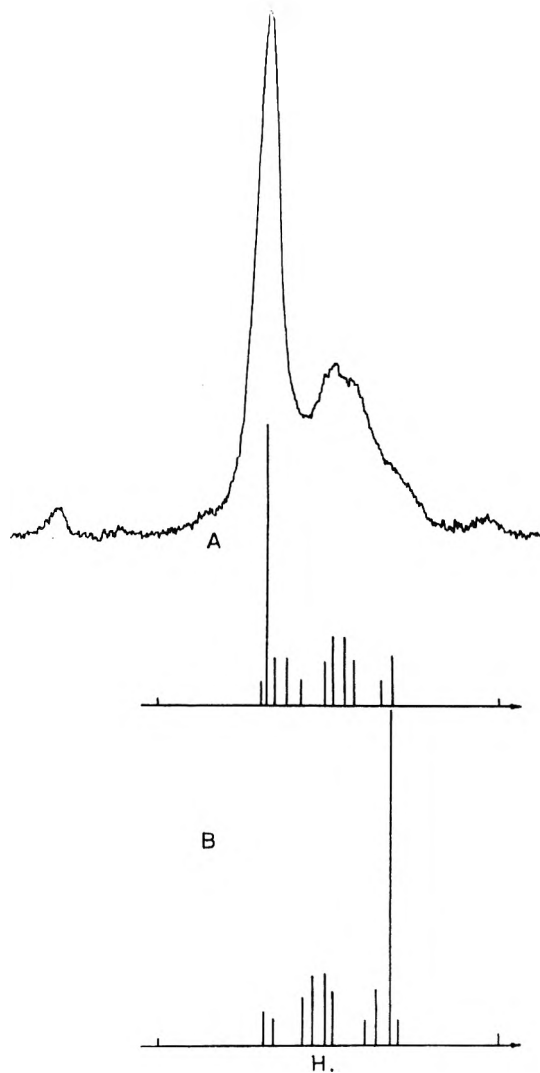
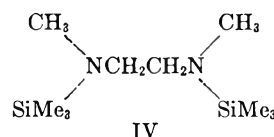


Fig. 2.—CH₂ bridge proton resonance of compound II, and spectra calculated for the A₂B₂X system with $J_{AA} = J_{BB} = 10.4$ c./sec., $J_{AB} = 6.9$ c./sec., $J_{BX} = 7.1$ c./sec., $J_{AX} = 0.5$ c./sec., and (A) $\delta_{AB} = -3.0$ c./sec. and (B) $\delta_{AB} = +3.0$ c./sec.



still may be asymmetrically substituted. The bridge proton resonance in this compound is a single sharp peak. Calculations performed for an ABA'B' system with $J_{AB} = J_{A'B'} = 10.4$ c./sec., and $J_{AA'} = J_{AB'} = 6.9$ c./sec. show that if δ_{AB} is larger than about 2 c./sec., additional detectable lines should be present in the spectrum. The spectrum calculated for the XABA'B'X' case using $\delta_{AB} = 2.0$ c./sec. and the same values of the coupling constants assumed for the XA₂A₂'X' calculation is also in agreement with the observed spectrum, as shown in Fig. 1.

It is also possible that with the large SiMe₃ substituents in compound I, the populations of the three conformers about the carbon-carbon bond of the bridge are different. The spectrum calculated for a *trans* arrangement of the nitrogen atoms with $\delta_{AB} = 0.0$ c./sec., $J_{AA'} = 15.0$ c./sec. (*trans* H-C-C-H coupling), and $J_{AB'} = 2.5$ c./sec. (*gauche* H-C-C-H coupling) is also in substantial agreement with the observed spectrum.

Since the wealth of structure that must be present

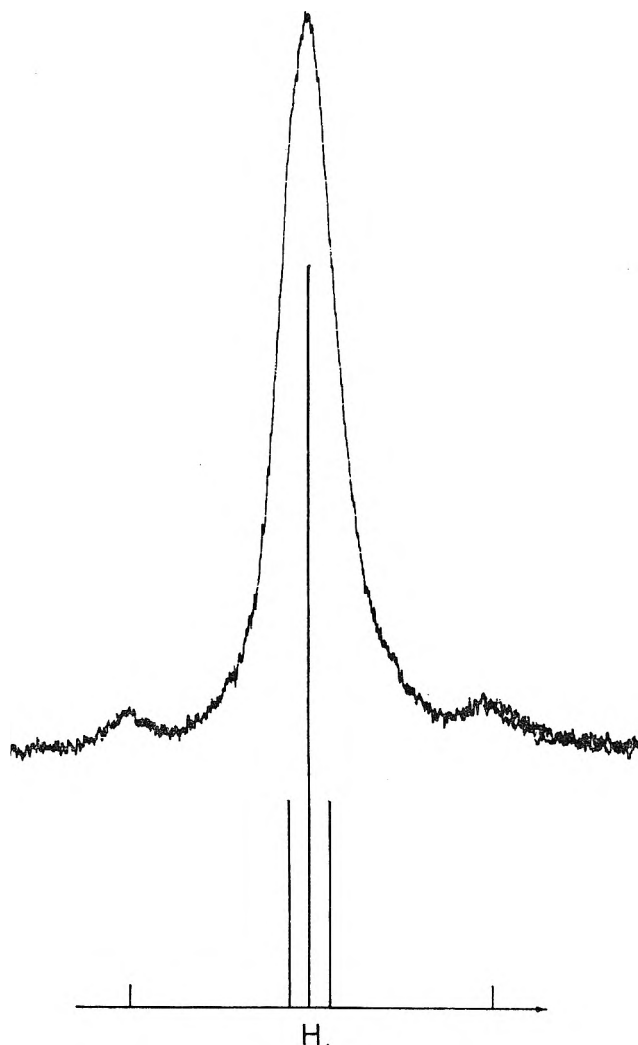
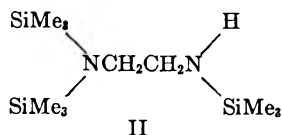


Fig. 3.—Ring CH₂ proton resonance of compound VI, and spectrum calculated for ABA'B' system with $J_{AB} = J_{A'B'} = 10.4$ c./sec., $J_{AA'} = J_{BB'} = 0.0$ c./sec., $J_{AB'} = J_{A'B} = 7.0$ c./sec., and $\delta_{AB} = 2.0$ c./sec.

in the CH₂ group resonance cannot be resolved, these interesting structural possibilities cannot be differentiated.

The assignment of the very broad resonance at 9.42 τ in compound I to the NH resonance has been confirmed by proton-nitrogen-14 double resonance.¹⁶ When a strong radiofrequency field is applied near the N¹⁴ resonance frequency, the NH resonance is sharpened considerably. The N¹⁴ resonance frequency can be measured by the double resonance method.¹⁷ The N¹⁴ resonance in I is 18.7 p.p.m. to low field of the N¹⁴ resonance in N¹⁴H₄⁺.¹⁸

The spectrum of compound II



includes two sharp peaks at 10.00 and 9.92 τ , and a complex multiplet at 7.40 τ . These resonances are readily assigned from intensity arguments to the single SiMe₃ group, the pair of SiMe₃ groups at one end of the mole-

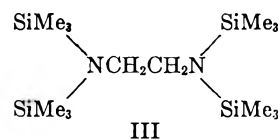
(16) E. W. Randall and J. D. Baldeschwieler, unpublished results.

(17) J. D. Baldeschwieler and E. W. Randall, *Proc. Chem. Soc.*, 303 (1961).

(18) E. W. Randall, "Studies in Electron Spin and Nuclear Spin Resonance Spectroscopy," Technical Report Nonr 1866(13), August, 1961.

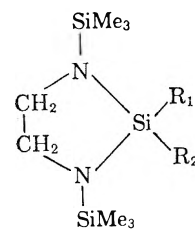
cule, and the CH₂ bridge protons, respectively. The bridge proton resonance is again complex, as shown in Fig. 2. Spectra calculated for an A₂B₂X system with $\delta_{AB} = \pm 3.0$, $J_{AA} = J_{BB} = 10.4$, $J_{AB} = 6.9$, $J_{BX} = 7.1$, and $J_{AX} = 0.5$ are also shown in Fig. 2 and indicate that the peak due to the CH₂ group closest to the —N—(SiMe₃)₂ group (the A₂ protons) lies at lower field than the resonance of the bridge protons adjacent to the —NHSiMe₃ group

The spectrum of compound III

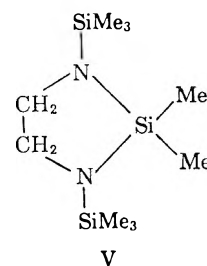


includes only two sharp lines at 9.94 and 7.29 τ . These are readily assigned to the SiMe₃ protons, and the bridge protons, respectively. The spectrum of compound IV consists simply of three sharp peaks at 9.99, 7.55, and 7.37 τ . These are again assigned on the basis of relative intensities to the SiMe₃, CH₃, and bridge protons, respectively.

Cyclic Silylamines.—The proton chemical shifts in four compounds of the type



where the R groups include CH₃, C₆H₅, and Cl are given in Table II. The preparation and chemical properties of these compounds have been discussed previously.^{5,6} The spectrum of compound V



consists of three sharp peaks at 9.94, 9.89, and 7.04 τ . These features can be assigned to the SiMe₃, CH₃, and ring CH₂ groups, respectively, from relative intensity arguments. Since the ring CH₂ resonance is a single sharp peak, the n.m.r. spectrum of V is consistent with the assumption that the five-membered ring is planar, and that the nitrogen atoms are either trigonally hybridized, or undergo rapid inversion. If the five-membered ring were non-planar, then the protons on the two CH₂ groups would not be equivalent and the CH₂ resonance would show a complex structure. Similarly, if the SiMe₃ groups were fixed above or below the plane, the CH₂ protons would again be non-equivalent, and two isomers of V might be expected with *cis* and *trans* arrangements of the SiMe₃ groups with respect to the plane of the ring. There is no evidence for these effects in the n.m.r. spectrum of V.

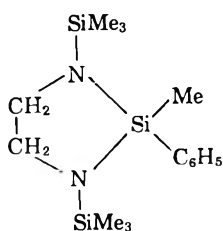
The spectrum of compound VI includes three peaks

TABLE I
PROTON CHEMICAL SHIFTS IN LINEAR SILYLAMINES

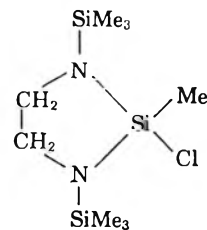
No.	R Groups				Chemical shifts, τ units, ± 0.02				
	R ₁	R ₃	R ₂	R ₄	CH ₂	R ₁	R ₂	R ₃	R ₄
I	SiMe ₃	H	SiMe ₃	H	7.38	9.99	9.42	9.99	9.42
II	SiMe ₃	SiMe ₃	SiMe ₃	H	7.40	9.92	9.92	10.00	9.42
III	SiMe ₃	SiMe ₃	SiMe ₃	SiMe ₃	7.29	9.94	9.94	9.94	9.94
IV	SiMe ₃	CH ₃	SiMe ₃	CH ₃	7.37	9.99	7.55	9.99	7.55

TABLE II
PROTON CHEMICAL SHIFTS IN CYCLIC SILYLAMINES

No.	R Groups		Chemical shifts, τ units, $+0.02$			
	R ₁	R ₂	CH ₂	SiMe ₃	R ₁	R ₂
V	CH ₃	CH ₃	7.04	9.94	9.89	9.89
VI	CH ₃	C ₆ H ₅	6.85	10.07	9.52	2.51, 2.83
VII	CH ₃	Cl	6.93	9.87	9.49	
VIII	Cl	Cl	6.84	9.82		



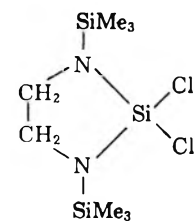
VI



VII

spectively. For this compound the CH₂ resonance is a single sharp peak, even though the substituents on the ring Si atom are different. Apparently for these substituents, δ_{AB} for the ring protons is too small for additional structure to be apparent.

The spectrum of compound VIII



VIII

centered at 10.07, 9.52, and 6.85 τ , as well as two groups of peaks centered at 2.83 and 2.51 τ . The two groups at 2.83 and 2.51 τ have an intensity ratio of 3:2, and are assigned to the phenyl protons. The peaks at 10.07, 9.52, and 6.85 τ can be assigned to the SiMe₃ group, the CH₃, and the ring CH₂ protons, respectively, on the basis of relative intensity.

The SiMe₃ and CH₃ resonances are single sharp peaks. However, the ring CH₂ resonance appears to be broadened, and to show some additional structure as shown in Fig. 3. Since the CH₃ and C₆H₅ substituents on the ring Si are very different, they destroy the plane of symmetry containing the ring. Thus the protons of the CH₂ groups above and below the ring are not equivalent, and structure due to the mutual coupling of these protons can appear. If the four protons are considered as an ABA'B' system, and the following constants are assumed: $\delta_{AB} = 2.0$, $J_{AB} = J_{A'B'} = 10.4$, $J_{AA'} = J_{BB'} = 0.0$, $J_{AB'} = J_{A'B} = 7.0$ c./sec., the calculated spectrum shown in Fig. 3 results. This calculation shows that the observed structure can result from non-equivalence of the CH₂ protons above and below the ring if reasonable values of the coupling constants are chosen.

The spectrum of compound VII consists of three sharp peaks at 9.87, 9.49, and 6.93 τ . These are readily assigned to the SiMe₃, CH₃, and ring CH₂ groups, re-

spectively. For this compound the CH₂ resonance is a single sharp peak, even though the substituents on the ring Si atom are different. Apparently for these substituents, δ_{AB} for the ring protons is too small for additional structure to be apparent.

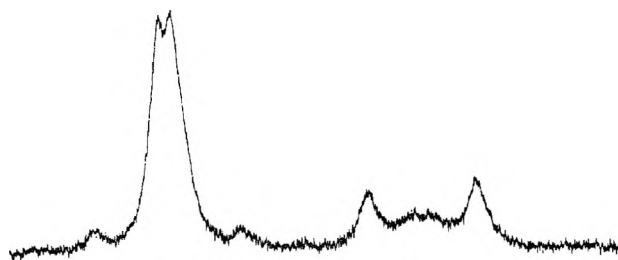
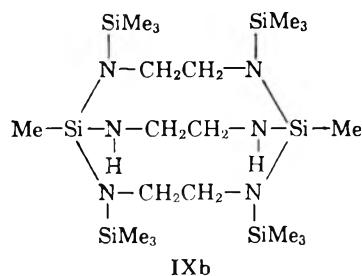
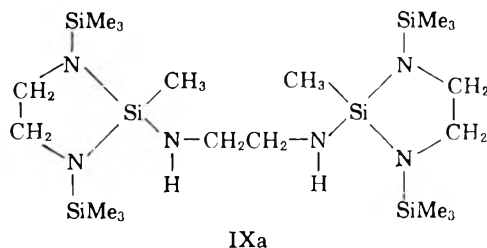
The spectrum of compound VIII includes only two sharp peaks at 9.82 and 6.84 τ , which are assigned to the SiMe₃ and ring CH₂ groups. The CH₂ resonance shows no structure as would be expected for symmetrical substitution of the ring Si atom.

A comparison of the chemical shifts given in Tables I and II indicates that the ring CH₂ resonances seem to be generally about 0.30 p.p.m. downfield from the CH₂ resonances in the linear compounds. This fact is particularly useful in distinguishing between linear and cyclic ethylenediamine groupings in more complex molecules.

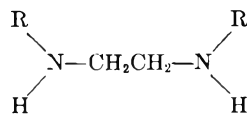
Mixed Linear and Cyclic Silylamines.—The reaction of Me₃SiNHCH₂CH₂NHSiMe₃ with MeSiCl₂ gives a complex silylamine with the formula Si₆C₂₀H₅₆N₆, based on chemical analysis and molecular weight.⁵ From chemical evidence, two structures can reasonably be proposed for this compound.

The spectrum of compound IX consists of peaks centered at 9.98, 9.93, 9.44, 7.27, and 6.97 τ . The peaks at 9.98 and 9.93 τ have a relative intensity of about 1:6, and must be assigned to the SiMe₃ and CH₃ resonances in either structure. The resonance at 9.44 τ is very broad and weak, and could arise from the NH protons in either structure.

The resonances at 7.27 and 6.97 τ have a relative intensity of 1:2, and both show additional structure as shown in Fig. 4. These peaks must be assigned to the remaining CH₂ groups. The resonance centered at

Fig. 4.—CH₂ proton resonances of compound IX.

7.27 consists of an asymmetric "triplet" pattern that is characteristic of the CH₂ protons of the six-proton system

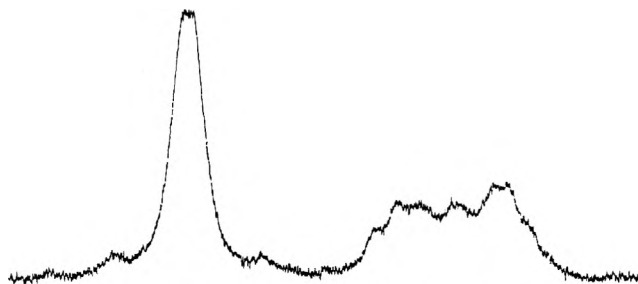


as illustrated by compound I. This feature clearly must be assigned to a $\begin{matrix} \diagup & & \diagdown \\ & \text{N}-\text{CH}_2\text{CH}_2-\text{N} & \\ \diagdown & & \diagup \\ & \text{H} & \end{matrix}$ group,

which, however, is also present in both IXa and IXb.

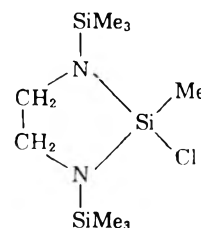
A decision between IXa and IXb must then be based on the resonance at 6.97 τ . This peak is in the range of chemical shifts observed for ring CH₂ groups in compounds V through VIII, as given in Table II. In compound IXa, the two substituents on the ring silicon atoms ($-\text{CH}_3$ and $-\text{NHCH}_2\dots$) are very different. Thus the structure that is observed on the peak at 6.97 τ could arise from non-equivalence of the ring CH₂ protons as in compound VI. In fact, the structure on the 6.97 τ peak is very similar in appearance to the CH₂ structure in compound VI as shown in Fig. 3. Thus, the n.m.r. spectrum is consistent in every detail with the proposed structure IXa.

If it is assumed that the $\begin{matrix} \diagup & & \diagdown \\ & \text{N}-\text{CH}_2\text{CH}_2-\text{N} & \\ \diagdown & & \diagup \\ & \text{H} & \end{matrix}$ group in structure IXb is analogous to the similar group in compound I, then it is reasonable to suggest that the remaining $\begin{matrix} \diagup & & \diagdown \\ & \text{N}-\text{CH}_2\text{CH}_2-\text{N} & \\ \diagdown & & \diagup \\ & \text{SiMe}_3 & \end{matrix}$ groups must

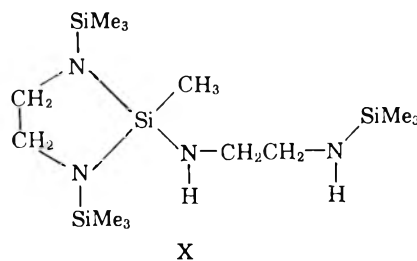
Fig. 5.—CH₂ proton resonances of compound X.

be similar to compound III. Thus a shift of the CH₂ protons 0.30 τ downfield in structure IXb is difficult to justify. No structure was observed on the CH₂ resonances in compound IV. It seems unlikely that the additional constraints imposed by structure IXb could cause the non-equivalence of the CH₂ protons required to give the structure on the 6.97 τ peak. Thus the n.m.r. spectrum indicates that IXa is the more probable structure for this compound.

In the reaction of



with $\text{NH}_2\text{CH}_2\text{CH}_2\text{NH}_2$, a product is obtained with the formula $\text{Si}_4\text{C}_{14}\text{H}_{40}\text{N}_4$ based on analysis and molecular weight.⁵ The probable structure of this compound from chemical arguments⁵ is



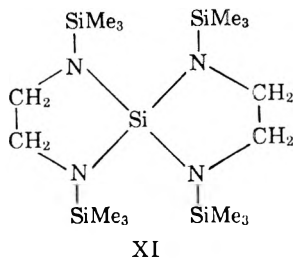
The spectrum of this compound consists of resonances centered at 9.97, 9.94, 9.91, 7.31, and 7.01 τ . The peaks at 9.97, 9.94, and 9.91 τ can be assigned to the SiMe₃ protons on the chain, the $-\text{CH}_3$ group, and the ring SiMe₃ groups, respectively. The features centered at 7.31 and 7.01 τ show structure as indicated in Fig. 5. The peak at 7.31 τ is assigned to the linear

$\begin{matrix} \diagup & & \diagdown \\ & \text{N}-\text{CH}_2\text{CH}_2-\text{N} & \\ \diagdown & & \diagup \\ & \text{H} & \end{matrix}$ grouping. The structure arises

from the coupling of the six protons which must be considered for example as an XA₂B₂Y grouping, since the groups R and R' are quite different. The feature at 7.01 τ is assigned to the ring CH₂ groups which show structure as in compound IXa since the substituents of the ring Si atom ($-\text{CH}_3$ and $-\text{NHCH}_2\dots$) are quite different. Thus the n.m.r. spectrum of compound X is consistent with the most probable structure predicted from chemical evidence.⁵ A comparison of the proton spectra of compounds VII, VI, X, and IX,

where the substituents on the ring Si atom are Me, Cl; Me, C₆H₅; Me, NHCH₂CH₂NHSiMe₃; and Me, NHCH₂CH₂NHSiCH₃(NSiMe₃CH₂—)₂ shows very clearly the effect of increasing the size of one substituent on the non-equivalence of the ring protons.

In the reaction of Me₃SiNHCH₂CH₂NHSiMe₃ with SiCl₄, a crystalline compound is obtained with a formula given by analysis and molecular weight as Si₅C₁₆H₄₄N₄.⁵ On the basis of chemical arguments, only one reasonable structure can be proposed for this compound



The spectrum of this compound consists of only two sharp peaks at 9.94 and 6.91 τ . These must be assigned to the SiMe₃ and ring CH₂ groups. Since the planes of symmetry of both rings are maintained in this struc-

ture, no structure is expected on the CH₂ resonances. Thus the n.m.r. spectrum of compound XI is in good agreement with the proposed structure.

Conclusion

Compounds I through VIII illustrate a number of characteristic features of the n.m.r. spectra of linear and cyclic silylamines. These features include both proton chemical shifts and structure arising from proton spin-spin coupling in certain functional groupings. The utility of these features in differentiating structures that involve both cyclic and linear diamine groupings has been illustrated with three new compounds. A detailed analysis of the n.m.r. spectra of functional groups of this type is of particular use in the determination of the structures of silicon-nitrogen polymers.¹⁹

Acknowledgments.—The assistance of Professor E. G. Rochow in this study is gratefully acknowledged. The work was carried out with the financial support of the National Science Foundation and the Office of Naval Research. The computations were performed with the I.B.M. 7090 computer of the Massachusetts Institute of Technology Computation Center.

(19) E. G. Rochow and D. Kummer, to be published.

VAPOR PRESSURE AND HEAT OF SUBLIMATION OF CALCIUM FLUORIDE^{1,2}

By DAVID A. SCHULZ AND ALAN W. SEARCY

Department of Mineral Technology and Inorganic Materials Research Division, Lawrence Radiation Laboratory, University of California, Berkeley, California

Received June 4, 1962

The vapor pressure of CaF₂ was investigated in the temperature range 1400 to 1850°K. by the torsion-effusion method. The vapor pressure (in atmospheres) of β -CaF₂ is given by the equation $\log P = -19.973/T + 7.8717$ in the experimental range. Extrapolation yields a calculated normal boiling point of 2786°K. and a heat of sublimation at 298°K. of 101.2 kcal. by the third-law method and 101.4 kcal. by the second-law method. Molecular-streaming conditions were demonstrated to break down when the mean free path became about as short as the orifice diameter, but a dependence on orifice length as well as orifice diameter was observed.

Introduction

The only vapor pressure measurements that have been available for calcium fluoride were obtained by Ruff and Le Boucher by use of a dynamic method.³ Their method entailed observation of the temperature at which a substance begins to boil when under an experimentally fixed ambient pressure and could be applied only for determination of vapor pressures of liquids. The lowest temperature of measurement by Ruff and Le Boucher was 2086°K.

It seemed desirable to measure the vapor pressure of CaF₂ at lower temperatures in order to check the reported pressures and obtain a value for the heat of sublimation at 298°K. from data that required less extrapolation. The torsion-effusion method was applied in the research reported here.^{4,5}

Experimental

In the torsion-effusion method, an effusion cell is suspended in a vacuum furnace by a fine wire. Upon heating, vapor escapes through eccentrically placed orifices in the cell, thereby exerting a

torsional force on the wire. The angle through which the cell is turned is measured, and from this angle the vapor pressure can be calculated by means of the formula $P = 2\phi D / (\Sigma qaf)$, where P is the vapor pressure, D is the torsion constant of the wire, q is the perpendicular distance from the cell center to the axis of the effusion hole, a is the area of the orifice, f is the force-reduction factor due to finite orifice channel length, and ϕ is the angle through which the cell has rotated. Values for f have been tabulated by Freeman and Searcy,⁶ Detkov,⁷ and Schulz and Searcy.⁸

For this research, the suspension thread was 17 in. of 2-ml. diam. tungsten wire. Components of the effusion cell and cell block were of National Carbon AUC premium graphite. Four chambers with axes $7/16$ in. from the center of the cell block were drilled into the side of the block, two each on opposing faces. Two loaded effusion cells with effusion orifices oriented to yield additive torques were fitted into two of the four chambers of the cell block. Empty cells were fitted into the other two chambers. In other runs the positions of the effusion cells and of the empty cells were reversed in order to evaluate and subtract the influence of a residual torque that resulted from electromagnetic repulsion of the torsion assembly by the alternating field of the furnace element.⁹

The calcium fluoride used in this work was supplied by Dr. K. K. Kelley of the U. S. Bureau of Mines and was from the same lot as that on which Naylor performed heat-content experiments.¹⁰

(1) This work was done under the auspices of the U. S. Atomic Energy Commission.

(2) From the thesis submitted by D. A. Schulz in partial fulfillment of the requirements of the Ph.D. degree.

(3) O. Ruff and L. Le Boucher, *Z. anorg. allgem. Chem.*, **219**, 376 (1934).

(4) H. Mayer, *Z. Physik*, **67**, 240 (1931).

(5) M. Vollmer, *Z. physik. Chem., Bodenst. Festband*, 863 (1931).

(6) R. D. Freeman and A. W. Searcy, *J. Chem. Phys.*, **22**, 762 (1954).

(7) S. P. Detkov, *Zh. Fiz. Khim.*, **34**, 1634 (1960).

(8) D. A. Schulz and A. W. Searcy, *J. Chem. Phys.*, **36**, 3099 (1962).

(9) A. W. Searcy and D. A. Schulz, to be submitted to *J. Chem. Phys.*

(10) B. Naylor, *J. Am. Chem. Soc.*, **67**, 150 (1945).

TABLE I: TEMPERATURE, PRESSURES, AND RATIOS OF MEAN FREE PATH TO ORIFICE DIAMETER

Temp., °K.	Pressure, atm.	λ/d	ΔH_{298}° , kcal.	Temp., °K.	Pressure, atm.	λ/d	ΔH_{298}° , kcal.
1624	4.284×10^{-6}	0.63	100.77 ^a	1788	4.816×10^{-4}	.25	100.86 ^a
1612	3.256×10^{-6}	0.83	100.98 ^a	1779	4.157×10^{-4}	.29	100.96 ^a
1598	2.494×10^{-6}	1.07	101.03	1770	3.576×10^{-4}	.33	101.05 ^a
1584	1.862×10^{-6}	1.42	101.15	1762	3.109×10^{-4}	.38	101.17 ^a
1564	1.251×10^{-6}	2.09	101.25	1748	2.566×10^{-4}	.46	101.17 ^a
1550	9.652×10^{-6}	2.69	101.23	1734	2.069×10^{-4}	.56	101.27 ^a
1530	6.614×10^{-6}	3.87	101.16	1715	1.453×10^{-4}	.80	101.58 ^a
1516	4.927×10^{-6}	5.15	101.22	1700	1.200×10^{-4}	.96	101.51 ^a
1497	3.472×10^{-6}	7.23	101.06	1696	1.163×10^{-4}	.98	101.39 ^a
1477	2.308×10^{-6}	10.73	101.04	1679	9.163×10^{-5}	1.24	101.31
1467	1.793×10^{-6}	13.72	101.12	1668	7.750×10^{-5}	1.45	101.25
1449	1.240×10^{-6}	19.61	101.08	1656	6.337×10^{-5}	1.76	101.25
1435	8.724×10^{-7}	27.61	101.21	1640	4.881×10^{-5}	2.27	101.25
1421	6.175×10^{-7}	38.64	101.25	1346	1.185×10^{-3}	0.10	100.20 ^a
1630	4.804×10^{-6}	0.57	100.77 ^a	1833	1.003×10^{-3}	.12	100.25 ^a
1616	3.578×10^{-6}	0.76	100.90 ^a	1820	8.204×10^{-4}	.15	100.39 ^a
1610	3.083×10^{-6}	0.87	101.04 ^a	1805	6.434×10^{-4}	.19	100.61 ^a
1592	2.174×10^{-6}	1.23	101.12	1795	5.415×10^{-4}	.22	100.74 ^a
1576	1.605×10^{-6}	1.64	101.16	1781	4.313×10^{-4}	.25	100.56 ^a
1556	1.087×10^{-6}	2.40	101.17	1765	3.252×10^{-4}	.32	100.69 ^a
1541	8.336×10^{-6}	3.10	101.11	1753	2.714×10^{-4}	.44	101.25 ^a
1518	5.306×10^{-6}	4.79	101.10	1739	2.224×10^{-4}	.53	101.28 ^a
1506	3.937×10^{-6}	6.41	101.25	1729	1.897×10^{-4}	.61	101.32 ^a
1484	2.670×10^{-6}	9.32	101.08	1721	1.575×10^{-4}	.74	101.63 ^a
1470	1.986×10^{-6}	12.42	101.03	1711	1.359×10^{-4}	.85	101.62 ^a
1456	1.475×10^{-6}	16.56	101.03	1689	1.054×10^{-4}	1.08	101.36
1442	1.047×10^{-6}	23.13	101.11	1676	8.747×10^{-5}	1.29	101.28
1427	7.089×10^{-7}	33.79	101.26	1664	7.181×10^{-5}	1.56	101.27
1830	9.479×10^{-4}	0.13	100.28 ^a	1649	5.814×10^{-5}	1.92	101.13
1821	8.013×10^{-4}	.15	100.50 ^a	1634	4.540×10^{-5}	2.43	101.13
1812	6.954×10^{-4}	.18	100.55 ^a	1625	3.883×10^{-5}	2.83	101.12
1795	5.423×10^{-4}	.22	100.74 ^a	1611	3.106×10^{-5}	3.51	101.07

^a All heats bearing this symbol were calculated from experimental data for which the mean free path was less than the diameter of the effusion hole. These heats were not considered in the computation of the average therefore. The first 28 measurements were made with the larger orifices.

Two sets of lids were used. One set had orifices that were 0.08 cm. in diameter and 0.04 cm. thick, and the other had orifices 0.32 cm. in diameter and 0.04 cm. long. The cell block, crucibles, and lids were degassed at 1900°. Samples were heated in cells whose lids contained no holes, in order to check for torque produced by sample leakage; none was found.

In a typical run, about 1 g. of calcium fluoride was loaded into each of the two effusion cells. Covers were placed over the apertures in the cells, and the cells then were fitted into the selected pair of holes in the cell block. Counter cells, containing no sample, were placed in the remaining pair of holes. In making a run, the power was turned on and gradually raised, while the ambient pressure was kept below 5×10^{-6} mm. until a deflection of about 1 radian was noted on the circular scale. The cell was allowed to remain at this power setting for about 1 hr.; then the deflection and temperature were recorded. The temperature was lowered in steps of 10 to 20°, and allowed to equilibrate at each temperature for 20 min. Deflection and temperature readings were taken, the temperature was again lowered 10 to 20°, and the procedure was repeated until the deflection became too small to measure. After the system had reached room temperature, the zero-point position was noted.

To obtain corrections for the residual deflection, runs were made in which the effusion holes were placed to reverse the direction of torque. With this arrangement, the residual deflection became subtractive. The two orientations of effusion holes yielded pairs of flaring deflections *vs.* $1/T$ curves, very close together at high pressures and parting at lower ones. Smooth curves were drawn through both sets of points. For every data point in each set, an isothermal line was drawn intersecting the smoothed curve through the other set. The data points of each curve then were averaged with the intercepts of the smoothed curve with the other curve to obtain corrected deflections. These corrected deflections then were converted into pressures. These pressures, corrected for thermal expansion of the cell parameters,

are shown in Table I and Fig. 1. A more detailed description of the apparatus and techniques is given in a previous paper.⁹

Results and Discussion

Studies on low-pressure gas flow have demonstrated that the molecular flow equations become inapplicable when the mean free path of the vapor approximately equals the diameter of the effusion orifice. Table I, therefore, shows for each measurement the calculated ratios λ/d of the mean free path to the average orifice diameter in addition to the pressure and the third-law value of the heat of sublimation at 298°K. Orifice lengths l and diameters d for each cell are listed in Table II. These ratios were calculated by using the hard-sphere approximation,¹¹ with the molecular diameter of CaF_2 taken as 7.4 Å., the sum of ionic diameters at room temperature. The numerical values of λ/d calculated by this approximation cannot be quantitatively correct, but they are satisfactory for internal comparisons.

In Fig. 1, open circles and squares indicate those points with calculated λ/d ratios less than unity; those with ratios greater than unity are shown as closed circles and squares. The solid line of the graph is calculated from heats of sublimation obtained from the low-temperature data. As can be seen from this graph, when the larger orifice was used, molecular flow prevailed to just the temperature for which λ/d is calculated to be unity. When the smaller orifice was used, molecular flow prevailed to a temperature for which λ/d is calculated to be about 0.3.

TABLE II
 ORIFICE DIMENSIONS^a

Cell	Hole diameter <i>d</i> , cm.		Lid thickness <i>l</i> , cm.		Channel factor <i>f</i>		Moment arm <i>q</i> , cm.	
	(1)	(2)	(1)	(2)	(1)	(2)	(1)	(2)
1	0.32160	0.32314	0.03759	0.04064	0.92704	0.92171	0.8684	0.8700
2	.32160	.32314	.03759	.04064	.92704	.92171	.8827	.8827
3	.07984	.07939	.04115	.04064	.72645	.72788	.8684	.8700
4	.07984	.07939	.04115	.04064	.72645	.72788	.8827	.8827

^a The torsion constant for these runs was 1.9897 dyne-cm.-rad.⁻¹.

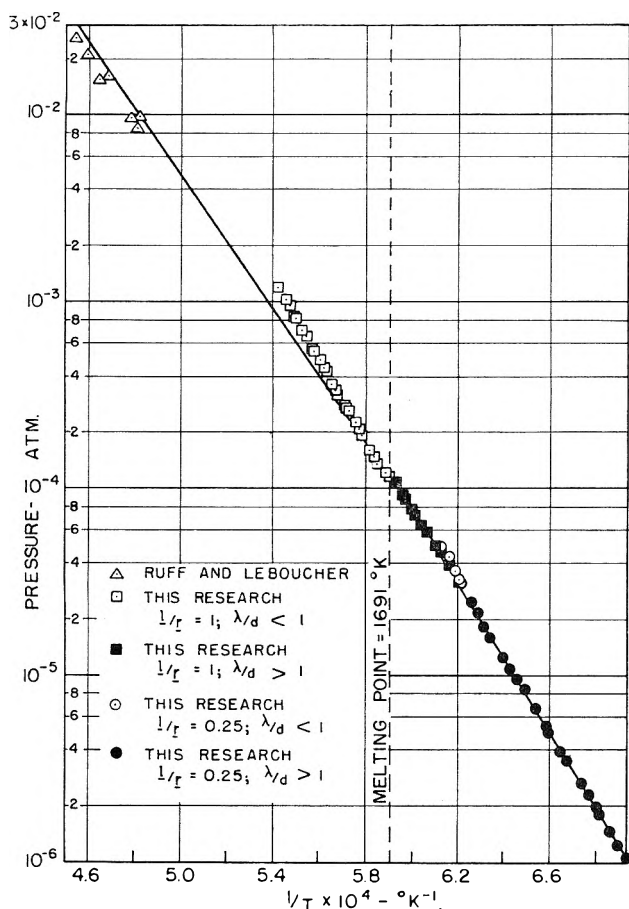


Fig. 1.—The vapor pressure of calcium fluoride.

For β -CaF₂ the vapor pressure in atmospheres is given by the expression $\log P = -19,973/T + 7.8717$. The heat of sublimation of α -CaF₂ at 298°K. was calculated from the lower-temperature data for each orifice by both the second-law (sigma-plot) method and third-law method. For the sigma-plot method the equation

$$\Sigma = -R \ln p + \Delta a \ln T + \frac{1}{2} \Delta b T = \frac{\Delta H_1^0}{T} + I$$

was used. In this equation ΔH_1^0 and I are constants from which the heat and entropies of sublimation can be calculated, and a and b are the constants in the heat-capacity equation $C_p = a + bT$.

For β -CaF₂ Kelley¹² reports that $C_p = 25.81 + 2.50 \times 10^{-3}T$ ($\pm 0.1\%$) in the range from 1424 to 1691°K. Brewer, *et al.*,¹³ have estimated the vibration frequencies for gaseous CaF₂ to be 484, 95(2), and 675 cm.⁻¹. Heat capacities were calculated from these frequencies at 50° intervals.

(11) S. Dushman, "Scientific Foundations of Vacuum Technique," John Wiley & Sons, Inc., New York, N. Y., 1949, Chapter 1.

(12) K. K. Kelley, U. S. Bureau of Mines Bulletin 584, 39 (1960).

(13) L. Brewer, G. Somayajulu, and E. Brackett, Lawrence Radiation Laboratory Report UCRL-9840, September, 1961.

The least-squares calculation yields $\Sigma = (111,615)/T - 133.27$, from which $\Delta H_1^0 = 111,615$, and $\Delta H_{1543}^0 = 91.50$ kcal. This compares with $\Delta H_{1543}^0 = 91.39$, which is calculated from the assumption that $\Delta C_p = 0$ in the experimental range. Graphical integration of the heat capacities from 298 to 1543°K. yields 17.99 kcal. The difference in heat content between α -CaF₂ at 298° and β -CaF₂ at 1543° is 27.93 kcal.¹² Therefore, ΔH_{298}^0 for sublimation of α -CaF₂ is calculated to be 101.44 kcal.

Free-energy functions for the third-law calculations were available for the gas at 500° intervals,¹³ and heat-content and entropy data were available for the solid at 100° intervals.¹² Kelley and King list 16.46 ± 0.08 e.u. as the entropy of α -CaF₂ at 298°K.¹⁴ Free-energy functions were plotted for the condensed phases and the gas, and smooth curves were drawn through each set. Free-energy functions read from the curves were combined with the individual pressure values in the equation

$$\Delta H_{298}^0 = -RT \ln p - T \frac{\Delta F_{298}^0 - \Delta H_{298}^0}{T}$$

to yield ΔH_{298}^0 values. The average third-law ΔH_{298}^0 value with standard deviation from the 11 lowest-temperature vapor-pressure points obtained with the small effusion holes is 101.22 ± 0.02 kcal. The average from 23 points when a hole 16 times greater in area was used is 101.14 ± 0.02 kcal. The apparent error is therefore ± 0.06 kcal. between the two sets or the average ΔH_{298}^0 is 101.17 ± 0.06 kcal. The sum of the errors made in measuring orifice areas, lid thicknesses, moment arms, and torsion constants should not contribute more than a 2% error in the calculated vapor pressures. Deflections were read to the nearest 0.001 radian and therefore contribute possible errors of 0.1% at the higher deflections and 10% for 0.01 radian deflections. Pressure errors then should vary from 2 to 12%, depending upon the magnitude of the deflection. Black-body conditions for temperature measurement were established by use of several holes of varied depths. No dependence of measured temperature on hole depth was found. The National Bureau of Standards certifies the corrected table of temperatures for the pyrometer used to be accurate to within $\pm 3^\circ$ in the temperature range investigated. An error of about $\pm 3^\circ$ arises from the problem of matching brightness in our experiments. Since the $\pm 3^\circ$ calibration uncertainty arises largely from the same problem of matching brightnesses, a total error of $\pm 5^\circ$ in temperature is estimated.

The pressure and temperature errors could therefore amount to uncertainties of 0.4% in the ΔH_{298}^0 values obtained from large deflections and 0.7% in values from

(14) K. K. Kelley and E. G. King, U. S. Bureau of Mines Bulletin 592 (1961).

the smallest deflections used. Other errors to be considered are those contained in the free-energy functions. If all estimated errors are taken into account, a gross uncertainty of 1 kcal. is estimated for the heat of sublimation at 298°K.

From the third-law average value $\Delta H_{298}^0 = 101.17 \pm 1.0$, the heat of sublimation of β -CaF₂ at its melting point is calculated to be 89.01 kcal.

Extrapolation with heat-capacity data for the liquid and gas yields calculated vapor pressures in the liquid range. The normal boiling point and heat of vaporization at the boiling point are calculated to be 2786°K. and 72.0 kcal. In Fig. 1, the liquid pressure curve calculated from the third-law data is seen to be in good agreement with experimental points of Ruff and Le Boucher.³ The low-temperature data extrapolated over 300° from below the melting point yield pressure values higher by less than 30% than those of Ruff and Le Boucher.

In these calculations it is assumed that CaF₂(g) was the vaporizing species. The only gaseous calcium fluoride molecule yet observed spectroscopically is CaF(g).¹⁵ However, thermodynamic calculations show that the total pressure to be expected from the reaction $\text{CaF}_2(l) \rightarrow \text{CaF}(g) + \text{F}(g)$ would be at least several orders of magnitude below the observed pressures. Calculations also demonstrate that dissociation to elemental calcium and fluorine gas is negligible. Hammer found magnesium fluoride vapor to have the molecular weight of MgF₂ monomer molecules.¹⁶ Calcium fluoride was expected, therefore, to evaporate primarily to CaF₂ monomer molecules.

The upturn in apparent pressures that was observed when the mean free path λ became small relative to orifice dimensions could be due to increased importance of a second vapor species. However, the temperature at which a second species reaches measurable concentrations would be independent of orifice area if the second species evaporated with a high evaporation coefficient. If the second species evaporated with a low evaporation coefficient, the increase in apparent pressure should appear at lower pressures with the smaller orifice rather than at higher pressures.

An upturn in apparent pressures when λ reaches lengths comparable with the orifice dimension has been observed by us for tin and has been studied in some detail.⁹ The results of that study and this one are easily understood in terms of onset of viscous flow, and no other explanation appears equally plausible.

The excellent agreement between heats of sublimation calculated by the second- and third-law methods and between our extrapolated pressures and the measured pressures of Ruff and Le Boucher lend confidence to the conclusion that the correct evaporation reaction has been chosen.

(15) G. Herzberg, "Molecular Spectra and Molecular Structure. I. Spectra of Diatomic Molecules," D. Van Nostrand Co., New York, N. Y., 1950.

(16) R. R. Hammer, "The Vapor Pressure of Magnesium Fluoride," Ph.D. Thesis, University of California, September, 1961.

More important than the thermodynamic information *per se* is the clear demonstration obtained here of the breakdown in applicability of the molecular streaming conditions which are necessary for validity of the torsion-effusion method. Apparently, this work and a second study by us⁹ constitute the only detailed investigations yet made of the high pressure limit to the force-of-effusion equations, although an important study by Carlson (under the guidance of P. W. Gilles and R. J. Thorn) of the high pressure limit to the Knudsen effusion weight loss equation provides closely related information.¹⁷

Our two studies demonstrate that the limiting mean free path at which the force equations can be applied may be much more sensitive to l/d than is the path in measurements of the total weight loss.¹⁷ A change of the ratio of channel length l to orifice diameter d in this study from $1/2$ to $1/8$ increased the limiting value of λ/d from 0.3 to 1. Shortening the orifice length appears definitely to reduce the upper pressure limit to which the force-of-effusion equation can be applied. This difference may arise because the force measurements are more sensitive than total weight loss measurements to scattering of molecules traveling at small angles relative to the axis of the orifice.

Carlson has hypothesized that the presently unexplained upturn in apparent vapor pressures of uranium dioxide¹⁸ may have arisen from onset of viscous flow, but he did not feel justified in a firm conclusion, probably because the upturn in the uranium dioxide study was pronounced when λ/d was as high as 6 (assuming a linear ionic model for the gas collision diameter) and was observable when λ/d was about 60. Carlson's own results indicated that the upturn should begin when λ/d was approximately 1.

However, for the investigation of uranium oxide, the pressures were calculated from the quantity of material that effused through a very thin orifice in a cone whose sides made an angle of only about five degrees with the orifice axis. We conclude that, for short orifices and small angles to the normal, deviations from molecular streaming conditions may well be observable under the conditions for which the uranium oxide pressure upturn was observed.

The inference drawn¹⁸ from the research of Johnson¹⁹ that molecular streaming equations may be used for short orifices when values of λ/d are less than 0.1 appears definitely disproved, although for orifices with longer channels the equations may possibly be applied in force or collection measurements when λ/d is of the order of 0.1. This last point requires further study.

Acknowledgment.—We gratefully acknowledge the valuable counsel of Dr. David J. Meschi in the design and operation of the equipment.

(17) K. D. Carlson, "The Molecular and Viscous Effusion of Saturated Vapors," ANL-6156, April, 1960.

(18) R. J. Ackermann, P. W. Gilles, and R. J. Thorn, *J. Chem. Phys.*, **25**, 1089 (1956).

(19) T. H. Johnson, *Phys. Rev.*, **31**, 103 (1928).

THE SURFACE COMPOSITION OF A DILUTE SOLID SOLUTION OF CALCIUM CHLORIDE IN SODIUM CHLORIDE

By J. T. KUMMER AND J. D. YOUNGS

Scientific Laboratory, Ford Motor Company, Dearborn, Michigan

Received June 4, 1962

It is shown that the surface of a dilute solid solution of CaCl_2 in NaCl contains a higher concentration of calcium than the bulk. The higher catalytic activity of the solid solution toward ethyl chloride dehydrohalogenation than NaCl alone can be accounted for by the high concentration of calcium ions on the surface of the solid solution.

It has been shown by Grimm and Schwamberger¹ that a number of ionic crystals including NaCl and CaCl_2 can be used as catalysts for the dehydrohalogenation of ethyl chloride. Since this initial work, the dehydrohalogenation of ethyl chloride and other organic chlorides over ionic crystals has been the subject of a number of different investigations,²⁻⁷ and it has, in general, been found that monovalent alkali halides have high activation energies and low rates, whereas divalent halides have lower activation energies and higher rates, and that the activation energy increases with increased size of the cation. Schwab and Noller⁵ have related the catalytic activity to the magnitude of the dipole moment at the surface, Noller and Ostermeier⁶ to the donor, acceptor properties of the surface ions, and Hauße⁷ to the presence of free electrons and anion vacancies in the ionic crystals.

It was shown by Schwab and Noller⁵ that the addition of 0.12 mole % sodium chloride to calcium chloride increased the activation energy for the ethyl chloride dehydrohalogenation from 11.4 to 23.3 kcal. mole. An explanation of the effect of the sodium chloride was given by Hauße.⁷ He proposed that the addition of NaCl to CaCl_2 reduces the free electron concentration of the solid and results in a higher activation energy for ethyl chloride chemisorption which he views as the slow step in the reaction.

It is the purpose of this paper to show that, although the mechanism proposed by Hauße is attractive, the results of Schwab and Noller⁵ may find another explanation. It is proposed that the surface composition of the dilute solid solution is very different from the bulk composition and that the catalytic activity is still determined by the dipole moments at the surface as proposed by Schwab and Noller⁵ or by the donor-acceptor properties as proposed by Noller and Ostermeier.⁶

Instead of working with dilute solutions of NaCl in CaCl_2 , as used by Schwab and Noller, we have used dilute solutions of CaCl_2 in NaCl because of the ease of preparing and handling such crystals, due to their non-hygroscopic nature and because a convenient way to analyze the surface concentration of these crystals, using the very small solubility of NaCl and CaCl_2 in acetone, has been found. From our experimental results, we will show that a small amount of CaCl_2 in NaCl greatly increases the catalytic activity per unit

area of the crystal and this can be a result of the high concentration of calcium ion on the surface of the crystal as compared to the bulk concentration.

Experimental

Small cubes of NaCl were made⁸ by adding saturated sodium chloride solution to an alcohol-water mixture. Small cubes of NaCl containing $\sim 0.2\%$ CaCl_2 were made by mixing a saturated sodium chloride solution with a saturated calcium chloride solution. Some of the cubes appeared perfect under the microscope, others appeared to have stepwise depressions on the surface. In addition, finely divided NaCl , CaCl_2 , and $\text{NaCl} + \text{CaCl}_2$ were made by fusion, rapid quenching, and grinding. In the latter case, the material was treated with anhydrous HCl at 500° before use in order to destroy the small amount of sodium or calcium hydroxide that was inevitably the result of fusion in air.

The surface area of the solid material was measured by krypton adsorption at 77°K . In a typical adsorption isotherm, the amount of Kr adsorbed increased almost linearly up to 0.2 relative pressure and then changed very little in the range 0.2-0.35 relative pressure. Because these isotherms did not plot as well as the usual B.E.T. plot, we have arbitrarily used the value adsorbed at $p/p_0 = 0.25$ for the monolayer and have used 20.8 \AA^2 for the area of the Kr molecule. A size distribution of precipitated cubes was obtained by microscopic observation and the area was calculated as $410 \text{ cm}^2/\text{g}$. From the krypton isotherm, a value of adsorption at $p/p_0 = 0.25$ was obtained corresponding to $720 \text{ cm}^2/\text{g}$. This difference may be due to the presence of stepwise depressions in the surface of some of the cubes. The precipitated cubes were stable in laboratory air ($<50\%$ relative humidity), whereas the ground salt lost surface area after exposure to laboratory air. For the catalytic runs, the salt samples (1-3 g.) were placed in a 1-cm. i.d. Vycor tube with a sintered Vycor disk to hold the sample and the Vycor tube was inserted into an aluminum core in a furnace. Ethyl chloride at $\sim 20 \text{ cc./min.}$ was passed through the sample and through distilled water to collect the HCl produced. It was necessary to wash down all the exit tubing (all glass, no rubber tubing) after a run, in order to get reproducible results.

The technique used for measuring surface composition is as follows. The salt sample (3 to 4 g.) containing a small amount of calcium chloride was heated in the apparatus of Fig. 1 to 500° for several hours in oxygen-free nitrogen (in some runs in anhydrous HCl) and then held at a given temperature for a given time after which the nitrogen was replaced by helium and the sample tube quenched in ice water, so as to freeze the surface composition. This sample was washed with four 50-cc. portions of acetone. The solubility of calcium chloride in the acetone we used is $\sim 10 \text{ \mu g./cc.}$ and of sodium chloride is $\sim 0.9 \text{ \mu g./cc.}$ These small solubilities have enabled us to dissolve, remove, and analyze the calcium chloride in the surface layer of the salt. The acetone was evaporated to dryness in Pyrex beakers (the initial use of platinum crucibles was found unnecessary), triple-distilled water added, and both the conductivity and the calcium content of the water determined. The conductivity measured the sum of the calcium and sodium ion concentrations, which together with the calcium concentration can be used to determine the sodium concentration. The calcium was titrated with the sodium salt of ethylenediaminetetraacetic acid using Eriochrome Black T as an indicator. The sample was held in the same container for the heat treatment and acetone wash which was

(1) H. G. Grimm and E. Schwamberger, *Réunion interphys. Chim. Paris*, 214 (1928).

(2) G. M. Schwab, *Trans. Faraday Soc.*, **42**, 689 (1946).

(3) G. M. Schwab and A. Karatzes, *J. Phys. Colloid Chem.*, **52**, 1053 (1948).

(4) E. Cremer and R. Baldt, *Z. Naturforsch.*, **4a**, 337 (1949).

(5) G. M. Schwab and H. Noller, *Z. Elektrochem.*, **58**, 762 (1954).

(6) H. Noller and K. Ostermeier, *ibid.*, **60**, 921 (1956); **63**, 191 (1960).

(7) K. Hauße, *Dechema Monograph.*, **26**, 328 (1956).

(8) Fitz-Hugh Marshall, *Phys. Rev.*, **58**, 642 (1940).

TABLE I
CATALYTIC ACTIVITY FOR ETHYL CHLORIDE DEHYDROHALOGENATION
Ethyl chloride flow rate ~ 20 cc. STP per min.

Reaction temp., °C.	Empty reactor Moles of HCl in 30 min. $\times 10^6$	—NaCl— 3 g. 870 cm. ² /g.		—NaCl + 0.11 mole % CaCl ₂ 2 g. 650 cm. ² /g.		—NaCl + 0.11 mole % CaCl ₂ 3 g. 1200 cm. ² /g.		—NaCl + 0.19 mole % CaCl ₂ 3 g. 2700 cm. ² /g.		Av. of various samples 1800 to 12,000 cm. ² /g. Moles HCl per min. $\times 10^{11}$
		Moles HCl in 30 min. $\times 10^6$	Moles HCl per cm. ² $\times 10^{11}$	Moles HCl in 30 min. $\times 10^6$	Moles ^a HCl per cm. ² $\times 10^{11}$	Moles HCl in 30 min. $\times 10^6$	Moles ^a HCl per cm. ² $\times 10^{11}$	Moles HCl in 30 min. $\times 10^6$	Moles ^a HCl per cm. ² $\times 10^{11}$	
300	1.3	1.8	2	3	7.7	4.8	4.4	10	4.1	47
350	1.5	2.1	2.7	7.5	19	15.5	14.5	36	14.8	
400	6.7	3.4	4.3	25	64	56	52	115 ^a	47	700

115 $\times 10^{-8}$ mole of HCl per 30 min. corresponds to a per cent decomposition of ethyl chloride $\sim 0.4\%$.

^a Not corrected for homogeneous reaction.

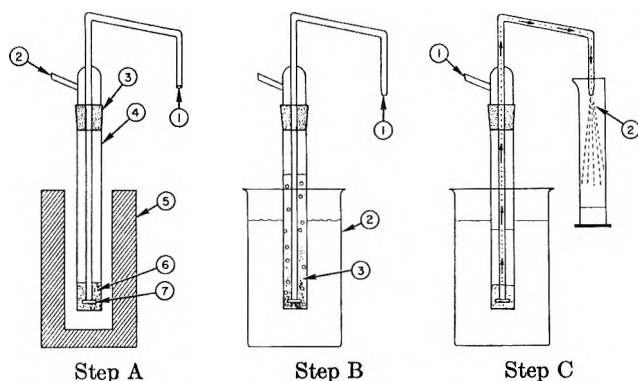


Fig. 1.—Step A, anneal sample: (1) inlet, prepurified N₂; (2) outlet, N₂; (3) ground glass joint; (4) Vycor reactor tube; (5) furnace; (6) sample; (7) UF fritted disk. Step B, sample washed with acetone: (1) inlet, acetone-saturated N₂; (2) water bath, 25°; (3) acetone washing sample. Step C, acetone pumped off for analysis: (1) inlet, acetone-saturated N₂; (2) outlet, wash acetone.

done in the absence of air (see Fig. 1). It is necessary to use at least four acetone washes since the equilibrium between the calcium chloride dissolved in the acetone and calcium chloride adsorbed on the salt surface does not completely favor calcium in solution. If, for example, one contacts 50 cc. of acetone containing 200 μ g. of calcium (as CaCl₂) with 4 g. of NaCl of total area 1.1 m.², then approximately half of the CaCl₂ will be adsorbed and half will remain in solution. The adsorbed material can be recovered by subsequent washes.

Results and Discussion

The catalytic results are given in Table I. Three different size precipitated sodium chloride cubes were used of areas 2700, 1200, and 650 cm.²/g. The high area crystals contained 0.19 mole % CaCl₂ and the two low area crystals 0.11 mole % CaCl₂. In addition, there are data for pure sodium chloride cubes (<30 p.p.m. of calcium chloride) and for the empty reactor. The rate for the empty reactor is larger than for the sodium chloride cubes at 400°, because the cubes have very low catalytic activity; in both cases we are measuring the homogeneous⁹ reaction and the time of contact is longer in the empty tube. The amount of HCl produced is proportional to the total area of salt in the catalyst tube. Since the largest per cent decomposition of the ethyl chloride is only $\sim 0.4\%$, the reaction rate is independent of flow rate. The data show that a small mole per cent calcium chloride has very greatly increased the catalytic activity. We will propose an explanation for this increased activity in terms of a surface concentration of calcium ion on the

salt surface that is much larger than the bulk composition.

Table II gives some typical results for the surface analysis experiments. The total surface of the sample was ~ 1.1 m.² and this corresponds to 0.012 mmole of Na ions if the total surface consisted of the 100 face. In order to see, from geometrical considerations only, what is the maximum amount of calcium a NaCl 100 face can contain without forming a new 3-dimensional compound of NaCl and CaCl₂, such as NaCaCl₃ (isomorphous with KCaCl₃), one can draw two types of surfaces. In one, there are all chloride ions with an equal number of cation vacancies made by replacing Na⁺ with CaCl⁺. In the other, which has one-half

TABLE II
SURFACE ANALYSIS USING ACETONE WASH

Fused sample of NaCl with 0.19 mole % CaCl₂ (0.13 wt. % Ca) used for the experiments. Pretreated with anhydrous HCl and washed with acetone before the experiment. Surface area 2700 cm.²/g.; 4.24 g. used. Total calcium in the salt = 5500 μ g. In all cases ~ 45 μ g. of NaCl removed per 50 cc. of acetone.

Heated to 500° for 3.5 hr. and quenched

- 1st 50 cc. acetone wash contains 25 μ g. of calcium
- 2nd 50 cc. acetone wash contains 9 μ g. of calcium
- 3rd 50 cc. acetone wash contains 6 μ g. of calcium
- 4th 50 cc. acetone wash contains 3 μ g. of calcium

Total calcium removed = 43 μ g.

Heated to 150° for 4.75 days and quenched

- 1st 50 cc. acetone wash contains 323 μ g. of calcium
- 2nd 50 cc. acetone wash contains 250 μ g. of calcium
- 3rd 50 cc. acetone wash contains 102 μ g. of calcium
- 4th 50 cc. acetone wash contains 26 μ g. of calcium
- 5th 50 cc. acetone wash contains 30)
- 6th 50 cc. acetone wash contains 17) these done 24 hr. after
- 7th 50 cc. acetone wash contains 8) first four washes
- 8th 50 cc. acetone wash contains 4)

Total calcium removed = 760 μ g.

as much calcium per unit area, we have replaced two sodium ions with a calcium ion and a cation vacancy. If each sodium were replaced by a calcium ion together with a chloride ion, the surface could hold 480 μ g. of calcium. Since in the experiment at 150° we have observed a removal of ~ 760 μ g. one might conclude that a separate phase of CaCl₂ (saturated with NaCl) is formed and that 0.19 mole % calcium chloride is above the solubility at 150°. Such a conclusion cannot be made with confidence, however, since the absolute value of our surface area is in doubt by perhaps the difference between 480 and 760 (although the relative

(9) D. H. R. Barton and K. E. Howlett, *J. Chem. Soc.*, 165 (1949).

values can be determined much more accurately). In the case of the 500° pretreatment, it also can be seen that the surface concentration of calcium is higher than the bulk. If the surface contained the same per cent calcium as the bulk, it would have $\sim 1 \mu\text{g.}$ of calcium instead of the $\sim 43 \mu\text{g.}$ observed. The alternate explanation that the surface had the same composition as the bulk and that we obtained the $43 \mu\text{g.}$ as a result of a rapid exchange 43 layers deep (presumably due to recrystallization) seems very unlikely for two reasons: (1) if this were so, we might expect to obtain the same result independent of the annealing temperature, which is not the case, and (2) exchange between poorly soluble ionic surfaces and ions in aqueous solution usually only involves the monolayer,¹⁰ since recrystallization is slow.

Table III shows the results of some experiments with fused NaCl containing 0.19 mole % CaCl_2 in which the sample has been annealed for various times and temperatures. Approximately $180 \mu\text{g.}$ of sodium chloride was removed in each experiment (4 acetone washes). The total area of the sample was $2.1 \times 10^4 \text{ cm.}^2$ which corresponds to $1288 \mu\text{g.}$ of NaCl on the cube faces or to $866 \mu\text{g.}$ of Ca if each sodium ion were replaced by CaCl^+ . If the surface had the same composition as the bulk, it would contain $1.6 \mu\text{g.}$ of calcium. One can see that the surface concentration of calcium ion is larger than the bulk concentration and increases with lower annealing temperatures and that above 250° the surface and bulk reach equilibrium in several hours. The interior and surface of a NaCl crystal can accommodate a Ca ion from CaCl_2 if there is associated with the Ca ion a cation vacancy. In addition, a Ca ion can appear at or near the surface without a cation vacancy if there is a chloride ion on the surface to keep electrical neutrality. The difference between bulk and surface calcium concentration may reflect the greater ease of making a cation vacancy with its associated Ca ion on the surface than in the bulk and this effect increases with lower temperature because the energy required for the surface cation vacancy formation is lower than for the bulk vacancy formation. A theoretical treatment of this difference in bulk and surface composition of ionic crystals has been given by Schwab.¹¹

It is interesting to note that at the end of this series the calcium chloride content of the solid was only 45% of the initial concentration. The concentration of undesirable ions at the surface of a solid and subsequent removal offers possibilities for purification of solids. After the final 150° treatment in Table II, the sample was annealed at 300° and only $11 \mu\text{g.}$ of calcium was recovered from the surface. It was thought that this low value may be a result of some impurity accumulating on the surface of the salt that was insoluble in acetone, such as $\text{Ca}(\text{OH})\text{Cl}$ or CaO (the solubility of CaO , for example, is $0.02 \mu\text{g./cc.}$ of acetone at room temperature) so the sample was treated with anhydrous HCl at 500° for 1.7 hr. After this treatment, the value of calcium appearing on the surface after a 300° anneal increased to $26 \mu\text{g.}$

Table IV gives some values for the concentration of calcium on the surface of precipitated NaCl cubes which behave similarly to the fused and ground material. The cubes also showed (data not given in the

(10) A. C. Wahl and N. A. Bonner, "Radioactivity Applied to Chemistry," John Wiley and Sons, New York, N. Y., 1951, p. 312.

(11) G. M. Schwab, Z. *Elektrochem.*, **56**, 297 (1952).

TABLE III

SURFACE COMPOSITION EXPERIMENTS ON 4.21 GRAMS OF FUSED $\text{NaCl} + 0.19 \text{ MOLE } \% \text{CaCl}_2$
Surface area $5000 \text{ cm.}^2/\text{g.}$

Annealing temp., $^\circ\text{C.}$	Duration of anneal	Micrograms of Ca removed in expt.	Total cumulative $\mu\text{g.}$ of Ca removed	Total $\mu\text{g.}$ left in sample
	Initial acetone wash	34	34	5560
500	17 hr.	56	90	5470
300	16 hr.	95	185	5275
300	5 days	103	288	5172
300	2 hr.	88	376	5084
400	18 hr.	63	439	5021
400	2 hr.	60	499	4961
500	1 hr.	48	547	4913
250	16 hr.	124	671	4789
250	2 hr.	101	772	4738
250	69 hr.	114	886	4574
200	16 hr.	445	1331	4129
200	3.5 hr.	227	1558	3902
200	91 hr.	399	1957	3503
150	15 hr.	287	2244	3216
150	64 hr.	419	2663	2797
150	11 days	434	3097	2363
300	2.3 hr.	11		2352
300	2.5 hr.	26 after HCl treatment ^a		

^a Solid analyzed at this point and found to contain 2090 $\mu\text{g.}$ of calcium; 4.10 grams of the original sample was recovered from the reactor at this point.

table) the same effect as the fused material, in that after a number of low temperature anneals in which considerable calcium was rejected to the surface, the sample then gave abnormally low calcium surface concentration values for $300\text{--}500^\circ$ anneals. The low values were increased by treatment with anhydrous HCl at 500° .

TABLE IV

SURFACE CALCIUM ANALYSIS OF SMALL NaCl CUBES CONTAINING 0.19 MOLE % CaCl_2

Area is $2700 \text{ cm.}^2/\text{g.}$; weight of sample used is 5 g.

Anneal temp., $^\circ\text{C.}$	Time, hr.	Micrograms of Ca on surface	Micrograms of Ca in bulk ^a
200	64	407	3452
200	17	307	3145
200	2	101	3044

^a This sample had originally $6450 \mu\text{g.}$ of Ca in the bulk but had been used for a number of preliminary runs. The calcium content of the solid was found by analysis at the end of the experiment.

The high value of surface calcium ion concentrations as compared to the bulk concentration can be used to explain the catalytic results of Table I. At 400° the salt with low mole per cent CaCl_2 has $\sim 7\%$ of the activity of calcium chloride per unit area. From the surface analysis figures of Table III, one would estimate that the surface contained $\sim 60 \mu\text{g.}$ of calcium out of a possible $866 \mu\text{g.}$ or that 7% of the surface is calcium ion. Since the calcium concentration on the surface varies with temperature, the apparent activation energy for the reaction will involve the energy change for this process. The exact agreement of 7% in both cases is most likely fortuitous, but the fact remains that in the case of the dehydrohalogenation of ethyl chloride by these ionic surfaces, the chemical composition of the surface appears to give a satisfactory explanation for the catalytic activity without the necessity for involving the free electron picture of Hauffe.⁷

NUCLEAR MAGNETIC RESONANCE SPECTRA OF SOME ALKYL VINYL ETHERS AND METHYL VINYL SULFIDE

BY R. T. HOBGOOD, JR., G. S. REDDY, AND J. H. GOLDSTEIN

Department of Chemistry, Emory University, Atlanta 22, Georgia

Received June 8, 1962

The n.m.r. spectra of methyl vinyl sulfide, methyl vinyl ether, ethyl vinyl ether, and isobutyl vinyl ether have been observed and analyzed in tetramethylsilane solution. From the chemical shift data, it appears that lone-pair conjugation with the π -electron system is more important in the case of oxygen than sulfur. In methyl vinyl ether a coupling constant between the methyl group and the α -proton of 0.3 c.p.s. is observed, with no detectable coupling between the methyl group and the β -protons. However, in methyl vinyl sulfide the methyl group couples with the β -protons, 0.4 c.p.s. (*cis*) and 0.2 c.p.s. (*trans*), with no coupling being observed between the methyl group and the α -proton. This long-range coupling is thought to reflect the participation of structures involving the d-orbitals of sulfur.

Introduction

This communication reports the results of a nuclear magnetic resonance (n.m.r.) study of methyl vinyl sulfide, methyl vinyl ether, ethyl vinyl ether, and isobutyl vinyl ether under comparable conditions in the inert solvent tetramethylsilane. N.m.r. spectra, as well as many other physical techniques, have been used previously in efforts to discover the relative mesomeric and inductive effects of substituents on an ethylenic system.¹⁻³ Analyses for the ethers have been performed previously,^{4,5} but due to differences in solvents and methods of referencing, it was necessary to re-analyze them as ABC systems under the conditions employed here. The long-range coupling constants through the hetero atom have been determined by first-order perturbation methods. The chemical shifts and coupling constants have been examined in an effort to deduce the difference in the manner and extent of interaction of sulfur and oxygen with the π -electron system.

Experimental

All spectra were observed on a Varian Model A-60 high-resolution spectrometer operating at 60 Mc./sec. The spectra of methyl vinyl ether and methyl vinyl sulfide were calibrated on a Varian Model 4300 B high-resolution spectrometer operating at 40 Mc./sec. by the usual side-band technique⁶ while the spectra of the remaining compounds were calibrated on the A-60 spectrometer by the same method. The spectra of the ethers and the sulfide were observed in 10% solution (by volume) in tetramethylsilane used as solvent and internal reference.

The 40 Mc./sec. spectrum of methyl vinyl sulfide is shown in Fig. 1 and 2. Figure 1 is the vinylic portion under medium resolution, *i.e.*, the splittings due to the methyl protons are not resolved. Figure 2 is the spectrum of the methyl group under conditions of very high resolution. The splitting between each pair of consecutive lines is 0.2 c.p.s., which is produced by two coupling constants (0.4 and 0.2 c.p.s.) with two of the vinylic protons.

Results and Discussion

In all pertinent cases, the vinylic portion of the spectrum was analyzed as an ABC system with any further splitting due to alkyl substituents being treated by first-order perturbation theory. The values of the

chemical shifts and coupling constants, shown in Table I, were obtained by numerically fitting the observed spectra. The maximum discrepancy between observed and calculated shifts, 0.2 c.p.s., occurred for only a few peaks, and the over-all agreement is within the mean deviation of the measurements. The observed ABC intensities were obtained numerically by a triangular approximation of the peak area. Considering approximations due to further splittings by the substituents, the observed ABC intensities agree quite well with the calculated ones. All the chemical shifts in the table have been converted to 60 Mc./sec. for comparison purposes.

Coupling constants for methyl vinyl ether have been reported previously⁴ which do not differ significantly from those obtained here. Complete ABC analyses for the three ethers reported here have been published earlier.⁵ However, due to differences in solvents and references used, individual chemical shifts vary from 5-15 c.p.s. from those listed in Table I.

The most striking feature of the values in Table I is the extreme high-field position of the β -protons in the ethers ($\sim 75-85$ c.p.s.) above ethylene.⁷ It is difficult to conceive of an anisotropy effect of oxygen which would produce an up-field shift this great. In acrylonitrile, where the anisotropy of the $-\text{C}\equiv\text{N}$ group is expected to be larger or certainly not smaller than that for oxygen, the calculated anisotropy shift of the β -protons⁸ is much smaller (11.5 c.p.s. for the *cis* and 15.0 c.p.s. for the *trans* position in the upfield direction) than the observed upfield shift in the case of the ethers. It is more likely that lone-pair conjugation of the oxygen with the unsaturated system with its resulting flow of charge into the β -position is responsible for this observed upfield shift.

In methyl vinyl sulfide the β -protons are 14-28 c.p.s. above ethylene, which is in sharp contrast with the corresponding ether (β -shifts $\sim 75-85$ c.p.s. above ethylene). The relative electronegativities of sulfur and oxygen would suggest that any inductive effect operating on the β -position should be in the opposite direction. Indeed, the α -proton shift does follow the order of electronegativities and since any inductive effect would probably be short-range, one might assume that the inductive effect is the controlling factor on the α -shift. Conceivably, however, the α -proton shift in the two compounds might be due to a difference in the anisot-

(1) L. Pauling, "The Nature of the Chemical Bond," 3rd Ed., Cornell University Press, Ithaca, N. Y., 1960, pp. 288-290.

(2) E. B. Whipple, W. E. Stewart, G. S. Reddy, and J. H. Goldstein, *J. Chem. Phys.*, **34**, 2136 (1961).

(3) C. N. Banwell and N. Sheppard, *J. Mol. Phys.*, **3**, 351 (1960).

(4) C. N. Banwell, N. Sheppard, and J. J. Turner, *Spectrochim. Acta*, **16**, 794 (1960).

(5) W. Brugel, Th. Ankel, and F. Kruckeberg, *Z. Elektrochem.*, **64**, 1121 (1960).

(6) J. A. Pople, W. G. Schneider, and H. J. Bernstein, "High-resolution Nuclear Magnetic Resonance," McGraw-Hill Book Co., Inc., New York, N. Y. 1959, p. 74.

(7) G. S. Reddy and J. H. Goldstein, *J. Am. Chem. Soc.*, **83**, 2045 (1961).

(8) G. S. Reddy, J. H. Goldstein, and L. Mandell, *ibid.*, **83**, 1300 (1961).

TABLE I^a

N.M.R. SPECTRAL PARAMETERS FOR METHYL VINYL SULFIDE AND SOME ALKYL VINYL ETHERS

	(c)	(c)	(c)	(c)	(c)
ω_a	-380.7	-386.0	-381.6	-383.0	-104.0
ω_b	-290.4	-241.8	-242.7	-242.8	-225.0
ω_c	-304.5	-232.7	-231.0	-230.4	-225.0
ω_d	-127.2	-189.8	-219.2	...	-205.5
J_{ab}	16.4	14.1	14.5	14.4	0.5
J_{ac}	10.3	7.0	7.0	6.9	0.5
J_{bc}	-0.3	-2.0	-1.7	-1.8	
J_{ad}	0.0	0.3	...	0.5	
J_{bd}	0.4	0.0	
J_{cd}	0.2	0.0	

^a All chemical shifts and coupling constants are expressed in c.p.s. at 60 Mc./sec. with respect to internal tetramethylsilane.

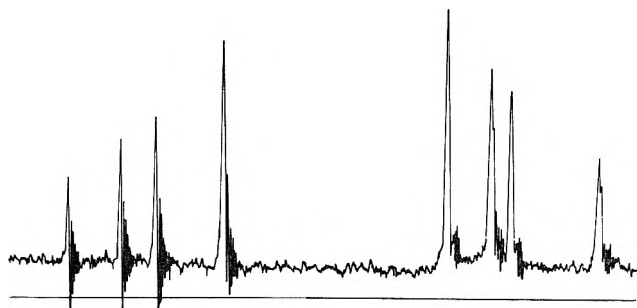


Fig. 1.—The observed vinyl spectrum of methyl vinyl sulfide in tetramethylsilane at 40 Mc./sec. Linearity should not be assumed in the observed spectrum. The direction of increasing field is from left to right.

copy of the two hetero atoms. The β -shift differences in the two compounds probably can be explained best by the difference in lone-pair conjugation of oxygen and sulfur. Previous n.m.r. data for the vinyl halides indicate that the smaller the halide, the greater the capability for lone-pair conjugation.² It therefore seems quite reasonable to expect that oxygen, because of its smaller size, would show a greater tendency for lone-pair conjugation than sulfur.

Ethyl vinyl ether and isobutyl vinyl ether in general have the same chemical shifts as methyl vinyl ether. Since no dilution studies were made in the present work, it is difficult to ascertain the chemical shift differences with a great degree of certainty. However, it appears that the R group does not have any significant effect on the β -shifts, implying that the R groups studied here do not alter the capacity for lone-pair conjugation of oxygen significantly and that oxygen acts as a buffer between the two groups.

It has previously been observed⁷ that the total methyl substituent effect on the two β -protons in an unsaturated system is generally 30 c.p.s. However, in isopropenyl methyl ether the total α -methyl effect is only 16 c.p.s., perhaps implying, since the methyl and the methoxy groups are cross-conjugated, that the charge transfer from the methyl group is reduced.

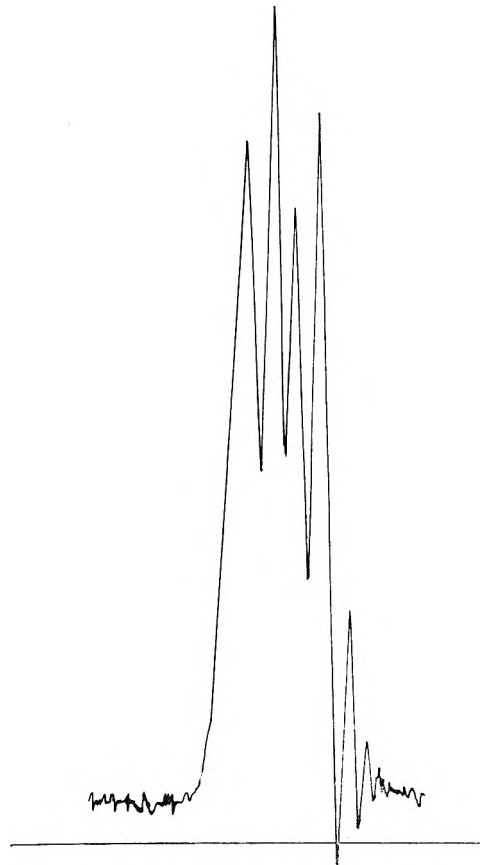


Fig. 2.—The observed methyl group spectrum of methyl vinyl sulfide in tetramethylsilane at 40 Mc./sec. The separation of the left-most peak from its nearest neighbor is 0.23 c.p.s. The direction of increasing field is from left to right.

The *gem* coupling constant in methyl vinyl sulfide has a greater degree of uncertainty than any of the other parameters due to the coupling of the β -protons with the methyl group. It may vary from -0.5 to 0.0 c.p.s. without changing the calculated spectrum significantly. The value of -0.3 c.p.s. was chosen in order that the pairs of lines which are primarily influenced by this coupling constant would coincide exactly. It

should be pointed out that a value of +0.3 c.p.s. will not produce exact coincidence of these lines. Since each of these peaks is further split by the methyl group, any value from -0.5 to 0.0 c.p.s. could be used without serious divergence from the observed spectrum.

One of the most surprising features about the spectrum of methyl vinyl sulfide is that the β -protons couple with the methyl group (0.4 c.p.s. *cis* and 0.2 c.p.s. *trans*) while there is no evidence of coupling between the α -proton and the methyl group. The absence of the latter might be due to the angles involved.⁹ In Fig. 1, it can be seen clearly that there is no coupling between the α -proton and the methyl group. The α -proton quartet shows no evidence of further splitting since the ringing produced by a fast sweep does not show the effect of two or more frequencies beating against one another.¹⁰ The long-range coupling to the β -protons is reminiscent of similar long-range interactions through conjugated systems.¹¹ Since it is well known that the S atom interacts with unsaturated structures as if it were itself pseudo-ethylenic in charac-

ter,¹² the transmission of spin-spin coupling across methyl vinyl sulfide appears to be not unreasonable. The cited behavior of S may involve the participation of its d-orbitals and the methyl group can be pictured as hyperconjugating with these orbitals to produce a

structure of the form $\text{CH}_2=\text{CH}-\bar{\text{S}}=\overset{\oplus}{\text{C}}\text{H}_3$. From energetic considerations, structures of this type involving the d-orbitals are more reasonable for sulfur than for oxygen. Consequently, if long-range methyl coupling depends significantly on such a structure, it will be expected to be larger for the sulfide than for the ether. The greater upfield displacement of the β -protons in the ether, it should be remarked, results from a correspondingly larger mesomeric transfer of p-electrons from the hetero atom, which is not related to the above mechanism of coupling.

It should be noted that the question of the relative signs of the long-range coupling constants in methyl vinyl sulfide cannot be resolved with our present procedure and data.

Acknowledgment.—The research described in this report was supported in part by grants from the National Institutes of Health (A-2397(C-3)) and Schering Corporation, Bloomfield, N. J.

(12) H. C. Longuet-Higgins, *Trans. Faraday Soc.*, **45**, 173 (1949); V. Schomaker and L. Pauling, *J. Am. Chem. Soc.*, **61**, 1778 (1939).

(9) H. S. Gutowsky, M. Karplus, and D. M. Grant, *J. Chem. Phys.*, **31**, 1278 (1959).

(10) J. J. Turner, *J. Mol. Phys.*, **3**, 417 (1960).

(11) H. J. Bernstein, J. A. Pople, and W. G. Schneider, *Can. J. Chem.*, **35**, 65 (1957); R. R. Fraser, *ibid.*, **38**, 549 (1960).

CARBON-13 SPLITTINGS IN FLUORINE NUCLEAR MAGNETIC RESONANCE SPECTRA¹

BY NORBERT MULLER AND DUANE T. CARR

Department of Chemistry, Purdue University, Lafayette, Indiana

Received June 8, 1962

Spin-spin coupling constants between F^{19} and directly bonded C^{13} nuclei have been measured for a wide variety of organofluorine compounds. The coupling constants tend to decrease with increasing fluorine chemical shifts. It is suggested that the degree of C-F double bond character is the most important single parameter influencing both of these observed quantities, with increased double bonding leading to stronger C-F coupling and decreased fluorine magnetic shielding. Increasing C^+-F^- ionic character apparently entails increased fluorine shielding and reduced C-F coupling, but this effect is quantitatively less important. Increasing the s-character of the carbon orbital used in the C-F bond also appears to reduce the magnitude of the C-F coupling constant. A number of long-range C-F, H-F, and F-F coupling constants also are reported.

Considerable effort has been devoted to discovering, both by theoretical and empirical methods, how the chemical shifts and spin-spin coupling constants which characterize nuclear magnetic resonance (n.m.r.) spectra are related to parameters describing the electronic wave functions of molecules. In particular, spin-spin coupling constants, J_{MF} , between an F^{19} nucleus and the nucleus of a directly bonded atom, M, have been measured for a variety of substances.²⁻⁴ The results were interpreted with the hypothesis that the coupling constants depend primarily on the fractional p-character of the atomic orbital of atom M that is used in the M-F bond. Although data for organic fluorine compounds are particularly well suited to test this hypothesis, only a few scattered observations of C^{13} -F

coupling constants (J_{CF}) have been published.⁵⁻⁹ The aim of the present research was to make a systematic study of J_{CF} values for a variety of organofluorine compounds and to attempt to determine how these values depend on changes in the nature of the C-F bond.

Experimental

The experimental procedures were analogous to those used to study C^{13} -H coupling constants,¹⁰ that is, they involved measurements of the spacings between " C^{13} -satellites" in the F^{19} n.m.r. spectra recorded at 56.4 Mc.p.s. The compounds were either commercial samples or were prepared in our Laboratory using standard methods.¹¹ Most of the observations were made with liquid samples at room temperature, but several of the fluoromethanes were studied as gases, and liquid formyl fluoride was

(1) Support of this work by the National Science Foundation is gratefully acknowledged.

(2) H. S. Gutowsky, D. W. McCall, and C. P. Slichter, *J. Chem. Phys.*, **21**, 279 (1953).

(3) J. A. Pople, W. G. Schneider, and H. J. Bernstein, "High-Resolution Nuclear Magnetic Resonance," McGraw-Hill Book Co., Inc., New York, N. Y., 1959, p. 196.

(4) E. L. Muetterties and W. D. Phillips, *J. Am. Chem. Soc.*, **81**, 1084 (1959).

(5) P. C. Lauterbur, *J. Chem. Phys.*, **26**, 217 (1957).

(6) G. V. D. Tiers, *J. Phys. Soc. Japan*, **15**, 354 (1960).

(7) G. V. D. Tiers and P. C. Lauterbur, *J. Chem. Phys.*, **36**, 1110 (1962).

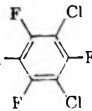
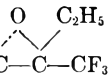
(8) P. C. Lauterbur, in "Determination of Organic Structures by Physical Methods," F. C. Nachod and W. D. Phillips, Ed., Academic Press, New York, N. Y., 1962, p. 505.

(9) A survey including eighteen compounds has appeared since this study was completed: R. K. Harris, *J. Phys. Chem.*, **66**, 768 (1962).

(10) N. Muller and D. E. Pritchard, *J. Chem. Phys.*, **31**, 768, 1471 (1959).

(11) D. T. Carr, Ph.D. Thesis, Purdue University, 1962.

TABLE I
OBSERVED C¹³-F COUPLING CONSTANTS AND CHEMICAL SHIFTS
FOR ORGANOFLUORINE COMPOUNDS LISTED IN ORDER OF INCREAS-
ING J_{CF} VALUES

No.	Compound Formula	Coupling constants		δ_F ,	Isotope
		J_{CF} ,	J_{CCF} ,	p.p.m.	shift,
		c.p.s.	c.p.s. ^a		p.p.m. ^b
1	CH ₃ F	158	276	0.067
2	C ₆ H ₅ CH ₂ F	165	207	.107
3	(CH ₃) ₃ CF	167	132	.114
4	CH ₂ F ₂	232	148	.143
5	<i>p</i> -CH ₃ OC ₆ H ₄ F	237	125	...
6	<i>p</i> -CH ₃ C ₆ H ₄ F	241	119	...
7	<i>o</i> -ClC ₆ H ₄ F	244	116	...
8	C ₆ H ₅ F	244 ^c	114
9	<i>p</i> -BrC ₆ H ₄ F	247	116	...
10	<i>m</i> -ClC ₆ H ₄ F	248	111	...
11	<i>p</i> -CF ₃ C ₆ H ₄ F	252 ^c	109	...
12	<i>p</i> -CH ₃ C(O)C ₆ H ₄ F	253	107	...
13		253	-21.6	98	.090
14	CF ₃ -C≡C-CF ₃	256	-57.2	57	.142
15	CF ₄	257	69	.105
16	<i>p</i> -NO ₂ C ₆ H ₄ F	257	103	...
17	CF ₃ N=SF ₂	263	50	.147
18	(CF ₃) ₂ CF ₂	265	-32.5	134	.115
19	(CF ₃) ₂ O	265	62	.116
20	(CF ₃) ₃ N	269	59	.125
21	<i>p</i> -NH ₂ C ₆ H ₄ CF ₃	270	-32.4
22	<i>p</i> -FC ₆ H ₄ CF ₃	271	-33.2
23	<i>p</i> -(CF ₃) ₂ C ₆ H ₄	271	-32.9	65	.128
24	CF ₃ CH ₃	271	65	.128
25	CF ₃ H	272	84	.133
26	CF ₃ CH ₂ Br	272	-38.5	71	.129
27	<i>m</i> -(CF ₃) ₂ C ₆ H ₄	272	65	.128
28	CF ₃ CH ₂ Cl	274	74	.108
29	CF ₃ CCl=CCl ₂	274	-39.2	62	.140
30	CF ₃ CH ₂ OH	278116
31		278	78	.106
32	CF ₃ CCl ₃	283 ^d	-43.1 ^d	82 ^e	.131 ^d
33	CF ₃ COOH	283	-44.1 ^d	79	.129 ^d
34	CF ₃ COOC ₂ H ₅	284	-44.1	78	.130
35	(CF ₃) ₂ CF ₂	285	-40.0	86	.106
36	CF ₂ =CD ₂	287	88	...
37	CF ₂ ClCH ₃	288	47	.147
38	CF ₂ =CCl ₂	289 ^d	-44.2 ^d	89 ^d	.103 ^d
39	CF ₃ C(O)CH ₃	289	83	.120
40	Cyclic C ₄ F ₈	298	-25.8	138	...
41	CF ₃ Cl	299	33	.152
42	Cyclic C ₄ F ₄ Cl ₄	300	114	.152
43	CFCl=CCl ₂	303 ^d	-43.7 ^d	79 ^d	.112 ^d
44	CF ₃ Br	324	21	.152
45	CF ₂ Cl ₂	325	8	.164
46	CFCl ₃	337	0	.192
47	C ₆ H ₅ C(O)F	344	-61.0	-17	.118
48	CF ₃ I	344	5	.132
49	CH ₃ C(O)F	353	-59.7	-47	.125
50	CF ₂ Br ₂	358	-7	.168
51	HC(O)F	369	-41	.128
52	CFBr ₃	372 ^f	-7 ^e	...

^a Negative signs have been chosen for J_{CCF} on the basis of conclusions reported in ref. 7. ^b δ_F is greater for the C¹³-containing than for the normal isotopic species. ^c ± 5 c.p.s. Other values are ± 1 c.p.s. or better. ^d From ref. 6. ^e From ref. 13. ^f From ref. 8.

studied at about -60° using a low-temperature probe accessory.¹² No indication was found that the J_{CF} values are affected by the presence of solvents or impurities or by moderate changes of temperature.

The measured values of J_{CF} span a range from 158 to 372 c.p.s. They are collected in Table I together with a few values from other laboratories. The table also contains chemical-shift values for the respective fluorine resonances, defined using trichlorofluoromethane as the reference. Most of these shifts were measured in this Laboratory using pure liquid samples and external references without corrections for dilution or bulk-susceptibility effects. They may therefore differ from the "best" values¹³ by a few units (p.p.m.) but the accuracy is adequate to show to what extent the chemical shifts and coupling constants are correlated (see Discussion.) The coupling constants themselves were rounded off to the nearest whole number of c.p.s. and should be in error by not more than 1.0 c.p.s. in most cases.

The center of gravity of the C¹³ sidebands in the fluorine n.m.r. spectrum usually falls at an appreciably higher field than the signal from the C¹²-containing species.⁵ Such isotope shifts, generally of the order of 0.1 p.p.m. but varying noticeably from compound to compound, are also reported in Table I. A number of the spectra included "extra" C¹³ sidebands due to spin-spin coupling in the isotopically substituted species containing the fragment C¹³-C¹²-F. These long-range coupling constants, J_{CCF} , are included in Table I. They are listed with negative signs on the assumption that J_{CF} and J_{CCF} will in general have opposite sign, though this has been proved only in two cases.⁷ No attempt was made to measure the C¹³-C¹²-F isotope shifts which are expected^{6,7} to be of the order of 0.02 p.p.m.

A number of long-range H-F and F-F coupling constants were also measured, and these are presented in Table II. Some of the F-F couplings can be detected only by studying the C¹³ sidebands because of equivalence of the relevant fluorine atoms in the isotopically unsubstituted molecule, as for example in CF₃-O-C¹³F₃.

TABLE II
OBSERVED LONG-RANGE COUPLING CONSTANTS

Compound	J_{H-F} (c.p.s.)			J_{FF} (c.p.s.)
	H-C-F	H-C-C-F	H-C-C-C-F	
CFH ₃	46.5
CF ₂ H ₂	50.4
CF ₃ H	79.0
C ₆ H ₅ CH ₂ F	48.0
H ₂ C(O)F	182
CH ₃ C(O)F	...	6.9
CF ₃ CH ₂ Cl	...	8.5
CF ₃ CH ₂ Br	...	9.0
CF ₃ CH ₂ OH	...	8.9
CF ₃ CH ₃	...	12.8
CF ₂ ClCH ₃	...	14.8
(CH ₃) ₃ CF	...	20.4
<i>p</i> -CH ₃ C(O)C ₆ H ₄ F	...	8.7	5.5	..
<i>p</i> -NO ₂ C ₆ H ₄ F	...	8.2	4.8	..
<i>p</i> -CH ₃ OC ₆ H ₄ F	...	7.8	4.8	..
<i>p</i> -CF ₃ C ₆ H ₄ F	...	8.5	5.1	..
<i>p</i> -BrC ₆ H ₄ F	...	8.1	4.9	..
CF ₃ -C≡C-CF ₃	2.2
(CF ₃) ₂ O	8.0
(CF ₃) ₃ N	10.8
CF ₃ N=SF ₂	10.7
CF ₃ -CF ₂ -CF ₃	7.6

Discussion

A preliminary examination of the data in Table I shows no simple relation between J_{CF} and any single parameter, such as the carbon-orbital hybridization coefficient, that may be used to characterize the C-F bond. Instead, the magnitude¹⁴ of J_{CF} must depend

(12) Varian Associates, Palo Alto, California.

(13) G. Filipovich and G. V. D. Tiers, *J. Phys. Chem.*, **63**, 761 (1959).

(14) It must be borne in mind that the measurements determine the magnitude but not the sign of J_{CF} and that the symbol J_{CF} is used here in place of $|J_{CF}|$ only for the sake of convenience.

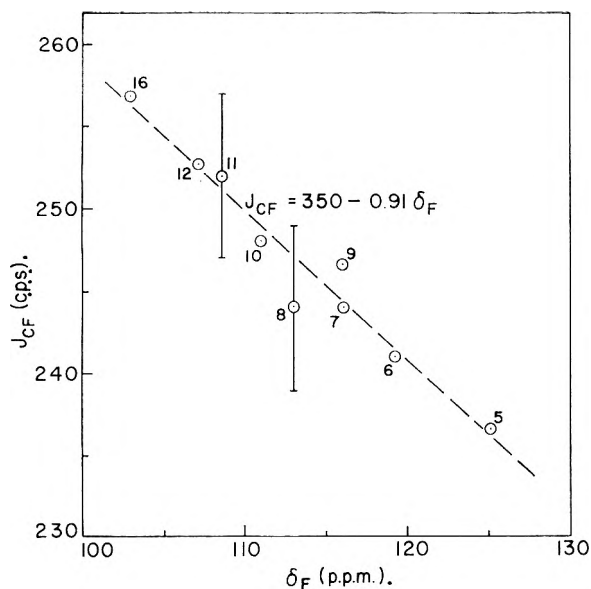


Fig. 1.— ^{13}C - ^{19}F coupling constants, J_{CF} , as a function of fluorine chemical shift, δ_{F} , for monosubstituted fluorobenzenes. The numbers labeling the points identify the compounds in accordance with the sequence in Table I. J_{CF} values are accurate to within 1 c.p.s. except for the two points with large error bars.

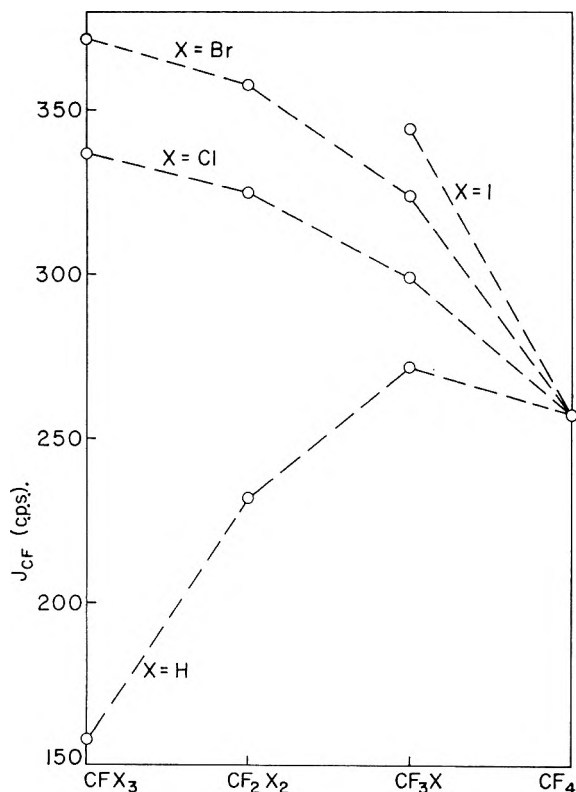


Fig. 2.— J_{CF} values of the halogenated methanes as a function of the number of fluorine atoms.

on several such variables, also including at least ionic character and double-bond character. The evaluation of the data is hindered by the fact that reliable values of such parameters are not available from other sources. It is possible at best to call attention to certain empirical regularities and to draw some tentative conclusions regarding the relative importance of various factors which may influence J_{CF} .

The largest values of J_{CF} in Table I are associated with the most negative values of δ_{F} , the fluorine chemical shift, and there is a marked tendency for J_{CF} to decrease uniformly as δ_{F} becomes more positive. How-

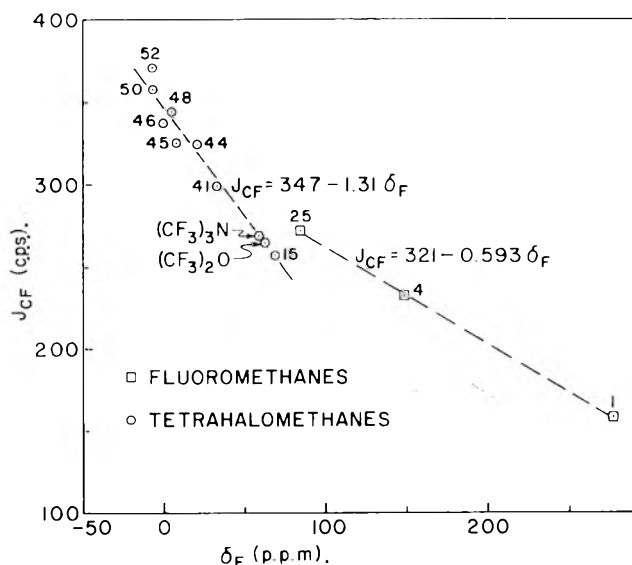


Fig. 3.— J_{CF} values of the halogenated methanes and $(\text{CF}_3)_2\text{O}$ and $(\text{CF}_3)_3\text{N}$ as a function of δ_{F} .

ever, if J_{CF} is plotted against δ_{F} , the points representing the data do not define a single straight line but rather a set of lines each corresponding to a group of structurally similar molecules. For example, Fig. 1 shows such a plot for fluorobenzene and several monosubstituted fluorobenzenes. The points fall quite close to the line $J_{\text{CF}} = 350 - 0.91\delta_{\text{F}}$. Within this series, the hybridization of the fluorine-substituted carbon probably varies very little. It seems then that with constant carbon-orbital hybridization, those changes in the C-F bond which increase δ_{F} reduce J_{CF} . Empirical¹⁵ and approximate theoretical considerations¹⁶ show that δ_{F} rises with either increasing C^+-F^- ionic character or decreasing C-F double-bond character. It follows that decreasing the C^+-F^- polarity or increasing the amount of pi-bonding results in larger values of J_{CF} .

Another class of closely related compound comprises the halogenated methanes, $\text{CF}_n\text{X}_{(4-n)}$, where X stands for hydrogen or a halogen atom and $n = 1, 2, 3,$ or 4 . Figure 2 is a plot of J_{CF} as a function of n for these compounds which shows that the effects of successive substitutions of other atoms for the fluorines of CF_4 are not additive.⁹ For the series $\text{CF}_n\text{H}_{(4-n)}$, J_{CF} has a maximum at $n = 3$. Since each of the relevant bonding parameters should vary monotonically (but not linearly) with increasing fluorination, this suggests again that at least two factors exert opposing effects on the coupling constant.

In Fig. 3, the J_{CF} values for the halogenated methanes are plotted against the chemical shifts. Roughly, the data for compounds containing four halogen atoms determine a straight line, which also passes through the points representing $(\text{CF}_3)_2\text{O}$ and $(\text{CF}_3)_3\text{N}$, and those for CH_3F , CH_2F_2 , and CHF_3 determine another. In the tetrahalomethanes, each bond is made with a carbon orbital with very nearly sp^3 hybridization, but in the $\text{CF}_n\text{H}_{(4-n)}$ series, the carbon orbital used in the C-F bond probably has increasing s-character with increasing fluorination.¹⁰ The relative positions and slopes of the lines in Fig. 3 then suggest that, other things being equal, reducing the s-character of the carbon orbital increases J_{CF} .¹⁷

(15) L. H. Meyer and H. S. Gutowsky, *J. Phys. Chem.*, **57**, 481 (1953).

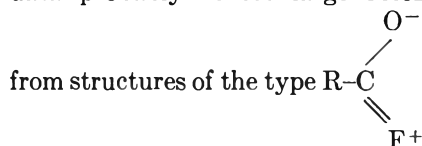
(16) M. Karplus and T. P. Das, *J. Chem. Phys.*, **34**, 1683 (1961).

The tetrahalomethane data may be used to estimate the relative importance of changes in pi-bond order and changes in sigma-bond polarity as factors affecting J_{CF} and δ_F . The trend in the series $CF_nCl_{(4-n)}$ is toward both increased C⁺-F⁻ ionic character and increased C-F double bonding with increasing chlorination.¹⁵ These factors exert opposing influences on δ_F and also on J_{CF} . In each case, the pi-bonding effect overwhelms the effect of the sigma-bond polarity change. Double-bond character emerges as probably the most important single parameter influencing both J_{CF} and δ_F . Apparently, this is true for most organofluorine compounds although it has only been explicitly recognized for the chlorofluoromethanes.^{15,18}

The slope of the "tetrahalomethane" line in Fig. 3 differs from that of the "fluorobenzene" line of Fig. 1. This may be due in part to intramolecular van der Waals forces whose effect on δ_F has been discussed by Evans.¹⁹ For the six compounds of type CF_3Y included in Fig. 3, both J_{CF} and δ_F are well correlated with the size (covalent radius) of Y.

The thirteen compounds studied which contain the fragment CF_3-C- behave very differently from the other CF_3Y compounds. The plot of J_{CF} vs. δ_F , Fig. 4, shows a fairly good linear correlation but with the two quantities increasing together. No explanation for this oddity is offered.

The three acid fluorides included in this study have very low δ_F values and large coupling constants. These data probably reflect large resonance contributions



The monofluorinated hydrocarbons CH_3F , $C_6H_5-CH_2F$, and $(CH_3)_3CF$ should have quite similar C-F bonds, and the observed J_{CF} values are nearly the same. Surprisingly, the δ_F values are 276, 209, and 132 p.p.m., respectively. They cannot be rationalized in a satisfactory way at this time.

In summary, many but not all of the data are consistent with the following conclusions. (1) Increasing the extent of pi-bond formation between C and F raises J_{CF} . (2) Increasing the sigma-bond ionic character in the sense C⁺-F⁻ tends to reduce J_{CF} , but this effect often is overpowered by the pi-bonding effect. (3) Increasing the carbon-orbital s-character in the C-F bond reduces J_{CF} .

These ideas may serve to explain qualitatively the puzzling fact that the isoelectronic species CF_4 and BF_4^-

(17) Approximate calculations¹¹ show that there is a large, positive contact contribution to J_{CF} which increases with increasing carbon s-character. Hence there is a strong possibility that the sign of J_{CF} is actually negative.

NOTE ADDED IN PROOF.—Evidence supporting this possibility has now been found independently by G. V. D. Tiers, *J. Am. Chem. Soc.*, **84**, 3972 (1962).

(18) For a discussion of the large variations in C-F double-bond character in the series $CF_nH_{(4-n)}$ see L. Pauling, "The Nature of the Chemical Bond," 2nd Ed., Cornell University Press, Ithaca, N. Y., 1960, p. 314.

(19) D. F. Evans, *J. Chem. Soc.*, 877 (1960).

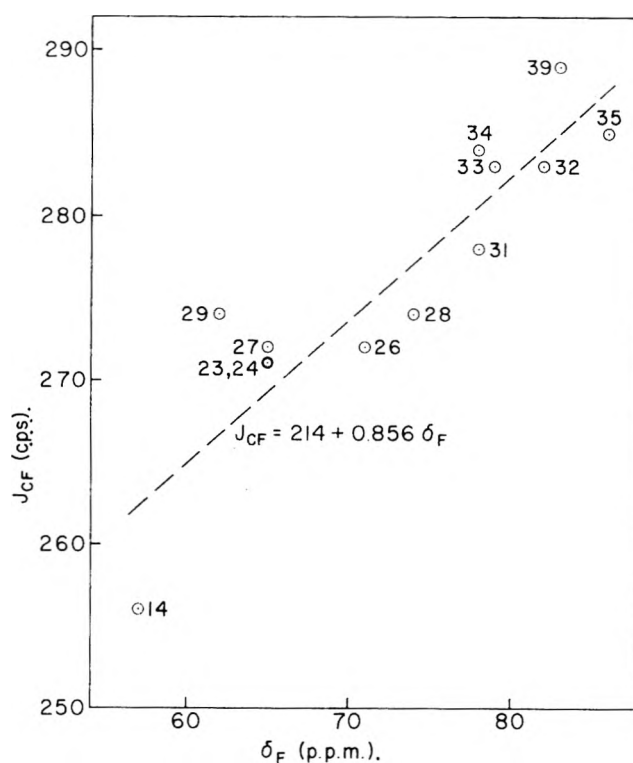
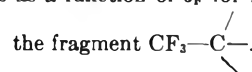


Fig. 4. J_{CF} values as a function of δ_F for molecules containing



have, respectively, $J_{CF} = 257$ c.p.s. and $J_{BF} = 4$ c.p.s.²⁰ Since the magnetogyric ratios are 1.40 nuclear magnetons for C¹³ and 1.79 for B¹¹, comparable values of these coupling constants might be expected. However, pi-bonding in an MF_4 molecule entails a transfer of electrons from the fluorines to the central atom, and since boron has a smaller nuclear charge than carbon one expects less double-bond character in the B-F bond of BF_4^- than in the C-F bond of CF_4 . It is likely that the value of J_{BF} , like that of J_{CF} , is determined by several contributions with unlike signs, and a reduction of the pi-bond order may then produce a situation where the remaining contributions just cancel one another. Upon passing from BF_4^- to BF_3 one expects an increase in boron-orbital s-character and also in B-F double-bond character. The above discussion suggests that these changes tend to produce opposite effects on J_{BF} . Indeed, the coupling constant in BF_3 is 15 c.p.s., nearly the same as in BF_4^- .^{20,21}

The long-range coupling constants obtained here are in line with values reported earlier^{3,6,7,22} except that the J_{CCF} values vary over a wider range than previously reported. The J_{CCF} values are not well correlated with estimated values of the C-C-F angle nor with the C-C bond order. There is a rough correlation between values of J_{CF} and J_{CCF} involving the same fluorine, but the values for $CF_3C \equiv CCF_3$ and for cyclo- C_4F_8 are out of line.

(20) D. E. Pritchard, Ph.D. Thesis, Purdue University, 1960.

(21) The idea that B¹¹-F coupling constants primarily reflect changes in the degree of multiple bonding was also suggested to the authors in a personal communication by P. C. Lauterbur.

(22) L. Petrakis and C. H. Sederholm, *J. Chem. Phys.*, **35**, 1243 (1961).

THE IONIZATION CONSTANTS FOR THE LIGAND 2,2',2''-TRIPYRIDINE

BY PETER O'D. OFFENHARTZ, PHILIP GEORGE, AND GILBERT P. HAIGHT, JR.

Chemistry Departments, University of Pennsylvania, Philadelphia, Pennsylvania, and Swarthmore College, Swarthmore, Pennsylvania

Received June 2, 1962

The ionization constants for the ligand 2,2',2''-tripyridine have been redetermined, using a spectrophotometric method which does not require the direct observation of the extinction coefficients of the singly-protonated forms. The new pK values are significantly larger than those previously reported in the literature. Accurate values of the ionization constants are necessary to obtain the stoichiometry and binding constants of tripyridine with transition metal ions.

Introduction

The stability constants of many nitrogenous bidentate ligands with transition metal ions have been determined, including 2,2'-dipyridine,¹ 1,10-phenanthroline,² and several substituted phenanthrolines. 2,2',2''-Tripyridine is one of the few tridentate nitrogenous ligands studied thus far. A recent report³ indicated that in moderately strong acid, the bis-(2,2',2''-tripyridine)-iron(II) complex existed mainly in a doubly protonated form, despite a very high stability. This would seem very unlikely, since there is no evidence that any of the bidentate ligands complex with the ferrous ion in this modification except in concentrated perchloric acid.⁴ Since an apparent stoichiometry of the bis complex which includes two protons could be produced by incorrect values of the ionization constant of the ligand, it was decided to remeasure the first two ionization constants of tripyridine, using more accurate techniques and more rigorous methods to analyze the data.

Theoretical

Since there is good evidence that 2,2'-dipyridine accepts only one proton in up to 0.1 *N* hydrochloric acid,¹ it will be assumed that 2,2',2''-tripyridine can accept two protons only when they are in non-adjacent positions. Thus, the asymmetric doubly-protonated form is assumed to have no appreciable formation in the pH region studied. The symmetric form, abbreviated tripyH₂⁺², dissociates to form the asymmetric singly-protonated base, abbreviated tripy_AH⁺, which is in tautomeric equilibrium with the symmetric form, tripy_SH⁺. Both of the singly-protonated compounds dissociate to form the free base, tripy.

Let

$$K_{1A} = \frac{[\text{tripy}][\text{H}^+]}{[\text{tripy}_A\text{H}^+]} \quad K_{1S} = \frac{[\text{tripy}][\text{H}^+]}{[\text{tripy}_S\text{H}^+]}$$

$$K_2 = \frac{[\text{tripy}_A\text{H}^+][\text{H}^+]}{[\text{tripyH}_2^{+2}]}$$

where [H⁺] is operationally defined as [H⁺] = antilog (-pH), and the constants *K*_{1A}, *K*_{1S}, and *K*₂ are implicit concentration constants. Also let

$$D = \epsilon_0[\text{tripy}] + \epsilon_{1A}[\text{tripy}_A\text{H}^+] + \epsilon_{1S}[\text{tripy}_S\text{H}^+] + \epsilon_2[\text{tripyH}_2^{+2}]$$

and

$$T = [\text{tripy}] + [\text{tripy}_A\text{H}^+] + [\text{tripy}_S\text{H}^+] + [\text{tripyH}_2^{+2}]$$

(1) J. H. Baxendale and P. George, *Trans. Faraday Soc.*, **46**, 55 (1950).

(2) T. S. Lee, I. M. Kolthoff, and D. L. Leussing, *J. Am. Chem. Soc.*, **70**, 2348 (1948).

(3) R. B. Martin and J. A. Lissfelt, *ibid.*, **78**, 938 (1956).

(4) E. A. Healy and R. K. Murmann, *ibid.*, **79**, 5827 (1957).

where *D* is the observed optical density and ϵ_0 , ϵ_{1A} , etc., are the extinction coefficients of the various species.

As is readily shown

$$[\text{tripy}] = T \frac{1}{1 + [\text{H}^+] \left(\frac{1}{K_{1A}} + \frac{1}{K_{1S}} \right) + \frac{[\text{H}^+]^2}{K_{1A}K_2}}$$

If all experiments are carried out at the same total concentration of tripyridine, then the quantities *D*₀, *D*_{1A}, *D*_{1S}, and *D*₂ can be defined analogously to their respective extinction coefficients as

$$D_0 = \epsilon_0 T \quad D_{1A} = \epsilon_{1A} T \quad D_{1S} = \epsilon_{1S} T \quad D_2 = \epsilon_2 T$$

Then

$$\left[1 + \text{H}^+ \left(\frac{1}{K_{1A}} + \frac{1}{K_{1S}} \right) + \frac{[\text{H}^+]^2}{K_{1A}K_2} \right] D = D_0 + \frac{[\text{H}^+]}{K_{1A}} D_{1A} + \frac{[\text{H}^+]}{K_{1S}} D_{1S} + \frac{[\text{H}^+]^2}{K_{1A}K_2} D_2$$

or

$$D - \delta = \frac{K_{1S}}{K_2} \frac{1}{K_{1A} + K_{1S}} [\text{H}^+] (D_2 - D) + \frac{K_{1A}D_{1S} + K_{1S}D_{1A}}{K_{1A} + K_{1S}} \quad (1)$$

$$\text{where } \delta = \frac{K_{1A}K_{1S}}{K_{1A} + K_{1S}} \frac{(D_0 - D)}{[\text{H}^+]}$$

This expression is useful at low pH values where δ is small. Also, defining

$$\delta' = \frac{K_{1S}}{K_2} \frac{1}{K_{1A} + K_{1S}} [\text{H}^+] (D_2 - D)$$

it is easily shown that

$$D - \delta' = \frac{K_{1A}D_{1S} + K_{1S}D_{1A}}{K_{1A} + K_{1S}} - \frac{K_{1A}K_{1S}}{K_{1A} + K_{1S}} \frac{(D - D_0)}{[\text{H}^+]} \quad (2)$$

Equation 2 is useful at higher pH values where δ' is small. *D*, *D*₀, *D*₂, and the pH are directly observable. The quantities δ and δ' can be calculated by re-iteration. (*K*_{1S}/*K*₂)/(*K*_{1A} + *K*_{1S}) and (*K*_{1A}*K*_{1S})/(*K*_{1A} + *K*_{1S}) can be obtained from the straight line plots of *D* - δ vs. [H⁺](*D*₂ - *D*) and *D* - δ' vs. (*D* - *D*₀)/[H⁺], respectively.

It is obviously impossible, by spectrophotometric means, to solve for either *K*_{1A}, *K*_{1S}, or *K*₂ without

additional information or assumptions. Therefore, it is useful to define the operational constants k_1 , k_2 , and D_1

$$k_1 = \frac{K_{1A}K_{1S}}{K_{1A} + K_{1S}} \quad k_2 = K_2 \frac{K_{1A} + K_{1S}}{K_{1S}}$$

$$D_1 = \frac{K_{1A}D_{1S} + K_{1S}D_{1A}}{K_{1S} + K_{1A}}$$

D_1 , the intercept in the plots of either eq. 1 or 2, is in general dependent upon temperature and ionic strength.

Thus

$$[\text{tripy}] = T \frac{1}{1 + \frac{[\text{H}^+]}{k_1} + \frac{[\text{H}^+]^2}{k_1 k_2}}$$

so the concentration of free base can always be calculated when the total tripyridine concentration and the pH are known.

Experimental

A sample of 2,2',2''-tripyridine was obtained from the G. Frederick Smith Chemical Co., and was recrystallized from a 40–60° cut of petroleum ether, removing an insoluble brown oil. The material was further recrystallized from an aqueous methanol solution, in which it was soluble at room temperature but only moderately soluble at 5°. The resulting crystals were very pale yellow in color. Calcd. for $\text{C}_{16}\text{H}_{11}\text{N}_3$: C, 77.23; H, 4.75; N, 18.02. Found: C, 76.96; H, 4.85; N, 18.12.

Stock solutions of tripyridine were prepared by dissolving several milligrams of the base in hydrochloric acid and diluting with conductivity water; the pH of such solutions was about 3. All experiments were carried out at a total concentration of tripyridine less than 10^{-4} molar to prevent precipitation of the free base.

Measurements of the pH were made on a Beckman Model GS pH meter, using the expanded scale. The electrodes were standardized with 0.05 M potassium acid phthalate, according to the recommendations of the National Bureau of Standards.⁵ Buffers were prepared from potassium acid phthalate–sodium hydroxide mixtures in the region around pH 4.5, and from hydrochloric acid–sodium chloride mixtures in the region around pH 3.2. The measured pH values probably are precise to 0.01 or better.

Measurements of the optical density were made on a Beckman Model DU spectrophotometer. Care was taken to ensure that all measurements in a particular run were made at exactly the same wave length and slit width. Small corrections were made for the absorption of the phthalate buffer. Measurements of the optical density probably are precise to 0.005 or better. The spectra of tripyH_2^{+2} and the free base tripy are shown in Fig. 1, along with the calculated values of D_1/T at 25.0° and ionic strength 0.01. The observed extinctions vary with slit width, and so are only valid at the experimental value of 0.26 mm.

Results

pK_1 was measured at $25.0 \pm 0.1^\circ$ and ionic strengths of 0.01 and 0.05, and, at the lower ionic strength, at $13.2 \pm 0.2^\circ$. pK_2 was measured at $25.0 \pm 0.1^\circ$ at ionic strengths 0.001 and 0.01, and, at the lower ionic strength, at $36.6 \pm 0.1^\circ$ and $13.2 \pm 0.2^\circ$. All data were subjected to least squares analysis, and the mean errors were computed. The possible inaccuracy in the results is considered to be about 0.02 greater than the mean error in the case of pK_2 , due to an uncertainty in the absolute value of the pH caused by unknown liquid junction potentials, and about 0.04 greater in the

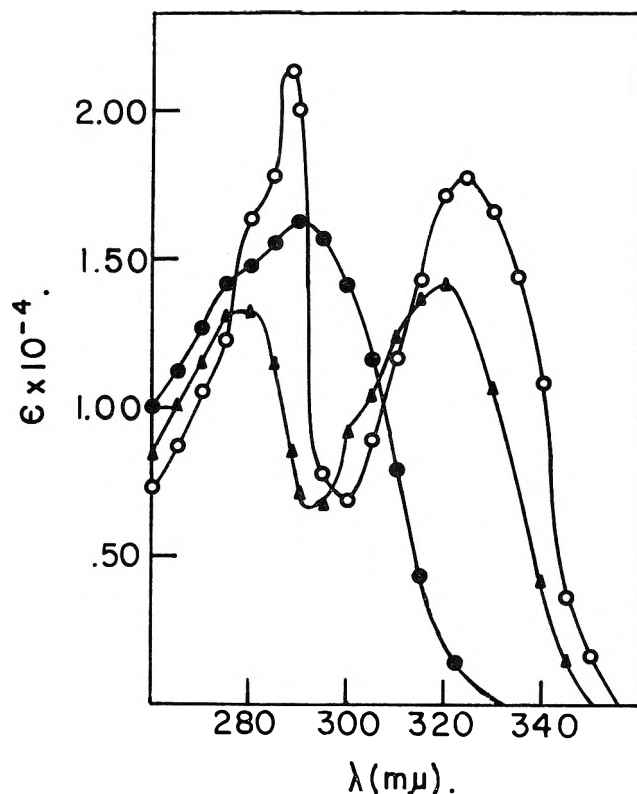


Fig. 1.—Absorption spectra of 2,2',2''-tripyridine and its acid derivatives. Key: open circles, tripyH_2^{+2} ; solid circles, tripy; solid triangles, D_1 (see text).

case of pK_1 , due to both the uncertainty in the pH and uncertainty in δ' . However, the sum of these errors never exceeded ± 0.07 , so both the pK values can be considered accurate within this amount. The data are summarized in Table I, and the results in Table II. All measurements of pK_1 were made at 322 $m\mu$, slit width 0.20 mm., and all measurements of pK_2 were made at 288.5 $m\mu$, slit width 0.26 mm. According to Fig. 1, these are the two most favorable wave lengths.

TABLE I

pK_1					
D	pH	D	pH	D	pH
0.392	4.644	0.494	4.304	0.550	4.295
.340	4.817	.424	4.504	.460	4.495
.310	4.939	.368	4.666	.410	4.656
.267	5.033	.292	4.876	.323	4.865
.240	5.125	.263	4.962	.290	4.951
.218	5.209				
$I = 0.05$		$I = 0.01$		$I = 0.01$	
$t = 25.0 \pm 0.1^\circ$		$t = 25.0 \pm 0.1^\circ$		$t = 13.2 \pm 0.2^\circ$	
$\lambda = 322 m\mu$, slit width = 0.20 mm., $D_0 = 0.066$, $D_2 = 0.838$					
$T \sim 5 \times 10^{-5} M$					

pK_2							
D	pH	D	pH	D	pH	D	pH
0.394	3.064	0.357	3.064	0.421	3.064	0.409	3.045
.370	3.169	.333	3.169	.393	3.169	.393	3.142
.349	3.284	.314	3.284	.370	3.402	.373	3.252
.326	3.402	.285	3.538	.343	3.538	.355	3.366
.314	3.538	.263	3.677			.341	3.470
						.327	3.575

$I = 0.001$		$I = 0.001$		$I = 0.001$		$I = 0.01$	
$t = 25.0 \pm 0.1^\circ$	$t = 36.6 \pm 0.2^\circ$	$t = 13.2 \pm 0.2^\circ$	$t = 13.2 \pm 0.2^\circ$	$t = 25.0 \pm 0.1^\circ$	$t = 25.0 \pm 0.1^\circ$	$t = 25.0 \pm 0.1^\circ$	$t = 25.0 \pm 0.1^\circ$
$\lambda = 288.5 m\mu$, slit width = 0.26 mm., $D_0 = 0.390$, $D_2 = 0.515$							
$T \sim 2.5 \times 10^{-5} M$							

(5) W. J. Hamer, G. D. Pinching, and S. F. Acree, *J. Res. Natl. Bur. Std.*, **36**, 47 (1946), RP 1690.

TABLE II

	pK_1	R.m.s. error	D_1	R.m.s. error
$I = 0.05$ $t = 25.0^\circ$	4.81	0.02	0.584	0.004
$I = 0.01$ $t = 25.0^\circ$	4.66	.01	.654	.004
$I = 0.01$ $t = 13.2^\circ$	4.68	.03	.694	.008
	pK_2			
$I = 0.01$ $t = 25.0^\circ$	3.28	.02	.224	.005
$I = 0.001$ $t = 25.0^\circ$	3.27	.05	.192	.015
$I = 0.001$ $t = 36.6^\circ$	3.08	.04	.188	.005
$I = 0.001$ $t = 13.2^\circ$	3.46	.05	(0.196 used)	

Discussion

Three other measurements of the ionization constants of 2,2',2''-tripyridine have been made.^{3,6,7} One of these measurements⁶ apparently was based on the extrapolation of potentiometric data in partially aqueous solutions to pure water, and so cannot be compared rigorously with the present results. The value of $pK_1 + pK_2$ was 7.1, compared to the value (for $pK_1 + pK_2$) of about 7.9 at 25° , $I = 0.01$, obtained above.

Martin and Lissfelt,³ using an experimental method similar to the present technique, found $pK_1 = 4.33$, $pK_2 = 2.64$ (both values corrected to $I = 0$). Their values for the extinction coefficients of the singly-protonated base apparently were assumed rather than measured by extrapolation as in the present paper. These assumed values are in serious disagreement with

(6) W. W. Brandt and J. P. Wright, *J. Am. Chem. Soc.*, **76**, 3082 (1954).

(7) P. Offenhardt, G. P. Haight, and P. George, Paper No. 55, Division of Physical Chemistry, American Chemical Society National Meeting, New York, N. Y., 1960.

the calculated values shown in Fig. 1 and Table II. The disagreement in the pK values probably can be traced to the difference in extinction coefficients used.

A preliminary value for pK_1 of 5.04 at 25° and $I = 0.1$ was reported previously by the present authors.⁷ No correction for the effect of pK_2 on the data was made in this earlier value, and the inaccuracy in the pH determination was much greater.

It is of interest to note that if $2K_{1A} = K_{1S}$, the statistical ratio of the constants, then, from the expression $k_1 = K_{1A}K_{1S}/(K_{1A} + K_{1S})$, it follows that $pK_{1A} = 4.48$ and $pK_{1S} = 4.18$ at 25° and $I = 0.01$. The pK for 2,2'-dipyridine at this temperature and ionic strength is 4.30,¹ so that, as expected, the first ionization constants of dipyridine and tripyridine are not much different. A second possible assumption is that $pK_{1A} = pK_{dipy} = 4.30$; this gives $pK_{1S} = 4.41$.

Although k_1 and k_2 are not true thermodynamic constants, it is possible to define $\Delta F = -RT \ln k = \Delta H - T\Delta S$, where $\Delta H = -RT^2 (d \ln k/dT)$. Values of the pK 's, free energies, heats, and entropies of ionization for pyridine,⁸ 2,2'-dipyridine,¹ and 2,2',2''-tripyridine are summarized in Table III. The more positive entropy change for the ionization of the doubly-protonated tripyridine is in keeping with the different charge type; that is, in this reaction, an ion with a +2 charge dissociates to two +1 ions, whereas each of the other ionizations in Table III is the dissociation of a +1 ion to a proton and a neutral compound.

TABLE III

	pK ($I = 0.01$)	ΔF (kcal.)	ΔH (kcal.)	ΔS (e.u.)
Pyridine	5.24	7.07	3.86	-10.8
2,2'-Dipyridine	4.30	5.80	2.0	-13
2,2',2''-Tripyridine, pK_1	4.66	6.36	0.7	-19
pK_2	3.28	4.47	6.8	+8

(8) F. L. Hahn and R. Klockman, *Z. physik. Chem.*, **146**, 373 (1930).

THERMODYNAMICS OF LIQUID SOLUTIONS OF BISMUTH AND SULFUR¹

BY DANIEL CUBICCIOTTI

Stanford Research Institute, Menlo Park, California

Received June 13, 1962

The pressure of S_2 in equilibrium with bismuth-sulfur melts has been determined at 705, 740, and 800° over the concentration range from pure bismuth to the composition at which a second phase formed—solid Bi_2S_3 at 705 and 740° , and liquid sulfur at 800° . A transpiration method was used in the lower pressure range and a dew-point method for the higher pressures. The thermodynamic quantities for solution of sulfur and bismuth in the melt were derived; these are discussed with regard to the possible nature of their binding in the melt. Evidence was found for the gaseous molecule BiS and its heat of dissociation was obtained.

Introduction

We have been studying the chemistry of metals dissolved in their molten halides in this Laboratory for some time.² It seemed of interest to investigate the bismuth-sulfur system since the phase diagram reported in the literature³ indicated that liquid Bi_2S_3 was completely miscible with liquid bismuth. Our re-investigation of the phase diagram already has

been reported.⁴ The present article describes the chemistry of the system as derived from measurement of the sulfur pressure.

Experimental

The thermodynamic properties of these bismuth-sulfur melts were characterized by measuring the pressure of sulfur and its temperature coefficient over the liquid composition range. For most of the range, from zero to about 50 atom % sulfur, the partial pressure of sulfur was determined by a transpiration method. At greater sulfur concentrations, the pressure became too large for that method, so a dew-point method was used.

Transpiration Method.—A stream of nitrogen was passed through a bulb containing the melt and then through a col-

(1) This work was made possible by the financial support of the Research Division of the United States Atomic Energy Commission.

(2) Consult for earlier references, D. Cubicciotti and F. J. Keneshea, Jr., *J. Phys. Chem.*, **63**, 295 (1959).

(3) M. Hansen, "Constitution of Binary Alloys," 2nd Ed., McGraw-Hill Book Co., New York, N. Y., 1958.

(4) D. Cubicciotti, *J. Phys. Chem.*, **66**, 1205 (1962).

lector tube. The volume of nitrogen and the weight of sulfur collected provided the information to calculate the pressure of sulfur. The container was a silica glass bulb having a nitrogen inlet tube and an outlet tube which had a ball-joint end. A collector tube with a matching ball-joint end led the gas out of the hot zone and collected the condensable vapors. The container bulb and the ball joint to the collector were in the constant temperature zone of the furnace; thus all condensation occurred in the collector well downstream from the joint. The amount of condensed material in the collector was determined by weight, and the nitrogen by volume in a gas buret arranged so that the gas was collected at constant pressure.

A glass sleeve was sealed to the cell in order that the ball joint could be blanketed with an atmosphere of nitrogen to keep air from diffusing into the cell. This sleeve was joined to a plastic glove-box filled with nitrogen. The arrangement was such that a collector could be introduced to or removed from the cell at the ball joint and the system exposed only to an atmosphere of nitrogen.

The cell was enclosed in a heavy-walled nickel tube to equalize the temperature. The system was heated in a three-section tube furnace. The temperature of each section was controlled by a potentiometer-controller and Chrome-Alumel thermocouple. The temperature of the cell was measured with a Pt-Rh thermocouple that had been calibrated at the Zn, Pb, and Al freezing points.

The cell was charged initially with a weighed amount of bismuth, about 100 g. The cell was sealed into position and flushed with nitrogen. Then determinations of the vapor density of bismuth were made before any sulfur was added. Sulfur was added to change the composition of the melt by approximately 7 percentage units after each set of determinations. The addition of sulfur was accomplished by distilling weighed amounts into the nitrogen upstream from the cell. The sulfur that was not condensed in the melt was caught in a collector downstream, and weighed. The distillation took 0.5–1.0 hr., and the system was allowed 2 or 3 hr. to come to steady state before the next determination of sulfur pressure was made.

A typical experiment lasted about 1000 min. and 0.1 to 0.25 g. of sample was collected. For each composition, determinations were made at 705, 740, and 800°. Since these temperatures were not reproduced exactly from one determination to the next, small corrections were made on the final pressures to adjust them to those temperatures.

In a transpiration experiment, the condensable vapors reach the collection tube by diffusion, as well as by being carried by the gas stream. The importance of the diffusion was evaluated by making determinations in which the nitrogen flow was stopped but conditions were otherwise unchanged. The diffusion correction was a function of the partial pressure of sulfur in the cell but was not otherwise sensitive to temperature. The correction amounted to as much as 9%; however, only in a few cases was it more than 5% of the sample collected.

It was observed that some bismuth condensed in the collector along with sulfur. This appeared as metallic crystals in the collector just upstream from the sulfur. X-Ray analysis showed the crystals to be Bi_2S_3 . The amount of bismuth in each sample was determined by burning off the sulfur in a stream of oxygen and reducing the residue to bismuth in a stream of hydrogen at 600°. The weight of the residue was equal to the amount of bismuth and the difference from the total weight was equal to the sulfur.

Dew-Point Method.—When the sulfur pressure became too great for the transpiration method, a dew-point method was used. The cell was a silica glass bulb with a side arm bent in the form of a "J." The bulb was maintained at constant temperature in a nickel sleeve in a furnace. The side arm extended horizontally into a second furnace whose temperature was independently controlled. A window was placed so that the bend in the side arm could be observed. As the bend was the coolest part of the system, sulfur condensed there first. A calibrated Pt-Rh thermocouple was tied with glass thread where condensation was first observed to occur. A similar thermocouple was attached to the bulb next to the liquid sample.

The cell was filled with weighed amounts of bismuth and sulfur, pumped out, and sealed. The whole cell was heated to temperature and then the side arm was slowly cooled until sulfur condensed, just below the thermocouple. The temperatures of the bulb and side arm were quickly measured. The side arm was then heated and the performance was repeated. Repeated

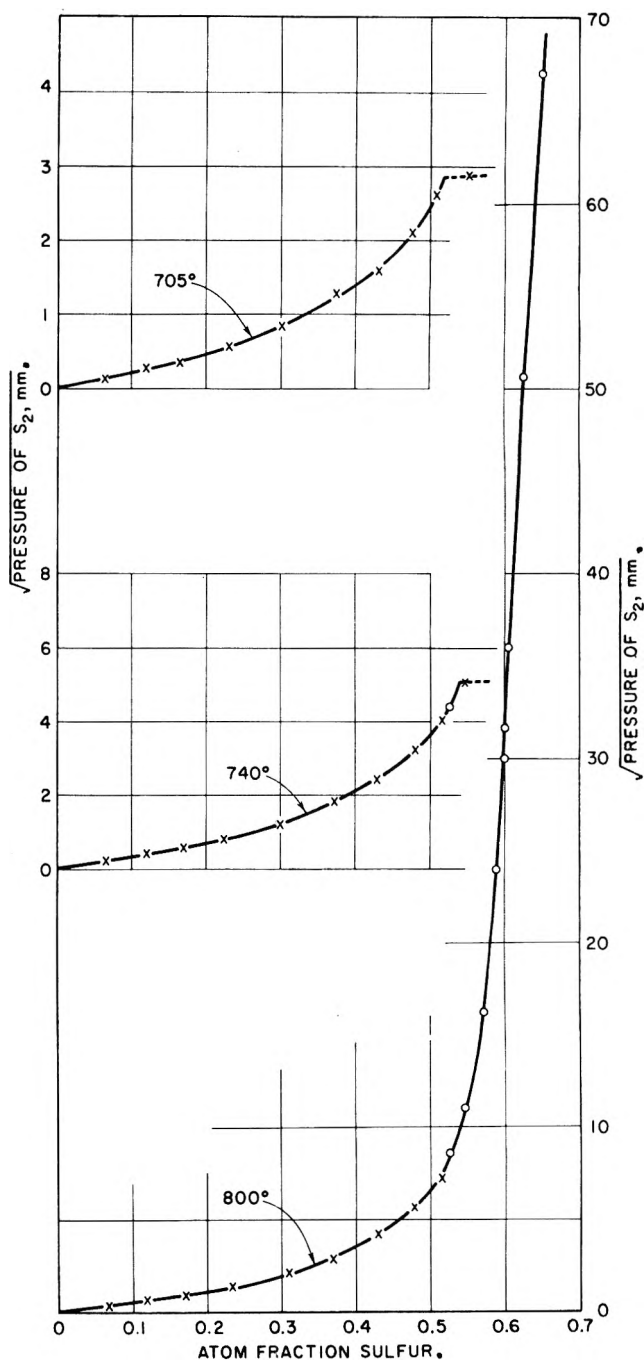


Fig. 1.—The square root of the partial pressure of S_2 over bismuth-sulfur melts. Crosses are results from transpiration experiments; they were corrected for the small amount of sulfur as BiS . Circles are results from dew point measurements.

measurements of the condensation temperature generally agreed to within 0.5 degree. (The temperature at which the sulfur began to evaporate also was observed. It was not sufficiently reproducible nor did it agree with the condensation temperature.)

To check the system, measurements were made on pure sulfur from 300 to 450°. The dew points measured were from 1.7 to 2.1° higher than the temperature of the liquid sulfur. This was because the condensation occurred below the point where the thermocouple was attached, *i.e.*, the thermocouple region was warmer because of the glass thread insulation. The position of the first condensation relative to the thermocouple was reproducible. Therefore, it was decided that a correction of 2° should be subtracted from all dew point measurements to correct for that effect.

The amount of sulfur in the vapor, which would reduce the amount in the liquid phase, was estimated from vapor density information. It was always small compared with the amount of

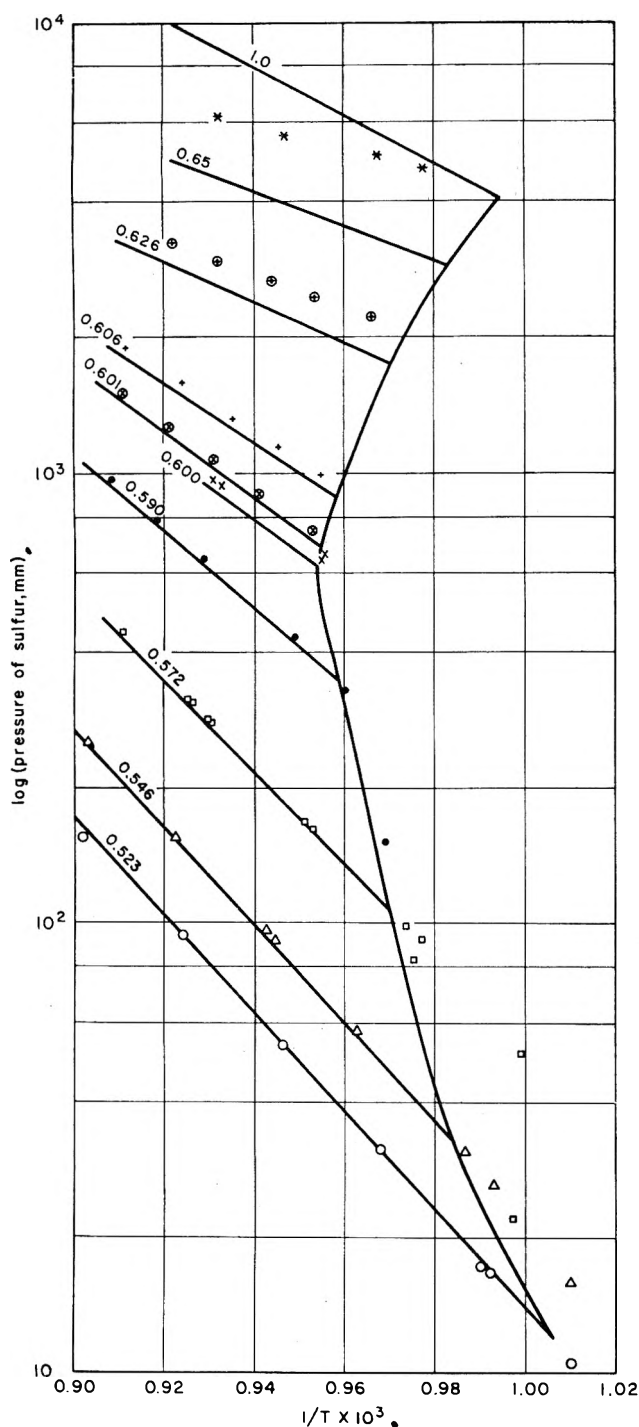


Fig. 2.—Sulfur pressures obtained from dew points. The data points are total sulfur pressures. The straight lines represent partial pressures of S_2 calculated from the total pressures. Numbers on the lines refer to atom fraction sulfur in the melt. The vertical curved line represents a phase boundary. To its left there is one condensed phase—liquid; to its right, two condensed phases—liquid and solid Bi_2S_3 .

sulfur in the cell and thus made a negligible correction to the composition of the melt.

Materials.—The bismuth and sulfur were "High Purity Elements" obtained from the American Smelting and Refining Co. They were quoted to be 99.999% pure and were used without further treatment. The nitrogen was "high purity" gas (99.99%). It was passed through silica gel at -80° to dry it.

Results

Transpiration.—Under the conditions of the transpiration measurements the results of this study indicate that the only important gaseous molecules were S_2

and BiS . The relative importances of the other possible sulfur species, such as S , S_3 , S_4 , etc., were evaluated from their thermodynamic functions (see below). Their contributions to the vapor were negligible. The pressure of S_2 was determined from the amount of sulfur in the samples after the small amount attributed to BiS was subtracted. The evidence for BiS , and its partial pressure will be discussed below.

The results of the transpiration experiments are given in Fig. 1 as crosses. The data are reported as the square root of S_2 pressure because that function is proportional to the activity of sulfur in the system. At all three temperatures, the square root of S_2 pressure was proportional to the atom fraction of sulfur in the liquid from zero to almost 0.2. At greater sulfur concentrations there were increasing positive deviations from this (Henry's law) region.

Dew Point.—The total pressures of all sulfur species were evaluated from the dew points using the vapor pressure equation reported by West and Menzies.⁵ It was necessary to use their equation to extrapolate beyond their measurements to obtain values greater than 2700 mm. The total pressure of sulfur obtained in that way is shown in Fig. 2 as a function of reciprocal of absolute temperature for several melt compositions.

The almost vertical curved line in Fig. 2 separates the region of one condensed phase from that of two condensed phases. The data for this line were taken from the liquidus of the phase diagram.⁴ It was found that sulfur pressures to the right of that line, *i.e.*, for samples in which solid Bi_2S_3 was present, were not consistent with one another. The points in that region are some of those obtained and illustrate the lack of consistency. Therefore measurements in that region were not pursued.

In the region of one condensed phase (to the left of the vertical curve) the logarithms of total sulfur pressure *vs.* reciprocal of temperature fell reasonably close to straight lines. Since the pressures derived from the data of West and Menzies represent the total pressure of all sulfur polymers, further calculation was necessary to derive the partial pressures of S_2 to compare with the transpiration results and to evaluate the activity of sulfur in the system.

The partial pressure of S_2 at each dew point was evaluated as follows. It was assumed that the total pressure of sulfur species was equal to the vapor pressure measured by the dew point. The relative partial pressures of the several sulfur species were quite different at the hot end and cold end of the dew point cell because the equilibria among the sulfur species were temperature dependent. The mean free paths of the molecules, under the conditions of these experiments, were very much shorter than the dimensions of the cell. Therefore, the partial pressures of the individual sulfur species at one end of the cell were independent of those at the other end. Because of the short mean free path, a molecule makes many collisions in traveling from one end of the tube to the other. These collisions cause it to come into equilibrium with the surrounding local molecules. Only if a molecule had a long free path and could traverse large fractions of the distance between the hot and cold end without col-

(5) W. A. West and A. W. C. Menzies, *J. Phys. Chem.*, **33**, 1880 (1929).

lision could the partial pressures of individual species at the two ends of the tube be equal. Thus under the conditions of these experiments, the only relationship was that the total pressure of sulfur species at the two ends was equal.⁶

The partial pressure of S_2 over the melt (hot end of cell) was calculated from the total pressure of sulfur together with the thermodynamic information for the sulfur species. Thermodynamic data for the species S , S_2 , and S_8 were obtained from the JANAF tables⁷ and those for S_3 , S_4 , and S_6 from the work of Luft.⁸ The partial pressure of S_2 was calculated for each dew-point measurement, and for each melt composition a straight line was drawn through the data. The lines obtained are shown in Fig. 2. The partial pressures of S_2 over pure liquid sulfur were taken from ref. 7.

The pressures of S_2 over melts of 0.52 to 0.67 atom fraction sulfur were read from the lines of Fig. 2 at 705, 740, and 800° and added to Fig. 1 so that those curves of S_2 pressure could be extended over the entire liquid range from pure bismuth to the composition at which a second phase forms (solid Bi_2S_3 at the two lower temperatures and liquid sulfur at the highest).

BiS in Vapor.—In the transpiration experiments, bismuth was found in the samples collected, as noted above. The apparent pressure of bismuth increased as the sulfur concentration in the melt was increased. Thus some species containing both bismuth and sulfur must have been present in the vapor. The nature of that species was discovered as follows.

The apparent pressures of bismuth over the pure liquid as calculated from the transpiration results on the assumption that Bi was the only vapor species are shown in the second column of Table I. Under the conditions of these experiments it is known that bismuth vapor consists of comparable amounts of Bi and Bi_2 molecules. Therefore, the apparent pressures expressed as Bi should equal the sum of the true pressures of the Bi species plus twice those of the Bi_2 . The partial pressures of these species were evaluated from the total vapor density measured by transpiration and the equilibrium constants relating them at each temperature. The equilibrium constants were obtained from the thermodynamic data for those gaseous species given by Brewer.⁹ The partial pressures of Bi and Bi_2 over pure, liquid bismuth so calculated are given in the last two columns of Table I.

For each transpiration experiment it was then possible to calculate the pressures of Bi and Bi_2 expected for each melt; hence, the pressure of Bi would equal the partial pressure of Bi over pure bismuth times the activity of bismuth in the liquid, and that of Bi_2 would equal its partial pressure over pure bismuth times the square of the activity of bismuth in the liquid. The amount of bismuth expected in the sample from such calculations was subtracted from the total amount and the difference was that due to a

(6) In these experiments the pressure of BiS was negligible compared with the pressure of sulfur species. The partial pressure of BiS was never more than a few mm., while the sulfur pressure was at least an atmosphere.

(7) JANAF Interim Thermochemical Tables, prepared by members of the staff of the Thermal Laboratory, the Dow Chemical Co., Midland, Mich. Revision as of September, 1961.

(8) N. W. Luft, *Monatsh.*, **86**, 474 (1955).

(9) L. Brewer and K. Pitzer, Revision of G. N. Lewis and M. Randall, "Thermodynamics," McGraw-Hill Book Co., New York, N. Y., 1961, p. 672.

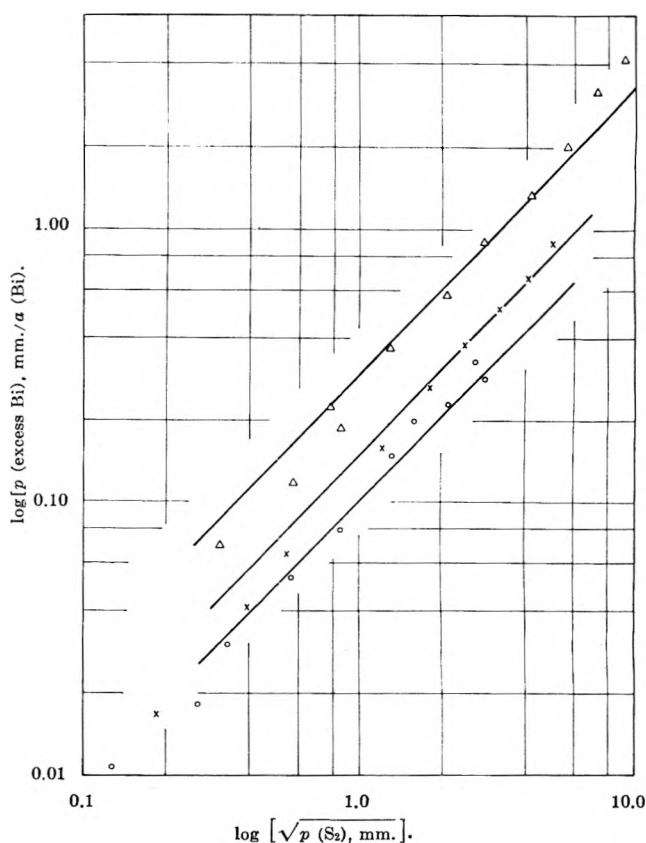


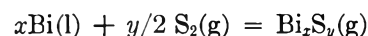
Fig. 3.—Excess bismuth in vapor. Log-log graph of [pressure of excess bismuth in vapor/activity of bismuth in liquid] vs. [square root of sulfur pressure] at 705° (lowest set of data), 740°, and 800° (uppermost set). Straight lines drawn with unit slope.

TABLE I
PRESSURES OVER PURE BISMUTH

Temp., °C.	Total measured by transpiration, expressed as mm. Bi	Partial press. Bi, calcd., mm.	Partial press. Bi_2 , calcd., mm.
705	0.028	0.0084	0.0098
740	.062	.018	.022
800	.20	.063	.068

gaseous Bi-S species. From this difference a pressure of "excess" bismuth (as monomeric Bi) was calculated.

To establish the formula of this molecule, the equilibrium:



was considered. Its equilibrium expression

$$K = \frac{(\text{Bi}_x\text{S}_y)}{(\text{Bi})^x(\text{S}_2)^{y/2}} \propto \frac{[\text{pressure of excess Bi}]}{[\text{activity Bi in liquid}]^x [p(\text{S}_2)]^{y/2}}$$

should be a constant. Thus a graph of $\log [\text{excess Bi pressure}/(\text{activity Bi})^x]$ vs. $\log [p^{1/2}(\text{S}_2)]$ should give a straight line of slope equal to the exponent y .

Such a graph was drawn assuming x equal to one. The data could be fit by straight lines of unit slope, indicating the molecule to be BiS. The results showed that a small fraction of the sulfur in the low pressure range had to be attributed to BiS. The lower pressures of sulfur were corrected for this BiS (the higher values were unaffected) and the data replotted to give the graph shown in Fig. 3. The precision of these data is not very high because the pressure of excess bismuth for low sulfur pressures is only a fraction of the total

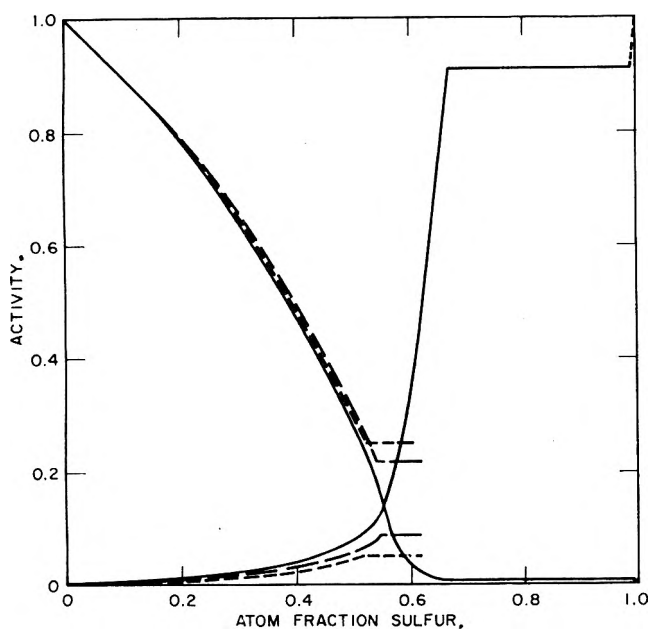
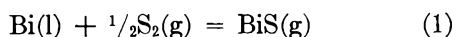


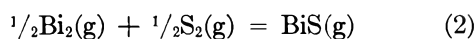
Fig. 4.—Activities of sulfur and bismuth at 705° (dotted), 740° (dashed), and 800° (full curve).

bismuth pressure, while at high sulfur pressures the total weight of bismuth collected was small. The data do fall reasonably close to straight lines. The equilibrium constants for the reaction



were, respectively, 0.10, 0.15, 0.31 (pressures in mm.) at 705, 740, and 800°.

It should be noted that a graph in which x had been assumed to be two gave a set of equally good straight lines of slope, y , equal to two, which would indicate the species to be Bi_2S_2 . Thus, this method only gives the ratio of bismuth to sulfur in the molecule, namely unity. The argument that led the writer to believe the BiS was monomeric is as follows. The entropy change, calculated from the data, for the reaction



was 3 e.u. The entropy change calculated from the same data for the reaction



that is, if a dimer were formed, was about -13 e.u. The entropy change for a reaction in which the net number of gas molecules does not change (*i.e.*, eq. 2) would be expected to be about zero and the 3 e.u. observed is close to zero, whereas for a reaction in which two gas molecules become one (*i.e.*, eq. 3) a value closer to -25 or -30 e.u. would be expected, as contrasted to the value -13 calculated from the data.

The amount of sulfur as BiS in the vapor was a small fraction of the total sulfur. The small, almost negligible correction required was made on the data shown in Fig. 3.

Thermodynamic Data.—The activity of sulfur in the melts relative to pure, liquid sulfur is equal to the square root of the pressure of S_2 divided by its value for liquid sulfur at the temperature in question. The activity of sulfur in the melts at the three temperatures studied is shown in Fig. 4. The curves have the

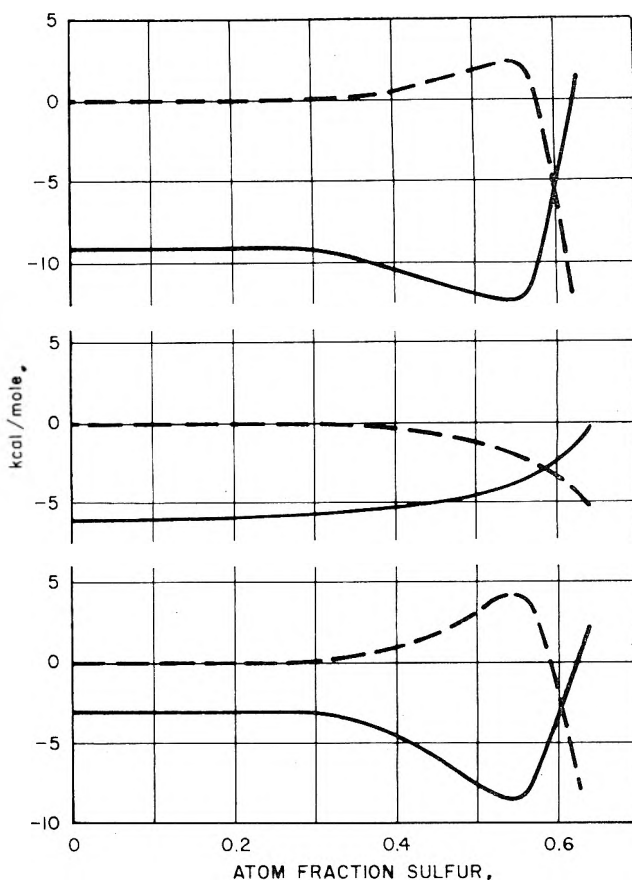


Fig. 5.—The partial molal quantities of solution at 800°: top, enthalpy; middle, excess free energy; bottom, excess entropy times temperature. Full curves for sulfur, referred to pure liquid sulfur. Dashed curves for bismuth referred to pure liquid bismuth.

same characteristics as those for the partial pressures of S_2 . The horizontal portions of the curves indicate the region in which two condensed phases existed.

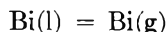
The activity of sulfur followed Henry's law up to almost 20 atom % sulfur. The Henry's law constants, k in the relation: activity of sulfur = $k \times$ atom fraction, were 0.039, 0.047, and 0.059 at 705, 740, and 800°.

The enthalpy of solution of liquid sulfur in the melts was derived from the change of logarithm of activity with reciprocal of absolute temperature. For the transpiration results these enthalpies were derived from the highest and lowest temperature data, while for the dew-point work the slopes of the lines of Fig. 2 were used. A smoothed curve drawn through the enthalpies is shown in Fig. 5. The excess partial molal free energy of solution of liquid sulfur in the melts was taken as $RT \ln$ [activity of sulfur/atom fraction of sulfur]. The curve for this function for 800° is the middle one of Fig. 5. The excess partial molal entropy times the temperature (at 800°) is the lowest curve of Fig. 5. It is the difference of the upper two curves.

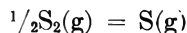
The activity of bismuth in the melts was calculated from that of sulfur using a graphical Gibbs-Duhem method. The curves for the three temperatures are shown in Fig. 4. The activity of bismuth followed Raoult's law over the same concentration range in which sulfur followed Henry's law. The partial molal enthalpy, excess free energy, and excess entropy times temperature of solution of bismuth were calculated from those of sulfur using a Gibbs-Duhem equation

for each thermodynamic quantity.¹⁰ They are also shown in Fig. 5.

The enthalpy of dissociation of gaseous BiS was obtained as follows. The change of the logarithm of the equilibrium constant with reciprocal of temperature for reaction 1 gave an enthalpy change of 25 ± 5 kcal. at the mid-temperature, about 1000°K. For the reaction



Brewer⁹ gives $\Delta H(298^\circ) = 49.5$ kcal. At 1000°K. this becomes 45.3 kcal., using Stull and Sinke's¹¹ heat content values. For the reaction



the JANAF tables⁷ give $\Delta H(1000^\circ) = 51.0$ kcal. Therefore, for the dissociation reaction



The heat of dissociation of the S₂ molecule is 102 kcal. and that of the Bi₂ molecule is 47 kcal.^{9,11} The average of these is 75 kcal. Thus the heat of dissociation of BiS is equal to the average of the heats of dissociation of Bi₂ and S₂.

Discussion

Some insight into the nature of these bismuth-sulfur melts can be obtained from the results presented above. The activity of sulfur followed Henry's law up to almost 20 atom % sulfur. This behavior indicates that the sulfur is monatomically dispersed in the melts. It also indicates that there is little interaction between the sulfurs even when there are as many as one sulfur atom to five bismuths. From this it would seem that the sulfur valences are of the short-range saturated type. Thus, it is unlikely that the sulfur species are ions since ions would show relatively long-range interactions.

Bismuth showed ideal solution behavior over the range from 0 to almost 20 atom % sulfur. Thus in a melt with as many as one sulfur to five bismuth atoms there was no heat of solution of bismuth and the entropy of solution was that for random mixing of the bismuths and the sulfurs; so the positions available to a bismuth atom—whether completely surrounded only by bismuth or with one or perhaps two sulfurs in the coordination shell—were equivalent.

As more sulfur is added, its activity increases more rapidly than Henry's law until, at temperatures below 775°, solid Bi₂S₃ precipitates. In solid Bi₂S₃ there are chains in which bismuth and sulfur alternate.¹² Pauling¹³ suggests that the metallic luster of substances of this type is due to metal-metal binding. Since these melts were metallic-looking,⁴ even those saturated with liquid sulfur, it might be presumed that bismuth-bismuth bonds exist even in melts with as high a sulfur atom fraction as 0.67.

(10) See ref. 9, eq. (20-20).

(11) D. R. Stull and G. C. Sinke, "Thermodynamic Properties of the Elements," American Chemical Society, Washington, D. C., 1956.

(12) A. F. Wells, "Structural Inorganic Chemistry," Oxford Press, London, England, 1945, p. 392.

(13) L. Pauling, "The Nature of the Chemical Bond," Third Ed., Cornell Univ. Press, Ithaca, N. Y., 1960, p. 442 ff.

The behavior of sulfur in the system changes in the region of 65 atom %. At smaller sulfur concentrations it shows negative deviations from Raoult's law and negative heats of solution relative to pure, liquid sulfur. Thus the sulfur is more stably bound in those bismuth-sulfur melts than in pure sulfur. At concentrations greater than 65 atom % the sulfur shows positive deviations from Raoult's law and the heat of solution becomes positive—typical of a system exhibiting two-liquid immiscibility. The environment for the sulfur in such melts is energetically less favorable than in liquid sulfur, but the favorable entropy factor overrides the energy up to 67%. It may be that the sulfur added beyond about 60 atom % would form primarily sulfur-sulfur bonds, as in polysulfides. Thus the nature of the binding of the additional sulfur would change from primarily bismuth-sulfur to sulfur-sulfur bonds in the region in which the enthalpy of solution increased sharply.

Rosenqvist¹⁴ has made measurements very similar to these for the silver-sulfur system over the range from Ag to Ag₂S. He found positive deviations from Raoult's law as contrasted to the negative deviations found here in the range Bi to Bi₂S₃. Otherwise the systems behave similarly.

The ratio of the relative concentration of sulfur to bismuth in the vapor to that in the melt is useful in considering the vaporization process as a means of purifying bismuth from sulfur. If that ratio is greater than unity, the melt becomes richer in bismuth when evaporation occurs; if less than unity, the vapor (or distillate) is richer in bismuth. In the present case the vapor is always richer in sulfur than the melt. The ratio, R , is expressed as

$$R = \frac{\left(\frac{\text{S}}{\text{Bi}}\right)_{\text{vapor}}}{\left(\frac{\text{S}}{\text{Bi}}\right)_{\text{melt}}} = \frac{p(\text{BiS}) + 2p(\text{S}_2) + 3p(\text{S}_3) + \dots}{p(\text{BiS}) + p(\text{Bi}) + 2p(\text{Bi}_2)} \cdot \frac{X(\text{S})}{X(\text{Bi})}$$

in which p is the partial pressure of a species and X the atom fraction of a component in the liquid. In the numerator the dashes indicate other sulfur species. Except for quite low sulfur atom fractions the predominant species in the vapor is S₂, so R is greater than unity and increases with atom fraction sulfur. At sufficiently low sulfur atom fractions, BiS becomes the important sulfur-containing vapor species, and its pressure is proportional to the sulfur atom fraction; the important bismuth-containing species are Bi and Bi₂, whose pressures are essentially independent of melt composition. The ratio reaches a finite limiting value for infinite dilution of sulfur. The limiting values are about the same at all three temperatures studied and equal to about 8. Thus over the entire range, R is greater than unity and the melt is always enriched in bismuth when some of it is removed by evaporation (under equilibrium conditions).

Acknowledgment.—The author is indebted to Mr. William E. Robbins for assistance in the experimental work, and to Professor Leo Brewer for important corrections on the original manuscript.

(14) T. Rosenqvist, *Trans. AIME*, **185**, 451 (1949).

IONIZATION AND DISSOCIATION PROCESSES IN PHOSPHORUS TRICHLORIDE AND DIPHOSPHORUS TETRACHLORIDE¹

BY ANTONIO A. SANDOVAL, H. C. MOSER, AND ROBERT W. KISER

Department of Chemistry, Kansas State University, Manhattan, Kansas

Received June 18, 1962

Appearance potentials and relative abundances are reported for the principal positive ions in the mass spectra of phosphorus trichloride and diphosphorus tetrachloride. Probable ionization and dissociation processes are deduced from the energetics, and the heats of formation of the various ions are given. The following molecular ionization potentials are given: phosphorus trichloride, 10.75 ± 0.2 and diphosphorus tetrachloride, 9.36 ± 0.2 e.v. Ionization potentials of PCl, PCl₂, and P₂ are calculated to be 9.6, 9.0, and 11.1 e.v., respectively. $D(\text{Cl}_2\text{P}-\text{PCl}_2) = 58$ kcal./mole.

Introduction

The preparation and properties of diphosphorus tetrachloride have been described in two publications.^{2,3} Recently, an improved synthesis and a mass spectral cracking pattern for P₂Cl₄ were reported by Sandoval and Moser giving additional evidence for the existence of this compound.⁴ We therefore undertook a detailed mass spectrometric investigation of the positive ions produced from P₂Cl₄ in order to define the ionization and dissociation processes occurring in P₂Cl₄ under electron impact. We report here the results of this study of P₂Cl₄, as well as a re-investigation of the electron impact processes in PCl₃.

Experimental

The preparation of the diphosphorus tetrachloride was accomplished by using two different synthetic techniques. One of these has already been described⁴ and the other method will be considered in a separate publication.⁵ The results of the 70 e.v. mass spectrometric analyses of both preparations were identical.

Phosphorus trichloride (Baker and Adamson Reagent Grade) was purified by using repetitive vacuum distillation and condensation techniques. Mass spectrometric analysis did not indicate any gross impurities in the samples to be used for the electron impact studies.

The ionization and appearance potentials were determined by the extrapolated voltage differences analysis⁶ of the ionization efficiency curves obtained using a time-of-flight mass spectrometer described previously.⁷ The energy compensation technique⁸ also was employed in these determinations. Spectroscopically pure xenon (Linde Co.) and nitrogen were employed as calibrating gases by comparing their observed ionization potentials with their known spectroscopic values. The gas used as the calibrating standard was intimately mixed with the PCl₃ or the P₂Cl₄ during the determinations of the appearance potentials of the various ions formed. The chlorine-37 isotope provided a convenient internal m/e reference; however, the appearance potentials were determined from ion currents due to those positive ions containing the chlorine-35 isotope (except for m/e 31 and 138 in PCl₃ and m/e 62 in P₂Cl₄). Negative ions were not studied.

Results

The results of the mass spectral data (partial mass spectra only) and the appearance potential determinations are presented in Tables I and II. The principal

(1) This work was supported in part by the United States Atomic Energy Commission under Contracts AT(11-1)-584 and AT(11-1)-751 with Kansas State University. Portion of a dissertation presented by A. A. Sandoval to the Graduate School of Kansas State University in partial fulfillment for the degree of Doctor of Philosophy in Chemistry.

(2) A. Besson and L. Fournier, *Compt. rend.*, **160**, 102 (1910).

(3) A. Finch, *Can. J. Chem.*, **37**, 1795 (1959).

(4) A. A. Sandoval and H. C. Moser, *Abstr. of Papers, 141st National Meeting of the American Chemical Society, Washington, D. C., March 21-29, 1962*, p. 21-M.

(5) A. A. Sandoval and H. C. Moser, *Inorg. Chem.*, **2**, 27 (1963).

(6) J. W. Warren, *Nature*, **165**, 810 (1950).

(7) E. J. Gallegos and R. W. Kiser, *J. Am. Chem. Soc.*, **83**, 773 (1961).

(8) R. W. Kiser and E. J. Gallegos, *J. Phys. Chem.*, **66**, 947 (1962).

positive ions and their relative abundances in the mass spectrum for 70 e.v. electrons are given in columns 1 and 2, respectively, of each table. The appearance potentials of the various positive ions and the probable processes by which the ions are formed at the threshold appear in columns 3 and 4. Column 5 gives the determined heat of formation of the ion; ΔH_f^+ was calculated from the appearance potential according to the process shown (see Discussion, below). Negative ions were not studied. The error values shown indicate the precision of successive determinations and do not necessarily reflect the absolute error involved in the measurements.

TABLE I

IONIZATION AND DISSOCIATION PROCESSES OF PHOSPHORUS TRICHLORIDE

m/e	R.A.	A.P., e.v.	Process	ΔH_f^+ , kcal./mole
138	31.5	10.75 ± 0.2	$\text{PCl}_3 \rightarrow \text{PCl}_3^+$	175
136	30.8			
101	100.0	$12.32 \pm .2$	$\rightarrow \text{PCl}_2^+ + \text{Cl}$	182
66	29.2	$16.83 \pm .3$	$\rightarrow \text{PCl}^+ + 2\text{Cl}$	257
35	48.3	$20.2 \pm .4$	$\rightarrow \text{Cl}^+ + \text{P} + \text{Cl}_2$	317
			$\rightarrow \text{Cl}^+ + \text{PCl} + \text{Cl}$	(35) ^a
31	20.9	$21.2 \pm .5$	$\rightarrow \text{P}^+ + 3\text{Cl}$	329

^a The value in brackets refers to the heat of formation of the PCl radical.

In the thermochemical calculations for the heats of formation of the gaseous ions and radicals, we have taken -73.22 kcal./mole for the heat of formation of phosphorus trichloride (g).⁹ From the appearance potentials for $m/e = 101$ and 66 in P₂Cl₄ and PCl₃, and assuming that $E(\text{P}-\text{Cl})$ in PCl₃ = 78 kcal./mole¹⁰ may be taken as $D(\text{Cl}_2\text{P}-\text{Cl})$, we estimate the heat of formation of diphosphorus tetrachloride to be -106 kcal./mole. In addition, heats of formation of Cl(g), P(g), and P₂(g), of 29.01 , 75.18 , and 33.82 kcal./mole,⁹ respectively, were employed in our calculations.

Discussion

Mass Spectra.—The 70 e.v. mass spectrum (partial) of phosphorus trichloride reported in Table I is in essential agreement with that of Kusch, Hustrulid, and Tate¹¹ (taken at 120 e.v.) considering the electron energy difference. The partial mass spectrum (at 70 e.v.) of diphosphorus tetrachloride reported here is

(9) F. D. Rossini, D. D. Wagman, W. H. Evans, S. Levine, and I. Jaffe, "Selected Values of Chemical Thermodynamic Properties," National Bureau of Standards Circular 500, U. S. Government Printing Office, Washington, D. C., 1952.

(10) T. L. Cottrell, "The Strengths of Chemical Bonds," 2nd Ed., Butterworths Scientific Publications, London, 1958, p. 283.

(11) P. Kusch, A. Hustrulid, and J. T. Tate, *Phys. Rev.*, **62**, 840 (1937).

TABLE II

IONIZATION AND DISSOCIATION PROCESSES OF DIPHOSPHORUS TETRACHLORIDE

m/e	R.A.	A.P., e.v.	Process	ΔH_f^\dagger , kcal./mole
202	4.6	9.36 \pm 0.2	$P_2Cl_4 \rightarrow P_2Cl_4^+$	110
167	5.3	11.7 \pm .3	$\rightarrow P_2Cl_3^+ + Cl$	135
132	1.5	13.9 \pm .3	$\rightarrow P_2Cl_2^+ + Cl_2$	215
101	100.0	11.68 \pm .2	$\rightarrow PCl_2^+ + PCl_2$	(-19) ^a
97	5.8	16.1 \pm .4	$\rightarrow P_2Cl^+ + Cl_2 + Cl$	236
66	36.5	15.7 \pm .3	$\rightarrow PCl^+ + PCl_2 + Cl$	(-30) ^a
62	9.9	19.7 \pm .4	$\rightarrow P_2^+ + Cl_2 + 2Cl$	290

^a The values in brackets refer to the heat of formation of the PCl_2 radical.

new. It is particularly significant that the PCl_2^+ at $m/e = 101$ is of greatest intensity in the spectrum. No significant quantities of PCl_3^+ ions were observed in the mass spectrum of P_2Cl_4 . Further remarks on this feature are given following the consideration of the appearance potentials of the various ions.

Appearance Potentials. $m/e = 31$.—The appearance potential of 21.2 e.v. for the P^+ ion was determined only in the case of PCl_3 , although it had a relative abundance of more than 15% in the P_2Cl_4 spectrum. The value of $\Delta H_f^\dagger(P) = 329$ kcal./mole, obtained from the observed appearance potential is in excellent agreement with the literature.⁹ We note that our appearance potential for P^+ from PCl_3 is nearly an electron volt lower than that determined by Kusch, Hustrulid, and Tate.¹¹

$m/e = 35$.—The appearance potential of Cl^+ from PCl_3 of 20.2 e.v. leads to a calculated $\Delta H_f^\dagger(Cl) = 317$ kcal./mole, approximately 10 kcal./mole lower than the literature value.⁹ For this reason, we believe some contribution, possibly significant in nature, may also be made by the process involving PCl and Cl as neutral fragments; if this is so, we calculate the heat of formation of PCl to be +35 kcal./mole, a value which appears to be not unreasonable. $E(P-Cl)$ from PCl_3 is given by Cottrell¹⁰ as 78 kcal./mole. Since $\Delta H_f^\dagger(PCl_3) = -73$ kcal./mole, the $\Delta H_f^\dagger(PCl)$ is expected to be in the neighborhood of +25 kcal./mole.

$m/e = 62$.—The heat of formation of P_2^+ , derived from the appearance potential and process given in Table II, is 290 kcal./mole. Combination of this result with $\Delta H_f^\dagger(P_2) = 33.82$ kcal./mole leads to an ionization potential of 11.1 e.v. for P_2 , in fair agreement with 11.8 ± 0.5 e.v. reported by Gutbier.¹²

$m/e = 66$.— $\Delta H_f^\dagger(PCl) = 257$, as determined from the appearance potential for the PCl^+ ion from PCl_3 . Utilization of this value with the appearance potential of PCl^+ from P_2Cl_4 leads to a heat of formation of the PCl_2 radical of -30 kcal./mole. This value is very close to $\Delta H_f^\dagger(PCl_2) = -24$ kcal./mole, calculated from $E(P-Cl) = 78$ kcal./mole and $\Delta H_f^\dagger(PCl_3) = -73$ kcal./mole. Therefore, we believe that the possible formation of Cl^- (or PCl_2^-) in an ion pair formation process does not, in fact, occur. Our value of $\Delta H_f^\dagger(PCl)$ is about 15 kcal./mole lower than that derived from Kusch, Hustrulid, and Tate's data.^{11,13} From the values of $\Delta H_f^\dagger(PCl)$ and $\Delta H_f^\dagger(PCl)$ given in Table II, $I(PCl) = 9.6$ e.v.

$m/e = 97$.—From the process shown in Table II, we deduce $\Delta H_f^\dagger(P_2Cl) = 236$ kcal./mole. The proc-

ess in which $3Cl$ are formed as the neutral fragments leads to a value of $\Delta H_f^\dagger(P_2Cl) = 178$ kcal./mole, a value which appears to be significantly too low. If ion pair formation is involved, $\Delta H_f^\dagger(P_2Cl) = 324$ or 266 kcal./mole, respectively. Both of these values appear too great; certainly the value of 324 kcal./mole is beyond reasonable expectations. We believe, therefore, that an ion pair formation process does not make a significant contribution in the formation of P_2Cl^+ .

$m/e = 101$.—This ion is the ion of greatest abundance in the spectra of both PCl_3 and P_2Cl_4 , and is the PCl_2^+ ion. From the PCl_3 study, $\Delta H_f^\dagger(PCl_2) = 182$ kcal./mole. This value may be compared to the value of 189 kcal./mole reported in the literature.^{11,13} Combination of our result of $\Delta H_f^\dagger(PCl_2) = 182$ kcal./mole with the appearance potential of 11.68 e.v. for $m/e = 101$ from P_2Cl_4 leads to $\Delta H_f^\dagger(PCl_2) = -19$ kcal./mole. From the appearance potentials of the $m/e = 66$ ions, we derived a value of -30 kcal./mole for $\Delta H_f^\dagger(PCl_2)$. Hence, we believe that $\Delta H_f^\dagger(PCl_2) = -25$ kcal./mole. From this, we see that the ionization potential of PCl_2 is about 9.0 e.v.

Using $E(P-Cl) = 78$ kcal./mole,¹⁰ $\Delta H_f^\dagger(PCl_3) = -73$ kcal./mole, and $\Delta H_f^\dagger(Cl) = 29$ kcal./mole, we calculate $\Delta H_f^\dagger(PCl_2) = -24$ kcal./mole, in good agreement with our average value of -25 kcal./mole. We conclude that the process is that given in Table II and ion pair formation processes do not make a significant contribution.

$m/e = 132$.—From the appearance potential of 13.9 e.v. for $P_2Cl_2^+$ from P_2Cl_4 , we calculate $\Delta H_f^\dagger(P_2Cl_2) = 157$ kcal./mole, assuming $2Cl$ as the neutral fragments. However, we slightly favor the process involving the formation of a chlorine molecule; this gives a $\Delta H_f^\dagger(P_2Cl_2) = 215$ kcal./mole. Clearly, no certain assignment of one process or the other process can be derived from the data here presented. If an ion pair formation process were involved in the formation of $P_2Cl_2^+$, $\Delta H_f^\dagger(P_2Cl_2)$ would be closer to 245 kcal./mole, a value which we believe to be too great in comparison to ΔH_f^\dagger values of the other $P_2Cl_2^+$ ions.

$m/e = 138$.—The ionization potential of PCl_3 was determined to be 10.75 ± 0.2 e.v. This leads to $\Delta H_f^\dagger(PCl_3) = 175$ kcal./mole. Our results are not in agreement with the earlier work of Kusch, Hustrulid, and Tate.¹¹ We repeatedly observed a difference of 1.5 to 1.6 e.v. for $[AP(PCl_2^+) - AP(PCl_3^+)]$ from the PCl_3 study, whereas Kusch, Hustrulid, and Tate¹¹ observed only 0.3 e.v. difference. We cannot offer any explanation for the difference of our results with those of the earlier workers, but we do observe that a recent determination of the ionization potential of $AsCl_3$

(12) H. Gutbier, *Z. Naturforsch.*, **16A**, 268 (1961).

(13) F. H. Field and J. L. Franklin, "Electron Impact Phenomena and the Properties of Gaseous Ions," Academic Press, Inc., New York, N. Y., 1957, p. 299.

by Cullen and Frost¹⁴ gave a result 0.6 e.v. lower than that determined by Kusch, Hustrulid, and Tate.¹¹

$m/e = 167$.—The dissociative ionization of P_2Cl_4 to form $P_2Cl_3^+$ was observed to require 11.7 e.v. This result leads to $\Delta H_f^+(P_2Cl_3) = 135$ kcal./mole. Energetic considerations indicate that Cl^- is not formed as an accompanying fragment in the formation of $P_2Cl_3^+$.

$m/e = 202$.—The ionization potential of P_2Cl_4 was observed to be 9.36 ± 0.2 e.v. This gives a calculated $\Delta H_f^+(P_2Cl_4) = 110$ kcal./mole. Although the intensity of this ion in the mass spectrum of P_2Cl_4 is only about 5% of the base peak ($m/e = 101, PCl_2$), it was quite sufficient in intensity to afford a precise determination of the ionization potential. The background at $m/e = 202$ due to mercury from the diffusion pump was very small; in addition, the ionization potential of 9.36 e.v., one electron volt lower than the ionization potential of mercury, indicates no significant contribution to the $m/e = 202$ peak from mercury in the region of the ionization threshold.

(14) W. R. Cullen and D. C. Frost, *Can. J. Chem.*, **40**, 390 (1962).

Combining the appearance potential of PCl_2^+ from PCl_3 and of PCl_2^+ from P_2Cl_4 with $D(Cl_2P-Cl) = 78$ kcal./mole, we calculate $D(Cl_2P-PCl_2) = 63$ kcal./mole. A value of $D(Cl_2P-PCl_2) = 52$ may be obtained using $AP(PCl^+)$ from both PCl_3 and P_2Cl_4 and $D(Cl_2P-Cl)$. Hence we take $D(Cl_2P-PCl_2) = 58$ kcal./mole. Cottrell¹⁰ lists $E(P-P)$ in P_4 as 48 kcal./mole and $D(P-P)$ as 116 kcal./mole (from P_2). From our data and using $E(P-Cl) = 78$ kcal./mole, we calculate $D(P-P)$ in P_2 to be 113 kcal./mole.

The P-P sigma bond energy is 58 kcal./mole from our study of P_2Cl_4 . This would indicate that the P-P bond in P_2 has π character, and we estimate this π character to be about 1.1–1.2 π bonds, in agreement with Van Wazer's value of 1.3 π bonds.¹⁵

Acknowledgments.—The authors wish to express their appreciation to B. G. Hobrock for his aid in obtaining some of the experimental data.

(15) J. R. Van Wazer, "Phosphorus and Its Compounds," Vol. I, Interscience Publishers, Inc., New York, N. Y., 1958, p. 35.

ONSAGER'S RELATION AND THE NON-ISOTHERMAL DIFFUSION OF WATER VAPOR¹

BY J. W. CARY

Southwest Branch, Soil and Water Conservation Research Division, Agriculture Research Service, USDA, Logan, Utah

Received June 18, 1962

The problem of thermally induced water vapor diffusion is analyzed with thermodynamics of irreversible processes and Onsager's relation. The rate equations are developed to account for the effect of significant thermal gradients on the free energy-temperature function. This effect has been isolated from other potential fields and the rate equations evaluated with appropriate data. The Onsager reciprocity relation was tested and found to be valid within the bounds of experimental error for a particular system.

I. Introduction

Consider a system in which two moist porous disks are separated by a small air space. The temperature of each disk may be adjusted individually to create small thermal gradients. The system is oriented in the gravitational field such that no convective currents are present in the air gap at steady state. There then will be a simultaneous diffusion of heat and moisture from the warm air-water interface to the cool air-water interface. For very small thermal gradients, the rate of vapor diffusion through the air space may be described approximately by Fick's law. A more complete treatment of the phenomena including the specific effects of the temperature difference has been well developed from the kinetic theory of gases and has been reviewed in the monograph by Grew and Ibbs.² The flow of heat across the air space may be accounted for satisfactorily by summing up the components of heat transferred by thermal conduction, by radiation, and as latent heat of vaporization.

The purpose of this paper is to combine some of these more classical results with rate equations developed from irreversible thermodynamics such that a test of the validity of the Onsager reciprocity relation can be made. While Onsager's reciprocity relation has been verified experimentally for a number of isothermal sys-

tems, as reviewed by Miller,³ there still is little proof of its validity when applied to processes complicated by thermal gradients.

In order to suspect reasonably that the system described at the beginning of this discussion is suitable for analysis with thermodynamics of irreversible processes, consideration must be given to several criteria such as linearity, independence of fluxes or driving forces, the degree of displacement from equilibrium, etc. These result from assumptions made in the development of the general theory and have been discussed by de Groot and Mazur⁴ and Prigogine.⁵ Because these criteria are as yet more qualitative than quantitative, it usually is necessary to test each particular case against experimental evidence before a final conclusion can be drawn. In this case it is convenient to argue the justification for applying the Onsager identity by pointing out the analogy between the system in question and electro-osmosis. Suppose that the water was being transported across a porous plug rather than an air space and that it was flowing in response to an electrical potential rather than a thermal potential. Thus, the thermal potential could be analogous to electrical potential, heat flux analogous to electron flux, and the air gap analogous to the porous plug when the mobile mass component is

(3) D. G. Miller, *Chem. Rev.*, **60**, 15 (1960).

(4) S. R. de Groot and P. Mazur, "Non-equilibrium Thermodynamics," John Wiley and Sons, New York, N. Y., 1962.

(5) I. Prigogine, "Introduction to Thermodynamics of Irreversible Processes," Charles C. Thomas, Springfield, Illinois, 1955.

(1) Approved by the Director, Utah Agricultural Experiment Station, as Journal Paper 265.

(2) K. E. Grew and T. L. Ibbs, "Thermal Diffusion in Gases," Cambridge University Press, New York, N. Y., 1952.

water. If, on the other hand, an osmotic or other external force were applied across the air gap, a spontaneous thermal gradient could develop (diffusion thermo-effect and latent heat transfer), which would be analogous to the forced flow of water through a porous plug giving rise to an electrical gradient. Onsager's relation is, as shown by Miller,³ well established for many electro-osmotic systems. Furthermore, Scheer⁶ recently has argued that a flux across parallel phase boundaries may be expressed as a linear function of the differences in electrochemical potential across the system.

Similarities between the problem presented here and thermal osmosis and thermomechanical effects are also obvious. The use of thermodynamics of irreversible processes in the analysis of thermal osmosis of gas through a membrane has led Denbigh and Raumann,⁷ and Bearman,⁸ to workable relations between the temperature gradient, pressure gradient, and the heat of transfer. The problem of thermal diffusion in liquids has been approached through the theory of irreversible processes in a particularly interesting manner by Dougherty and Drichamer,^{9,10} and the literature on this subject has been reviewed thoroughly by von Halle.¹¹ Hutchison, Nixon, and Denbigh,¹² Spanner,¹³ and Taylor and Cary¹⁴ have studied the thermomechanical phenomena arising in various porous systems with irreversible thermodynamics. Good use has been made of the general theory for developing rate and steady state equations for these non-isotherm problems; however, experimental verification of the Onsager reciprocity relation for these applications is lacking. As pointed out by Miller,³ only Kapitza,¹⁵ Meyer and Mellink,¹⁶ and Brewer and Edwards,¹⁷ working with liquid helium, have reported data suitable for testing the Onsager hypothesis as related to the thermomechanical effect. In this case the reciprocity relation appeared to be valid.

Expressions already well known for the thermomechanical effect are not applicable to the problem under discussion here. The rigorous development of these equations requires either infinitesimally small thermal gradients or a free energy function that is independent of temperature. While these conditions are not strictly complied with in most thermomechanical experiments, the errors may be reduced to second order by a significant pressure difference or other force field across the dividing barrier. None of these criteria are met by the system in question here, *i.e.*, there is no significant pressure difference, the temperature gradient is not infinitesimally small, and the free energy of water

is a function of temperature. Therefore, the development of rate equations for the flux of heat and water must begin with the entropy function for this particular case.

II. Theoretical

Following the analysis of Prigogine,⁵ the rate of internal entropy production, σ , due to the flow of mass and energy across the air gap may be written as

$$\sigma = -J_w \Delta \frac{\mu_w}{T} + J_e \Delta \frac{1}{T} \quad (1)$$

or

$$\sigma = -J_w \Delta \frac{\mu_w}{T} + J_w H_0 \Delta \frac{1}{T} + J_q \Delta \frac{1}{T} \quad (2)$$

where J is flux, μ_w the chemical potential of water, T the absolute temperature, H_0 the absolute enthalpy per mole of the pure water in the cool plate, Δ indicates the difference between the two plate faces; and the subscripts w, e, and q denote water, energy, and heat, respectively. The system so described is discontinuous, *i.e.*, two liquid water films supported by the porous plates and separated by a gas phase.

Integrating the Gibbs-Helmholtz equation at a constant 1-atm. pressure over the temperature difference between the plates gives

$$\Delta \frac{\mu_w}{T} = -C_p \Delta \ln T + (H_0 - C_p T_0) \Delta \frac{1}{T} \quad (3)$$

provided the temperatures lie between 273.16 and 373.16°K. and the heat capacity of liquid water, C_p , is taken as constant so that $H = C_p(T - T_0) + H_0$. Putting eq. 3 into 2 results in

$$\sigma = J_w \left(C_p \Delta \ln T + C_p T_0 \Delta \frac{1}{T} \right) + J_q \Delta \frac{1}{T} \quad (4)$$

The phenomenological equations for heat and mass transfer then may be written, as shown by Prigogine,⁵ as

$$J_w = L_w \left(C_p \Delta \ln T + C_p T_0 \Delta \frac{1}{T} \right) + L_{wq} \Delta \frac{1}{T} \quad (5)$$

$$J_q = L_{qw} \left(C_p \Delta \ln T + C_p T_0 \Delta \frac{1}{T} \right) + L_q \Delta \frac{1}{T} \quad (6)$$

where L is a phenomenological coefficient.

In this case physical significance can be assigned to L_w , L_{qw} , and L_q through the following arguments.

Suppose that for the system described in the Introduction the water were driven across the air space only by an osmotic pressure difference between the water reservoirs. Equation 1 then would become simply

$$\sigma = -J_w \Delta \frac{\mu_w}{T} = -J_w R \Delta \ln p \quad (7)$$

where p is vapor pressure of water and R is the gas constant. In this case eq. 5 would become

$$J_w = -L_w R \Delta \ln p \quad (8)$$

For this isothermal process, the vapor flux also may be represented by Fick's law

$$J_w = -D \frac{dc}{dl} = -\frac{D}{RT} dp = -\frac{Dp}{RT} d \ln p \quad (9)$$

(6) B. T. Scheer, *Science*, **135**, 313 (1962).

(7) K. G. Denbigh and G. Raumann, *Proc. Roy. Soc. (London)*, **A210**, 377, 518 (1952).

(8) R. J. Bearman, *J. Phys. Chem.*, **61**, 708 (1957).

(9) E. L. Dougherty and H. G. Drichamer, *ibid.*, **59**, 443 (1955).

(10) E. L. Dougherty and H. G. Drichamer, *J. Chem. Phys.*, **23**, 295 (1955).

(11) E. von Halle, "A New Apparatus for Liquid Phase Thermal Diffusion," available from the Office of Technical Service, U. S. Dept. of Commerce, Washington, D. C., 1959.

(12) H. P. Hutchison, I. S. Nixon, and K. G. Denbigh, *Discussions Faraday Soc.*, **3**, 86 (1948).

(13) D. C. Spanner, *Symp. Exptl. Biol.*, **VIII**, 76 (1954).

(14) S. A. Taylor and J. W. Cary, *Trans. 7th Intern. Congr. of Soil Sci.*, **I**, 80 (1960).

(15) P. Kapitza, *Phys. Rev.*, **60**, 354 (1941).

(16) L. Meyer and J. Mellink, *J. Physica*, **12**, 197 (1947).

(17) D. F. Brewer and D. O. Edwards, *Proc. Phys. Soc. (London)*, **71**, 117 (1958).

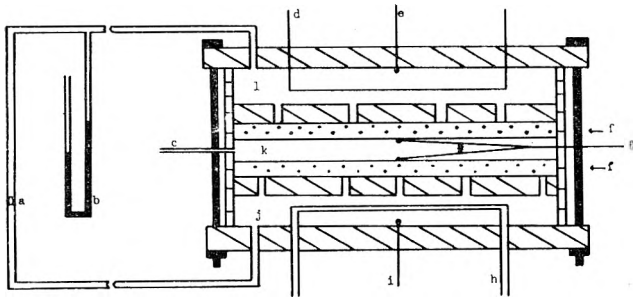


Fig. 1.—Cross-sectional diagram of the vapor diffusion apparatus. It is described in detail in section III, Experimental.

where D is the diffusion coefficient for water vapor in air, c the concentration of water vapor, and l the distance between the plates. Comparison of eq. 8 and 9 suggests that for small vapor pressure gradients, the approximation

$$L_w = \frac{Dp}{R^2lT} \quad (10)$$

will be useful.

When the system operates under a thermal gradient such that there is a steady state flux of both heat and vapor, the net heat flux across the air space must be the sum of three components: that transferred by the vapor as latent heat (ΔH_v), that flowing by thermal conduction through the gas, and that transferred by thermal radiation. For small thermal differences, the radiation flux is approximately proportional to the temperature difference, ΔT , which may be taken as $T^2 \Delta (1/T)$. Thus the net heat flux per unit area may be written as

$$J_q = \Delta H_v J_w + (K + \beta) \frac{T^2}{1} \Delta \frac{1}{T} \quad (11)$$

where K is Fourier's thermal conductivity of air and β is the proportionality constant for radiation.¹⁸ Replacing J_w with its equivalent from eq. 5, eq. 11 becomes

$$J_q = \Delta H_v L_w C_p \Delta \ln T + \left[\Delta H_v L_w C_p T_0 + \Delta H_v L_w q + (K + \beta) \frac{T^2}{l} \right] \Delta \frac{1}{T} \quad (12)$$

Comparison of eq. 6 and 12 leads to the conclusions that for this system

$$L_{qw} = \Delta H_v L_w = \frac{\Delta H_v D p}{R^2 l T} \quad (13)$$

and

$$L_q = \Delta H_v L_w q + (K + \beta) \frac{T^2}{l} \quad (14)$$

The linear phenomenological equations for the net flux of water and heat across the air space of this system may be rewritten then as

$$J_w = \frac{2.3C_p D p}{R^2 l T} \Delta \log T + \left(\frac{C_p T_0 D p}{R^2 l T} + L_{wq} \right) \Delta \frac{1}{T} \quad (15)$$

(18) In this analysis $\Delta 1/T > 0$ when J_q is chosen as positive since the term, $J_q \Delta 1/T$, in eq. 4 must be positive.

and

$$J_q = \frac{2.3C_p \Delta H_v D p}{R^2 l T} \Delta \log T + \left[\frac{C_p T_0 \Delta H_v D p}{R^2 l T} + (K + \beta) \frac{T^2}{l} \right] \Delta \frac{1}{T} \quad (16)$$

Equations 15 and 16 account for the most significant mechanisms of transfer across the air space and should give good approximations of the water and heat fluxes due to small thermal gradients. Use of eq. 13 and 15 provides a direct test of the Onsager reciprocity relation provided one value of J_w as a function of T is available.

III. Experimental

The simultaneous fluxes of heat and water vapor were measured with the apparatus diagrammed in Fig. 1. The upper water chamber, l, was warmed to a steady-state temperature by applying a constant voltage across the heater, d. The lower water chamber, j, was cooled to a steady state temperature by circulating constant temperature water through a copper coil, h. The resulting thermal gradient between the porous ceramic disks, f, caused a diffusion of water vapor across the air space, k. This flux produced a corresponding movement of a mineral oil bubble through the calibrated flow tube, a, and so the rate of vapor transfer between the porous plates could be measured. The mercury manometer, b, was connected into the circulating water system to prevent liquid phase water from moving into the air space and also to assure a negligible total pressure difference between the two water reservoirs, j and l. The apparatus, except for the external flow tube and manometer, was covered with aluminum foil and supported in a vacuum chamber. To calibrate the apparatus for heat loss to its surroundings, the air space, k, was filled with water. The steady-state temperature in the warm chamber was recorded as a function of voltage across the heater with the cool chamber temperature held constant. The power input minus the heat conducted across the water-filled air gap was plotted against warm chamber temperature. This formed a heat loss calibration curve. The steady-state heat flux across the air gap then was known from the difference between the electrical energy input and the apparatus' heat loss.

The temperature of the water reservoirs was measured with thermistors, e and i. The temperature of the air-water interface was measured with the thermistors, g. These were small bead sensors enclosed in slender glass rods. They were held in contact with the air-water interface by a spring, as shown in Fig. 1. Atmospheric pressure was maintained by the vent, c, which was covered with a flexible rubber membrane. The vapor gap was 1.5 cm. across and 19.8 cm. in diameter. It was bounded horizontally by ceramic filter plates. These plates were supported by perforated 0.5-in. lucite disks. The covers for the water reservoirs were also made from 0.5-in. lucite plates. The vertical boundaries of water chambers and air space were made from rings of 1/8-in. wall lucite tube. Rubber gaskets were used where necessary, and the apparatus was held together with 12 1/4-in. bolts. It was always placed in the vacuum chamber with the cool side downward to prevent convection currents from developing in the air space. The vacuum chamber was placed in a constant temperature air bath, and the whole assembly was housed in a constant temperature room.

Measurements of heat and water flow were made by first applying a constant a.c. voltage to the 4.43-ohm heating element. The power source was an electronic voltage regulator and rheostat. The voltage across the heater was measured with an a.c. meter which had been calibrated with a standard calorimeter assembly. At least 16 hr. was allowed for the system to reach steady state. The flow rate through the external tube, the level of the mercury manometer, and the temperature distribution across the apparatus were measured periodically for the next 6 to 8 hr. to assure that the system was at steady state. The simultaneous fluxes of heat and moisture measured as a function of temperature at the air-water interfaces are shown in Table I.

IV. Results

Numerical values for L_{qw} were calculated from eq. 13. Corresponding values of L_{wq} were calculated from eq. 15 using the temperature and water flux data given

TABLE I
 EXPERIMENTAL OBSERVATIONS AND CALCULATED VALUES

T Warm film, °C.	T Cool film, °C.	J_w Measured, moles/sec. cm. ²	J_w		L_{qw}	L_{wq}	(L_{wq}/L_{qw})	J_q	
			Predicted					Measured (mjoules/sec. cm. ²)	Predicted
13.83	11.95	1.44×10^{-8}	1.43×10^{-8}		0.626×10^{-3}	0.628×10^{-3}	1.00		
20.60	15.55	5.06	5.01		0.773	0.782	1.01		
27.22	26.37	1.56	1.45		1.527	1.642	1.08	0.49	0.85
28.68	27.23	2.74	2.61		1.632	1.712	1.05	1.51	1.42
30.43	28.30	4.16	4.17		1.803	1.796	1.00	2.24	2.38
31.67	28.95	5.25	5.59		1.895	1.888	1.00	2.83	3.16
33.15	29.88	6.90	7.21		2.055	1.967	0.96	3.75	4.01
33.35	30.32	6.22	6.69		2.050	1.917	0.94	4.06	3.72
34.26	30.53	8.15	8.44		2.122	2.060	0.97	4.73	4.67
35.06	31.10	9.35	9.29		2.208	2.264	1.03	5.40	5.10
37.00	36.20	2.17	2.25		2.699	2.614	0.97	1.58	1.19
43.48	40.60	11.03	10.47		3.622	3.816	1.05	4.80	5.29

in Table I. The results and the ratio (L_{wq}/L_{qw}) are included in Table I. Values of ΔH_v and p were taken from the "Handbook of Chemistry and Physics,"¹⁹ and values of D came from Dorsey.²⁰ They were chosen in accordance with the average temperature between the two air-water interfaces. The coefficient, D , was taken as inversely proportional to the atmospheric pressure, in this case, 64 cm. It was also considered to be unaffected by the small thermally induced concentration differences of the gases in the air space.

If one assumes that the Onsager reciprocity relation is valid for this system, eq. 15 may be written as

$$J_w = \frac{DpC_p}{R^2T} \left[\Delta \ln T + \left(T_0 + \frac{\Delta H_v}{C_p} \right) \Delta \frac{1}{T} \right] \quad (17)$$

The steady-state vapor flux may be predicted from this equation for any given temperatures of the air-water interfaces without any prior measurements of flux in the system. The values of J_w so calculated are shown in Table I.

Equation 12 may be used to find values of heat flux, provided the value of the constant ($K + \beta$) is known. The value of β depends on the particular system used and so must be measured. For this case a reasonable estimate of ($K + \beta$) is 4×10^{-4} joule per sec. cm. °C. Values for the simultaneous heat flow calculated from eq. 12 also are listed in Table I.

Before drawing any conclusions based on these results, the magnitude of the experimental errors must be

(19) "Handbook of Chemistry and Physics," Chemical Rubber Publishing Co., 35th Edition, 1953-1954.

(20) N. E. Dorsey, ACS Monograph 81 (1940).

considered. Random variations in water flux measurements were generally less than $\pm 0.15 \times 10^{-8}$ mole per sec. cm.². The difficulties in reproducing heat flux measurements were greater. Variations of 0.5 mjoule per sec. cm.² sometimes occurred. However, the measured values of heat flux were not necessary for testing the validity of Onsager's reciprocity relation. The fourth significant figure in the temperature measurements must be regarded as an estimation. Variations in the steady-state temperatures shown in Table I were not greater than $\pm 0.05^\circ$. The accuracy of the vapor flux measurement may have been affected by the vertical boundaries of the air space, though it is believed that this was less than the error developed by random variations. The accuracy of the heat flux measurements was largely dependent on the validity of the heat loss calibration. This could have been in error by as much as 10%. The temperature recorded by the thermistors may have been slightly different from the true temperature of the air-water interface, though it is not likely that this error was greater than 0.1° .

Considering these experimental difficulties and the approximations required in using isothermal values of p , D , ΔH_v , C_p , and T in non-isothermal equations, the variation of the ratio L_{wq}/L_{qw} is not unreasonable. The differences between the measured and predicted values of heat and vapor fluxes are also within the limits of experimental and theoretical errors. The author concludes that the Onsager reciprocity relation is valid for this system, and that eq. 12 and 15 give reliable estimates of the simultaneous fluxes of heat and water across the air space.

INVESTIGATION OF SOLUTION ADSORPTION ON PLATINUM OF PURE AND MIXED FILMS OF FATTY AMINES BY CONTACT POTENTIALS¹

BY K. W. BEWIG AND W. A. ZISMAN

U. S. Naval Research Laboratory, Washington 25, D. C.

Received June 20, 1962

A homologous series of pure, primary, fatty amines from C₄ to C₂₂ has been studied in the form of retracted monomolecular films adsorbed on pure polished platinum. The change in the contact potential difference between the platinum electrode and a stable reference electrode of gold coated with FEP Teflon as the result of the adsorption of each condensed monolayer was measured at 20° and 50% relative humidity in filtered air carefully freed from organic contaminants. The molecular packing of amine molecules in each monolayer was measured conveniently although indirectly by obtaining the contact angle of pure methylene iodide as in our previous investigations. Contact potential differences were reproduced readily under these conditions in independent measurements within ±2% provided the electrode temperature and the relative humidity were controlled appropriately. Monolayers were deposited on the platinum electrode by retraction from a variety of pure solvents. Plots of the contact angle vs. the number of carbon atoms per amine molecule and of the contact potential differences vs. the contact angle were found most informative about the effects of homology, molecular packing, and orientation, as well as of solvent inclusion through molecular adlineation in the monolayers. The molecular adlineation of solvents containing a phenyl group as well as branching of the hydrocarbon chain were compared with that of straight chain alkane solvents.

Introduction

After a metal surface has been coated with a film of either Teflon or FEP Teflon, there is practically no tendency to adsorb gases or vapors which are above their boiling points.² An unreactive metal, like gold, when so coated is an effective reference electrode for studying the adsorption of molecules on an uncoated or "active" metal electrode by means of measurements of change in the contact potential difference between the electrodes. This useful surface property of fluorocarbon resins follows from their extraordinarily low surface energies (or low critical surface tensions of wetting). For example, the critical surface tension of wetting of Teflon is 18.5 dynes/cm.,³ and of FEP Teflon only 16.2 dynes/cm.⁴ Recently, Martinet⁵ and Graham⁶ have shown that Teflon has low gas adsorptivity at ordinary temperatures. We report here the changes observed in the contact potential difference between such a reference electrode and the clean polished surface of platinum (the active electrode) upon which a close-packed monolayer of each of the homologous fatty amines has been adsorbed. Results are also presented on the effects of varying the solvent from which the amine is adsorbed, the time allowed for adsorption, the conditions under which mixed condensed films of solute and solvent are adsorbed, and on the relation between structure of amine and solvent molecules for stable mixed films to form.

Experimental

Materials and Procedures.—The primary fatty amine compounds used as adsorbates in this investigation were of unusual purity; when each was melted and recrystallized in flowing dry nitrogen gas, a melting point range within 1 or 2° of the best literature values was obtained. All of the contact potential measurements were made using the vibrating condenser method^{7,8} in a room ventilated with filtered air freed of adsorbable vapors and controlled to 50 ± 5% relative humidity and 20 ± 1°.

The platinum surface on which each monolayer was adsorbed was prepared by polishing it on a wet "kitten's ear" cloth with levigated alumina having an average particle size of 0.3 μ; it then was scrubbed on a clean, grease-free cloth, rinsed in flowing distilled water, and dried in clean air. In the carefully controlled air used, this treatment gave adequately reproducible contact potential differences between the reference electrode and the clean platinum electrode and also the platinum electrode after having been coated with an adsorbed monolayer of the amine. Reproducibility was always within ±10 mv. even after 24 hr. When platinum was cleaned in this way, much more reproducible data were obtained than after flaming, or after various etching treatments, or after cleaning with redistilled solvents. Of course, none of these treatments in the air produced platinum surfaces free of oxide.

Each of the fatty amines studied was adsorbed on the platinum by retraction⁹⁻¹¹ from a solution in pure nitromethane or in each of a variety of pure hydrocarbons. The contact potential difference referred to throughout this report was obtained by first allowing a freshly cleaned, plane, platinum electrode which was 3/8 in. in diameter and 1/16 in. thick to come to equilibrium with the room atmosphere for 30 min., at which time the difference in contact potential between it and the coated reference electrode was measured. Next, the electrode was removed from the vibrating condenser and placed in a solution of the amine for the desired immersion time. Finally, the electrode was removed slowly from the solution with its plane face held vertically in order to allow the liquid to retract, and the resulting dry, monolayer-covered electrode was inserted in the vibrating condenser. The resulting potential difference was found to be constant for a long time and so could be measured readily. The difference in the contact potential before and after the platinum had been so immersed and retracted from the adsorbing solution will be denoted as Δ*V*.

The contact angle (θ) reported here is the value measured with a sessile drop of pure, colorless, methylene iodide (surface tension, 50.8 dynes/cm. at 20°) resting on the film-coated, horizontal, platinum surface of the active electrode. A contact angle of from 68 to 70° always is obtained with methylene iodide when resting under equilibrium conditions on the close-packed methyl terminal groups of a film comprised of paraffinic polar molecules.¹¹⁻¹³ We have used methylene iodide extensively for measurements of contact angles on films because its high surface tension leads to large values of θ, the approximate spherical shape of the molecule minimizes any tendency to molecular ad-

(1) Presented at the National Meeting, Division of Colloid and Surface Chemistry, American Chemical Society, Washington, D. C., March 29, 1962.

(2) (a) K. W. Bewig and W. A. Zisman, NRL Report 5383, "Metals Coated with Films of Low Surface Energy as Reference Electrodes for the Measurements of Contact Potential Differences," October 23, 1959; (b) K. W. Bewig and W. A. Zisman, *Advances in Chemistry Series*, No. 33, American Chemical Society, Washington, D. C., 1961, p. 100.

(3) H. W. Fox and W. A. Zisman, *J. Colloid Sci.*, **5**, 514 (1950).

(4) M. K. Burnett and W. A. Zisman, *J. Phys. Chem.*, **65**, 2266 (1961).

(5) J. M. Martinet, Rapport CEA 888, Centre D'Etudes Nucleaires de Saclay, 1958.

(6) D. Graham, *J. Phys. Chem.*, **66**, 1815 (1962).

(7) W. A. Zisman, *Rev. Sci. Instr.*, **3**, 369 (1932).

(8) K. Bewig, NRL Report 5096, "Improvements in the Vibrating Condenser Method of Measuring Contact Potential Differences," February 4, 1958.

(9) W. C. Bigelow, D. L. Pickett, and W. A. Zisman, *J. Colloid Sci.*, **1**, 513 (1946).

(10) W. C. Bigelow, E. G. Glass, and W. A. Zisman, *ibid.*, **2**, 563 (1947).

(11) E. G. Shafrin and W. A. Zisman, *J. Phys. Chem.*, **64**, 519 (1960).

(12) O. Levine and W. A. Zisman, *ibid.*, **61**, 1068 (1957).

(13) O. Levine and W. A. Zisman, *ibid.*, **61**, 1188 (1957).

lineation in films of polar paraffinic compounds, and the large size of the methylene iodide molecule prevents liquid or vapor permeation into close-packed monolayers of paraffinic derivatives.

The alkane solvents used in these experiments were 99+ % olefin-free; they were obtained from Phillips Petroleum Corp., Humphrey-Wilkinson, and Matheson, Coleman and Bell, and before each sample was used it was percolated through a column of activated silica gel and adsorption alumina. An exception was *n*-octadecane, which has a melting point of 28°; this compound was liquefied at 35° and it was used as obtained from the supplier. The nitromethane solvent was Eastman spectro grade and it was also used without further purification.

Results with Adsorbed Films which Are Free of Solvents.—Figure 1 is a plot of the values of ΔV obtained for the homologous series of primary fatty amines when plotted against the number (*N*) of carbon atoms in the amine molecule. Each monolayer was adsorbed from a 0.10 wt. % solution in 10 ml. of nitromethane. Previous research⁹⁻¹³ had shown that this concentration was more than sufficient to guarantee adsorption of each amine on platinum in the form of a close-packed monolayer. Nitromethane has a surface tension at 20° of 36.2 dynes/cm., which is sufficiently greater than the critical surface tension of wetting of 24 dynes/cm. observed with close-packed paraffinic films to permit isolating the platinum coated with its adsorbed monolayer from the solution by the retraction method.¹¹⁻¹³ Each graphical point in Fig. 1 was unchanged when the time of immersion before retraction was varied from 12 min. up to 24 hr.; consequently, with the 0.1% concentration of amine used, the equilibrium adsorbed film was always obtained within the first few minutes of immersion of the platinum. However, to be certain that the time of adsorption would not be a factor in plotting Fig. 1 for every member of the homologous series of amines, an immersion time of 30 min. was always used.

The reset accuracy of any one measurement of ΔV was within 2 or 3 mv.; the the spread of a series of independent experiments is shown in Fig. 1, the average deviation from the curve being ± 20 mv. The graph reveals an asymptotic maximum for tetradecylamine (C_{14}) and its higher homologs. Because of the non-linear shape of nitromethane and its volatility, mixed films of solute and solvent would not be expected at adsorption equilibrium at the high solute concentrations used; the following results will show that no evidence to the contrary was found. Hence, the observed values of ΔV must result from the change in the surface density of amine dipoles adsorbed on the platinum. Since there is no variation in the dipole moment of the higher fatty amines, the conclusion appears unavoidable that the number and orientation of the adsorbed amine molecules must be identical in all monolayers for which $N \geq 14$. The simplest interpretation is that these films are close-packed monolayers. The progressive decrease in ΔV for the amines below C_{14} must mean that the decreasing lateral attractions by hydrocarbon "tails" having values of *N* below 14 permit either large, lateral, thermal movements in the chains or tilting of the molecular axes in the adsorbed film. Therefore, the surface density of the adsorbed amine dipoles must decrease with *N*. The positive sign of the values of ΔV means that the adsorbed amine molecules were oriented in all cases so that the positive pole was directed away from the metal substrate.²

A condensed monolayer of octadecylamine on an aqueous substrate at pH 8.2 has a value of $\Delta V = 0.600$

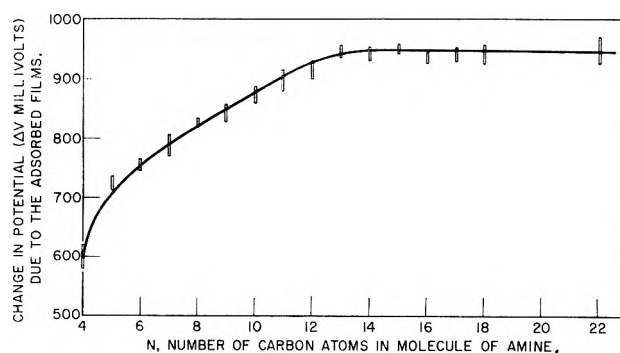


Fig. 1.—Contact potentials of homologous amines adsorbed on platinum from nitromethane.

v. and a limiting area per molecule of 20.4 \AA^2 at zero compression.¹⁴ Using the Helmholtz relation, $\Delta V = 4\pi\eta\mu_{\perp}$, to compute μ_{\perp} , the normal component of the dipole moment of the molecules adsorbed on the aqueous substrate, where $\eta = 1/(20.4 \times 10^{-16})$ or 4.9×10^{14} adsorbed molecules per cm^2 , we obtain $\mu_{\perp} = 0.324 \text{ D}$. The literature value of the dipole moment of octadecylamine in the gaseous state is 1.3 D.¹⁵ The smaller value of μ_{\perp} of octadecylamine when adsorbed on water probably is the resultant of the induced dipoles caused by proximity of the amines and also the effects of dipoles in the surface layer of the liquid substrate which originate in hydrogen bonding and also in orientation in the local field of the amine dipoles.

The situation of a condensed monolayer on a metal substrate is analogous to that of an aqueous substrate. Different metals have different work functions so that the interaction energy between a condensed monolayer and the underlying solid would be different for each metal; consequently, the resultant of the dipole polarization effects would change in each case. A further complication arises from the fact that metals react differently with any one reference atmosphere so that their apparent work functions would differ from the values obtained from a nascent state surface. For these reasons, when the Helmholtz relation is used to compute μ_{\perp} , the apparent normal component of the dipole moment of the adsorbed molecules would be expected to change for different metal adsorbents and there would not necessarily be a one to one correspondence with the work function sequence of the metals. In any case, μ_{\perp} would differ from the dipole moment, μ , of a molecule determined from dielectric constant measurements of its vapor or of its solution in a non-polar solvent.

Using a multiple-dip technique, Bigelow, Pickett, and Zisman⁹ adsorbed octadecylamine on a platinum dipper from solution in dicyclohexyl and determined the average cross sectional area per adsorbed molecule to be about 30 \AA^2 . Brockway and Karle¹⁶ and Bigelow and Brockway¹⁷ have shown by electron diffraction experiments that there is a random tilt of several degrees in the axes of polar molecules adsorbed by retraction on solid substrates. Consistent with this is the structural model of micelles of such films proposed by Epstein.¹⁸ Either such a micellar structure or a slight random tilt of the adsorbed molecular axes could account for less

(14) H. W. Fox, *J. Phys. Chem.*, **61**, 1058 (1957).

(15) J. W. Smith, *J. Chem. Soc.*, 1567 (1933).

(16) L. O. Brockway and J. Karle, *J. Colloid Sci.*, **2**, 277 (1947).

(17) W. C. Bigelow and L. O. Brockway, *ibid.*, **11**, 60 (1956).

(18) H. T. Epstein, *J. Phys. Colloid Chem.*, **54**, 1053 (1950).

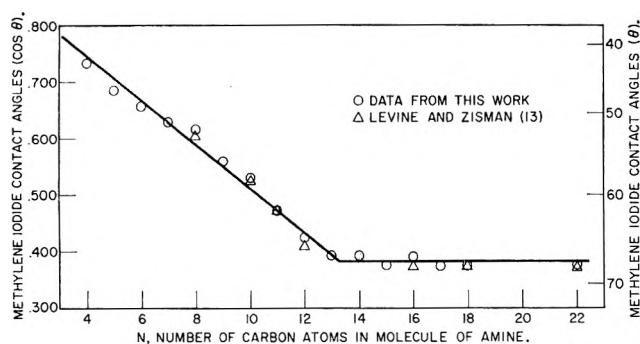


Fig. 2.—Contact angles of homologous amines adsorbed on platinum from nitromethane.

dense films adsorbed on solids than on liquid substrates, thereby producing the apparent area per molecule of 30 \AA^2 on platinum as compared to 20.4 \AA^2 per molecule of the aqueous substrate.

From Fig. 1 for the higher homologs of the aliphatic amines, $\Delta V = 0.945 \text{ v}$. If it is assumed that the average area per molecule is 30 \AA^2 , $\eta = 3.33 \times 10^{14}$ adsorbed molecules per cm^2 , and $\mu_{\perp} = 0.753 \text{ D}$., which is much closer to the dipole moment in gaseous states than ever found before. Bowden and Throssell¹⁹ have reported that platinum surfaces cleaned by polishing and washing methods have hygroscopic impurities on the surface because of which at room temperature and 80% relative humidity there results adsorption of about 20 molecular layers of water. When such impurities were absent, only one monolayer of water was adsorbed. The adsorbed water present on such a surface would be more rigidly bound and its orientation polarization and dipole induction effects would be less than that of the bulk water substrate; therefore, μ_{\perp} for the adsorbed amine monolayer should be between the value obtained on bulk water and that of the gaseous amine molecules as has been indicated by the above experiments.

Whereas the values of ΔV result from the electrostatic field originating principally in the polar terminal groups of the adsorbed amine molecules, the values of θ are determined essentially by the nature and packing of methyl groups on the opposite terminal of each molecule adsorbed on the monolayer.²⁰ The cosines of the contact angles of methylene iodide observed on the same adsorbed films studied in obtaining the data of Fig. 1 are plotted in Fig. 2 against N . Again an asymptotic maximum is seen for C_{14} and higher amines. This result can be explained readily if the monolayers comprised of the C_{14} and higher amines are solid close-packed films, whereas those having $N < 14$ are less densely packed. On comparing Fig. 1 and 2 it will be evident that $\cos \theta$ vs. N varies linearly for $N < 14$, whereas ΔV vs. N varies in a curvilinear manner. The triangular data points in Fig. 2 show the excellent agreement of our data for films on platinum with the results of Levine and Zisman¹³ obtained on condensed monolayers of the same compounds adsorbed by retraction on glass from the pure liquid amines.

Results on Monolayers Containing Solvent Molecules.—Bartell and co-workers²¹⁻²³ have used an

(19) F. P. Bowden and W. R. Throssell, *Nature*, **167**, 601 (1951).

(20) W. A. Zisman, "Relation of Chemical Constitution to the Wetting and Spreading of Liquids on Solids," NRL Report 4932, May 15, 1957; published in "A Decade of Basic and Applied Science in the Navy," Office of Naval Research, Rept. ONR-2, 30 (1957), Supt. of Documents, U. S. Govt. Printing Office, Washington, D. C.

(21) L. S. Bartell and R. J. Ruch *J. Phys. Chem.*, **60**, 1231 (1956).

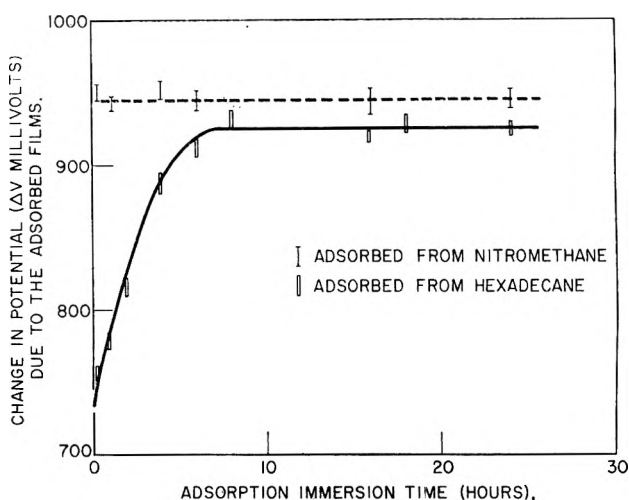


Fig. 3.—Contact potentials of octadecylamine adsorbed on platinum from nitromethane and hexadecane.

optical interference spectrometer to show that octadecylamine films adsorbed and retracted from hexadecane solutions on polished chromium were mixtures of solute and solvent molecules. Levine and Zisman¹³ found that such mixed films also could be formed on glass surfaces and could be detected and studied readily by multiple-traverse, boundary friction measurements of film durability. Their mixed films were metastable, for they did not occur if sufficient immersion time was allowed before retraction to attain true adsorption equilibrium. An immersion time of around 24 hr. was required before all of the hexadecane was replaced by fatty amine molecules.

In Fig. 3 the observed value of ΔV for octadecylamine adsorbed from solution is plotted against the immersion time, and each curve describes the results obtained using a different solvent. The dotted curve shows the results obtained using a 0.1% by weight solution in nitromethane. As mentioned before, molecules of this solvent would not be expected to adlineate with octadecylamine to form a retracted monolayer. This conclusion was verified upon observing that, for immersion times varying from 12 min. to 24 hr., ΔV had a constant value of 945 mv. and θ a constant value of between 68 and 69° . It also will be noted that these values agree well with the asymptotic maximum values shown for pure films of the fatty amines in Fig. 1 and 2, respectively. Since nitromethane has a dipole moment of 3.4 D. and octadecylamine 1.2 D., any significant proportion of the nitromethane included in the film would cause a significant change in ΔV . Hence it can be concluded that the octadecylamine films retracted from such nitromethane solutions are devoid of solvent.

The lower curve of Fig. 3 is for the results obtained upon retracting octadecylamine from a 1.0 wt. % solution in *n*-hexadecane; this large solute concentration was used because it is fairly close to the solubility of the amine at 20° and hence created favorable conditions for guaranteeing the adsorption on platinum of a close-packed film. The contact angles of the resulting retracted films were from 68 to 69° over the entire range of immersion times studied (up to 24 hours). However, ΔV increased with the immersion time from 760 mv. after 12 min. to a maximum of 925 mv. after 6 hr.

(22) L. S. Bartell and R. J. Ruch, *ibid.*, **63**, 1045 (1959).

(23) L. S. Bartell and J. F. Betts, *ibid.*, **64**, 1075 (1960).

Note that this maximum value is about 20 mv. less than obtained for the condensed film adsorbed from solutions in nitromethane. Whereas the contact angles indicate a close-packed film of outermost methyl groups, the measurements of ΔV reveal that during the first few hours of immersion, the amine molecules in the adsorbed film were not close packed but gradually became nearly so after 6 hr.

A saturated alkane has a zero dipole moment in the vapor state,²⁴ and a reasonable assumption is that the moment is nil in the mixed adlineated films described here. However, if the terminal methyl group of the alkane is in contact with the platinum, it may become polarized by the electrostatic field of the metal. If no contact is made, the induced polarization moment probably is negligible. Assuming the adlineated alkanes do not contribute to ΔV , it is evident that ΔV is determined solely by the number of amine molecules adsorbed per unit area and by the normal component of the amine-platinum dipole moment. If the adlineated alkane molecules are so located that the outermost methyl groups are situated approximately in the same plane as the methyl terminals of the adsorbed amine molecules, then the surface density of outermost methyl groups in the mixed film would be the same as in the pure film because the cross sectional areas of amine and alkane are nearly the same; hence unlike ΔV , θ would not be affected by the presence of the adlineated alkane molecules.

Since the ΔV value of 945 mv. obtained from the study of octadecylamine in nitromethane is due solely to the oriented dipoles of close-packed amine molecules adsorbed on the surface of the platinum, this value can be used as a reference for computing the proportion of amine molecules to adlineated alkane molecules in the mixed film. Thus, from the increase in ΔV with immersion time shown in Fig. 3, one can compute how the percentage of alkane molecules in the mixed film decreases as the time of immersion increases. The results calculated on the basis that the cross-sectional area of adsorbed amine molecules and of alkane molecules is about the same are given in Fig. 4.

Figure 4 makes it evident that after 1 hr. immersion time, about 20 mole % of the adsorbed film consists of adlineated hexadecane molecules. Bartell and Betts²³ also found that octadecylamine adsorbed from hexadecane contained approximately 20% of the solvent in the films. However, our results show that the included hexadecane is gradually replaced by octadecylamine until after 6 hours 1% or less of the hexadecane remains in the adsorbed film. The fact that the asymptotic maximum is 925 mv. rather than the value of 945 mv. for a condensed retracted amine monolayer may mean that the solute concentration is not high enough to give closest packing of the amine molecules; however, the 1.0 wt. % solution was about the maximum concentration at room temperature at which octadecylamine could be dissolved in hexadecane.

In attempting to study the effects on mixed film formation of using lower *n*-alkanes such as tetradecane, dodecane, etc., a difficulty encountered was that retracted films could not be obtained below tetradecane. The reason for this result is that retraction becomes

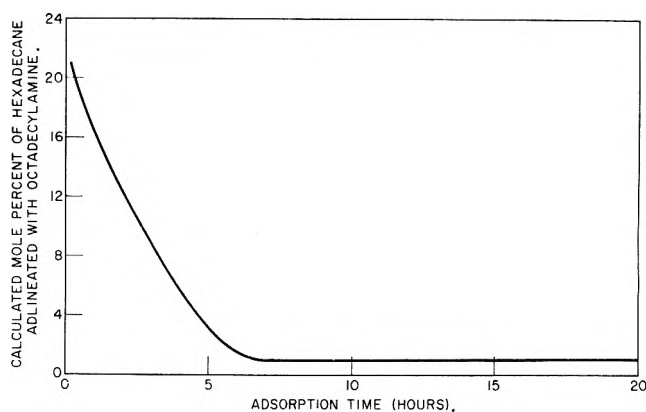


Fig. 4.—Calculated mole per cent of hexadecane adlineated with octadecylamine adsorbed on platinum.

more difficult the smaller the difference between the surface tension of the solution and the critical surface tension of wetting of 24 dynes/cm. which is characteristic for a surface of close-packed methyl groups.²⁵ In the family of *n*-alkanes, the surface tension of hexadecane is 27.6 dynes/cm. and of heptane is 20.3 dynes/cm.²⁶; hence retraction is impossible below tetradecane. Despite this limitation, we have managed to study adlineation for these and other related solvent-solute systems by using a simple technique which has a good experimental foundation. Levine and Zisman¹² have demonstrated that solid monolayers can be rubbed repeatedly and vigorously with clean tissue paper without changing the coefficient of boundary friction, the film durability, and the contact angles with various liquids; they also showed the equivalence of solid films retracted from solution with those obtained by rubbing away any excess of the solution placed on the smooth adsorbing surface. The same technique was used here to prepare mixed films of the fatty amines with the lower *n*-alkane liquids. Added justification for so doing is our observation that a clean platinum surface can be rubbed vigorously with a clean tissue paper without any more change in ΔV than 7 or 8 mv. maximum deviation as a result of much repeated handling and rubbing. Furthermore, the adsorbed monolayers of amines and alkanes described below were not changed any more than this small amount as a result of the same repeated rubbing treatment with tissue paper.

Table I summarizes the results obtained with monolayers of the fatty amines adsorbed from solution in various pure alkane solvents; those relating to heptane, decane, or dodecane were obtained by the above-mentioned tissue-rubbing method. In the first row of Table I the data for octadecylamine adsorbed from nitromethane are tabulated for reference. Values of ΔV given in the third and fourth columns were determined in each case for immersion times of 12 min. and 24 hr. In the fifth column is the methylene iodide contact angle (θ) which was measured after each immersion time; it will be noted that θ was usually 68 or 69° and was never below 67°, which indicates that the outermost composition of each mixed film is a close-packed surface of methyl groups. Hence, it is not likely that the lower terminal of the adlineated alkane molecule was in contact with the platinum substrate.

In the last two columns are given the estimated mole

(24) C. J. F. Bottcher, "Theory of Electric Polarization," Elsevier Publishing Co., 1952, p. 329.

(25) E. G. Shafrin and W. A. Zisman, *J. Colloid Sci.*, **7**, 166 (1952).

(26) O. R. Quayle, *Chem. Rev.*, **53**, 439 (1953).

TABLE I

COMPARISON OF SEVERAL AMINES ADSORBED ON PLATINUM FROM VARIOUS ALKANES COMPARED WITH OCTADECYLAMINE ADSORBED FROM NITROMETHANE

Solute	Solvent	ΔV , 12 min.	ΔV , 24 hr.	CH_2I_2 θ	Mole % alkane in film after 12 min.	Mole % alkane in film after 24 hr.
0.1% C_{18} amine	CH_3NO_2	0.945	0.945	69°	0	0
1% C_{14} amine	C_{12} alkane	.710	.880	67°	24.9	7.0
	C_{14} alkane	.510	.805	68°	46.0	14.9
	C_{16} alkane	.645	.840	68°	31.8	11.1
1% C_{16} amine	C_{12} alkane	.735	.910	69°	22.3	3.6
	C_{14} alkane	.730	.935	69°	22.8	1.0
	C_{16} alkane	.710	.800	69°	24.9	15.4
1% C_{18} amine	C_7 alkane	.937	.955	68°	1.0	0
	C_{10} alkane	.913	.934	68°	3.4	1.1
	C_{12} alkane	.840	.920	69°	11.1	2.6
	C_{16} alkane	.760	.925	69°	19.5	2.1
	C_{18} alkane ^a	.778	.819	68°	17.7	13.4

^a Adsorbed from solution at 35°.

TABLE II

DATA FROM THREE AMINES ADSORBED ON PLATINUM FROM EQUAL CHAIN LENGTH ALKANES

Solute	Solvent	ΔV , 12 min.	ΔV , 24 hr.	ΔV , 48 hr.	Mole % alkane in film after 24 hr.	Mole % alkane in film after 48 hr.
1% C_{14} amine	C_{14} alkane ^a	0.510	0.805	0.806	14.9	14.7
	^b	.517	.808	.805	14.5	14.9
1% C_{16} amine	C_{16} alkane ^a	.710	.800	.804	15.4	15.0
	^b	.702	.798	.792	15.5	16.1
1% C_{18} amine	C_{18} alkane ^b	.778	.819	.814	13.4	13.9

^a Adsorbed from solution at 20°. ^b Adsorbed from solution at 35°.

TABLE III

DATA FOR THREE AMINES ADSORBED ON PLATINUM FROM 1-PHENYLDODECANE AND TWO BRANCHED CHAIN HYDROCARBONS

Solute	Solvent	ΔV , 12 min.	ΔV , 24 hr.	ΔV , 48 hr.	CH_2I_2 θ	Mole % solv. in film after 24 hr.	Mole % solv. in film after 48 hr.
1% C_{18} amine	1-Phenyldodecane	0.926	0.939	0.942	68°	0.7	0
1% C_{15} amine	Pristane	.748	.950	.935	62-67°	0	1.0
1% C_{12} amine	Squalane	.847	.917	.929	61-66°	3.0	1.8

per cent of alkanes in the mixed film. When the length of the *n*-alkane molecule was much smaller than that of the alkyl amine molecule—as, for example, in the combination of a C_7 alkane with a C_{18} amine—then little solvent adlineation took place since ΔV after a 12-min. immersion and again after 24 hr. was not significantly different from 945 mv., the value for a condensed film free from solvent molecules. As the number of carbon atoms in the amine and alkane molecules became more nearly equal, the rate of change in ΔV with the immersion time increased as shown in Table I by the progressive changes in the series formed by C_{18} amine dissolved in the alkanes from C_7 to C_{18} . When both chains contain the same number of carbon atoms, adlineation of the solvent is the most marked and most tenacious as shown by the fact that ΔV after 24 hr. immersion is far less than 945 mv. for the pair C_{14} alkane and C_{14} amine, the pair C_{16} amine and C_{16} alkane, and C_{18} amine with C_{18} alkane.

Table II summarizes the results obtained with these three most stable systems. On extending the immersion time from 24 to 48 hr., no significant change in the mixed film occurred. Since *n*-octadecane is solid at room temperature, it was necessary to liquefy and use it at 35° as a solvent for the study summarized in Table II. Therefore, in order to obtain comparable data for Table II, the systems C_{14} alkane with C_{14} amine and the C_{16} amine with the C_{16} alkane also were studied at 35°.

No significant temperature effect occurred in going from 25 to 35° with these systems; all the contact angles at both temperatures were 68 to 69°. The persistent value in Table II, last two columns, of about 15 mole % of alkanes in the stable mixed films suggests there is some kind of regular structure involved in the steady-state condition encountered in these solute-solvent systems. One such system is a two-dimensional cluster or mixed micelle consisting of one central alkane molecule surrounded by six adhering symmetrically placed fatty amine molecules. If the alkane made no contribution to ΔV , a surface covered by these close-packed micelle groups would indicate an inclusion of 14.3 mole % of alkane molecules for such a hypothetical structure.

Branching of the solvent molecules would be expected to decrease the adlineation in mixed films; hence the effect on the ΔV vs. time curves was examined. The results obtained with 1% solutions of octadecylamine in 1-phenyldodecane, pristane (2,6,10,14-tetramethylpentadecane), and squalane (2,6,10,15,19,23-hexamethyltetracosane) are summarized in Table III. Solutions in 1-phenyldodecane showed practically no evidence of solvent adlineation as indicated by ΔV in the third and fourth columns of the table and the methylene iodide contact angles given in the fifth column. The mole per cent of solvent in the film after 12 min. and 24 hr. was calculated from the estimated cross section of the phenyl

group obtained from Stuart-Brigleb ball model measurements. The behavior indicates that the size, 27.5 \AA^2 , and shape of the phenyl group does not allow the 1-phenyldodecane to adlineate with the octadecylamine, which has an estimated ball model cross section of 20.4 \AA^2 . However, the two hydrocarbons, pristane and squalane, each having many methyl side chains, showed adlineation comparable to that of the mismatched pairs of straight chain hydrocarbons and amines. Although the cross sectional areas of pristane and squalane, estimated 30 \AA^2 , are greater than that of the alkane solvents, 20.4 \AA^2 , nevertheless the linear close packing with the hydrocarbon tails of the amine molecules appears to be quite similar to that of the alkanes as determined from ball model studies. This compatibility of the two mo-

lecular systems probably accounts for the adlineation of these solvents. In the case of pristane and squalane, the contact angle (in the fifth column) corresponding to immersion times of 12 minutes is only from 61 to 62° for the branched chain solvents; thus these adlineated solvents reduced the contact angle, whereas the alkanes presented an outermost methyl group which did not disturb the close-packed methyl surfaces of the alkane-amine systems. It should be observed that the ball model shows that because of tilting of the terminal methyl groups of pristane and squalane there would be fewer methyl groups expected per square centimeter of surface, and this may account for the 61 to 62° contact angles.

COULOSTATIC STUDY OF ADSORPTION KINETICS AT A METAL-ELECTROLYTE INTERFACE

BY PAUL DELAHAY

Coates Chemical Laboratory, Louisiana State University, Baton Rouge, Louisiana

Received June 22, 1962

Variations of the surface concentration and potential with time are derived for the coulostatic method for an adsorption process, obeying the logarithmic Temkin isotherm at equilibrium, at an ideal polarized electrode and for mixed control by semi-infinite linear diffusion and adsorption kinetics. It is assumed that the charge density on the electrode varies according to a step-function of time in such a way that the cell with the ideal polarized electrode is essentially at open circuit after the abrupt change of charge density. Limiting cases corresponding to pure control by either adsorption kinetics or diffusion also are considered. The evaluation of the adsorption exchange rate, v^0 , from potential-time variations is indicated. It should be possible to determine values of $v^0 \leq 10^{-5}$ mole cm^{-2} sec^{-1} for observations with $t \leq 1 \mu\text{sec}$. Faster processes might be investigated with shorter measurement times.

A coulostatic method was recently suggested in a paper from this Laboratory¹ for the study of adsorption kinetics of a neutral substance at a metal-electrolyte interface. The influence of mass transfer control was not considered. The more general case with control by adsorption kinetics and mass transfer, as determined by semi-infinite linear diffusion, is analyzed here.

Principle and Boundary Value Problem.—Consider an ideal polarized electrode on which a neutral substance other than the solvent is adsorbed. Further, assume that the charge density on the electrode is changed according to a step-function of time in such a way that the cell with the ideal polarized electrode is essentially at open circuit immediately after the change of charge density. The surface concentration of adsorbed substance progressively reaches its equilibrium value after the step-variation of the charge density, and the potential varies accordingly. Parameters for adsorption kinetics can be deduced from the potential-time variations. The kinetics of adsorption processes obeying the logarithmic Temkin isotherm at equilibrium will be discussed here, but the method can be extended to processes obeying other isotherms. The method also may be applied when a specific form of the rate equation for adsorption is not postulated provided only a small departure from equilibrium is considered; the adsorption rate then is expressed in terms of the partial derivatives with respect to the variables on

which the rate depends.² It will be assumed here that the rate equation previously derived¹ for processes obeying the logarithmic Temkin isotherm applies.

The logarithmic Temkin isotherm is

$$b\Gamma = -\Delta G^0 + RT \ln C^0 \quad (1)$$

where Γ is the surface concentration of adsorbed substance; C^0 is the bulk concentration of adsorbed substance; ΔG^0 is the standard free energy of adsorption; b is a parameter characteristic of adsorption; and R and T are as usual. Equation 1 is written in terms of C^0 rather than the corresponding activity on the assumption that the activity coefficient in solution is constant (dilute solution of a neutral substance). The net adsorption rate per unit area for a small departure from equilibrium, with which we are concerned here, is¹

$$v = v_i^0 [(\delta C_{x=0}/C^0) - (b/RT)\delta\Gamma - (1/RT)\delta(\Delta G^q)] \quad (2)$$

where

$$\delta C_{x=0} = C_{x=0} - C^0 \quad (3)$$

$$\delta\Gamma = \Gamma - \Gamma_i \quad (4)$$

$$\delta(\Delta G^q) = \Delta G^q - \Delta G_i^q \quad (5)$$

In the preceding equations v^0 is the exchange rate per unit area; ΔG^q is the charge-dependent part of

(1) P. Delahay and D. M. Mohilner, *J. Phys. Chem.*, **66**, 959 (1962); *J. Am. Chem. Soc.*, **84**, 4247 (1962).

(2) Cf. W. Lorenz, *Z. Elektrochem.*, **62**, 192 (1958), who used this approach in the study of adsorption kinetics by the non-faradaic impedance method.

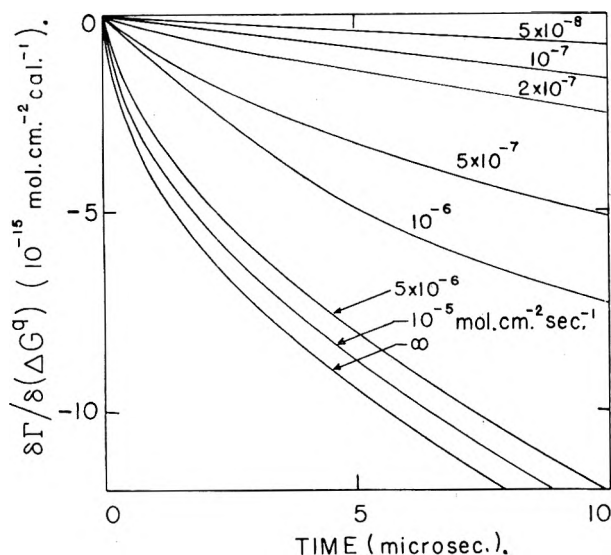


Fig. 1.—Variations of $\delta\Gamma/\delta(\Delta G^q)$ with time for mixed control by adsorption kinetics and diffusion for different adsorption exchange rates. Data: $b = 5 \times 10^{12}$ mole $^{-1}$ cm. 2 cal., $c = 10^{-6}$ mole cm. $^{-3}$, $d = 5 \times 10^{-6}$ cm. 2 sec. $^{-1}$, $T = 25^\circ$.

ΔG^0 , and $C_{x=0}$ is the volume concentration, at the electrode surface, of the adsorbed substance. The subscript i indicates the initial values of v^0 and ΔG^q which prevail before variation of the charge density. One has $v \geq 0$ for net adsorption or desorption, respectively. The values C^0 , Γ_i , and ΔG_i^q correspond to initial conditions at which there is equilibrium according to the isotherm of eq. 1. Since $\delta(\Delta G^q)$ varies abruptly because of the change of the charge density q , Γ , $C_{x=0}$, and E vary until equilibrium corresponding to the new value q is reached. The change of potential from its initial value before charging to the value at time t after charging is¹ for small variations of q

$$\delta E = (\partial E/\partial q)_\Gamma \delta q + (\partial E/\partial \Gamma)_q \delta \Gamma \quad (6)$$

where the partial derivatives are taken for the initial charge density and surface concentration.

The concentration C for mass transfer controlled by semi-infinite linear diffusion is the solution of Fick's equation for the following initial and boundary conditions: $C = C^0$ for $x \geq 0$ and $t = 0$; $C \rightarrow C^0$ for $x \rightarrow \infty$ and $t \geq 0$, and

$$D \left(\frac{\partial C}{\partial x} \right)_{x=0} = v_i^0 \left[\frac{C_{x=0}}{C^0} - \frac{bD}{RT} \int_0^t \left(\frac{\partial C}{\partial x} \right)_{x=0} dt - \frac{\delta(\Delta G^q)}{RT} - 1 \right] \quad (7)$$

for $x = 0$ and $t > 0$. The notations are C^0 , concentration of the adsorbable substance in the bulk of the solution; D is the diffusion coefficient of this substance; x is the distance from the electrode (more rigorously, distance from the plane of closest approach for the adsorbed substance). The boundary condition 7 was derived from eq. 2 by reckoning that the rate $d\delta\Gamma/dt$ for $t > 0$ is equal to the flux of the adsorbed substance at $x = 0$, i.e., that $\delta\Gamma$ is the integral from 0 to t of the flux at $x = 0$.

Variations of Surface Concentration. General Equation.—The flux at the electrode surface $(\partial C/\partial x)_{x=0}$ was derived by Laplace transformation, and the rate $d\delta\Gamma/dt$ ($= D (\partial C/\partial x)_{x=0}$) was obtained. The varia-

tion of surface concentration $\delta\Gamma$ was obtained by integration. Thus

$$\delta\Gamma = v_i^0 \frac{\delta(\Delta G^q)}{RT} \frac{1}{m-p} \times \left\{ \frac{\frac{1}{m} [1 - \exp(m^2 t) \operatorname{erfc}(mt^{1/2})]}{-\frac{1}{p} [1 - \exp(p^2 t) \operatorname{erfc}(pt^{1/2})]} \right\} \quad (8)$$

where

$$m = \frac{v_i^0}{2C^0 D^{1/2}} + \left[\left(\frac{v_i^0}{2C^0 D^{1/2}} \right)^2 - \frac{bv_i^0}{RT} \right]^{1/2} \quad (9)$$

$$p = (bv_i^0/RT)(1/m) \quad (10)$$

The function $y = 1 - \exp(\lambda^2) \operatorname{erfc}(\lambda)$ is such that $y = 0$ for $\lambda = 0$ and $y = 1$ for $\lambda \rightarrow \infty$. Hence (Fig. 1) $\delta\Gamma = 0$ for $t = 0$ and $\delta\Gamma = -\delta(\Delta G^q)/b$ for $t \rightarrow \infty$ (since $mp = bv_i^0/RT$ according to eq. 10). The latter value of $\delta\Gamma$ corresponds to the variation of Γ at equilibrium as deduced from the isotherm of eq. 1. One readily ascertains from eq. 8 that $\delta\Gamma$, at any time, has always the same sign as $-\delta(\Delta G^q)/b$.

Adsorption Control vs. Diffusion Control.—When (cf. eq. 9)

$$v_i^0 \gg \frac{4bC^0 D}{RT} \quad (11)$$

$$\frac{v_i^0}{C^0 D^{1/2}} t^{1/2} \gg 1 \quad (12)$$

there is pure diffusion control. The function $\exp(m^2 t) \operatorname{erfc}(mt^{1/2})$ in eq. 8 vanishes, and eq. 8 becomes after introduction of the corresponding values of m and p

$$\delta\Gamma = -\frac{\delta(\Delta G^q)}{b} \left\{ 1 - \exp \left[\left(\frac{bC^0 D^{1/2}}{RT} \right)^2 t \right] \operatorname{erfc} \left[\left(\frac{bC^0 D^{1/2}}{RT} \right) t^{1/2} \right] \right\} \quad (13)$$

One has, as for the general case, $\delta\Gamma = 0$ at $t = 0$, and $\delta\Gamma = -\delta(\Delta G^q)/b$ for $t \rightarrow \infty$.

Condition 11 is satisfied at room temperature, for instance, for $v_i^0 \geq 10^{-4}$ mole cm. $^{-2}$ sec. $^{-1}$ for $b = 5 \times 10^{12}$ mole $^{-1}$ cm. 2 cal., $C^0 = 10^{-6}$ mole cm. $^{-3}$, and $D = 5 \times 10^{-6}$ cm. 2 sec. $^{-1}$ (Fig. 1). Condition 12 then is satisfied for $t > 10^{-8}$ sec.

There is pure control by adsorption kinetics (Fig. 2) when (cf. eq. 9)

$$v_i^0 \ll \frac{4bC^0 D}{RT} \quad (14)$$

The quantities m and p of eq. 9 and 10 then are imaginary but it can be easily shown³ that eq. 8 reduces to

$$\delta\Gamma = -[\delta(\Delta G^q)/b] \{1 - \exp[-(v_i^0 b/RT)t]\} \quad (15)$$

(3) Note that

$$\operatorname{erf}(i\lambda) = \frac{2i}{\pi^{1/2}} \int_0^\lambda e^{-z^2} dz$$

This result was directly derived in a previous paper¹ for pure adsorption control.

Small and Large Arguments and Imaginary Arguments.—One obtains after expansion of the exponential and error functions

$$\delta\Gamma = v_i^0 \frac{\delta(\Delta G^0)}{RT} \left[-t + \frac{4}{3\pi^{1/2}} (m+p)t^{3/2} - \frac{1}{2} (m^2 + mp + p^2)t^2 + \frac{1}{3\pi^{1/2}} (m^2 + p^2)(m+p)t^{5/2} \dots \right] \quad (16)$$

Conversely, one has for $mt^{1/2} \gg 1$ and $pt^{1/2} \gg 1$

$$\delta\Gamma = -\frac{\delta(\Delta G^0)}{b} \left[1 - \frac{1}{\pi^{1/2}} \left(\frac{1}{m} + \frac{1}{p} \right) \frac{1}{t^{1/2}} \dots \right] \quad (17)$$

Similar equations can be written for pure diffusion control, but $\delta\Gamma$ varies with $t^{1/2}$ for small arguments since this term does not cancel out as in eq. 16. It follows eq. 17 and the corresponding equations for pure diffusion control that the adsorption rate $d\delta\Gamma/dt$ varies with $t^{-3/2}$ for sufficiently long times, whether there is control by diffusion only or by diffusion and adsorption kinetics.

When (cf. eq. 9 and 10)

$$v_i^0 < \frac{4bC^0D}{RT} \quad (18)$$

m and p are imaginary, and it can be shown easily that the coefficients of the series of eq. 16 are real. Thus

$$m + p = \frac{v_i^0}{C^0D^{1/2}} \quad (19)$$

$$m^2 + mp + p^2 = \left(\frac{v_i^0}{C^0D^{1/2}} \right)^2 - \frac{bv_i^0}{RT} \quad (20)$$

$$(m^2 + p^2)(m + p) = \left[\left(\frac{v_i^0}{C^0D^{1/2}} \right)^2 - 2 \frac{bv_i^0}{RT} \right] \frac{v_i^0}{C^0D^{1/2}} \quad (21)$$

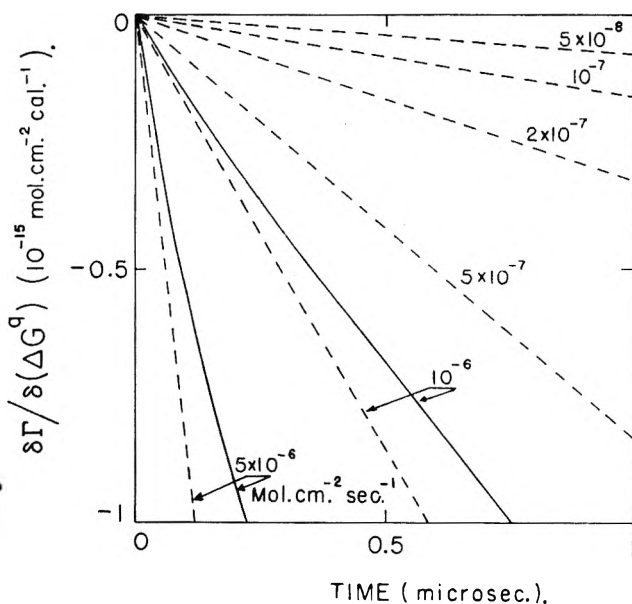


Fig. 2.—Initial segments of the curves of Fig. 1 (solid curves) and corresponding curves for pure control by adsorption kinetics. The curves for mixed control by adsorption and diffusion for the lowest four adsorption exchange rates practically coincide with those shown for pure control by adsorption.

Potential-Time Variations and Determination of v_i^0 .—The potential-time variations are directly deduced by introduction of $\delta\Gamma$, as given above, in eq. 6. The first term on the right hand side corresponds to the variation of E at $t = 0$ upon the change of the charge density. The adsorption exchange rate v_i^0 is deduced from the potential-time variations.

Conclusion

Exchange rates for adsorption of neutral molecules at a metal-electrolyte interface can be determined by the present coulostatic method provided the rate is appreciably smaller than the limit for pure diffusion given by conditions 11 and 12 (e.g., $v_i^0 \leq 10^{-5}$ mole cm^{-2} sec^{-1} , $t \leq 1$ μsec).

Acknowledgment.—This work was supported by the Office of Naval Research. The author is indebted to Dr. Y. Takemori for the numerical calculations for the preparation of Fig. 1 and 2.

KINETIC STUDIES ON THE DECARBOXYLATION OF SEVERAL UNSTABLE ACIDS IN THE MOLTEN STATE

BY LOUIS WATTS CLARK

Department of Chemistry, Western Carolina College, Cullowhee, N. C.

Received July 2, 1962

Kinetic data are reported on the decarboxylation of anthranilic acid, *p*-aminobenzoic acid, benzylmalonic acid, and malonic acid in the molten state. The malonic acid study was undertaken in order to up-date previous data reported 42 years ago. An enthalpy-entropy plot of the data for these four acids plus those for picolinic acid and oxanilic acid reported previously yielded two straight lines. The isokinetic temperatures were calculated from the slopes of the lines and calculated ΔF^0 values were found to agree with the theoretical. Information regarding the nature of the activated states was deduced based upon the position of any acid of a given series on one of the lines. The malonic acid data were found to be at variance with those reported previously, indicating that older kinetic data in the literature are in need of rechecking.

Numerous kinetic studies have been carried out by many investigators on the decarboxylation of a large number of unstable acids in a variety of solvents.¹ Although data on the decarboxylation of the free acids in the molten state or in inert solvents are needed also in order to obtain a more complete understanding of the effect of solvent and structure on the reaction, it appears that relatively few such compounds have been investigated. These include malonic acid,² trichloroacetic acid,³ oxanilic acid,⁴ and picolinic acid.⁵

The present paper reports results of kinetic studies which have been carried out in this Laboratory on the decarboxylation of three additional acids in the molten state, namely, anthranilic acid, *p*-aminobenzoic acid, and benzylmalonic acid. Efforts to correlate the data obtained in this research with those for the decarboxylation of malonic acid reported by Hinshelwood² in 1920 were unsuccessful, and prompted a recheck of the behavior of this compound using the more up-to-date equipment now available. The data for the malonic acid reaction thus obtained are included in this report.

Experimental

Reagents.—The benzylmalonic acid and anthranilic acid used in this research were highest purity or reagent chemicals and were used without any further purification. The *p*-aminobenzoic acid was technical grade. However, before use, it was carefully recrystallized from ethanol, and a pure, dry sample of m.p. 187–188° was easily obtained. The malonic acid was reagent grade, 100.0% assay, m.p. 134.0°. The benzylmalonic acid, anthranilic acid, and *p*-aminobenzoic acid used yielded the theoretical amount of CO₂ on complete decarboxylation, but in the case of malonic acid the additive vapor pressure of the acetic acid released during decarboxylation caused a slight increase in the volume toward the end of the reaction.

Apparatus and Technique.—The apparatus employed in the present investigation was the same as that which has been used in previous studies.⁶ It consists of a thermostated oil bath provided with a thermometer calibrated by the U. S. Bureau of Standards. The steam point of the thermometer is carefully rechecked at frequent intervals to ensure reliability. The reaction vessel was the same as that used in studying the decarboxylation of molten oxanilic acid⁴ and picolinic acid.⁵ It was connected by standard taper joints to a condenser, the condenser being connected to the water-jacketed buret by a short

rubber hose. A piece of flexible tubing joined the buret to a leveling bulb holding an entraining liquid. This liquid consisted of a solution 20% by weight of sodium sulfate and 5% by volume of sulfuric acid in which CO₂ is insoluble. The vapor pressure of this solution was calculated using Raoult's law and activity coefficients of the two solutes. It was found to be 91.0% of the vapor pressure of pure water. In converting the observed gas volumes to STP, the vapor pressure of this solution was subtracted from the observed corrected barometric pressure.

In each decarboxylation experiment a sample of the required acid was used which would yield 40.0 ml. of CO₂ on complete reaction.⁷ The weights of these samples in grams were as follows: malonic acid, 0.1870; benzylmalonic acid, 0.3489; anthranilic acid and *p*-aminobenzoic acid, 0.2464.

Results

The decarboxylation of anthranilic acid, *p*-aminobenzoic acid, and benzylmalonic acid was studied at three different temperatures over a 10–20° temperature range. The experiments were performed two or three times at each temperature. The evolved CO₂ (converted to STP) was plotted against time for each experiment. The plot of $\log(V_{\infty} - V_t)$ vs. time, taken from representative points on the smoothed experimental plots, yielded straight lines over most of the reaction in each case.

The decomposition of molten malonic acid was studied at four different temperatures between 140 and 150°. At higher temperatures the reaction was too rapid to be measured with precision and lower temperatures were impractical because of the slowness of the melting. Two or three experiments were performed at each temperature. As in all rate studies, the beginning of the reaction was somewhat erratic, the first few milliliters of evolved CO₂ occurring prior to the complete melting of the sample. This necessitated an extrapolation back to zero time for the first 5–10% of the reaction. In a typical experiment with malonic acid, for example, the sample was added to the reaction flask at 146.03° (cor.) and was completely melted in 5 min. No readings were taken before the melting was complete. At this time 1.4 ml. of CO₂ (uncorrected) were evolved. To complicate the situation further, as acetic acid accumulated from the reaction, its vapor pressure became appreciable toward the end of the experiment so that a linear logarithmic plot was obtainable only over about the first 60–70% of the reaction. Figure 1 is a typical plot of the experimental data, showing the decomposition of molten malonic acid at 150.93° (cor.). A slight downward trend of the logarithmic plot toward the end of the reaction is evident.

(7) These weights were calculated, based not upon the ideal gas laws, but upon the actual molar volume of CO₂, 22, 264 ml. at STP.

(1) For reviews, cf., E. F. Gould, "Mechanism and Structure in Organic Chemistry," Henry Holt and Company, New York, N. Y., 1959, pp. 346 ff.; S. L. Friess and A. Weissberger, Ed., "Technique of Organic Chemistry; Volume VIII, Investigation of Rates and Mechanisms of Reactions," Interscience Publishers, Inc., New York, N. Y., 1st Ed., 1953, pp. 382 ff.; J. Hine, "Physical Organic Chemistry," McGraw-Hill Book Co., Inc., New York, N. Y., 1956, pp. 283 ff.

(2) C. N. Hinshelwood, *J. Chem. Soc.*, **117**, 156 (1920).

(3) L. W. Clark, *J. Am. Chem. Soc.*, **77**, 3130 (1955).

(4) L. W. Clark, *J. Phys. Chem.*, **66**, 1543 (1962).

(5) L. W. Clark, *ibid.*, **66**, 125 (1962).

(6) L. W. Clark, *ibid.*, **60**, 1150 (1956).

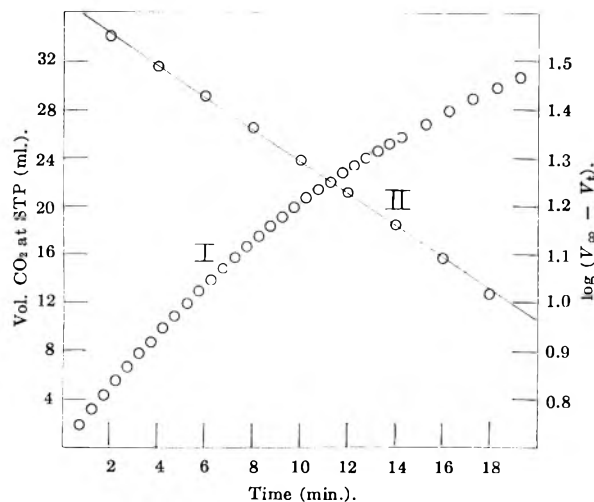


Fig. 1.—Experimental data for the decarboxylation of 0.1860 g. of malonic acid at 150.93° (cor.): I, volume of CO₂ at STP (ml.); II, log (V_∞ - V_t).

The average values of the apparent first-order rate constant for each compound at each temperature were obtained from the slope of the experimental logarithmic plot. The values thus obtained are shown in Table I. An Eyring plot of the kinetic data for the decarboxylation of malonic acid at the four temperatures studied is shown in Fig. 2. The parameters of the Eyring equation, based upon the data in Table I, are shown in Table II, along with comparative data previously reported for oxanilic acid and picolinic acid.

TABLE I

APPARENT FIRST-ORDER RATE CONSTANTS FOR THE DECARBOXYLATION OF SEVERAL UNSTABLE ACIDS IN THE MOLTEN STATE

Acid	Temp., °C. (cor.)	$k \times 10^4$, sec. ⁻¹	Av. dev.
Malonic acid	139.63	3.87	±0.03
	144.40	6.39	± .04
	146.03	7.34	± .04
	149.93	12.7	± .05
Benzylmalonic acid	141.03	7.37	± .04
	150.78	17.0	± .05
	161.12	40.2	± .1
Anthranilic acid	171.57	3.69	± .02
	181.78	6.51	± .02
	191.65	11.04	± .05
<i>p</i> -Aminobenzoic acid	189.64	7.62	± .04
	194.59	9.75	± .04
	200.11	14.12	± .05

TABLE II

KINETIC DATA FOR THE DECARBOXYLATION OF SEVERAL UNSTABLE ACIDS IN THE MOLTEN STATE

Acid	ΔH^* (kcal./mole)	ΔS^* (e.u./mole)
Oxanilic acid ⁴	40.1	+21.4
Picolinic acid ¹	39.8	+13.2
Malonic acid ^a	35.8	+11.9
Benzylmalonic acid	29.4	-2.6
<i>p</i> -Aminobenzoic acid	24.9	-19.9
Anthranilic acid	21.6	-26.5

^a The data of Hinshelwood (ref. 2) for this reaction yield $\Delta H^* = 33.0$ and $\Delta S^* = +4.5$.

Discussion of Results

It is not surprising to find that the data obtained in this present investigation on the decarboxylation of molten malonic acid (see line 3 of Table II) differ

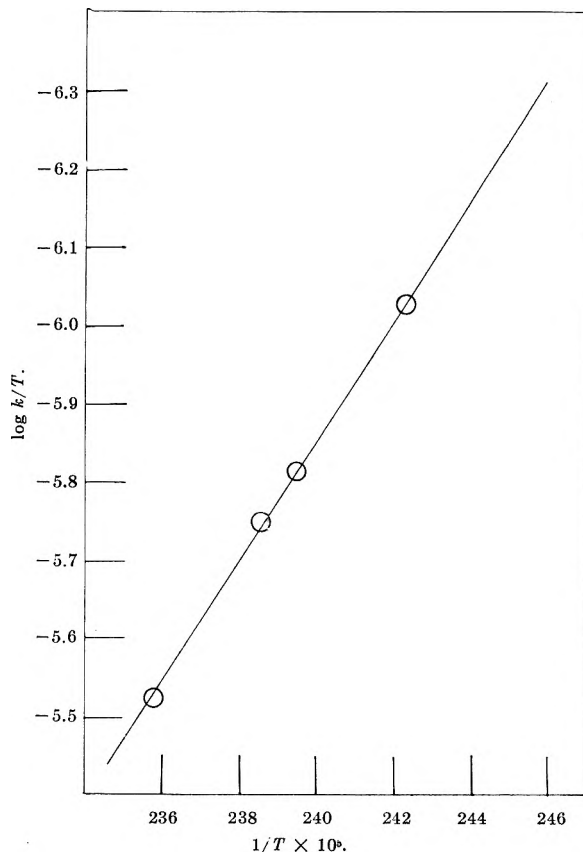


Fig. 2.—Eyring plot for the decarboxylation of molten malonic acid at different temperatures.

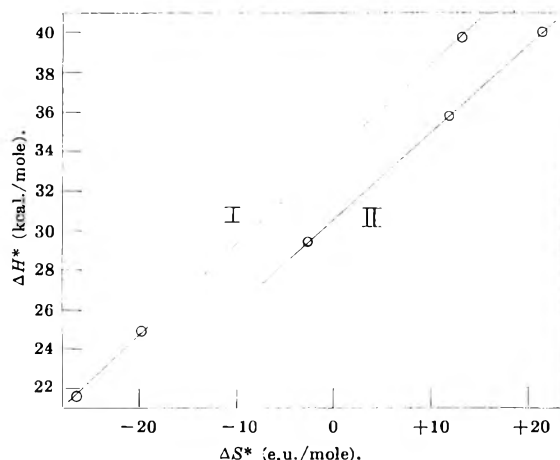


Fig. 3.—Enthalpy-entropy plot for the decarboxylation of several acids: I, amino acids (anthranilic, *p*-aminobenzoic, and picolinic); II, keto acids (benzylmalonic, malonic, and oxanilic).

somewhat from that reported by Hinshelwood 42 years ago. This result points out the fact that many of the older kinetic data in the literature are in need of careful rechecking.

It has been well established that the mechanism of the decarboxylation of malonic acid in basic type solvents is a bimolecular reaction, the rate-determining step being the formation of an intermediate complex between solute and solvent species.⁸ It is logical to assume that the decarboxylation of the molten acid is bimolecular also, the complex in this case being formed by the coordination of two "supermolecules" of malonic acid—a polarized, electrophilic, carbonyl carbon atom

(8) G. Fraenkel, R. L. Belford, and P. E. Yankwich, *J. Am. Chem. Soc.*, **76**, 15 (1954).

of one molecule attracted to the unshared pair of electrons on the nucleophilic hydroxyl oxygen atom of another—both electrophilic and nucleophilic species existing as associated complexes composed of two or more molecules each.⁹ There is no reason to doubt but that an analogous mechanism obtains in the case of the decarboxylation of the other acids listed in Table II.⁴

Figure 3 is an enthalpy-entropy plot of the data shown in Table II. It will be observed that the data for the two amino acids and the one imino acid fit on one straight line, of slope 460°K. or 187°C., the so-called isokinetic temperature¹⁰ (line I of Fig. 3). This temperature corresponds to the melting point of *p*-aminobenzoic acid. The zero intercept of line I in Fig. 3 is 33.9 kcal./mole. This is equal to $\Delta H^0 = \Delta F^0$, or the free-energy change of the reaction at the isokinetic temperature. The experimental values of $\Delta F^0_{187^\circ}$ for anthranilic acid, *p*-aminobenzoic acid, and picolinic acid turn out to be, respectively, 33.8, 34.0, and 33.8 kcal./mole, agreeing well with the theoretical values.

Benzylmalonic acid and malonic acid may be regarded as types of β -keto acids, while oxanilic acid is analogous to an α -keto acid. The $\Delta H^* - \Delta S^*$ plots of these three acids fit on a separate straight line (line II of Fig. 3) of slope 445°K. or 172°C. The zero intercept of line II is 30.5 kcal./mole, and the $\Delta F^0_{172^\circ}$ values for benzylmalonic acid, malonic acid, and oxanilic acid are, respectively, 30.4, 30.5, and 30.6 kcal./mole. These results suggest the possibility that other substituted malonic acids, substituted oxamic acids, and α - and β -keto acids should also fall on this same line.

The position of any acid of a given series on one of the lines in Fig. 3 affords information on the nature of the activated state. We see that picolinic acid has a relatively high activation energy, and also a high probability of formation of the intermediate complex as shown by the large positive value of ΔS^* . The high ΔH^* may be attributed to the relatively weak electron attracting power of the α -imino group, on the one hand, and the weak basicity of the nitrogen due to resonance on the other. The large ΔS^* indicates relatively little association of the picolinic acid molecules or

zwitterions. There is a very large decrease in both ΔH^* and ΔS^* on going from picolinic acid to *p*-aminobenzoic acid. The large negative value of ΔS^* in this case may be ascribed to the association of the *p*-aminobenzoic acid to form long chain clusters. The low enthalpy of activation may be explained on the basis of the carbonyl group of a zwitterion coördinating with one of the amino nitrogen atoms of a cluster of un-ionized molecules. If an amino group captures a proton the resulting $-\text{NH}_3^+$ group will have an electron attracting effect which will increase the effective positive charge on the carbonyl carbon atom of the carboxylate ion, thus causing a lowering of ΔH^* . A similar explanation undoubtedly holds in the case of the isomer, anthranilic acid. The lower ΔH^* for this reaction is consistent with the closer proximity of the amino group to the carboxyl group, and the decrease in ΔS^* is indicative of an ortho effect.

A comparison of the data for oxanilic acid and picolinic acid shows them to have very nearly equal enthalpies of activation. Picolinic acid is actually smaller than oxanilic acid, and the fact that the former has a lower value of ΔS^* than the latter points to an ortho effect arising from the relative positions of the imino and carboxyl groups in the molecule.

Although oxanilic acid has a more complex structure than does malonic acid a comparison of the ΔS^* values of these two reactions shows that the intermediate complex of the former has the simpler structure. This points again to the tendency of dibasic acids to associate past the dimer stage to form "supermolecule" clusters composed of an aggregation of molecules.¹¹ The lowering of ΔS^* on going from malonic acid to benzylmalonic acid reflects the large steric hindrance produced by the dangling benzyl group in the latter. The benzyl substituent also produces a rather large lowering of ΔH^+ as would be anticipated in view of the $-I$ effect of the phenyl moiety.

Acknowledgments.—The support of this research by the National Science Foundation, Washington, D. C., is gratefully acknowledged. Virgil Snell carried out the purification of the *p*-aminobenzoic acid.

(11) W. Hückel, "Theoretical Principles of Organic Chemistry," Vol. II, Elsevier Publ. Co., New York, N. Y., 1958, p. 341.

(9) L. W. Clark, *J. Phys. Chem.*, **64**, 692 (1960).
 (10) J. E. Leffler, *J. Org. Chem.*, **20**, 1202 (1955).

VARIATION IN THE K_A -VALUE OF A SALT WITH COMPOSITION OF A BINARY SOLVENT

By H. K. BODENSEH¹ AND J. B. RAMSEY

Department of Chemistry of the University of California at Los Angeles, Los Angeles, California

Received July 2, 1962

The association constants at 25° of tetra-*n*-butylammonium perchlorate have been determined in $\text{C}_6\text{H}_5\text{CN}$ ($D = 25.2$), $o\text{-Cl}_2\text{C}_6\text{H}_4$ ($D = 10.1$), and in six mixtures of these two solvents with dielectric constants 18.6, 16.0, 13.8, 11.4, 10.8, and 10.2. It is found that the association constants (K_A -values) in mixtures having D -values less than 18.6 do not satisfy a linear relation between $\log K_A$ and $1/D$ (known for this salt) in that the K_A -values are less than those given by this linear relation. This deviation from linearity is shown to be consistent with the assumption previously made to account for the divergences from linearity found for this salt in $\text{C}_2\text{H}_4\text{Cl}_2$ and $\text{CH}_3\text{CHClCH}_2\text{Cl}$, namely that the effective dielectric constants of these mixtures in the salt solutions are greater than their measured dielectric constants in the absence of salt.

Recent results obtained in this Laboratory² have shown that the variation in the values of K_A , the associa-

tion constant, of tetra-*n*-butylammonium perchlorate, $(n\text{-Bu})_4\text{NClO}_4$, found in six one-component solvents, each consisting of but one molecular species and ranging in dielectric constant (D -value) from 9.9 to 25.2 at 25°,

(1) Postdoctoral Fellow at U.C.L.A., 1961-1962.

(2) Y. H. Inami, H. K. Bodenseh, and J. B. Ramsey, *J. Am. Chem. Soc.*, **83**, 4745 (1961).

is represented by a linear relation between $\log K_A$ and $1/D$. It also was shown that the K_A -values of tetra-*n*-butylammonium picrate, $(n\text{-Bu})_4\text{NPI}$, found by other investigators in six one-component monomolecular solvents, covering a range of D -values from 5.04 to 34.69, conform to this same linear relation.

This linear relation between $\log K_A$ and $1/D$ has been derived in two different ways^{3,4} on the basis of the following assumptions: (1) two oppositely charged ions constitute an associated ion pair when and only when their distance of separation is so small that no solvent molecules exist between them (the distance commonly referred to as the "contact distance" and designated by the letter a); at separation distances greater than a they behave as free ions, namely as ions which are available to contribute to the conductance of a solution, (2) the "contact distance" of a given salt has the same value in different solvents, *i.e.*, is independent of the dielectric constant of the solvent, and (3) the predominant interaction between oppositely charged ions is a charge-charge interaction.

In several investigations during recent years, Fuoss and collaborators have determined the effect of varying the dielectric constant of the solvent on the K_A -value of various salts by use of a series of mixtures of two miscible solvents which in their pure state differ appreciably in dielectric constant. In the report of one of the more recent of these investigations, Hirsch and Fuoss⁵ noted that the points given in a plot of $\log K_A$ against $1/D$ (for each of the three salts $(n\text{-Bu})_4\text{NPI}$, $(n\text{-Bu})_4\text{NI}$, and $(n\text{-Bu})_4\text{NNO}_3$ in $\text{C}_6\text{H}_5\text{NO}_2\text{-CCl}_4$ mixtures) are better represented by a curve, concave downward, than by a straight line. A consideration of the results obtained in two other of these investigations^{6,7} shows unmistakably, although not so pronouncedly, that the points (in a plot of $\log K_A$ vs. $1/D$) deviate from linearity in the same sense.

That such deviation from a linear relation between $\log K_A$ and $1/D$ will be found to exist whenever a series of mixtures of two solvents, having considerably different dielectric constants, is used seems quite probable in view of the following considerations. It has been found² that the K_A -values of $(n\text{-Bu})_4\text{ClO}_4$ in ethylene chloride ($D = 10.23$) and in propylene chloride ($D = 8.78$), also of $(n\text{-Bu})_4\text{NPI}$ in ethylene chloride, are appreciably less at the respective dielectric constants of these pure solvents than the values to be expected from the established² linear relations. A probable explanation of these divergences has been found in the assumption that the dielectric constant of that portion of each of these two solvents which exists near enough to an ion to be appreciably influenced by its electric field is distinctly *greater* than the macroscopic dielectric constant of the pure solvent (an assumption not applicable to solvents which consist of but one molecular species). Incidentally, independent non-conductimetric evidence has been adduced⁸ which substantiates this assumption. If the justification given² for this assumption is valid for the solvents, ethylene chloride and propylene chloride, (each known to consist of two molecular species

which differ appreciably in polarity) then it seems reasonable to presume that it (this assumption) is likewise applicable to mixtures of two solvents, each consisting of but one molecular species and differing appreciably in dielectric constant. Thereby the downward curvature of the graphs obtained on plotting $\log K_A$ vs. $1/D$ when using such solvent mixtures may be accounted for.

It has been the purpose of this investigation to determine whether the K_A -values of a salt in a series of mixtures of two such solvents deviate as expected from a linear relation between $\log K_A$ and $1/D$. Other investigations with two-component solvent mixtures, including the three referred to above, have not provided the information desired due to the facts: (1) that the dielectric constant of one of the components was too small to permit determination of the K_A -values over the entire range of composition and (2) that the linear relation between $\log K_A$ and $1/D$ to be expected for the salt in a series of one-component monomolecular solvents, covering the range of dielectric constants involved, had not been established (and could not be if the dielectric constant of one of the components was too small). It has been shown² that these essential requirements are fulfilled by the salt, $(n\text{-Bu})_4\text{NClO}_4$, and by the two solvents, benzonitrile, $\text{C}_6\text{H}_5\text{CN}$, ($D_{25^\circ} = 25.2$) and *o*-dichlorobenzene, $o\text{-C}_6\text{H}_4\text{Cl}_2$ ($D_{25^\circ} = 10.1$).

Experimental

The methods of preparation, purification, desiccation, and identification of $(n\text{-Bu})_4\text{NClO}_4$ were those used previously.²

Treatment of Solvents.—The *o*-dichlorobenzene was obtained (as previously described²) from the Eastman product (White Label grade) by fractional distillation (b.p. 81.0–82.0° at 30.9 to 32 mm.) and found *via* gas chromatography to contain less than 0.5 mole % of *p*-dichlorobenzene as the only foreign organic substance present. The benzonitrile, Eastman (Yellow Label grade), required more elaborate purification. Prior to fractional distillation, it was treated with benzoyl chloride and sodium hydroxide (somewhat in excess of that needed to hydrolyze any unreacted benzoyl chloride). This heterogeneous mixture was stirred for several hours at room temperature and finally over a steam bath. The resulting organic layer was washed twice with concentrated NaCl solution after which it was dried over CaCl_2 for 24 hr. On fractional distillation a colorless product (b.p. 84° at 22 mm.) was obtained in which no impurity was detectable in its gas chromatogram.

Both of these solvents were dried and stored in contact with Davison silica gel. The specific conductances of the $\text{C}_6\text{H}_5\text{CN}$ and of the *o*- $\text{C}_6\text{H}_4\text{Cl}_2$ were 5.4×10^{-8} and 5×10^{-10} ohm⁻¹ cm.⁻¹, respectively, and those of the mixtures were between these two values.

The density (at 25°) of each of these solvents and of each of their mixtures was determined with a Lipkin-type pycnometer (volume, 3 ml.) which was calibrated with conductance water. The Ubbelohde viscometer, used to determine viscosities, had the flow time for conductance water at 25° of 106.6 sec. The density and viscosity found for each of the pure components agreed well within experimental error with their presently accepted values.

Conductance Measurements.—These were made with the Shedlovsky⁹ alternating current bridge modified as previously described.² The conductance cell was the Kraus erlenmeyer type¹⁰ which had a cell constant equal to 0.1473 cm.⁻¹.

Dielectric Constant Measurements.—A bridge method was chosen which permits determination of the dielectric constants with sufficient accuracy ($\pm 1\%$) for the purposes of this investigation. It involved the use of a General Radio Twin-T Impedance Measuring Circuit (type 821-A), a Bendix Radio Frequency Meter (type BC-221M) as an oscillator, and a Signal Corps radio receiver (type BC-348Q) as a detector. Both the oscillator and the detector were connected with the impedance circuit by coaxial cables supplied with the twin-T circuit.

(3) J. T. Denison and J. B. Ramsey, *J. Am. Chem. Soc.*, **77**, 2615 (1955); see also ref. 2.

(4) R. M. Fuoss, *ibid.*, **80**, 5059 (1958).

(5) E. Hirsch and R. M. Fuoss, *ibid.*, **82**, 1021 (1960).

(6) F. Accuscina, S. Petrucci, and R. M. Fuoss, *ibid.*, **81**, 1301 (1959).

(7) R. M. Fuoss and E. Hirsch, *ibid.*, **82**, 1013 (1960).

(8) Y. H. Inami and J. B. Ramsey, *J. Chem. Phys.*, **31**, 1297 (1959).

(9) T. Shedlovsky, *J. Am. Chem. Soc.*, **52**, 1793 (1930).

(10) C. A. Kraus and R. M. Fuoss, *ibid.*, **55**, 21 (1933).

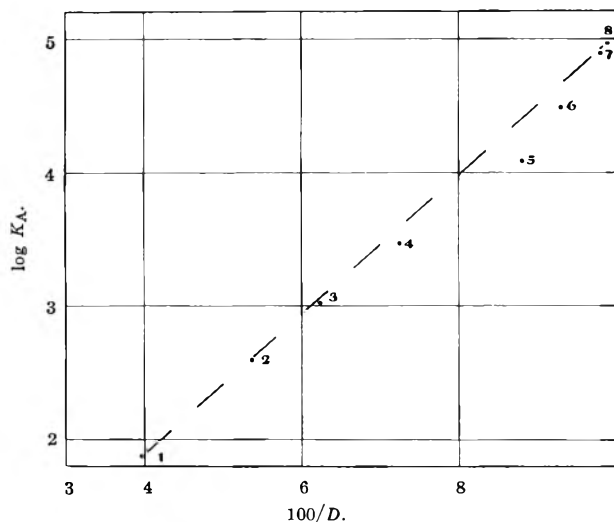


Fig. 1.—Dependence of the association constant of $(n\text{-Bu})_4\text{NClO}_4$ on the dielectric constant of the solvent. Point numbers correspond to those given to the solvents in Table I.

The Pyrex capacitance cell (requiring ~ 35 ml. of liquid) which consisted of three concentric platinum cylinders was made in accordance with the specifications given by Smyth.¹¹ This cell can be filled and emptied, *via* suction, without altering its position in the oil-filled thermostat (maintained at $25 \pm 0.01^\circ$). Before each determination the cell was flushed out with pure acetone and dried with a stream of filtered dry air.

To fix the geometry of the circuit between the bridge and the cell rigid copper bars ($1 \times \frac{1}{8}$ in.) were used. The grounded connection, which remained unbroken, consisted entirely of such a bar. For the other connection a cam was mounted near the end of a somewhat shorter bar. To this cam a copper wire (B.&S. gage 11), bent to a half circle (radius ~ 7 in.), was attached in such a way that contact between the end of the copper wire (sharpened to a point) and the mercury in contact with the ungrounded cell terminal could be made and broken by a small turn of the cam, thereby producing but a very small (and reproducible) change in the mutual position of the two leads.

The air capacitance of the cell was determined at 0.50 Mc./sec. with benzene as the reference and found to be 50.8 pf. For adequate calibration of the cell it was necessary to use a series of liquids with dielectric constants covering the range from 2 to 26. Those were benzene ($D = 2.274$), chlorobenzene ($D = 5.621$), acetone ($D = 20.7$), benzonitrile ($D = 25.2$), and four mixtures of nitrobenzene and anisole, chosen to provide D -values between 5 and 20. The D -values of the four one-component liquids are those given by Maryott and Smith.¹² Those of the four mixtures of nitrobenzene and anisole were readily obtainable from the results of Powell and Martell,¹³ who have determined the D -values of eleven mixtures of these two liquids covering the entire range of composition. From the smooth curve given by plotting these D -values against the weight per cent, w , of nitrobenzene the following values were found for the four mixtures used: $w = 29.24$, $D = 10.05$; $w = 41.02$, $D = 12.9$; $w = 52.01$, $D = 16.0$; $w = 60.97$, $D = 18.8$.

The benzonitrile used was that obtained by the procedure described above. All the other liquids, except acetone which was Baker Analyzed Reagent grade, were initially Eastman White Label products. The acetone was merely dried thoroughly with Davison silica gel. Before fractionally distilling, the benzene and the chlorobenzene were treated in the way described by Brown, Levina, and Abrahamson.¹⁴ After the nitrobenzene had been dried over silica gel for 24 hr., it was twice fractionally distilled at reduced pressure (~ 12 mm.). The anisole was washed once with 2 *N* NaOH, three times with water, and then dried with CaCl_2 for 15 hr. before being fractionally distilled.

(11) C. P. Smyth and A. Weissberger, "Technique of Organic Chemistry; Physical Methods," Vol. I, Part 3, 3rd Ed., Interscience Publishers, Inc., New York, N. Y., 1959, p. 2567 and pp. 2631–2632.

(12) A. A. Maryott and E. R. Smith, Natl. Bur. Std. Circular No. 514, 1951.

(13) A. L. Powell and A. E. Martell, *J. Am. Chem. Soc.*, **79**, 2118 (1957).

(14) A. S. Brown, P. M. Levina, and E. W. Abrahamson, *J. Chem. Phys.*, **19**, 1226 (1951).

The boiling point of each of these liquids agreed with their well established values.

To ascertain that errors due to lead inductance were insignificant, all calibrations and measurements were carried out at four different frequencies, *viz.*, 0.50, 1.80, 3.00, and 5.00 Mc./sec. The dielectric constants obtained at these four frequencies agreed within $\pm 0.4\%$, which is well within the desired accuracy.

The capacitance of the cell containing a liquid having a greater dielectric constant than 18 exceeded the range of the precision condenser in the twin-T circuit. With such liquids ($D > 18$) calibrations and measurements were made with a small fixed condenser in series with the cell. It was essential that the condenser, so used, should be small dimensionally, have a very small temperature coefficient, and have a constant capacity during the time in use. In every case two such condensers were used separately, one having a capacity of 244 pf. and the other, 480 pf. With each of these condensers, in series, measurements for a given liquid were made at each of the four frequencies (specified above). The results obtained showed the same good agreement as did those obtained in the direct reading range (*i.e.*, where a series condenser was not required).

Properties of Solvents.—The values obtained for the density, d , the dielectric constant, D , and the viscosity, η , of the solvents used in the conductance measurements are given in Table I. The symbol, w , represents the weight per cent of benzonitrile [$(100 - w)$ equals the weight per cent of *o*-dichlorobenzene].

TABLE I

PROPERTIES OF SOLVENTS AT 25°				
	w	d , g./ml.	D	η , poise
(1)	100.00	1.008	25.20 ^a	0.01246
(2)	44.99	1.1505	18.64	.01272
(3)	30.04	1.2003	16.04	.01275
(4)	17.51	1.2406	13.80	.01281
(5)	7.53	1.2811	11.36	.01284
(6)	4.99	1.2906	10.75	.01285
(7)	1.51	1.2991	10.21	.01285
(8)	0.00	1.3005	10.12 ^b	.01284

^a Value given by Maryott and Smith.¹² Not redetermined in this investigation. ^b Value found in this investigation which is larger than that, 9.93, accepted by Maryott and Smith.¹²

Results

The values of the association constant, K_A , and the limiting equivalent conductance, Λ_0 , were determined by use of the equation developed by Shedlovsky,¹⁵ namely

$$1/\Lambda S(z) = [c\Lambda f^2 S(z)]K_A/\Lambda_0^2 + 1/\Lambda_0$$

In each of the eight solvents the conductances at five concentrations of the perchlorate, covering the range from $\sim 10^{-4}$ to $\sim 10^{-5}$ volume formal, were measured. Evaluations of K_A and Λ_0 were very greatly expedited by use of the I.B.M. computer, No. 7090, available on campus at the UCLA Computing Facility. The maximum probable error in the value of K_A thus was found to be in no case greater than 2%; in most cases it was less.

In Table II are given the values of K_A and Λ_0 obtained, along with those of $\log K_A$ and $100/D_{\text{macro}}$. The solvents are designated by the code numbers used in Table I. Duplicate runs were carried out with each of the two pure components; not with any of the mixtures. Since the duplicate values of K_A found in each of the pure components differed by less than 1%, it was presumed that duplicate values of K_A in each of the mixtures would exhibit no greater disagreement.

In Fig. 1 the values of $\log K_A$ are plotted against $100/D_{\text{macro}}$. With the ordinate scale used the maximum difference between duplicate values of $\log K_A$, presumed possible, is too small to be indicated by open circles. Since it has been found² that the values of $\log K_A$ of

(15) T. Shedlovsky, *J. Franklin Inst.*, **220**, 739 (1938).

TABLE II

CONSTANTS OF $(n\text{-Bu})_4\text{NClO}_4$ IN THE SOLVENTS AT 25°

Solvent	λ_0	$K_A \times 10^{-3}$	$\log K_A$	$100/D_{\text{macro}}$
(1)	46.02	0.0753	1.877	3.97
(2)	42.53	0.400	2.602	5.37
(3)	41.84	1.067	3.028	6.23
(4)	40.75	2.94	3.468	7.25
(5)	41.78	12.32	4.091	8.80
(6)	40.00	30.7	4.487	9.30
(7)	45.31	78.1	4.893	9.79
(8)	42.3	93.4	4.970	9.88

$(n\text{-Bu})_4\text{NClO}_4$ in six monomolecular solvents, including $\text{C}_6\text{H}_5\text{CN}$ and $o\text{-C}_6\text{H}_4\text{Cl}_2$, vary linearly with $1/D_{\text{macro}}$, the dashed straight line in Fig. 1 which is drawn through the points given by $\text{C}_6\text{H}_5\text{CN}$ and by $o\text{-C}_6\text{H}_4\text{Cl}_2$ should represent this linear relation quite closely. That it does so is confirmed by the fact that its slope is only slightly ($\sim 3.5\%$) greater than that of the most probable straight line found² to be given by the six monomolecular solvents.

It is seen that in a series of mixtures of $\text{C}_6\text{H}_5\text{CN}$ and $o\text{-C}_6\text{H}_4\text{Cl}_2$ the variation of $\log K_A$ and $1/D_{\text{macro}}$ cannot be represented by a straight line. Also in each of the mixtures containing less than ~ 45 weight % of $\text{C}_6\text{H}_5\text{CN}$ ($100/D_{\text{macro}} > 5.37$) the value of $\log K_A$ is distinctly less than it would be if $\log K_A$ varied linearly with $1/D_{\text{macro}}$. It also is noteworthy that deviation from linearity would be practically undetectable in mixtures containing more than ~ 45 weight % of $\text{C}_6\text{H}_5\text{CN}$.

Discussion

These results substantiate the prediction that the values of $\log K_A$ of a salt in a series of mixtures of two solvents having appreciably different dielectric constants should deviate from the linear relation between $\log K_A$ of this salt and $1/D$ in the sense that their values, over a considerable range of composition, should be less than those to be expected from this linear relation. The prediction is a consequence of the assumption that molecules of that component of the mixture which has the larger dielectric constant would have a greater tendency to accumulate in the neighborhood (or near vicinity) of an ion than would the component with the lower dielectric constant. This would result in making the dielectric constant of this small portion of a solvent mixture (which is effective in determining the stability of the associated ion pair) greater than that of the pure solvent mixture, *i.e.*, of the solvent mixture in the absence of ions; thereby causing the K_A -value of a salt to be smaller than expected.

This assumption has been shown² to provide a probable interpretation for the deviations from linearity found to exist with $(n\text{-Bu})_4\text{NClO}_4$ in each of the solvents, ethylene chloride and propylene chloride, and with $(n\text{-Bu})_4\text{NPi}$ in ethylene chloride. Each of these two one-component solvents consists of two molecular species, one distinctly more polar than the other.

It is apparent (from Fig. 1) that deviation from linearity would not be detectable with $(n\text{-Bu})_4\text{NClO}_4$ in mixtures of $\text{C}_6\text{H}_5\text{CN}$ and $o\text{-C}_6\text{H}_4\text{Cl}_2$ which have dielectric constants greater than 18.6 ($100/D < \sim 5.4$). That such a linear portion of the graph would exist in mixtures with D -values in the higher range might have been expected from the results obtained by Fuoss, *et al.*⁵⁻⁷ Their results show that the points given by each of the salts used in the several mixtures with D -values in the higher range are well represented by a straight line. However, it was not known whether this linear portion of their graphs would coincide with the straight line to be expected when $\log K_A$ of the salt is plotted against $100/D$ of a series of one-component solvents with D -values covering the same range as that of these mixtures. From the results of this investigation it is concluded that such coincidence would exist. If this conclusion is valid, it follows that the α -parameter of a given salt may be evaluated from the slope ($= \epsilon^2/230.3akT$) of this initial straight line portion of such graphs. Also the extrapolation of this linear portion to the value of $100/D$ corresponding to that of the component having the smaller D -value should give the K_A -value of the salt in this pure component which cannot be determined directly due to the smallness of its dielectric constant.

This linear portion of these graphs may be interpreted to mean that the effective (microscopic) dielectric constants of those mixtures to which this linear portion pertains do not differ perceptibly from the dielectric constants of these pure solvent mixtures. The conclusion that this condition would exist only in those solvent mixtures which have D -values in the higher range seems reasonable since in these mixtures the molecules of the component having the higher dielectric constant would be expected to have the least (and very small) tendency to accumulate in the near vicinity of an ion.

The results show that deviation from the linear relation between $\log K_A$ and $100/D$, which is known for $(n\text{-Bu})_4\text{NClO}_4$ (the dashed straight line in Fig. 1), exists to a measurable extent in mixtures of $\text{C}_6\text{H}_5\text{CN}$ and $o\text{-C}_6\text{H}_4\text{Cl}_2$ which have D -values less than ~ 18.6 ($w \approx 42.5$). Over the range of D -values from 18.5 to about 12.5 this deviation is seen to be represented by a curve which is concave downward. It is recalled that Hirsch and Fuoss⁵ noted deviations from linearity in this same sense with three different salts in a series of mixtures of $\text{C}_6\text{H}_5\text{NO}_2$ and CCl_4 . That no change in curvature (from downward to upward) was observed by these investigators may be attributed to the fact that it was impossible to determine K_A -values in $\text{C}_6\text{H}_5\text{NO}_2\text{-CCl}_4$ mixtures containing sufficiently low weight per cent of $\text{C}_6\text{H}_5\text{NO}_2$ since the D -values of such mixtures were too small to permit their evaluation. It is seen that this reversal in curvature with $(n\text{-Bu})_4\text{NClO}_4$ in the $o\text{-Cl}_2\text{-C}_6\text{H}_4\text{-C}_6\text{H}_5\text{CN}$ system occurs at a composition near 12.2% $\text{C}_6\text{H}_5\text{CN}$ ($100/D \approx 8$).

APPLICATION OF FLASH-DESORPTION METHOD TO CATALYST STUDIES. I. ETHYLENE-ALUMINA SYSTEM¹

BY Y. AMENOMIYA AND R. J. CVETANOVIC

Division of Applied Chemistry, National Research Council, Ottawa, Canada

Received July 6, 1962

The flash-desorption technique was applied to the ethylene-alumina system to investigate the surface of alumina. The apparatus consisted of a programming controller increasing the catalyst temperature linearly with time at various speeds and of a thermistor type thermal conductivity cell for measuring the rate of desorption of ethylene. The existence of two different sites for the adsorption of ethylene on alumina was established. On one of these sites the activation energy of desorption was 26.8 kcal./mole (I), and on the other 36.4 kcal./mole (II). These sites occupy 2.8% of the total surface area, 60% of which belongs to I, 40% to II.

Introduction

Flash-desorption technique has been used by several investigators²⁻⁸ to obtain kinetic information on adsorption and desorption of gases on metals. Very interesting information recently was obtained with this technique by Redhead,⁸ who studied desorption of gases from a metal filament using ultrahigh vacuum techniques. The desorption was followed by measuring pressure changes by means of an ionization gage. The filament temperature was increased linearly with time and the activation energy of desorption was obtained by assuming the temperature independent factor in the Arrhenius equation to be 10^{13} .

The present work has been carried out under conditions much more similar to those ordinarily employed in catalytic reactions. Desorption of ethylene has been studied in an attempt to obtain information on the properties of the catalyst surface of alumina. A thermistor type thermal conductivity cell was used to detect the ethylene desorbed from the catalyst in a stream of helium. The speed of increase of catalyst temperature was variable and considerably slower than used by previous authors.

Experimental

Apparatus.—The apparatus used is shown in Fig. 1. The reactor, R, is a quartz tube of 8-mm. i.d. provided with a perforated disk on which a small amount of alumina is placed. The part of the apparatus to the right of stopcocks S_1 and S_2 is an ordinary static system which can be used to measure the adsorption when S_1 and S_2 are closed. The amount of ethylene adsorbed on the catalyst was measured in the usual way using the manometer, M, and a cathetometer. Following this, the catalyst was evacuated and then the stream of helium was admitted through S_1 , over the catalyst in R, through S_2 , the thermal conductivity cell, D, and finally through the liquid nitrogen trap, T_1 . Helium from the cylinder was passed through silica gel at liquid nitrogen temperature to remove traces of water. The flow rate of helium was measured by a soap film flow-meter attached to the outlet of the rotary pump.

When the catalyst temperature is raised at a uniform rate by means of the programming controller, ethylene desorbs from the catalyst and is carried with helium past the thermal conductivity cell, D, by means of which the concentration of ethylene in helium is determined in the same manner as in gas chromatography and is recorded on a recorder (Leeds & Northrup Speedomax, full scale: 1 mv., response time: 1 sec.). Since the flow rate of helium is constant, the deflection of the recorder due to the pres-

ence of ethylene in the carrier should be proportional to the rate of its desorption. The rate of desorption increases with temperature at first but eventually begins to decrease as a result of depletion of adsorbed gas so that a peak is recorded. The recorded peaks will be called in the present paper the flash-desorption chromatogram. Simultaneously, the temperature of the catalyst is recorded by means of a second recorder which is connected to an Alumel-Chromel thermocouple, TC_2 , inserted directly into the center of catalyst bed, as shown in the inset of Fig. 1. As the charts of the two recorders are driven at the same speed, the temperature at any point of the flash-desorption chromatogram can be determined. The temperature at which peak maximum appears is related to the activation energy of desorption, as will be discussed later. The surface area of the thermocouple, TC_2 , and of its leads was so small that their effect on the adsorption was neglected. The temperature indicated by the inside thermocouple TC_2 was always a little higher than that indicated by TC_1 . The temperatures reported here are those read by means of TC_2 . The speed of raising the catalyst temperature could be varied from 0.5 to 40°/min.

The detector used was a conventional thermal conductivity cell of thermistor type, AEL 9677 of the Gow-Mac Instrument Co.

Materials.—Alumina was prepared by adding an excess of a 10% ammonium hydroxide solution to a 20% aluminum nitrate solution at room temperature. The precipitate was washed with distilled water several times,⁹ dried at 110°, and crushed to small cubes of about 2 mm. The weight of alumina placed into the reactor was 0.253 g. and the length of the catalyst bed was 13 mm.

Before use, alumina was treated with air for 2 hr. at 600° and evacuated at the same temperature for more than 60 hr., until no more water condensed in the trap T_1 during evacuation. After each run the catalyst was evacuated for 2 hr. at 600° and this was followed by evacuation for 12 hr. at 550°. The total BET surface area of the catalyst after this treatment was 41.7 m.² for the sample of 0.253 g. used. The amount of ethylene adsorbed in each run under the same conditions was found to be constant within the experimental error, indicating that the above pretreatment was adequate for the cleaning of the catalyst surface.

Phillips research grade ethylene was passed through activated charcoal, condensed in a liquid nitrogen trap, and evacuated. A trace impurity of ethane was present but no attempt was made at further purification.

Procedure.—In every run the adsorption of ethylene was first measured. When ethylene was admitted to the catalyst, a pressure change was observable only within 2 or 3 min.; the amounts adsorbed reported here all were measured after 10 min. After this measurement the catalyst was evacuated for 10 min. at room temperature (series I), and then exposed to the helium flow. When the recorder base line of the thermistor detector became stable after several minutes, indicating that no gas was evolved from the catalyst, the flash-desorption was started.

In the experiment series II, the catalyst was heated up quickly to 100° *in vacuo* after the adsorption measurement and evacuated for 60 min. at the same temperature instead of the evacuation for 10 min. at room temperature in series I. The subsequent procedure was the same as in series I.

The amount of gas desorbed by flash-desorption can be measured by either (1) trapping in the trap T_1 , followed by gas chromatographic analysis, or (2) measuring the area of the flash-

(1) Contribution no. 7142 from the National Research Council, Ottawa, Canada.

(2) G. Ehrlich, *J. Phys. Chem.*, **60**, 1388 (1956).

(3) (a) T. W. Hickmott and G. Ehrlich, *J. Chem. Phys.*, **24**, 1263 (1956);

(b) J. Eisinger, *ibid.*, **27**, 1206 (1957).

(4) R. E. Schlier, *J. Appl. Phys.*, **29**, 1162 (1958).

(5) T. W. Hickmott and G. Ehrlich, *J. Phys. Chem. Solids*, **5**, 47 (1958).

(6) G. Ehrlich, *J. Appl. Phys.*, **32**, 4 (1961).

(7) G. Ehrlich, *J. Chem. Phys.*, **34**, 29, 39 (1961).

(8) P. A. Redhead, *Trans. Faraday Soc.*, **57**, 641 (1961).

(9) The final pH of the wash water was between 8 and 9. No analysis was carried out for residual nitrate.

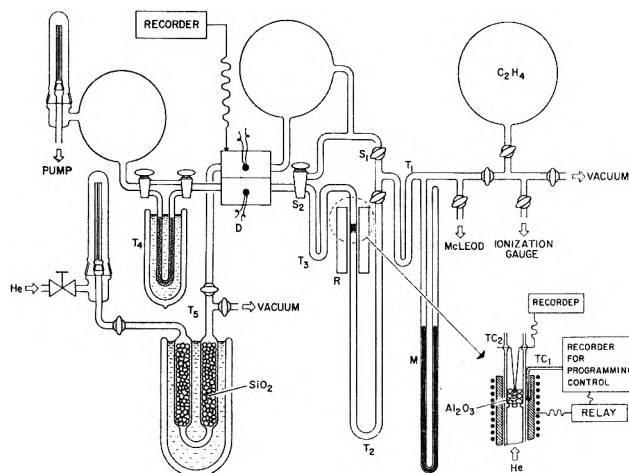


Fig. 1.—Diagram of the apparatus.

desorption chromatogram. The latter method contained, however, some uncertainty due to the shift of the base line during flashing, although this agreed with the result of the former method within the experimental error of about 10%. The values reported in this paper all were obtained by the former method.

Results and Discussion

Figure 2(a) shows the typical flash-desorption chromatogram of an experiment in series I, *i.e.*, with the catalyst evacuated for 10 min. at room temperature before the flash-desorption. Figure 2(b) was obtained at a different speed of flashing. The speed of raising temperature is given in the figures as β ($^{\circ}\text{C./min.}$). It is seen that two superposed peaks are obtained. The results of series I are summarized in Table I in which T_{M1} is the temperature at which the first peak maximum appeared. The amount of gas desorbed during the flashing was measured as described above.

When the catalyst was evacuated for 60 min. at 100° before the flash-desorption (series II), the first peak disappeared and only the second peak was left as seen in Fig. 2(c). This peak can be well superposed onto the second peak of Fig. 2(b) obtained at approximately the same β , as shown in Fig. 2(d). The results of series II are listed in Table II in which T_{M2} is the temperature at which the second peak maximum appeared. T_{M2} values taken from the chromatograms of series I were slightly different from those listed in Table II due to the influence of superposition of the first peak upon the second peak. In similar experiments with ethane instead of ethylene, no peaks such as with ethylene were observed.

If ethylene was introduced to the catalyst under higher pressure than 50 mm. for a long time, the main peak of the flash-desorption chromatogram appeared at higher temperature and the gas chromatographic analysis showed that the desorbed material consisted almost entirely of butenes. However, the present experiments were done at pressures below 10 mm. and both peaks in series I and II were identified by gas chromatography as ethylene containing less than 0.5% of C_3 and a trace of C_4 hydrocarbons.

When the temperature, T , of the catalyst is raised, the following general relation should hold

$$d^2\theta/dt^2 = \partial^2\theta/\partial t^2 + (\partial^2\theta/\partial t\partial T + \partial^2\theta/\partial T\partial t)dT/dt + \partial^2\theta/\partial T^2(dT/dt)^2 + \partial\theta/\partial T \cdot d^2T/dt^2$$

where θ is the surface coverage and t is the time.

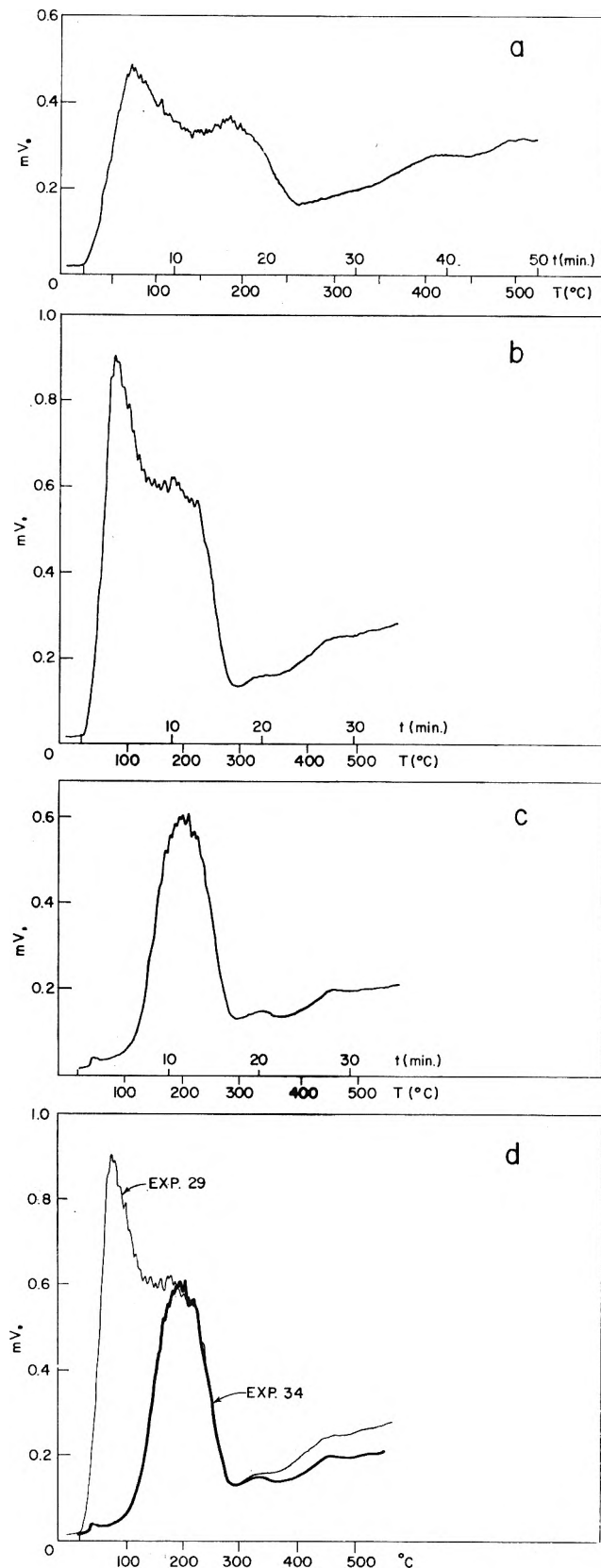


Fig. 2.—Flash-desorption chromatograms. (a) Expt. no. 22: evacuated before flashing 10 min. at room temperature; $\beta = 10.08^{\circ}/\text{min.}$ (b) Expt. no. 29: evacuated before flashing 10 min. at room temp., $\beta = 16.03^{\circ}/\text{min.}$ (c) Expt. no. 34: evacuated before flashing 60 min. at 100° , $\beta = 15.90^{\circ}/\text{min.}$ (d) Superposition of chromatograms from Expt. no. 29 and 34.

If the temperature is increased linearly with time, so that $T = T_0 + \beta t$, where T and T_0 are, respectively, the temperature at time t and the initial temperature, and if it is assumed that $\partial\theta/\partial t \gg \partial\theta/\partial T$ throughout

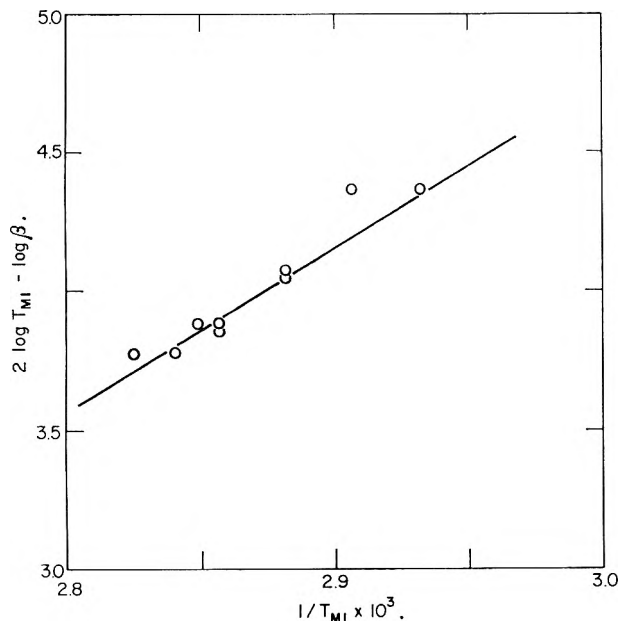


Fig. 3.—Plot of eq. 3 for series I.

the course of an experiment,⁷ the above equation can be simplified to

$$d^2\theta/dt^2 = \partial^2\theta/\partial t^2 + \beta\partial^2\theta/\partial T\partial t \quad (1)$$

At the same time the rate of desorption, r_d , is written as

$$r_d = -v_m d\theta/dt = k_0\theta \exp(-E_d/RT) \quad (2)$$

where k_0 is a constant, E_d is the activation energy of desorption, and v_m is the amount of gas adsorbed at $\theta = 1$. From (1) and (2), and putting $d^2\theta/dt^2 = 0$ at $T = T_M$, we have

$$E_d\beta v_m/RT_M^2 k_0 = \exp(-E_d/RT_M)$$

which is the same as Redhead's result,⁸ or

$$2 \log T_M - \log \beta = E_d/2.303 RT_M + \log E_d v_m/Rk_0 \quad (3)$$

The plot of the left hand side of eq. 3 against $1/T_M$ gives, therefore, a straight line, from which E_d and k_0/v_m are obtained.

The assumption that $\partial\theta/\partial t \gg \partial\theta/\partial T$ appears reasonable because in a fast flow of helium the rate of readsorption should be negligible. If the rate of readsorption had an effect, T_M and the shape of the peak would be altered by a change in the flow rate of helium similarly to the changes occurring in adsorption gas chromatography. However, expt. no. 44 in Table I, which was done at more than twice the flow rate than in the remaining experiments, gave the same T_M and peak shape. In addition, the good linearity of the plot of eq. 3 also supports the above assumption, as will be shown later.

In Fig. 3, $2 \log T_M - \log \beta$ was plotted against $1/T_M$ for the first peak (Table I). From the slope and intercept E_d and k_0/v_m were found to be 26.8 kcal./mole and 1.6×10^{15} sec.⁻¹, respectively. Assuming that the adsorption of ethylene on alumina is non-dissociative and localized, the absolute rate of desorption is written as

$$r_d = c_a(kT/h)(f_*/f_a) \exp(-E_d/RT)$$

TABLE I

ADSORPTION AND FLASH-DESORPTION OF ETHYLENE. SERIES I
(Alumina evacuated for 10 min. at room temperature before flash-desorption, flow-rate of He 45.7 ± 0.3 cc./min.)

Expt. no.	Adsorption			Flash-Desorption		
	Temp., °C.	Pressure, mm.	Amt. of gas adsorbed, cc. (NTP)	β , °C./min.	T_M , °C.	Amt. of gas desorbed, cc. (NTP)
22	24.9	6.13	0.218	10.08	74	...
23	24.8	6.34	.227	20.70	79	...
24	24.7	6.37	.239	5.05	68	...
26	25.2	5.28	.273	5.14	72	...
27	26.2	5.63	.259	21.05	81	...
28	26.5	5.38	.251	10.40	74	0.091
29	25.8	5.96	.266	16.03	77	.095
44 ^a	24.0	5.73	.323	16.35	77	...
45	24.8	1.43	.212	16.10	..	.102
46	24.2	9.00	.344	16.05	78	.105
50	25.0	0.002 ^b	.097	15.78	..	.099

^a Flow-rate of He, 102.5 cc./min. ^b Measured by McLeod gage.

where f_* and f_a are the partition functions of the activated complex (excluding $kT/h\nu$) and adsorbed molecule, respectively, c_a is the surface concentration of the adsorbed molecule, and k and h are the Boltzmann and Planck constants, respectively. Also assuming that the freedom of both the activated complex and the adsorbed molecules is so small that $f_* = f_a = 1$, we have

$$r_d = c_a(kT/h) \exp(-E_d/RT)$$

where kT/h corresponds to k_0/v_m in eq. 2. The calculated value of kT/h at 350°K. is 0.73×10^{13} sec.⁻¹ and is in reasonable agreement with the observed $k_0/v_m = 1.6 \times 10^{15}$ sec.⁻¹ considering that the freedom of the activated complex might be greater than that of adsorbed molecules, i.e., $f_*/f_a > 1$.

Unfortunately, a good linear plot as in Fig. 3 was not obtained for the second peak (series II). In this case the activation energy of desorption was calculated from eq. 3 assuming that k_0/v_m was 1.6×10^{15} as obtained for the first peak. The values of E_d are given in the last column of Table II and the mean value is 36.4 kcal./mole. Since the adsorption reached equilibrium very quickly (usually within a few minutes),

TABLE II

ADSORPTION AND FLASH-DESORPTION OF ETHYLENE. SERIES II
(Alumina evacuated for 60 min. at 100° before flash-desorption; flow-rate of He 45.7 ± 0.3 cc./min.)

Expt. no.	Adsorption			Flash-Desorption			Acti- vation energy of desorption, kcal./ mole
	Temp., °C.	Pres- sure, mm.	Amt. of gas ad- sorbed, cc. (NTP)	β , °C./ min.	T_M , °C.	Amt. of gas de- sorbed, cc. (NTP)	
33	26.1	5.77	0.278	17.00	202	0.044	36.6
34	25.9	5.61	.285	15.90	203	.045	36.8
35	25.4	6.33	.307	19.80	207	.044	36.8
36	26.0	5.87	.311	9.87	186	.041	35.8
38	26.0	5.72	.289	31.95	210	.041	36.6
39	25.5	6.05	.306	40.32	208	.041	36.3
42	26.0	5.76	.305	16.00	194	...	36.0
47	25.0	2.03	.214	15.55	200	.041	36.5
48	25.0	2.22	.234	15.80	203	.042	36.7
49	25.0	10.11	.377	15.50	195	.039	36.1
						Mean	36.4

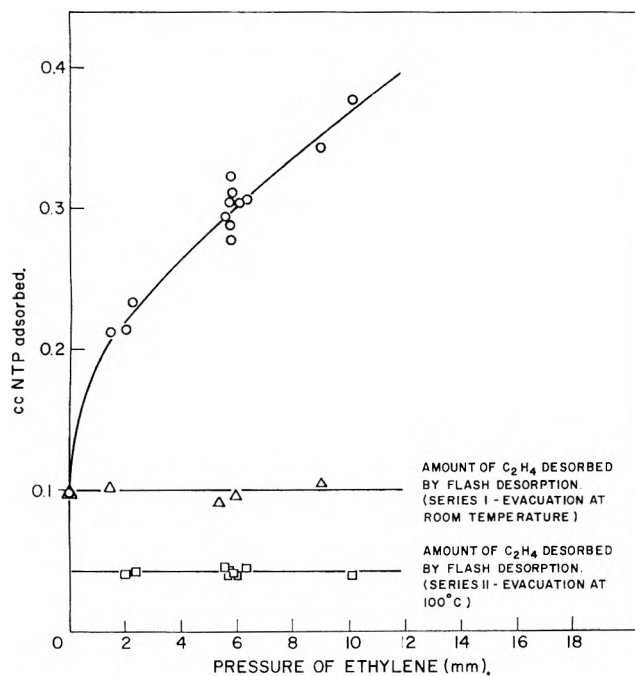


Fig. 4.—Isotherm of ethylene at room temperature.

the observed activation energies of desorption will be approximately equal to the heats of adsorption.

In Fig. 4 the amount of gas desorbed by flashing and the amount of adsorbed gas are plotted against the pressure at which the adsorption was measured. It is seen that the amount of the gas desorbed is constant and independent of the pressure at which adsorption was carried out. This indicates that the strong adsorption (chemisorption) which is not removed by evacuation at room temperature is already saturated at a pressure as low as 0.002 mm. There exist, therefore, two types of chemisorption of ethylene on alumina: one corresponds to 0.058 cc./0.253 g. of alumina with a heat of adsorption of 26.8 kcal./mole, the other to 0.042 cc./0.253 g. with a heat of adsorption of 36.4 kcal./mole. The BET area of this catalyst was 41.7 m.²/0.253 g., as mentioned before. v_m was found to be 3.64 cc./0.253 g. from the Langmuir plot ranging from 30 to 150 mm. of ethylene. Combining this v_m with BET area, 43 Å.² is obtained as the sectional area of an

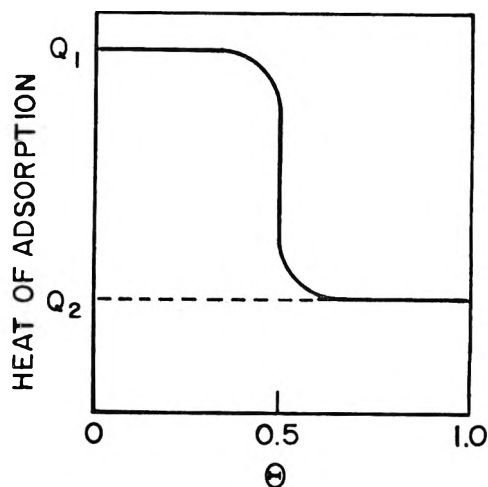


Fig. 5.—Change of the heat of adsorption with surface coverage (ref. 10).

adsorbed molecule. Although this value seems to be a little too large, it is of the right order of magnitude. If 3.64 cc. is adopted as v_m , 0.058 and 0.042 cc. correspond to surface coverages of 1.6 and 1.2%, respectively.

If an adsorbed molecule experiences the repulsive force from a molecule adsorbed on an adjacent site and not from other molecules, the heat of adsorption varies with the surface coverage as shown in Fig. 5, so that two distinctly different heats of adsorption may be observed on homogeneous surfaces.¹⁰ In the present case, however, the distance between chemisorbed molecules is at least about 29 Å., provided ethylene molecules are dispersed homogeneously on the surface. This distance is too large for the repulsive forces between molecules to be effective. Therefore it is unlikely that the existence of two different heats of adsorption depends on the interaction between adsorbed molecules except if the active sites on which ethylene chemisorbs are dispersed patchwise on the surface.

The shapes of the two peaks on the flash-desorption chromatograms were broader than calculated assuming a constant E_d . In view of this, it may be possible that a heterogeneity of the surface is involved. This matter, however, cannot be discussed at present.

(10) K. J. Laidler, "Catalysis" (P. H. Emmett), Vol. 1, Chap. 3, Reinhold Publ. Corp., New York, N. Y., 1954.

SOLVENT EFFECTS IN THE ELECTRONIC SPECTRUM OF ORGANOLITHIUM COMPOUNDS¹

BY R. WAACK AND M. A. DORAN

*Eastern Research Laboratory, The Dow Chemical Company, Framingham, Massachusetts**Received July 6, 1962*

We have found that the absorption maximum in the electronic spectrum of di- or triphenylmethyl lithium compounds is shifted to longer wave lengths by more polar solvents. For the most thoroughly studied species, 1,1-diphenylhexyllithium, the shifts in absorption maximum are approximately proportional to the solvent dielectric constant. Two factors are considered to account for the observed red shift in absorption maximum: first, a decrease in the energy required for the electronic excitation resulting from increased solvation of the excited state due to the polarizability and dipole orientation of the solvent; and second, the more polar (basic) solvents promote ionization of the carbon-lithium bond, raising the ground state energy of this electron pair relative to the excited state. A solvent induced shift in the absorption spectrum cannot be considered to be a general phenomenon for all organolithium compounds. The position of the absorption maximum of monophenylmethyl lithium species, *e.g.*, polystyryllithium, poly- α -methylstyryllithium, benzyl lithium, and α -methylbenzyl lithium is insensitive to solvent. A lack of increase in dipole moment on electronic excitation of these species or a preference of these less sterically hindered species toward self solvation is suggested to be responsible for the insensitivity of their spectrum to solvent. Consideration of solvation effects can improve the agreement between the spectrum of the cation and anion of a given species or the correlation of the absorption with calculated transition energy.

Ultraviolet spectra of polar molecules usually are altered by changes in polarity of the solvent media. In general, the K-bands of conjugated compounds are shifted to the red by more polar solvents.² A report of the spectrum of the polar organolithium compound, polystyryllithium, showed the spectrum to be insensitive to solvent changes, *i.e.*, in tetrahydrofuran and benzene.³ Our measurements of the spectrum of this species also show it to be solvent insensitive. In addition we have found this same solvent insensitivity in the spectrum of other monophenylmethyl organolithium species such as benzyl lithium, α -methylbenzyl lithium, and poly- α -methylstyryllithium. On the other hand, we have found the electronic spectrum of di- and triphenylmethyl lithium compounds to be very sensitive to solvent. For these species a more polar solvent produces a pronounced red shift in the absorption maxima. There appears to be a linear relationship between the frequency of the absorption maximum and the dielectric constant of the solvent for 1,1-diphenylhexyllithium in the seven solvents examined. These experiments indicate that a lack of solvent sensitivity is characteristic of the electronic spectrum of monophenylmethyl organolithium species, whereas a pronounced solvent dependence is typical of the spectrum of di- and triphenylmethyl lithium species.

Experimental

The spectra were measured in a closed cell apparatus⁴ consisting of a 0.2-cm. path length quartz cell, sealed to a side arm of a 25-ml. flask. This was connected to a high vacuum system *via* an attached vacuum stopcock for alternate evacuation and flushing with argon. The spectra were measured under an argon atmosphere. A removable 0.18-cm. quartz spacer was sealed in the side arm, thus permitting a change in cell path length. This apparatus is illustrated elsewhere.⁵ A Cary Model 14 spectrophotometer was used to record the spectrum.

The standard procedure followed to form 1,1-diphenyl-*n*-hexyllithium, polystyryllithium, and poly- α -methylstyryllithium

was to add *n*-butyllithium to a solution of the corresponding olefin in the desired solvent. The solvents were distilled from lithium aluminum hydride or liquid sodium under argon. The olefins, 1,1-diphenylethylene, styrene, and α -methylstyrene were vacuum distilled from calcium hydride and stored under argon. With α -methylstyrene, the concentration of the monomer was well below its equilibrium value.⁶ Hence, the initiation product should predominate. A stoichiometric amount of *n*-butyllithium to olefin was used, except with styrene where excess olefin was used to ensure consumption of the *n*-butyllithium. If the previous procedure is reversed, there are no differences in the spectrum, but in the standard procedure the spectrum of the olefin was recorded and its subsequent disappearance observed on addition of the *n*-butyllithium.⁷ Butyllithium in hexane solution was obtained from Foote Mineral Corporation. A small amount of hexane therefore was present in each experiment. This should not affect the absorption spectrum as the active center is expected to be preferentially solvated by the more abundant higher polarity solvents. Gas-tight syringes (Hamilton Co.) were used to transfer the solvent, olefin, and organolithium solutions.

Benzyl lithium was prepared from tribenzyltin chloride and phenyllithium in ether,⁸ chilling the reaction after 2 hr. to precipitate the tetraphenyltin and filtering. α -Methylbenzyl lithium was prepared in an analogous manner from α -methylbenzyltriphenyltin.⁹ The yields of tetraphenyltin in these reactions were 95 to 100%. Carbonation of benzyl lithium resulted in a 70% yield of phenylacetic acid. Phenyllithium was prepared from bromobenzene and lithium metal in ether at 10°. Carbonation produced benzoic acid in greater than 90% yield. Triphenylmethyl lithium was prepared in tetrahydrofuran from triphenylmethyl chloride and lithium metal at 0°, filtering after 4 hr. Benzyl lithium and α -methylbenzyl lithium, which were prepared directly in the cell apparatus by reacting stoichiometric amounts of phenyllithium (or butyllithium) with the appropriate tin compound, gave long wave length absorption identical with the previous preparations. The tetraphenyltin so produced does not interfere although its spectrum is observed. The rate of the transmetalation reaction is directly observable from the build-up of lithium compound. It is very rapid in THF but becomes progressively slower in the less polar solvents, analogous to the olefin addition reaction.⁵ Each experiment was completed by the addition of several drops of ethanol, destroying the long wave length absorption of the carbanion and producing the spectrum for the hydrocarbon.

(1) Preliminary communication: R. Waack and M. A. Doran, *Chem. Ind.* (London), 1290 (1962).

(2) L. Lang, Ed., "Absorption Spectra in the Ultraviolet and Visible Region," Academic Press, New York, N. Y., 1961, p. 53.

(3) D. J. Worsfold and S. Bywater, *Can. J. Chem.*, **38**, 1891 (1960).

(4) The high reactivity of organolithium compounds requires the use of an absorption cell that prevents contact with air or moisture.

(5) R. Waack and M. A. Doran, to be published (1963).

(6) H. W. McCormick, *J. Polymer Sci.*, **25**, 488 (1957).

(7) In THF and dimethoxyethane, maximum intensity is obtained immediately. In the less polar solvents, the addition reaction is progressively slower and the disappearance of the olefin can be followed. For example, see A. G. Evans and D. B. George, *J. Chem. Soc.*, 4653 (1961).

(8) H. Gilman and S. B. Rosenberg, *J. Org. Chem.*, **24**, 2063 (1959).

(9) This tin compound was kindly supplied by Dr. F. C. Leavitt and Miss Priscilla A. Carney of this Laboratory.

Results

The position of the principal absorption maximum of 1,1-diphenyl-*n*-hexyllithium (I) in seven different solvents is listed in Table I. In the five most polar solvents, a weaker absorption band at shorter wave length is also evident, *e.g.*, λ_{\max} 315 $m\mu$ in THF which shifted to 300 $m\mu$ in isopropyl ether. This band is not observed in the two low polarity solvents. It is apparent that a more polar solvent medium causes a bathochromic shift in the absorption maximum. The 81 $m\mu$ shift between the most polar and least polar solvent is unusually large. The ionic strength of the solution apparently is of lesser importance, because excess amounts of butyllithium have no effect on the position of the absorption maximum of I.

TABLE I

THE POSITION OF THE ABSORPTION MAXIMUM IN THE ELECTRONIC SPECTRUM OF 1,1-DIPHENYL-*n*-HEXYLLITHIUM IN SOLVENTS OF DIFFERENT POLARITY

Solvent	Primary absorption max., $m\mu$	Dielectric constant (20°)
Tetrahydrofuran	496	7.58 ^a
1,2-Dimethoxyethane	495	^b
Diethyl ether	438	4.335 ^c
Isopropyl ether	428	3.88 ^c
<i>n</i> -Butyl ether	435	3.06 (25°) ^c
Benzene	426 ^d	2.286 ^e
<i>n</i> -Hexane	415 (broad)	1.890 ^e

^a F. E. Critchfield, J. A. Gibson, Jr., and J. L. Hall, *J. Am. Chem. Soc.*, **75**, 6044 (1953). ^b The dielectric constant of 1,2-dimethoxyethane has been determined as 5.50 and that of THF as 6.00: J. L. Downs, J. Lewis, B. Moore, and G. Wilkinson, *J. Chem. Soc.*, 1367 (1959). The small difference between the dielectric constant of these two solvents corroborates our observation of their similar solvation properties. However, the above value for the dielectric constant of THF is quite different from that determined by Critchfield, *et al.*^a We have chosen to use this latter value. ^c A. A. Maryott and E. R. Smith, "Table of Dielectric Constants of Pure Liquids," N.B.S. Circ. 514 (1951). ^d This measurement in benzene agrees with the recent report for the spectrum of I in benzene, *i.e.*, λ_{\max} 428 $m\mu$: A. G. Evans and D. B. George, *J. Chem. Soc.*, 4653 (1961). ^e P. Debye and H. Sack, "Constantes Dielectriques Moments Electriques," Hermann and Cie, Paris, 1937.

The dependence of the position of the absorption maximum, in reciprocal centimeters, on solvent polarity, as expressed by solvent dielectric constant, is illustrated in Fig. 1. The linearity of Fig. 1 might be expected from the relationship $\Delta E = h\nu$, providing the solvent dielectric constant is a consistent measure of the extent of solvent interaction on the transition energy. The faster rate of development of absorption intensity in the higher dielectric media is also illustrative of such solvation ability.⁵ The slope of the line measures the average lowering in electronic transition energy by solvent interaction, per unit dielectric constant. One might expect that extrapolating to zero dielectric constant would best estimate the transition energy in the absence of solvent effects. The limits of $\pm 5 m\mu$ shown in Fig. 1 are an estimate of the possible variation in locating the maximum of these rather broad absorption curves. The scatter shown by the data is perhaps caused by steric effects, which are not expressed in the dielectric constant, but which are a prominent factor in the ability of the medium to solvate. There is no simple relationship between the absorption maxima and solvent refractive index.

Another species similar to I is triphenylmethylithium

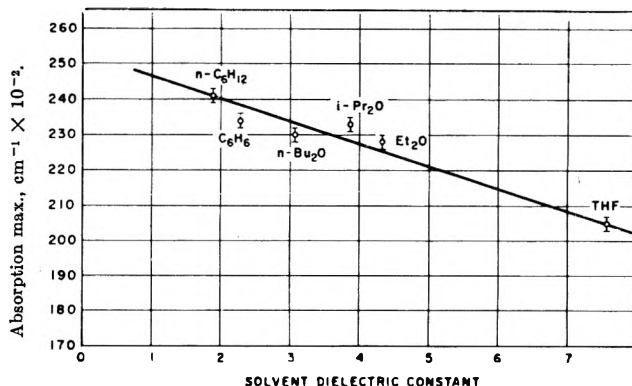


Fig. 1.—Absorption maximum in ultraviolet spectrum of 1,1-diphenyl-*n*-hexyllithium.

(II). This is reported to show maximum absorption at 475 and 410 $m\mu$ in diethyl ether,¹⁰ whereas we observe the absorption maximum of II at 500 and 425 $m\mu$ in THF; thus, the absorption of II also experiences a red shift with increasing solvent polarity.

The spectrum of the diphenylmethyl anion (the gegenion is not specified, but is assumed to be Na) is reported to have an absorption maximum at 435 $m\mu$ in diethyl ether,¹⁰ which is almost identical with our observation of I in ether. The small 3 $m\mu$ difference is explicable in terms of the usual bathochromic effect of substituting an alkyl group for a hydrogen.^{2,5}

In liquid ammonia, the position of maximum absorption of diphenylmethyl potassium is reported as 440 $m\mu$,¹¹ strikingly similar to that in diethyl ether. In view of the high dielectric constant of ammonia, however, (22.5 at -33.4° , see Table I, ref. c) it is apparent that the relationship of Fig. 1 does not hold; this is perhaps due to the larger gegenion or the dual solvating behavior of NH_3 , *i.e.*, it can act as a base to solvate the cation or H-bond with the lone pair electrons of the ionized C-Li bond.

The spectrum of the alkali metal-benzophenone ketyl (III) is also reported to experience a red shift (of the order 30–35 $m\mu$) on changing solvent from 1,4-dioxane (ϵ^{26° 2.209^c) to THF.¹² The π -electron system of III is quite similar to that of I. The electronic transition observed for this radical-ion system is suggested to be the excitation of an electron from the lowest antibonding π -orbital to one of higher energy.¹³

In contrast to the di- and triphenylmethylithium species, the electronic absorption spectra of monophenylmethylithium compounds are comparatively insensitive to solvent. The first reported example was polystyryllithium.³ We observe this species to have a single well defined absorption maximum at 335 $m\mu$ in THF and similarly at 334 $m\mu$ in benzene. The only solvent effect is a broadening of the band in the more polar medium. We have measured the spectrum of other monophenylmethylithium compounds in three different polarity solvents. These data are summarized in Table II.

It is apparent that these monophenylmethyl organolithiums do not show a pronounced solvent sensitivity in their electronic spectra. In fact there appears to

(10) S. F. Mason, *Quart. Rev.*, **15**, 336 (1961).

(11) I. V. Astaf'ev and A. I. Shtenshtein, *Opt. Spectr.* (English Translation), **6**, 410 (1959).

(12) H. V. Carter, B. J. McClelland, and E. Warhurst, *Trans. Faraday Soc.*, **56**, 455 (1960).

(13) B. J. McClelland, *ibid.*, **57**, 1458 (1961).

TABLE II

THE POSITION OF THE ABSORPTION MAXIMUM IN THE ELECTRONIC SPECTRA OF MONOPHENYLMETHYL ORGANOLITHIUM COMPOUNDS IN SOLVENTS OF DIFFERENT POLARITY

Solvent	Position of maximum absorption, $m\mu$		
	Benzyl lithium	α -Methylbenzyl lithium	Poly- α -methylstyryl lithium
THF	330	335	340
Et ₂ O	328	335	337
Benzene	..	344	349

be a small opposite (blue) shift in the least polar solvent.

Another organo-alkali metal system in which the spectrum does not appear to be solvent sensitive is the alkali metal-aromatic hydrocarbon radical-ions. The major absorption band of sodium-anthracene radical-ion is identical in 1,4-dioxane¹² and in THF^{14a} or dimethoxyethane.^{14b}

Discussion

Although the solvent effects in the electronic spectrum of organolithium compounds (carbon-lithium bond) have not been studied previously, the effect of solvents on electronic spectra in general has received considerable attention. Some of the highly conjugated organic dyes show pronounced solvent effects in their spectra.¹⁵ The shifts usually are less pronounced than that observed here. For example, phenol blue, which consists of both homopolar and charged zwitterionic resonance structures, undergoes a pronounced red shift in absorption maximum in more polar solvents. On the other hand the spectrum of Bindschellers' green, which has a formal charge in both the ground state and excited state, is relatively insensitive to solvent changes. These different behaviors are readily explained by the ability of the solvent to stabilize their different resonance structures.^{16,17} The odd alternant organolithium species are a very interesting example of a class of compounds all of similar structure (in having analogous resonance forms) but for which we find individuals that behave in different manners regarding spectral shifts due to solvent. Thus, the explanation here is not simply the preferred stabilization or destabilization by the solvent of a certain resonance structure.

In each of these organolithium species delocalization of the carbon-lithium bond electrons throughout the π -system is a stabilizing factor. This tendency to delocalize the unshared pair, for example in I, is reflected in the high "acidity" observed for the corresponding hydrocarbon. Along with its stabilizing effect, electron delocalization moves the bonding and antibonding π -orbitals closer together.¹⁸ Thus, we assume that the observed long wave length absorption in each of these compounds is due to the excitation of an

electron from the highest occupied π -orbital to the lowest antibonding π -orbital.

The absorption of ultraviolet light by a molecule results in its electronic excitation from some ground state energy to a more energetic excited state. In solution, the extent of the solvation of the molecule in each of these two electronic states influences their relative positions in energy. It is apparent that in di- and triphenylmethyl lithium compounds, the more polar medium reduces the energy difference between the ground and excited states, thus causing a red shift in absorption maximum. We consider that the pronounced red shift in absorption maximum of such species, with more polar solvents, might be explained in two ways which are somewhat interrelated. First, note that the organolithium systems under discussion consist of a polar solute in both polar and non-polar solvent medium. As we mentioned, conjugation bands in electronic spectra frequently are shifted toward the visible by a more polar solvent. This is because the absorbing molecule (to be considered in the classical sense as an oscillating electron) which is imbedded in a dielectric medium polarizes the medium and thus decreases the work required for electronic excitation.^{19,20} The lowering in energy is dependent on the polarizability of the solvent. There may also be a solvent effect due to orientation of the solvent dipoles by the solute. In the spectrum of a polar solute in a polar solvent, a strong red shift may be expected if the solute experiences an increase in dipole moment on excitation.²¹ The increase in solute dipole in the excited state results in a gain in solvation energy for this state, relative to the ground state, through increased interaction with the oriented solvent molecules. On the other hand, should the solute dipole decrease during electronic excitation, the oriented solvent would cause a blue shift due to "orientation strain," which will be superimposed on the polarization red shift.²¹ Such may be the case for the monophenylmethyl organolithium compounds discussed later. Another factor, the promotion of ionization of the carbon-lithium bond by more polar solvents,²² might also be considered as contributing to the observed solvent effect in the spectra of organolithium compounds. Consider that an organolithium compound may be described, in valence bond language, by a wave function containing contributions from covalent and ionic structures, *i.e.*

$$\psi_{R-Li} = a\psi_{(cov.)} (R-Li) + b\psi_{(ionic)} (R^{\ominus}Li^{\oplus})$$

Presumably, in the ground state —a— is large whereas in the electronic excited state —b— would be of greater importance. Thus, an increase in ionic character of the ground state, *via* solvent-promoted ionization, should lower the electronic transition energy (keeping in mind that the transition is suggested to be $\pi \rightarrow \pi^*$ of the delocalized electrons). To say this in another way, bond formation lowers the energy of the carbon-lithium bond electrons, whereas ionization raises the energy of these electrons, relative

(14) (a) P. Balk, G. J. Hooijink, and J. W. H. Schreurs, *Rec. trav. chim.*, **76**, 813 (1957); (b) E. DeBoer and S. I. Weissman, *ibid.*, **76**, 824 (1957).

(15) L. G. S. Brooker and R. H. Sprague, *J. Am. Chem. Soc.*, **63**, 3214 (1941).

(16) G. W. Wheland, "Resonance in Organic Chemistry," John Wiley and Sons, New York, N. Y., 1955, pp. 325-326.

(17) M. J. S. Dewar, *Chem. Soc. (London), Spec. Publ.*, **4**, 75 (1956).

(18) In an odd alternant molecule as I, the highest occupied orbital is non-bonding, so these electrons do not contribute to the resonance energy. It is the lowering of the other π -orbitals (relative to their position in the non-delocalized molecule) that produces increased stability. The occurrence of the non-bonding orbital between the bonding and antibonding orbitals is the reason odd alternants absorb at longer wave length than even alternants, for example see ref. 17, p. 78.

(19) F. A. Matsen, "Techniques of Organic Chemistry," Vol. IX, Interscience Publishers, Inc., New York, N. Y., 1956, p. 695.

(20) S. F. Mason, *Quart. Rev.*, **15**, 368 (1961).

(21) N. S. Bayliss and E. G. McRae, *J. Chem. Phys.*, **58**, 1002 (1954).

(22) D. J. Kelley and A. V. Tobolsky, *J. Am. Chem. Soc.*, **81**, 1597 (1959).

to the non-delocalized structure.²³ This concept is analogous to the well known blue shift caused by hydrogen bonding solvents on carbonyl $n \rightarrow \pi^*$ -transitions.²⁴ In this latter system, the energy of the non-bonding electron pair is lowered in the ground state by H-bond formation, whereas there is little H-bonding in the excited state.^{25,26} The result is an increase in transition energy observed as a blue shift. The ability of the solvent to promote ionization of the organolithium compound is related to its basicity,²⁷ which is determined by such properties as permanent dipole and polarizability as well as steric factors which regulate the closeness of approach or the number of closest solvent molecules. In Table I, solvent basicity decreases in the same order as the dielectric constant. From this discussion, the observed red shift in the absorption maximum of di- and triphenylmethyl lithium species, with increasing solvent polarity, might be attributed to a decrease in the energy required for the electronic excitation resulting from increased solvation of the excited state due to the polarizability and dipole orientation of the solvent, or the more polar (basic) solvents promote ionization of the carbon-lithium bond thus raising the ground state energy of this electron pair relative to the excited state.

Following the foregoing discussion, two possible explanations may be considered to account for the insensitivity to solvent of the monophenylmethyl organolithium compounds. The first possibility is that in these solvent insensitive species, electronic excitation is not accompanied by an increase in dipole moment, so solvent orientation would not cause a lowering of the excited state energy. If the dipole moment decreases on excitation, the effect of solvent "orientation strain" may be superimposed on the "red" polarization shift and if the former dominates,

(23) Electron delocalization stabilizes the excited state to a greater extent than the ground state, and results in a smaller difference in energy between these two states. Bond formation of the C-Li bond is analogous to twisting components of a conjugated system out of plane, resulting in reduced interaction. This usually causes a hypsochromic shift in $\pi \rightarrow \pi^*$ transition and a loss of intensity. See, for example, M. J. S. Dewar, "Steric Effects in Conjugated Systems," Academic Press, Inc., New York, N. Y., 1958, p. 46.

(24) M. Kasha, *Discussions Faraday Soc.*, **9**, 15 (1950).

(25) H. McConnell, *J. Chem. Phys.*, **20**, 700 (1952).

(26) C. J. Brealey and M. Kasha, *J. Am. Chem. Soc.*, **77**, 4462 (1955).

(27) H. C. Brown and R. M. Adams, *ibid.*, **64**, 2557 (1942).

a small red shift with decreasing solvent polarity may be realized. Such a trend is indicated by the data in Table II. Another approach, which is in keeping with the second explanation of the solvent effect discussed previously, is based on the well known tendency of organolithium compounds to form clusters.²⁸ The species which show strong solvent dependence are very bulky, and consequently may be sterically prohibited from cluster formation. The organolithium function of the bulkier species thus is available for coordination with the smaller solvent molecules. On the other hand, the monophenyl species should have little steric inhibition to cluster formation, so they preferentially solvate themselves and are less sensitive to the solvent environment. Thus, we consider that the insensitivity of the spectrum of monophenylmethyl lithium compounds to solvent may result from a lack of increase in dipole moment on electronic excitation or a preference of the less sterically hindered species toward self solvation.

One important consequence of these findings bears directly on the correlation of the absorption spectrum of cations, anions, or free-radicals of odd or even alternant hydrocarbons with each other²⁹ or with transition energies calculated by molecular orbital methods.³⁰ The solvent in which the spectrum is measured has a pronounced effect on the observed transition energy. It is apparent that in comparing the spectrum of the cation or anion of a species, which is solvent sensitive, the solvent medium of the cation and anion must have similar solvating properties. For example, comparing the spectra of the diphenylmethylcarbonium ion in sulfuric acid (λ_{\max} 429 $m\mu$)³¹ and the anion in isopropyl ether (λ_{\max} 428 $m\mu$) gives quite good agreement, but the agreement is not good when the anion spectrum is taken in the higher solvating medium THF (λ_{\max} 496). The correlation of absorption frequency and transition energy calculated by Hückel M.O. method also may be improved by considering solvent effects.

(28) R. G. Wittig, F. J. Meyer, and G. Lange, *Ann.*, **571**, 167 (1951).

(29) M. J. S. Dewar and H. C. Longuet-Higgins, *Proc. Phys. Soc. (London)*, **A67**, 795 (1954).

(30) A. Streitwieser, "Molecular Orbital Theory for Organic Chemists," John Wiley and Sons, Inc., New York, N. Y., 1961, p. 228.

(31) N. C. Deno, J. J. Jaruzelski, and A. Schriesheim, *J. Org. Chem.*, **19**, 155 (1954).

DYNAMIC MECHANICAL PROPERTIES OF POLYVINYL ACETATE IN SHEAR IN THE GLASS TRANSITION TEMPERATURE RANGE

BY A. J. KOVACS,¹ ROBERT A. STRATTON,² AND JOHN D. FERRY

Department of Chemistry, University of Wisconsin, Madison, Wisconsin

Received July 6, 1962

The storage shear modulus and loss tangent of polyvinyl acetate (weight-average molecular weight 2×10^6) were measured at radian frequencies between 0.7 and 40 sec.⁻¹ and at ten temperatures from 20.0 to 39.2°, using a modification of the torsion pendulum of Plazek, Vrancken, and Berge. Parallel dilatometric experiments were made to measure the isothermal volume contraction at most of these temperatures after quenching from well above the glass transition (T_g). From 31.25 to 39.2°, dynamic shear measurements were made under conditions of voluminal equilibrium. Above about 33°, the temperature dependence could be described by the method of reduced variables and the temperature shift factors followed the WLF equation with the parameters $\alpha_f = 5.3 \times 10^{-4}$ deg.⁻¹, $f_{36} = 0.0225$ (the subscript 35 referring to centigrade temperature). These parameters are somewhat different from those derived from shear measurements far above T_g , indicating that the WLF equation requires some modification in the immediate vicinity of T_g . Below 33°, the method of reduced variables was inapplicable; the behavior could be ascribed to a change in the shape of the relaxation spectrum with decreasing temperature, namely, a depression of the plateau on the left side of the maximum. In the vicinity of its maximum, the relaxation spectrum as obtained from both storage and loss components of the shear modulus (G' , G'') agreed well with that derived from earlier shear measurements at higher temperatures by Williams and Ferry. From 20 to 33.8°, dynamic shear measurements were made repeatedly during isothermal volume contraction after quenching. Such experiments in principle provide for separation of the temperature dependence of relaxation times into the effect attributable to free volume and the effect of temperature at constant free volume. Correlation of the dependences of storage modulus and loss tangent on temperature and on elapsed time (at constant frequency) indicated that the relaxation times were essentially functions of free volume alone. However, about 20% of the total temperature dependence of relaxation times may be ascribed to an effect which is either independent of free volume or else associated with a small change in free volume with temperature which is achieved instantaneously, the same above and below T_g . The method of reduced variables was applied to the frequency dependence of G' and G'' at various temperatures using shift factors a_{T_i} calculated from the Doolittle equation taking into account the dependence of free volume on both temperature and time. For G' , which is negligibly affected by changes in the shape of the relaxation spectrum at short times, all the data fell nearly on a single composite curve. For G'' , there were deviations corresponding to those observed under conditions of volume equilibrium, but the positions of the curves at all temperatures and elapsed times showed that these deviations (attributable to changes in spectral shape) were also functions of free volume alone. Finally, in an isothermal volume expansion experiment at 39°, the time dependence of G' and loss tangent showed the same autocatalytic character as the volume expansion itself, and corresponded to a time-dependent shift factor a_t which again agreed closely (after establishment of thermal equilibrium) with that calculated from the change in free volume.

Although extensive studies³ of the frequency dependence of the storage and loss shear moduli of amorphous polymers have been made above the glass transition temperature (T_g), there are very few data below T_g . (In referring to T_g , it is of course recognized that this characteristic temperature is not unique but is a function of the time scale of the experiment. It can be cited qualitatively as the upper boundary of the glassy state, but for more precise considerations its time dependence must be explicitly formulated.)

Most measurements on glassy polymers have been made at essentially constant frequency and have ignored the frequency dependence.⁴ Below T_g , a polymer is in general not in a state of equilibrium with respect to its volume at a given temperature,⁵ and the dynamic shear properties may be expected to depend on the thermal and mechanical history of the sample. Such effects were noted by McLoughlin and Tobolsky in the (tensile) stress relaxation of polymethyl methacrylate,⁶ and attributed to the differences in free volume. The apparent maximum in activation energy for viscoelastic relaxation processes as a function of temperature^{7,8} must therefore be interpreted with caution.

The very large increases in viscosity and the temperature derivative of viscosity in glasses as T is diminished approaching T_g , noted long ago by Vogel⁹ and Tammann,¹⁰ are accompanied by similar increases in viscoelastic relaxation times. According to the free space concept of Doolittle,^{11,12} these quantities depend on the fractional free volume. Recently,⁵ isothermal time-dependent volume changes have been observed following temperature changes in the vicinity of T_g . Such time-dependent contractions or expansions reflect primarily changes in free volume and therefore should be accompanied by marked changes in viscoelastic relaxation times. From the Doolittle equation^{11,12} it can be estimated that a relative volume change of 3×10^{-3} would alter a relaxation time or viscosity by a factor of about 400.

Time-dependent effects for the viscosity of glucose were reported by Parks¹³ and for borosilicate glasses by Prod'homme,¹⁴ but have not been investigated in detail for polymers. By combining shear viscoelastic measurements with direct dilatometric measurements of volume changes, it should be possible to determine the effects of isothermal volume changes on viscoelastic properties, and by comparison with the effects of temperature to

(1) Centre de Recherches sur les Macromolécules, Strasbourg, France.
 (2) Minnesota Mining and Manufacturing Company Fellow, 1961-1962.
 (3) J. D. Ferry, "Viscoelastic Properties of Polymers," John Wiley and Sons, New York, N. Y., 1961, Chapter 12.
 (4) A. E. Woodward and J. A. Sauer, *Advan. Polymer Sci.*, **1**, 114 (1958).
 (5) A. J. Kovacs, *J. Polymer Sci.*, **30**, 131 (1958).
 (6) J. R. McLoughlin and A. V. Tobolsky, *ibid.*, **7**, 658 (1951).
 (7) A. V. Tobolsky and J. R. McLoughlin, *J. Am. Chem. Soc.*, **74**, 3378 (1952).
 (8) S. Saito and T. Nakajima, *J. Appl. Polymer Sci.*, **2**, 93 (1959).

(9) H. Vogel, *Physik. Z.*, **22**, 645 (1921).
 (10) G. Tammann and G. Hesse, *Z. anorg. allgem. Chem.*, **156**, 245 (1926).
 (11) A. K. Doolittle, *J. Appl. Phys.*, **22**, 1471 (1951).
 (12) M. L. Williams, R. F. Landel, and J. D. Ferry, *J. Am. Chem. Soc.*, **77**, 3701 (1955).
 (13) G. S. Parks, L. E. Barton, M. E. Spaght, and J. W. Richardson, *Physics*, **5**, 193 (1934).
 (14) N. Prod'homme, *Verres Refractaires*, **14**, 261 (1960).

decide whether the latter are solely attributable to free volume changes as assumed in the treatment of Doolittle¹¹ and related developments.¹²

The present study is devoted to measurements of shear viscoelastic properties of polyvinyl acetate near T_g , both under conditions of volume equilibrium and during time-dependent isothermal contraction or expansion processes. By measuring the frequency dependence of the storage and loss moduli, the effects of temperature and thermal history on the relaxation times and relaxation spectrum can be determined.

Material and Method.—The polymer investigated was an unfractionated polyvinyl acetate with weight-average molecular weight 2.0×10^6 , identical with that designated as PVAc II in reference 5. It was compression molded at 120° into sheets about $1/8$ in. thick and slowly cooled to room temperature. The sheets were examined carefully in polarized light for absence of imperfections. From these, several nearly identical prism-shaped samples were cut, about $1/8$ in. wide and $1-1/4$ in. long.

The conditioning and installation of each sample were carried out as follows. The ends were clamped in holders as illustrated in Fig. 1. Very little compressive stress was used, but the terminal surfaces of the sample were cemented in the holders with an epoxy resin, the proper alignment being maintained while mounted in a jig during setting of the cement. The sample then was annealed in the jig at 45° for several days (far enough above T_g to permit complete volume equilibration and removal of stresses, but not far enough for danger of sagging), in an air thermostat containing silica gel. This annealing was repeated after each experiment in the torsion pendulum, to erase the previous thermal and mechanical history.

The torsion pendulum of Plazek, Vrancken, and Berge,¹⁵ originally designed for soft, disk-shaped samples, and providing for measurements at different frequencies by changing the moment of inertia, was modified as follows for hard, prism-shaped samples. Mountings were provided in which the sample end holders shown in Fig. 1 could be securely clamped. Since it is necessary to control the tension in a rigid sample (increased tensile strain can cause volume expansion when Poisson's ratio is less than $1/2$, and attendant changes in relaxation times from this source^{16,17}), the lower mounting was attached to a thin plate (tension control spring) which provided a slight vertical flexibility while maintaining torsional rigidity. The top of the torsion wire was attached to a vertical screw carrying a large engraved disk, to provide for small controlled vertical displacements. Four strain gages, each about 500 ohms, were cemented to the tension control spring (Fig. 2) and were connected in a Wheatstone bridge so that the displacement of the plate and hence the tensile stress could be monitored. With suitable calibration, the stress could be controlled within 5×10^3 dynes/cm.², corresponding to a relative change in sample length of 2×10^{-7} . In practice, the tensile stress was maintained near zero by adjustments of the top vertical screw. In experiments where time-dependent isothermal volume changes took place, intermittent adjustments were necessary throughout the measurements.

One sample was placed in a dilatometer, filled with mercury under vacuum, and its specific volume was measured as a function of temperature and time with its thermal history paralleling as closely as possible that of the sample in the torsion pendulum. This technique has been described in detail elsewhere.⁵ The precision of volume measurements was about 3×10^{-6} cm.³.

Experimental Procedure.—Each series of dynamic measurements, covering a range of radian frequencies (ω) from about 0.7 to 40 radians/sec., was preceded by a standard thermal treatment. First the sample was heated while held in the jig at 45° for at least 1 hr. (in some cases 3 hr.), to erase previous history, and then the jig was placed on Dry Ice for about 1 min. to bring the sample quickly to room temperature. The jig mounting permitted longitudinal motion of the sample to allow for thermal expansion and contraction in this direction. Within about 5 min., the sample could be removed from the jig and installed in the torsion pendulum, which had been preheated to the temperature

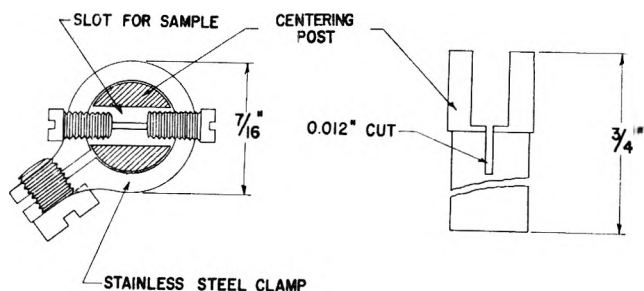


Fig. 1.—Holder for each end of the sample to clamp it in jig for cementing and conditioning, and in torsion pendulum for measurements.

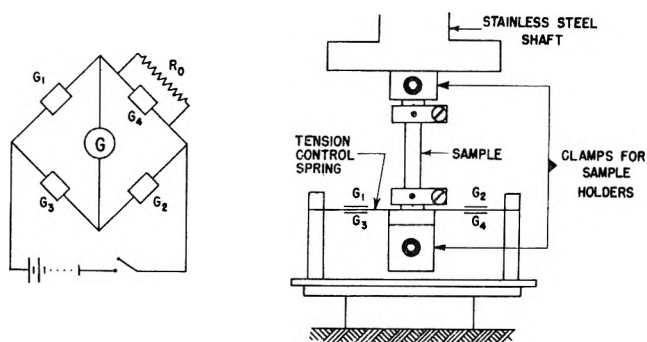


Fig. 2.—Installation of sample in torsion pendulum with tension control spring and strain gages.

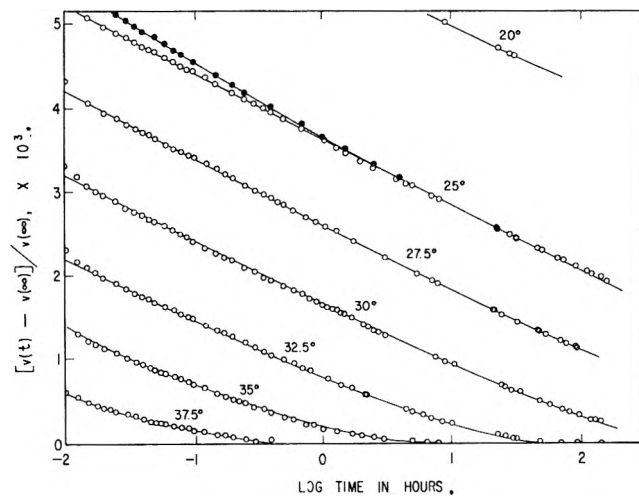


Fig. 3.—Isothermal volume contraction of samples in dilatometer at temperatures indicated: open circles, quenched from 40° ; black circles, quenched from 50° .

at which the dynamic measurements were to be made. The elapsed time of the experiment was counted from the moment of quench, although thermal equilibrium in the torsion pendulum was reached only 30 to 40 min. later. Time-dependent dynamic measurements were significant only after attainment of thermal equilibrium, of course. The parallel dilatometric measurements were not strictly comparable in the early stages, because thermal equilibrium is reached in the dilatometer in less than 2 min. However, the importance of this difference diminishes with increasing elapsed time and the approach toward voluminal equilibrium.

The results of shear measurements after attainment of voluminal equilibrium and the time-dependent results during approach to voluminal equilibrium are described and discussed separately. For the former, it was necessary to keep the sample at constant temperature first for a period which varied from about 30 min. at 37.5° to a month at 30.0° (cf. Fig. 3 below). If the equilibration period was longer than a day, the sample was equilibrated in a dry air thermostat rather than in the torsion pendulum itself, and then quickly installed in the preheated torsion pendulum. Measurements were not begun, of course, until a few hours had elapsed to eliminate the disturbance in thermal history caused by brief exposure to room temperature. Measurements

(15) D. J. Plazek, M. N. Vrancken, and J. W. Berge, *Trans. Soc. Rheology*, **2**, 39 (1958).

(16) J. D. Ferry and R. A. Stratton, *Kolloid-Z.*, **171**, 107 (1960).

(17) G. M. Bryant, *Textile Res. J.*, **31**, 399 (1961).

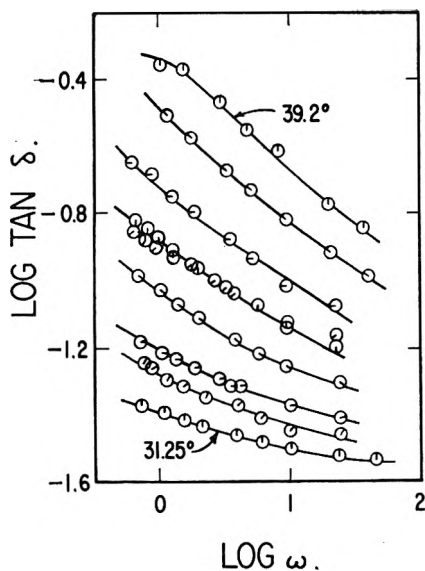


Fig. 4.—Loss tangent plotted logarithmically against radian frequency at nine different temperatures, at voluminal equilibrium: pip up, 31.25° (*); successive 45° rotations clockwise correspond to 32.45°, 32.6° (*), 33.8°, 35.0°, 35.06° (*), 36.35°, 37.6°, and 39.2°; (*) indicates different sample.

were repeated a few hours later to make sure that the shear properties were not changing with elapsed time.

Precautions were taken to avoid absorption of water by the sample during annealing, equilibration, and dynamic measurements.

The loss tangent ($\tan \delta = G''/G'$) and storage shear modulus (G') were calculated from the frequency and logarithmic decrement by the equations previously given¹⁵ except that for a sample of rectangular cross-section the sample coefficient¹⁸ is $K = 16 L/\mu cd^3$, where L is the length, c the width, and d the thickness ($d < c$). The coefficient μ depends on the ratio c/d , and was calculated by a well known formula¹⁹; for most of the samples it was close to 2.3. The sample width and thickness were measured at room temperature by a micrometer, taking the average of several readings at different points, and the length between the clamps was measured with calipers. Corrections at other temperatures were made from the dilatometric data, assuming isotropic dimensional changes.

Dilatometric Measurements.—The results of a series of dilatometric measurements are presented in Fig. 3, where the relative difference between the volume $v(t)$ at an elapsed time t after the quench and final equilibrium volume $v(\infty)$ is plotted against $\log t$. As usual,^{5,20} $v(\infty)$ was obtained directly at temperatures high enough so that voluminal equilibrium was reached within the experimental time scale, and at lower temperatures by a suitable extrapolation against T . In most of these experiments, the temperature before quench was 40° instead of 45° as in the torsion pendulum experiments, but this difference produces negligible deviations except in the early stages of the isothermal contraction, as shown by the comparison at 25° in Fig. 3. More extended dilatometric studies of polyvinyl acetate have been reported elsewhere.^{5,20}

The data of Fig. 3 will be used in analyzing the dynamic shear data, as described below.

Dynamic Shear Measurements at Voluminal Equilibrium

Experimental Results.—The loss tangent and storage modulus, measured after attainment of voluminal equilibrium, are plotted against frequency at nine temperatures in Fig. 4 and 5. Two different samples were employed, as identified in the legend of Fig. 4; at nearly identical temperatures (35.0°), the values of

(18) L. E. Nielsen, *Bull. Am. Soc. Testing Materials*, **165**, 48 (1950).

(19) S. Timoshenko, "Theory of Elasticity," McGraw-Hill Book Co., New York, N. Y., 1934, p. 349.

(20) A. J. Kovacs, "Phénomènes de Relaxation et de Fluage en Rheologie Non-Lineaire," Editions du Centre National de la Recherche Scientifique, Paris, 1961, p. 191.

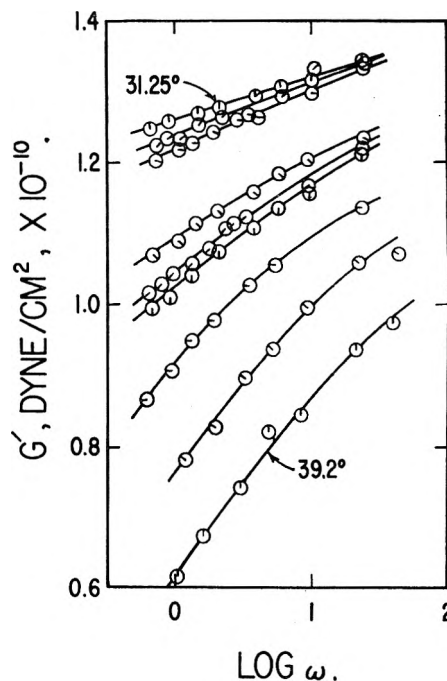


Fig. 5.—Storage shear modulus plotted against logarithm of radian frequency. Key to temperatures same as in Fig. 4.

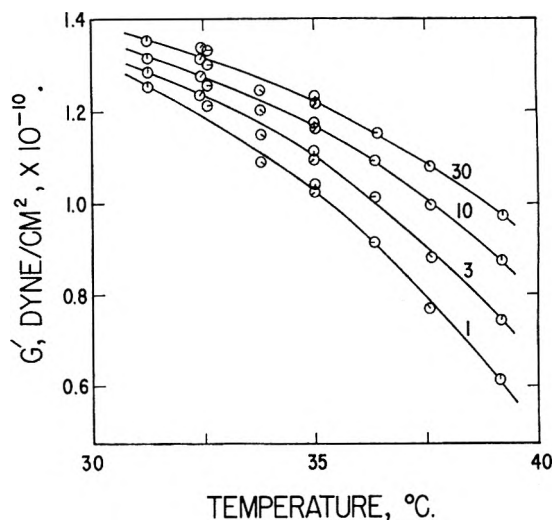


Fig. 6.—Storage shear modulus plotted against temperature at several radian frequencies as indicated.

$\tan \delta$ from the two samples agree rather well, but those of G' show a small consistent difference. A comparison with a third sample at 37.6° (not shown) revealed a similar discrepancy. Since G' , unlike $\tan \delta$, depends critically on sample dimensions, it may be estimated that its absolute accuracy cannot be expected to be better than 2%, and these differences are attributed to small errors in the sample coefficients.

Small empirical corrections were made to the values of G' , therefore, to bring them into relative consistency; the small uncertainty in the absolute value of G' is of no consequence. In Fig. 6, G' is plotted against temperature at several selected values of the frequency. From this plot empirical factors can be estimated to adjust the measured values at certain temperatures to agree with the best curves drawn through all the points, as follows: at 32.45°, 0.968; at 32.6°, 0.978; and at 33.8°, 1.020. These factors were used in subsequent calculations based on the G' data.

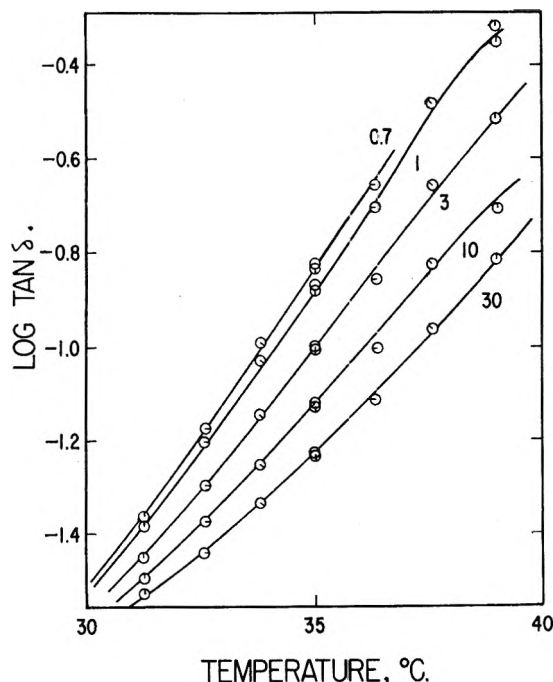


Fig. 7.—Logarithm of loss tangent plotted against temperature at several radian frequencies as indicated.

In Fig. 7, $\tan \delta$ is plotted against temperature at constant frequency, and since it does not depend on sample dimensions, no deviations such as those in Fig. 6 are apparent. The data at 32.45° did not agree with the others, however, and have been omitted from further consideration.

Application of Reduced Variables.—The G' curves in Fig. 5 are closely parallel and shift factors $\log a_T$ can be measured from their separations on the frequency scale in the usual way, taking 35° as the reference temperature. The magnitude of G' was not reduced for this purpose by the $T\rho/T_0\rho_0$ factor commonly used in the transition zone of viscoelastic properties, since the elasticity in the glassy state is not of a rubber-like nature. Approximate shift factors also could be obtained from $\tan \delta$ in Fig. 4; the a_T values from the two sources agreed above 33° , but diverged at lower temperatures, as shown in Fig. 8. It may be concluded that the shape of the relaxation spectrum changes with temperature below 33° , so that the method of reduced variables becomes inapplicable.

Above 33° , the a_T values can be closely fitted by the WLF equation¹² in the form

$$\log a_T = - \frac{(1/2.303f_{35})(T - 308.2)}{f_{35}/\alpha_f + T - 308.2} \quad (1)$$

where the reference temperature of 35° (308.2°K.) plays the role of T_g in the usual formulation. (Since the present treatment deals with data in the immediate vicinity of the glass transition, the fact that there is no unique value of T_g must be explicitly recognized.) Here f_{35} is the fractional free volume at 35° , and α_f its thermal expansion coefficient. A satisfactory fit is obtained with $f_{35} = 0.0225$ and $\alpha_f = 5.3 \times 10^{-4} \text{ deg.}^{-1}$, as shown by the curve in Fig. 8. In fact, the calculated curve agrees with the a_T values obtained from G' over the whole temperature range; this is to be expected since a change in the shape of the relaxation spectrum at short times will affect G' much less than G'' . It also

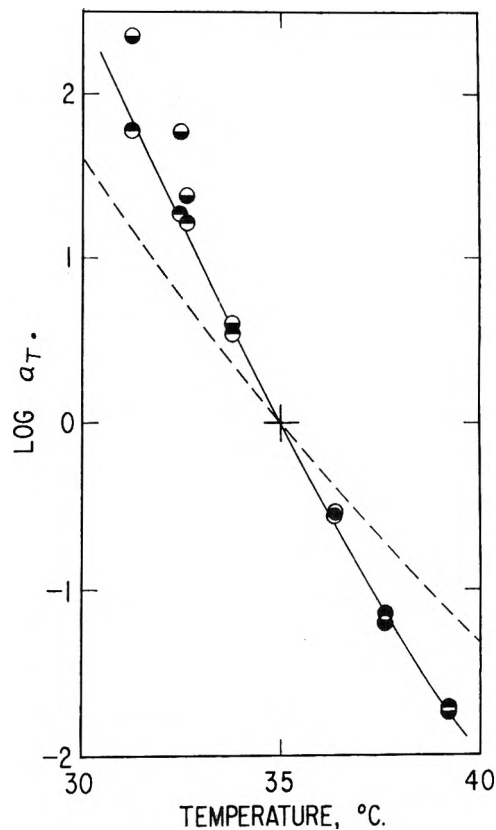


Fig. 8.—Log a_T plotted against temperature: points top black, from empirical shifts of G' ; bottom black, from shifts of $\tan \delta$; solid line, calculated from WLF equation with $\alpha_f = 5.3 \times 10^{-4}$, $f_{35} = 0.0225$; dashed line, calculated from WLF equation with parameters from shear measurements at higher temperatures by Williams and Ferry.

agrees almost exactly with a_T calculated from the time-scale separation of the isothermal bulk contraction curves in Fig. 3.

The ratio f_{35}^2/α_f is rather precisely determined as $0.96 \pm 0.04 \text{ deg.}$ by the slope of Fig. 8 at 35° . This value also agrees with that calculated from the inflectional slopes^{5,20} of the curves of Fig. 3, and, of course, that from the separation of these curves on the time scale. However, there is some latitude in the choice of the individual parameters f_{35} and α_f from the data of Fig. 8, because of the limited temperature range; a 10% decrease in f_{35} and a 20% decrease in α_f would leave the solid curve essentially unchanged. Actually, the analysis of the time-dependent experiments to be presented below determines α_f independently as 5.3×10^{-4} with an accuracy of about 4%. From the inflectional slope of the isothermal contraction, on the other hand, one obtains $f_{35} = 0.0195$ and $\alpha_f = 4.2 \times 10^{-4}$. This discrepancy probably is not serious because the calculation is based on an oversimplified model.^{5,20}

The values of f_{35} and α_f obtained from earlier dynamic shear measurements on polyvinyl acetate by Williams and Ferry,²¹ made between 45 and 90° in the transition zone of viscoelastic behavior, are 0.0298 and 5.9×10^{-4} , and from these a rather different curve for $\log a_T$ is obtained as shown by the dashed curve in Fig. 8. If a best fit of the WLF equation is made to the earlier data at the low-temperature end of the range, from 45 to 57° , we obtain $f_{35} = 0.0286$ and $\alpha_f = 5.0 \times 10^{-4}$, somewhat closer to values from the new data in the range from 33

(21) M. L. Williams and J. D. Ferry, *J. Colloid Sci.*, **9**, 479 (1954).

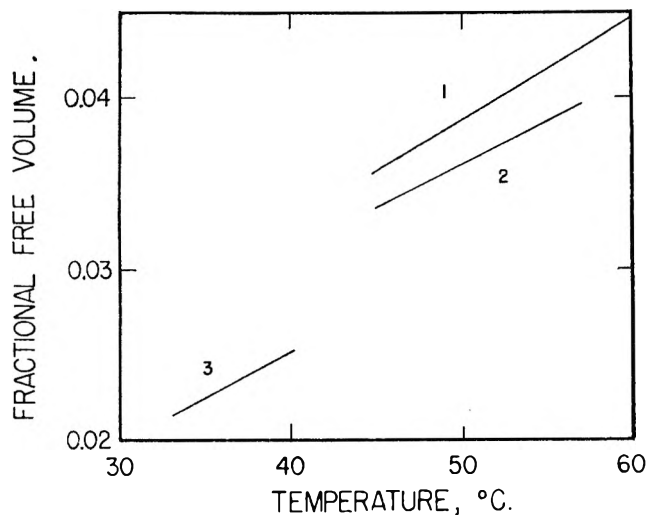


Fig. 9.—Fractional free volume plotted against temperature, from WLF parameters as follows: 1, Williams and Ferry, best fit 45 to 90°; 2, Williams and Ferry, best fit 45 to 57°; 3, present measurements.

to 39°. It is evident that the WLF equation cannot be applied in the immediate vicinity of T_g with the same parameters that apply far above this temperature. Although the rule of thumb is often stated¹² that the WLF equation holds from T_g to $T_g + 100^\circ$, the lower limit probably should be raised to $T_g + 10^\circ$, while there is some evidence²² that the upper limit also can be raised.

If the fractional free volume is calculated as $f = f_{35} + \alpha_f(T - 308.2)$ with these different pairs of parameters and plotted against temperature, the results (Fig. 9) suggest a small abrupt increase in f about 10° above the conventional identification of T_g (which for polyvinyl acetate²³ is about 32°). Since there is no physical evidence of such a transition in the free volume (the total volume does not undergo a discontinuity, and the occupied volume can hardly decrease with increasing temperature), this probably means only that the absolute value of the free volume does not have precise physical significance.

It is an important conclusion that the temperature shift factors for shear and volume (bulk) deformations near T_g are identical, indicating that the molecular motions by which these respective deformations are accomplished are very similar.

Reduced Shear Moduli.—Values of G' and the loss modulus G'' are plotted in Fig. 10 against the frequency reduced to 35° in accordance with the calculated curve of Fig. 8. A single composite curve is obtained for G' ; for G'' , as expected from Fig. 8, there are divergences of the data taken below 33°. These correspond to a drop in the magnitude of G'' with decreasing temperature.

From earlier shear measurements²¹ at higher temperatures with the Fitzgerald transducer apparatus,²⁴ reduced plots were obtained which located the maximum in $\log G''$ as 9.47 and the magnitude of $\log G'$ at the same frequency as 9.74. The corresponding values from Fig. 10 are 9.46 and 9.83, respectively, representing gratifying agreement since the experimental methods are entirely different. (The average molecular weight of the earlier sample was lower, and its distribution

(22) L. J. Garfield, S. E. Petrie, and D. W. Vanas, *Trans. Soc. Rheology*, **6**, 131 (1962).

(23) Reference 3, p. 222.

(24) E. R. Fitzgerald and J. D. Ferry, *J. Colloid Sci.*, **8**, 1 (1953).

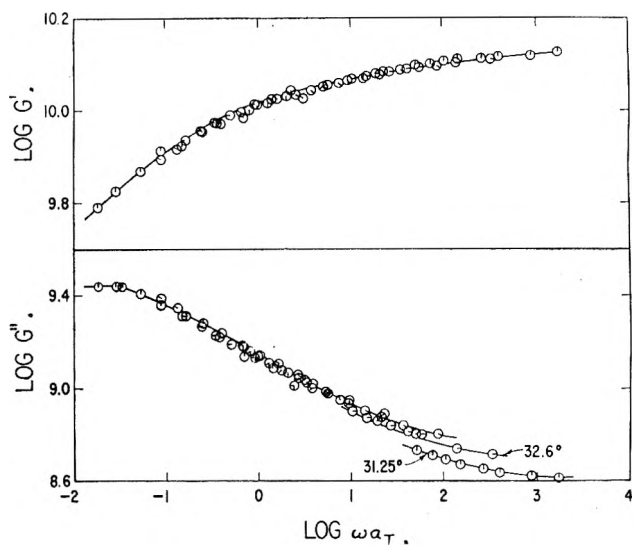


Fig. 10.—Composite plots of G' and G'' reduced to 35°, using shift factors a_T from WLF equation with $\alpha_f = 5.3 \times 10^{-4}$, $f_{35} = 0.0225$. Key to temperatures same as in Fig. 4-7.

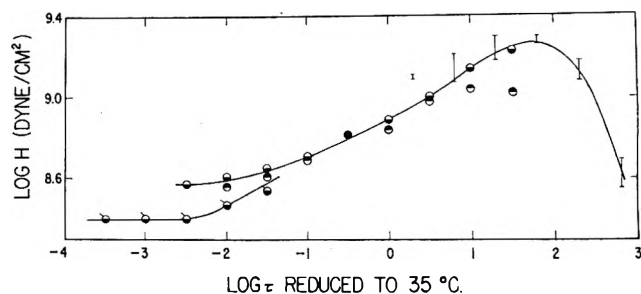


Fig. 11.—Relaxation spectrum reduced to 35°: Points top black, from G' ; bottom black, from G'' . Tagged points are from G'' at 31.25° (Fig. 10). Vertical bars are values from previous measurements by Williams and Ferry, reduced from 75 to 35° by $\Delta \log a_T = 7.8$.

probably broader, but these differences should not affect the viscoelastic properties near the maximum of G'' .)

The location of the maximum on the reduced frequency scale is at $\log \omega a_T = -1.5$ from Fig. 10, reduced to 35°, and at 6.3 from the measurements at higher temperatures, reduced to 75°. Thus $\Delta \log a_T$ between the two reference temperatures appears to be 7.8. This value is in fact obtained from the WLF equation provided that the low-temperature parameters ($f_{35} = 0.0225$, $\alpha_f = 5.3 \times 10^{-4}$) are applied from 35 to 45° and the high-temperature pair (0.0298 and 5.9×10^{-4}) from 45 to 75°. The latter assignment seems reasonable in view of the preceding discussion, and thus confirms the applicability of reduced variables where the two types of measurement overlap.

Relaxation Spectrum. The relaxation spectrum H , calculated from the data of Fig. 10 by the Williams-Ferry approximation method,²⁵ is plotted in Fig. 11. The agreement between values from G' and from G'' is in most cases very satisfactory. Near the maximum, the data agree quite well with those from the earlier measurements²¹ reduced as described above. The shape of H on the left side of the maximum is clearly delineated; it flattens to a plateau, and the height of the plateau drops somewhat at lower temperatures where the method of reduced variables fails. Evidence will be presented in the next section that the latter anomaly also is associated with free volume changes.

(25) M. L. Williams and J. D. Ferry, *J. Polymer Sci.*, **11**, 169 (1953).

Dynamic Shear Measurements during Isothermal Contraction and Expansion

Dynamic measurements as functions of elapsed time during approach to voluminal equilibrium were carried out in three ways. (1) Measurements at constant moment of inertia were made repeatedly at constant temperature following the quench. Since G' changes only slightly during the isothermal contraction, and ω is proportional to $\sqrt{G'}$, these represent time-dependent data at nearly constant frequency. (2) A sample which had been kept at room temperature for 72 days after molding was installed in the torsion pendulum and brought as rapidly as possible to 39° . Measurements were made repeatedly at constant moment of inertia during the isothermal expansion²⁰ which ensued. (3) Measurements were made during isothermal contraction at various frequencies and elapsed times, by changing the moment of inertia repeatedly. By interpolation, values of G' and G'' corresponding to fixed intervals of elapsed time were calculated, to obtain the frequency dependence of the viscoelastic properties at constant temperature and elapsed time.²⁶

Time-Dependent Measurements during Isothermal Contraction at Essentially Constant Frequency.—In Fig. 12, the loss tangent is plotted logarithmically against elapsed time following quench from 45° to room temperature and installation in the torsion pendulum at the temperature indicated on each curve. Measurements were started about 10 min. after the quench, but thermal equilibrium is reached only after 30 min. additional time, as shown by the vertical dashed line. Thus the curves all start from about the same point, reflecting the reproducibility of the quench to room temperature, and then diverge. The delay in reaching thermal equilibrium may cause some after-effects,²⁸ as exemplified in the curve at 33.8° where isothermal expansion followed by the normal slow contraction process causes $\tan \delta$ to pass through a maximum. Such disturbances should have no effect, however, after a lapse of 2 hr. By this time, the curves are nearly linear and are characterized by slopes which will be used in subsequent calculations.

A few values of the individual frequencies are shown; the extreme range in these experiments was from 1.38 to 1.50 radians/sec., and the differences in $\tan \delta$ corresponding to this range were within experimental error.

The small changes in oscillation frequency reflect changes in G' , which is plotted against the logarithm of elapsed time in Fig. 13. It is clear by comparing Fig. 12 and 13 with Fig. 6 and 7 that the effects of an increase in elapsed time on both G' and $\tan \delta$ are qualitatively equivalent to those of a decrease in temperature at voluminal equilibrium, as would be expected if these effects reflect primarily changes in free volume. The time-dependent viscoelastic properties approach limiting values (at 32.5° and above) within elapsed times which are similar in magnitude to those needed to achieve voluminal equilibrium as measured in the dilatometer (Fig. 3).

Time-Dependent Measurements during Isothermal Expansion.—In Fig. 14, G' and $\log \tan \delta$ are plotted

(26) Such functions may be termed *isoaeonal*, as distinguished from *isochronal* functions which give²⁷ the temperature dependence of viscoelastic properties at a fixed point on the viscoelastic time scale (for dynamic properties, at fixed frequency).

(27) Reference 3, pp. 243, 315.

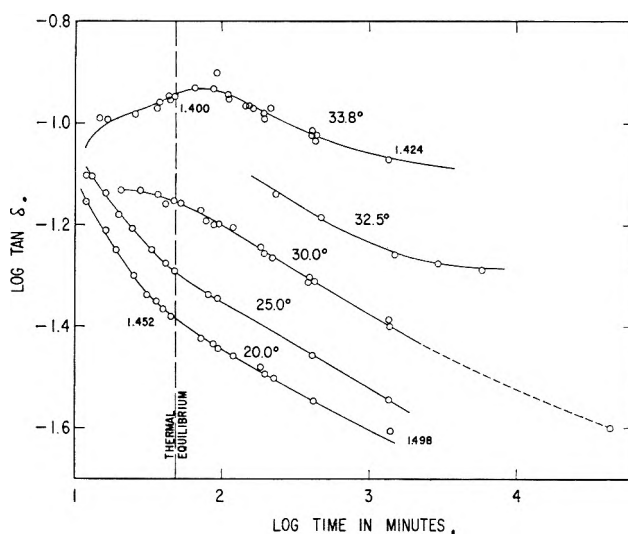


Fig. 12.—Loss tangent plotted logarithmically against elapsed time during isothermal contraction, following quench to room temperature and installation in the torsion pendulum at the temperature indicated on each curve. Vertical dashed line indicates time required for thermal equilibrium. Small numbers (1.400, etc.) are examples of actual radian frequencies in measurements at constant moment of inertia.

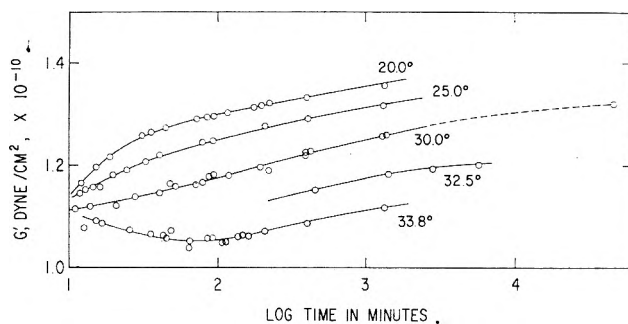


Fig. 13.—Storage shear modulus plotted against logarithm of elapsed time as in Fig. 12, at five different temperatures.

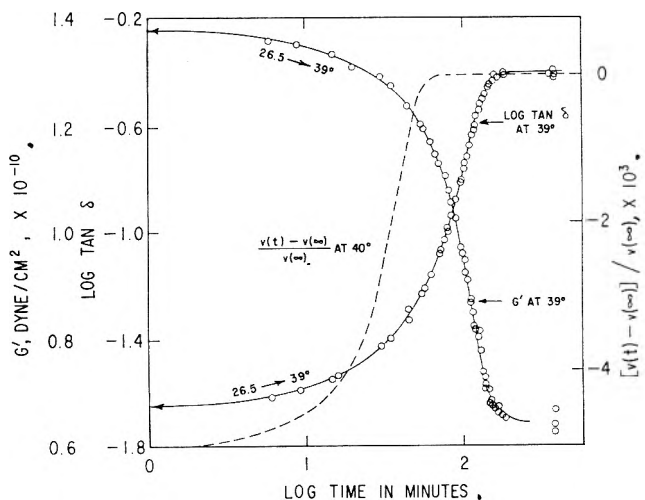


Fig. 14.—Storage modulus and logarithm of loss tangent plotted against logarithm of elapsed time during isothermal expansion at 39° . The temperature change from 26.5 to 39° reached thermal equilibrium at about $\log t = 1.6$. The dashed line shows the actual relative volume expansion in a comparable dilatometric experiment at 40° .

against $\log t$ for the sample which had been kept 72 days at $27 \pm 2^\circ$ and then heated in the torsion pendulum to 39° . For the first 40 min., the temperature is coming

(28) A. J. Kovacs, *Compt. rend.*, **235**, 1127 (1952).

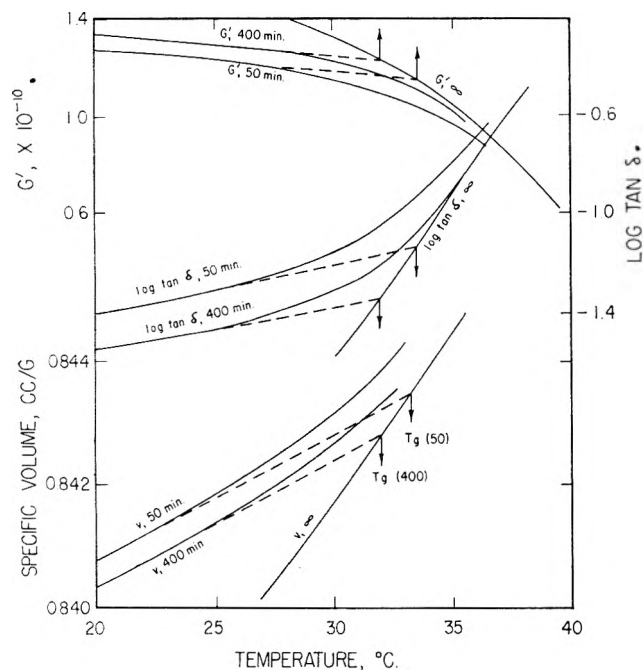


Fig. 15.—Storage modulus, logarithm of loss tangent, and specific volume plotted against temperature, at elapsed times of 50 min., 400 min., and ∞ (complete volume equilibration). Frequency for dynamic measurements about 1.45 radians/sec.

to equilibrium, but the major parts of the changes in G' and $\tan \delta$ occur isothermally after the final temperature is reached.

The relative change in specific volume measured in a similar isothermal expansion experiment carried out in a dilatometer is shown by the dashed curve in Fig. 14. It is not strictly comparable, since the temperature is different by 1° and thermal equilibrium is reached much more quickly in the dilatometer. Also, the previous conditioning was slightly different, at 25° for 48 days. Nevertheless, it is clear that the autocatalytic character of the time dependence, characteristic of an isothermal expansion whose rate is controlled by free volume,²⁰ is mirrored in both the specific volume and the viscoelastic properties, reinforcing the view that the latter are controlled by the free volume.

Glass Transition Temperature Defined by Dynamic Measurements.—Attempts to specify the glass transition temperature in terms of time-dependent shear properties by specifying a particular magnitude of the modulus or the location of maximum in $\tan \delta$ at a given frequency can be ambiguous because of the gradual nature of the transition in shear properties and the difficulty of comparing magnitudes in different systems.²⁹ However, by adopting a convention similar to that used in dilatometry, values of T_g can be obtained from shear properties which agree quite well with the usual dilatometric definition.

In Fig. 15, values of G' and $\tan \delta$ interpolated from Fig. 4, 5, 16, and 17 at $\omega = 1.45$ radians/sec., as well as values of specific volume, are plotted against temperature at elapsed times of 50 min., 400 min., and ∞ (*i.e.*, voluminal equilibrium). The limited-time values at low temperatures are extrapolated linearly to intersect, as in the conventional dilatometric plot for v , the equilibrium values at high temperatures. Virtually the same value of T_g is obtained for all three experimental

quantities: 33.3° at an elapsed time of 50 min., and 32.0° at 400 min. In this construction, the frequency of the dynamic measurement is of course irrelevant, if the time-dependent and voluminal equilibrium values of the dynamic shear properties are plotted for the same frequency; the value of T_g depends only on the elapsed time after quench. The "transition" in each quantity reflects the free volume.

Analysis of the Dependence of Viscoelastic Properties on Temperature and Elapsed Time.—In general, the dependence of G' on frequency, temperature, and elapsed time t may be written

$$dG' = (\partial G'/\partial \log \omega)_{T,t} d \log \omega + (\partial G'/\partial T)_{\omega,t} dT + (\partial G'/\partial \log t)_{T,\omega} d \log t \quad (2)$$

In Fig. 6, 7, 12, and 13 the frequency is essentially constant, so the term in $d \log \omega$ and the ω subscripts can be omitted. We then can define a correlation derivative $(\partial \log t/\partial T)_{G',\infty}$ which compares the effects of temperature and elapsed time as

$$(\partial \log t/\partial T)_{G',\infty} = -(\partial G'/\partial T)_{t=\infty}/(\partial G'/\partial \log t)_T \quad (3)$$

where the derivatives on the right are taken from Fig. 6 and 13, and the subscript G', ∞ signifies that the temperature derivative is taken at $t = \infty$, *viz.*, at voluminal equilibrium. The derivative $(\partial \log t/\partial T)_{\tan \delta, \infty}$ is defined in an analogous way with slopes taken from Fig. 7 and 12.

If G' and $\tan \delta$ depend on free volume alone when either T or t is varied, then the three derivatives should be equal

$$(\partial \log t/\partial T)_{G',\infty} = (\partial \log t/\partial T)_{\tan \delta, \infty} = (\partial \log t/\partial T)_{t,\infty} \quad (4)$$

where

$$(\partial \log t/\partial T)_{t,\infty} = -(\partial f/\partial T)_{t=\infty}/(\partial f/\partial \log t)_T = \alpha_t/\bar{\beta} \quad (5)$$

Here $\bar{\beta}$ is the negative of the inflectional slope of the plot in Fig. 3, since the quantity $(v - v_\infty)/v_\infty$ is the same as $f - f_\infty$ if the time-dependent volume changes are due to collapse of free volume only.²⁰

From the slopes in Fig. 6, 7, 12, and 13 at a radian frequency of about 1.45 radians/sec., the derivatives $(\partial \log t/\partial T)_{G',\infty}$ and $(\partial \log t/\partial T)_{\tan \delta, \infty}$ have been calculated and are compared in Table I with the ratio $\alpha_t/\bar{\beta}$, taking α_t as 5.3×10^{-4} deg.⁻¹. While there is some scatter, it appears that at each temperature the three derivatives are equal within experimental error and therefore the effects of temperature seem to be attributable to free volume entirely.

TABLE I
CORRELATION DERIVATIVES FOR EFFECTS OF TEMPERATURE AND ELAPSED TIME

Temp., °C.	$(\partial \log t/\partial T)_{G',\infty}$	$(\partial \log t/\partial T)_{\tan \delta, \infty}$	$\alpha_t/\bar{\beta}$
20.0	0.67	0.78	0.68
25.0	.69	.76	.68
30.0	.67	.73	.69
32.5	.86	.75	.75
33.8	.92	.83	.79

There are, however, some inconsistencies showing that this conclusion is not strictly correct. The thermal

expansion coefficient above T_g is $6.9 \times 10^{-4} \text{ deg.}^{-1}$, from dilatometric data and extensive earlier work^{5,20}; that for the glassy state is 2.5×10^{-4} , from dilatometry far below the glass transition^{5,20} as well as the temperature expansion which precedes an isothermal expansion experiment (Fig. 14). If the difference, $\Delta\alpha = 4.4 \times 10^{-4}$, can be identified with the true thermal expansion coefficient of f , then the apparent value of $\alpha_f = 5.3 \times 10^{-4}$ which gives such good agreement in Table I probably includes a fictitious contribution of 0.9×10^{-4} representing an additional contribution to the temperature dependence of the relaxation times—about 20% of the total. This could be an isochoric temperature dependence, but the latter cannot be distinguished from an effect associated with expansion of the occupied volume or a contribution to the thermal expansion of free volume which is instantaneous and is the same above and below T_g . According to this last interpretation, the value of 2.5×10^{-4} below T_g would include 0.9×10^{-4} for expansion of free volume and 1.6×10^{-4} for expansion of the rigid structure. Whatever the interpretation of the discrepancy, the value of 5.3×10^{-4} for α_f reproduces the over-all temperature dependence of all the observed phenomena very satisfactorily.

Similar conclusions can be reached from Fig. 15. Since the expansion coefficients of $v(t)$ between 20 and 25° for $t = 50$ and 400 min. are equal within experimental error to that for the glassy state, the free volume governed by the coefficient $\Delta\alpha$ is constant in this region of temperature.³⁰ If the shear properties depended on this free volume only, $(\partial G'/\partial T)_{t,\omega}$ and $(\partial \log \tan \delta/\partial T)_{t,\omega}$ should be zero from 20 to 25°; moreover, the shear isotherms in Fig. 12 and 13 should coincide at these temperatures. (Here the subscript t denotes constant elapsed time of a magnitude much smaller than that needed for voluminal equilibrium.) In fact, neither of these conditions is fulfilled, and the relative positions of the curves in Fig. 13 correspond to a correlation derivative $(\partial \log t/\partial T)_{G',t}$ of about 0.13 deg.⁻¹. This value is about one-fifth of those in Table I. Thus, by considering the total effect of temperature as due only in part to free volume changes with a residual effect of temperature at constant free volume—*e.g.*, for G'

$$\frac{dG'}{dT} = \left(\frac{\partial G'}{\partial T}\right)_f + \left(\frac{\partial G'}{\partial f}\right)_T \left(\frac{df}{dT}\right) \quad (6)$$

where frequency is of course constant and $t = \infty$, it can be shown that the first term on the right is then 20% of the total.

The alternative interpretation here is that the free volume is governed by the coefficient α_f which includes a contribution of 0.9×10^{-4} even below T_g , accounting for the temperature dependence of the shear properties between 20 and 25°. In this case, the extrapolated lines in Fig. 15 do not represent states of iso-free-volume. However, on the basis of the present data there appears to be no way of distinguishing between the two alternatives.

It should be emphasized, of course, that the effects of free volume changes on G' and $\tan \delta$ at constant frequency are considered to arise entirely from modifications of the shear relaxation times, at least for free volumes greater than that corresponding to voluminal

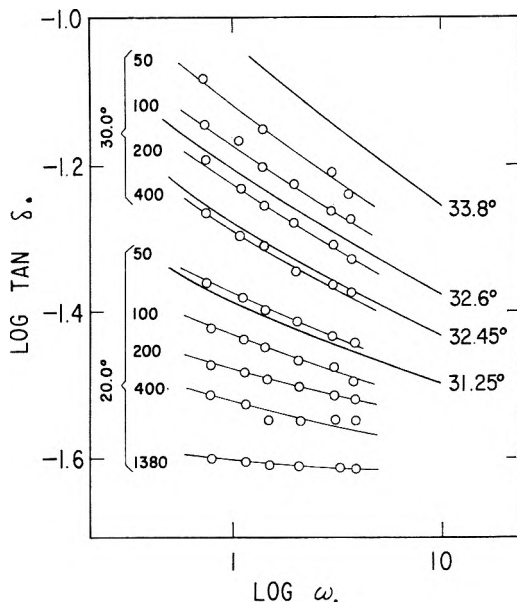


Fig. 16.—Loss tangent plotted logarithmically against radian frequency at various elapsed times in minutes as shown, at 20 and 30°. Heavy curves denote measurements at voluminal equilibrium at the temperatures indicated.

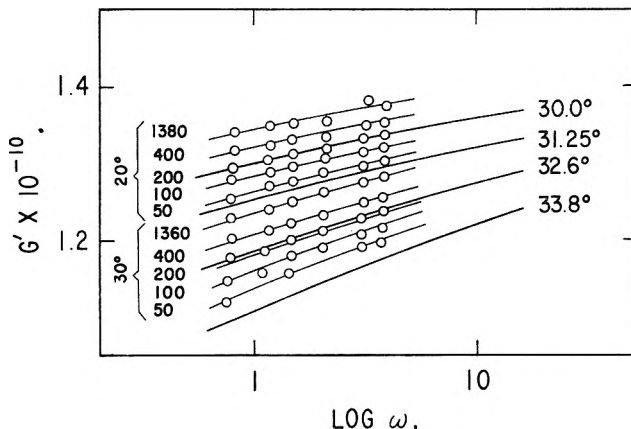


Fig. 17.—Storage shear modulus plotted against logarithm of radian frequency at various elapsed times at 20 and 30° as in Fig. 15.

equilibrium at 33°, since above that temperature reduced variables are applicable (Fig. 10). The magnitude of G' is supposed to be inherently independent of temperature, since the proportionality to $T\rho$ commonly used for treating viscoelastic properties in the transition zone has been omitted in the reduction. Assumption of a small *negative* temperature dependence for the magnitude of G' , which would not be unreasonable for a glassy structure, also could resolve the discrepancy and represents a third alternative for interpretation which requires further study for resolution.

Frequency Dependence of Dynamic Shear Properties as a Function of Elapsed Time.—From much more extensive measurements with different moments of inertia during isothermal contraction at 20, 25, and 30°, values of G' and $\tan \delta$ were determined over a range of frequencies at periods of 50, 100, 200, 400, and 1360–1380 min. after quench. The isoeonal curves at 20 and 30° are plotted against $\log \omega$ in Fig. 16 and 17 together with curves at voluminal equilibrium from Fig. 4 and 5. The measurements at 25° were similar and will be introduced later in reduced plots. It is evident that each set of curves forms a coherent family.

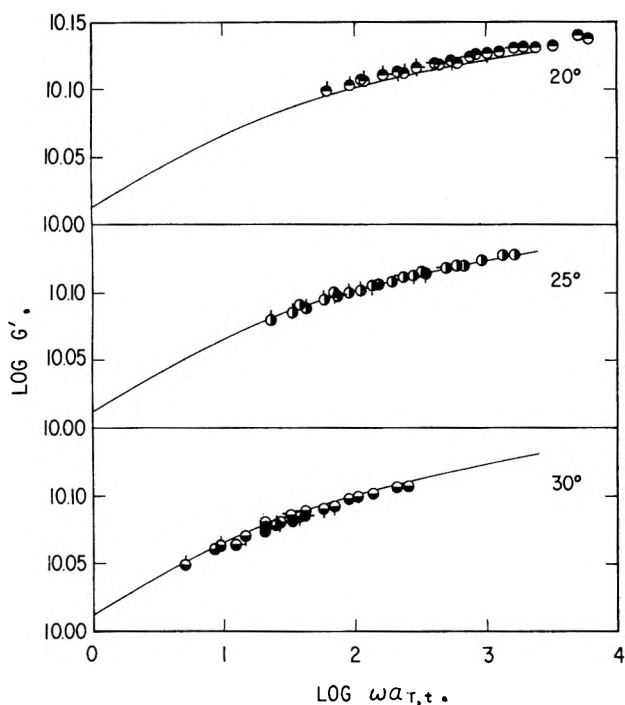


Fig. 18.—Composite plot of G' from data of Fig. 16 and similar data at 25° , reduced to 35° and complete volume equilibration by shift factors $a_{T,t}$ calculated from free volume as described in text; solid curve corresponds to Fig. 10: points top black, 20° ; right black, 25° ; bottom black, 30° ; tag up, 50 min.; right, 100 min.; down, 200 min.; left, 400 min.; no tag, 1360–1380 min. For clarity of presentation, some points falling very close to others have been omitted.

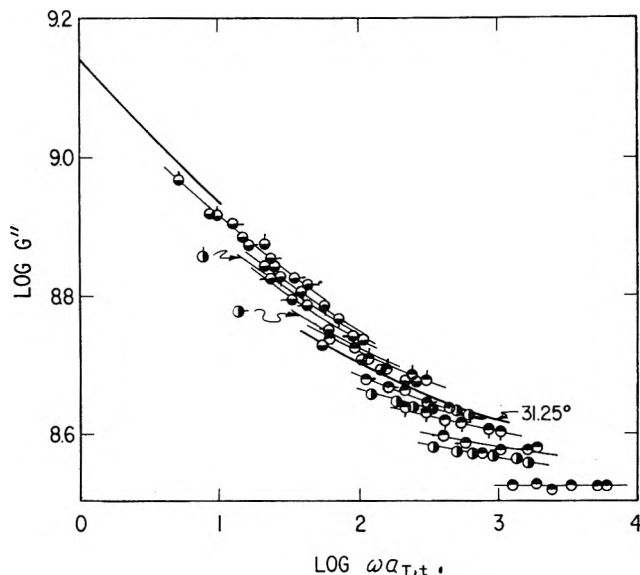


Fig. 19.—Composite plot of G'' from data measured during isothermal contraction as in Fig. 18, with the same key for temperatures and elapsed times after quench. Heavy curves refer to data at voluminal equilibrium.

Reduced Variables for Temperature and Elapsed Time.—We choose voluminal equilibrium at 35° as a reference state and define a factor $a_{T,t}$ as the ratio of any relaxation time at temperature T and elapsed time t to its value in the reference state. The shifts $\log a_{T,t}$ could be obtained empirically by measuring the separations on Fig. 16 and 17, but to test again the hypothesis that the relaxation times are controlled by free volume we have instead calculated them from the modified Doolittle equation^{12,16}

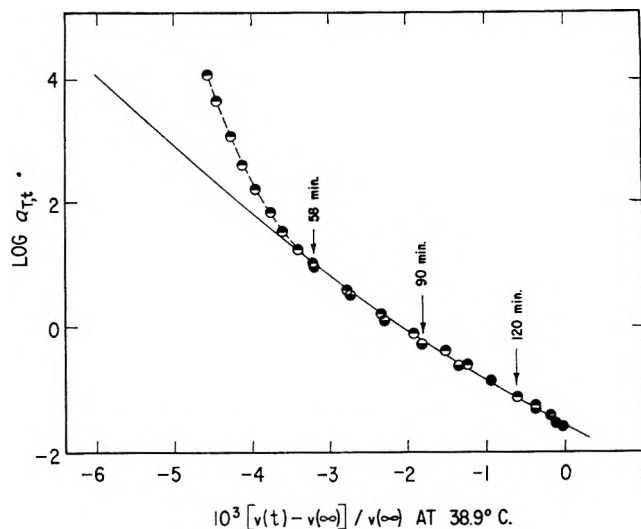


Fig. 20.—Analysis of data of Fig. 14: $\log a_{T,t}$ obtained empirically from G' (top black) and $\tan \delta$ (bottom black) plotted against relative volume measured dilatometrically, and compared with values calculated from the Doolittle equation (solid curve).

$$\log a_{T,t} = (1/2.303)(1/f_{T,t} - 1/f_{35,\infty}) \quad (7)$$

where $f_{35,\infty}$ is taken as 0.0225 and $f_{T,t}$ is obtained from $\alpha_f = 5.3 \times 10^{-4}$ together with the isothermal contraction data of Fig. 3, noting again that $(v_t - v_\infty)/v_\infty = f_t - f_\infty$. Thus, $f_{T,t} = f_{35,\infty} + \alpha_f(T - 308.2) + [(v_t - v_\infty)/v_\infty]_T$. In this calculation, the value of α_f used gives the correct temperature dependence of a_T independently of the uncertainties discussed above.

Reduced plots of G' and G'' against $\omega a_{T,t}$ derived in this way are presented in Fig. 18 and 19. For G' the superposition is rather satisfactory and confirms again the role of free volume. For G'' , the divergences at long elapsed times are analogous to those at voluminal equilibrium at low temperatures; these will be further discussed below.

Reduced Variable Analysis of Isothermal Expansion Experiment.—The data of Fig. 14 have been analyzed similarly, except that here values of $a_{T,t}$ have been obtained empirically and compared with a curve calculated from eq. 7, both plotted in Fig. 20 against the parallel dilatometric data from which the necessary values of $f_{T,t}$ were derived at 38.9° .

To obtain $\log a_{T,t}$ empirically from $\tan \delta$, the value of $\log \omega a_{T,t}$ corresponding to a measured $\tan \delta$ was read from a master curve for $\tan \delta$ at voluminal equilibrium (i.e., G''/G' from the graphs in Fig. 10), and $\log \omega$ was subtracted from it. This calculation is limited to $t > 70$ min., after which time the free volume corresponds to a temperature above 33° at voluminal equilibrium and the method of reduced variables can be safely applied. $\log a_{T,t}$ was obtained from G' in a similar manner except that minor corrections were made for the change of the sample coefficient, taking into account the changes of sample dimensions with temperature and time. The calculations from G' were made over the entire range of the experiment, since the composite curve for G' in Fig. 10 shows superposition within experimental error at low temperatures even though the method of reduced variables is not strictly applicable. The gratifying agreement between $\log a_{T,t}$ estimated from G' and from $\tan \delta$ data lends confidence to the method of calculation.

In calculating $f_{T,t}$ as a function of time, it was necessary to correct for the fact that the dilatometric experiment was made at 40° after keeping the sample at 25° for 48 days, while the dynamic shear measurements were made at 38.9° after 72 days at room temperature. The small differences in the magnitude of the free volume and in the time scale of the isothermal expansion process arising from these discrepancies were estimated from the thermal expansion coefficients and the data of Fig. 3, and the time scale of the isothermal expansion process at 40° was corrected using the $\log a_T$ function to the corresponding time scale at 38.9° where the shear experiments were performed.

After about 50 min., when thermal equilibrium has been reached in the torsion pendulum, the agreement between the empirical values of $\log a_{T,t}$ and those calculated from eq. 7 is excellent, providing quantitative evidence that the shear relaxation times during the isothermal expansion are controlled by the average free volume. At earlier times, where the temperature is changing, the empirical values are larger than those calculated. The difference shows again an additional temperature effect, which appears immediately upon change of temperature before the time-dependent free volume changes become effective. The magnitude of this instantaneous effect is again about 20% of the total.

Reduction Anomaly at Low Temperatures and Long Elapsed Times.—The drop in the magnitude of G'' at voluminal equilibrium at temperatures below 33° , seen in Fig. 10, which reflects a depression in the short-time plateau of H as in Fig. 11, is seen also in Fig. 19 at long elapsed times. The similarity in behavior suggests that this reduction anomaly is associated with free volume alone, just as the relaxation time shift factors are. As a crude test of this hypothesis, the vertical separations of the various curves below the high-temperature equilibrium composite curve in Fig. 19 have been measured and the total vertical displacement from the latter curve is plotted in Fig. 21 against the fractional free volume. The points for voluminal equilibrium at various temperatures and for systems in the course of isothermal contraction at various times all fall on the same curve, so that whatever the nature of the anomaly it appears to be related to free volume alone. The same conclusion can be drawn from the close agreement of the second and third columns in Table I, since at the lower temperatures the method of reduced variables does not apply and $\tan \delta$ is affected

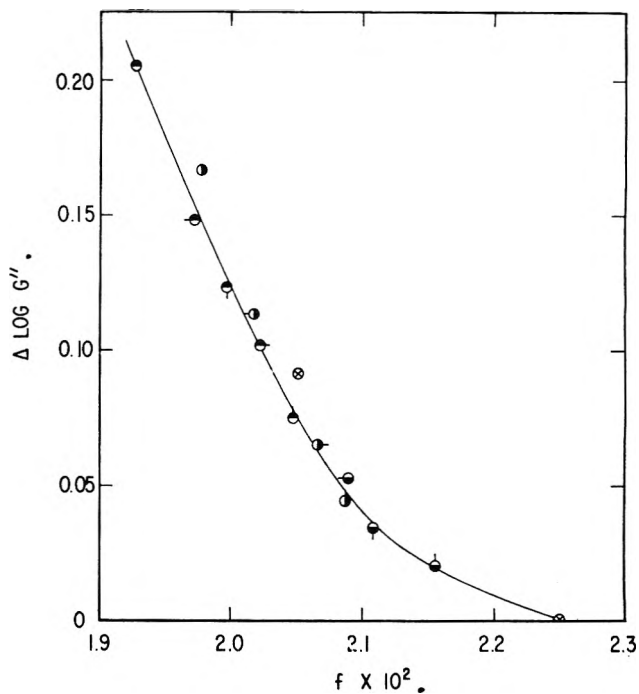


Fig. 21.—Vertical displacement of $\log G''$ in Fig. 19, measured from curve at voluminal equilibrium above 33.8° , plotted against fractional free volume. Key for temperatures and elapsed times same as in Fig. 18. Crossed points refer to data at voluminal equilibrium.

by both relaxation time shifts and change in the shape of the relaxation spectrum.

The different curves in Fig. 19 correspond to a progressive depression of the plateau in H (Fig. 11) with decrease in free volume. If the retardation spectrum L is calculated, it is found that this also undergoes a progressive drop in magnitude while remaining fairly flat. The symptoms are not those of a β mechanism^{31,32}; it is difficult to interpret them without more understanding of the molecular origin of viscoelasticity in the glassy state.

Acknowledgments.—This work was supported in part by the National Science Foundation and in part by the Army Research Office. We are much indebted to Dr. T. P. Yin and Mr. R. Schmelzer for work on the apparatus, to Mr. P. Mangin for help with some of the experiments, and to Mr. L. R. Shultis for making many calculations.

(31) J. D. Ferry, W. C. Child, Jr., R. Zand, D. M. Stern, M. L. Williams, and R. F. Landel, *J. Colloid Sci.*, **12**, 327 (1957).

(32) J. D. Ferry and K. Ninomiya, in J. T. Bergen, "Viscoelasticity—Phenomenological Aspects," Academic Press, New York, N. Y., 1960, p. 55.

THE THERMAL ISOMERIZATION OF CYCLOPROPANE AT LOW PRESSURES

By A. D. KENNEDY AND H. O. PRITCHARD

Chemistry Department, University of Manchester, Manchester 13, England

Received July 13, 1962

The isomerization of cyclopropane has been studied in a 1-l. vessel at 490° down to a pressure of 6×10^{-4} mm. At these low pressures, the rate constant becomes first order again in cyclopropane, and dependent on surface area, because the molecules are predominantly energized by collisions with the walls instead of collisions with other gas molecules. The activation energy was measured in this low pressure first-order region.

Some years ago, one of us¹ collaborated in an attempt to study the isomerization of cyclopropane at 5×10^{-3} mm. in a flow system; the experiment failed, apparently

(1) H. O. Pritchard, R. G. Sowden, and A. F. Trotman-Dickenson *Discussions Faraday Soc.*, **17**, 90 (1954).

because of some kind of streaming phenomenon, such as has recently been observed at higher pressures by Batten.² However, with the development of gas chromatography using very high sensitivity ionization

(2) J. J. Batten, *Australian J. Appl. Sci.*, **12**, 11 (1961).



Fig. 1.—●, points taken from ref. 3; ○, experiments in unpacked vessel; ●, experiments in packed vessel.

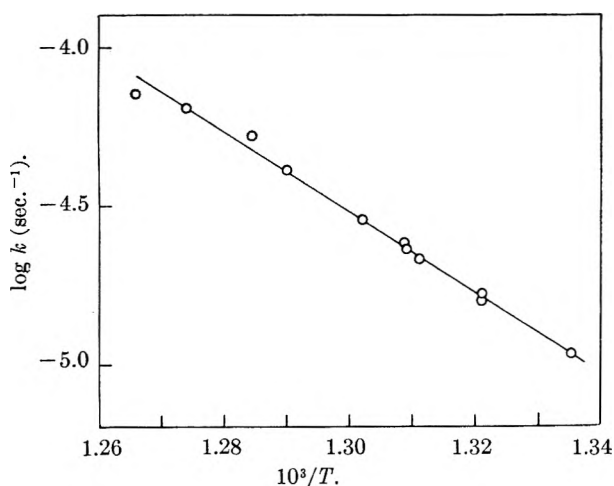


Fig. 2.—Arrhenius plot for thermal isomerization of cyclopropane in a packed reaction vessel at 8×10^{-3} mm. pressure.

detectors, it is now possible to analyze the products of a reaction carried out in a static system at less than 10^{-3} mm. pressure. Our aim in these experiments was to observe the change in kinetics which must occur when the mean free path exceeds the size of the reaction vessel and energization becomes principally a wall process instead of a gas phase one.

Experimental

The apparatus and procedure were similar in principle to experiments performed previously in this Laboratory³ except that a 1-l. spherical Pyrex vessel was used instead of the original 2-l. cylindrical one. The required pressure of cyclopropane was introduced into the reaction vessel by performing a series of expansions on a known quantity of gas: the gas buret in which the cyclopropane was originally measured and the whole series of expansion volumes were fitted with polythene diaphragm valves to reduce any loss of gas by absorption. The reaction vessel itself was isolated from the pumping system by a wide-bore mercury cut-off and a trap cooled in solid CO_2 to prevent mercury vapor from entering the reaction zone. The sampling section likewise consisted of a set of expansion volumes isolated by polythene diaphragm valves, leading to a 4-ft. chromatographic column which was built into the vacuum line: the column was packed with 20% of molar $\text{AgNO}_3/\text{glycol}$ on firebrick and was operated at -30° . The detector used was the Pye Argon system which is accurate to approximately $\pm 10\%$ for hydrocarbon analyses on the small quantities that were available.

(3) H. O. Pritchard, R. G. Sowden, and A. F. Trotman-Dickenson, *Proc. Roy. Soc. (London)*, **A217**, 563 (1953).

Experiments were carried out in the region of 490° from 7 mm. pressure down to 6×10^{-4} mm. At the higher pressures, the rate constants coincide with those obtained previously³; as the pressure is reduced, the rate constant falls toward the second-order limit, but before this is reached, the rate constant levels off and the reaction becomes first order again in cyclopropane, as shown by the plot of $\log k/k_\infty$ vs. $\log p$ in Fig. 1. The reaction is essentially first order at 10^{-3} mm., when the mean free path is about 7 cm., compared with the diameter of the vessel, which is 13 cm.

The measurements then were repeated with the reaction vessel packed. The vessel was completely filled with 169 4-cm. lengths of 10 mm. o.d. Pyrex tubes (8 mm. i.d.) so that the total surface area was increased from 530 to 4390 cm^2 and the reaction volume fell from 1060 to 870 ml. The reaction now became first order slightly above 10^{-2} mm. pressure, when the mean free path was about 0.7 cm. compared with the mean free travel of the order of 1 cm. The rate constant for the formation of propylene in the low-pressure first-order region increased by a factor of about 2.5 on packing the vessel.

The activation energy in the low pressure first order region was measured at 8×10^{-3} mm. in the packed vessel over the temperature range 477 – 517° . The use of the packed vessel meant that we could operate at a higher pressure, thus allowing us to make more than one analysis for each run; also, since the rate constant is higher, the length of each run is shortened considerably. The activation energy was found to be 57.2 ± 2 kcal. with a frequency factor of $10^{11.6}$ sec^{-1} ; the frequency factor is of course dependent on the geometry of the packing. The Arrhenius plot is shown in Fig. 2.

Discussion

We conclude, for reasons advanced below, that in the low pressure first-order region, the nature of the isomerization of cyclopropane is unchanged, the only difference being that energization takes place predominantly on the walls instead of in the gas phase.

First, it is necessary to discuss the possibility of some systematic experimental error in these observations. We do not think that there is any significant error in our estimate of the cyclopropane pressure: this was obtained from the original quantity of gas measured out, and the appropriate expansion ratio; we did not find any discrepancy between the amount of gas we assumed went into the reaction vessel, and the amount that was available for analysis afterward. Nor is it likely that the total pressure in the reaction vessel differed much from the cyclopropane pressure. The lowest pressure at which we could operate was 6×10^{-4} mm., which is much in excess of the attainable vacuum in the reaction vessel (better than 10^{-5} mm.); also the pressure of mercury vapor in the vessel should be well below 10^{-6} mm. Nor is there likely to be much error in our estimate of the reaction time. At the low pressures, where the pumping speed is likely to be slow, runs usually lasted about 20 or about 40 hr. so that errors due to slow pumping would be negligible. Even at the highest temperature of 517° , the shortest run was 3 hr., so that even here, no significant error is likely.

Two alternative interpretations of the observations are possible, one that we have a wall energized reaction, and the other that we have a true heterogeneous reaction involving an adsorbed species; the third possibility envisaged by Butler⁴ in a recent paper is ruled out because we never observed any product other than propylene in any of our experiments. We believe that in this reaction, the second postulate is unnecessary because the observations fit the wall energization scheme quite well. In the unpacked vessel, the number of molecule-wall collisions equals the number of mole-

(4) J. N. Butler, *J. Am. Chem. Soc.*, **84**, 1393 (1962).

cule-molecule collisions at about 5×10^{-3} mm.; the corresponding figure for the packed vessel is about 5×10^{-2} mm. These are approximately the pressures where the low pressure first-order regions begin in each case and this is consistent with the interpretation that collisions with the walls are some 3-5 times as efficient as collisions with other cyclopropane molecules. Furthermore, if we regard the walls as acting instead of gas molecules as far as energization is concerned, the temperature coefficient of the reaction shows the expected behavior. The variation in temperature

coefficient with pressure has been observed for azo-methane⁵ and 1,1-dimethylcyclopropane.⁶ In both cases, as the pressure is reduced, the activation energy falls by about 5 to 7 kcal. and the frequency factor falls by a factor of 10^2 to 10^4 . Our activation energy is 8 ± 2 kcal. below the high pressure value, and the frequency factor, although it is to some extent dependent on the surface area, is down by a factor of about 10^3 to 10^4 .

(5) C. Steel and A. F. Trotman-Dickenson, *J. Chem. Soc.*, 975 (1959).

(6) M. C. Flowers and H. M. Frey, *ibid.*, 1157 (1962).

INTRAMOLECULAR REARRANGEMENTS. V. FORMATION OF ETHYLENE IN THE PHOTOLYSIS OF ETHYL ACETATE FROM 4 TO 500°K.¹

By P. AUSLOOS AND RICHARD E. REBBERT

National Bureau of Standards, Washington, D. C.

Received July 16, 1962

The formation of ethylene in the gas, liquid, and solid phase photolysis of $\text{CH}_3\text{COOC}_2\text{H}_5$, $\text{CH}_3\text{COOCD}_2\text{CD}_2\text{H}$, and $\text{CH}_3\text{COOC}_2\text{D}_5$ has been investigated at various wave lengths and temperatures. The intramolecular isotope effect increases with a decrease in temperature in both the gas and liquid phase photolysis. In the liquid phase, an activation energy difference of 1.0 kcal./mole was obtained for D and H-atom transfer in the photolysis of $\text{CH}_3\text{COOCD}_2\text{CD}_2\text{H}$. A variation in wave length influences the formation of ethylene in the gas and solid phases but does not affect the intra- and intermolecular isotope effects in the liquid phase. A comparison of the product yields in the mercury sensitized decomposition with those obtained in the direct photolysis, as well as a study of the effect of biacetyl on the ethylene yield, indicates that the formation of ethylene by an intramolecular rearrangement of the ester molecule excited to an upper triplet state cannot be ruled out.

Introduction

It is now well established² that esters containing one or more β -hydrogen atoms in the alkyl group may decompose photochemically by an intramolecular rearrangement into an olefin and the corresponding acid.

In the present work, the gas, liquid, and solid phase photochemical decompositions of $\text{CH}_3\text{COOC}_2\text{H}_5$, $\text{CH}_3\text{COOCD}_2\text{CD}_2\text{H}$, and $\text{CH}_3\text{COOC}_2\text{D}_5$ have been investigated in order to obtain a better understanding of the intra- and intermolecular isotope effects on the primary process. The comparison of these results with those obtained on the photolysis of $\text{CH}_3\text{COCH}_2\text{CHDCD}_2\text{H}$,³ and on the pyrolysis of isotopically labeled ethyl acetate,⁴ was expected to lead to interesting correlations.

Experimental

Apparatus.—The gas phase was photolyzed in a quartz cell (10 cm. in length, 5 cm. in diameter) enclosed in a heavy aluminum furnace provided with double quartz windows. The temperature was automatically controlled within half a degree.

The liquid phase was irradiated in a quartz cell (0.05 cm. in depth, 2.5 cm. in diameter) provided with two outlets, one of which was sealed after filling and the other closed by a break seal. The liquid cell was immersed in a Pyrex dewar flask with double quartz windows. Cold ethyl alcohol was the refrigerant for experiments carried out from 193 to 273°K.

The solid phase experiments were carried out in a stainless steel low-temperature dewar.⁵ The ethyl acetate was deposited on a gold plated brass plate, in order to ensure good thermal conduction. The flow rate for deposition of the sample was

about 2 cc. (STP)/min. In most experiments about 30 cc. (STP) of gas was deposited on the brass plate.

In the mercury photosensitized experiments a flat spiral low-pressure mercury arc was used in conjunction with a Corning filter 7-54. A Hanovia SH-100 lamp was used in all other experiments. The incident wave length range was varied by using Corning filters 9-54 and 7-54, transmitting radiation at wave lengths greater than 2150 and 2250 Å., respectively. Because ethyl acetate absorbs mostly below 2350 Å., the effective wave length regions were roughly 2150-2350 Å. and 2250-2350 Å.

Materials.—Ethyl-*d*₅ acetate and ethyl-*d*₄ acetate were obtained from Merck, Sharp & Dohme of Canada, Ltd. Mass spectrometric analysis showed that the three batches of ethyl-*d*₄ acetate used in this work contained about 5% ethyl-*d*₃ acetate, the remainder consisted of $\text{CH}_3\text{COOCD}_2\text{CD}_2\text{H}$. It was not possible to tell what fraction of the ethyl-*d*₃ acetate was $\text{CH}_3\text{COOCD}_2\text{CDH}_2$ or $\text{CH}_3\text{COOCHDCD}_2\text{H}$; consequently, the results have not been corrected for the presence of this impurity. At any rate, this correction would only be a minor one and certainly would not affect any of the conclusions drawn in this paper. The ethyl-*d*₅ acetate batch contained 2.5% ethyl-*d*₄ acetate. Chromatographic analysis indicated that after a trap-to-trap distillation at -80°, the total chemical impurities amounted to not more than 1%, ethanol being the major impurity.

$\text{CH}_3\text{COOC}_2\text{H}_5$ was obtained from Eastman Kodak Co. After distillation the impurities did not exceed 0.1%.

Analysis.—The analytical system consisted of a solid nitrogen trap, a modified Ward still, an automatic Toepler pump, and a Toepler gas buret. The carbon monoxide-methane-hydrogen fraction was removed at -210°. Ethylene and ethane subsequently were distilled off at -180°. Propane and carbon dioxide were removed at -150°. All fractions were analyzed mass spectrometrically using a Consolidated mass spectrometer Model 21-101. Standard samples of C_2D_4 and $\text{C}_2\text{D}_3\text{H}$ obtained from Merck, Sharp & Dohme were run on the same mass spectrometer in order to calculate the isotopic distribution of the ethylenes.

Results

In order to study the relative importance of a H atom to a D atom transfer in the intramolecular rearrangements of the labeled ethyl acetates, ethylene

(1) This research was supported by a grant from the U. S. Public Health Service, Department of Health, Education, and Welfare.

(2) (a) P. Ausloos, *Can. J. Chem.*, **36**, 383 (1958); (b) P. Ausloos, *J. Am. Chem. Soc.*, **80**, 1310 (1958); (c) M. H. J. Wijnen, *ibid.*, **82**, 3034 (1960); (d) R. Borkowski and P. Ausloos, *ibid.*, **83**, 1053 (1961).

(3) R. P. Borkowski and P. Ausloos, *J. Phys. Chem.*, **65**, 2257 (1961).

(4) (a) A. T. Blades and P. W. Gilderson, *Can. J. Chem.*, **38**, 1401 (1960); (b) A. T. Blades and P. W. Gilderson, *ibid.*, **38**, 1407 (1960).

(5) Hofman Free Radical Research Dewar, D-1288.

rather than acetic acid has been determined quantitatively. It may be noted that acetic acid has been observed as a product in the liquid phase experiments, but the fast exchange of CH_3COOD to CH_3COOH during the analytical procedure reduces the usefulness of a systematic analysis of this compound.

In order to inhibit radical reactions which may eventually lead to the formation of ethylene, oxygen was present in nearly all vapor phase photolysis experiments. Under these conditions, ethylene was the only hydrocarbon product formed in the gas-phase photolysis of ethyl acetate. In the liquid phase experiments, no radical scavengers have been used, because ethylene always accounted for more than 95% of the hydrocarbon products. All vapor phase experiments were carried out at conversions varying between 0.03 and 0.1%. The extent of decomposition in the liquid phase experiments was always less than 0.02%.

(A) **Vapor Phase Photolysis.**—In order to obtain information on the relative importance of the olefin elimination process, $\text{CH}_3\text{COOC}_2\text{H}_5$ has been photolyzed in the absence of oxygen at 135° and at a pressure of 5 cm. At this temperature the relative distribution of CO , CO_2 , and C_2H_4 is

Full arc: CO , 1.0; CO_2 , 0.25; C_2H_4 , 0.39

$\text{Hg}(^3\text{P}_1)$ sensitized: CO , 1.0; CO_2 , 0.15; C_2H_4 , 0.83

In the mercury photosensitized decomposition at 135° , the formation of ethane, propane, and butane was completely inhibited by the addition of 1% oxygen, while the yield of ethylene was reduced by only 6%.

In the mercury sensitized decomposition at 30° carried out in absence of oxygen the ethane, propane, and butane yields were, respectively, 1.1, 3.0, and 1.5% of the ethylene yield.

The results⁶ given in Table I can be summarized as follows:

A variation in the pressure of oxygen from 0.1 to 1 cm. has within experimental error no effect on the yield as well as on the distribution of the ethylenes.

Absorption of shorter wave lengths by $\text{CH}_3\text{COOC}_2\text{D}_4\text{H}$ or an increase in temperature reduces the ratio $\text{C}_2\text{D}_4/\text{C}_2\text{D}_3\text{H}$ to a value which approaches the chance value of 0.5.

TABLE I
GAS PHASE PHOTOLYSIS

T °K.	—Pressure, cm.—		Wave lengths, Å.	Ethylene, cc./min. × 10 ⁴	Ratio
	[Ethyl acetate]	[O ₂]			
$\text{CH}_3\text{COOCD}_2\text{CD}_2\text{H}$					
315	3.0	0.1	Full arc	22.5	0.665
315	3.0	0.1	2150–2350	9.0	0.805
315	3.0	1.0	2150–2350	9.1	0.803
431	3.6	0.1	2150–2350	9.3	0.74
315	3.0	0.1	2250–2350	0.2	1.06
315	2.9	0.05	2537 $\text{Hg}(^3\text{P}_1)$	4.0	2.10
315	3.1	None	2537 $\text{Hg}(^3\text{P}_1)$	4.0	2.15
$\text{CH}_3\text{COOC}_2\text{H}_5\text{—CH}_3\text{COOC}_2\text{D}_5$ (1:1)					
315	3.2	0.1	Full arc	33.2	2.40
315	3.1	0.1	2150–2350	10.0	2.35
500	4.4	0.1	2150–2350	10.6	2.55
315	3.2	0.1	2250–2350	1.3	2.25
315	3.2	None	2537 $\text{Hg}(^3\text{P}_1)$..	1.75

(6) A variation of the total ethylene rates given in the tables, for experiments performed in the same wave length range, reflect a variation in the relative quantum yields.

In the photolysis of equimolar mixtures of $\text{CH}_3\text{COOC}_2\text{H}_5$ and $\text{CH}_3\text{COOC}_2\text{D}_5$ the intermolecular isotope effect as evidenced by the ratio $\text{C}_2\text{D}_4/\text{C}_2\text{H}_4$ increases slightly with decrease in wave length and increase in temperature.

(B) **Liquid Phase Photolysis.**—The incident intensity was kept constant for all experiments carried out in the wave length range 2150–2350 Å. For these experiments the rates of formation of ethylene may thus be considered as relative quantum yields. The following conclusions can be drawn from the results given in Table II.

TABLE II
LIQUID PHASE PHOTOLYSIS

T, °K.	Filter	Ethylene, cc./min.	Ratio
$\text{CH}_3\text{COOCD}_2\text{CD}_2\text{H}$			
322.5	9-54	3.00	2.35
302.5	None	..	2.57
302.5	7-54	..	2.54
302.5	9-54	2.88	2.56
273.0	9-54	2.46	3.07
270.0	9-54	2.40	3.10
244.0	9-54	2.20	3.70
224.0	9-54	2.09	4.50
198.0	9-54	1.72	5.95
$\text{CH}_3\text{COOC}_2\text{H}_5$			
273.0	9-54	2.95	
273.0 ^a	9-54	0.79	
193.0	9-54	2.45	
$\text{CH}_3\text{COOC}_2\text{D}_5$			
295.0	9-54	1.62	
273.0	9-54	1.58	
238.0	9-54	1.02	
193.0	9-54	0.56	
$\text{CH}_3\text{COOC}_2\text{H}_5\text{—CH}_3\text{COOC}_2\text{D}_5$ (1:1)			
322.5	9-54	1.86	$\text{C}_2\text{H}_4/\text{C}_2\text{D}_4$ 1.84
302.5	9-54	2.05	1.82
302.5	None	..	1.80
273	9-54	2.03	1.87
273 ^a	9-54	0.40	7.10
238	9-54	1.90	2.98
198	9-54	1.39	4.20
198	7-54	..	4.25

^a 2% by volume biacetyl added.

A variation of the incident wave length has no effect on the ratios $\text{C}_2\text{D}_4/\text{C}_2\text{D}_3\text{H}$ and $\text{C}_2\text{H}_4/\text{C}_2\text{D}_4$ obtained in the photolysis of $\text{CH}_3\text{COOC}_2\text{D}_4\text{H}$ and $\text{CH}_3\text{COOC}_2\text{H}_5\text{—CH}_3\text{COOC}_2\text{D}_5$ mixtures, respectively.

In the photolysis of $\text{CH}_3\text{COOC}_2\text{D}_4\text{H}$ the total ethylene undergoes a gradual increase with increase in temperature, while the ratio $\text{C}_2\text{D}_4/\text{C}_2\text{D}_3\text{H}$ diminishes with a raise in temperature. A plot of $\log \text{C}_2\text{D}_4/\text{C}_2\text{D}_3\text{H}$ against $1/T$ corresponds to 1.0 kcal/mole.

The effect of temperature on the yield of ethylene is more pronounced in the photolysis of $\text{CH}_3\text{COOC}_2\text{D}_5$ than in the photolysis of $\text{CH}_3\text{COOC}_2\text{H}_5$.

In the photolysis of equimolar mixtures of $\text{CH}_3\text{COOC}_2\text{H}_5$ and $\text{CH}_3\text{COOC}_2\text{D}_5$, the ratio $\text{C}_2\text{H}_4/\text{C}_2\text{D}_4$ decreases with increase in temperature until it reaches, around 273°K ., a constant temperature independent value of ~ 1.83 . The same value is obtained by taking the ratio of the yields of C_2H_4 and C_2D_4 produced in the photolysis of $\text{CH}_3\text{COOC}_2\text{H}_5$ and $\text{CH}_3\text{COOC}_2\text{D}_5$ at 273° .

Addition of 2% biacetyl reduces the yield of ethylene produced in the photolysis of $\text{CH}_3\text{COOC}_2\text{H}_5$ by 80%. A similar reduction is observed upon addition of biacetyl to an equimolar mixture of $\text{CH}_3\text{COOC}_2\text{H}_5$ and $\text{CH}_3\text{COOC}_2\text{D}_5$. In the latter case addition of biacetyl also increases the ratio $\text{C}_2\text{H}_4/\text{C}_2\text{D}_4$.

(C) **Solid Phase.**—In Table III several experiments have been presented, which have been performed at various temperatures of deposition and irradiation. For comparison, a few experiments carried out on $\text{CH}_3\text{COCH}_2\text{CHDCD}_2\text{H}$ have been included as well. Products other than ethylene were only observed in the photolysis of ethyl acetate at 4°K.

TABLE III
SOLID PHASE PHOTOLYSIS

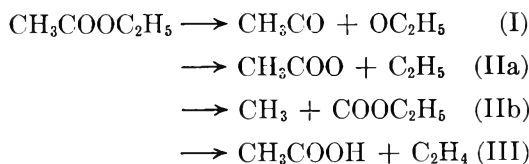
Wave lengths	T, °K. (depos.)	T, °K. (irrad.)	Ethylene, cc./min. × 10 ⁴	Ratio
$\text{CH}_3\text{COOC}_2\text{D}_2\text{CD}_2\text{H}$				
Full arc	77	77	2.0	$\text{C}_2\text{D}_4/\text{C}_2\text{D}_3\text{H}$ 10.4
Full arc	4	77	1.9	8.9
Full arc	77	4	1.0	3.5
Full arc	4	4	1.6	2.0
$\text{CH}_3\text{COOC}_2\text{H}_5-\text{CH}_3\text{COOC}_2\text{D}_5$ (1:1)				
Full arc	77	77	..	$\text{C}_2\text{H}_4/\text{C}_2\text{D}_4$ 25.6
Full arc	77	4	..	10.0
$\text{CH}_3\text{COCH}_2\text{CHDCD}_2\text{H}$				
3130 Å.	77	77	1.2	$\text{C}_2\text{D}_3\text{H}/\text{C}_2\text{D}_3\text{H}_2$ 11.4
2537 Å.	77	77	..	5.0
3130 Å.	77	4	0.52	7.4
3130 Å.	4	4	.56	5.6

The results show that: (1) At an irradiation temperature of 77°K., the ratios $\text{C}_2\text{D}_4/\text{C}_2\text{H}_4$ and $\text{C}_2\text{D}_4/\text{C}_2\text{D}_3\text{H}$ obtained in the photolysis of an equimolar mixture of $\text{CH}_3\text{COOC}_2\text{H}_5$ and $\text{CH}_3\text{COOC}_2\text{D}_5$ and in the photolysis of $\text{CH}_3\text{COOC}_2\text{D}_2\text{CD}_2\text{H}$, are still considerably higher than those observed in the liquid phase at temperatures close to the melting point. (2) A decrease in the temperature of deposition from 77 to 4°K. apparently reduces the ratio $\text{C}_2\text{D}_4/\text{C}_2\text{D}_3\text{H}$ in the photolysis of $\text{CH}_3\text{COOC}_2\text{D}_2\text{CD}_2\text{H}$. A similar effect is observed in the photolysis of $\text{CH}_3\text{COCH}_2\text{CHDCD}_2\text{H}$. In the latter case there seems to be a decrease in quantum yield as well. (3) In the photolysis of $\text{CH}_3\text{COOC}_2\text{D}_2\text{CD}_2\text{H}$ a decrease in temperature of irradiation from 77 to 4°K. strongly reduces the ratio $\text{C}_2\text{D}_4/\text{C}_2\text{D}_3\text{H}$. At this temperature other products, besides ethylene, are produced in significant amounts.⁷

Discussion

I. The Nature of the Upper Electronic State.

(A).—The following primary processes have been reported to occur in the vapor and liquid phase photolysis of ethyl acetate.² From the vapor phase experi-



(7) The distribution of the gaseous products formed in the photolysis of $\text{CH}_3\text{COOC}_2\text{D}_2\text{CD}_2\text{H}$ carried out at 4°K. is as follows: CO, 50%; methane, 24.2%; hydrogen, 12.3%; ethylene ~10%; ethane ~3.5%. The isotopic compositions of the hydrogen and methane fractions were as follows: CD_4 , 3.1%; CD_3H , 19.9%; CD_2H_2 , 15.8%; CH_3D , 23.2%; CH_4 , 38.0%; D_2 , 13.7%; HD , 37.3%; H_2 , 48.9%.

ments^{2a} it could not be decided if either (IIa) or (IIb) or both occur. However, the fact that above 124° the ratio $\text{C}_2\text{H}_4/\text{CO}_2$ as well as the yields of CO_2 and CO were within experimental error independent of temperature indicates that at these temperatures and at moderate intensities, CO_2 and CO may be taken as a measure of processes (IIa) + (IIb) and (I), respectively. Also the earlier observation^{2a} that addition of iodine reduces the yield of ethylene by not more than 20% demonstrates that even in absence of scavengers ethylene is mainly produced by process III. It thus follows from a comparison of the relative yields of CO , CO_2 , and C_2H_4 produced in the direct photolysis at 135° with those observed in the $\text{Hg}(^3\text{P}_1)$ sensitized photolysis, that the intramolecular rearrangement process is relatively more important in the mercury photosensitized decomposition than in the direct photolysis. If as it has been suggested⁸ one assumes that the Wigner spin conservation rule can be applied in the case of the photosensitized excitation, one is forced to conclude that contrary to a recent prediction,⁹ an ethyl acetate molecule excited to an upper triplet state does decompose according to process III.

It may be argued that the independence of the yield of ethylene (Table I) with a variation of the pressure of oxygen seems to rule out the occurrence of the olefin elimination process by way of a triplet state.¹⁰ However, it should be noted that the transition from the upper singlet formed in the primary photochemical act to the triplet state may lead to the production of a molecule excited to a high vibrational level of the triplet state with a short dissociative lifetime. Such a vibrationally excited molecule may decompose before suffering a quenching collision with oxygen. In this connection it may be pointed out that oxygen does quench the intramolecular rearrangement in the photolysis of 2-pentanone, provided that temperature is low enough and that only the longer wave lengths are absorbed by the ketone molecule.¹¹

Other evidence for the elimination of an olefin from compounds containing carbonyl which are excited to a triplet level follows from the recent observation¹² that traces of biacetyl readily quench the formation of ethylene in the photolysis of *n*-butyraldehyde at 3340 Å.

It is obvious that it is experimentally difficult to determine at any particular wave length, temperature, and pressure if a certain mode of decomposition in the gas phase occurs from a molecule excited to an upper singlet state or to a high vibrational level of the triplet state, or both. At any rate, the $\text{Hg}(^3\text{P}_1)$ sensitized experiments presented in this paper indicate that the formation of ethylene from a molecule excited to an upper triplet state cannot be ruled out.

(B) **Liquid Phase.**—Recent gas phase photolysis studies¹³ have demonstrated that energy transfer from a triplet excited ketone molecule to biacetyl occurs readily at the longer wave length and low temperatures.

(8) P. Borrell and R. G. W. Norrish, *Proc. Roy. Soc. (London)*, **A262**, 19 (1961).

(9) P. Borrell, *Nature*, **188**, 1002 (1960).

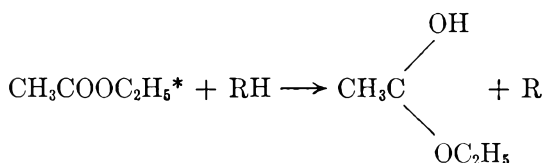
(10) V. Brunet and W. A. Noyes, Jr., *Bull. soc. chim. France*, 121 (1958).

(11) R. Borkowski and P. Ausloos, *J. Phys. Chem.*, **65**, 2257 (1961).

(12) R. Borkowski and P. Ausloos, *J. Am. Chem. Soc.*, **84**, 4044 (1962).

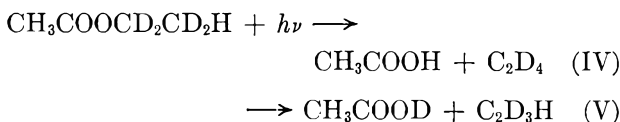
(13) (a) H. Okabe and W. A. Noyes, Jr., *ibid.*, **79**, 801 (1957); (b) J. Heicklen and W. A. Noyes, Jr., *ibid.*, **81**, 3858 (1959); (c) D. S. Weir, *ibid.*, **83**, 2629 (1961).

In the liquid phase, because of extensive degradation of the vibrational energy,² one may expect that the energy transfer reaction between a triplet excited molecule and biacetyl will have a relatively high efficiency at all wave lengths. This is indeed demonstrated by the pronounced reduction (Table II) in the relative quantum yield of ethylene caused by the addition of 2% biacetyl.¹⁴ Although these experiments only demonstrate that transfer of electronic energy from ethyl acetate to biacetyl is an efficient process, it may be said that on the basis of the relatively long lifetime of the triplet state as well as in view of the recent gas phase experiments,^{11,12} an excited triplet rather than an upper singlet state is involved in this process. In this connection it may be pointed out that in an earlier investigation of the liquid phase photolysis of esters, a quenching of process (III) by a number of solvents has been observed.¹⁵ Evidence was presented which indicated that this quenching process actually consisted of a photochemical reaction involving an ester molecule excited to a higher electronic level



This reaction is analogous to the H-atom abstraction from solvent molecules by electronically excited acetone,¹⁶ biacetyl,¹⁷ and benzophenone.¹⁸ These reactions have been ascribed^{17,18c} to a triplet state of the compound containing carbonyl.

II. Intra- and Intermolecular Isotope Effect. (A) Vapor Phase. $\text{CH}_3\text{COOCD}_2\text{CD}_2\text{H}$.—In the presence of oxygen, C_2D_4 and $\text{C}_2\text{D}_3\text{H}$ are formed by the following two processes



A chance occurrence of these two processes would lead to a value of 0.5 for the ratio $\text{C}_2\text{D}_4/\text{C}_2\text{D}_3\text{H}$. It can be seen (Table I) that this value is only approached in the gas phase photolysis at the shorter wave lengths. It is obvious that the increase of the ratio $\text{C}_2\text{D}_4/\text{C}_2\text{D}_3\text{H}$ with increasing wave lengths and decreasing temperatures is related to the difference in bond strength between the C-H and C-D bond. Rupture of the C-H bond apparently is favored at long wave lengths and low

(14) The importance of this quenching effect for other compounds containing carbonyl has been demonstrated by recent experiments carried out in this Laboratory. It was found that the addition of 2% biacetyl to 2-pentanone, photolyzed in the liquid phase at 2537 Å. and 0°, reduced the quantum yield of ethylene by 90%.

(15) It should be noted that the quenching effect of these solvents (methanol, ethanol, *n*-heptane) is at least one order of magnitude smaller than the effect of biacetyl. Also, the efficiency of this process increases with decreasing C-H bond strength in the solvent molecule. This would make biacetyl a rather ineffective additive.

(16) P. E. Frankenburg and W. A. Noyes, Jr., *J. Am. Chem. Soc.*, **75**, 2847 (1953).

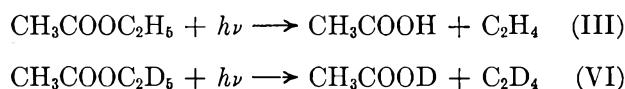
(17) H. L. J. Bäckström and K. Sandros, *Acta Chem. Scand.*, **12**, 823 (1958).

(18) See for instance: (a) H. L. J. Bäckström, *Z. physik. Chem.*, **B25**, 19 (1934); (b) Y. Hirschberg and L. Farkas, *J. Am. Chem. Soc.*, **59**, 2453 (1937); (c) H. L. J. Bäckström, A. Steneryr, and P. Perlmann, *Acta Chem. Scand.*, **12**, 8 (1958); (d) J. N. Pitts, R. L. Letsinger, R. P. Taylor, J. M. Patterson, G. Recktenwald, and R. B. Martin, *J. Am. Chem. Soc.*, **81**, 1068 (1959).

temperatures. Similar observations have been made in the course of a recent investigation of the photolysis of $\text{CH}_3\text{COCH}_2\text{CHD}_2\text{H}$.¹¹

As may be expected, the value for the ratio $\text{C}_2\text{D}_4/\text{C}_2\text{D}_3\text{H}$, obtained in the $\text{Hg}(^3\text{P}_1)$ sensitized experiments, is larger than that found in the direct photolysis experiments which have been carried out at shorter wave lengths. It is interesting to note that the intramolecular isotope effect in $\text{Hg}(^3\text{P}_1)$ sensitized decomposition of ethyl- d_4 acetate is nearly twice as large as that observed under comparable experimental conditions in the photolysis of $\text{CH}_3\text{COCH}_2\text{CHD}_2\text{H}$. This may be related to a difference in the degree of vibrational deactivation of these two compounds, prior to decomposition. As will be shown later in the discussion, in the liquid phase the ester and the ketone show about the same intramolecular isotope effect.

$\text{CH}_3\text{COOC}_2\text{H}_5-\text{CH}_3\text{COOC}_2\text{D}_5$ (1:1).—From the results of Table I it can be deduced that there is an appreciable intermolecular isotope effect¹⁹ for the two processes



In the direct photolysis, the variations of the ratio $\text{C}_2\text{H}_4/\text{C}_2\text{D}_4$ with wave length and temperature are rather small and do not warrant any further discussion.

(B) Liquid Phase. $\text{CH}_3\text{COOCD}_2\text{CD}_2\text{H}$.—The fact that the ratio $\text{C}_2\text{D}_4/\text{C}_2\text{D}_3\text{H}$ is independent of wave length indicates that in the liquid phase, the ethyl acetate molecule excited to an upper electronic state undergoes a collision induced degradation to a lower lying energy level. The degree of excitation of the molecule which decomposes apparently is independent of the exciting wave length. However, a variation in temperature has a pronounced effect on the ratio $\text{C}_2\text{D}_4/\text{C}_2\text{D}_3\text{H}$ as well as on the total ethylene yield. In this respect there is a similarity between the photolysis and pyrolysis of ethyl acetate. Apparently, in the liquid phase the excited molecules undergo a sufficient number of collisions prior to decomposition to achieve equilibration of the vibrational energy in the upper electronic state. From the results of Table II, the following expression can be deduced

$$k_{\text{H}}/k_{\text{D}} = 0.95e^{1000/RT}$$

where k_{H} and k_{D} stand for the relative rates of formation of C_2D_4 and $\text{C}_2\text{D}_3\text{H}$ per β -deuterium atom, respectively.

It is of interest to note that this rate expression is very similar to the one obtained by Blades and Gilder-son⁴ in their investigation of the gas-phase pyrolysis of $\text{CH}_3\text{COOCD}_2\text{CD}_2\text{H}$

$$k_{\text{H}}/k_{\text{D}} = 0.99e^{1145/RT}$$

Similarly, the liquid phase photolysis of $\text{CH}_3\text{COCH}_2\text{CHD}_2\text{H}$ yielded a value of 1.15 ± 0.15 kcal./mole for the difference in activation energy between the transfer of a D and H-atom.³ The actual values of $\text{C}_2\text{D}_3\text{H}/\text{C}_2\text{H}_2\text{D}_2$ obtained in photolysis of this ketone,

(19) At 2200 Å. the extinction coefficients of the two compounds do not differ by more than 5% as measured on a Cary-15 spectrophotometer. The quenching cross sections in mercury sensitized decomposition have not been determined.

at a given temperature, agree closely with the ratios C_2D_4/C_2D_3H given in Table II. These similarities are not unexpected if one considers that in all cases, decomposition occurs by way of a similar six-centered intermediate. The actual mechanism of this process in the pyrolysis has been discussed in detail by Blades and Gilderson.⁴

In the vapor phase photolysis of $CH_3COOCD_2CD_2H$, the effect of temperature on the ratio C_2D_4/C_2D_3H is much less pronounced than in the liquid phase. This is not surprising in view of the fact that in the vapor phase, as indicated by the wave length effect, collisional degradation of the vibrational energy levels is not as effective as in the liquid phase. It obviously may be expected that the magnitude of the temperature effect diminishes with a decrease of the incident wave length.³

$CH_3COOC_2H_5-CH_3COOC_2D_5$ (1:1).—The data of Table II demonstrate that there exists a considerable intermolecular isotope effect. In view of the fact that at 273 and 193°K., the values obtained for the ratio C_2H_4/C_2D_4 in the photolysis of equimolar mixtures of $CH_3COOC_2H_5$ and $CH_3COOC_2D_5$ are the same as those which can be deduced from the yields of ethylene observed in the photochemical decomposition of $CH_3COOC_2H_5$ and of $CH_3COOC_2D_5$, it may be concluded that the intermolecular isotope effects are not due to a transfer of energy from $CH_3COOC_2D_5$ to $CH_3COOC_2H_5$.

A comparison of the ethylene yields given in Table II shows that below 273°K., the magnitude of the effect of temperature on the relative quantum yields of the intramolecular processes varies according to the following sequence



This trend probably is related to a difference in activation energy of decomposition between the various excited molecules, which can be accounted for qualitatively by considering the C–H and C–D bond strengths and the number of β -deuterium and hydrogen atoms in the molecule. This interpretation is substantiated by the observation that biacetyl quenches the decomposition of $CH_3COOC_2D_5$ more strongly than that of $CH_3COOC_2H_5$. The higher activation energy for the decomposition of the deuterium labeled compound implies a longer dissociative lifetime and a larger probability to take part in energy transfer processes.

In this connection it may be noted that the more pronounced quenching effect of oxygen on the photochemical decomposition of $CH_3COCH_2CHD_2H$ ³ as

compared to $CH_3COC_3H_7$, also has been ascribed to a longer dissociative lifetime of the labeled compound.

It may finally be pointed out that the decrease of the relative quantum yield of ethylene in the liquid photolysis of ethyl acetate and 2-pentanone³ clearly demonstrates that besides cage effects, deactivation processes have to be considered as well to account for the low quantum yields of the dissociative processes in some of the compounds containing carbonyl.

(C) Solid Phase.—The results of Table III show that although the values of the ratio C_2D_4/C_2D_3H obtained in the solid phase photolysis of $CH_3COOCD_2CD_2H$ at 77°K. are larger than those obtained in the liquid phase, they are considerably smaller than the expected value of 330 which can be extrapolated from the liquid phase data. The fact that the intermolecular isotope effect is also considerably lower than may be predicted from a consideration of the liquid phase data indicates that a hindered rotation cannot entirely account for the low intramolecular isotope effect. Apparently, an ineffective collisional deactivation prior to decomposition could explain the observed trends. In agreement with this interpretation is the significant observation that the quantum yield of the formation of ethylene is not greatly affected by a decrease in temperature from 77 to 4°K., indicating that the energy requirement for decomposition observed in the liquid phase is of less importance in the solid phase. More direct evidence for a less efficient energy degradation in the solid phase as compared to the liquid phase follows from the observed effect of wave length on the solid phase photolysis of $CH_3COCH_2CHD_2H$.²⁰ These experiments show that in contrast with the liquid phase data,³ the intramolecular isotope effect varies with wave length, and actually, just as in the gas phase, increases with increase in wave length.

The lowering of the intra- and intermolecular isotope effects with a decrease of the temperature of irradiation probably is indicative of a less efficient energy transfer. The fact that at constant irradiation temperature but for different temperatures of deposition similar trends are observed demonstrates that besides the irradiation temperature the structure of the solid may also affect the intramolecular isotope effect.

(20) It should be noted that the appearance of non-condensable products in the solid phase photolysis of ethylacetate at 4°K. implies that at this temperature some of the ethylene may eventually be produced by secondary radical reactions. The ketone experiments have been carried out for comparison because in this case no other products have been observed besides ethylene, acetone, and 1-methylcyclobutanol. Also, the absence of ethyl radicals in the photolysis of 2-pentanone excludes the formation of ethylene by radical disproportionation reactions.

THE REACTIONS OF METHYL RADICALS WITH AROMATIC COMPOUNDS. I. TOLUENE, ETHYLBENZENE, AND CUMENE¹

BY ISABEL B. BURKLEY² AND R. E. REBBERT²

Chemistry Department, Georgetown University, Washington, D. C.

Received July 16, 1962

Acetone was photolyzed in the presence of toluene, ethylbenzene, and cumene between 80 and 250° in the gas phase. The activation energies for the reactions of the type $\text{CH}_3 + \text{RH} \rightarrow \text{CH}_4 + \text{R}$ are 7.4 ± 0.3 , 7.0 ± 0.3 , and 6.4 ± 0.5 kcal./mole, respectively. The difference in the activation energy for the abstraction of a primary hydrogen compared to a tertiary hydrogen both alpha to a benzene ring is much smaller than in the corresponding aliphatic hydrocarbons.

Introduction

In the past ten years, a considerable amount of effort has been expended in measuring the rate constants and activation energies for the hydrogen abstraction reactions of the methyl radical.³ So far, the published works have not dealt to any great extent with the hydrogen abstraction from aromatic compounds except benzene and toluene. The present investigations were undertaken with a view toward including in the available literature a better representation of aromatic compounds. Toluene, ethylbenzene, and cumene were chosen so that the activation energies and rate of hydrogen abstractions from primary, secondary, and tertiary positions alpha to the benzene ring could be determined for the methyl radical. In the case of aliphatic hydrocarbons, the activation energies for reactions of this type are approximately 10.0, 8.0, and 7.0 kcal./mole, respectively.³

Experimental

Apparatus.—A conventional vacuum apparatus was used. A cylindrical quartz reaction cell (186 cc.) was placed inside an aluminum block furnace. The maximum temperature variation along the cell was 2.5°. The connecting tubing was heated to 100° and the pressure was measured by means of an all-glass spoon gage in conjunction with a mercury manometer. A glass covered iron plunger was manipulated manually to ensure good mixing of the two compounds which were introduced into the reaction cell.

A Hanovia S-100 medium pressure mercury arc was the light source. No filters were used. The beam was roughly collimated with an aluminum pipe.

Analysis.—Methane, ethane, and carbon monoxide were analyzed by means of a Ward still,⁴ gas buret, and copper oxide furnace. Carbon monoxide and methane were distilled over at -196° and measured together. The carbon monoxide was oxidized to carbon dioxide in the copper oxide furnace and the carbon dioxide was condensed in liquid nitrogen. The methane then was measured and the amount of carbon monoxide was the difference in the two measurements. Ethane was brought over at -170°. No more than 3% of the acetone was decomposed during any experiment.

Materials.—The acetone used in this study was Mallinckrodt analytical reagent grade. Impurities were stated to be less than 0.06%, mainly in the form of methanol. The acetone was introduced into the vacuum system and thoroughly degassed.

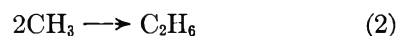
The toluene was Phillips research grade and was stated to be 99.96 mole % pure.

The ethylbenzene and cumene were standard samples from the National Bureau of Standards and were listed as 99.96 ± 0.02 and 99.93 ± 0.03 mole % pure, respectively.

Results

When acetone is photolyzed in the presence of a

hydrocarbon, the following reactions account for the formation of methane and ethane



If we assume that these are the only reactions forming methane and ethane, we have

$$\frac{R_{\text{CH}_4}}{R_{\text{C}_2\text{H}_6}^{1/2}} = \frac{k_1}{k_2^{1/2}} [\text{CH}_3\text{COCH}_3] + \frac{k_3}{k_2^{1/2}} [\text{RH}]$$

where R_{CH_4} and $R_{\text{C}_2\text{H}_6}$ are the rates of formation of methane and ethane, respectively. The ratio $k_1/k_2^{1/2}$ was determined by photolyzing acetone by itself. Since all other parameters are measurable, the above equation can be used to calculate $k_3/k_2^{1/2}$.

In the present investigation the results of the photolysis of acetone alone gave the following straight line which was determined by the method of least squares

$$13 + \log \frac{k_1}{k_2^{1/2}} = 6.130 - \frac{2171}{T}$$

All rate constants are in molecules, cubic centimeters, and seconds. This equation corresponds to an acti-

TABLE I

Temp., °K.	[Acetone] [RH]			Time, sec.	(μmoles)			CH ₄ + C ₂ H ₆ CO	$\frac{k_3}{k_2^{1/2}} \times 10^{13}$ cc. ^{1/2} molecules ^{-1/2} sec. ^{-1/2}
	Temp., °K.	(μmoles/ cc.)	Time, sec.		CO	CH ₄	C ₂ H ₆		
Toluene									
372.7	2.01	1.40	900	7.58	0.80	6.95	1.02	3.90	
395.6	2.05	2.00	900	8.99	1.79	6.96	0.97	6.19	
423.9	1.93	2.03	900	9.02	3.12	5.65	0.97	13.2	
447.8	2.03	1.32	900	9.34	4.48	5.27	1.04	17.0	
482.8	1.97	1.30	900	9.22	7.60	3.21	1.17	37.5	
502.3	2.04	1.33	900	9.02	9.02	2.02	1.22	52.8	
526.0	1.91	1.31	900	8.99	9.64	1.18	1.20	66.4	
Ethylbenzene									
358.0	1.80	1.80	3600	4.77	2.51	3.26	1.21	11.0	
360.1	2.15	2.08	900	4.87	1.66	3.59	1.08	11.6	
370.3	2.03	1.74	900	7.71	2.10	5.99	1.05	13.3	
384.2	1.85	1.85	9144	5.72	2.52	3.69	1.09	19.2	
393.8	2.16	2.15	900	8.00	4.02	4.70	1.09	23.0	
403.9	2.02	2.02	900	5.53	3.82	2.80	1.20	29.9	
429.4	1.96	1.96	900	10.28	7.18	3.99	1.09	45.9	
449.8	2.00	2.09	900	11.65	9.80	2.69	1.07	70.7	
455.5	2.04	2.04	900	5.93	7.38	1.18	1.45	81.9	
Cumene									
396.2	2.00	1.12	900	8.71	2.91	4.74	0.88	42.5	
413.6	1.97	1.44	900	7.10	5.32	3.36	1.22	53.0	
420.6	2.04	1.26	900	8.07	6.37	3.72	1.25	67.3	
443.3	1.97	0.89	900	7.47	7.02	2.68	1.30	114	
475.0	2.12	1.33	900	8.86	11.14	1.60	1.44	151	
500.4	2.01	0.71	900	8.71	10.73	1.22	1.37	255	
522.0	1.97	0.90	900	7.87	11.82	0.58	1.58	339	

(1) Abstracted from a thesis submitted to the Graduate School of Georgetown University in partial fulfillment of the requirements of the M.S. degree.

(2) Division of Physical Chemistry, National Bureau of Standards, Washington 25, D. C.

(3) A. F. Trotman-Dickenson, *Quart. Rev.*, **7**, 198 (1953).

(4) D. J. LeRoy, *Can. J. Res.*, **B28**, 492 (1950).

vation energy of 9.9 kcal./mole for $E_1 - \frac{1}{2}E_2$, compared to 9.7 kcal./mole reported by Trotman-Dickenson and Steacie.⁵ The results of the photolysis of acetone in the presence of toluene, ethylbenzene, and cumene are given in Table I. The following equations also obtained by the method of least squares give the best straight lines through the experimental points

$$\text{For toluene: } 13 + \log k_3/k_2^{1/2} = 4.913 - \frac{1620}{T}$$

$$\text{For ethylbenzene: } 13 + \log k_3/k_2^{1/2} = 5.260 - \frac{1527}{T}$$

$$\text{For cumene: } 13 + \log k_3/k_2^{1/2} = 5.197 - \frac{1407}{T}$$

The activation energies for the hydrogen abstraction reactions are 7.4 ± 0.3 , 7.0 ± 0.3 , and 6.4 ± 0.5 kcal./mole, respectively. These results of course assume zero activation energy for the recombination of two methyl radicals. The limits of precision of the activation energies were calculated from the average deviation of the experimental points.

Discussion

It is assumed throughout this discussion that the methyl radical abstracts the hydrogen atom in the aliphatic side chain alpha to the benzene ring and that it does not abstract the hydrogen atom within the ring to any great extent. The reasonableness of this assumption is based on the following.

(1) The activation energy for abstracting a hydrogen atom from benzene is 9.2 kcal./mole³ compared to 7.4 or less for the three aromatic compounds mentioned in this paper. Moreover, the ratio k_3 (toluene)/ k_3 (benzene) at 182° is 11.6 and even greater for ethylbenzene and cumene.

(2) The ratio of rates $k_3/k_2^{1/2}$ per active hydrogen atom increases by a factor of 5.7 from toluene to ethylbenzene and by a factor of 3.2 from ethylbenzene to cumene. Changes in rate of this order of magnitude are expected in these cases for abstraction from the side chains but not for abstraction from the ring.

(3) Berezin, Kazanskaya, and Martinek⁶ have shown that the ratio of the rate of abstraction of a tritium atom in the side chain compared to the rate of abstraction from the *para* position in the ring in toluene is 156 at 85°. The difference in activation energy for these two reactions is 2.6 kcal./mole. These results were obtained by the thermal decomposition of acetyl peroxide which was dissolved in toluene over the temperature range from 60 to 96°.

Recently some evidence for the abstraction of a hydrogen atom from the ring has appeared in the literature.^{7,8} In these cases toluene- α - d_3 was used

(5) A. F. Trotman-Dickenson and E. W. R. Steacie, *J. Chem. Phys.*, **18**, 1097 (1950).

(6) I. V. Berezin, N. F. Kazanskaya, and K. Martinek, *Zh. Obshch. Khim.*, **30**, 4092 (1960).

to show that hydrogen abstraction from the ring occurs. This is not too surprising since all this work was done in the liquid phase where it is known that methyl radicals add to the benzene ring.⁹ Thus hydrogen abstraction from the ring probably occurs after addition as has been suggested by Levy, Steinberg, and Szwarc¹⁰ as well as others. However, in our work in the gas phase, a methyl radical addition to the benzene ring cannot be occurring to any large extent. It probably occurs to a minor extent. If radical addition occurs to a large extent in the gas phase, the equation for the material balance, $(\text{CH}_4 + \text{C}_2\text{H}_6)/\text{CO}$, should fall below unity. In fact, this ratio usually is greater than one, especially at the higher temperatures. This can be accounted for by the reactions



At low temperature the steady-state concentration of R is low and R is lost by the recombination reaction (4). Thus, the ratio $(\text{CH}_4 + \text{C}_2\text{H}_6)/\text{CO}$ is near one. At higher temperatures, the steady-state concentration of R increases and some of the radicals, R, are lost by the recombination reaction 5. The net effect is to increase the ratio of $(\text{CH}_4 + \text{C}_2\text{H}_6)/\text{CO}$.

It is interesting to compare the reactions of methyl radicals with aromatic compounds to the reactions of the perfluoromethyl radicals. Whittle and co-workers¹¹ have shown that the perfluoromethyl radicals add very easily to the benzene ring in the gas phase and that abstraction from the ring probably occurs through the addition product. As mentioned previously, there is no evidence in our results which would indicate that methyl radicals add to the benzene ring in the gas phase to any large extent.

As in the case of aliphatic hydrocarbons, the activation energy for the abstraction of hydrogen atom decreases in the sequence primary, secondary, tertiary, while the rate of reaction increases for the same sequence. However, it is to be noted that the effect of the attached phenyl group is so strong that the difference in activation energy and in rate constant from the primary to tertiary compound is small compared to the same reactions in aliphatic compounds. There is only a 1.0 kcal./mole difference in activation energy for aromatic compounds compared to 3.0 kcal./mole for aliphatic compounds. Moreover, the ratio of the rate of abstraction from tertiary to primary compound is about 18 for aromatic compounds while it is 50 for aliphatic compounds.

(7) S. H. Wilen and E. L. Eliel, *J. Am. Chem. Soc.*, **80**, 3309 (1958).

(8) J. H. T. Brook and R. W. Glazebrook, *Trans. Faraday Soc.*, **56**, 1014 (1960).

(9) R. P. Buckley, F. Leavitt, and M. Szwarc, *J. Am. Chem. Soc.*, **78**, 5557 (1956).

(10) M. Levy, M. Steinberg, and M. Szwarc, *ibid.*, **76**, 3439 (1954).

(11) S. W. Charles and E. Whittle, *Trans. Faraday Soc.*, **56**, 794 (1960); S. W. Charles, J. T. Pearson, and E. Whittle, *ibid.*, **57**, 1356 (1961).

THE REACTIONS OF METHYL RADICALS WITH AROMATIC COMPOUNDS. II. THE XYLENES¹

BY WILLIAM A. SANDERS AND R. E. REBBERT²

Chemistry Department, Georgetown University, Washington 7, D. C.

Received July 30, 1962

Acetone was photolyzed in the presence of the *p*-, *o*-, and *m*-xylenes between 100 and 200°. The activation energies for the reactions of the type $\text{CH}_3 + \text{RH} \rightarrow \text{CH}_4 + \text{R}$ are 7.4 ± 0.2 , 7.8 ± 0.3 , and 8.5 ± 0.3 kcal./mole, respectively. The observed order of the activation energies for the three xylenes is consistent with a hyperconjugation mechanism. It should be noted that the pre-exponential factors for the three xylenes are not constant but vary by a factor of four.

Introduction

As in part I,³ this investigation was undertaken so that a better representation of the rates of hydrogen atom abstraction by methyl radicals from aromatic compounds would be available. The xylenes were chosen so that the effect of the *para*-, *ortho*-, and *meta*-substitutions could be determined. The observed activation energies should give some indication of the C-H bond strength of the molecule from which the hydrogen atom is abstracted. Szwarc⁴ has determined the bond dissociation energies for the hydrogen atom on the methyl groups of the *p*-, *o*-, and *m*-xylenes to be 75.0, 74.0, and 77.5 kcal./mole, respectively.

Experimental

The same apparatus and general procedure as described in part I³ were used. The *p*- and *o*-xylenes were standard samples from the National Bureau of Standards. The *m*-xylene was Phillips Petroleum research grade.

Results

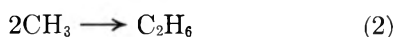
The results of the photolysis of acetone in the presence of the three xylenes are given in Tables I and II. The following equations obtained by the least squares method give the best straight lines through the experimental points

$$\text{For } p\text{-xylene: } 13 + \log \frac{k_3}{k_2^{1/2}} = 5.262 - \frac{1619}{T}$$

$$\text{For } o\text{-xylene: } 13 + \log \frac{k_3}{k_2^{1/2}} = 5.566 - \frac{1712}{T}$$

$$\text{For } m\text{-xylene: } 13 + \log \frac{k_3}{k_2^{1/2}} = 5.886 - \frac{1863}{T}$$

All rate constants are in molecules, cubic centimeters, and seconds; k_3 and k_2 refer to reactions 2 and 3 of part I



The activation energies for the hydrogen abstraction reactions are 7.4 ± 0.2 , 7.8 ± 0.3 , and 8.5 ± 0.3 kcal./mole, respectively, for *p*-, *o*-, and *m*-xylenes. The pre-exponential factors, $A_3/A_2^{1/2}$, for these three reactions are $1.8 \pm 0.5 \times 10^{-8}$, $3.7 \pm 1.5 \times 10^{-8}$, and $7.7 \pm 1.6 \times 10^{-8}$ molecule^{-1/2} cc.^{1/2} sec.^{-1/2}. The limits of precision of the activation energies and the

pre-exponential factors were calculated from the average deviation of the experimental points.

TABLE I

Temp., °K.	Ace- tone pres- sure, mm.	Xylene pres- sure, mm.	Time, sec.	Product molecules cc.-sec. $\times 10^{-13}$			CH ₄ + C ₂ H ₆ CO	$k_3/k_2^{1/2}$ $\times 10^{13}$, cc. ^{1/2} mole- cules ^{1/2} - sec. ^{1/2}
				CO	CH ₄	C ₂ H ₆		
<i>p</i> -Xylene								
372.0	44.3	49.3	900	2.73	0.56	1.91	0.91	8.3
395.6	46.7	45.6	900	3.11	0.99	2.12	1.00	14.8
417.7	49.0	48.1	900	3.47	1.62	2.04	1.05	23.5
447.5	52.3	48.5	900	3.82	2.72	1.62	1.14	44.0
469.5	53.9	44.9	900	4.01	3.47	1.27	1.18	66.7
<i>o</i> -Xylene								
374.3	43.1	46.1	900	2.50	0.60	1.77	0.95	10.1
397.2	46.3	50.2	900	2.86	1.10	1.85	1.03	16.8
421.5	45.9	40.7	900	3.53	1.69	1.80	0.99	32.0
428.8	47.6	25.7	900	3.81	1.69	2.23	1.03	40.3
452.5	51.3	42.7	900	3.55	2.79	1.39	1.18	56.4
467.2	57.0	44.7	900	3.71	3.37	0.96	1.17	79.4
477.6	52.1	28.8	900	3.57	3.14	1.03	1.17	98.1
<i>m</i> -Xylene								
373.1	44.8	56.6	900	2.00	0.52	1.34	0.93	8.0
399.0	46.1	47.2	900	2.39	0.93	1.45	1.00	16.5
421.5	48.7	53.0	900	2.64	1.54	1.19	1.03	27.9
447.4	52.6	51.9	900	2.87	2.39	0.91	1.15	51.7
469.6	54.3	43.8	900	2.76	2.70	0.56	1.18	86.3

TABLE II

Compound	$k_3/k_2^{1/2}$ $\times 10^{13}$ (at 182°)	$A_3 \times 10^8 / A_2^{1/2}$	$E_3 - 1/2 E_2$
<i>p</i> -Xylene	50.8	1.8 ± 0.5	7.4 ± 0.2
<i>o</i> -Xylene	63.6	3.7 ± 1.5	$7.8 \pm .3$
<i>m</i> -Xylene	62.1	7.7 ± 1.6	$8.5 \pm .3$
Toluene ³	22	0.8	7.4

Discussion

Insofar as the activation energies of the hydrogen abstraction reactions by methyl radicals are related to the C-H bond dissociation energies, the results indicate that the bond dissociation energies of the hydrogen atom on the methyl group of the xylenes should follow the order *para*, *ortho*, *meta* from the lowest to the highest. Szwarc⁴ has studied the kinetics of this pyrolysis of the xylenes by his toluene carrier technique. He reported the following values of the bond dissociation energies of a hydrogen atom from the methyl group: 75.0, 74.0, and 77.5 kcal./mole, respectively, for *p*-, *o*-, and *m*-xylenes. In support of the order indicated by his results, Szwarc cited the work of Dobryanskii and Saprykin,⁵ who studied the isom-

(5) A. F. Dobryanskii and F. Y. Saprykin, *J. Gen. Chem. (USSR)*, **9**, 1313 (1939).

(1) Abstracted from a thesis submitted to the Graduate School of Georgetown University in partial fulfillment of the requirements of the M.S. degree.

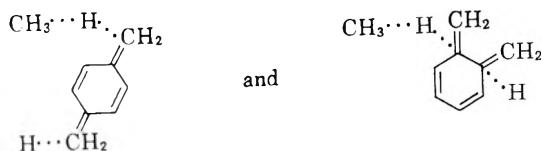
(2) Division of Physical Chemistry, National Bureau of Standards, Washington 25, D. C.

(3) I. B. Burkley and R. E. Rebbert, *J. Phys. Chem.*, **67**, 168 (1963).

(4) M. Szwarc, *J. Chem. Phys.*, **16**, 128 (1948); **16**, 637 (1948).

erization of the xylenes. They found that the *ortho* isomer isomerized most readily, while the *meta* isomer showed no tendency to isomerize and the *para* isomer was between the two. Although the experimental error in our results (about 0.2 kcal./mole) leaves the *para-ortho* order somewhat uncertain, two other investigators in our Laboratory^{6,7} have found this same order with the fluorotoluenes and the ethyltoluenes.

The order for the activation energy of the hydrogen abstraction reaction increasing from the *para* to *meta* isomer can be explained on the assumption that a hyperconjugation mechanism is involved in the stabilization of the transition state complex. Szwarc⁴ originally put forth this explanation in his study of the kinetics of the pyrolysis of the xylenes. Thus, for *p*- and *o*-xylenes we can write the resonance structures



No such structure can be written for the *meta*-isomer. Moreover, there is the possibility that there is some steric hindrance in the transition state complex of the *o*-xylene structure which lessens the full effect of the hyperconjugation. In this regard, it is interesting to note that for the fluorotoluenes the activation energies for the *ortho* and *para* isomers are relatively closer to one another and farther from the *meta* isomer.⁶ In the case of the ethyltoluenes just the opposite is true, that is, the activation energies for the *ortho-meta* isomers are closer together and farther from the *para* isomer.⁷ If steric hindrance is the reason for the difference in activation energy between the *ortho* and *para* isomers, a smaller difference would be expected with the fluorotoluenes and a larger one with the ethyltoluenes.

It is interesting to compare the results of this investigation with the data obtained from studies of the analogous reaction with toluene. In Table II a sum-

(6) F. J. Wunderlich and R. E. Rebbert, to be published.

(7) I. B. Burkley, Ph.D. Thesis, 1962, Georgetown University.

mary of these results is given. The ratio of rate constants of the xylenes to toluene amounts to somewhat more than the statistical factor of two which may have been expected if the only change were the presence of an additional methyl group.

Throughout this paper we have assumed that it is the hydrogen atom on the methyl groups which are abstracted and not the hydrogen atoms on the benzene ring. The reasons for this assumption were given in part I.³ It should also be mentioned that for all three xylenes a positive deviation was noticed above 200°. However, the amounts of ethane produced at these high temperatures are very small. This makes accurate measurements difficult, since a small absolute error in the ethane measurement would produce a large error in the rate constant. A more recent investigation⁷ of the *o*- and *m*-xylenes with acetone-*d*₆ did not show any curvature in the Arrhenius plots up to 275°. In this case, the ratio of CD₃H/CD₄ was measured on a mass spectrometer and the results, therefore, should be more accurate.

Finally, it should be pointed out that the pre-exponential factors for these three very similar reactions are quite different. As seen in Table II, the pre-exponential factors vary by a factor of four from *p*- to *m*-xylene. Again this same variation in pre-exponential factors was obtained by two other investigators with the fluorotoluenes⁶ and the ethyltoluenes.⁷ The consistency of these three investigations rules out experimental error as the cause of these differences in the pre-exponential factors. Although at the present time we have no explanation for these differences, it is important to note that the pre-exponential factors are different since in the past many authors have assumed constant pre-exponential factors for similar reactions. Thus, they have calculated activation energies from rate constants at one temperature. Activation energies so obtained may be considerably in error.

It is interesting to note that the activation energy and the pre-exponential factor for *p*-xylene are almost the same as those obtained for toluene itself,³ while the *ortho* and *meta* isomers have higher activation energies and also higher pre-exponential factors. It is not immediately obvious why this should be.

THE ACTIVE NITROGEN AFTERGLOW AND THE QUENCHING EFFECT OF ADDED AMMONIA^{1,2}

BY A. N. WRIGHT³ AND C. A. WINKLER

Upper Atmosphere Chemistry Research Group, Physical Chemistry Laboratory, McGill University, Montreal, Canada

Received July 23, 1962

The intensity of light emission in the visible region, and for emission from the 11th and 6th vibrational levels of $N_2(B^3\Pi_g)$, varies linearly with the square of the N atom concentration in such a way as to suggest that collision with an unpoisoned Pyrex wall may induce transition from the $^5\Sigma_g^+$ state to the B state at vibrational levels less than eleven. The results further suggest that as many as 10^6 collisions with $N_2(X^1\Sigma_g^+)$ may be necessary to induce the conversion of the quintet state of nitrogen to a triplet state capable of causing light emission. When NH_3 is added to active nitrogen in an unpoisoned system, its effect on light emission in the first positive system is complicated by the role of NH_3 as an effective wall poison against surface recombination of N atoms, as well as its quenching action in the gas phase. However, in a system well poisoned against surface recombination, the quenching effect of NH_3 on light emission over the visible region, and particularly in the 5820 and 6630-Å. regions, suggests that NH_3 deactivates the quintet state of nitrogen with a collision efficiency of about 10^{-6} . The quenching efficiency of NH_3 for $N_2(^5\Sigma_g^+)$ is reduced in the presence of significant concentrations of $N_2(A^3\Sigma_u^+)$, and it appears that most chemical decomposition of NH_3 is induced by a collision of the Second Kind with the A state molecule.

Introduction

It has been established conclusively^{4,5} that the intensity of the Lewis-Rayleigh nitrogen afterglow, for total emission and also for emission from the 11th or 6th vibrational levels of the $B^3\Pi_g$ state, depends on the square of the concentration of N(⁴S). The characteristic vibrational distribution of the $N_2(B^3\Pi_g \rightarrow A^3\Sigma_u^+)$ 1st positive bands appears to remain unchanged during 140 sec. of decay,⁶ and the infrared, vacuum ultraviolet, and visible afterglows all decay⁷ identically with time. Although nitrogen atom concentrations were not determined in the recent studies in static systems,⁶⁻⁸ they were estimated at a point downstream in some of the studies⁴ that have been made in flow systems, in which the afterglow intensities were measured by viewing longitudinally^{4,9,10} a decay tube of at least 25-cm. length.

Recent work¹⁰ supports the postulate^{4,11} that ⁴S nitrogen atoms first recombine to form weakly bound $^5\Sigma_g^+$ nitrogen molecules as a stable intermediate in the emission of the afterglow, and these then populate directly the $v = 12, 11, 10$ (group 1) levels of the B state through a radiationless collision-induced transition. On the other hand, the strong emission from the lower vibrational levels of the $B^3\Pi_g$ state, *i.e.*, $v = 7, 6, 5$ (group 4) and $v = 4$ (groups 3a and 3b), appears to arise from population of these levels of the B state through intermediate electronic states of lower energy content than $^5\Sigma_g^+$. Bayes and Kistiakowsky have pointed out¹⁰ that further progress in elucidating the initial steps of the afterglow mechanism requires experiments in which the nitrogen atom concentration and

the intensities in the afterglow spectrum are simultaneously measured.

The intensity of the afterglow in active nitrogen produced by a microwave discharge is quenched¹² by the addition of NH_3 , especially¹⁰ the bands originating from the lowest vibrational levels of the $B^3\Pi_g$ state. This interaction does not appear¹² to involve N atoms and the pressure dependence of the quenching efficiency of added NH_3 has been attributed¹⁰ to interaction between NH_3 and $N_2(^5\Sigma_g^+)$. On the other hand, the chemical decomposition of NH_3 , in active nitrogen produced by a condensed discharge,¹³⁻¹⁵ appears to be caused mainly by collisions between $N_2(A^3\Sigma_u^+)$ and NH_3 , with an over-all rate constant¹⁵ of about 10^{10} cc. mole⁻¹ sec.⁻¹. The reaction apparently does not involve N atoms,¹⁵ although the addition of NH_3 does quench the CN emission from the reactions of active nitrogen with many carbon-containing compounds.^{17,18} The negligible extent of NH_3 decomposition in active nitrogen of microwave origin has been attributed¹⁶ to the low concentration of N atoms, and hence low concentration of excited nitrogen molecules formed by atom recombination, in such systems.

The present paper reports measurements on the afterglow intensities at different levels in a flow system, corresponding to known times of decay of the active nitrogen, for a system in which values had previously been obtained for both the N-atom concentrations,¹⁵ and the concentrations of NH_3 left unreacted¹⁶ at these levels, for different initial flow rates of added NH_3 .

Experimental

The afterglow was monitored by a 1P21 photomultiplier tube used in conjunction with an Eldorado photometer. The phototube was mounted on guide rails inside a dark box constructed around a straight tube reaction vessel. This permitted positioning of the phototube, so as always to view the center of the reaction vessel at any level between 0.2 and 45 cm. below the reactant inlet. The nitrogen was activated by a condensed discharge and the linear flow rate of the gas through the cylindrical flow system

(1) This investigation was supported by the National Research Council of Canada and the Defence Research Board of Canada.

(2) Presented at the Edmonton Conference of the Chemical Institute of Canada, May 28, 1962.

(3) Postdoctoral Fellow.

(4) J. Berkowitz, W. A. Chupka, and G. B. Kistiakowsky, *J. Chem. Phys.*, **25**, 457 (1956).

(5) G. B. Kistiakowsky and P. Warneck, *ibid.*, **27**, 1417 (1957).

(6) R. A. Young and K. C. Clark, *ibid.*, **32**, 604 (1960).

(7) R. A. Young, *ibid.*, **33**, 1112 (1960).

(8) T. Wentink, Jr., J. O. Sullivan, and K. L. Wray, *ibid.*, **29**, 231 (1958).

(9) U. H. Kurzweg and H. P. Broida, *J. Mol. Spectroscopy*, **3**, 388 (1959).

(10) K. D. Bayes and G. B. Kistiakowsky, *J. Chem. Phys.*, **32**, 992 (1960).

(11) A. G. Gaydon, "Dissociation Energies and Spectra of Diatomic Molecules," Chapman and Hall, Ltd., London, 1953, 2nd Ed., p. 157; *Nature*, **153**, 407 (1944).

(12) G. B. Kistiakowsky and G. G. Volpi, *J. Chem. Phys.*, **28**, 665 (1958).

(13) G. R. Freeman and C. A. Winkler, *J. Phys. Chem.*, **59**, 371 (1955).

(14) R. Kelly and C. A. Winkler, *Can. J. Chem.*, **38**, 2514 (1960).

(15) A. N. Wright, R. L. Nelson, and C. A. Winkler, *ibid.*, **40**, 1032 (1962).

(16) A. N. Wright and C. A. Winkler, *ibid.*, **40**, 5 (1962).

(17) K. D. Bayes, *ibid.*, **39**, 1074 (1961).

(18) A. N. Wright and C. A. Winkler, *ibid.*, **40**, 1291 (1962).

was 478 cm. sec.⁻¹. All experiments were conducted at a pressure of 3 mm. and, in all other respects, the system was identical with that described previously.^{16,18} Experiments involving introduction of NH₃ were initiated after the condensed discharge had been allowed to operate for about 20 min., at which time the temperature of the active nitrogen had reached a maximum value, constant for about 5 min.

With suitable collimation by a pin hole through 1/4-in. thick lucite in front of the phototube, readings were obtained for the unfiltered afterglow that approached the upper limit of the photometer, while the readings in the presence of filters were always at least a factor of 10 higher than the background values. Although the afterglow emission is given by the photomultiplier in terms of "% transmission," and consequently offers only a measure proportional to the light intensity, the readings were all made under similar geometrical conditions and comparisons between them therefore are valid.

Optical filters, constructed by Spectrolab of California for transmission peaked at 5820 and 6630 Å., and with less than 25 Å. transmission widths, permitted⁴ intensity measurements of the emission centered about the 11th and 6th vibrational levels, respectively, of the B³Π state. Readings were made for the visible afterglow (unfiltered system) and at the two chosen wave lengths at selected positions for the unpoisoned Pyrex system and for the system when it was poisoned against atom recombination with a minute amount of water vapor.¹⁵ The photomultiplier readings decreased with time of operation of the condensed discharge but, after approximately 22 min., reached values that were constant for the subsequent 8 min. Only these steady values are recorded in the results. Similar readings were made, down to the 45-cm. level below the reactant inlet, in the presence of known amounts of added NH₃. The NH₃ flow was continued for as long as 2 min, *i.e.*, until three readings of the photomultiplier, spaced 30 sec. apart, were identical.

Results

Dependence of Afterglow Intensity on [N] in the Absence of NH₃.—Photomultiplier (PM) readings at the various levels may be compared with a measure of the N atom flow rates at the same levels, estimated from the extent of HCN production during the C₂H₄ reaction.¹⁵

For the unfiltered afterglow, plots of the PM readings against the square of the N atom flow rates yield reasonably straight lines, as expected (*cf.* Fig. 1A, for the poisoned system).¹⁹ These lines appear not to pass exactly through (0,0),²⁰ and therefore have been described (Table I) by parameters *a* and *b* in the linear equation

$$\text{PM readings} = a(\text{N atoms flow rate})^2 + b$$

For emission from *v* = 11 (5820 Å.) and from *v* = 6 (6630 Å.), the values of *a* and *b* for the straight lines obtained up to the 15 cm. level also are given in Table I. At levels above 15 cm., however, the PM readings fell off markedly, as shown by the typical data plotted in Fig. 1B and 1C for the poisoned system. This behavior was almost certainly due to an increase in the

(19) The vertical height of the larger symbol in these figures corresponds to the limits of variation of a considerable number of experiments, while the circles represent a single experiment. Note that the origin in these plots is not at (0,0).

(20) It is of interest that equally good straight lines may be obtained if the PM readings are plotted against the N atom flow rate as determined by the NO titration method,¹⁶ in which case there is a considerable intercept on the ordinate, the sign of which is different for the poisoned and unpoisoned systems. These intercepts are in agreement with the suggestion¹⁶ that the destruction of NO may be due to both N₂(A) and N atoms, with the concentration of N₂(A), relative to that of N atoms, increasing with decay time of the active nitrogen in an unpoisoned system. If the NO method indicates a considerable value for the N-atom flow rate after decay times for which it had, in fact, decreased to low values in the unpoisoned system, a negative intercept would result. On the other hand, the proportionately greater concentration of N₂(A) after shorter decay times¹⁶ in the poisoned system would tend to produce a line of too small slope, and hence extrapolate to a positive intercept.

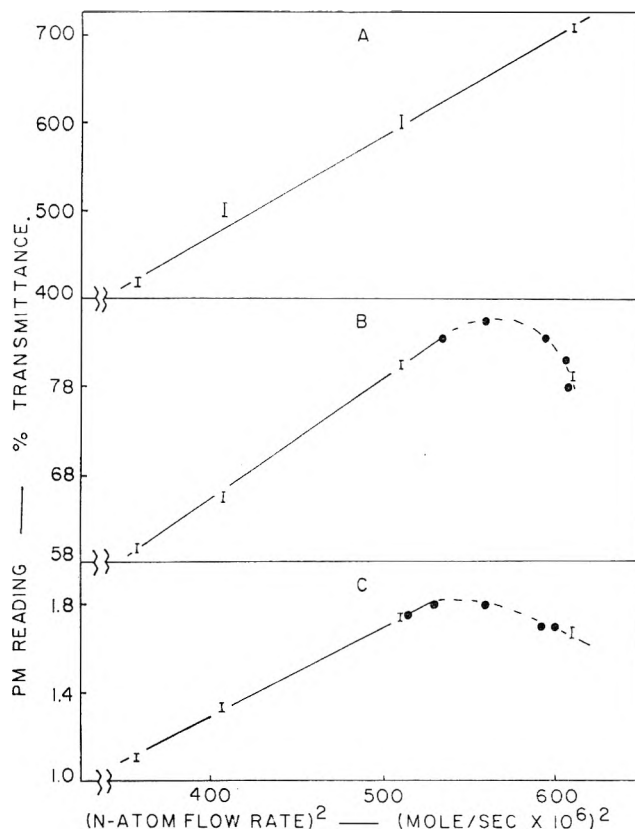


Fig. 1.—Plot of PM reading against the square of the N-atom flow rate, as given by HCN production from C₂H₄: A, unfiltered afterglow; B, afterglow at 5820 Å.; C, afterglow at 6630 Å.

surface:volume ratio in the flow system in the vicinity of the bulbous inlet jet in the active nitrogen stream.¹⁶

TABLE I
PARAMETERS FOR THE DEPENDENCE OF THE AFTERGLOW INTENSITY ON THE SQUARE OF THE N-ATOM FLOW RATE

	Slope <i>a</i> (% trans.) / (mole/sec. × 10 ⁻³) ²		Intercept <i>b</i> (% trans.)	
	Poisoned	Unpoisoned	Poisoned	Unpoisoned
Unfiltered afterglow				
HCN data	1.14	2.03	15.0	42.0
NO data	0.253	1.17	198	-104
Afterglow at 5820 Å.				
HCN data	0.137	0.328	10.3	0.70
Afterglow at 6630 Å.				
HCN data	4.14 × 10 ⁻³	5.48 × 10 ⁻³	-0.36	0.25

Quenching of the Afterglow in the Presence of NH₃.—The introduction of NH₃ invariably caused considerable decrease in the afterglow intensity in the poisoned system (Table II), but an increase in the PM reading (minus sign) frequently was observed in the unpoisoned system. While this increase may be explained in terms of a "poisoning" effect of added NH₃ (see Discussion), the behavior renders uncertain any estimate of the quenching influence of NH₃ in the unpoisoned system, and such efforts have been limited, therefore, to the poisoned system.

The quenching efficiency of NH₃ in the poisoned system may be determined from the dependence of the ratio *I*₀/*I* upon the amount of NH₃ present, where *I*₀ and *I* are the PM readings in the absence and presence of NH₃, respectively. The flow rates of NH₃ unreacted at various levels, for different initial flow rates of NH₃, were obtained from the results of the earlier study¹⁶ and were expressed in terms of concentrations by an appropriate factor (3.79 × 10⁻⁴ sec. cc.⁻¹). Good

TABLE II
DECREASE IN PM READINGS (% TRANSMISSION) AT THE DIFFERENT LEVELS IN THE PRESENCE OF ADDED NH₃

Initial NH ₃ flow rate, mole sec. ⁻¹ × 10 ⁶	Unfiltered afterglow				Afterglow at 5820 Å.						Afterglow at 6630 Å.			
	0.5 cm.	15 cm.	30 cm.	45 cm.	0.2 cm.	2 cm.	5 cm.	15 cm.	30 cm.	45 cm.	0.5 cm.	15 cm.	30 cm.	45 cm.
	Unpoisoned system													
0 ^a	270	240	160	120	26.5	31.5	31.0	26.0	19.0	13.5	0.70	0.66	0.55	0.45
2.5	-5	-50	-60	-85	1.0	-1.0	-2.0	-5.0	-5.0	-10.5	.05	-0.06	-.07	-.10
6.1	25	-30	-40	-60	5.0	3.5	2.0	-1.5	-2.0	-5.5	.10	0	-.01	-.03
8.0	40	-30	-25	-45	7.0	6.5	4.0	0	0	-4.0	.15	0.04	.05	0
12.5	50	0	-10	-25	10.5	9.5	7.0	2.5	2.5	-1.0	.20	0.08	.09	0
	Poisoned system													
	0.5 cm.													
0 ^a	710	595	510	420	81.0	80.5	64.5	59.5	1.65	1.70	1.35	1.10
2.5	40	45	55	50	7.5	9.0	7.5	8.0	0.15	0.10	0	0
6.1	90	80	110	100	16.0	15.0	16.0	17.0	.30	.25	0.20	0.15
8.0	105	100	130	110	20.0	17.5	19.5	19.5	.40	.30	.30	.20
12.5	150	130	170	140	27.0	22.5	26.0	24.5	.55	.35	.40	.30

^a Values at 0 flow rate of NH₃ correspond to the PM reading in the absence of NH₃. This reading was reproduced prior to introduction of NH₃ and within 4 minutes of turning off the NH₃ flow.

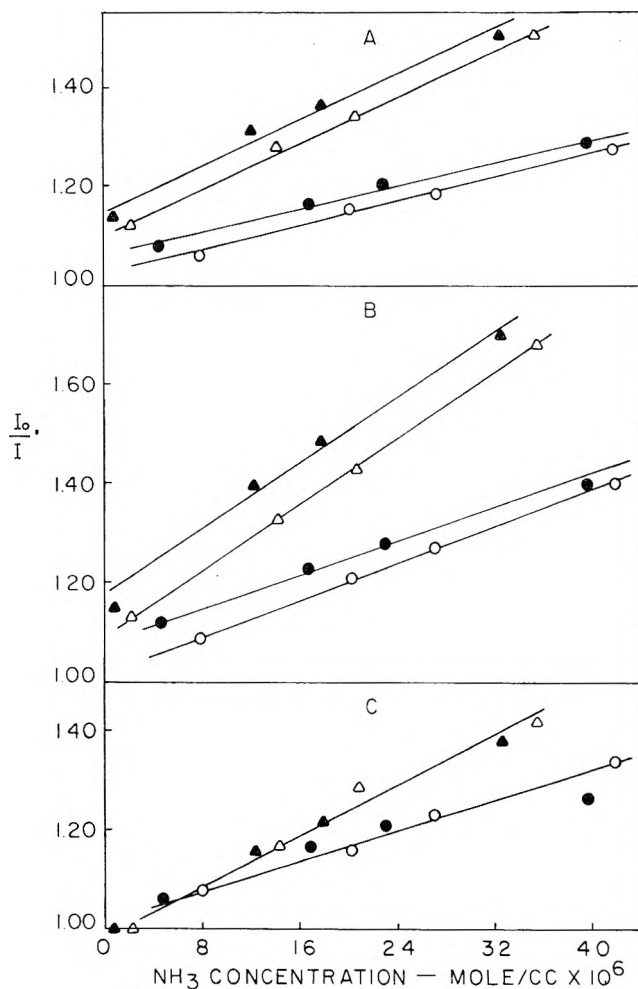


Fig. 2.—Plot of I_0/I against the concentration of NH₃ left unreacted at the levels: ○, 0.5 cm.; ●, 15 cm.; △, 30 cm.; ▲, 45 cm. Subdivided for the spectral conditions: A, unfiltered afterglow; B, afterglow at 5820 Å.; C, afterglow at 6630 Å.

straight lines were obtained when I_0/I values at a given level were plotted against the corresponding concentrations of unreacted NH₃ in the system, as shown in Fig. 2A (unfiltered afterglow), Fig. 2B (afterglow at 5820 Å.), and Fig. 2C (afterglow at 6630 Å.).²¹ The slopes of these straight lines are summarized in Table III.

For both the unfiltered afterglow, and the selected wave lengths, the slopes (quenching efficiencies) are quite similar at the 0.5 and 15-cm. levels, but increase to a considerably higher value for the 30 and 45-cm. levels.

TABLE III
SLOPES OF I_0/I AGAINST CONCENTRATION OF UNREACTED NH₃ AT THE VARIOUS LEVELS

Level (cm.)	Unfiltered afterglow	Afterglow at 5820 Å.	Afterglow at 6630 Å.
0.5	5.8 ^a	9.2	7.9
15	5.8	8.4	
30	11	16	12
45	11	17	

^a Units are cc./mole × 10⁷.

The variation in I_0/I with distance below the NH₃ inlet depends strongly upon the initial concentration of NH₃ added to the system, as illustrated in Fig. 3. It should be noted that, for the unfiltered afterglow (Fig. 3A) and the afterglow at 5820 Å. (Fig. 3B), marked increases in I_0/I between the 15 and 30-cm. levels occur only for initial concentrations of NH₃ > 9.5 × 10⁻¹⁰ mole cc.⁻¹.

Discussion

The Active Nitrogen Afterglow.—The linear relation between PM readings and the square of the N-atom flow rate, as illustrated in Fig. 1, demonstrates that the intensity of the visible²² afterglow depends only on the extent of homogeneous recombination of N atoms. Obviously, there is no important contribution to the visible afterglow from A state molecules formed on the Pyrex walls, in contrast to the emission from the $v = 8$ and 6 levels of the B state following recombination on a cobalt surface.²³

The ratios of the slopes, a , for the unpoisoned system to those for the poisoned system are 1.78, 2.40, and 1.32

(21) Values of I_0 were obtained for the filtered afterglows at any given upper level (i.e., close to the reactant inlet), where Fig. 1B and 1C show a fall-off in the absence of NH₃, by extrapolating the linear relations for the lower levels and reading the PM value for the N-atom concentration which the previous work¹⁵ showed to correspond to the upper level. The corrected value of I then was obtained by subtracting from this value of I_0 the decrease in intensity observed in the presence of the added NH₃ at the same level.

(22) The spectral response of the phototube was limited to the range 3000 to 6200 Å.

for the unfiltered afterglow, and the emissions from the 5820 and 6630-Å. regions, respectively. The greater values for the unpoisoned system, for emission in all three spectral regions used, probably results from the greater proportion of the N atom decay (approximately 0.9 of the total)¹⁵ that occurs without light emission by surface recombination, which is first or zero-order in N atoms.²⁴ The greater effect of a change of wall condition on the values of a for the 5820 Å. region, in particular, might be explained if the unpoisoned Pyrex walls were more effective than the poisoned walls for inducing an electronic transition from the quintet state to the $^3\Pi_g$ state²⁵ (cf. ref. 27). The wall-induced change of spin would have to be accompanied by a loss of energy greater than the negligible loss that occurs^{4,10} during the radiationless collision-induced transition between $N_2(^5\Sigma_g^+)$ and $N_2(X^1\Sigma_g^+)$ in the gas phase, so as to populate the B state into vibrational levels less than $v = 11$, rather than directly into the $v = 12, 11, 10$ levels, as assumed by Bayes and Kistiakowsky.¹⁰ The currently accepted theory of the afterglow^{4,10} requires that the $^5\Sigma_g^+$ molecule make many collisions with $N_2(X)$ during a considerable lifetime and, at a pressure of 3 mm., with a mean free path of about 10^{-3} cm., it is possible that it might make a substantial number of collisions with the wall during its lifetime in the present system.

With similar wall conditions, the linear relation between $[N]^2$ and the intensity of the afterglow does show some dependence upon the spectral region under investigation. If the change in PM readings, down to the 45-cm. level, is expressed in terms of a percentage decrease in light emission from that observed at the 15-cm. level (a change of 153 and 38.8×10^{-6} mole/sec.² in the abscissas for the poisoned and unpoisoned systems, respectively), the following variation is obtained

	Unfiltered afterglow	Emission from $v = 11$ (5820 Å.)	Emission from $v = 6$ (6630 Å.)
Poisoned system	30	26	36
Unpoisoned system	40	48	31

Emission from $v = 11$ in the unpoisoned system is more dependent upon $[N]^2$ than is the emission in this same system from the unfiltered afterglow or from $v = 6$, while the reverse is true in the poisoned system.²⁸ This might again suggest that a collision of $N_2(^5\Sigma_g^+)$ with the unpoisoned walls effectively induced transition to the B state at $v < 11$.

That the manner of populating the B state is modified by wall collisions of a precursor of the afterglow is

(23) (a) P. Harteck, R. R. Reeves, and G. Mannella, *Can. J. Chem.*, **38**, 1648 (1960); (b) Although NO may be destroyed by excited nitrogen molecules produced by wall recombination,¹⁶ light emission, if initiated at all by A state molecules in such low vibrational levels, would occur in the infrared (group 3b) and not be detectable in the present study.

(24) R. A. Back, W. Dutton, and C. A. Wirkler, *Can. J. Chem.*, **37**, 2059 (1959).

(25) Although water vapor is known²⁶ to be very effective for inducing vibrational relaxation in the gas phase, it is assumed that, because of the very short lifetime⁷ of the B state, the vibrational distribution within this state will not be affected significantly, at the pressure of 3 mm., by collision of $N_2(B)$ with the trace of water vapor present in the poisoned system. This property of water vapor would not be expected to operate for collisions with the much longer lived quintet state, because of the very shallow potential energy well associated¹⁰ with this nitrogen molecule.

(26) S. J. Lukasik and J. E. Young, *J. Chem. Phys.*, **27**, 1149 (1957).

(27) E. R. V. Milton, H. B. Dunford, and A. E. Douglas, *ibid.*, **35**, 1202 (1961).

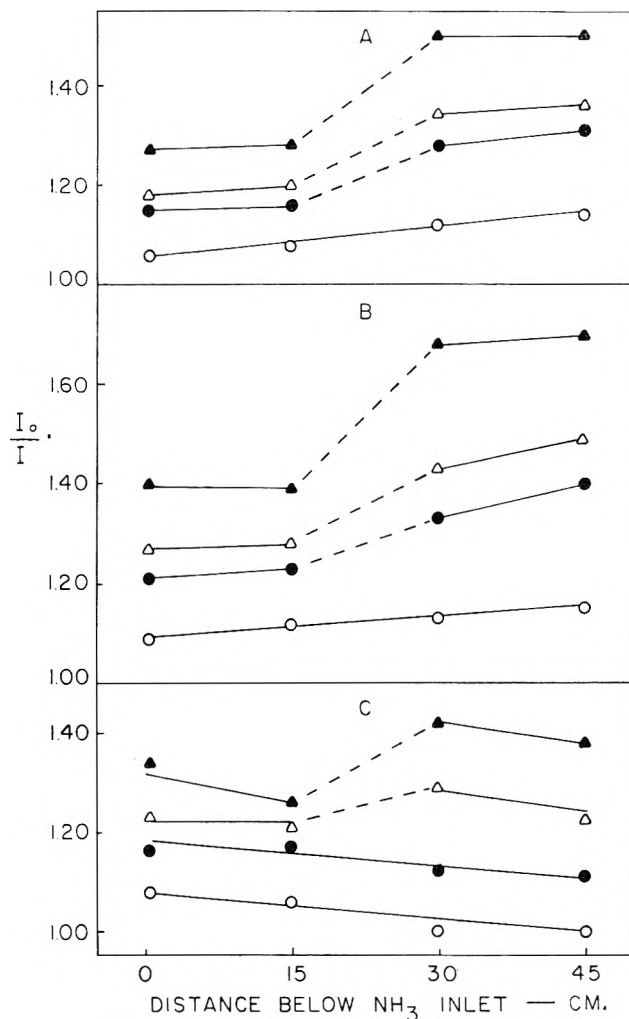


Fig. 3.—Plot of I_0/I against distance below the point of introduction of NH_3 at the initial concentrations given by: \circ , 9.5×10^{-10} mole cc.⁻¹; \bullet , 23×10^{-10} mole cc.⁻¹; \blacktriangle , 47×10^{-10} mole cc.⁻¹. Subdivided for the spectral conditions: A, unfiltered afterglow; B, afterglow at 5820 Å.; C, afterglow at 6630 Å.

further indicated by the observation that, for positions close to the inlet jet, the emission from particular spectral regions (5820 and 6630 Å.), but not the total visible afterglow emission,²⁹ showed a falling-off from the linear dependence of intensity on $[N]^2$ (Fig. 1). In the poisoned system, this fall-off occurs, for emission from either $v = 11$ or $v = 6$, at a value of $(N\text{-atom flow rate})^2$ that corresponds to a decay time of about 18 msec. In the unpoisoned system, the corresponding decay time is about 24 msec.

(28) This variation is not explicable by the temperature dependence of the intensity of the group 1 bands in active nitrogen,¹⁰ since the decrease in temperature between the 0.2 and 45 cm. levels was only 43 and 36° in the poisoned and unpoisoned systems,¹⁵ respectively. It is conceivable, in view of the effect of added foreign gases,¹⁰ that the introduction of even the trace of H_2O vapor ($< 0.3 \times 10^{-6}$ mole sec.⁻¹ in the presence of a flow rate of molecular nitrogen of 378×10^{-6} mole sec.⁻¹) might influence the manner in which the quintet state populates the triplet states, and hence the $B^1\Pi_g$ state by collisions in the gas phase. However, in the absence of low-lying triplet states for the water molecule, such as would permit a resonance exchange of energy and the conservation of resultant total spin of the collision partners, there is little reason to expect H_2O to induce the *electronic* transition from the quintet state much more effectively than ground state nitrogen molecules themselves. Moreover, H_2O vapor was present at all levels in the poisoned system. It is assumed, therefore, that the values of the slope a , for emission in groups 1 and 4, are not greatly affected by the presence of the trace of poisoning agent in the gas phase.

(29) Neglecting the small variation in sensitivity of the phototube over the spectral regions studied, approximately 13 and 0.35% of the visible afterglow was emitted in the spectral regions centered at 5820 and 6630 Å., respectively.

An approximate minimum lifetime for the precursors of light emission may be estimated from the above fall-off behavior. The similarity in times over which collisions with the wall upstream may affect the vibrational distribution within the B state supports the view¹⁰ that both $v = 11$ and $v = 6$ are populated by the same precursor of long life, rather than the postulate^{23a} that the 6th level is populated through A state molecules of high vibrational energy content. If it is assumed that recombination of N atoms yields $N_2(^5\Sigma_g^+)$, and that the intermediates between the quintet state and light emission in the first positive system are of negligible lifetimes, as established^{7,30} for the B state ($\sim 10^{-7}$ sec.) and assumed¹⁰ for the $^3\Delta_u$ state, the average measured time interval for emission, about 21 msec., may be taken as an approximate *minimum* lifetime for the $^5\Sigma_g^+$ state.

A lifetime of 21 msec. for $N_2(^5\Sigma_g^+)$ indicates that about 10^6 collisions with $N_2(X)$ are necessary to induce conversion of spin and transition to the triplet states, $B^3\Pi_g$ or $^3\Delta_u$. This may be compared with a probability factor of $< 10^{-3}$ derived⁴ for the radiationless collision-induced transition to the B state, and with the number of collisions ($\sim 10^9$) with $N_2(X)$ required³¹ to induce the analogous transition from the $A^3\Sigma_u^+$ state to the ground $X^1\Sigma_g^+$ state. It also may be concluded that, if the $v = 6$ level is populated through the $^3\Delta_u$ state as suggested by Bayes and Kistiakowsky,¹⁰ this state cannot have the long life of 1–2 sec. recently ascribed to it.³²

The Quenching Effect of Ammonia.—There appear to be two effects when NH_3 is added to the active nitrogen stream in an *unpoisoned* system.

(i). An increase is observed in the PM readings, which becomes greater with distance downstream from the inlet jet, for a given initial flow rate of NH_3 . This enhancement in afterglow intensity may be attributed to the ability of NH_3 to poison the wall of the reaction tube against surface recombination of N atoms, as suggested¹⁵ previously to explain the increased extent of HCN production in the C_2H_4 reaction when NH_3 was added upstream.³³

(ii). A decrease in PM reading is observed when the flow rate of NH_3 is increased at a given position in the reaction tube. This decrease is to be expected when the quenching effect of NH_3 on the 1st positive system *predominates* over the increase in afterglow intensity that results from the poisoning effect of NH_3 as in (i) above. The *decrease* in intensity is observed, even at low initial flow rates of NH_3 , for positions close to the NH_3 inlet, presumably because the effect of NH_3 as a wall poison, to promote an increased N atom concentration in the gas stream, is not pronounced for short times of decay. The effect of added NH_3 on the afterglow is therefore quite complicated in an unpoisoned system, and only the results obtained in a poisoned system are amenable to satisfactory interpretation.

In the poisoned system, where the addition of NH_3 has little effect in altering the small extent of wall recombination of N atoms that occurs,¹⁵ a decrease in

light intensity for all three spectral regions was observed at all positions, and for all initial flow rates of NH_3 (Table II). Since the quenching effect of NH_3 on the unfiltered afterglow, and particularly on emission from the 6th vibrational level, is similar to that on the emission from the 11th vibrational level of the B state (Fig. 2 and ref. 10), it may be attributed¹⁰ to collisional deactivation of $N_2(^5\Sigma_g^+)$ to a state incapable of causing light emission in the visible region. The similar quenching efficiencies for the unfiltered and filtered afterglows (Table III) indicate that, for the conditions of these experiments, the quenching is accompanied by relatively little alteration in the population distribution among the higher vibrational levels of the $B^3\Pi_g$ state. However, the quenching efficiency for emission from the $v = 11$ level is somewhat greater than for the other emissions (Table III), and this might reflect an enhanced effect of high flow rates of NH_3 on emission from this level, near which the maximum of the fully modified population curve¹⁰ occurs.

There is evidence that the quenching efficiency of NH_3 for $N_2(^5\Sigma_g^+)$ is decreased by the presence of $N_2(A^3\Sigma_u^+)$. This is suggested by calculating the amount of NH_3 that would be destroyed at the different levels using the results of the previous study¹⁶ and comparing the values with the amount of $N_2(A)$ present initially, also inferred from the earlier data. It is found that the marked increase in I_0/I between the 15 and 30-cm. levels (Fig. 3) corresponds, except with the lowest concentration of NH_3 used, to the depletion that might be expected, by reaction with NH_3 , of most of the $N_2(A)$ originally present in the active nitrogen.³⁴ In a similar way, emission in the infrared, originating from the lowest vibrational levels of the B state, is more strongly quenched by NH_3 than any other part of the afterglow spectrum.¹⁰ This might be due also to removal, by reaction, of $N_2(A)$ which otherwise serves to populate¹⁰ these levels (group 3b) of the B state. It is interesting that, although decomposition of NH_3 by $N_2(^5\Sigma_g^+)$ cannot be ruled out, both resultant spin and extent of energy transfer could not be maintained between these collision partners, and it appears that most of the decomposition results from the collisions with electronically excited nitrogen molecules that are not responsible for emission in the *visible* afterglow.

An approximation to the rate constant for $N_2(^5\Sigma_g^+) + NH_3 \xrightarrow{k_2} N_2(\text{deactivated}) + ?$ (eq. 12 of ref. 10), may be obtained from the measured quenching efficiencies. Bayes and Kistiakowsky have derived a rather complex relation between I_0/I and added NH_3 (eq. 1 of ref. 10). However, in the present system, NH_3 exerts mainly a quenching, rather than a distributional effect, on the afterglow intensity, and the variation in k_2 (distributional rate constants) of their mechanism, in the presence of added NH_3 , may be neglected. Similarly, the apparently negligible change in the rate of homogeneous recombination of N atoms, when NH_3 is added to the poisoned system,¹⁵ suggests that the processes

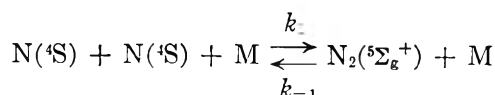
(34) The small, but apparently steady, *decrease* in the rate I_0/I with distance below the NH_3 inlet, at the two lower initial flow rates of NH_3 , for emission in the 6630-Å. region (Fig. 3C) might be a consequence of the ability of NH_3 to alter¹⁰ the vibrational distribution within the $B^3\Pi_g$ state. In these experiments, only a very small fraction of the light emission occurs at 6630 Å. and, at lower flow rates, the *apparent* effectiveness¹⁰ of NH_3 in drastically reducing the population peak at $v = \sim 6$ might make a significant contribution to the over-all quenching effect.

(30) J. C. Keck, J. C. Cammon, B. Kivel, and T. Wentlink, *Ann. Phys.*, **7**, 1 (1959).

(31) J. Noxon, *J. Chem. Phys.*, **36**, 926 (1962).

(32) C. Kenty, *ibid.*, **35**, 2267 (1961).

(33) An increase in the N-atom concentration downstream resulting from the admixture of small amounts of O_2 upstream in a flow system was similarly attributed⁴ to a reduced rate of recombination of N atoms on walls deactivated by O_2 .



(eq. 1 of ref. 10) are little effected by the presence of NH_3 . With these approximations, it may be readily deduced that the slopes given in Table III give a measure of $k_{12}/k_3 [\text{N}_2]$, where k_3 is the rate constant for transition of the quintet state, induced by collision with $\text{N}_2(\text{X})$, to a triplet state capable of causing light emission. The value for the unfiltered afterglow, at the lower positions where the influence of $\text{N}_2(\text{A})$ is reduced, indicates a value³⁵ for k_{12} equal to about $16k_3$. As outlined previously, the present work yields a collision efficiency of about 10^{-6} , for deactivation of $\text{N}_2(^5\Sigma_g^+)$ by $\text{N}_2(\text{X})$, corresponding to the rate constant k_3 , and, since neither this reaction, nor reaction 12, would be subject to a significant activation energy, it follows that NH_3 deactivates the quintet state with a collision efficiency about 16 times that of $\text{N}_2(\text{X})$, *i.e.*, about 10^{-5} . This rather low probability reflects the impossibility of a resonant energy exchange, and concomitant conservation of total resultant spin, during a collision of the Second Kind between $\text{N}_2(^5\Sigma_g^+)$ and NH_3 . Since the

(35) The quenching efficiency for emission at 5820 Å., which might be subject to the distributional effect of added N_2 , would increase this approximate value by about 50%.

lifetime inferred for the $^5\Sigma_g^+$ state would permit a considerable concentration of these molecules, the apparent factor of about 10 between the "probability factors" for reaction of NH_3 with the quintet state, and for reaction with $\text{N}_2(\text{A})$, parallels the reduced quenching efficiency for $\text{N}_2(^5\Sigma_g^+)$ in the presence of relatively large concentrations of $\text{N}_2(\text{A})$.

This paper has presented data obtained from a system in which the N-atom concentrations, the concentrations of NH_3 introduced or left unreacted, and changes in afterglow emission over different spectral regions, are simultaneously measured. The variation in the dependence of the intensity of light emission upon $[\text{N}]^2$ for different spectral regions, and for different wall conditions, has led to the conclusion that an unpoisoned Pyrex wall tends to induce transition from $\text{N}_2(^5\Sigma_g^+)$ to the B state at $v < 11$. A change in the vibrational distribution within the B state with a greater surface to volume ratio in the flow system would appear to indicate a considerable lifetime for the quintet state of nitrogen at the pressure of these experiments (~ 3 mm.). The quenching effect of NH_3 on the afterglow emission also indicated a considerable lifetime for the quintet state before it is converted to a triplet or the singlet state of nitrogen by collision with the NH_3 molecule.

MASS SPECTROMETRIC STUDY OF HIGH TEMPERATURE REACTIONS IN THE BORON-HYDROGEN-OXYGEN SYSTEM¹

BY WILLIAM P. SHOLETTE AND RICHARD F. PORTER²

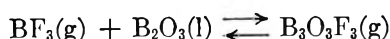
Department of Chemistry, Cornell University, Ithaca, New York

Received July 2, 1962

Low pressure reactions of $\text{H}_2(\text{g})$ with B-B₂O₃ mixtures and of $\text{H}_2\text{O}(\text{g})$ with elemental boron in the temperature range 1000 to 1400°K. have been investigated. The experimental technique involves flowing the reactant gas at pressures between 10^{-6} and 10^{-3} atm. into a Knudsen-type vessel containing a condensed sample, and observing the gaseous products effusing from the oven mass spectrometrically. The major product formed with either $\text{H}_2(\text{g})$ or $\text{H}_2\text{O}(\text{g})$ as reactant is $\text{B}_3\text{O}_3\text{H}_3$ (boroxine). A smaller yield of $\text{B}_3\text{O}_4\text{H}_3$ (hydroxyboroxine) also is observed. In separate experiments, the products of these reactions have been collected in a cold trap at liquid nitrogen temperature. Upon warming, the condensed material evolves diborane and hydrogen. The heats of formation of $\text{B}_3\text{O}_3\text{H}_3(\text{g})$ and $\text{B}_3\text{O}_4\text{H}_3(\text{g})$ at 298°K. are -302 ± 7 and -393 ± 7 kcal./mole, respectively.

Introduction

Substituted boroxines ($\text{B}_3\text{O}_3\text{X}_3$) have been synthesized and studied by several investigators.³ These derivatives include the trimethyl, trimethoxy, and trihalogenated compounds, which are presumed to have six-membered ring structures. Gaseous trihydroxyboroxine also has been reported as a product in the high temperature reaction of $\text{H}_2\text{O}(\text{g})$ with liquid B_2O_3 .⁴ Recently some attention has been directed toward $\text{B}_3\text{O}_3\text{F}_3$, which is generated in the reaction



The trifluoro derivative is quite stable thermally, as noted by the fact that the above reaction proceeds at temperatures between about 500 and 1000°K. with

$\text{BF}_3(\text{g})$ pressures between 10^{-5} and 1 atm.^{5,6} The unsubstituted boroxine ($\text{B}_3\text{O}_3\text{H}_3$) has not been reported as an isolated compound although there is evidence that it is produced in low yield in the oxidation of pentaborane.⁷

The present investigation was prompted by some recent mass spectrometric studies of the low pressure reaction of $\text{H}_2(\text{g})$ - $\text{BF}_3(\text{g})$ mixtures with $\text{B}_2\text{O}_3(\text{l})$.⁸ The gaseous products in this reaction are $\text{B}_3\text{O}_3\text{F}_3$, $\text{B}_3\text{O}_3\text{F}_2\text{H}$, $\text{B}_3\text{O}_3\text{FH}_2$, and $\text{B}_3\text{O}_3\text{H}_3$. From the data obtained it was possible to compare the relative stabilities of the four species. The heat of formation of $\text{B}_3\text{O}_3\text{H}_3(\text{g})$ was found to be -307 ± 8 kcal./mole. If we compare this value with the available thermochemical data for B_2O_3 and boron, it is evident that $\text{B}_3\text{O}_3\text{H}_3(\text{g})$ is thermodynamically stable with respect to the

(1) Supported by the Advanced Research Projects Agency.

(2) Alfred P. Sloan Fellow.

(3) (a) A. B. Burg, *J. Am. Chem. Soc.*, **62**, 2228 (1940); (b) P. Baumgarten and W. Bruns, *Chem. Ber.*, **74**, 1232 (1940); (c) Von J. Goubeau and H. Keller, *Z. anorg. allgem. Chem.*, **267**, 1 (1951); **272**, 303 (1953).

(4) D. J. Meschi, W. A. Chupka, and J. Berkowitz, *J. Chem. Phys.*, **33**, 530 (1960).

(5) D. L. Hildenbrand, L. P. Theard, and A. M. Saul, XVIII International Congress of Pure and Applied Chemistry, Montreal, 1961.

(6) R. F. Porter, D. R. Bidinosti, and K. F. Watterson, *J. Chem. Phys.*, **36**, 2104 (1962).

(7) J. F. Ditter and I. Shapiro, *J. Am. Chem. Soc.*, **81**, 1022 (1959).

(8) R. F. Porter and W. P. Sholette, *J. Chem. Phys.*, **37**, 198 (1962).

system $H_2(g)$, $B(s)$, and $B_2O_3(l)$ at high temperatures.⁹ Thus a further examination of high temperature reactions in the B-H-O system was undertaken. Boroxine is also of fundamental interest because of its analogy to the isoelectronic molecules, borazine and benzene.

Experimental

The mass spectrometer, high temperature assembly, and gas inlet system have been described previously.^{6,10,11} For these experiments a molybdenum reaction vessel was used. Its construction was similar to that of previous crucibles¹¹; however, a small molybdenum cup was placed inside the vessel to contain the sample. Where B_2O_3 was used, this served to prevent the molten sample from clogging the gas inlet tube.

Samples of B_2O_3 were prepared as in previous experiments,⁶ *i.e.*, by decomposing and fusing Mallinckrodt reagent grade boric acid and dehydrating further inside the mass spectrometer. Boron was added to the molten B_2O_3 just before placing the sample in the mass spectrometer. For experiments using only ^{10}B ,¹² the sample was packed into the molybdenum cup and dehydrated inside the mass spectrometer. Water vapor or hydrogen was admitted through the inlet tube and its pressure was controlled by a Hoke valve. In some experiments the valve was eliminated and water vapor at a known "slush bath" temperature was admitted directly into the reaction vessel, allowing a calibration of the cell pressure. This calibration will be described in a later section. Hydrogen, supplied by the Matheson Co., was purified by passing through a liquid nitrogen trap before being admitted to the reaction cell.

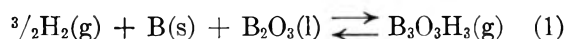
Results

Identification of gaseous products issuing from the hot reaction vessel was made from their mass spectral patterns. In Table I we show a typical mass spectrum obtained in the reaction of $H_2O(g)$ on an isotopically enriched sample of ^{10}B . Spectra of products from the reaction of H_2 and B- B_2O_3 mixtures were similar. A series of spectral patterns for $m/e = 79$ to 84 is given in Table II. Comparison of the isotope structure obtained for various experimental conditions shows that the sequence of ions arises from a species containing three boron atoms. The spectral patterns are consistent with that for a molecule $B_3O_3H_3$ (boroxine). The spectra are somewhat complicated by the fact that a hydrogen atom is removed on electron impact. This gives rise to overlap of peaks arising from the

parent ion ($B_3O_3H_3^+$) and $B_3O_3H_2^+$. This behavior also is observed with the isoelectronic borazine. Comparing the data in Table II also shows that when H_2 reacts with $^{10}B(s) + B_2O_3(l)$ with a natural ^{10}B and ^{11}B abundance, mixing and exchange of the boron atoms must occur to account for the appearance of relatively intense peaks at $m/e = 82$ and 83.

A second but less abundant product has ion peaks in the $m/e = 96$ to 100 range. This is identified as $B_3O_4H_3$ (hydroxyboroxine). The product appears in reactions of H_2 with (B + B_2O_3) and H_2O with elemental boron. The lower mass peaks were characterized as ion fragments. The relatively intense peak at $m/e = 53$ is assumed to be $B_2O_2H^+$ and has an appearance potential above 20 v. Appearance potentials for $B_3O_3H_3^+$ and $B_3O_3H_2^+$ were obtained by extrapolation of appearance potential curves using H_2O^+ as a voltage calibration. These were found to be 13.5 ± 0.5 and 14.5 ± 0.5 v., respectively.

Boroxine, $B_3O_3H_3$.—For temperatures above 1100°K. gaseous boroxine is generated by the reactions



and



Reaction 1 is not meant to imply that either pure boron solid or pure boric oxide liquid is necessarily present under the experimental conditions. For $H_2(g)$ pressures of about 0.1 mm. the ratio of $B_3O_3H_3^+/H_2^+$ for reaction 1 was generally between 0.01 and 0.1 in the temperature range 1100 to 1400°K. When $H_2O(g)$ was passed into a cell containing boron, the initial ratio of $B_3O_3H_3^+$ to H_2^+ was considerably below 0.01. As H_2O was continually passed over the sample the yield of $B_3O_3H_3$ increased to a point which nearly coincided with the yield obtained when H_2 was passed over a mixture of B- B_2O_3 . In reactions of H_2O with boron, molecular hydrogen was always in greater yield than $B_3O_3H_3$. This indicated that at least one additional reaction was occurring to produce $H_2(g)$. At the high temperature employed, unreacted H_2O was never observed in the effusing gases. After H_2O was allowed to react with boron for several hours, $H_2(g)$ was then passed into the oven. This again resulted in the production of $B_3O_3H_3$ in maximum yield. These observations show that the boron sample within the reaction vessel was partially converted to oxide. In Fig. 1 the $\log(B_3O_3H_3^+)/(H_2^+)$ is plotted as a function of temperature. The data as indicated were taken from reactions of H_2 and B- B_2O_3 mixtures and H_2O with boron after the latter reaction was allowed to proceed for several minutes. Background levels of both reactant and product gases were generally present after reaction had proceeded for some time. The following experimental procedure for eliminating the background contributions at each temperature therefore was employed. Upon opening the leak to admit reactant gas, the ion intensities would rise continuously for a while, finally becoming constant. This was accompanied by a slight decrease in temperature in the reaction cell. When steady conditions were reached, equilibrium was assumed to have been established, and the data were recorded. The leak was then closed and the ion intensities allowed to decrease again to

TABLE I

MASS SPECTRUM OF GASEOUS PRODUCTS IN THE REACTION OF $H_2O(g)$ WITH $^{10}B(s)$ (ENRICHED)^a

$T = 1250^\circ K.$, ionizing electron energy = 75 v.

m/e	Ion	Intensity (relative units)
97		3.7
96	$B_3O_4H_2^+$	12.9
82		6.3
81		40.0
80	$B_3O_3H_2^+$	100.0
79		5.5
70		1.1
69	$B_2O_3H^+$	4.8
68		1.8
54		6.6
53	$B_2O_2H^+$	36.0
52		4.0
27	BOH^+	17.3

^a Sample is about 92% ^{10}B and 8% ^{11}B .

(9) J.A.N.A.F. Thermochemical Data, Thermal Laboratory, Dow Chemical Co., Midland, Michigan, 1960.

(10) R. F. Porter and R. C. Schoonmaker, *J. Phys. Chem.*, **62**, 234 (1958).

(11) D. R. Bidinosti and R. F. Porter, *J. Am. Chem. Soc.*, **83**, 3737 (1961).

(12) Obtained from Oak Ridge National Laboratories.

TABLE II

EFFECT OF BORON ISOTOPE COMPOSITION ON THE MASS SPECTRUM OF GASEOUS BOROXINE

 $(m/e$ range = 79-84; ionizing electron energy = 75 v.; reaction temperature approximately 1200°K.; intensities in relative units)

Reaction	$m/e = 79$	80	81	82	83	84
$H_2O(g) + {}^{10}B^a$	5.5	100.0	38.2	5.9	1.2	...
$H_2O(g) + (B + B_2O_3)$, natural B abundance	..	3.8	24.2	77.3	100.0	18.1
$H_2(g) + {}^{10}B^a + B_2O_3$ (natural B abundance)	..	19.6	98.5	100.0	54.9	5.9

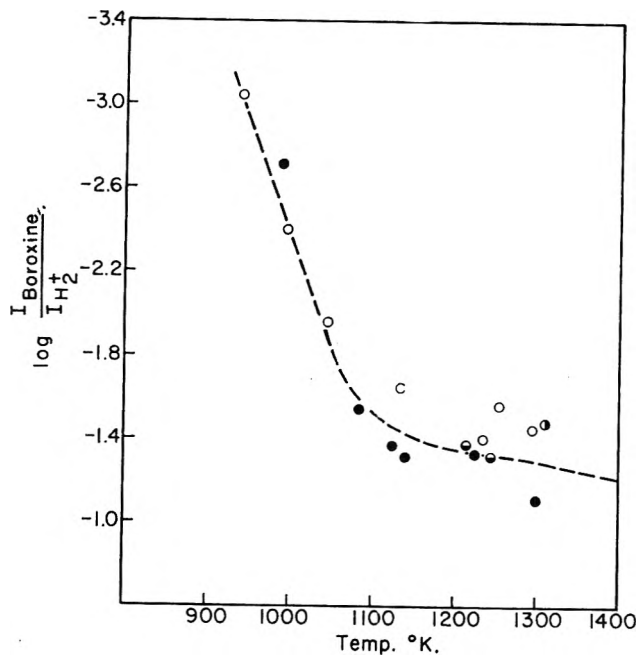
^a Mass spectral analyses indicate sample is about 92% ¹⁰B.

Fig. 1.—Relative temperature dependence of boroxine and hydrogen in reactions of: $H_2O(g)$ with $B(s)$ [O, ●]; $H_2(g)$ with $(B + B_2O_3)$ [◐]; $H_2(g)$ with B after $H_2O(g)$ had reacted with it [◑].

steady values, these being subtracted out as background.

The pressure of $H_2(g)$ in these experiments was approximately 10^{-4} atm. with fluctuations of about 25%. Since the experimental conditions within the reaction vessel containing $B-B_2O_3$ mixture also eventually are approached in the reaction of H_2O with boron, thermodynamic data obtained for either of these sets of conditions should then be equivalent. From the data in Fig. 1, we note that the yield increases quite rapidly in the lower temperature range, but tends to flatten off in the high temperature range. This effect may be attributable to either kinetic effect at the lower temperatures or thermodynamic changes occurring within the condensed phase in the reaction vessel. Further discussion of these effects will be deferred until later. From the second law procedure we can evaluate ΔH^0 for reaction 1 from the slope of a plot of

$$\log \frac{P_{B_3O_3H_3}}{P_{H_2}^{3/2}} = \log \frac{(I_{B_3O_3H_3})}{(I_{H_2})^{3/2}} + \text{constant vs. } 1/T$$

A plot of this type is given in Fig. 2. At low temperatures the curve drops off as is expected from similar data in Fig. 1. In the higher temperature range $(I_{B_3O_3H_3})/(I_{H_2})^{3/2}$ increases by a factor of between 2 and 3 for a 100° rise in temperature. These data give an apparent heat for reaction 1 of 22 ± 5 kcal./mole of $B_3O_3H_3(g)$.

As an alternative method for evaluating H^0_T of reaction 1 third law calculations were made from data ob-

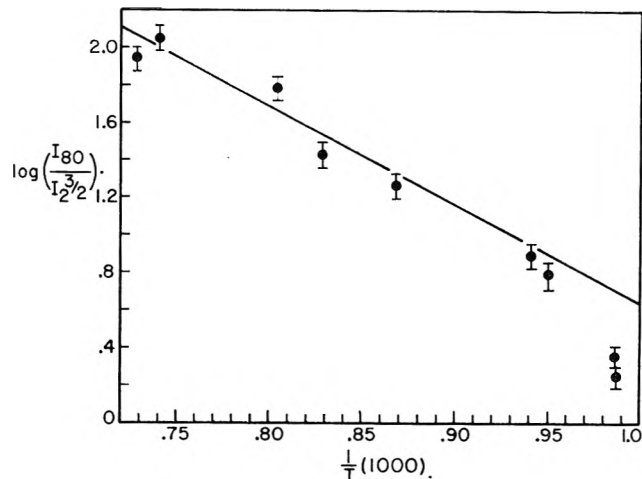


Fig. 2.—Second law data for the reaction: $3/2 H_2(g) + (B + B_2O_3) \rightleftharpoons B_3O_3H_3(g)$.

served at several temperatures. The equilibrium constant for this reaction is

$$K_1 = (P_{B_3O_3H_3}) / (P_{H_2})^{3/2} a_B a_{B_2O_3}$$

For initial calculations, the activities a_B and $a_{B_2O_3}$ were assumed equal to unity and were defined relative to amorphous boron and liquid boric oxide. Pressure calibration was achieved by admitting water vapor directly into the reaction vessel from a "thumb" of ice at known temperature. Dry Ice-carbon tetrachloride and Dry Ice-dichloroethane slush baths were used to control the temperature of the ice. Since H_2O was converted entirely to H_2 inside the crucible at reaction temperatures, P_{H_2} was taken as the vapor pressure of water in equilibrium with ice at the known temperature. The pressure of $B_3O_3H_3$ then was found from the relation

$$P_{B_3O_3H_3} = C \frac{I_{B_3O_3H_3}}{I_{H_2}} P_{H_2}$$

where $I_{B_3O_3H_3}$ and I_{H_2} are the total ion intensities of the respective molecules and C is a constant including the relative collision cross sections for electron impact and the relative sensitivities for ion detection. The constant C was estimated to be the same as that for the similar system C_6H_6 and H_2 , the latter being readily evaluated by studying the pyrolysis of benzene in the mass spectrometer. Benzene was admitted at low pressure into the reaction vessel and pyrolyzed to yield a H_2 pressure three times that of the C_6H_6 reacted. From the relation

$$\frac{P_{H_2 \text{ formed}}}{P_{C_6H_6 \text{ reacted}}} = 3 = C \frac{I_{H_2 \text{ formed}}}{I_{C_6H_6 \text{ reacted}}}$$

C was found to be 6.8. From the values of the equilibrium constant thus calculated, ΔF^0 was evaluated using the relation $\Delta F^0 = -RT \ln K$.

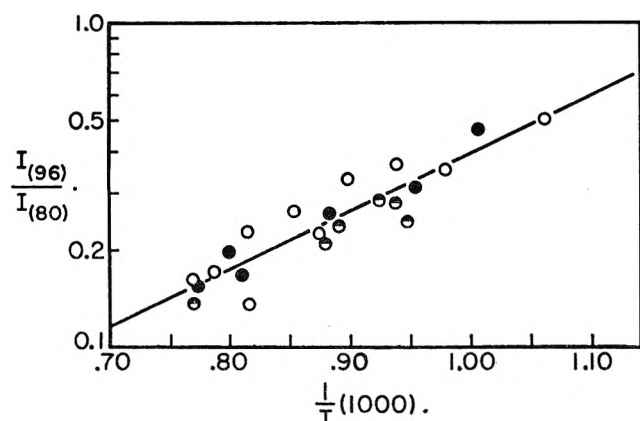
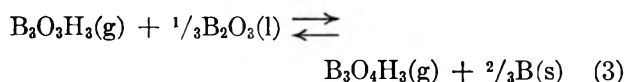


Fig. 3.—Second law data for the reaction: $B_3O_3H_3(g) + \frac{1}{3}B_2O_3(l) \rightleftharpoons B_3O_4H_3(g) + \frac{2}{3}B(s)$.

The standard entropy of $B_3O_3H_3$ has been estimated at various temperatures by statistical thermodynamical comparison with three similar molecules whose entropies are tabulated, *viz.*, $B_3O_3F_3$, $B_3N_3H_6$, and $B_3O_6H_3$.⁹ In the case of $B_3O_3F_3$, for example, this calculation consisted chiefly of two parts: (1) replacing the contributions of the three B-F bonds toward the moment of inertia with those of B-H bonds, and (2) replacing nine assumed vibrational frequencies for the B-F bonds with those for B-H bonds. The calculation from $B_3O_6H_3$ was similar, B-O and O-H bonds being replaced in this case. With $B_3N_3H_6$ the known N-H frequencies were simply subtracted out, the contributions of the BN and BO rings being assumed equal. The agreement among the three sets of values thus obtained was very good. The mean values calculated for $S^0_{B_3O_3H_3}$ at absolute temperatures 300, 600, 1000, 1200, and 1400° were 67.8, 87.3, 107.1, 114.7, and 121.3 e.u., respectively. Using tabulated values of S^0 for B, B_2O_3 , and H_2 , $T\Delta S^0$ for each temperature was calculated and combined with ΔF^0 to give ΔH^0_T . The thermochemical data are summarized in Table III, from which we find the average value: $\Delta H^0_{1400} = -16.3 \pm 1.5$ kcal./mole of $B_3O_3H_3$. (The three highest values of ΔH^0_T from the table were not given full weight in the averaging, since they do not seem to be in line with the other values.)

Hydroxyboroxine, $B_3O_4H_3$.—The production of hydroxyboroxine, $B_3O_4H_3$, also was investigated as a function of temperature and related to the production of $B_3O_3H_3$. The following equilibrium may be considered



for which the equilibrium constant is

$$K_3 = \frac{P_{B_3O_4H_3}(a_B)^{2/3}}{P_{B_3O_3H_3}(a_{B_2O_3})^{1/3}} = C \frac{(I_{B_3O_4H_3})^{2/3}(a_B)^{2/3}}{(I_{B_3O_3H_3})^{1/3}(a_{B_2O_3})^{1/3}}$$

Here a_B and $a_{B_2O_3}$ were assumed to be unity for initial calculations. Since the two gaseous molecules would be expected to have similar cross sections and sensitivities, C also may be assumed equal to unity. An apparent ΔH_T was found from the slope of a plot of $\log K_3$ vs. $1/T$, shown in Fig. 3; three separate sets of data are included in the one plot. This calculation gives $\Delta H_T = -8 \pm 3$ kcal./mole of $B_3O_4H_3$ for the temperature range 900 to 1300°K.

TABLE III
THERMOCHEMICAL DATA FOR THE REACTION
 $3/2H_2(g) + (B + B_2O_3) \rightarrow B_3O_3H_3(g)$

Temp., °K.	P_{H_2} (atm.) $\times 10^4$	$P_{B_3O_3H_3}$ (atm.) $\times 10^6$	K_{eq}	ΔF^0 (kcal./ mole)	ΔS^0 (e.u.)	ΔH^0 (kcal./ mole)
1290	3.2	14.9	2.6	-2.5	-10.0	-15.4
1294	2.7	15.4	3.4	-3.2	-10.0	-16.1
1333	6.6	33.4	2.0	-1.8	-10.2	-15.4
1341	6.6	26.9	1.6	-1.3	-10.2	-15.0
1368	3.0	10.4	2.0	-1.8	-10.3	-15.9
1450	3.4	17.4	2.8	-3.0	-10.8	-18.7
1452	3.4	24.4	4.0	-4.0	-10.8	-19.7
1469	3.4	21.6	3.5	-3.6	-10.8	-19.5
1454	7.2	15.6	0.8	+0.65	-10.8	-15.1
1481	7.2	24.5	1.3	-0.7	-10.9	-16.8

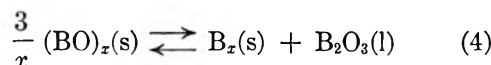
The third law method was also used to calculate ΔH^0_T for one set of the same experimental data. The quantity $(S^0_{B_3O_4H_3} - S^0_{B_3O_3H_3})$ was estimated *via* statistical thermodynamics to be 15.3 e.u. at 1200°K. $T\Delta S^0$ then was calculated for each temperature and combined with ΔF^0 to give ΔH^0_T , as summarized in Table IV. This treatment gives the average value: $\Delta H^0_{1150} = 6.3 \pm 1.0$ kcal./mole of $B_3O_4H_3$.

Heats of Formation.—Appreciable discrepancies are found between second law and third law calculations of ΔH^0_T for reactions 1 and 3, even when only the high temperature data are considered. This seems to indicate that thermodynamic changes occur within the condensed phase of the reaction system, thus invalidating the assumption of unit activity for B and B_2O_3 . Such an activity effect could be due to the solution of B in B_2O_3 , for example, or to some chemical combination between the two such as $(BO)_x$. Assuming a polymer

TABLE IV
THERMOCHEMICAL DATA FOR THE REACTION
 $B_3O_3H_3(g) + \frac{1}{3}B_2O_3(l) \rightarrow B_3O_4H_3(g) + \frac{2}{3}B(s)$

Temp., °K.	K_{eq}	ΔF^0 , kcal./mole	ΔS^0 , e.u.	ΔH^0 , kcal./mole
1020	0.32	2.3	2.6	5.0
1021	.31	2.3	2.6	5.0
1065	.33	2.3	2.6	5.1
1112	.30	2.7	2.6	5.5
1143	.21	3.6	2.5	6.5
1173	.24	3.3	2.5	6.3
1230	.21	3.9	2.5	7.0
1272	.16	4.7	2.5	7.9
1303	.15	5.0	2.5	8.2

formation of this type, we might postulate the following endothermic equilibrium to occur within the reaction vessel at higher temperatures

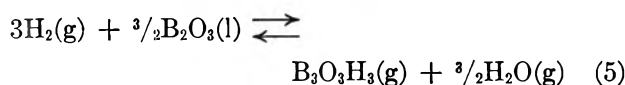


This would result in an increase in the activities of B and B_2O_3 —and therefore of $(a_B a_{B_2O_3})$ as in K_1 , and $(a_B^{2/3}/a_{B_2O_3}^{1/3})$ as in K_3 —with increasing temperature. Neglecting these factors then would lead to an overestimation of ΔH^0_T for reaction 1 and an underestimation of ΔH^0_T for reaction 3, the discrepancies being much larger in the case of the second law calculations. This is consistent with the experimental findings reported here. For reaction 1, then, the value of ΔH^0_T obtained from the second law calculation would actually include ΔH^0_T for reaction 4, whereas that obtained from

the third law calculation would be a reasonable upper limit for ΔH^0_T of reaction 1 itself. For reaction 3, the third law calculation would provide a lower limit for ΔH^0_T .

From the third law values of ΔH^c_T , heats of formation of $B_3O_3H_3$ and $B_3O_4H_3$ have been calculated using tabulated values for ΔH^0_f of B_2O_3 .⁹ Corrections to ΔH^0_{f298} were made from estimated values of $(H^0_T - H^0_{298})$ for the boroxines and tabulated values for B, O_2 , and H_2 . Using this treatment for $B_3O_3H_3$ gives $\Delta H^0_{f298} = -308 \pm 6$ kcal./mole, and for $B_3O_4H_3$ $\Delta H^0_{f298} = -399 \pm 6$ kcal./mole. The value for $B_3O_3H_3$ is seen to be in good agreement with that found previously in the study of the fluoroboroxines,⁸ although the coincidence of nearly identical values is fortuitous considering the over-all uncertainties involved.

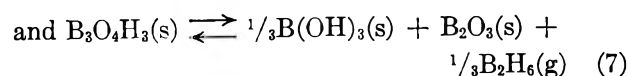
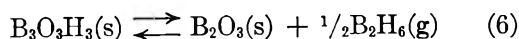
An attempt to produce boroxine by passing H_2 over B_2O_3 alone has resulted in the calculation of a lower limit for ΔH^0_{f298} of $B_3O_3H_3$. The equation for the reaction is



Since only B_2O_3 was in the reaction cell, $a_{B_2O_3}$ could be assumed equal to unity, and the partial pressures of H_2 , $B_3O_3H_3$, and H_2O could be calculated readily from the intensities of the corresponding ions in the mass spectrum. Moreover, the intensity of $B_3O_3H_3$ —which was very low even at the highest temperatures—represented a maximum yield since it included the background contribution. A third law calculation gives $\Delta H^0_{1200} \geq 27.3$ kcal./mole of $B_3O_3H_3$ for reaction 5, from which $\Delta H^0_{f298} \geq -324$ kcal./mole for $B_3O_3H_3$.

Preliminary experiments¹³ have been conducted in an effort to isolate the products of reactions 1 and 3. A sample consisting of a mixture of boron and B_2O_3 contained in a molybdenum boat was heated in a quartz tube to a temperature of 1325°K. Water vapor was introduced into the system through a glass frit and the system was pumped through a liquid nitrogen trap, maintaining a pressure of about 1 mm. A white solid condensed in the trap and on warming the trap to room temperature a gas evolved, which was shown by mass spectrometric analysis to be mainly diborane. Upon further heating of the white residue to about 200°, hydrogen was evolved along with additional diborane and there was some discoloration of the solid. The evolution of hydrogen is presumably accompanied by the production of a suboxide of boron. Accordingly, the remaining solid was analyzed by permanganate titration to give the approximate composition $BO_{1.38}$.

These results indicate that at room temperature the condensed products probably disproportionate according to the reactions



From the equilibrium pressure of diborane observed, about 20 mm., ΔF^0_{298} for reaction 6 was calculated and combined with tabulated values of S^0_{298} for $B_2O_3(s)$ and $B_2H_6(g)$ and an estimated value of S^0_{298} for $B_3O_3H_3(s)$ of

(13) S. Gupta and R. F. Porter (further work in progress).

41 e.u., to give an approximate value for the heat of the reaction. The heat of formation of $B_3O_3H_3(s)$ at 298°K. was then found to be -304 kcal./mole. The heat of formation of gaseous boroxine would be assumed to be 8 to 10 kcal. more positive, leading to a value of about -295 kcal./mole. This result suggests that $B_3O_3H_3(g)$ is somewhat less stable than was indicated by the previous experimental data. In view of this we suggest as the most probable value $\Delta H^0_{f298} = -302 \pm 7$ kcal./mole for $B_3O_3H_3(g)$. This also requires lowering the value for $B_3O_4H_3(g)$ to $\Delta H^0_{f298} = -393 \pm 7$ kcal./mole.

Table V is a list of best values presently available for the heats of formation at 298°K. for boroxine, the fluoroboroxines, and the hydroxyboroxines. Bond energies were estimated, utilizing the experimental heats of formation listed in column two of the table. The B-H bond energy was assumed to be the same as that in BH_3 , 90 kcal./mole, and Cottrell's value of 110.6 kcal. was used for the O-H bond energy.¹⁴ Using these, the values for the remaining bond energies most consistent with the experimental heats of formation are as follows: B-O (in ring), 128 kcal.; B-O (out of ring), 120 kcal.; and B-F, 144 kcal. The last column of Table V lists the heats of formation obtained by using the above bond energies. Cottrell¹⁴ lists bond energies of 128 kcal. for B-O in alkyl borates, and 154 kcal. for B-F in BF_3 . The difference between the B-F bond strength in BF_3 and that in $B_3O_3F_3$ is consistent with the difference in B-F stretching frequencies reported for the two molecules.¹⁵ A difference of this magnitude between the B-H bond strengths in $B_3O_3H_3$ and in BH_3 would not be expected, since the interaction of the external bonds with the ring should be less in this case.

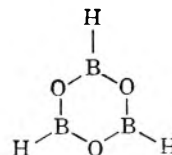
TABLE V
HEATS OF FORMATION OF GASEOUS BOROXINES AT 298°K.

Gaseous molecule	ΔH^0_{f298} (kcal./mole)	
	Experimental	Calcd. from bond energies
$B_3O_3H_3$	$-302 \pm 7^{a,b}$	-305
$B_3O_4H_3OH$	-393 ± 7^a	-386
$B_3O_3H(OH)_2$		-467
$B_3O_3(OH)_3$	-541 ± 10^c	-548
$B_3O_3H_2F$	-392 ± 6^b	-392
$B_3O_3HF_2$	-479 ± 5^b	-480
$B_3O_3F_3$	-567 ± 2^c	-567

^a This work. ^b Reference 8. ^c Reference 9.

Discussion

The structure of boroxine is assumed to be basically a six-membered ring of alternate atoms as in borazine, $B_3N_3H_6$, although the bond angles within the ring are not necessarily equal. More likely, the B-O-B angles



are somewhat less than 120° and the O-B-O angles greater than 120°. The mass spectral pattern of

(14) T. L. Cottrell, "Strengths of Chemical Bonds," 2nd Ed., Butterworths, London, 1958.

(15) H. D. Fisher, W. J. Lehmann, and I. Shapiro, *J. Phys. Chem.*, **65**, 1166 (1961).

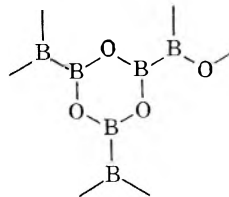
boroxine is found to be analogous to that of borazine¹⁶ rather than that of trifluoroboroxine, $B_3O_3F_3$. As with borazine the major ion peak in the spectrum of $B_3O_3H_3$ is that resulting from loss of a H atom. This behavior also has been found with $B_3O_3FH_2$ and $B_3O_3F_2H$, whereas with $B_3O_3F_3$ the major peak observed is the parent ion. The second most abundant fragment ion from boroxine, $B_2O_2H^+$, corresponds to $B_2N_2H_3^+$ in the borazine spectrum. The size of this peak has been explained in part for borazine by the fact that stable neutral fragments result from such a fragmentation, which involves the breaking of alternate bonds in the ring. No important rearrangement process is evident in the spectrum of boroxine, as occurs with trifluoroboroxine where $B_2OF_3^+$ is the major fragment ion observed. The analog of the only other appreciable fragment peak found here, BOH^+ , is not so abundant in the borazine spectrum.

The observed appearance potentials for $B_3O_3H_3^+$ and $B_3O_3H_2^+$ (13.5 and 14.5 e.v., respectively) may be compared with those for the corresponding ions of $B_3N_3H_6$ (10.2 and 11.5 e.v.) and C_6H_6 (9.6 and 14.5 e.v.). A difference of only about 1 e.v. exists between the appearance of the parent and the parent-minus-H ions for both boroxine and borazine, whereas for benzene this difference is about 5 e.v. This is reflected in the apparent ease with which $B_3O_3H_3$ and $B_3N_3H_6$ lose an H atom upon ionization, thus giving large parent-minus-H peaks, while for C_6H_6 the parent ion peak is the most abundant.¹⁶

No evidence was found for the formation of the molecule $B_2O_3H_2$ reported by Ditter and Shapiro as an intermediate in the oxidation of pentaborane.⁷ The small ion peaks at $m/e = 68-70$ are most likely fragments belonging to the $B_3O_3H_3$ spectrum. At best, the amount of $B_2O_3H_2$ present would be only a few per cent of that of boroxine.

There have been several reports¹⁷⁻²⁰ of a condensed $(BO)_x$ polymer of the type postulated in the preceding section. Indirect evidence for a condensed $B-B_2O_3$ phase also has been reported by Inghram, *et al.*,²¹

who observed that the addition of boron greatly reduced the vapor pressure of B_2O_3 at high temperatures. A three-dimensional pattern of "boroxole rings" has been suggested¹³ as a possible structure for the $(BO)_x$ polymer



This structure of alternate boron and oxygen atoms in a six-membered ring also has been postulated as the basic unit in polyborates, and is considered to have unusual stability in the crystalline polyborates as well as in aqueous solution.²² The formation of boroxine from such a structure is easily visualized.

The species $B_2O_2(g)$ has been reported to be highly stable at high temperatures in the vapor from a $B-B_2O_3$ mixture.²¹ The contribution of this molecule was negligible in our experiments, however, since at the temperatures employed here its vapor pressure was low compared to that of the product, $B_3O_3H_3$. At higher temperatures $B_2O_2(g)$ would be expected to become predominant, unless the hydrogen pressure were increased to overcome this. The best yield of boroxine should therefore be expected with high H_2 pressures and temperatures around 1200°K.

The third law calculations for reactions 1 and 3 tend to minimize errors due to either activity effects or kinetic effects. The discrepancy between the second law and third law values for reaction 1 might be used to calculate a heat for reaction 4. However, part of this discrepancy is likely due to kinetic effects; therefore, such a calculation would be highly speculative.

(17) T. Wartik and E. F. Apple, *J. Am. Chem. Soc.*, **77**, 6400 (1955).

(18) A. L. McCloskey, R. J. Brotherton, and J. L. Boone, *ibid.*, **83**, 4750 (1961).

(19) F. A. Kanda, A. J. King, V. A. Russell, and W. Katz, *ibid.*, **78**, 1509 (1956).

(20) M. D. Scheer, *J. Phys. Chem.*, **62**, 490 (1958).

(21) M. G. Inghram, R. F. Porter, and W. A. Chupka, *J. Chem. Phys.*, **25**, 498 (1956).

(22) J. O. Edwards and V. Ross, *J. Inorg. Nucl. Chem.*, **15**, 329 (1960).

(16) E. D. Loughran, C. L. Mader, and W. E. McQuiston, Atomic Energy Commission Report IA-2368 (1960).

COMPARISON OF MASS SPECTRAL REGULARITIES FOR *n*-PARAFFINS AND *n*-TERMINAL OLEFINS¹

BY NORMAN D. COGGESHALL

Guif Research & Development Company, Pittsburgh, Pennsylvania

Received August 1, 1962

The mass spectra of *n*-paraffins and *n*-terminal olefins in the C₁₀ to C₂₀ range, inclusive, have been studied to establish the quantitative relationships that must be predicted by a satisfactory theory of mass spectra. The *n*-terminal olefin spectra are generically similar to those for the *n*-paraffins but systematically have a higher center of gravity (based on $C(M,n)$ plots). The linear behavior of classes upon M (carbon number of parent molecule) previously observed for *n*-paraffins has been confirmed by this investigation. The same type of class dependence upon M was observed for the olefins. Subclasses defined by $Y(M,n,j)$, each of which represents specific ions, showed, for both classes of compounds, a linear dependence on M expressible as $Y(M,n,j) = f_j(n) \cdot (M - n_j')$. The postulate that the molecules first dissociate into C_{*n*}H_{2*n*+1} ions with subsequent dissociation into ions of different stoichiometry is shown to be untenable for some classes of ions but not for others. The data indicate that the presence of the double bond probably affects the molecule as a whole in all its dissociation modes rather than just those modes involving the double bond. Classes of ions defined by particular stoichiometric relationships and summed over all *n* are shown to be independent of or linearly dependent upon M . This suggests that the molecules may first dissociate to a particular stoichiometry and then to the final values of *n*.

The theoretical studies aimed at formulating and quantitatively testing a complete theory of the fragmentation and ionization by electron impact need systematically obtained data obtained under controlled conditions. Steiner,^{2a} *et al.*, and Schug,^{2b} *et al.*, discussed some of the difficulties in the application of the statistical theory prior to its reformulation.³ It is believed that the data taken for events near and just beyond onset of fragmentation should be supplemented by observations at higher electron voltages wherein the structure type or molecular weight of the molecule are systematically varied. The purpose of this is to establish the quantitative relationships between mass spectral parameters and structural parameters. This report constitutes an extension of studies previously reported⁴ on *n*-paraffin spectra.

Source and Treatment of Data.—In the previous study⁴ the data were largely taken from existing API Research Project 44 spectral files. In this study, the data were taken at this Laboratory on a C.E.C. Model 21-103 instrument. The conditions were as follows: electron current = 10.5 μ a.; ionizing voltage = 70 volts; ion chamber temperature = 250°; vapor temperature = 200°; first scan, m/e 12 through 90, magnet current 230 ma. (2200 gauss); second scan, m/e 60 through 500, magnet current 530 ma. (5067 gauss); and collector slit width = 7 mils.

The compounds examined comprised the *n*-paraffins and the normal terminal olefins, C₁₀ through C₂₀, excepting the C₁₉ members of both types which were unavailable. The compounds were obtained from the Phillips Petroleum Company, the Aldrich Chemical Company, and the American Petroleum Institute. Infrared examination indicated the possibility of several per cent of olefin types other than the *n*-terminal olefins in the higher molecular weight members. However, this test⁵ is not highly accurate, and it cannot be reli-

ably calibrated in this range due to the unavailability of reference compounds. There was no mass spectral evidence for any isoölefins. In consideration of all the data obtained, it is believed that if impurity olefins were present that they were of the *cis* and *trans* *n*-olefin type.

Relative to the latter point, an examination of the API data for terminal *vs.* internal double bond *n*-olefins of the C₇, C₈, and C₉ classes showed spectral variations for the internal bond types which were not observed in the present studies. To our knowledge the spectra obtained therefore represent the best that can be obtained for the normal terminal olefins in the mass range studied until further, more highly purified materials become available.

As in the previous study⁴ we denote by $P_{M,n,j}$ the normalized ion intensity for an ion of stoichiometry C_{*n*}H_{2*n*+2-*j*} coming from a compound of M carbon atoms. An ion sum $C(M,n)$ is the summation of normalized intensities of all ions of *n* carbon atoms. The yield $Y(M,n) = MC(M,n)$ represents the yield of all ions of *n* carbon numbers being produced from a compound of M carbon atoms per unit of ionizing current and per mole.

A C.E.C. Mascot digitized the data for punching onto IBM cards. The cards were handled by machine calculations and tabulation to yield the data in a variety of forms. The intensities were given as percentages of total ionization, as monoisotopic peak heights, and as monoisotopic percentages of total ionization. Also, the ion summations ($C(M,n) = \sum_j P_{M,n,j}$) by carbon number on a monoisotopic basis were calculated.

General Behavior.—In Fig. 1 may be seen plotted the $C(M,n)$ values for both *n*-octadecane and octadecene-1. The relative behavior seen here is typical of the entire series of paraffins and olefins. The differences always observed comprised the olefin $C(M,n)$ values being lower through $n = 4$, being higher for the region $n = 5$ to 9, and lower throughout the remainder. Clearly the centers of gravity of the $C(M,n)$ plots are shifted to higher values for the olefins. In Table I are given the n values for the centers of gravity (CG) of all members and the shift for each carbon number. It is interesting to note that the CG is shifting progressively to larger n values for both classes but that the difference between

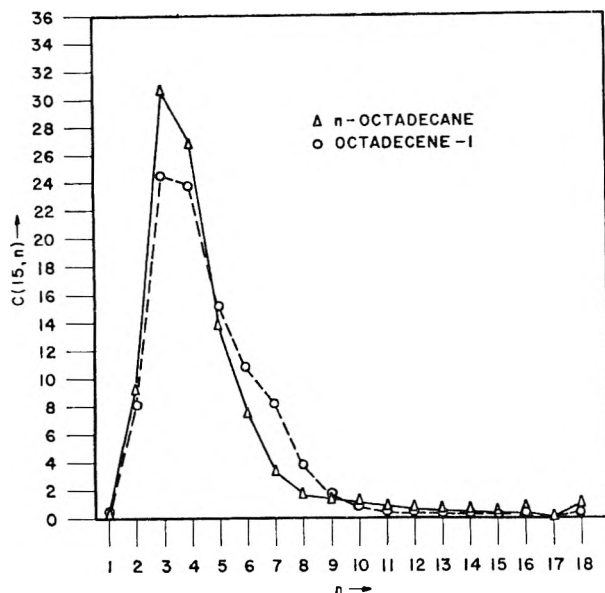
(1) This material was presented at the 1961 meeting of ASTM E-14, Mass Spectrometry, Chicago, Ill., as paper no. 26.

(2) (a) B. Steiner, C. Giese, and M. Inghram, *J. Chem. Phys.*, **34**, 189, (1961); (b) J. C. Schug and N. D. Coggeshall, *ibid.*, **35**, 1146 (1961).

(3) M. Vestal, A. Wahrhaftig, and W. Johnson, paper no. 19 presented at the 1961 meeting of ASTM E-14 on Mass Spectrometry at Chicago, Ill., 1961.

(4) N. D. Coggeshall, *J. Chem. Phys.*, **33**, 1247 (1960).

(5) E. L. Saier, A. Pozefsky, and N. D. Coggeshall, *Anal. Chem.*, **26**, 1258 (1954).

Fig. 1.— $C(M,n)$ values for n -octadecane and for 1-octadecene.

corresponding members reaches a maximum for $n = 16$ and then progressively decreases.

TABLE I
CENTERS OF GRAVITY OF THE $C(M,n)$ PLOTS

Carbon no.	n -Paraffin	n -Terminal olefin	Difference
C_{10}	3.73	3.89	0.16
C_{11}	3.83	4.02	.15
C_{12}	3.94	4.13	.19
C_{13}	4.04	4.26	.22
C_{14}	4.15	4.37	.22
C_{15}	4.24	4.48	.24
C_{16}	4.36	4.57	.31
C_{17}	4.47	4.67	.20
C_{18}	4.55	4.73	.18
C_{20}	4.82	4.96	.12

$Y(M,n)$ values were plotted vs. M and the types of relations observed previously for the n -paraffins⁴ again were obtained and the same generic type behavior also was obtained for the olefins. The data for the latter are seen in Fig. 2. Here it may be seen that the $Y(M,n)$ approximately obey the general type relation

$$Y(M,n) = f(n)(M - n') \quad (1)$$

In Table II are given the $f(n)$ values for both classes from this work as determined from the curve slopes, the $f(n)$ values from the previous work, and the n' values for the olefins. The latter were algebraically determined from the straight lines in Fig. 2. These were not determined for the paraffins as it is believed the larger range of M covered previously provides better n' values. Values of $f(n)$ and n' were not determined for $n > 9$ as the limited spread of M and the low $Y(M,n)$ values do not permit adequate accuracy.

It is interesting to note that for the paraffins the present $f(n)$ values are in fair agreement with those previously determined except for $n = 6$. In this case it is believed the previous value should be preferred due to the greater spread in M . A large difference in $f(n)$ behavior between the paraffins and olefins may be noted with $f(n)$ peaking at $n = 4$ for the latter and decreasing much more slowly with increasing n .

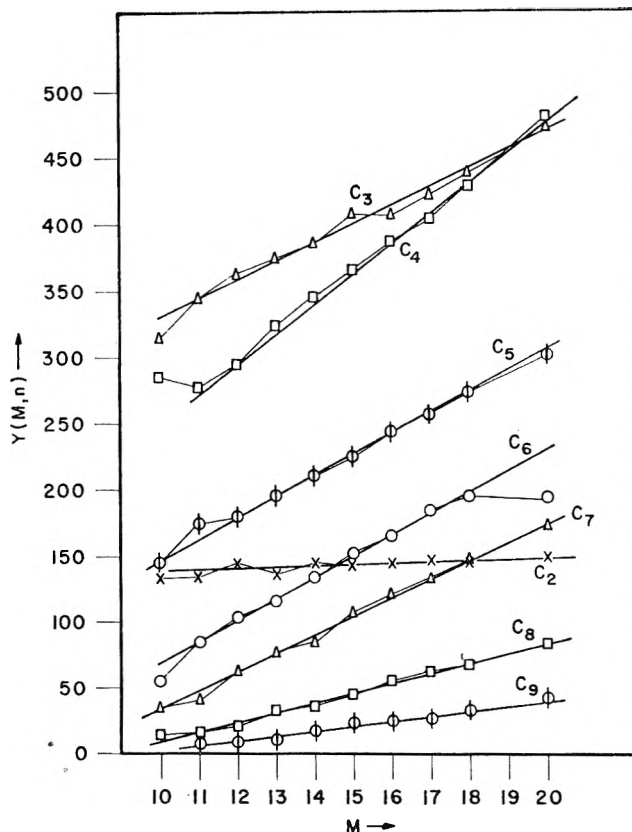
Fig. 2.— $Y(M,n)$ plots for various n 's for the n -terminal olefins.

TABLE II
 $f(n)$ VALUES FOR THE n -PARAFFINS AND n -TERMINAL OLEFINS
AND n' VALUES FOR THE LATTER

n	Paraffins— $f(n)$ values		Olefins	
	(This work)	Previous ⁴	$f(n)$	n'
2	2.0	..	0.55
3	21.6	23.2	13.9	-13.7
4	27.1	28.9	22.9	-0.9
5	19.8	20.6	16.2	0.9
6	10.3	14.9	16.0	5.6
7	6.4	6.8	14.0	7.6
8	3.4	3.6	7.3	8.6
9	2.5	2.1	3.7	8.8

The data of this study provided the behavior for the C_1 and C_2 type ions which could not be determined in the previous study. This is because data for these ions have been left out of most of the API spectra. In Table III are given the $Y(M,n)$ values for $n = 1$ and 2. When these are expressed as $C(M,n)$ values, it is clear that the data used to construct Fig. 1 of reference 4 were not very accurate and that curve which was used to interpolate for $C(M,1) + C(M,2)$ dips too steeply with increasing M . It is of interest to note for both types that the increase of $Y(M,n)$ with M is very small for $n = 2$ and that there is actually a negative slope for $n = 1$.

Subclass Behavior.—In the previous section we discussed the behavior of ion classes wherein a class was defined as all ions having a particular number, n , of carbon atoms. In this section will be compared the behavior of the types: C_nH_{2n+1} , C_nH_{2n} , C_nH_{2n-1} , C_nH_{2n-2} , and C_nH_{2n-3} which in each case account for practically all of the ions in a class. The comparative behavior of corresponding types within a class should reflect differences in dissociation behavior between a n -paraffin and a n -terminal olefin. For example, we may

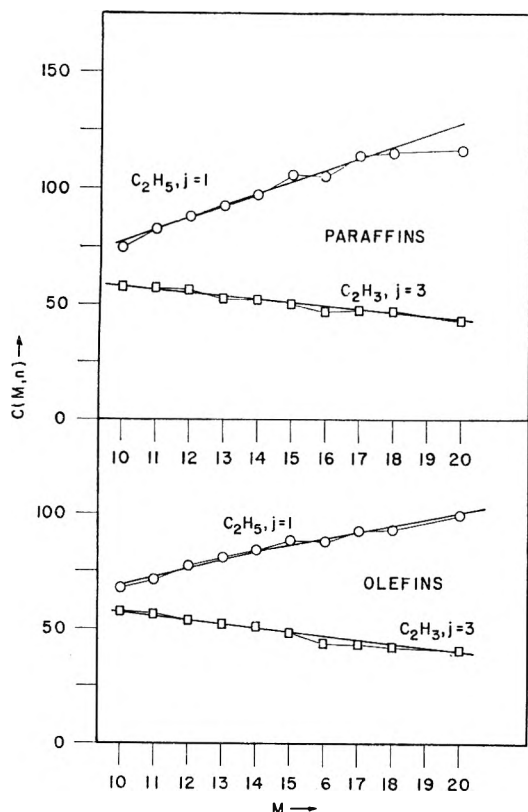


Fig. 3.—Subclass behavior for the principal ions for $n = 2$ for the paraffins and olefins.

TABLE III

VALUES OF $Y(M,1)$ AND $Y(M,2)$ FOR n -PARAFFINS AND n -TERMINAL OLEFINS

M	Paraffins		Olefins	
	$Y(M,1)$	$Y(M,2)$	$Y(M,1)$	$Y(M,2)$
10	3.8	136	4.8	132
11	3.6	146	4.2	134
12	3.4	154	4.0	144
13	3.0	159	3.5	138
14	2.7	155	3.4	144
15	2.3	159	2.9	143
16	2.2	156	2.7	144
17	2.6	164	3.2	148
18	2.3	164	2.9	146
20	1.9	165	2.4	150

postulate that the dissociation proceeds as follows: (1) first, a carbon-carbon bond is broken to yield C_nH_{2n+1} ions, and (2) the C_nH_{2n-1} ions then dissociate to yield C_nH_{2n} , C_nH_{2n-1} , etc., ions. If this were true, the yields of the C_nH_{2n+1} ions from olefins would be expected to be only one-half of the yields of the corresponding types from paraffins of equal molecular weight.

In Fig. 3 is given the behavior of the mass 29 and 27 ions (C_nH_{2n+1} and C_nH_{2n-1}) for the paraffins and olefins. It is to be noted that between types they are about equal in both magnitude and slope with increasing M . This would not be the case if the above postulate were true.

In contrast to the quite similar behavior of paraffins and olefins for the principal 2-carbon ions seen in Fig. 3, we may see large but systematic differences in the subclass behavior shown in Fig. 4 and 5. These give the subclass behavior for the 4- and 5-carbon ion types, respectively. One important observation which may be made immediately is that the individual ions are linear but not proportional to M . Thus, a subclass yield specified by $Y(M,n,j) = MP(M,n,j)$ is expressible as

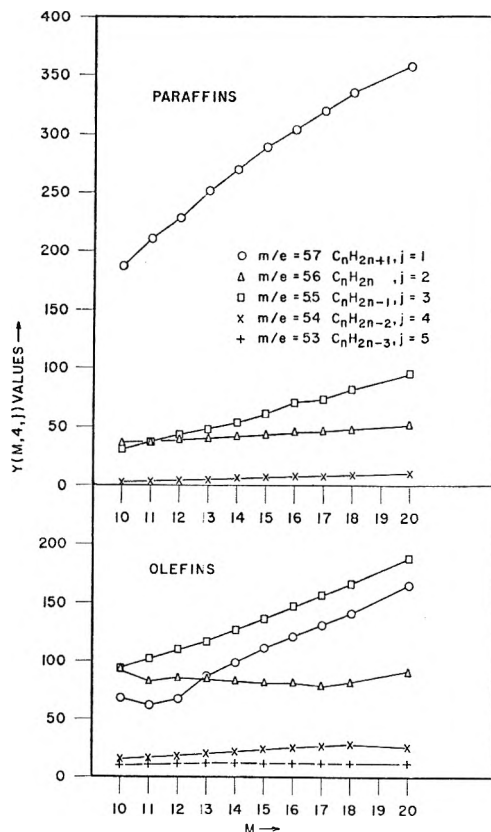


Fig. 4.—Subclass behavior for paraffins and olefins for $n = 4$.

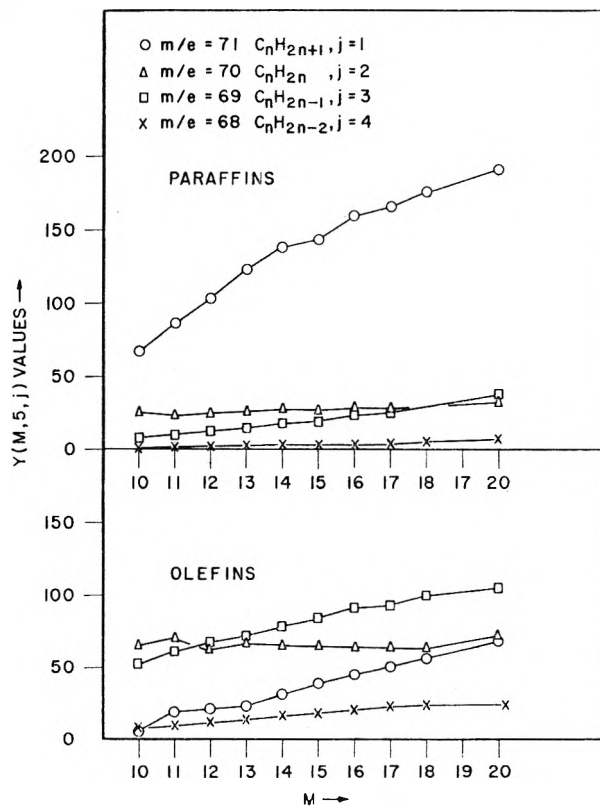


Fig. 5.—Subclass behavior for paraffins and olefins for $n = 5$.

$$Y(M,n,j) = f_j(n)(M - n_j')$$

Thus, we have the observation that the intensity of a subclass ion is linearly dependent, but not proportional to M , the total number of carbon atoms in the molecule. This general type of behavior is observed for both paraffins and n -terminal olefins. However, the numerical

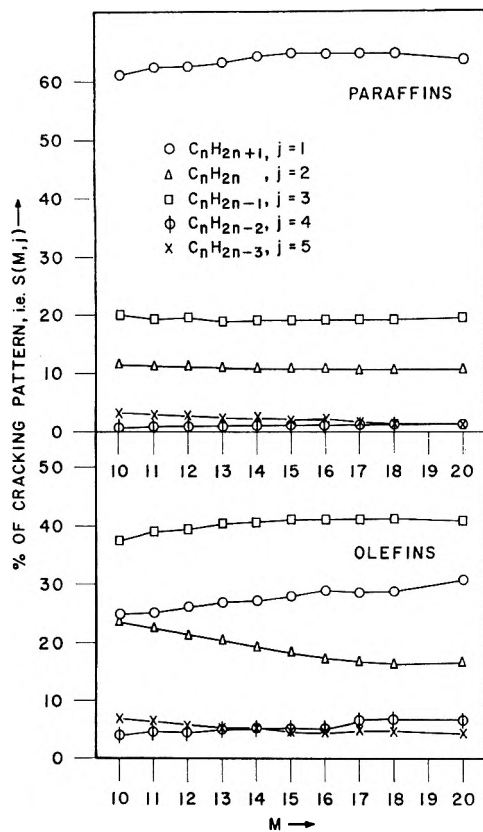
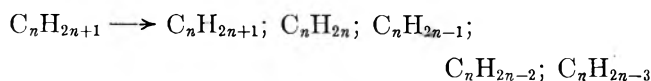


Fig. 6.— $S(M,j)$ behavior as dependent on M for paraffins and olefins.

values, $f(n)$ and n_j' , obviously differ widely for ions of the same type and mass originating from the two classes of compounds.

Slopes, *i.e.*, $f_j(n)$ values, were determined for subclasses up to $n = 7$, inclusive. These are given in Table IV. Due to the scatter of points and the limited mass range, these values should not be regarded as highly accurate, especially for ions of low intensity. Also included in Table IV are the Y values for the two C_{15} compounds, pentadecane and pentadecene-1. Using these and the $f_j(n)$'s, one can readily calculate the Y for any subclass type for any other molecule among those examined.

These data also provide evidence against the simple dissociation model postulated above. By it we would expect the initially formed C_nH_{2n+1} ions to divide into the various subclasses as



A simple ancillary postulate to this model would be that C_nH_{2n+1} ions would always divide into the subclasses with the same relative relationships. Since the yield of the C_nH_{2n+1} ions increases with molecular weight M of the parent molecule, each subclass would also increase with M . Thus all $f_j(n)$ values would be positive. Negative values have been clearly obtained for some classes and they constitute evidence against the above model and the ancillary postulate.

It seems very significant that the wide differences in slope occur within a subclass. In the previous work it was shown that class yields in terms of ions produced per unit of ionizing electron current and per mole of compound in the observation region are dependent in

TABLE IV
SLOPES FOR PRINCIPAL SUBCLASS IONS AND Y VALUES FOR IONS FROM C_{15} MOLECULES

Class n	Subclass	Ion mass	Slopes, f values		— Y values, C_{15} —	
			Paraffins	Olefins	Penta-decane	Penta-decene-1
2	C_nH_{2n+1}	29	5.1	3.3	106	88.9
	C_nH_{2n-1}	27	-1.4	-1.7	50.3	48.8
3	C_nH_{2n+1}	43	15.5	10.1	289	164
	C_nH_{2n}	42	0.6	-0.5	36.1	34.5
	C_nH_{2n-1}	41	7.6	6.2	139	168
	C_nH_{2n-2}	40	0.0	0.0	3.4	4.6
	C_nH_{2n-3}	39	-1.1	-1.3	21.6	36.2
4	C_nH_{2n+1}	57	17.9	11.4	289	111
	C_nH_{2n}	56	1.4	-1.0	43.4	81.3
	C_nH_{2n-1}	55	6.5	9.5	61.1	136
	C_nH_{2n-2}	54	1.0	1.8	6.4	24.0
	C_nH_{2n-3}	53	0.1	0.0	6.1	12.0
5	C_nH_{2n+1}	71	13.0	6.1	144	38.3
	C_nH_{2n}	70	0.3	-0.3	26.9	65.3
	C_nH_{2n-1}	69	3.0	6.1	19.6	84.8
	C_nH_{2n-2}	68	0.5	2.0	3.3	17.9
	C_nH_{2n-3}	67	0.5	2.0	3.7	16.8
6	C_nH_{2n+1}	85	8.0	3.3	77.0	15.6
	C_nH_{2n}	84	0.33	0.5	13.1	34.1
	C_nH_{2n-1}	83	2.1	8.4	8.3	75.5
	C_nH_{2n-2}	82	..	2.3	2.0	18.3
	C_nH_{2n-3}	81	..	1.2	0.6	5.9
7	C_nH_{2n+1}	99	2.5	1.2	18.4	1.7
	C_nH_{2n}	98	1.3	0.25	13.4	23.8
	C_nH_{2n-1}	97	2.4	9.1	6.9	69.0
	C_nH_{2n-2}	96	..	1.8	1.0	9.2
	C_nH_{2n-3}	95	0.5	3.1

some cases directly upon the size of the neutral fragments produced. However, in all cases observed there, the class yields varied linearly with total mass of the molecule. In Fig. 4 and 5 and in Table IV we see subclass yields which increase linearly with M or which are essentially independent of M as is the case for the C_nH_{2n} ions from both paraffins and olefins. In Fig. 3 we see, for the C_nH_{2n-1} ions from both compound types, an example of a decrease of yield with M . Other examples may be seen in Table IV. Thus, we see instances where increasing the size of the molecule may increase or decrease the probability of creation of particular ions.

The fact that subclasses depend differently upon M , or equivalently upon total mass, suggests that the subclass types each arise through different dissociation mechanisms. This in turn suggests that the summation of a particular subclass type over n should show a regular trend with M . We define such a summation as $S(M,j)$ which is given by

$$S(M,j) = (1/M) \sum_n Y(M,n,j) = \sum_n P_{m,n,j}$$

$S(M,j)$ thus represents the fraction, expressed in per cent, of all ions from a molecule of M carbon atoms that have the stoichiometry C_nH_{2n+2-j} , $n = 1, 2, 3, \dots, M$. In Fig. 6 are plotted the $S(M,j)$'s for the paraffins and olefins. By definition, $\sum_j S(M,j) = 100$. From

the observed behavior in Fig. 6, it is clear that $S(M,j)$ is approximately constant or a linear function of M in all cases. Thus, we may express

$$S(M,j) = a_j M + b_j$$

From above we know that

$$\frac{\partial}{\partial M} \sum_j S(m, j) = 0$$

so that $\sum a_i = 0$, which states that the negative slopes balance out the positive slopes. This is quite evident in both sets of curves in Fig. 6.

The data in Fig. 4, 5, and 6 and in Table IV all demonstrate the rather extensive differences in detail between the characteristics of n -paraffin and n -terminal olefin spectra. Let us assume that the existence of the terminal double bond did not in any way affect the dissociation mechanism involving bonds apart from the double bond itself. With this assumption it would be possible to calculate much of the olefin spectra from the n -paraffin spectra as the effect of the double bond would be a mere stoichiometric change for many ions. The observed differences are much more profound than this and they indicate that the presence of the terminal olefin bond affects the whole molecule in its dissociation behavior.

Conclusions

The observations of above may be summarized as follows: (a) the spectra plotted as $C(M, n)$ vs. M of the n -terminal olefins are generically similar to those of the n -paraffins in demonstrating the universal maxima in the C_3 - C_4 region with general decrease of intensities with increasing carbon number, (b) the $Y(M, n)$ for n -terminal olefins also depend linearly upon M , (c) the center of gravity of the $C(M, n)$ plots are always higher for the olefins than for the corresponding paraffins, (d)

the subclass behavior, expressible through $Y(M, n, j)$, for both paraffins and olefins was shown to be represented by

$$Y(M, n, j) = f_j(n)(M - n_j')$$

(e) the differences in subclass behavior between the two types of compounds show the invalidity of the postulate that the molecules first dissociate into C_nH_{2n+1} ions and these in turn dissociate further into C_nH_{2n} , C_nH_{2n-1} , C_nH_{2n-2} , etc., ions, (f) the subclass differences between the olefins and paraffins show that the double bond in the olefins has a general effect on the dissociation pattern that cannot be explained by a mere difference in stoichiometry, and (g) the subclass behavior for both types of compounds indicates that a molecule C_MH_{2M+2} may first dissociate into C_MH_{2M+1} , C_MH_{2M} , C_MH_{2M-2} , or C_MH_{2M-3} ions with further dissociations into ions of different n values but of the same stoichiometry; suitable changes in stoichiometry apply to the consideration of olefins.

Although some speculation is offered relative to dissociation mechanisms, the main purpose of this work has been to find and describe mass spectral regularities that have regular dependence on M , n , or j , as used above. Such regularities must be quantitatively explained by the unimolecular theory as it develops and they serve to guide the development and to provide tests of validity.

Acknowledgment.—Grateful acknowledgment is due to Dr. J. C. Schug for worthwhile discussions of this subject.

THE ROLE OF DISSOLVED WATER IN PARTITION EQUILIBRIA OF CARBOXYLIC ACIDS

BY SHERRIL D. CHRISTIAN, HAROLD E. AFFSPRUNG, AND STANTON A. TAYLOR

Department of Chemistry, University of Oklahoma, Norman, Oklahoma

Received August 16, 1962

Partition and water solubility data have been obtained for the system water-benzene-acetic acid, with the object of calculating the extent of hydration of the acetic acid species in the benzene phase. Results are consistent with the assumption that a monomer hydrate, but no dimer hydrate, forms in the organic phase at low acid concentrations. A general analytical treatment is presented for calculating hydration constants for solutes which associate in organic solvents.

Introduction

The partition, or distribution, method has been widely used in the determination of dimerization constants of carboxylic acids in solvents only slightly miscible with water.¹⁻⁴ In using the method, it is commonly assumed that the presence of small amounts of dissolved water in the non-aqueous phase does not interfere with the association of the acid.¹ However, we have noticed that literature values of dimerization constants calculated from partition data frequently are lower than those reported for the same acids in the corresponding anhydrous solvents.⁵

A plausible explanation for this discrepancy in dimerization constants is that dissolved water reacts with the acid monomer to form a hydrate. To test this theory, we decided to measure the solubility of water in benzene as a function of the concentration of dissolved acetic acid. The Karl Fischer method was employed to analyze for water. Equilibrium concentrations of acetic acid in the benzene phase and in the aqueous phase were determined using standard alkali. We observed that the total concentration of water in the benzene phase increases significantly as total acid concentration is increased.

Theory

Our solubility data can be explained on the basis of the assumption that the only species present as solutes in the benzene phase are CH_3COOH , $(CH_3COOH)_2$, H_2O , and $CH_3COOH \cdot H_2O$ (monomer hydrate). The

(1) M. Davis and H. E. Hallam, *J. Chem. Educ.*, **33**, 322 (1956).

(2) E. A. Moelwyn-Hughes, "Physical Chemistry," Pergamon Press, Oxford, Second Revised Edition, 1961, pp. 1078-1080.

(3) G. C. Pimentel and A. L. McClellan, "The Hydrogen Bond," Freeman and Company, San Francisco and London, 1960, pp. 45-49.

(4) E. A. Moelwyn-Hughes, *Trans. Chem. Soc.*, 850 (1940).

(5) Reference 3, Appendix C, pp. 368-376.

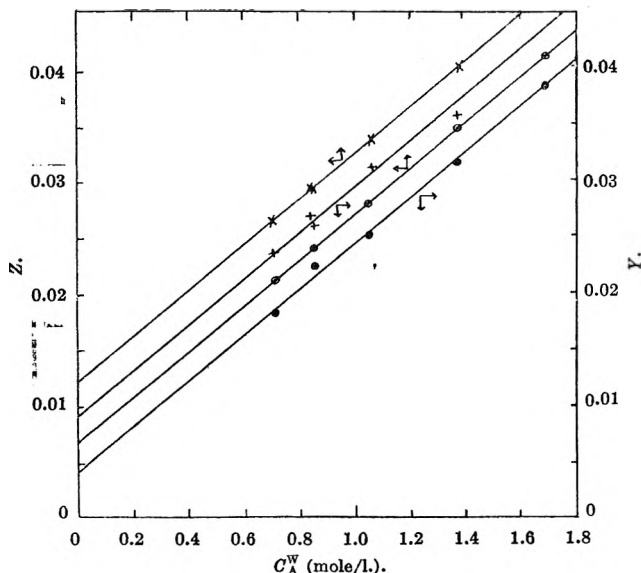


Fig. 1.—Dependence of Z and Y on C_A^w . Z values: \times , at 35° ; \circ at 15° . Y values: $+$ at 35° ; \bullet at 15° .

formal concentration of acetic acid in benzene can be expressed as

$$f_A^b = c_A^b + 2c_{A_2}^b + c_{AW}^b \quad (1)$$

and the formal concentration of water in benzene may be written as

$$f_W^b = c_{AW}^b + c_W^b \quad (2)$$

where c_A^b , $c_{A_2}^b$, c_W^b , and c_{AW}^b represent the molarities of the species CH_3COOH , $(\text{CH}_3\text{COOH})_2$, H_2O , and $\text{CH}_3\text{COOH}\cdot\text{H}_2\text{O}$, respectively, in the benzene phase at equilibrium. Further, the equilibrium quotients

$$K_2 = c_{A_2}^b/c_A^{b^2}, K_h = c_{AW}^b/c_A^b c_W^b, K_D = c_A^b/c_A^w \quad (3)$$

should remain constant in dilute solutions; where c_A^w represents the concentration of acetic acid monomer in the aqueous phase, K_2 and K_h are the acid dimerization constant and acid monomer hydration constant in benzene, and K_D is the distribution constant for the acid monomer.

Combining equations 1, 2, and 3, we may write

$$\frac{f_A^b - f_W^b + c_W^b}{c_A^w} = Y = K_D + 2K_D^2 K_2 c_A^w \quad (4)$$

and

$$f_A^b/c_A^w = Z = K_D + K_h c_W^b K_D + 2K_D^2 K_2 c_A^w \quad (5)$$

where Y and Z are defined in terms of measurable concentrations.⁶ Note that plots of Y vs. c_A^w and Z vs. c_A^w should be linear, with a common slope of $2K_D^2 K_2$. However, the intercept obtained from a plot of Z vs. c_A^w should exceed that determined from a plot of Y vs. c_A^w by the constant $K_h c_W^b K_D$.

Results

Table I contains the partition and solubility data for the system water-benzene-acetic acid at 15 and 35° . The upper limit of the concentration of acid in the organic phase is about $0.07 M$, corresponding to a con-

(6) In dilute solutions, c_W^b should be constant and equal to the solubility of water in pure benzene at the given temperature. Also, c_A^w (the acid monomer concentration in the aqueous phase) is equal to the formal concentration of acetic acid in water minus the concentration of the acetate ion, which can be computed from the ionization constant.

centration of about $1.7 M$ in the aqueous phase. Although the water solubility data scatter to a certain extent, the increase in water concentration in the organic phase is striking and parallels the increase in acid concentration.

TABLE I
PARTITION AND WATER SOLUBILITY DATA^a

f_A^b	c_A^w	f_W^b
At 15°		
0	0	0.0265
0.0152	0.709	.0287
.0206	0.851	.0280
.0294	1.047	.0291
.0474	1.366	.0307
.0691	1.680	.0310
At 35°		
0	0	0.0465
0.0187	0.700	.0485
.0248	.836	.0488
.0249	.841	.0495
.0355	1.048	.0490
.0549	1.361	.0527

^a All concentrations in mole/liter.

As a test of the hydration theory, the data are plotted in Fig. 1 in the form Y vs. c_A^w and Z vs. c_A^w . It can be seen that at each temperature the Y and Z points define nearly parallel curves; consequently, in curve-fitting data at each temperature, the curves were forced to have equal slopes. Table II summarizes results calculated from the parameters of these straight lines.

Except for the additive constant $K_h c_W^b K_D$, eq. 5 is identical with the expression commonly applied in treating partition data to obtain K_2 and K_D . Neglecting $K_h c_W^b K_D$ in comparison with K_D , one could calculate an apparent dimerization constant from the relation

$$K_2^{\text{apparent}} = \text{slope}/2 \cdot \text{intercept}^2 \quad (6)$$

where the slope and intercept are obtained from a plot of Z vs. c_A^w . However, in the present instance, an examination of Fig. 1 reveals that $K_h c_W^b K_D$ is not small compared to K_D ; and as a result, the partition method leads to a value of the dimerization constant that is too low. Values of K_2^{apparent} calculated from the present data by means of eq. 6, and dimerization constants reported by Davies, *et al.*,⁷ (from partition data) are included in Table II for comparison. Note that K_2 values

TABLE II
CURVE PARAMETERS AND CALCULATED EQUILIBRIUM CONSTANTS^a

t , $^\circ\text{C}$.	15	35
Slope from Fig. 1	0.0203	0.0205
Intercept from Fig. 1		
Z curve	0.0067	0.0121
Y curve	.0041	.0091
c_W^b (mole/l.)	.0265	.0465
K_h (l./mole)	26	7.1
K_D	0.0041	0.0091
K_2 (l./mole)	605	125
K_2^{apparent} (l./mole) from eq. 6	225	70
K_2^{apparent} (l./mole) from ref. 7	200 (extrap- olated)	81

^a All concentrations in mole/liter.

(7) M. Davies, P. Jones, D. Patniak, and E. A. Moelwyn-Hughes, *J. Chem. Soc.*, 1249 (1951).

obtained by the preceding analysis are greater by a factor of 2 or 3 than the apparent constants.

Discussion

The results given here cast serious doubt on the reliability of the conventional partition method as a means of determining association constants. We believe that systematic studies of the variation in water solubility with acid concentration in the organic phase should be undertaken in order that available partition data may be re-evaluated with due regard being given to hydration. We also wish to emphasize that the presence of tiny amounts of dissolved water can lead to erroneous results in the case of other methods for determining association constants for carboxylic acids. In fact, we suspect that a major reason for the lack of agreement between various literature values of association constants of carboxylic acids in solution is that small, variable amounts of dissolved water have been present in most of the systems investigated.

Since both the monomer and the dimer of many polar solutes may be expected to hydrate, an extended treatment of data which would allow the determination of the extent of hydration of each species is desirable. We may develop equations analogous to 1 through 5, without making the restrictive assumption that the monomer monohydrate is the only hydrated species in the organic phase. If both the monomer and the dimer form hydrates, with formulas AW_1 and A_2W_k , respectively, the hydration constants may be defined by the relations

$$K_{h1} = c_{AW_1}^b / c_A^b c_W^{b1} \text{ and } K_{h2} = c_{A_2W_k}^b / c_{A_2}^b c_W^{bk} \quad (7)$$

The following equations then may be developed in a manner similar to the development of relations 4 and 5

$$\frac{f_A^b - f_W^b + c_W^b}{c_A^w} = Y = K_D [1 + (1 - j)K_{h1}c_W^{b1}] + K_D^2 [2K_2 + (2 - k)K_{h2}c_W^{bk}] c_A^w \quad (8)$$

and

$$f_A^b / c_A^w = Z = K_D (1 + K_{h1}c_W^{b1}) + K_D^2 (2K_2 + 2K_{h2}c_W^{bk}) c_A^w \quad (9)$$

These equations indicate that even in the more complex situations where both the monomer and the dimer form hydrates, plots of Y and Z vs. c_A^w should be linear. If the monomer hydrates, the intercept of the Z plot will exceed that of the Y plot by the constant $jK_D K_{h1}c_W^{b1}$; and if the dimer hydrates, the slope of the Z plot will exceed that of the Y plot by the constant $kK_D^2 K_{h2}c_W^{bk}$. In order to determine j and k uniquely, further data would be required.

We anticipate that plots of Z and Y similar to those in Fig. 1 will prove to be of great utility in the interpretation of partition data for carboxylic acids and other polar solutes. These plots can be classified into these four types

- Type 1—Slope $Z =$ slope Y ; intercept $Z =$ intercept Y . No hydration of either A or A_2 occurs.
- Type 2—Slope $Z =$ slope Y ; intercept $Z >$ intercept Y . Hydration of A , but not of A_2 , occurs.
- Type 3—Slope $Z >$ slope Y ; intercept $Z =$ intercept Y . Hydration of A_2 , but not of A , occurs.
- Type 4—Slope $Z >$ slope Y ; intercept $Z >$ intercept Y . Hydration of both A_2 and A occurs.

Type 1 plots may be expected only in systems where the solute is not capable of forming hydrogen bonds. The data presented in this paper indicate that systems containing acetic acid, and perhaps other carboxylic acids, yield type 2 plots. In general, it is expected that the majority of systems will be characterized by type 4 plots; and that type 2 and 3 plots will result when hydration of either the monomer or the dimer predominates. Currently we are investigating other systems involving amides, carboxylic acids, and phenols, and in each case we find that the solubility of water in the non-polar solvent is greatly increased by the presence of small concentrations of the polar solute.

Acknowledgment.—This work was supported in part by the National Institutes of Health, and in part by the Research Corporation.

THE EFFECT OF UREA ON MICELLE FORMATION AND HYDROPHOBIC BONDING

BY PASUPATI MUKERJEE AND ASHOKA RAY

Department of Physical Chemistry, Indian Association for the Cultivation of Science, Jadavpur, Calcutta 32, India

Received May 2, 1962

Dissolved urea is suggested as a probe for studying water structure contributions to micelle formation and hydrophobic bonding. Critical micelle concentrations (c.m.c.) of dodecylpyridinium iodide in water and urea solutions at 25 and 45° determined by ultraviolet spectrophotometry are reported. The nature of the spectra and their intensities indicate that the nature of the micelles does not change drastically on the addition of urea. The c.m.c., however, is raised to a moderate extent, the effect being the same at 25 and 45°; urea thus weakens hydrophobic bonding and the effect seems to be independent of temperature. Arguments suggesting the importance of contributions other than those due to water structure are presented. The relation of these findings to the stability of proteins is briefly indicated.

Introduction

Recent investigations¹⁻⁵ have indicated that micelle formation in aqueous solution is primarily an entropy-directed process in which enthalpy changes play a minor role, although considerations based on the loss of interfacial energy, taken for granted until recently,⁶⁻⁹ predict large enthalpy changes. The currently accepted explanation³ invokes the iceberg picture of Frank and Evans.¹⁰ A wide variety of phenomena, including hydrophobic bonding in general,¹¹ can be explained qualitatively on this basis. The possibilities remain, however, that interfacial effects are not entirely negligible, that enthalpies from several sources cancel each other in part, that a proper evaluation of pre-micellar association¹² may alter the thermodynamic picture, and that a substantial entropy contribution, in the case of aliphatic systems, arises from the orientations and bendings of the chain, which may be restricted in water and freer in a non-aqueous environment.^{1,13}

The present paper deals with the use of dissolved urea as a probe for investigating the water structure contribution to micelle formation and hydrophobic bonding. The choice of urea rests on its two outstanding properties in aqueous solutions, namely, its great ability to undergo hydrogen bonding with water, due to the presence of three potential bonding centers on each molecule, and its small effect on the polarity of water. Urea actually increases the dielectric constant of water appreciably and surface tension slightly. At high concentrations, therefore, it should markedly reduce the cooperative structure of water itself, which is primarily due to hydrogen bonding and responsible for the solvent structure effects,^{10,14} without unduly af-

fecting the interfacial effects and the concomitant restrictions on the freedom of movement of organic solutes.

In view of the possibly great significance of hydrophobic bonding in the chemistry of proteins in aqueous solution,¹¹ the effect of urea on micelle formation may contribute to the understanding of the denaturing action of urea. From this point of view, a short study similar to ours has been published recently,¹⁵ after our work was completed. The object of our study is mainly to understand the detailed nature of hydrophobic bonding. The results are in fair agreement with the recent work¹⁵ but in strong disagreement with some older measurements.¹⁶

Experimental

Materials.—Dodecylpyridinium iodide was prepared from dodecylpyridinium chloride (purity better than 95%), obtained from Milton Industrial Chemicals, England, by washing with ether, recrystallization from dioxane, precipitation from concentrated potassium iodide solution in water by cooling, repeated twice, followed by three recrystallizations from water. Analytical reagent variety urea was used.

C.m.c. Determination.—On micelle formation, the spectra of long chain pyridinium iodides change.^{17,18} The c.m.c. values were determined by following this change in absorption, as shown in Fig. 1. Measurements at several wave lengths at 290 m μ and above were made in a Hilger spectrophotometer using silica cells of 1-cm. path lengths. The cell chambers were thermostated at 25.0 \pm 0.2° and 45.0 \pm 0.2°. Measurements at different wave lengths gave c.m.c. values in agreement to within 1%. The reproducibility of the c.m.c. was within 1-2%.

The measurements in pure water tended to be somewhat uncertain, presumably because of triiodide formation in small amounts. Some results, therefore, were obtained in dilute sodium thiosulfate solutions. The effect of changing the thiosulfate concentration was also studied.

Results and Discussion

The c.m.c. data are summarized in Table I. The effect of thiosulfate is small and negligible compared to the effect of the urea addition. Our value in water at 25° is about 5% higher than that reported by Harkins, *et al.*¹⁸

It is desirable to investigate if urea causes any change in the nature of micelles. The present spectrophotometric method can be adapted to give some information on this question. The investigations of Kosower and co-workers¹⁹ on short chain analogs such

(15) W. Bruning and A. Holtzer, *J. Am. Chem. Soc.*, **83**, 4865 (1961).

(16) M. L. Corrin and W. D. Harkins, *ibid.*, **69**, 683 (1947).

(17) G. S. Hartley, *Kolloid-Z.*, **88**, 22 (1939).

(18) W. D. Harkins, H. Krizek, and M. L. Corrin, *J. Colloid Sci.*, **6**, 576 (1951).

(19) E. M. Kosower and P. E. Klinedinst, Jr., *J. Am. Chem. Soc.*, **78**, 3493 (1956); E. M. Kosower and J. C. Burbach, *ibid.*, **78**, 5838 (1956).

(1) G. Stainsby and A. E. Alexander, *Trans. Faraday Soc.*, **46**, 587 (1950).

(2) E. D. Goddard and G. C. Benson, *Can. J. Chem.*, **35**, 986 (1957).

(3) E. D. Goddard, C. A. J. Hoeve, and G. C. Benson, *J. Phys. Chem.*, **61**, 593 (1957).

(4) P. White and G. C. Benson, *Trans. Faraday Soc.*, **55**, 1025 (1959).

(5) B. D. Flockhart, *J. Colloid Sci.*, **16**, 484 (1961).

(6) P. Debye, *Ann. N. Y. Acad. Sci.*, **51**, 575 (1949).

(7) M. Nakagaki, *J. Chem. Soc. Japan*, **72**, 113 (1951).

(8) Y. Ooshika, *J. Colloid Sci.*, **9**, 254 (1954).

(9) I. Reich, *J. Phys. Chem.*, **60**, 257 (1956).

(10) H. S. Frank and M. W. Evans, *J. Chem. Phys.*, **13**, 507 (1945).

(11) W. Kauzmann, *Advan. Protein Chem.*, **14**, 1 (1959).

(12) P. Mukerjee, K. J. Mysels, and C. I. Dulin, *J. Phys. Chem.*, **62**, 1390 (1958); P. Mukerjee, *ibid.*, **62**, 1397 (1958); P. Mukerjee and K. J. Mysels, *ibid.*, **62**, 1400 (1958); P. Mukerjee, *ibid.*, **62**, 1404 (1958); F. Van Voorst Vader, *Trans. Faraday Soc.*, **57**, 110 (1961); D. Eagland and F. Franks, *Nature*, **191**, 1003 (1961); K. J. Mysels and P. Kapauan, *J. Colloid Sci.*, **16**, 481 (1961); G. D. Parfitt and A. L. Smith, *J. Phys. Chem.*, **66**, 942 (1962).

(13) R. H. Aronow and L. Witten, *ibid.*, **64**, 1643 (1960).

(14) H. S. Frank and A. S. Quist, *J. Chem. Phys.*, **34**, 604 (1961).

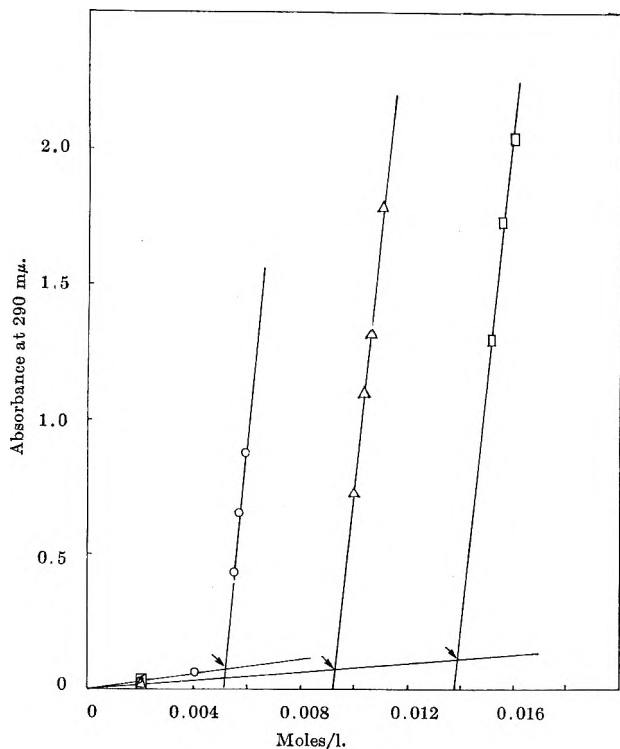


Fig. 1.—Absorbance of dodecylpyridinium iodide at 290 $m\mu$ as a function of its concentration in 0.0001 M sodium thiosulfate at 25° and varying concentrations of urea denoted by: \circ , 0 M ; Δ , 3.4 M ; \square , 5.9 M . The c.m.c. values are marked by arrows.

TABLE I
C.M.C. DATA ON DODECYLPYRIDINIUM IODIDE

Medium	Urea concentration, M				
	0	0.96	3.4	5.9	8.0
Water, 25°	0.00526	0.00934	0.0136
Water, 45°	.006700118	.0171	0.0213
0.0001 M					
$\text{Na}_2\text{S}_2\text{O}_3$, 25°	.0051500930	.0139
0.001 M					
$\text{Na}_2\text{S}_2\text{O}_3$, 25°	.00475	.00575	.00910	.0133
0.001 M					
$\text{Na}_2\text{S}_2\text{O}_3$, 45°	.00563	.00710	.0110	.0157

as methyl- and ethylpyridinium iodides leave little doubt that the appearance of the new absorption on micelle formation is due to charge transfer interactions between the iodide ions and the quaternary pyridinium ions. These short range interactions must be confined to the bound layer of the counterions on the micelle surface. They are also dependent on the polarity of the environment,²⁰ so that the micellar bands can be interpreted in terms of the effective polarity at the micelle surface.²¹ If urea changes the nature of these charge interactions then the nature of the spectrum should be affected. If it alters the degree of dissociation, which is of importance in any thermodynamic calculation,²² the intensity of the absorption should change.¹⁸

Figure 2 shows two different spectra in water and 5.9 M urea. These were obtained by measuring the absorption of a solution appreciably above the c.m.c. against one slightly above it. They are, therefore, characteristic of the micelles. The logarithms of the optical densities are plotted against the wave lengths such that

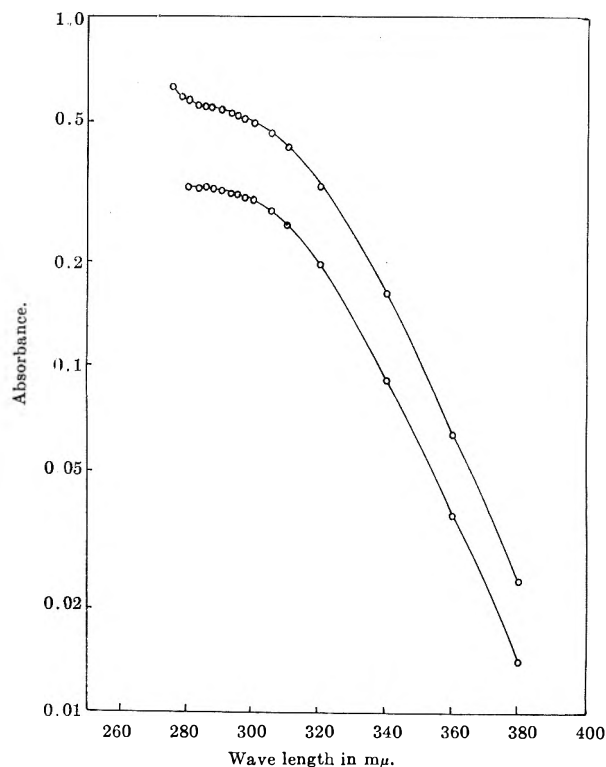


Fig. 2.—Difference spectra of the micelles of dodecylpyridinium iodide in 0.0001 M sodium thiosulfate. Lower curve in water and the upper curve in 5.9 M urea.

any variation in only the micellar concentrations shifts the whole curve equally in the vertical direction. The two different spectra in water and 8 M urea are superposable within experimental error on shifting only the vertical scale, showing that the spectra are the same and, therefore, the nature of the charge interactions in the bound layer at the micelle surface are similar.

The intensity of absorptions at any wave length increases linearly with concentration above the c.m.c. in the concentration ranges studied (Fig. 1). The slope of the lines above the c.m.c. decreases by about 25% on passing from water to 5.9 M urea. If the molecular extinction coefficients are assumed to be constant, an increase in the degree of dissociation of the micelles is indicated, which is in conformity with the increase of the dielectric constant of the medium on adding urea, and the resultant decrease in the strength of the long-range electrical interactions. The magnitude, however, is small for our system though it may be larger for others.²³

Figure 3 shows the relative increase in the c.m.c. with the concentration of urea. The results of Bruning and Holtzer¹⁵ on dodecyltrimethylammonium bromide are also shown. The trend of their data at low urea concentration is very similar to ours but their value for 6 M urea deviates appreciably. Some older measurements on sodium lauryl sulfate gave very different results,¹⁶ even a slight decrease in the c.m.c. in 3 M urea. We ascribe this discrepancy to the shortcomings of the dye-spectral change method employed for the c.m.c. determinations, which have been examined in detail.²⁴

(23) E. K. Mysels, of the University of Southern California, Los Angeles, has studied the conductivity of sodium lauryl sulfate in 6 M urea. The increase in dissociation in this case seems to be considerably more than in the case of dodecylpyridinium iodide (private communication).

(24) P. Mukerjee and K. J. Mysels, *J. Am. Chem. Soc.*, **77**, 2937 (1955).

(20) E. M. Kosower, *J. Am. Chem. Soc.*, **80**, 3253 (1958).

(21) P. Mukerjee and A. Ray, unpublished work.

(22) P. Mukerjee, *J. Phys. Chem.*, **66**, 1375 (1962).

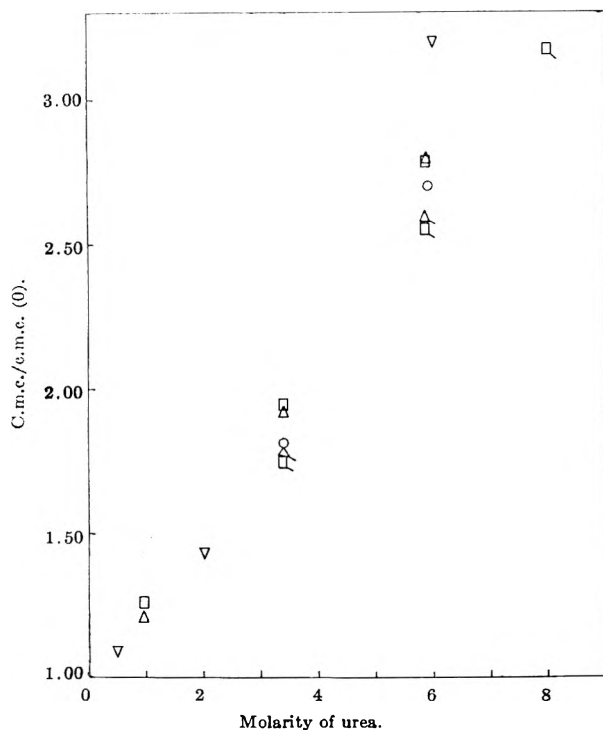


Fig. 3.—The ratio of the c.m.c. in urea to the c.m.c. in the absence of urea as a function of the concentration of urea: Δ , dodecylpyridinium iodide in water at 25°; \square , in water at 45°; \circ , in 0.0001 *M* sodium thiosulfate at 25°; \triangle , in 0.001 *M* sodium thiosulfate at 25°; \square , 0.001 *M* sodium thiosulfate at 45°; ∇ , dodecyltrimethylammonium bromide at 25°.¹⁶

The c.m.c. in our system increases almost linearly with urea concentration. Urea clearly has appreciable influence on micelle formation and hydrophobic bonding.

The effect of urea, moreover, seems to be independent of temperature. Measurements could not be carried out in 8 *M* urea at 25° because of the precipitation of a white solid, presumably an inclusion complex of dodecylpyridinium iodide in urea. Up to 5.9 *M* urea, however, while the c.m.c. increases by a maximum factor of 2.8, the ratio of the c.m.c.'s at the same urea and thiosulfate concentration at 25 and 45° remains constant to within 1.5% of the average value of about 20%. This variation is within experimental error. Although thermodynamic interpretations in terms of c.m.c.'s alone have been shown to be uncertain,²² since the change in the dissociation in our system is nearly the same at 25 and 45°, our results strongly indicate that urea affects mainly the entropy change in

micelle formation, and not the enthalpy change, in accordance with our expectation that it modifies primarily the icebergs.

Quantitatively, however, the effect of urea seems to be small, considering that in 8 *M* urea there are only five water molecules per molecule of urea, and that a decrease in the chain length by only two methylene groups raises the c.m.c. by a factor of 4. This suggests that water-structure effects may not be the whole cause of micelle formation. In support of the possible importance of interfacial effects and the chain-entropy, two other evidences may be cited. The effect of short-chain organic additives such as methanol, ethanol, or acetone,²⁵ at low molar concentrations, is much less than that of urea. The c.m.c. may even be lowered. At higher concentrations, however, in the 6–8 molar range and above, the c.m.c. increases much more steeply than with urea and to much higher values. The most likely explanation seems to be lowering of the surface tension of the medium in the case of the organic additives, and the consequent reduction of any interfacial energy and the chain-entropy contributions.

The other evidence comes from the recent study of Whitney and Tanford,²⁶ who found a considerably more pronounced effect of urea on the solubility of amino acids with aromatic side chains than one with an aliphatic one, although the expected entropy change on hydrophobic bonding is larger for the latter.¹¹ This greater vulnerability of the aromatic system, for which the chain-entropy should be negligible, to urea also argues for a substantial chain-entropy contribution to the hydrophobic bonding of aliphatic systems.

Finally, it may be remarked that the effects of urea and organic additives on micelle formation are clearly consistent with their denaturing effects on proteins¹¹ in terms of weakening of hydrophobic bonds, although different factors may be involved, as indicated above. If the effect of urea on hydrophobic bonding is independent of temperature, as is suggested by our work, a promising differentiating tool may be obtained for the study of the complicated features of protein stability and denaturation.

(25) A. F. H. Ward, *Proc. Roy. Soc. (London)*, **A176**, 412 (1940); A. W. Ralston and C. W. Hoerr, *J. Am. Chem. Soc.*, **68**, 2450 (1946); A. W. Ralston and D. N. Eggenberger, *J. Phys. Colloid Chem.*, **52**, 1492 (1948); E. C. Evers and C. A. Kraus, *J. Am. Chem. Soc.*, **70**, 3049 (1948); C. A. Kraus, *ibid.*, **70**, 3803 (1948); G. L. Brown, P. F. Grieger, and C. A. Kraus, *ibid.*, **71**, 95 (1949); H. S. Young, P. F. Grieger, and C. A. Kraus, *ibid.*, **71**, 309 (1949).

(26) P. L. Whitney and C. Tanford, *J. Biol. Chem.*, **237**, PC 1735 (1962).

THE EFFECT OF UREA ON METHYLENE BLUE, ITS SELF-ASSOCIATION, AND INTERACTION WITH POLYELECTROLYTES IN AQUEOUS SOLUTION

BY PASUPATI MUKERJEE AND ASHISH K. GHOSH

Department of Physical Chemistry, Indian Association for the Cultivation of Science, Calcutta 32, India

Received August 20, 1962

The effect of urea on the association of methylene blue in water, the extractability of methylene blue perchlorate into chloroform and its solubility, and the metachromatic interaction of methylene blue with polyacrylic acid have been investigated. Urea decreases the self-association of methylene blue and its metachromatic interactions very efficiently, and strongly influences the activity coefficient of monomeric methylene blue. These facts have been interpreted in terms of water-structure promotion around the dye ions and the consequent hydrophobic bonding in dye-association and metachromatic interactions. Several other lines of reasoning support the important role of water-structure effects in dye-association. The quantitatively smaller effect of urea on aliphatic systems as compared to aromatic systems has been interpreted in terms of the possible chain-entropy contribution for the former in hydrophobic bonding.

Introduction

The postulated presence of structured regions of low entropy, frequently called icebergs, around organic molecules or groups in water^{1,2} gives a fairly adequate explanation of observed facts regarding the transfer of such molecules or groups into non-aqueous environments. Similar considerations indicate the thermodynamic possibility of association of organic molecules in water or hydrophobic bonding, the primary driving force of which seems to be the gain in entropy when part of the icebergs disappear. Since hydrophobic bonding seems to be as likely for aliphatic systems as aromatic ones,² it is of interest to examine the possible role of this type of bonding in the frequently studied but little understood association of ionic dyes, which are mostly aromatic in nature, in aqueous solution. We have investigated, for this purpose, the effect of urea on the association of methylene blue (chloride) in water, the activity coefficient of monomeric methylene blue, and the metachromatic interaction of methylene blue chloride with polyacrylic acid and its sodium salt.

That urea weakens hydrophobic bonding has already been established.³⁻⁵ We have ascribed this effect to the outstanding capacity of urea for breaking up hydrogen bonds in water,⁵ and thus destroying the icebergs which presumably are associated with fairly large-scale coöperative structures stabilized by water-water hydrogen bonding.^{1,6} Since urea increases the surface tension of water slightly and the dielectric constant appreciably, effects due to the reduction of the polarity of the medium, which are known to affect dye-association strongly,⁷ should be absent. These arguments provide the rationale for the use of urea in investigating water-structure contributions to hydrophobic bonding.

A subsidiary point of interest is the possibility of a substantial chain-entropy contribution^{8,9} to hydrophobic bonding in aliphatic systems. Since aromatic systems are mostly non-flexible, this type of entropy change in their case should be small. *A priori*, therefore, it may be expected that if the chain-entropy con-

tribution, which is unlikely to be affected much by urea, is important for the aliphatic systems, then their hydrophobic bonding will be less vulnerable to urea.

Experimental

Materials.—Methylene blue was of commercial variety, used after three recrystallizations from distilled ethanol. Its molecular extinction coefficient at the band maximum in ethanol was 9.6×10^4 , which is slightly higher than the highest values mentioned in the literature.^{10,11}

Methylene blue perchlorate was prepared by precipitating methylene blue chloride with potassium perchlorate and was recrystallized from ethanol. The polyacrylic acid was prepared by bulk polymerization of acrylic acid with a trace of azo-bis-isobutyronitrile. Its equivalent weight was determined by titrating against sodium hydroxide. Merck's reagent variety urea was used.

Spectrophotometric Measurements.—These were carried out in a Hilger spectrophotometer using 1 and 0.1-cm. cells.

Results and Discussion

The spectrum of methylene blue in water in very dilute solutions, where association is negligible, is characterized by a prominent sharp peak at $660 \text{ m}\mu$, called the monomer peak, and a small shoulder at about $605 \text{ m}\mu$.

With increasing concentration, Beer's law is not obeyed: the extinction coefficient at $660 \text{ m}\mu$ diminishes and that at $605 \text{ m}\mu$ increases progressively.⁷ This is ascribed to the formation of dimers and higher multimers.^{7,11,12} The formation of these aggregates is quite pronounced in $1 \times 10^{-4} M$ solutions at ordinary temperature (ref. 7, also Fig. 1). With increasing proportion of an added organic solvent, the monomer peak intensifies at the expense of the dimer and multimer absorption. Figure 1 shows this effect for the addition of ethanol. The reduction of the association is generally ascribed to the reduced polarity of the medium.⁷

The effect of the addition of urea is qualitatively very similar to that of ethanol as shown in Fig. 2. Thus urea, at similar molar concentrations, breaks up the aggregates of methylene blue about as efficiently as ethanol. As with ethanol,^{10,11} a small part of the increase in the intensity at $660 \text{ m}\mu$ is due to a medium effect, which can be seen more clearly for a dilute system, $1 \times 10^{-5} M$ (Fig. 3). At this concentration there is still some association (3-4%) in water so that the medium effect is smaller than is apparent in Fig. 3.

(10) G. N. Lewis, T. T. Magel, O. Goldschmid, and J. Bigeleisen, *J. Am. Chem. Soc.*, **65**, 1150 (1943).

(11) L. Michaelis and S. Granick, *ibid.*, **67**, 1212 (1945).

(12) D. R. Lemin and T. Vickerstaff, *Trans. Faraday Soc.*, **43**, 491 (1947).

(1) H. S. Frank and M. W. Evans, *J. Chem. Phys.*, **13**, 507 (1945).

(2) W. Kauzmann, *Advan. Protein Chem.*, **14**, 1 (1959).

(3) W. Bruning and A. Holtzer, *J. Am. Chem. Soc.*, **83**, 4865 (1961).

(4) P. L. Whitney and C. Tanford, *J. Biol. Chem.*, **237**, PC 1735 (1962).

(5) P. Mukerjee and A. Ray, *J. Phys. Chem.*, **67**, 190 (1963).

(6) H. S. Frank and A. S. Quist, *J. Chem. Phys.*, **34**, 604 (1961).

(7) E. Rabinowitch and L. F. Epstein, *J. Am. Chem. Soc.*, **63**, 69 (1941).

(8) G. Stainsby and A. E. Alexander, *Trans. Faraday Soc.*, **46**, 587 (1950).

(9) R. H. Aronow and L. Witten, *J. Phys. Chem.*, **64**, 1643 (1960).

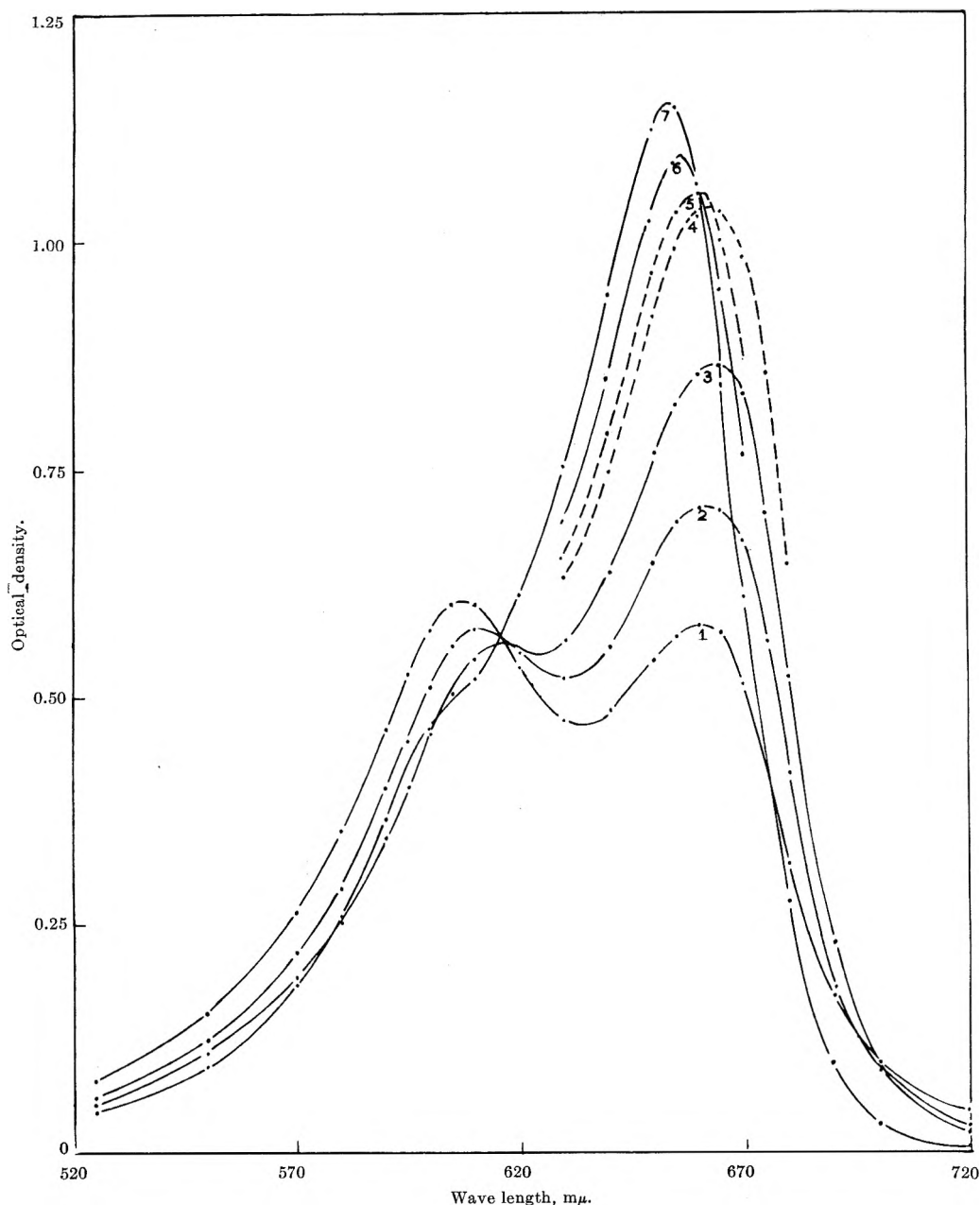


Fig. 1.—Spectrum of methylene blue in water-ethanol mixtures. Optical densities determined in 1-mm. cells. Concentration of methylene blue $1.20 \times 10^{-4} M$. Percentage of ethanol by volume: curve 1, 0%; 2, 8% (1.37 M); 3, 20% (3.43 M); 4, 40% (6.87 M); 5, 60% (10.3 M); 6, 80% (13.7 M); 7, 96% (16.5 M); temperature $20 \pm 1^\circ$.

Figure 3 also shows the effect of polyacrylic acid and its sodium salt on a dilute methylene blue solution. The monomer peak is considerably lower in intensity. At the same time the absorption at lower wave length region is higher (the metachromatic effect). In the presence of 8 M urea the metachromatic spectral effects with the polyelectrolytes disappear completely, and the absorption spectra become indistinguishable from that in the absence of the polyelectrolytes.

Figure 4 shows a more pronounced metachromatic effect in a more concentrated methylene blue solution where the monomer absorption becomes extremely small, and a flat peak at about 570 $m\mu$ is observed. On the addition of 6 M urea the absorption curve regains the characteristic shape of dilute solutions, showing very little association.

The metachromatic effect is presumably due to the extensive association of the dye ions with the poly-

electrolyte resulting in extended interactions of the dye chromophores.¹¹ Urea seems to inhibit this interaction in the same way as it inhibits aggregation in water alone.

Before these facts can be interpreted in terms of the non-specific effect of urea on the hydrophobic bonding between dye ions, two alternative explanations must be examined.

It has been suggested that the aggregation of dyes may involve sandwiched water molecules as intermediaries.¹³ Conceivably, urea may prevent aggregation by making such intermediary water molecules unavailable. The non-specific effect of urea on icebergs around the dye ions should, on the other hand, affect both monomers and the aggregated species. The other possible explanation is some specific reaction of urea with methylene blue.

(13) J. A. Bergeron and M. Singer, *J. Biophys. and Biochem. Cytol.*, **4**, 433 (1958).

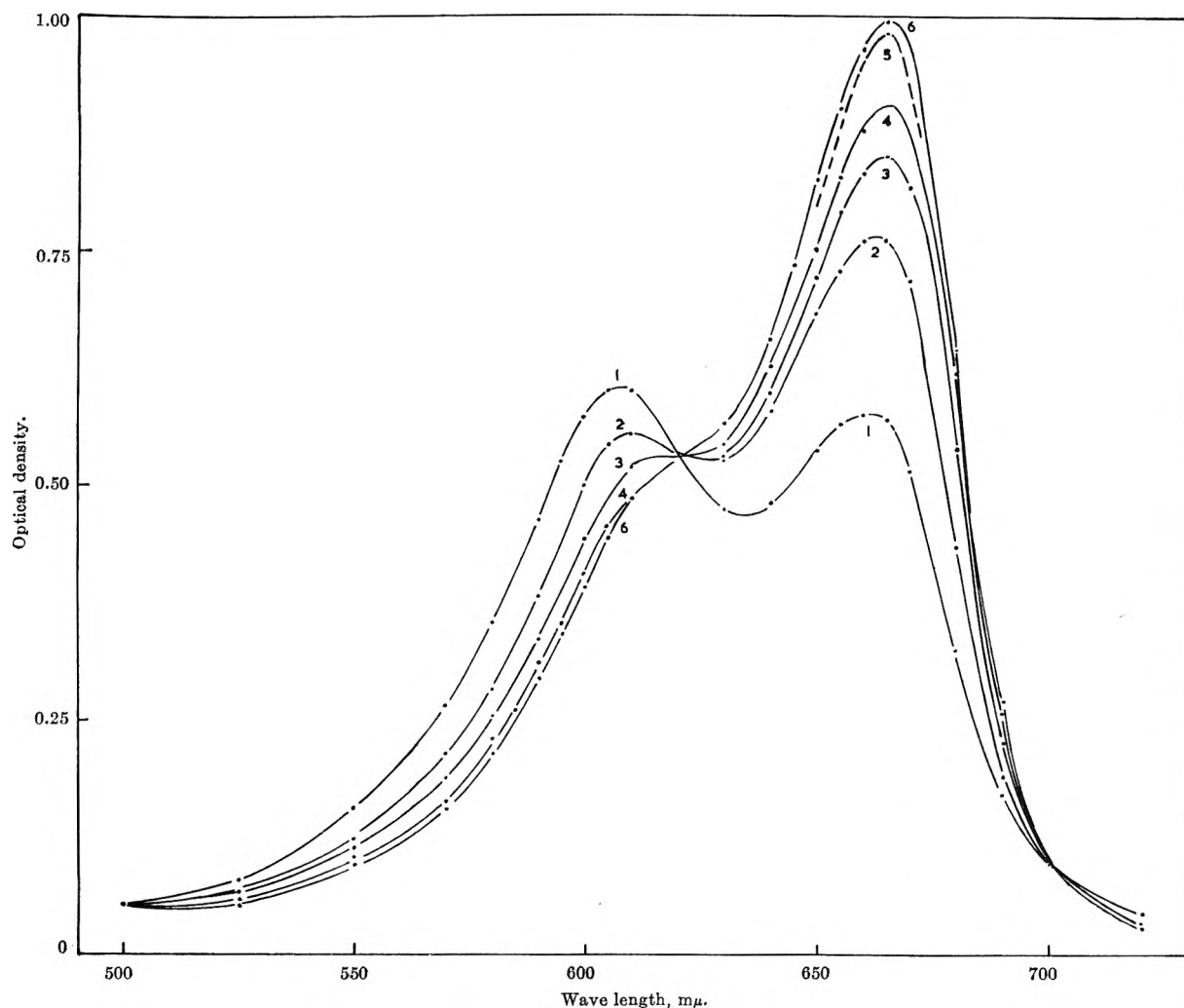


Fig. 2.—Effect of urea on the spectrum of methylene blue in aqueous solution. Optical densities determined in 1-mm. cells. Concentration of methylene blue $1.20 \times 10^{-4} M$. Concentration of urea: curve 1, 0 M ; 2, 1.77 M ; 3, 3.53 M ; 4, 5.30 M ; 5, 7.07 M ; 6, 8.45 M ; temperature $20 \pm 1^\circ$.

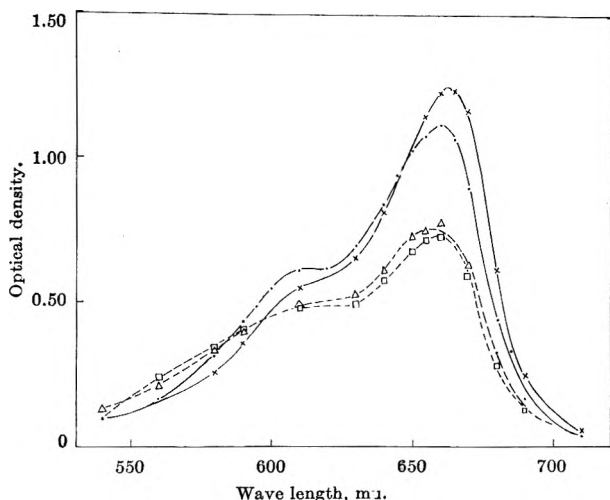


Fig. 3.—Spectrum of methylene blue in presence of polyelectrolytes and urea. Concentration of methylene blue $1.38 \times 10^{-5} M$. Optical densities determined in 1-cm. cells. ●, methylene blue in water; □, in $9.5 \times 10^{-4} N$ sodium polyacrylate; Δ, in $9.5 \times 10^{-4} N$ polyacrylic acid; ×, indistinguishable curves of the three previous systems in 8 M urea. Temperature $23 \pm 1^\circ$.

To investigate these points we have determined the solubility of methylene blue perchlorate, which is sparingly soluble in water ($\sim 1.3 \times 10^{-4} M$ at 30°) in 10 M urea, in which the solubility increases by a factor of 30. Considering that the association of the dye in

10 M urea is very little (see above), the activity coefficient of monomeric methylene blue perchlorate must be reduced by about this factor of 30 in 10 M urea. The effect of urea on the activity coefficient of a few simple electrolytes studied¹⁴ is much smaller in magnitude and often in the opposite direction, so that this lowering of the activity coefficient for methylene blue perchlorate cannot be ascribed to the effect of urea on charged systems in general.

We also have studied the effect of urea on the distribution coefficient of methylene blue perchlorate between water and chloroform. In these experiments we used an "iso-extraction" method developed in this Laboratory for the study of self-associating systems.¹⁵ A methylene blue chloride solution in dilute hydrochloric acid (0.001 M) is mixed with potassium perchlorate solution and equilibrated with chloroform. The extracting species is primarily methylene blue perchlorate ($MBClO_4$); the extraction of methylene blue chloride is small and can be corrected for from a blank experiment in which potassium perchlorate is not added. At different concentrations of urea, the amount of potassium perchlorate added is varied such that the absorbance in the chloroform layer, and hence

(14) A. Seidell, "Solubilities of Inorganic and Metal Organic Compounds," Vol. I, Third Ed., D. Van Nostrand Co., New York, N. Y., 1940, pp. 292, 1241, 1315.

(15) A. K. Ghosh and P. Mukerjee, unpublished results.

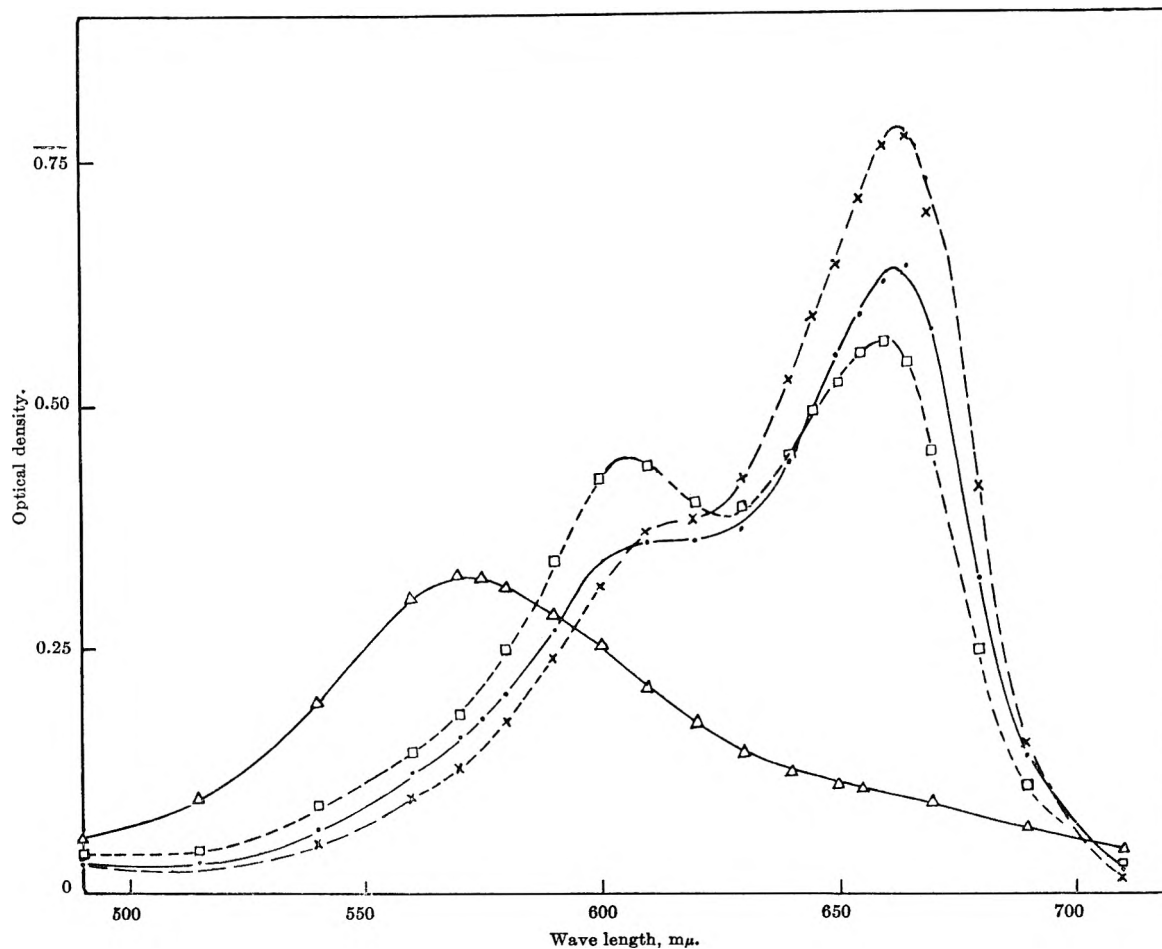


Fig. 4.—Spectrum of methylene blue in the presence of sodium polyacrylate and urea. Optical densities determined in 1-mm. cells. Concentration of methylene blue $1.0 \times 10^{-4} M$. \square , methylene blue in water; \times , in 6 M urea; Δ , in $9.4 \times 10^{-4} N$ sodium polyacrylate; \bullet , in $9.4 \times 10^{-4} N$ sodium polyacrylate and 6 M urea.

the concentration of methylene blue perchlorate in it, remains constant. Assuming that the addition of urea to the aqueous phase does not change the activity coefficients of the various species in chloroform, irrespective of the state of the solution of methylene blue perchlorate in chloroform, the activity of $MBClO_4$ in chloroform and therefore the product $(MB^+)(ClO_4^-)f_{\pm}^2$ in the aqueous phases in equilibrium must remain constant. Since the concentration product of $(MB^+)(ClO_4^-)$ is known from analytical balance, the mean activity coefficient, f_{\pm} , of $MBClO_4$ in the presence of urea is readily determinable. For our rough calculations, we have assumed the activity coefficient in the absence of urea to be unity (at the ionic strength of about 0.001 used any error should be less than 4%) and neglected all association (at the concentration of methylene blue used, $4 \times 10^{-5} M$, the maximum possible error due to this is about 7%).

Figure 5 shows a plot of f_{\pm} on a log scale, against the concentration of urea. The point obtained from the solubility of $MBClO_4$ in 10 M urea is also included. The effect of urea on f_{\pm} is pronounced. Typical salting-in or salting-out type equilibria, involving the activity coefficient f of a non-electrolyte in the presence of electrolytes, show linear variation of $\log f$ with the concentration of the electrolyte.¹⁶ From thermodynamic considerations,¹⁶ the reverse effect of a non-electrolyte

on $\log f_{\pm}$ of an electrolyte should show similar linearity as seems to be the case here (Fig. 5). Since salting-in or salting-out equilibria are explained in terms of various non-specific effects, a similar explanation seems to be indicated here also. The data do not seem to be easily explained if a mass-action controlled adduct-formation with urea is invoked. The effect of urea, moreover, seems to be quite general in lowering the activity coefficients and preventing aggregations of dye molecules of very different chemical constitutions. We have observed that the solubility of orange OT, a highly insoluble non-ionic azo dye (1-*o*-tolylazo-2-naphthol) is increased by a factor of roughly 10 in 10 M urea. Alexander and Stacey¹⁷ in their light scattering investigations on several highly aggregating dyes, anionic and cationic and of very different structures, found that urea causes generally extensive disaggregation. We have observed qualitatively that urea markedly lowers the association of pinacyanol, a carbocyanine dye. It is very unlikely that specific effects could be operating in all of these cases.

Hydrophobic Bonding in Dye Association.—Accepting on the basis of the previous arguments the non-specific nature of the effect of urea, all the observed facts now fit the explanation which invokes the existence of structured regions, or icebergs, around the dye ions which are partly destroyed by urea. Thus, in the presence of urea, the transfer of methylene blue to a solid form

(16) G. N. Lewis and M. Randall, "Thermodynamics," revised by K. S. Pitzer and L. Brewer, 2nd Ed., McGraw-Hill Book Co., Inc., New York, N. Y., 1961, pp. 584-586.

(17) P. Alexander and K. A. Stacey, *Proc. Roy. Soc. (London)*, **A212**, 274 (1952).

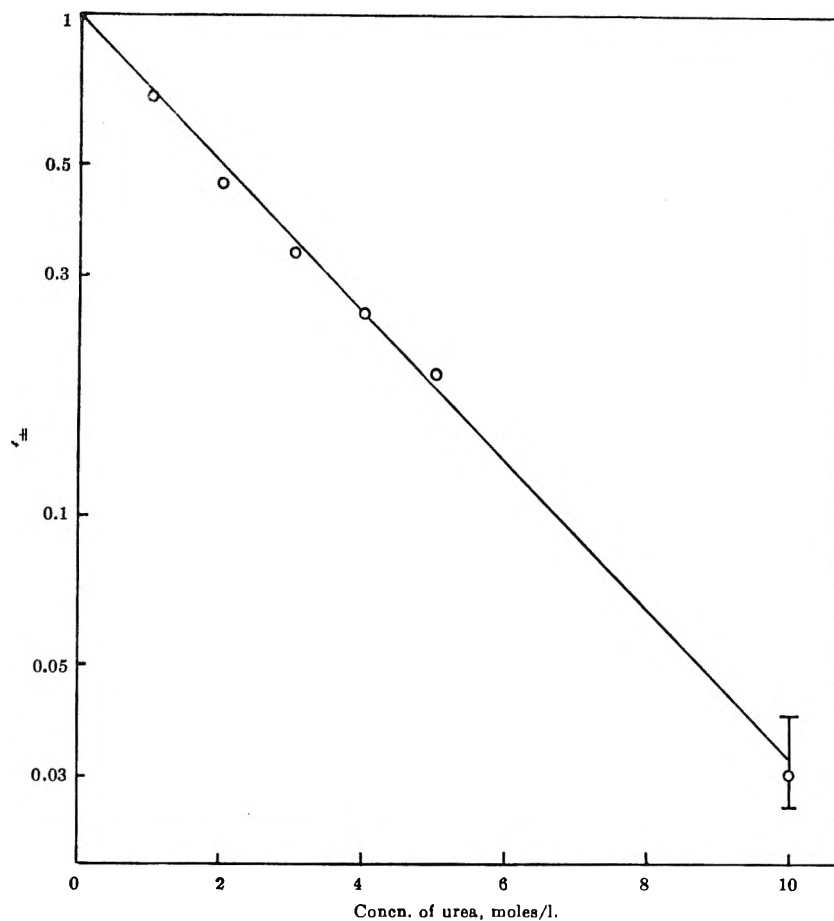


Fig. 5.—The variation of the mean molar activity coefficient (f_{\pm}) of MBClO_4 , plotted on a log scale, with concentration of urea. Point at 10 M urea derived from solubility, others from extraction studies; temperature, 30°.

or into a non-aqueous environment, or the association of methylene blue to form aggregates, are all made less favorable because there is less entropy to be gained. Thus solvent structure induced hydrophobic bonding seems to play an important part in the association of dyes, and presumably other aromatic type molecules.

Several other lines of reasoning suggest the likelihood of this conclusion. The association of dyes is known not to occur or to do so only to a very limited extent in non-aqueous media, such as hydroxylic solvents of intermediate polarity such as methanol, or even formamide,¹⁸ which has a dielectric constant greater than that of water. Thus an aqueous medium seems to be as particularly favorable for dye association as for micelle formation.

The detailed thermodynamics of association has not been satisfactorily worked out for any dye system. The primary reason for this is that the association, in all cases thoroughly investigated, seems to proceed stepwise to multimers higher than the dimer, and multimer equilibria of this kind are difficult to unravel. For thionine Rabinowitch and Epstein⁷ derived enthalpy and entropy values on the assumption of only dimerization taking place. When converted to the "unitary" scale,^{2,19} the entropy of association is slightly positive (~ 1 e.u.). Considering that the association of two

similarly charged species should result in a loss of entropy due to charge compaction over and above the loss of the translational entropy of one ion, the net positive entropy change indicates a large positive entropy contribution from some source, which is very likely to be a water structure contribution.

A further interesting point is the magnitude of the urea effect for the aromatic systems as compared to typical aliphatic systems. For dodecylpyridinium iodide the critical micelle concentration increases by only a factor of 3.1 in 8 M urea.⁵ Thus the activity coefficient of dodecylpyridinium iodide is lowered by about this factor, which is considerably less than the effect on methylene blue. In the recent study of Whitney and Tanford on the solubility of amino acids,⁴ it was found that the effect of urea was considerably more pronounced for phenylalanine than for leucine containing non-polar side chains benzyl and secondary butyl, respectively. The entropy changes for the transfer of toluene and butane from aqueous solutions to pure liquids are, on the other hand, 16 e.u. at 18° and 23 e.u. at 25°, respectively.² This greater sensitivity of the aromatic systems to the effect of urea is in line with the suggested substantial contribution of chain-entropy for flexible systems,^{8,9} as indicated in the Introduction.

Acknowledgment.—A. K. G. is grateful to the Council of Scientific and Industrial Research, New Delhi, for financial support.

(18) Kh. Z. Arvan and N. E. Zaitseva, *Opt. Spectr.* (USSR), **10**, 137 (1961).

(19) R. W. Gurney, "Ionic Processes in Solution," McGraw-Hill Book Co., Inc., New York, N. Y., 1953, p. 90.

NOTES

RADIATION DOSE AND IODINE SCAVENGER EFFECTS ON RECOIL C^{11} REACTIONS IN CYCLOHEXANE¹

BY EDWARD P. RACK AND ADOLF F. VOIGT

Contribution No. 1126 from The Institute for Atomic Research and Department of Chemistry, Iowa State University, Ames, Iowa

Received March 12, 1962

The chemistry of recoil carbon atoms has received considerable attention in recent years. The experiments of Wolfgang and his co-workers²⁻⁴ on the reactions of C^{11} with gaseous hydrocarbons have been interesting, in particular their discussion of the formation of products by C^{11} or C^{11} H insertions into a C-H bond in the target molecules.

This paper presents the results of a study of the C^{11} + liquid cyclohexane system in which the (γ , n) reaction was used as the method of activation. The relative yields of gaseous products were determined as a function of the radiation dose and of the concentration of iodine dissolved in the cyclohexane. During the irradiation, the samples were subjected to rather large radiation doses and it was important to establish the contribution of radiation damage to the observed yields.

Experimental

Materials.—Phillips research grade cyclohexane (99.94 mole % purity) was used after drying over sodium wire. "Baker Analyzed" iodine was used without further purification. The tantalum foil used as a beam monitor was from the Ethicon Suture Laboratory. The irradiated tantalum foil was shown to be free of radioactive impurities. Helium which was used as a carrier gas in the chromatograph had a stated purity in excess of 99.99%.

Sample Preparation.—The systems studied were cyclohexane, either pure or with dissolved iodine, prepared by vacuum-line techniques and sealed in Pyrex glass bulbets with a volume of about 0.5 ml. Iodine concentrations were determined by a Hellige Duboscq colorimeter.

Synchrotron Irradiations.—The samples were irradiated in a thin-walled thimble which projected into the cavity of the doughnut-shaped acceleration chamber of the Iowa State University electron synchrotron, operated at 47 Mev. Irradiations were for periods of 5 to 60 min. and all runs were made at room or ambient temperature. Tantalum foil strips used as X-ray dose monitors were placed around the bulbets at reproducible positions. A description of the irradiating position can be found elsewhere.⁵ In addition to the bremsstrahlung which cause the nuclear transformation in carbon, samples were exposed to a high electron flux. These fluxes combined with the recoiling C^{11} atoms, with a kinetic energy of ~ 0.5 Mev., to produce appreciable radiation decomposition in the samples. The only activity observed in the samples was that of C^{11} .

In previous work⁶ using this synchrotron irradiations were made on samples outside the doughnut. In that position the flux responsible for activating the C^{11} and producing decomposition was much lower.

Gaseous Product Analysis.—A radio-gas chromatograph designed and built by R. Clark and W. Stensland of this Laboratory was used. The only column used was a diisodecylphthalate-di-

methylsulfolane (DIDP-DMS) mixed column consisting of a 6-ft. section of DIDP and a 16-ft. section of DMS, both 40% by weight, on celite-22 (48-65 mesh). All the gaseous products appeared on a DIDP-DMS column, except that C_2H_4 and C_2H_6 appeared as one product peak because of similar retention times. No attempt was made to resolve these activities since earlier work has shown that about four times as much ethylene as ethane is produced in the C^{11} + cyclohexane reaction.

Activity Calculations.—The counting system was described by Lang and Voigt⁶; the gas stream was passed through a vial placed in the well of a NaI(Tl) crystal. For each radioactive product the count rate vs. time was recorded on a strip chart recorder or summed by a scaler, or both. The scaler sums and the areas on the recorder charts were in quite good agreement. These data were corrected for background and for decay to the end of the irradiation (using 20.4 min. for the half-life of C^{11}) and standardized to a 1-g. sample. The corrected areas were multiplied by the flow rate to obtain values for the activities of the products.

Results

Sixteen experiments were done with pure cyclohexane and seventeen with iodine at various initial concentrations, in mole fraction: 1.6×10^{-5} (6), 3.2×10^{-5} (5), and 2.1×10^{-3} (6). The labeled products observed were methane, ethane + ethylene, propylene, acetylene, and 4-carbon products. Tantalum foil monitors, in which the 8.15 hr. Ta^{180m} was produced, were used to correct for variations in irradiation time and beam intensity. However, there was considerable scatter in the results when this external monitor was used.

It was observed that the acetylene activity compared to tantalum and corrected for irradiation time with $(1 - e^{-\lambda t})$ terms was remarkably constant. In 12 experiments the acetylene/tantalum activity ratio was found not to depend on irradiation time (from 5 to 40 min.), on dose (over a 9-fold range), on dose rate (over a 2-fold range), or on iodine concentration. Hence, the acetylene yield could be and was used as an internal monitor, and the yields of other products are presented as ratios to acetylene. In this way agreement between experiments was greatly improved. Also, if the absolute yield of acetylene is known (Lang and Voigt estimate it as 14%)⁶ the absolute yields of other products can be obtained by multiplying the appropriate ratio by the absolute acetylene yield.

It is legitimate to use the acetylene activity as a measure of the total radiation dose as well. Although the total dose includes the contribution of electrons and bremsstrahlung of all energies, while the yield of acetylene measures only those X-rays of energy sufficient to induce the $C^{12}(\gamma, n)$ reaction, the method of producing the bremsstrahlung is the same in all experiments. Hence, the relative total doses in different experiments will be related to the acetylene activities, if these are corrected for C^{11} decay during irradiation with the factor $t/(1 - e^{-\lambda t})$.

The total radiation intensity in the system was estimated in two ways. The irradiation of cyclohexane containing low concentrations of iodine led to the disappearance of the iodine color after about 5 min. from an original concentration of 3.2×10^{-5} mole fraction. With the assumption that $G(-I_2) = 3.2$,⁷ this corresponds to an intensity of $\sim 1.5 \times 10^{13}$ e.v./g. min. Ex-

(7) E. H. Weber, P. F. Forsyth, and R. H. Schlier, *Radiation Res.*, **3**, 68 (1955).

(1) Work was performed in the Ames Laboratory of the U. S. Atomic Energy Commission.

(2) C. MacKay and R. Wolfgang, *J. Am. Chem. Soc.*, **83**, 2399 (1961).

(3) C. MacKay, M. Pandow, P. Polak, and R. Wolfgang, "Chemical Effects of Nuclear Transformations," Vol. II, International Atomic Energy Agency, Vienna, 1961, pp. 17-26.

(4) C. MacKay, P. Polak, H. E. Rosenberg, and R. Wolfgang, *J. Am. Chem. Soc.*, **84**, 308 (1962).

(5) A. J. Bureau and C. L. Hamner, *Rev. Sci. Instr.*, **32**, 93 (1961).

(6) C. E. Lang and A. F. Voigt, *J. Phys. Chem.*, **65**, 1542 (1961).

periments with the Fricke dosimeter indicated the oxidation of $\sim 6 \times 10^{-3}$ mole/l. min. of ferrous ion, corresponding to an intensity of $\sim 2 \times 10^{19}$ e.v./g. min. The actual dose rate probably lies between these limits.

Results on the effects of changing the radiation dose and the iodine concentration on the yields of CH_4 and $\text{C}_2\text{H}_4 + \text{C}_2\text{H}_6$ are shown in Fig. 1 and 2. In all of the experiments at 1.6×10^{-5} mole fraction iodine and in those for longer than 5 min. at 3.2×10^{-5} m.f., the iodine color disappeared. In these experiments yields lay between the upper and lower curves of Fig. 1 and 2. Since iodine was not present during the complete irradiation, the results are not included in the figures.

The yield of methane relative to acetylene can be extrapolated to 0.29 ± 0.05 at zero radiation dose, independent of the iodine concentration. Similarly, the yield of ethylene plus ethane extrapolates to 0.13 ± 0.03 . Experiments with a silica gel column which does separate them indicate that the ratio for ethylene is ~ 0.10 and that for ethane ~ 0.03 . The data for the production of propylene are similar to those of Fig. 1 and 2 giving, on extrapolation, ~ 0.08 for the propylene/acetylene ratio.

The yields of 4-carbon compounds show some variation, with an average of 0.40 ± 0.06 relative to acetylene for the iodine-free systems. *trans*-Butene-2 has been identified tentatively as one of the 4-carbon products. The data show that in the presence of sufficient iodine the yield is reduced to zero.

Experiments were conducted to determine what effect traces of oxygen might have on the shape of the yield vs. dose curve. Solvent extraction experiments on pure cyclohexane, with CHCl_3 and I_2 as one phase and an aqueous solution $0.5 M$ in Na_2SO_3 and in NaOH as the other, showed that about 99% of the C^{11} activity was organic. A gas chromatographic separation on a silica gel column showed that labeled CO and CO_2 , two products expected in the presence of oxygen, were not present. Experiments on cyclohexane saturated with oxygen at atmospheric pressure gave results similar to those from the 1.6×10^{-5} mole fraction I_2 systems, indicating that dissolved O_2 behaves similarly to I_2 .

Discussion

The results show that the radiation-induced portions of the yields of CH_4 , $\text{C}_2\text{H}_4 + \text{C}_2\text{H}_6$, and C_3H_6 are removed by iodine and hence involve species that react with iodine. While the short lives of the usual radicals exclude them from consideration as causing the build-up of yields to a maximum over a period of 20 to 30 min., other active species with lifetimes of a few minutes may be formed. In any case, additional data will be required before the nature of the radiation damage in this system is understood.

That portion of the yields which is produced at zero dose or in the presence of iodine can be considered as the true hot-atom yield, resulting from the fact that the C^{11} fragment has energy above that of its surroundings. Although the C^{11} fragment may lose electrons initially and start out as an ion, the ionization potentials of the various C-H radicals and cyclohexane are such that the radicals would be neutralized before reaching the energy range for reaction. Hence ion-molecule reactions can be eliminated. Since the steady state concentration of radicals is much less than the concentration of cyclohexane molecules, reaction of the

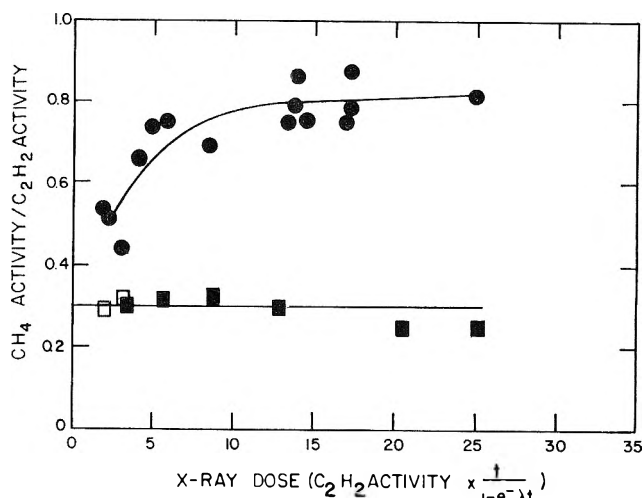


Fig. 1—Relative yields of CH_4 vs. radiation dose at various iodine concentrations. Mole fraction I_2 : ●, 0; □, 3.2×10^{-5} ; ■, 2.1×10^{-3} .

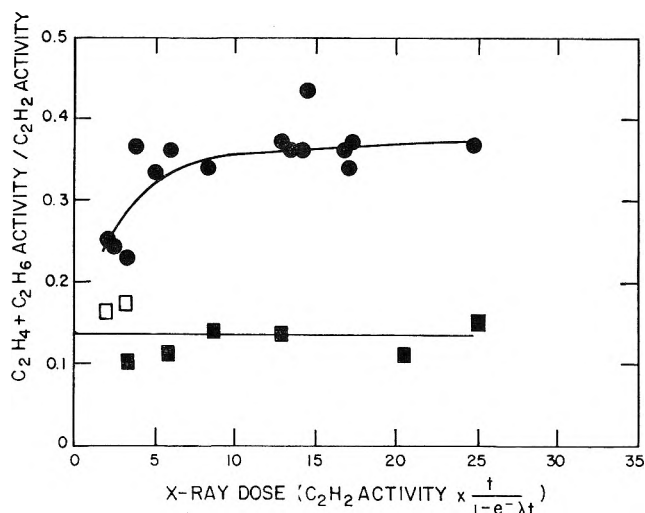


Fig. 2—Relative yields of $\text{C}_2\text{H}_4 + \text{C}_2\text{H}_6$ vs. X-ray dose at various iodine concentrations. Mole fraction I_2 : ●, 0; □, 3.2×10^{-5} ; ■, 2.1×10^{-3} .

C^{11} fragment with the latter is more probable, particularly since this reaction would be exothermic even when the C^{11} fragment is at thermal energies.

Thus, the various products appear to be formed predominantly by reactions of the recoiling fragment with the molecules of cyclohexane. Displacement and abstraction reactions can be expected to be important. The most abundant gaseous product, acetylene, could be formed by a reaction path involving displacement of hydrogen by a C^*H radical, or it could be considered as insertion of a carbon in a C-H bond. In this mechanism sufficient energy would be contributed to the intermediate so that two C-C ring bonds would be broken and the labeled product would rearrange to acetylene. The formation of the other two-carbon compounds could be quite similar, possibly involving C^*H_2 and C^*H radicals, or an energetic C_2^*H_x fragment could abstract hydrogens from the cyclohexane.

Of the other products, methane probably is produced by a series of abstraction reactions, as the C^{11} fragment cools down but is still above thermal energies, since its yield at zero dose is not reduced by the addition of iodine. Three-carbon compounds could result from the rupture of a $\text{C}_6\text{H}_{11} \cdot \text{C}^*\text{H}$ intermediate in such a way that a 3-carbon chain results, followed by stabilization of the

fragment by hydrogen abstraction. Since the yield of 4-carbon compounds was reduced to zero in the presence of iodine, reactions to form these are more likely radiation induced or thermal.

Acknowledgment.—The authors gratefully appreciate the assistance of Dr. A. Bureau and the synchrotron staff, particularly Mr. J. R. McConnell, who operated the synchrotron for the many irradiations, and Mr. D. Clark, who performed Fricke dosimetry in the synchrotron.

THE STATE OF PLATINUM IN RE-FORMING CATALYSTS

BY MARVIN F. L. JOHNSON AND CARL D. KEITH

Sinclair Research, Inc., Harvey, Illinois

Received August 9, 1962

Alumina with a small amount of platinum is widely used as a re-forming catalyst—to catalyze reactions of dehydrocyclization, dehydrogenation, isomerization, and hydrocracking of hydrocarbons.¹ Such catalysts normally are prepared by impregnating alumina with a soluble platinum compound, followed by calcination in air at an elevated temperature.

The chemical state and degree of dispersion of the platinum in platinum-alumina have been the subject of several recent papers. Since the catalysts are employed under reducing conditions, one presumes that platinum has been converted to the metallic state. Indeed, proposed mechanisms for the various re-forming reactions¹ presuppose the existence of metallic platinum as the dehydrogenation component of these dual-function catalysts. Hydrogen consumption measurements in these Laboratories and by Mills, *et al.*,² indicate nearly complete reduction of Pt⁴⁺ to Pt⁰ in a few minutes in hydrogen, at temperatures as low as 245°. As suggested by Kluksdahl and Houston,³ the darkening and dehydrogenation activity which appear upon reduction with hydrogen suggest the production of platinum metal. Furthermore, it has been observed in these Laboratories that hydrogen reduction at an elevated temperature is necessary to cause platinum-alumina to catalyze H₂-D₂ exchange; rate constants of the order of 20–30 min.⁻¹ at -195.5° and 518 mm. are observed for various preparations containing 0.6% Pt.

The above constitutes evidence for the existence of platinum metal upon treatment of platinum-alumina with hydrogen at elevated temperatures. Several workers have employed adsorption techniques to show that this platinum exists in a high degree of dispersion. Hughes, *et al.*,⁴ used carbon monoxide adsorption, while others^{5–7} employed hydrogen adsorption to draw this conclusion. Hughes, *et al.*,⁴ showed, in addition, that hydrogen reduction must be carried out above at least 200° to obtain adsorption by platinum metal; they showed further that a minimum extent of plati-

num area, as measured by carbon monoxide adsorption, is necessary to obtain activity for re-forming methylcyclopentane. Similarly, Mills, *et al.*,² observed that a loss of catalytic effectiveness paralleled the growth of platinum metal particles as observed by X-ray diffraction. Platinum surface area thus is an important factor in re-forming.

A different point of view has been proposed by McHenry, *et al.*,⁸ who postulated the active component of these catalysts to consist of a platinum-alumina complex. This conclusion was based on their finding that dehydrocyclization activity was dependent on the amount of complex present, defined as that portion of the platinum which was soluble with the alumina in aqueous hydrofluoric acid or acetylacetone.

The present paper presents evidence to show that this apparent discrepancy can be resolved if one considers the "complex" to exist in the oxidized state and to be responsible for high platinum metal dispersion upon subsequent reduction.

Experimental

Platinum solubilities of Table I were measured by the method described by McHenry, *et al.*⁸ Table II results were obtained by digestion in 1:4 H₂SO₄ at 60° for several days; the solutions and the residues each were analyzed.

Chemisorptions of carbon monoxide were performed after reduction for 12 hr. at 482° in flowing purified hydrogen, and evacuation for 9 hr. at 300°, at about 5 × 10⁻⁶ mm.; this temperature of evacuation was chosen to minimize adsorption by alumina to about 0.05 cc. (STP)/g. After cooling to room temperature in a few mm. of helium and evacuation of the helium, a measured quantity of carbon monoxide is admitted to the catalyst. One hour later, automatic Toepler pumping is started to return unadsorbed gas to the calibrated system. This pump-

TABLE I
EFFECT OF OXIDATION ON SOLUBLE PLATINUM

Sample	History	% soluble Pt ^a	CO chemisorption (cc. STP/g.)
A	Used catalyst	0.23	0.14
B	A + 3 hr., 440°, one atm. air	.27	.20
C	A + 3 hr., 480°, one atm. air	.32	.22
D	A + 3 hr., 505°, one atm. air	.34	.24
E	C + 20 hr., 505°, 10 atm. air	.48	.33

^a Solubility in HF; 0.6% total Pt.

TABLE II
EFFECT OF OXIDATIVE CONDITIONS ON SOLUBLE PLATINUM

Temp., °C.	Partial pressure of O ₂ , atm.	% soluble platinum ^a	H ₂ -D ₂ exchange rate ^b
427	0.015	0.27	..
427	0.11	.427 ^c	22
427	1.0	.452	30
482	0.21	.493	30
482	1.0	.509	46
510	0.015	.433	39
510	0.21	.508	50
510	1.0	.52	45
538	0.21	.504	57
538	1.0	.53	47
582	0.015	.367	18
582	0.21	.378	43
582	1.0	.533	44
650	1.0	.374	33

^a Solubility in H₂SO₄; 0.55% total Pt. ^b See text. ^c This sample was used for the other treatments.

(1) F. G. Ciapetta, R. M. Dobres, and R. W. Baker, "Catalysis," Vol. 6, ed. by P. H. Emmett, Reinhold Publ. Corp., New York, N. Y., 1958.

(2) G. A. Mills, S. Weller, and E. B. Cornelius, "Second International Congress on Catalysis," Vol. II, Paris, 1960, Paper 113.

(3) H. E. Kluksdahl and R. J. Houston, *J. Phys. Chem.*, **65**, 1469 (1961).

(4) T. R. Hughes, R. J. Houston, and R. P. Sieg, Preprints Pet. Div., ACS, April, 1959.

(5) L. Spenadel and M. Boudart, *J. Phys. Chem.*, **64**, 204 (1960).

(6) S. F. Adler and J. J. Keavney, *ibid.*, **64**, 208 (1960).

(7) H. L. Gruber, *ibid.*, **66**, 48 (1962).

(8) K. W. McHenry, R. J. Bertolacini, H. M. Brennan, J. L. Wilson, and H. S. Seelig, "Second International Congress on Catalysis," Vol. II, Paris, 1960, Paper 117.

ing is continued for 6–12 hr.; no further carbon monoxide is recovered after 6–8 hr. The chemisorption is defined as the difference between gas admitted and gas recovered.

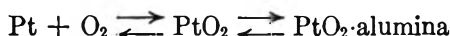
The H₂-D₂ exchange rates also are measured after reduction for 12 hr. at 482°. The catalyst is cooled to liquid nitrogen temperature in hydrogen, after which a mixture of 25% D₂ and 75% H₂ is passed over the catalyst at a constant rate and at a constant pressure of 518 mm.; the effluent is analyzed for HD by mass spectrometry. From several consecutive runs at varying flow rates, the exchange rate constant is attained as the slope of a linear plot of $-\ln(1 - X/X_e)$ vs. $1/SV$, where X is the conversion to HD, X_e the equilibrium conversion, and SV is expressed as cc. (STP)/g./min.

Results and Discussion

A commercial catalyst consisting of 0.6% Pt on alumina, partially deactivated by use and subsequent regenerations, was treated with dry air at various temperatures. The changes in carbon monoxide chemisorption and platinum solubility are shown in Table I.

Sample A, the regenerated catalyst, was found to have a small amount of platinum metal, barely detectable by X-ray diffraction; this plus the low carbon monoxide chemisorption value indicates that some growth of platinum crystallites has occurred. Correspondingly, less than half of the platinum was soluble, compared to nearly 100% for the fresh catalyst. As the severity of oxidative treatment was increased, the extent of platinum solubility increased. At the same time, the platinum surface area upon subsequent reduction increased. Thus, the formation of platinum-alumina complex results in greater platinum surface area, as measured by carbon monoxide chemisorption. The existence of a platinum-alumina complex is, therefore, desirable, not *per se*, but because it leads to a high dispersion of the platinum upon subsequent reduction.

Consider the reaction



It is clear that in the presence of an oxygen partial pressure, there will be a tendency for the oxide to form, and that the oxidized state will be stabilized by complex formation with alumina. Therefore, an increase in oxidation severity increases the extent of complex formation. At the same time, since the particles of platinum are dispersed by the complex formation, subsequent reduction produces more highly dispersed platinum metal.

There are limits to the improvements one can attain by increasing oxidation severity. As platinum-alumina is treated in a given oxygen partial pressure at successively higher temperatures, a temperature will be reached at which the oxygen pressure equals the decomposition pressure. Above this temperature, there will be decomposition to form platinum metal. The critical temperature will increase as oxygen partial pressure increases. If the reasonable assumption be made that mobility is greatest in the oxidized state, the treatment at a temperature such that the decomposition pressure exceeds the ambient pressure will result not only in the formation of platinum metal, but in an increase in crystallite size. Herrmann, *et al.*,⁹ have reported a decrease in the amount of soluble platinum on heating in air at 593 and 625°.

The results given in Table II illustrate this hypoth-

esis. As oxygen partial pressure is increased with temperature held constant, the amount of platinum-alumina complex increases. As in Table I, this increase is accompanied by a subsequent increase in platinum dispersion upon reduction, as measured by the rate of H₂-D₂ exchange. Also, as temperature is increased at constant oxygen pressure, the extent of complex formation passes through a maximum, as predicted. This critical temperature, at which the oxygen partial pressure equals the decomposition pressure, is near 510° at 0.21 atm. and near 580° at 1.0 atm.

It is concluded, therefore, that in the oxidized state a platinum-alumina complex does exist, but that it is converted to metal on treatment with hydrogen. Furthermore, the degree of dispersion of this metal increases with an increase in the fraction of platinum soluble in the oxidized state.

Acknowledgment.—The authors wish to acknowledge the assistance of J. S. Melik in determining rates of H₂-D₂ exchange.

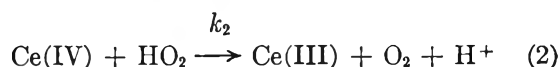
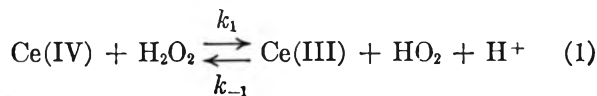
THE KINETICS OF THE OXIDATION OF HYDROGEN PEROXIDE BY CERIUM(IV)¹

BY G. CZAPSKI, B. H. J. BIELSKI, AND N. SUTIN

Chemistry Department, Brookhaven National Laboratory,
Upton, Long Island, New York

Received May 28, 1963

Baxendale has reported that the oxidation of hydrogen peroxide by cerium(IV) is complete within a few seconds at room temperature, even at micromolar concentrations of the two reactants, and has proposed that the reaction proceeds in two one-electron steps.² The kinetics of the hydrogen peroxide-induced cerium(III)-cerium(IV) exchange in 0.8 *N* sulfuric acid solutions have been studied by Sigler and Masters.³ Following Baxendale, they have proposed that the hydrogen peroxide-cerium(IV) reaction proceeds *via* the two-stage process



with $k_{-1}/k_2 = 0.129 \pm 0.013$ at 0°. According to Baer and Stein, on the other hand, the reverse of reaction 1 does not occur to any significant extent.⁴ The conclusions of Baer and Stein are based on studies of the stoichiometry of the hydrogen peroxide-cerium(IV) system. The formation of perhydroxyl radicals as intermediates in the hydrogen peroxide-cerium(IV) reaction, as required by the above reaction scheme, recently has been confirmed by means of electron spin resonance spectroscopy.^{5,6}

(1) Research performed under the auspices of the U. S. Atomic Energy Commission.

(2) J. H. Baxendale, *J. Chem. Soc. (London), Spec. Publ. No. 1*, 40 (1954).

(3) P. B. Sigler and B. J. Masters, *J. Am. Chem. Soc.*, **79**, 6353 (1957).

(4) S. Baer and G. Stein, *J. Chem. Soc.*, 3176 (1953).

(5) E. Saito and B. H. J. Bielski, *J. Am. Chem. Soc.*, **83**, 4467 (1961).

(6) B. H. J. Bielski and E. Saito, *J. Phys. Chem.*, **66**, 2266 (1962).

(9) R. A. Herrmann, S. F. Adler, M. S. Goldstein, and R. M. DeBaun, *J. Phys. Chem.*, **65**, 2189 (1961).

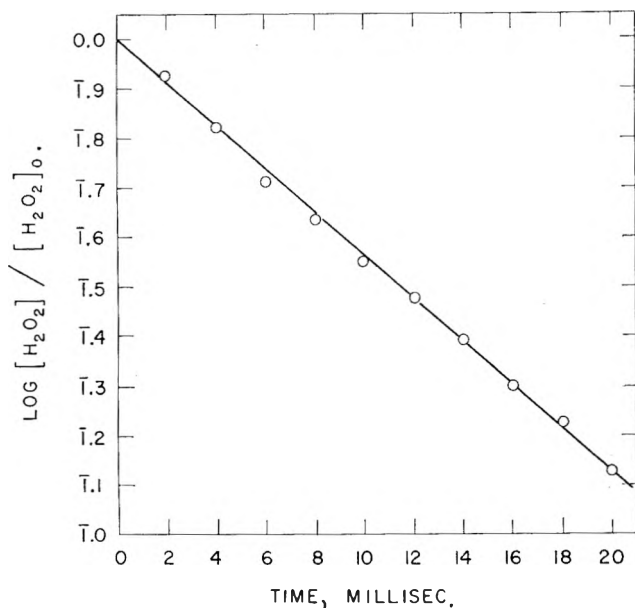


Fig. 1.—First-order plot of the kinetic data obtained in the first experiment of Table II. $[\text{Ce(IV)}]_0 = 92.5 \times 10^{-6} F$, $[\text{H}_2\text{O}_2]_0 = 7.50 \times 10^{-6} F$, $[\text{H}_2\text{SO}_4] = 0.8 N$, $T = 25.0^\circ$.

In order to obtain additional information, we have studied the kinetics of the hydrogen peroxide-cerium(IV) reaction in 0.8 *N* H_2SO_4 using a flow technique. The results obtained confirm the mechanism proposed by Sigler and Masters, and in addition establish that $k_1 = 1.0 \pm 0.1 \times 10^6 F^{-1} \text{sec.}^{-1}$ at 25.0° .

Experimental

Ceric sulfate (G. Frederick Smith), cerous sulfate (Amend Drug & Chemical Co.), hydrogen peroxide (Baker Analyzed Reagent), and sulfuric acid (Baker and Adamson) were used without further purification. The solutions for the kinetic measurements were prepared with triply-distilled water. The kinetics were studied in 0.8 *N* sulfuric acid; no attempt was made to keep the ionic strength of the solutions constant. The ceric sulfate solution was standardized spectrophotometrically; a value of 5580 was assumed for the extinction coefficient of ceric sulfate at 320 $m\mu$.⁷ The cerous sulfate and hydrogen peroxide were estimated either directly or indirectly as ceric sulfate; the cerous sulfate was estimated after the addition of excess potassium persulfate, and the hydrogen peroxide after the addition of excess ceric sulfate.

The disappearance of ceric sulfate was followed spectrophotometrically by means of a modified version of the rapid-mixing and flow apparatus which has been described previously.^{8,9} The modification allowed reactions with half-times down to a few milliseconds to be studied by means of the stopped-flow technique. All the kinetic measurements were made at 25.0° . A first-order plot of the kinetic data obtained in the first experiment of Table II is shown in Fig. 1.

Results and Discussion

If it is assumed that the hydrogen peroxide-cerium(IV) reaction proceeds *via* reactions 1 and 2, the rate of disappearance of cerium(IV) is given by

$$\frac{d[\text{Ce(IV)}]}{dt} = \{k_{-1}[\text{Ce(III)}] - k_2[\text{Ce(IV)}]\}[\text{HO}_2] - k_1[\text{Ce(IV)}][\text{H}_2\text{O}_2] \quad (3)$$

where the hydrogen ion and sulfate ion concentrations have been included in the appropriate rate constants and the reverse of reaction 2 has been neglected. The

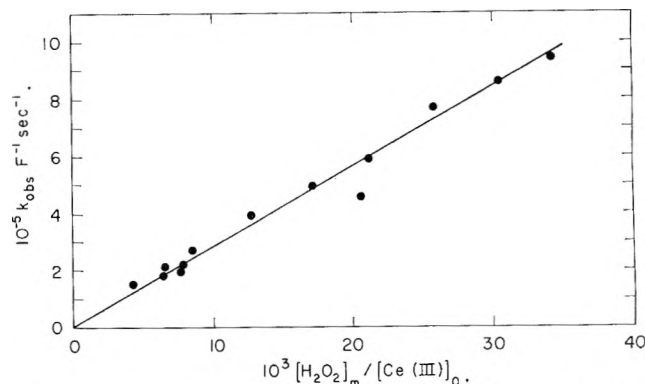


Fig. 2.—Dependence of k_{obs} on $[\text{H}_2\text{O}_2]_m/[\text{Ce(III)}]_0$ at 25.0° .

TABLE I
OXIDATION OF HYDROGEN PEROXIDE BY CERIC SULFATE
 $[\text{Ce(III)}] \gg [\text{Ce(IV)}]$, $[\text{H}_2\text{O}_2] > [\text{Ce(IV)}]$, $[\text{H}_2\text{SO}_4] = 0.8 N$,
 $T = 25.0^\circ$

$10^6[\text{Ce(IV)}]_0$, <i>F</i>	$10^2[\text{Ce(III)}]_0$, <i>F</i>	$10^4[\text{H}_2\text{O}_2]_0$, <i>F</i>	$10^{-3}k_{\text{obs}}$, $F^{-1} \text{sec.}^{-1}$
15.5	6.20	4.08	2.10
33.0	6.40	5.04	2.14
33.0	2.40	5.04	4.60
35.5	5.93	7.65	3.92
35.5	5.93	10.3	4.81
35.5	5.93	12.7	5.81
35.5	5.93	15.5	7.64
35.5	5.93	18.2	8.50
35.5	5.93	20.4	9.38
36.5	5.93	2.57	1.46
36.5	5.93	5.02	2.66
50.0	6.20	4.08	1.74
64.0	6.40	5.04	1.96

TABLE II
OXIDATION OF HYDROGEN PEROXIDE BY CERIC SULFATE
 $[\text{Ce(IV)}] > [\text{H}_2\text{O}_2]$, $[\text{H}_2\text{SO}_4] = 0.8 N$, $T = 25.0^\circ$

$10^6[\text{Ce(IV)}]_0$, <i>F</i>	$10^2[\text{Ce(III)}]_0$, <i>F</i>	$10^4[\text{H}_2\text{O}_2]_0$, <i>F</i>	k'_{obs} , sec.^{-1}
92.5	..	7.50	101
103	..	5.50	94.5
147	5.56	6.50	24.7
147	11.2	6.50	15.1
147	20.2	6.50	9.30
147	28.0	6.50	7.58
147	42.6	6.50	5.33
147	55.6	6.50	4.74
147	60.7	6.50	4.00
147	69.6	6.50	3.49
147	88.6	6.50	2.88
147	111.0	6.50	2.25
200	3.90	5.00	88.9
200	4.88	5.00	71.9
200	5.75	5.00	62.5
200	7.96	5.00	53.6
294	8.90	13.5	71.0
294	33.4	13.5	28.0
294	64.0	13.5	17.1
294	83.4	13.5	11.6

steady-state equation for the concentration of the perhydroxyl radical is

$$\frac{d[\text{HO}_2]}{dt} = 0 = k_1[\text{Ce(IV)}][\text{H}_2\text{O}_2] - \{k_{-1}[\text{Ce(III)}] + k_2[\text{Ce(IV)}]\}[\text{HO}_2] \quad (4)$$

Solving eq. 4 for the steady-state concentration of the perhydroxyl radical and introducing this value into eq. 3 gives

(7) A. I. Medalia and B. J. Byrne, *Anal. Chem.*, **23**, 453 (1951).

(8) N. Sutin and B. M. Gordon, *J. Am. Chem. Soc.*, **83**, 70 (1961).

(9) G. Dulz and N. Sutin, to be published.

$$\frac{d[\text{Ce(IV)}]}{dt} = -\frac{2k_1k_2[\text{Ce(IV)}]^2[\text{H}_2\text{O}_2]}{k_{-1}[\text{Ce(III)}] + k_2[\text{Ce(IV)}]} \quad (5)$$

The rate of disappearance of cerium(IV) will be given by eq. 5 provided eq. 3 and the steady-state approximation for the concentration of the perhydroxyl radical are valid. It is possible to derive two limiting kinetic expressions, which depend on the relative concentrations of cerous sulfate, ceric sulfate, and hydrogen peroxide, and these expressions will be discussed in turn.

Case 1.—In this case $[\text{Ce(III)}] \gg [\text{Ce(IV)}]$ and $[\text{H}_2\text{O}_2] > [\text{Ce(IV)}]$. If $k_{-1}[\text{Ce(III)}] \gg k_2[\text{Ce(IV)}]$ eq. 5 becomes

$$\frac{d[\text{Ce(IV)}]}{dt} = -\frac{2k_1k_2[\text{H}_2\text{O}_2][\text{Ce(IV)}]^2}{k_{-1}[\text{Ce(III)}]} = -k_{\text{obsd}}[\text{Ce(IV)}]^2 \quad (6)$$

where

$$k_{\text{obsd}} = \frac{2k_1k_2[\text{H}_2\text{O}_2]}{k_{-1}[\text{Ce(III)}]} \quad (7)$$

Values of k_{obsd} calculated from the integrated form of eq. 6 are presented in Table I. Each value of k_{obsd} presented in this table is the mean of four determinations. Individual determinations differed from the mean by less than 10%. The values of k_{obsd} are plotted against $[\text{H}_2\text{O}_2]_{\text{m}}/[\text{Ce(III)}]_0$ in Fig. 2, where $[\text{H}_2\text{O}_2]_{\text{m}}$ is the mean concentration of hydrogen peroxide during the run. It will be seen that the plot is linear, and of zero intercept, as required by eq. 7. The value of k_1k_2/k_{-1} at 25.0° calculated from the slope is $1.37 \times 10^7 F^{-1} \text{sec}^{-1}$.

Case II.—In this case $[\text{Ce(IV)}] > [\text{H}_2\text{O}_2]$. Under these conditions eq. 5 reduces to

$$\frac{d[\text{Ce(IV)}]}{dt} = 2\frac{d[\text{H}_2\text{O}_2]}{dt} = -2k'_{\text{obsd}}[\text{H}_2\text{O}_2] \quad (8)$$

where

$$k'_{\text{obsd}} = \frac{k_1k_2[\text{Ce(IV)}]^2}{k_{-1}[\text{Ce(III)}] + k_2[\text{Ce(IV)}]} \quad (9)$$

or

$$\frac{[\text{Ce(IV)}]}{k'_{\text{obsd}}} = \frac{1}{k_1} + \frac{k_{-1}[\text{Ce(III)}]}{k_1k_2[\text{Ce(IV)}]} \quad (10)$$

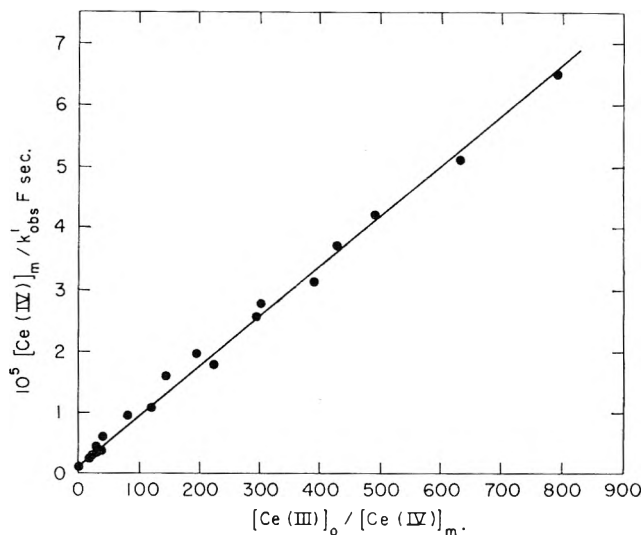


Fig. 3.—Dependence of $[\text{Ce(IV)}]_{\text{m}}/k'_{\text{obsd}}$ on $[\text{Ce(III)}]_0/[\text{Ce(IV)}]_{\text{m}}$ at 25.0°.

Values of k'_{obsd} calculated from the integrated form of eq. 8 are presented in Table II. As in case I, each value of k'_{obsd} is the mean of four determinations with the individual determinations differing from the mean by less than 10%. The values of $[\text{Ce(IV)}]/k'_{\text{obsd}}$ are plotted against $[\text{Ce(III)}]_0/[\text{Ce(IV)}]_{\text{m}}$ in Fig. 3, where $[\text{Ce(IV)}]_{\text{m}}$ is the mean concentration of cerium(IV) during the run. It will be seen that the plot is linear and of finite intercept, as required by eq. 10. Since the intercept is very small, the value of k_1 was determined directly by measuring the rate of the hydrogen peroxide–cerium(IV) reaction at high cerium(IV) concentrations, but in the absence of added cerium(III). The results of these measurements, which are included in Table II, give $k_1 = 1.0 \pm 0.1 \times 10^6 F^{-1} \text{sec}^{-1}$ at 25.0°. This value of k_1 is in good agreement with the value given by the intercept of Fig. 3. The slope of Fig. 3 gives $1.19 \times 10^7 F^{-1} \text{sec}^{-1}$ for the value of k_1k_2/k_{-1} at 25.0°, which is in good agreement with the value calculated from the slope of Fig. 2. The mean of these values is $1.28 \pm 0.1 \times 10^7 F^{-1} \text{sec}^{-1}$, corresponding to a value of 13 ± 2 for k_2/k_{-1} at 25.0°. This value is consistent with that obtained by Sigler and Masters at 0°.³

The studies described above are thus consistent with the mechanism proposed by Sigler and Masters and in addition establish that $k_1 = 1.0 \pm 0.1 \times 10^6 F^{-1} \text{sec}^{-1}$ in 0.8 N sulfuric acid at 25.0°.

COMMUNICATION TO THE EDITOR

ON LARGE DIFFERENCES IN THE EQUILIBRIUM SOLUBILITIES OF HYDROGEN AND DEUTERIUM IN PLATINUM-PALLADIUM ALLOYS

Sir:

The absorption of deuterium by palladium has been investigated recently, utilizing the technique of direct absorption of deuterium gas from acidic heavy water solutions.¹ The course of absorption was followed by

(1) T. B. Flanagan, *J. Phys. Chem.*, **65**, 280 (1961).

changes of relative resistance and electrode potential of the wire specimens. It previously has been demonstrated that equilibrium absorption data are obtained with this technique.² In agreement with earlier work, it was found that the final equilibrium solubility of deuterium in palladium does not differ appreciably from that of hydrogen in palladium, *i.e.*, $\text{D/Pd} = 0.65$, $\text{H/Pd} = 0.69$ (atomic ratios, 25°, 1 atm. pressure). Having regard to this difference in solubilities in

(2) T. B. Flanagan and F. A. Lewis, *Trans. Faraday Soc.*, **55**, 1409 (1959).

palladium (25°), a separation procedure for hydrogen isotopes is not particularly promising (barring special chromatographic procedures³).

Carson, *et al.*,⁴ have utilized the technique mentioned above to investigate the absorption of hydrogen by a series of platinum-palladium alloys. This communication reports the extension of this technique to the absorption of deuterium by these same alloys. These results are shown in Table I as compared to the equilibrium solubilities of hydrogen in the same alloys.

TABLE I
EQUILIBRIUM SOLUBILITIES OF HYDROGEN AND DEUTERIUM IN
PLATINUM-PALLADIUM ALLOYS (25°, 1 ATM.)

Atomic per cent platinum	Atomic ratios	
	H/Pd	D/Pd
0	0.69	0.65
2.79	.64	.51
5.73	.59	.38
8.80	.46	.03
12.03	.20	.02

It may be seen from Table I that there is a significant difference in the equilibrium solubilities of hydrogen and deuterium at certain alloy compositions, *i.e.*, 8.80 and 12.03% platinum. The equilibrium isotopic solubility ratio observed for these alloys, approximately 10:1, approaches the maximum kinetic separation factors previously observed.

This large difference in isotopic solubilities suggests that these alloys may be utilized to effect an isotopic

(3) E. Gluekauf and G. P. Kitt, *Proc. Intern. Symp. Isotope Separation Amsterdam*, 227 (1957).

(4) A. Carson, T. Flanagan, and F. Lewis, *Trans. Faraday Soc.*, **56**, 363, 371, 1332 (1960).

separation at 25°. To test the feasibility of such a separation the following experiments were performed. An acidic solution of light and heavy water (50% heavy water, 0.1 *N*) was electrolyzed with a platinum electrode as anode and a 12.03% platinum-palladium wire specimen as cathode. After electrolysis for 17 hr. at 1 ma. current, the relative resistance of the specimen increased from 1.000 to 1.567 ohms.⁴ The sample was removed from the electrolysis cell and degassed *in vacuo* (300°). The total gas evolved was analyzed with the aid of a mass spectrometer as: 83.5% H₂, 15.8% HD, and 0.7% D₂; it may be noted that these percentages are close to those predicted by assuming statistical equilibrium. The separation factor, $(C_H/C_D)_{II}/(C_H/C_D)_I$, is 10.6, where the subscript II refers to the ratio of the total concentrations of hydrogen and deuterium in the final state and the subscript I refers to their ratio in the initial state. A further electrolysis experiment was performed with a water mixture richer in heavy water (70% heavy water). The separation factor achieved in this experiment was 15.3.

Acknowledgment.—This research was supported in part by the U. S. Atomic Energy Commission, Contract No. AT(30-1)-3000. The author is indebted to Arnulf Maeland for assistance and F. J. Norton of the General Electric Research Laboratory for the mass spectrometric analyses.

DEPARTMENT OF CHEMISTRY
UNIVERSITY OF VERMONT
BURLINGTON, VERMONT

TED B. FLANAGAN

RECEIVED NOVEMBER 9, 1962